Titre: Title:	Inelastic seismic response of steel roof deck diaphragms including effects of non-structural components and end laps
Auteur: Author:	Wei Yang
Date:	2003
Type:	Mémoire ou thèse / Dissertation or Thesis
Référence: Citation:	Yang, W. (2003). Inelastic seismic response of steel roof deck diaphragms including effects of non-structural components and end laps [Mémoire de maîtrise, École Polytechnique de Montréal]. PolyPublie. https://publications.polymtl.ca/7307/

URL de PolyPublie: PolyPublie URL:	https://publications.polymtl.ca/7307/
Directeurs de recherche: Advisors:	Robert Tremblay, & Colin Rogers
Programme: Program:	Non spécifié

UNIVERSITÉ DE MONTRÉAL

Inelastic Seismic Response of Steel Roof Deck Diaphragms Including Effects of Non-Structural Components and End Laps

WEI YANG
DÉPARTEMENT DES GÉNIES CIVIL, GÉOLOGIQUE ET DES MINES
ÉCOLE POLYTECHNIQUE DE MONTRÉAL

MÉMOIRE PRÉSENTÉ EN VUE DE L'OBTENTION
DU DIPLÔME DE MAÎTRISE ÈS SCIENCES APPLIQUÉES
(GÉNIE CIVIL)
DECEMBER 2003

Your file Votre référence
ISBN: 0-612-90866-6
Our file Notre référence
ISBN: 0-612-90866-6

UNIVERSITÉ DE MONTRÉAL

ÉCOLE POLYTECHNIQUE DE MONTRÉAL

Ce mémoire intitulé :

Inelastic Seismic Response of Steel Roof Deck Diaphragms Including Effects of Non-Structural Components and End Laps

présenté par : YANG Wei

en vue de l'obtention du diplôme de : Maîtrise ès sciences appliquées

a été dûment accepté par le jury d'examen composé de :

M. MASSICOTTE Bruno, Ph.D., président

M. TREMBLAY Robert, Ph.D., membre et directeur de recherche

M. ROGERS Colin, Ph.D., membre et codirecteur de recherche

M. PROULX Jean, Ph.D., membre

ACKNOWLEDGEMENTS

I would like to give me thankfulness to all the people and groups who provided many helps, informations and funds.

I hope to express my heartfelt thanks to Prof. Robert Tremblay and Prof. Colin Rogers, my director and co-director for the project, for their specialized and all-rounded assistance.

I am also very grateful to M. Gérard Degrange, M. Denis Fortier et M. Patrice Bélanger, the technical staff at the Laboratoire de Structures de l'École Polytechnique, M. David Pearce, the student from McGill University, Ms. Marie-Christine Denis, M. Jerome Isabelle, and M. Benoit Turcotte, the students in École Polytechnique. Their efforts in the installation of specimen and tests are deserving of highly praise.

The following organizations and companies are highly appreciated for their contributions in the project : Natural Sciences and Engineering Research Council of Canada (NSERC); Canadian Institute of Steel Construction (CISC); Canadian Sheet Steel Building Institute (CSSBI); Steel Deck Institute (SDI); Canam Manac Group; Canadian Welding Bureau; Hilti Limited and ITW Buildex; Ontario Industrial Roofing Contractors Association (OIRCA); Association des Maitres Couvreurs du Quebec (AMCQ), etc.

RÉSUMÉ

Cette thèse porte sur le comportement dynamique non élastique des diaphragmes en acier utilisé dans la toiture des bâtiments en acier de faible hauteur. Au total, quatre groupes d'essais de diaphragme à grande échelle ont été effectués (12 spécimens). Les résultats de ces essais, combinés à ceux réalisés dans des études précédentes, démontrent que l'utilisation de feuilles de tablier de faible longueur (avec des joints de chevauchement d'extrémité) diminue de façon significative la rigidité en cisaillement des diaphragmes, mais n'influencera pas sensiblement leur résistance au cisaillement. Les matériaux d'enveloppe de la toiture dont les différents panneaux à base de bois ou de gypse, les panneaux d'isolation thermique, le pare-vapeur, les membranes imperméables etc, peuvent augmenter la résistance au cisaillement et la rigidité des diaphragmes lorsque fixé convenablement au tablier. On a observé que la barrière thermique, qui était constituée de panneaux de gypse rigides dans leur plan et fixés mécaniquement au tablier métallique dans les spécimens d'essais, influençait le plus les propriétés de diaphragme Cette observation a été également vérifiée par une analyse par éléments finis 3D du tablier métallique avec panneaux de gypse.

Les résultats d'analyses dynamiques non linéaires d'un bâtiment en acier d'étage simple réalisés dans cette étude ont permis de conclure qu'il est possible d'utiliser un diaphragme de toit avec assemblages par clous à la structure et vis entre les feuilles de tablier comme l'élément dissipateur d'énergie dans le système de résistance aux charges latérales.. Pour ce type de diaphragme, on suggère d'utiliser un facteur de modification des forces pour la ductilité, R_d, égal à 2.0 et le facteur de modification des forces pour la sur-résistance , R_o peut être posé $R_o = R_\phi = 1/\phi$. Pour les diaphragme avec soudures à la structure et joints sertis entre les feuilles de tablier, on recommande d'utiliser $R_o = R_d = 1.0$, c'est-à-dire que ce type de diaphragme de toit doit demeurer élastique sous les sollicitations sismiques de conception.

Une autre étude analytique réalisée dans le cadre de ce projet indique que les effets de la torsion sont habituellement moins importants dans les bâtiments d'un seul étage avec diaphragmes de toit flexibles par rapport à ce que l'on observe pour les mêmes bâtiments avec un diaphragme rigide. La pratique courante de supposer un diaphragme rigide au lieu d'un diaphragme flexible pour le calcul des effets de la torsion semble, en général, acceptable. Il est cependant important de vérifier les déformations en tenant compte des déformations du diaphragme et les niveaux de ductilité dans les contreventements peuvent être plus élevés pour les structures avec diaphragmes flexibles.

ABSTRACT

This thesis describes the topics that are closely relevant to the inelastic dynamic behaviour of steel roof deck diaphragms. In total, four groups (12 specimens) of large-scale diaphragm tests were carried out. These tests, together with the tests finished by earlier researchers, demonstrate that short sheet length (with end laps) will largely decrease the in-plane shear stiffness, but will not noticeably influence the shear strength. The roofing material composed of various wood or gypsum based panels, insulation boards, vapor barrier, waterproof membranes, etc. can increase both the diaphragm shear strength and stiffness if appropriately attached to the steel deck. The thermal barrier, e.g. the gypsum board in the test model, which is quite rigid in its plane and is mechanically fastened to the steel deck, was found to influence the diaphragm properties to the greatest extent. This was also verified by a 3-D stress and deformation analysis by FEM of deck panel-gypsum board assembly.

According to inelastic dynamic analyses of a single storey steel building performed in the study, it was found that it is possible to use a roof diaphragm system with nailed fasteners to the frame and screwed fasteners in side-lap as the energy-dissipating element in the seismic load carrying path. For this system, a ductility-related force modification factor, R_d, of 2.0 is suggested and the overstrength-related force modification factor, R_o can be taken as $R_o = R_\phi = 1 / \phi$. In the case of diaphragms with welded frame fasteners and button punched side laps, $R_o = R_d = 1.0$ is recommended, i.e. this type of roof diaphragm should be designed to remain elastic under design seismic load conditions.

Another analytical study performed in this research indicated that single-storey buildings constructed with flexible roof diaphragms usually results in less of torsion effects as compared with the same buildings with rigid roof diaphragms. The current design practice of using a rigid roof assumption instead of a flexible roof in

considering the building's torsion effects is, in general, acceptable. It is however important to include diaphragm deformations in the calculation of the storey drifts, and the ductility demand on the braces can be higher for buildings with flexible roof diaphragms.

CONDENSÉ EN FRANÇAIS

1. INTRODUCTION

Les toitures en acier sont largement utilisées dans les bâtiments en acier à faible hauteur que l'on retrouve dans les secteurs industriel léger, commercial ou récréationnel. Un arrangement structural typique d'un bâtiment en acier d'un seul étage est montré sur la Figure 1, où les unités de tablier métallique du toit sont supportées par les poutrelles de toit. Le tablier métallique du toit fournit une surface sur laquelle des matériaux de toiture tels que le pare-vapeur, l'isolation et la membrane imperméable à l'eau sont installés. La composition d'un toit typique peut être vue sur la Figure 2.

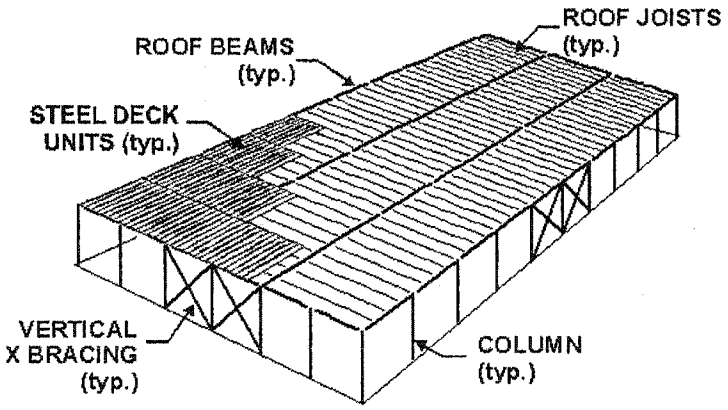

Figure 1. Arrangement structural typique d'un bâtiment en acier à un étage (de Rogers et de Tremblay, 2000)

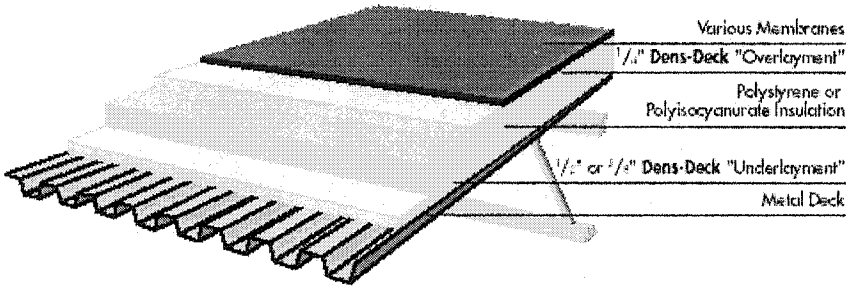

a) 3-D view of roof composition

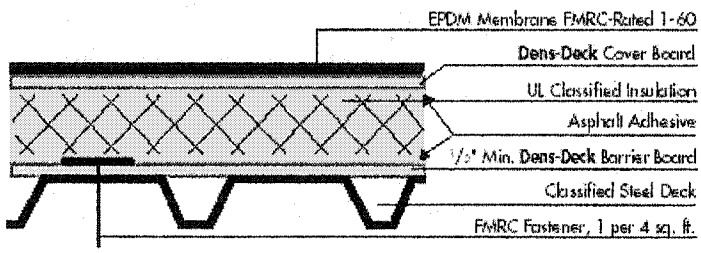

b)Section view of roof composition

Figure 2. Composition typique d'un toit (adaptée de G-P Gypsum Corporation, 2000)

Les feuilles de tablier métallique du toit doivent être bien reliées aux éléments porteurs sous-jacents (poutrelles, poutres ou fermes), ceci pour plusieurs raisons. Les feuilles de tablier froment un diaphragme quand le bâtiment est soumis aux charges latérales, et par conséquent, toutes les forces dans le diaphragme de toit doivent être transférées au système vertical qui le supporte. Les charges verticales de soulèvement dues au vent doivent aussi être transférées à la structure métallique principale. Finalement, le diaphragme de toit agit souvent en tant qu'appui latéral qui limite le déplacement latéral des membrures fléchies du toit.

D'après les résultats de recherche, un assemblage adéquat du tablier métallique est essentiel pour le fonctionnement approprié du diaphragme de toit. Ce composant du diaphragme peut résister aux forces de cisaillement importantes dans le plan du

diaphragme et permet d'éliminer le besoin d'un système supplémentaire de contreventement horizontal au toit. L'étude des diaphragmes de toit en acier a commencé il y'a un demi siècle. Cependant, presque toutes les recherches se sont intéressées au comportement statique des diaphragmes. Ce n'est qu'à partir des années 80 que le comportement dynamique des diaphragmes a été pris en considération (Mazzolani et Labini, 1983). La connaissance du comportement dynamique ou cyclique d'un diaphragme est important dans un contexte de conception parasismique. Pour s'assurer de l'efficacité de la structure, la pratique habituelle est basée sur l'approche de conception par capacité, selon laquelle une pièce de la charpente dans le système de résistance aux charges latérales est choisie et conçue pour agir en tant qu'élément absorbant et dissipant l'énergie sismique. Cet élément structural, également connu sous le nom du maillon faible de la chaine de résistance aux charges latérales, est supposé exhiber un comportement inélastique ductile de telle sorte que les charges sismiques sont reprises avec des grandes déformations sans perte de capacité du système de contreventement. Le reste des éléments structuraux est conçu pour demeurer élastique ou pour subir de faibles déformations inélastiques pendant une secousse sismique.

Depuis 1999, on a entrepris un programme de recherche à l'École Polytechnique de Montréal visant à étudier le comportement sismique inélastique des diaphragmes de toit en acier. Ce programme inclut l'étude du comportement au niveau des connexions du diaphragme. Cette thèse vient s'ajouter à une série de 37 essais de diaphragme à échelle réelle et plus de 400 essais réalisés sur les connexions. Elle se limite à l'étude du comportement structural des diaphragmes, incluant l'influence des composants non-structuraux. En outre, des détails de construction, tel que le chevauchement longitudinal aux extrémités des panneaux, n'ont pas encore été étudiés. Il est possible que ces deux facteurs aient une certaine influence sur le comportement sismique des diaphragmes, et une recherche bibliographique a été faite dans cette thèse pour vérifier si ces aspects ont été étudiés dans le passé.

La portée de cette thèse est limitée aux systèmes légers de tablier métallique pour les toits, aux matériaux communément utilisés pour la toiture (membrane et isolant) et aux bâtiments à un étage en acier. Au total, 12 essais sur des diaphragmes en porte-à-faux ont été réalisés. Les spécimens de diaphragme ont été construits avec des soudures ou des clous pour les assemblages tablier-charpente, et des points de sertissage ou des vis pour les joints de chevauchement longitudinaux. Les feuilles de tablier métallique avaient une profondeur de 38 millimètres avec une épaisseur nominale de 0.76 ou 0.91 millimètre et d'une résistance nominale de 230 MPa. Des essais ont aussi été réalisés avec du tablier métallique de 76 mm de profondeur. Les matériaux non-structuraux de toiture ont été choisis afin de représenter une composition typique du Canada, et par conséquent, ont été basés sur la conception SBS-34 de l'Association Maîtres Couvreurs du Québec (AMCQ).

Pour la phase analytique du projet, un bâtiment de taille moyenne situé à Victoria B.C. a été étudié. Le bâtiment a été conçu selon la nouvelle version proposée du code national du bâtiment 2005 (NRCC 2001), et la conception aux états limites des structures métalliques CAN/CSA-S16.1 (CSA, 2001). La configuration d'assemblage par clous/vis a été employée pour la conception du diaphragme. Le diaphragme de toit en acier a été choisi pour agir en tant qu'élément absorbant l'énergie sismique, et deux valeurs de facteur de modification de force reliés à la ductilité ont été considérés. Dans les analyses, les modèles de diaphragme ont été ajustés sur la base des résultats de neuf essais sur des diaphragmes et trois accélérogrammes sismiques ont été utilisés. Dans le mémoire, on a aussi réalisé des analyses par éléments finis (FEM) de diaphragme avec et sans l'apport des panneaux de gypse qui sont utilisés dans la construction des la toiture, ceci afin de reproduire les résultats des essais réalisés avec les matériaux non-structuraux.

Dans la dernière partie du mémoire, on a aussi étudié, à l'aide d'un modèle numérique, l'influence de la flexibilité du toit sur la réponse torsionelle d'un bâtiment

en acier d'un seul étage. Dans cette étude, on a considéré deux rigidités différentes de toitures et huit accélérogrammes sismiques.

2. ESSAIS SUR DIAPHRAGMES À ÉCHELLE RÉELLE

2.1. Montage d'essais

Le montage utilisé permet de réaliser des essais sur un spécimen de diaphragme qui travaille comme une poutre profonde en porte-à-faux. La surface du diaphragme est de 6.096 x 3.658 m. La longueur des feuilles de tablier est de 6.096 m. La largeur du diaphragme correspond à la largeur de 4 feuilles de tablier métallique P3615 de Canam, soit 4 x 914 = 3656 millimètres. L'espacement des poutres intermédiaires est de 1.524 m. Les membrures du cadre d'acier supportant le tablier métallique sont des membrures de type HSS (section en acier creuse) 101.6x50.8x4.78, deux cornières 100x75x10, un fer plat de 304 x 25.4 mm, et un HSS 203.2x203.2x7.96. Le cadre d'essais avant l'installation du tablier métallique est montré sur la Figure 3. Une photo du cadre d'essais avec le spécimen de diaphragme de toit installé est présentée à la Figure 4.

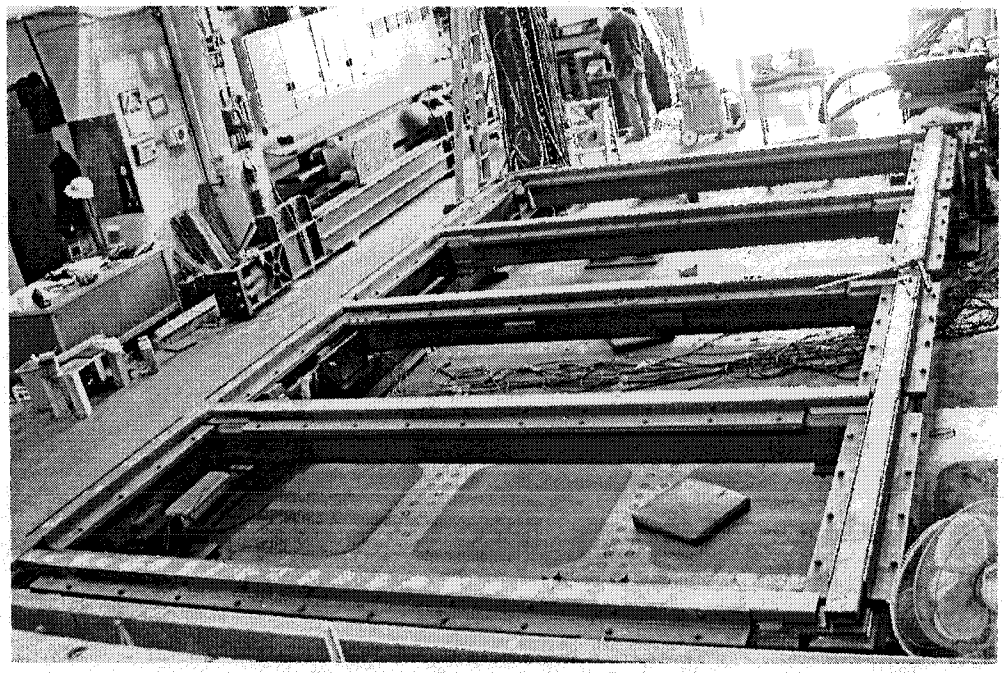

Figure 3. Photographie du cadre d'essais avant l'installation de plate-forme

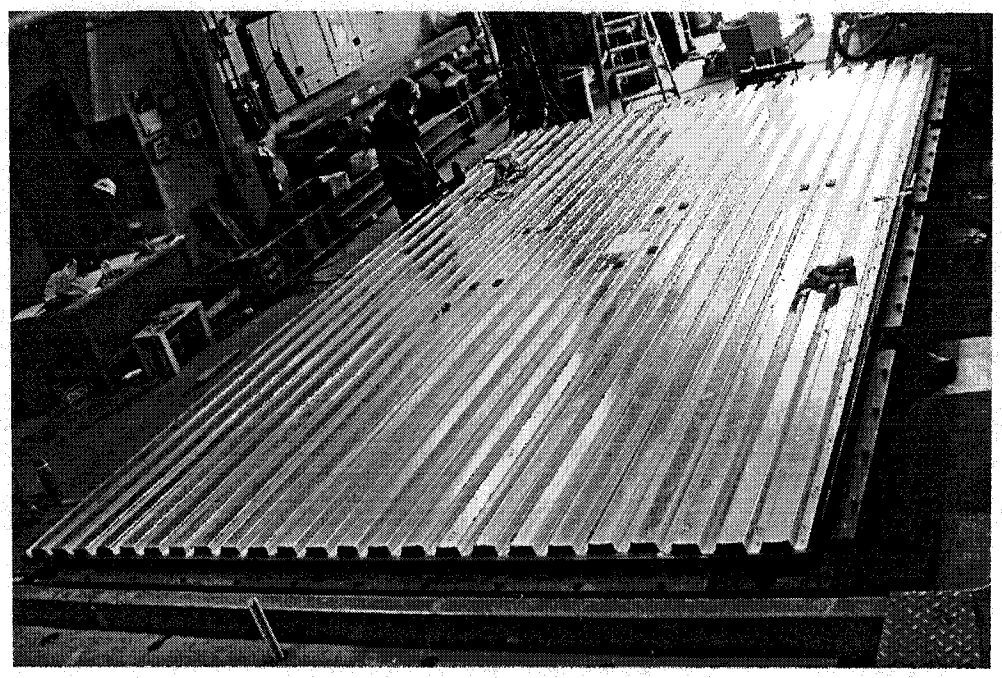

Figure 4. Installation finale du spécimen de diaphragme

2.2. L'installation matérielle de toiture

Avant cette recherche, aucun spécimen de diaphragme à l'École Polytechnique n'avait été construit avec des composantes non-structurales de toiture (isolation, membrane, etc.). Une combinaison de toiture, appelée SBS-34, de l'Association Maitres Couvreurs du Québec (AMCQ) a été choisie pour les spécimens d'essais. C'est un système courant et conventionnel de toit composé des couches suivantes (de haut en bas) :

- Deux couches (4 + 2.2 mm) d'une membrane SBS imperméable à l'eau;
- Un panneau de particules en bois inflammables de 25.4 mm d'épaisseur, collé à chaud avec un bitume de type 2;
- Une couche de 50.8 mm d'épaisseur d'isolation en polyisocyanate (ISO), adhérée à chaud avec un bitume de type 2 ;
- Un pare-vapeur constitué de deux couches en papier feutres asphaltés numéro 15 adhérées à chaud avec du bitume ;
- Une panneau de gypse de type X d'une épaisseur de 12.7 mm, fixé par 12 vis par panneau de 1.2 m x 2.4 m.
- Plancher d'acier.

Après la mise en place des feuilles de tablier métallique selon la configuration décrite précédemment pour former le diaphragme, le panneau de gypse a été fixé au diaphragme en acier avec les vis spéciales (Figure 5). Les vis sont de 4.76 millimètres de diamètre, 41 millimètres long, et ont 16 filets par pouce de longueur. La rondelle est faite d'un disque en acier galvanisé épais de 0.46 millimètres avec un diamètre de 76.2 millimètres (3"). Le cadre d'essais a exigé 2.5 morceaux de plaques de gypse standard (4'x8') dans la longue direction (2.5 x 8' = 20'), et 3 morceaux dans la plus

courte direction (3 x 4' = 12'). Pour chaque panneau complet de gypse, un total de 12 vis a été utilisée, Pour chacun des demi-panneaux de gypse, on a utilisé 9 vis. Une fois que les panneaux de gypse installés, les autres couches ont été placées les unes sur les autres. Le spécimen d'essai fini avec le diaphragme en acier et les composantes non-structurales est montré à la Figure 6.

Figure 5. Installation de panneaux de gypse sur le diaphragme en acier

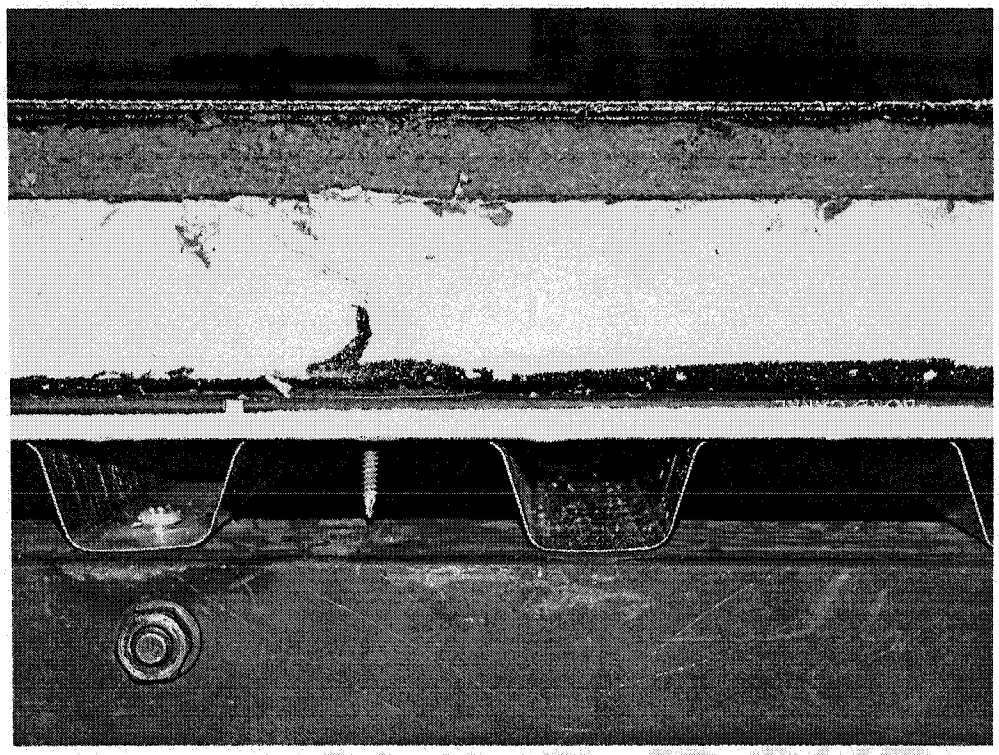

Figure 6. Vue en section du spécimen après l'installation de la toiture

2.3. Analyse des résultats des essais.

2.3.1. Influence des joints de chevauchement sur la résistance et la rigidité des diaphragmes

2.3.1.1. Diaphragmes assemblés par clou/vis

Dans le Tableau 1, les mesures de la résistance et de la rigidité au cisaillement des essais nos. 4 et 7 par Essa et al. (2001) et des essais nos. 28 et 29 par Martin (2002) sont comparés aux valeurs obtenues des essais nos. 39 et 40 réalisés dans le cadre de cette recherche. Dans les deux derniers essais, on avait un joint de chevauchement des feuilles de tablier à la mi-longueur du diaphragme (deux feuilles de 3048 mm de

longueur = 6096 mm). La longueur des feuilles de tablier était donc différente de celle que l'on avait dans les essais des études antérieures. Les cas de chargement étaient aussi différents. Cependant, on a utilisé le même tablier métallique et les mêmes connecteurs. D'après les résultats présentés, il est évident que la présence du joint de chevauchement longitudinal n'a pas influencé la résistance au cisaillement du spécimen de diaphragme, mais que la rigidité au cisaillement a été affectée à la baisse lors des essais monotonique (M, no. 39) et sismique de courte durée (SD, no. 40). On note également d'après le Tableau 1 que l'évaluation de la force et la rigidité selon les approches de SDI coïncide assez bien avec les résultats des essais 39 et 40, malgré que les joints de chevauchement d'extrémité ne sont pas pris en compte dans la méthode du SDI.

Tableau 1 : Comparaison de la résistance et de la rigidité pour les essais 39 et 40 avec essais d'études précédentes

Essai no.	Résultats		Rapport			
	Su	G'	Su	G'	Su	G'
	kN/m	kN/mm	Test/SDI	Test/SDI	Test/SDI*	Test/SDI*
38-76-6-NS-M-4	12.30	3.12	0.92	0.84	1.11	0.96
38-76-6-NS-Q-7	12.19	2.87	0.91	0.77	1.10	0.89
38-76-6-NS-SD-28	14.10	2.45	1.08	0.65	1.27	0.87
38-76-6-NS-LD-29	13.60	2.39	1.05	0.64	1.23	0.85
Moyenne 1 (Tests 4,7,28, et 29)	13.05	2.71	0.99	0.73	1.18	0.89
38-76-3-NS-M-39	11.28	1.73	0.88	1.02	1.01	1.08
38-76-3-NS-SD-40	12.68	1.58	0.99	0.93	1.13	0.98
Moyenne 2 (Tests 39, 40)	11.98	1.66	0.94	0.98	1.07	1.03
Rapport de la moyenne 2 à la moyenne 1	0.92	0.61	0.94	1.34	0.91	1.15

2.3.1.2. Diaphragmes assemblés avec soudures/sertissage

Dans le Tableau 2, on compare les mesures de la résistance et de la rigidité au cisaillement des essais nos. 1 et 2 par Essa et al. (2001) et de l'essai no. 20 par Martin (2002) à celles obtenues dans les essais nos. 41 et 42. Similairement, on trouve que le joint de chevauchement longitudinal n'a pas eu une influence significative sur la résistance au cisaillement. Toutefois, on observe une perte substantielle de rigidité de cisaillement. Encore là, l'approche du SDI donne des valeurs proches des essais.

Tableau 2 : Comparaison du cisaillement et de la rigidité pour les essais 41 et 42 avec d'autres essais

Essai no.	Résultats		Rapport			
	Su	G'	Su	G'	Su	G'
	kN/m	kN/mm	Test/SDI	Test/SDI	Test/SDI*	Test/SDI*
38-76-6-WB-M-1	8.05	2.14	0.83	0.77	0.71	0.78
38-76-6-WB-Q-2	7.53	2.15	0.78	0.78	0.66	0.78
38-76-6-WB-SD-20	9.81	2.44	1.07	0.74	0.86	0.88
Moyenne 1 (Tests 1,2 and 20)	8.46	2.24	0.89	0.76	0.74	0.81
38-76-3-WB-M-41	9.14	1.65	0.9	1.02	0.72	1.03
38-76-3-WB-SD-42	10.29	1.55	1.01	0.95	0.81	0.97
Mean 2 (Test 41, 42)	9.72	1.60	0.96	0.99	0.77	1.00
Rapport de la moyenne 2 à la moyenne 1	1.15	0.71	1.07	1.29	1.03	1.23

2.3.2. Influence des composantes non-structurales sur la résistance et la rigidité des diaphragmes

Les résultats d'essais sur diaphragme avec composantes non structurales sont présentés dans le Tableau 3 (essais nos. 45 et 46). Les résultats de plusieurs essais réalisés dans des études antérieures sur des tabliers sans composantes non structurales sont aussi donnés dans le tableau pour comparaison. Tous les essais ont été faits sur des diaphragmes construits avec le tablier métallique P3615B de Canam, avec acier de 0.76 millimètre d'épaisseur et assemblages avec clous et vis.

Dans le tableau 3, on observe généralement que les matériaux de toiture augmentent la résistance et la rigidité du diaphragme. Une augmentation moyenne approximative de 26 % de la résistance a été enregistrée, en plus d'une augmentation moyenne de rigidité de 46% pour les diaphragmes testés. Mais la valeur de la moyenne 1 pour la rigidité G', qui est basée sur huit essais avec diaphragmes sans composantes non structurales, est égale à 0.77 pour le SDI, et 0.88 pour SDI*. Ces valeurs sont plus petites que 1.0 et il semble que l'approche du SDI surestime la rigidité des diaphragmes sans composantes non structurales qui sont assemblés avec vis et clous. En comparant la moyenne 1 des rapports test/SDI et test/SDI*, il semble que le premier fournit une meilleure évaluation de la résistance, mais le second donne une meilleure évaluation de la rigidité.

Tableau 3 : Comparaison entre les essais 4, 7, 5, 8, 28, 29.43, 44, 45, et 46

Essai no.	Résultats		Rapport			
	Su	G'	Su	G'	Su	G'
	kN/m	kN/mm	Test/SDI	Test/SDI	Test/SDI*	Test/SDI*
38-76-6-NS-M-4	12.30	3.12	0.92	0.84	1.11	0.96
38-76-6-NS-Q-7	12.19	2.87	0.91	0.77	1.10	0.89
38-76-6-NS-M-5*	11.48	3.02	0.86	0.81	1.06	0.90
38-76-6-NS-Q-8*	12.29	2.80	0.92	0.75	1.13	0.84
38-76-6-NS-SD-28	14.10	2.45	1.08	0.65	1.27	0.87
38-76-6-NS-LD-29	13.60	2.39	1.05	0.64	1.23	0.85
38-76-6-NS-M-43	13.40	2.58	1.06	0.71	1.24	0.83
38-76-6-NS-C-44	10.47	2.85	0.83	0.78	0.97	0.91
Moyenne 1 (Tests 4, 5, 7, 8, 28, 29, 43, and 44)	**12.53**	**2.76**	**0.95**	**0.74**	**1.14**	**0.88**
C.d.V. des spécimens ci-dessus	0.09	0.10	0.10	0.10	0.09	0.05
38-76-6-NS-M-R-45	15.60	4.17	1.24	1.14	1.44	1.34
38-76-6-NS-C-R-46	15.90	3.90	1.26	1.07	1.47	1.25
Moyenne 2 (Tests 45, 46)	**15.75**	**4.03**	**1.25**	**1.11**	**1.46**	**1.30**
Rapport de la moyenne 2 à la moyenne 1	**1.26**	**1.46**	**1.31**	**1.49**	**1.28**	**1.47**

Note :

1) Essais 4, 5, 8, et 7 par Essa et al. (2001), essais 28 et 29 par Martin (2002). Seulement l'essai 5 et l'essai 8 utilisent des connecteurs de type ITW Buildex, les autres utilisent des connecteurs Hilti.

2) La moyenne 1 est la moyenne des essais avec des diaprhamges sans somposantes non structurales; la moyenne 2 est la moyenne des essais avec des matériaux de toiture.

3. COMPORTEMENT SISMIQUE INÉLASTIQUE DU DIAPHRAGME DE TOIT EN ACIER

Un bâtiment en acier de taille moyenne à un seul étage (Figure 7), situé à Victoria, B.C., a été analysé en utilisant le programme d'analyse dynamique non linéaire RUAUMOKO (Carr, 2000). Les loi force-déformation d'hystérésis ont été ajustées par rapport aux résultats d'essais pour tenir compte de l'influence du type de connecteurs, de la longueur des feuilles de tablier, de la forme du profil du tablier, et de la présence des composantes non structurales (matériaux de toiture).

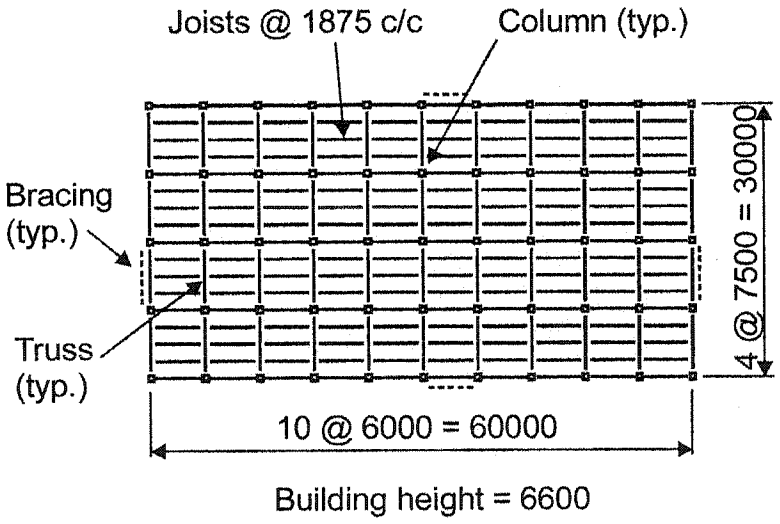

Figure 7. Vue en plan du bâtiment analysé (Martin, 2002)

Les analyses discutées dans cette section ont couvert un certain nombre de scénarios différents pour lesquels les combinaisons de facteurs suivants ont été utilisées :

- Deux valeurs de R_d, $R_d = 3.0$ et $R_d = 2.0$;
- Trois types d'assemblage de toit ;
  1) toit de type 1: tole sans composantes non structurales, aucun chevauchement, longueur des feuilles = 7500 mm;
  2) toit de type2 : tole sans composantes non structurales, avec joints de chevauchement, longueur des feuilles = 5625 mm;
  3) toit de type 3: avec composantes non structurales (toiture), aucun chevauchement, longueur des feuilles = 7500 mm.
- Trois accélérogrammes compatibles avec le spectre de dimensionnement sismique pour la ville de Victoria, C.-B.

Une illustration du modèle d'analyse de RUAUMOKO est montrée sur la Figure 8. Le modèle d'hystérésis de rigidité dégradante de Wayne Stewart (Stewart, 1987) fournit une bonne représentation du comportement observé dans des essais sur diaphragmes. Le toit du bâtiment a été discrétisé en des éléments de treillis de 3 x 3 m où le diaphragme était représenté par un élément diagonal de ressort de longueur LD = 4.243 m. Les membrures intérieures (verticales et horizontales) dans le modèle de treillis permettent de stabiliser les éléments ressort du diaphragme de toit.

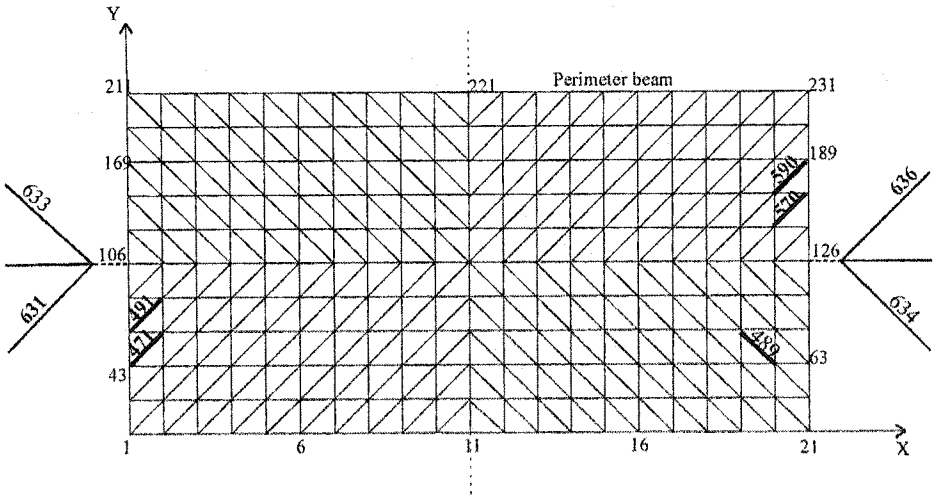

Figure 8. Modèle d'analyse de RUAUMOKO

Sur la Figure 8, les éléments de ressort représentés en gras représentent les éléments qui ont subi les plus grandes déformations lors des analyses dynamiques.

Après analyse dynamique, les aspects suivants ont été observés :

1) L'utilisation de feuilles de tablier plus courtes rend le diaphragme plus flexible. Les composantes non-structurales, si elles sont fixés convenablement au diaphragme, rendent le diaphragme plus rigide.

2) Concernant le comportement inélastique des diaphragmes en acier de toitutre, deux paramètres importants ont été introduits: la déformation plastique, γ_p, et le niveau de ductilité, μ_D. Les deux paramètres sont mesurés au niveau des éléments (local). Essa et al. (2001) ont recommandé que la déformation plastique ne dépasse pas γ_p = 10 rad/1000 pour les diaphragmes avec vis/clous. Cette valeur a été définie comme la déformation de cisaillement inélastique qui correspond à une résistance égale à 80% de la charge ultime, après avoir dépassé la résistance ultime. De ce point de vue, il semble que R_d=3.0 ne peut pas être employé pour le toit de type 1 parce que la déformation plastique obtenue des analyses excède cette limite. Cependant, R_d=3.0 peut être utilisé pour le toit de type 2 et pour le toit de type 3.

Concernant le niveau de ductilité, μ_D, les résultats des analyses indiquent que la ductilité est approximativement égale à R_d quand R_d=2.0, mais que la ductilité est beaucoup plus élevée et varie de manière significative quand R_d=3.0. Pour le toit de type 1, μ_D est beaucoup plus grand que prévu, c'est-à-dire que l'utilisation de R_d=3.0 pour le toit de type 1 peut causer des résultats inattendus comme, par exemple, une dégradation de la résistance due aux grandes déformations inélastiques. Les valeurs de μ_D pour le toit de type 2 et le toit de type 3 n'étaient pas consistantes non plus, mais les déformations inélastiques demeurent dans la gamme permise et, par conséquent, R_d=3.0 peut être employé pour ces deux types de toits.

4. ANALYSES STATIQUES DU DIAPHRAGME DE TOIT EN ACIER

Dans cette phase analytique, une portion d'une feuille de tablier métallique P3615B de Canam faisant 3200.4 mm de longueur et 952.5 mm de largeur a été analysée avec le logiciel d'éléments finis 3D SAP2000 (CSI, 2002). Dans l'une des analyse, les panneaux de gypse de la toiture ont été ajoutés au modèle pour fins de comparaisons. L'objectif de cette partie du projet était de mieux comprendre les effets des composantes non-structurales sur le comportement des diaphragmes de toit et de quantifier ces effets. L'analyse est statique et linéaire, et on examine seulement la rigidité en cisaillement de l'ensemble tablier-panneau de gypse et la distribution des forces dans les connecteurs. Le tablier a été divisé en 1596 éléments de coque, c'est-à-dire 38 éléments sur la largeur et 42 éléments sur la longueur (Figure 9). Comme mentionné, la dimension de la feuille de tablier est de 952.5 x 3200.4 mm, ce qui excède la dimension nominale de 914.4 x 3048 mm, soit la dimension en plan du cadre d'essais..

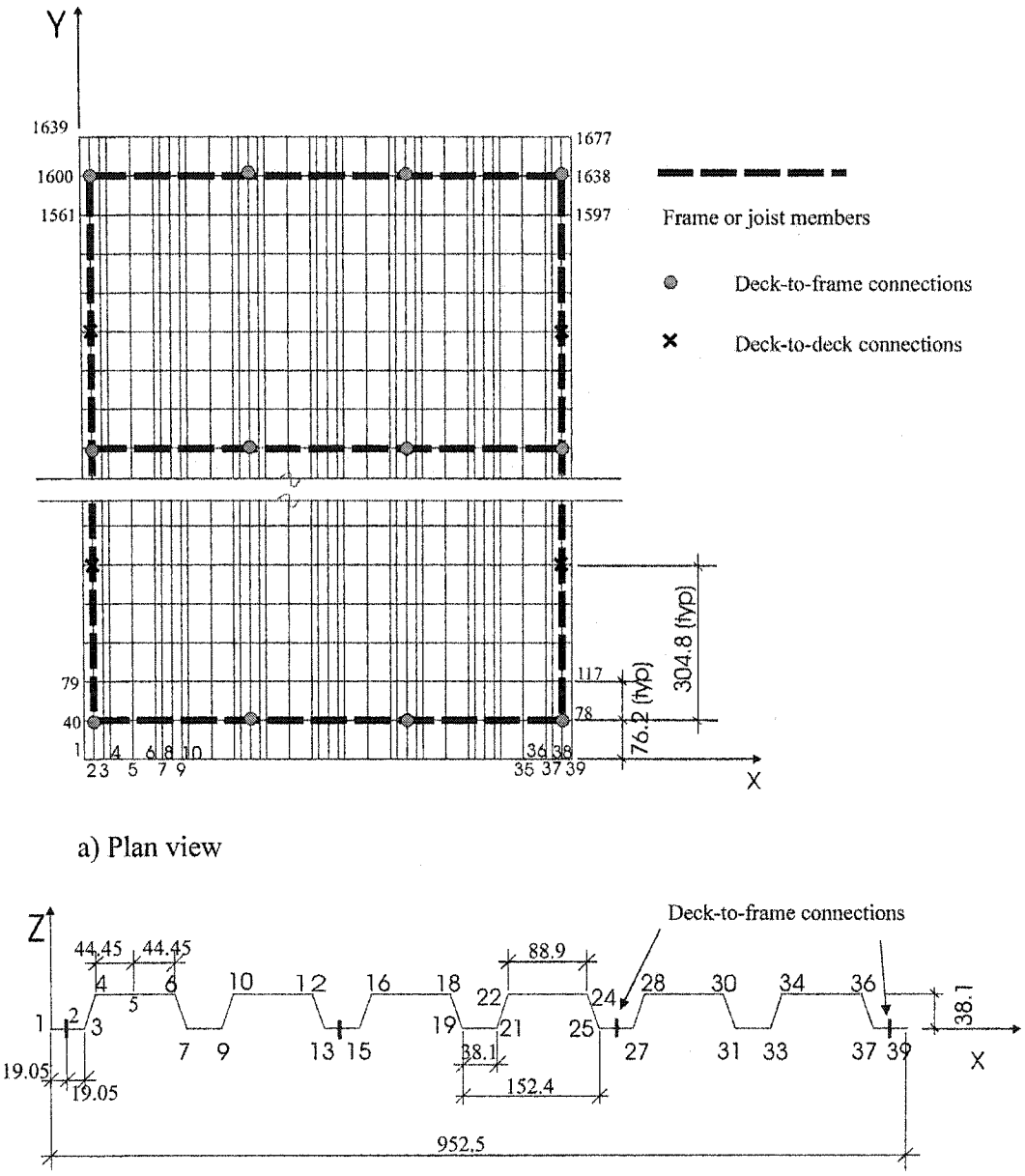

a) Plan view

b) Section view

Figure 9. Numérotation des noeuds des 1596 éléments de coque, charpentes, poutrelles et raccordements

Afin d'être compatible avec le maillage du tablier métallique qui comprenait 1596 éléments de coque, la même quantité d'éléments de coque a été employée pour le

panneau de gypse. Le raccordement tablier-panneau de gypse est montré au schéma de la Figure 10. Lors de la définition des propriétés des matériaux, il n'était pas possible d'obtenir de la littérature une valeur du module de cisaillement ou du module d'Young pour le panneau de gypse. Dans l'analyse, deux valeurs ont alors été considérées pour le module d'Young, E_g :

- $E_g = 1.0$ GPa ;
- $E_g = 0.293$ GPa.

La première valeur ($E_g = 1.0$ GPa) a été choisie sur la base de la similitude qui existe entre le panneau de gypse et le béton à faible densité, tous les deux étant des matériaux fragiles. Le coefficient de Poisson a été posé égal à 0.167. La deuxième valeur de E_g (= 0.293 GPa) a été estimée à partir du module de cisaillement G du panneau de gypse qui a été présentée dans "Racking Tests of High-Rise Building Partitions" (Freeman, 1977).

Figure 10. Raccordement tablier métallique-panneau de gypse

Des résultats de l'analyse, on observe que les composantes non-structurales limitent les déformations relatives en plan entre les nervures adjacentes du tablier métallique; elles limitent également les déformations verticales du tablier métallique (dues au gauchissement, aux extrémités des feuilles) par compression entre les matériaux ou par tension due aux vis reliant le tablier au panneau de gypse. Ces effets résultent en un diaphragme de toit plus rigide en cisaillement. La déformation principale du panneau de gypse est sous forme de flexion aux extrémités des feuilles, due à la tension des vis de raccordement tablier-panneau de gypse. L'augmentation de G' due au panneau de gypse se situe entre 1.0~1.82 kN/mm, selon la valeur de E_g retenue, ce

qui est comparable aux résultats des essais ($G'_{Test45} - G'_{Test43} = 1.59$ kN/mm). On recommande de faire des essais sur les composantes non-structurales pour mieux connaître leurs propriétés. Cette information est nécessaire pour fournir des paramètres de matériaux plus précis qui peuvent être utilisés pour améliorer les résultats des analyses par EF.

5. INFLUENCE DE LA FLEXIBILITÉ DES DIAPHRAGMES SUR LE COMPORTEMENT TORSIONNEL SISMIQUE

L'effet de torsion et l'influence de la flexibilité du diaphragme de toit en acier sur la réponse sismique d'un bâtiment en acier à un étage avec contreventements à rigidité asymétrique ont été étudiés en utilisant des méthodes d'analyse statiques et dynamiques. Le bâtiment décrit dans cette section a été conçu selon une philosophie d'un contreventement faible et d'un diaphragme rigide, reflétant la pratique courante de conception. Le logiciel DRAIN-2DX (Prakash et Powell 1993) a été employé pour l'analyse, et le modèle du bâtiment est représenté sur la Figure 11. Le diaphragme de toit a été divisé en éléments de membrane carrés de 3.75 x 3.75 m qui étaient reliés aux contreventements. La structure du toit était reliée au sol par des colonnes et des membrures de contreventement situées le long des quatre murs extérieurs. Comme dans le modèle Ruaumoko étudié précédemment, les éléments verticaux étaient placés dans le même plan que la toiture pour obtenir une représentation 2D de la structure.

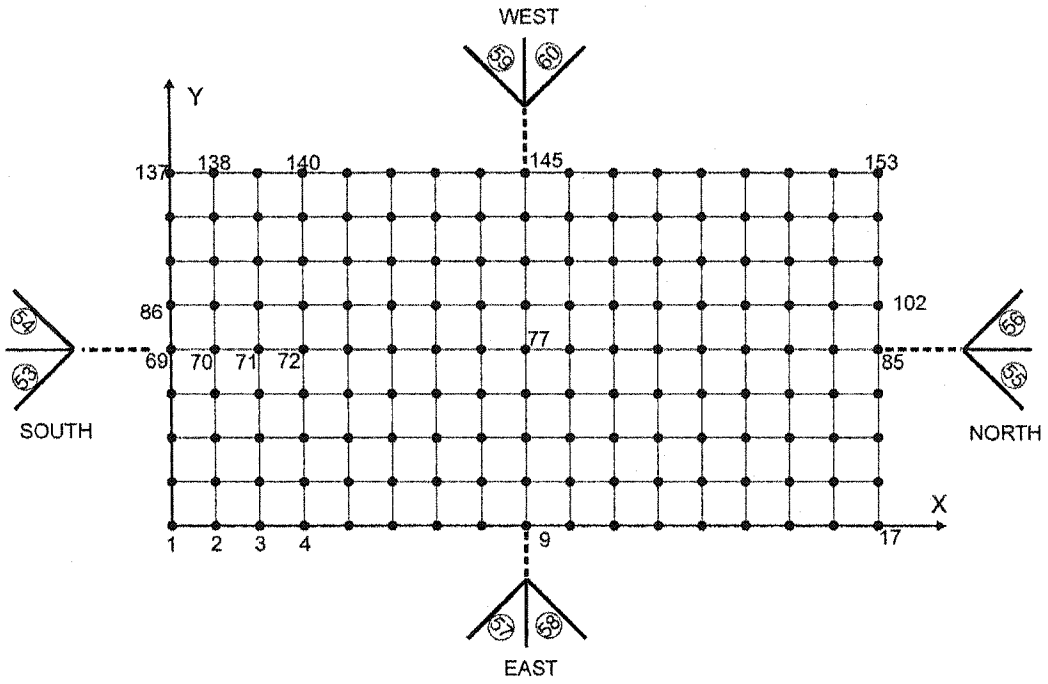

Figure 11. Modèle de DRAIN-2DX pour l'analyse numérique statique et dynamique

Les méthodes statiques linéaire et non linéaire, la méthode spectrale et la méthode temporelle non linéaire (avec huit accélérogrammes) ont été appliquées dans cette étude. Les résultats sont discutés ci-dessous :

1) Pour un bâtiment avec diaphragme de toit flexible, on a constaté que les effets de torsion sont généralement réduits, incluant le moment de torsion, les mouvements inter-étages, les forces de contreventement perpendiculaires à la direction du tremblement de terre et l'excentricité du centre d'inertie par rapport au centre de masse. Cependant, la flexibilité du diaphragme du plancher augmente le déplacement relatif du toit à mi-longueur du bâtiment. Elle peut également augmenter, mais pas dans tous les cas, le niveau de ductilité dans les contreventements travaillant dans la direction du séisme.

2) Dans la pratique courante, on assume généralement en conception que les diaphragmes de toit sont rigides, même si des toits flexibles sont utilisés. En général, cette pratique est adéquate, parce que les effets de la torsion sont moins importants. Cependant, il est important de vérifier les déplacements inter étages en tenant compte de la flexibilité du diaphragme, à l'aide d'une analyse statique ou bien une analyse spectrale

3) En comparant les méthodes statique linéaire, statique non linéaire, spectrale et les méthodes dynamiques mentionnées ci-dessus, la méthode statique linéaire est très simple, bien qu'elle ne puisse pas fournir la vraie distribution des forces pour quelques éléments structuraux de la charpente. Une méthode statique non linéaire permet d'améliorer ces résultats, mais l'effet de torsion considéré n'est pas adéquat. La méthode spectrale est un moyen d'analyse dynamique qui n'exige pas un temps significatif de calcul. Toutefois, l'information résultante n'est valable que pour un comportement élastique. La méthode dynamique temporelle non linéaire est la plus complète. Cependant, elle requiert un temps de calcul important. Les accélérogrammes doivent être choisis correctement par rapport à la période de vibration du bâtiment. Pour un bâtiment en général, les méthodes statique linéaire et non linéaire linéaire devraient être appliquées, de même qu'une des deux méthodes dynamiques.

TABLE OF CONTENTS

LIST OF TABLES

LIST OF FIGURES

LIST OF SYMBOLS

a:	Test frame width 3658mm
A:	Area; sheet width
A_g:	Gross area of a structural element
ALPHA:	Reloading or pinch power factor
APP:	Atactic Polypropylene
AS:	Effective shear area of the member section
a_{xi}:	X-direc. acce. component at node i
a_{yi}:	Y-direc. acce. component at node i
B:	Ratio used to determine torsional sensitivity; building width
BE:	Bearing failure
BETA:	Beta or softening factor
b.p.	Button punched
BU:	Buckling failure
BUR:	Built-Up Roof
C:	Connector slip parameter; cyclic plus monotonic load protocol
C:	Damping matrix of the whole structure
CSSBI:	Canadian Sheet Steel Building Institute
C_b:	Roof load parameter
CBF:	Concentrically braced frames
CI:	Centre of inertia forces

CSA:	Canadian Standard Association
CM:	Centre of mass
C.o.V.	Coefficient of variation
C_r:	Factored strength in compression
CR:	Centre of rigidity
d:	Corrugation pitch
D:	Diaphragm width; building width
D_{eq}:	Equivalent weld diameter
D_n:	Warping constant
D_{nx}:	Plan dimension of the building at level x perpendicular to the direction of seismic loading considered
D_s:	Horizontal bracing bent length
DL:	Roof dead load
DOF:	Degree of freedom
d_{u2}:	Shear deformations in local coordinate directions 2
d_{u3}:	Shear deformations in local coordinate directions 3
LL:	Roof snow and rain live load
e or e_x:	Distance measured perpendicular to the direction of earthquake loading between centre of mass and centre of rigidity at the level being considered
E:	Young's modulus
EA:	Effective horizontal extension stiffness
E_c:	Modulus of elasticity for concrete

E_d:	Energy dissipated
E_g:	Young's modulus for gypsum board
$E_H/(S_{U,SD})$	Cumulated hysteretic energy in segment I, II or III normalised to the maximum force measured in the SD loading protocol
E_h/E:	Strain hardening ratio
EI:	Flexual rigidity
EPDM:	Ethylene propylene diene monomer
EPS:	Expanded Polystyrene
F:	Foundation factor; flexibility; axial force in the spring
F_a:	Acceleration-based site coefficient
f_c':	Concrete compressive cylinder strength
F_E:	Brace horizontal forces in the east wall
FM:	Factory Mutual
F_N:	Brace horizontal forces in the north wall
F_S:	Brace horizontal forces in the south wall
F_W:	Brace horizontal forces in the west wall
F_x	Lateral force at Level x;
F_X:	X-component of the axial spring force
$F_{x,e-w}$:	Summed inertia force in the X-direction
F_{xi}:	X direction components of nodal inertial force at node i
F_v:	Velocity-based site coefficient
F_y:	Specified minimum yield stress; spring yield force in the axial direction;

F_Y:	Y-component of the axial spring force
F_{yi}:	Y direction components of nodal inertial force at node i
$F_{y,s\text{-}n}$:	Summed inertia force in the Y-direction
FI or F_i:	Intercept force
FU or F_u:	Ultimate force
f_{u2}:	Shear forces in local coordinate directions 2
f_{u3}:	Shear forces in local coordinate directions 3
FX:	Spring yield force in the x-direction
g:	Acceleration due to gravity
G:	Shear modulus of member material
G':	Diaphragm rigidity in shear
G'_b:	Shear stiffness of bare sheet diaphragm
G'_r:	Shear stiffness of roofed diaphragm
GAP+:	Initial slackness, positive axis
GAP-:	Initial slackness, negative axis
h_n:	Building height
h_s:	Interstorey height
HSS:	Hollow steel section
I:	Moment of inertia of diaphragm flanges (perimeter members) about centroidal axis of diaphragm, moment of inertia of section
I_E:	Earthquake importance factor of the structure
ISO:	Polyisocyanurate, or Polyurethane
j:	Mode j

J:	Numerical reduction coefficient for base overturning moment
k:	Effective length factor
K:	Stiffness matrix of the whole structure
K_B:	Total lateral stiffness of the vertical bracing
$K_{B,E}$:	Brace horizontal stiffness in the east wall
$K_{B,N}$:	Brace horizontal stiffness in the north wall
$K_{B,S}$:	Brace horizontal stiffness in the south wall
$K_{B,W}$:	Brace horizontal stiffness in the west wall
K_D:	Total lateral stiffness of the diaphragm
KE:	Linear effective stiffness
KX or K_0:	Spring stiffness in the local x-direction
K_y:	Translational stiffness
K_θ:	Rotational stiffness
L:	Length
LD:	Long duration
L_D:	Length of diagonal spring element for diaphragm
L.F.	Load factor, or safety factor
LFRS	Lateral force resistant system
L_v	Joist spacing
LVDT:	Linear Variable Differential Transformer
m:	Mass of the floor
M:	Monotonic
M:	Mass matrix

MB:	Modified bitumen roof
m_{xi}:	Lumped masses of node i in the X directions
M_v:	Factor to account for higher mode effect on base shear
m_{yi}:	Lumped masses of node i in the Y directions
n_e:	Number of edge connectors between cross supports
n_s:	Number of stitch connectors within sheet length
n_v:	Average number of connections over sheet width
N:	Total number of storeys above exterior grade to level n
NHS:	Nail Head Standoff
NS:	Screw-nail design
NW:	Weld with washer-nail design
P:	Load measured by the load cell
PGA:	Peak ground acceleration
PHA:	Unscaled peak horizontal acceleration
PHV:	Peak horizontal velocity
PMR:	Protected membrane roof system
PTRI:	Tri-linear factor beyond ultimate force
PUNL:	Unloading stiffness factor
P_u:	Peak load
q	Allowable shear strength
q_1	Contribution of strength from the connection at the ends of the deck sheet
q_2	Contribution of strength from the seam fasteners

q_3	Limit of shear strength for q_2
Q	Quasi-static
r:	Radius of gyration; bi-linear factor
R:	Force modification factor; with roofing case
R_d:	Ductility related force modification factor
$R_dR_o\Delta_{B:}$	Equivalent elastic disp. at braced bents
$R_dR_o\Delta_{TOT:}$	Equivalent elastic disp. at building mid-length
R_o:	Overstrength related force modification factor
R_ϕ:	$1 / \phi$
R_y:	Factor applied to F_y to estimate the probable yield stress
R_{yield}:	Ratio of probable yield strength to minimum specified yield strength
R_{sh}:	Overstrength due to strain hardening
R_{size}:	Overstrength due to discrete member sizes
R_{mech}:	Overstrength developed when a full collapse mechanism is formed
RF:	Bi-linear factor
s:	Girth of corrugation per rib
S:	Roof snow and rain live load, unit shear
SBS:	Styrene Butadiene Styrene
SD:	Short duration
S_{des}	Allowable design shear
SDI:	Steel Deck Institute

S_f:	Maximum unit shear force along the edge of the diaphragm
SF	Safety factor
SFRS	Seismic Force Resisting System
SS	Screw-screw design
S_F:	Scaling factor used
SH:	Nail shear
$S / S_{U, SD}$:	Ratio of the maximum force in largest excursion in segment I, II or III to the maximum measured force in the total SD signal
$S / S_{U, MON}$:	Ratio of the shear force to the maximum measured force in monotonic tests
S_r:	Rain load; factored required strength of diaphragm
S_s:	Ground snow load
S_u:	Deck ultimate shear strength
$S_{U,SDI*}$:	Deck ultimate shear strength predicted by the SDI method based on test values for connectors
$S_{U,SDI}$:	Deck ultimate shear strength predicted by the SDI method
$S_{U,MON}$:	Deck ultimate shear strength from monotonic test
$S_{U,SD}$:	Deck ultimate shear strength from test with a short duration (SD) loading protocol
$S_{U,LD}$:	Deck ultimate shear strength from test with a long duration (LD) loading protocol
Srequ:	Deck design force considered
S(T):	The design spectral response acceleration, expressed as a ratio to gravitational acceleration, for a period of T

S_a (T):	The 5% damped spectral response acceleration, expressed as a ratio to gravitational acceleration, for a period of T
S1:	Shear strength at γ_1
SD:	Standard deviation
S_{yc}:	Yield stress or buckling stress in compression
S_{yt}:	Yield stress in tension
t:	Base metal thickness
T:	Fundamental periods (sec.)
T_a:	Fundamental lateral period of vibration of the building or structure in the direction under consideration
$T_{CM,B}$:	Torsional moment about CM due to brace forces
$T_{CM,D}$:	Overall torsion moment about the centre of mass due to inertia forces
$T_{CM,DX}$:	Torsion moment about the centre of mass due to X-direction inertia forces
$T_{CM,DY}$:	Torsion moment about the centre of mass due to Y-direction inertia forces
$T_{CR,B}$:	Overall torsion moment about the centre of rigidity due to brace forces
$T_{CR,D}$:	Overall torsion moment about the centre of rigidity due to inertia forces
t_d:	Trifunac duration
T_{deck}:	Deck shear capacity in the direction of the brace elements
TE:	Tearing failure

T_f:	Tension force considered in design
T_r:	Factored tension capacity; torsional moment about the centre of rigidity
T_x:	Torsional moment at Level x
T_y:	Axial yield capacity of the braces
U_1:	Axial properties
U_2:	Shear properties in the 1-2 plane
U_3:	Shear properties in the 1-3 plane
UL:	Underwriters Laboratories
V:	Lateral earthquake design force at the base of the structure as determined by the equivalent static force procedure
V_d:	Lateral earthquake design force at the base of the structure as determined by a dynamic analysis procedure
V_e:	Lateral earthquake elastic force at the base of the structure as defined by a dynamic analysis procedure
V_f:	Design base shear force
V_{max}:	The yield capacity of brace elements
V_p:	Lateral force on a part of the structure
V_u:	Expected lateral strength of the structure
V_2:	Shear forces in the local coordinate 2-direction
V_3:	Shear forces in the local coordinate 3-direction
w:	Uniform load; density of concrete
W:	Seismic weight of the building

WB:	Button punch-weld design
WE:	Weld failure
W'W:	Weld with washer-weld with washer design
X:	Coordinate in horizontal direction
XEPS:	Extruded Expanded Polystyrene
$X_{INERTIA}$:	Offset distance of summed Y-direction inertia force to CM
X_n:	Distance from north wall to CM in a building
X_s:	Distance from south wall to CM in a building
Y:	Coordinate in vertical direction
$Y_{INERTIA}$:	Offset distance of summed X-direction inertia force to CM
Z:	Plastic section modulus
Z_a:	Acceleration-related seismic zone
Z_v:	Velocity-related seismic zone
α:	Damping coefficient for mass matrix
α_1:	End distribution factor (SDI, 1991)
α_2:	Purlin distribution factor (SDI, 1991)
β:	Damping coefficient for stiffness matrix
δ_{ave}:	Average of the displacements at the extreme points of the structure at level x
δ_{max}, or Δ_{max}:	Maximum displacement of the structure at level x
δ_n:	North wall roof displacement
δ_s:	South wall roof displacement

Δ:	Real diaphragm displacement
Δt:	Time interval
Δ_B:	Lateral deflection of braced walls
Δ_{centre}:	Storey drifts in load direction
Δ_F:	Flexural lateral deflection
Δ_L:	Axial deformation in the spring element of diaphragm
Δ_{Tr}:	transversal displacement in the spring element of diaphragm
Δ_w:	Shear deflection of diaphragm
Δ_{TOT}:	Total lateral deflection of the structure
Δ_{LIMIT}:	Limit criteria for the lateral deflection of the structure
Δ_Y:	Yield extension for brace elements
ϕ:	Resistance factor, purlin effect factor on warping
γ :	Average shear strain
γ_p:	Inelastic distortion starting from γ_u
γ_{max}:	Maximum shear deformation in SD load protocol
γ_u:	Shear deformation obtained from S_u/G'
γ_1:	Shear deformation where stiffness deterioration starts
γ_2:	Shear deformation where shear strength reaches its peak value
γ_{slip}:	Shear deformation due to slip between decks
γ_{total}:	Total shear distortion
$\gamma_{0.8Su}$:	Shear distortion related to a load degrading to 80% of the peak load

μ:	Ductility demand
μ_B:	Ductility demand for brace elements
μ_D:	Ductility demand in deck panels
μ_T:	Target ductility demand
μ/μ_T:	Ductility Amplification Ratio
σ_y	Specified minimum yield stress of steel
ω_j:	Frequency of j^{th} mode
ω_y:	Translational (in the earthquake direction) frequency
ω_θ:	Rotational (about the centre of resistance) frequency
θ:	Slope angle of the brace with respect to horizontal
ν:	Poisson's ratio
ρ:	Ratio of the wall mass to the total mass of the system
Ω:	Ratio of the uncoupled torsional and translational frequencies

LIST OF APPENDICES

CHAPTER 1 INTRODUCTION

1.1 GENERAL

Steel roof decks are widely used in low-rise steel buildings, which are often intended for light industrial, commercial, or recreational use. One typical structural arrangement of a single storey steel building is shown in Figure 1.1, where the steel deck units span between the roof joists. The roof deck provides a surface on which roofing materials such as the vapour retarder, the insulation and the waterproof membrane are installed. The composition of a typical roof assembly can be seen in Figure 1.2.

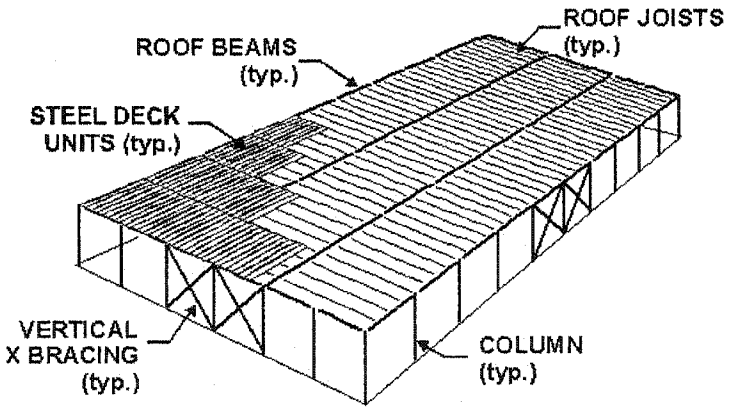

Figure 1.1. Typical structural arrangement of a single storey steel building (from Rogers & Tremblay, 2000)

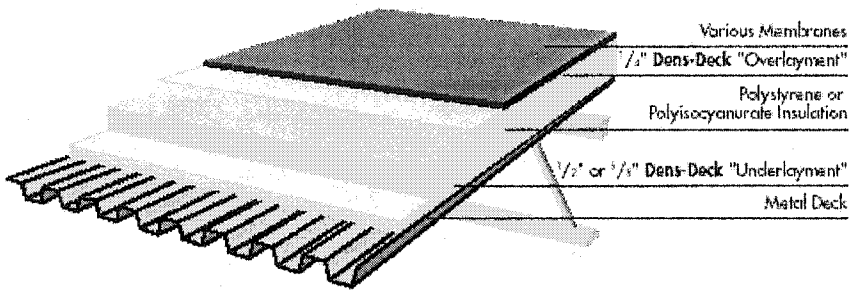

a) 3-D view of roof composition

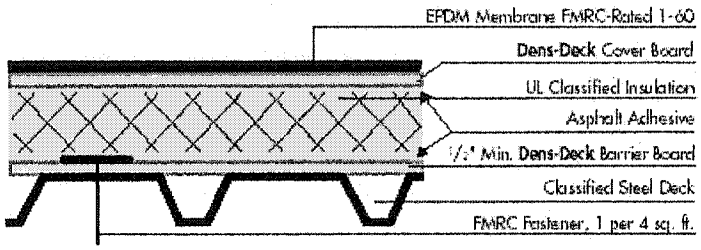

b)Section view of roof composition

Figure 1.2. Typical roof composition (adapted from G-P Gypsum Corporation, 2000)

The steel roof deck panels should be adequately connected to the underlying framing members (joists, beams or trusses) for a number of reasons. The roof deck panels act as a diaphragm when the building is subjected to lateral loads, and hence, any forces in the roof must be transferred to the supporting vertical bracing system. Direct loads from wind uplift must be transferred to the main steel structure. In addition, the roof deck often acts as a means of lateral support to limit the lateral displacement of the flexural roof members. One example of deck attachment is given in Figure 1.3.

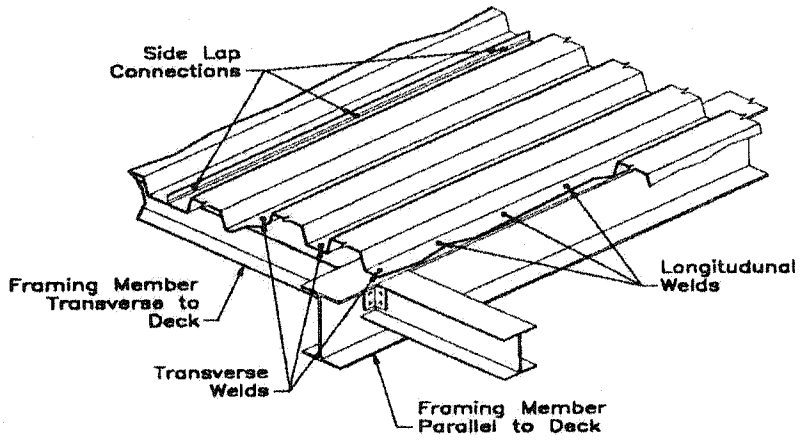

Figure 1.3. Typical deck attachment (adapted from CSSBI, 1991)

In light of the research that has been carried out for this thesis, an adequately fastened roof deck assembly is vital for the proper functioning of the roof diaphragm. The diaphragm component of the structure is able to resist significant in-plane shear forces, and in effect may eliminate the need for a separate horizontal roof bracing system.

The first recorded test of a light gauge steel diaphragm under in-plane shear loading was performed by Johnson and Converse in 1947 (Nilson, 1960). In their report, it was indicated that the work would hopefully provide "*the stimulus for continued research and experimentation along these lines*". From 1955 to 1960, Nilson (1960) performed approximately 39 full-scale diaphragm tests using both the simple beam and cantilever beam test frame assembly. The first design guide for light gauge steel diaphragms in North America, published by the American Iron and Steel Institute (AISI), was based on the findings of Nilson (AISI, 1967).

Currently, the most widely used document for the design of steel panel diaphragms is published by the Steel Deck Institute (SDI) under the name "Diaphragm Design

Manual" (SDI, 1987). This manual is based mostly on the research of Luttrell, which dates back to the early 1960s, (SDI, 1981). In Canada, the Canadian Sheet Steel Building Institute (CSSBI) has made the Design of Steel Deck Diaphragms (CSSBI, 1991) and the Standard for Steel Roof Deck (CSSBI, 1996) publications available to aid engineers in the design and construction of these roof structures.

The study of steel roof deck diaphragms has been ongoing for the past half century, however, it should be noted that in almost all investigations only the static performance was evaluated. It was not until the 1980s that the dynamic performance of roof diaphragms was researched (Mazzolani and Labini, 1983). Knowledge of the dynamic or cyclic behaviour of a diaphragm has specific benefits in terms of earthquake resistant design. In Canada, a structure is currently designed to resist the earthquake forces caused by a peak ground acceleration (PGA) with a 10% probability of exceedance in a 50 year time span, *i.e.* a recurrence of 475 years (NRCC, 1995). This probability of exceedance will be adjusted to 2% in a 50 year time span in version 2005 of the National Building Code (NRCC, 2001), with a much longer recurrence of 2475 years. To ensure that the structure is safe but cost efficient, the usual practice is to employ the capacity based design approach, whereby one of the structural members in the lateral load carrying path is specified and sized to act as the earthquake energy dissipating element. This structural element, also know as the weak link or fuse in the lateral force resisting system, is typically expected to perform in the inelastic behaviour range such that seismic loads can be carried over large displacements of the building without a loss in the capacity of the steel framing system. Other structural elements are designed to remain elastic or to endure very limited inelastic response during a seismic event. Traditionally, in low-rise steel buildings, diagonal bracing members in the walls (the vertical X bracing shown in Figure1.1) are selected as the energy dissipating element, while the steel roof deck is designed to remain elastic and have a shear capacity that exceeds the ultimate capacity of the brace elements. It is possible for brace members to be oversized due to

a limitation in the cross-section sizes available and because of slenderness limits imposed in steel design codes. A brace that has an over-strength may require that the steel roof deck be increased in thickness or be connected at more locations such that its behaviour remains elastic. The result is an increase in the cost of constructing the building. One possible solution is to consider the steel deck diaphragm as the weak link in the lateral load carrying path, while designing the brace elements to remain elastic under earthquake loading. That is to say, the steel roof deck diaphragm must be able to undergo inelastic deformations without a significant loss in shear resistance, and hence, dissipate the dynamic energy caused by severe ground motion.

Since 1999 a research program has been carried out at École Polytechnique de Montréal in the area of inelastic seismic behaviour of steel roof deck diaphragms under dynamic load conditions. This research includes both the behaviour of the connections and the deck assembly. Prior to the writing of this thesis, 37 full-scale cantilever diaphragm tests and over 400 connection tests had been completed. A summary of these investigations is contained in Chapter 2. One limitation of the above research is that the influence of the non-structural components had not been considered. In addition, construction details such as the longitudinal overlap at the ends of panels had not been studied. It is likely that these two factors have a significant influence on the behaviour of diaphragms, and for this reason, the research documented in this thesis was carried out.

1.2 OBJECTIVES AND SCOPE

The main purpose for carrying out the research reported in this thesis is to better understand the inelastic behaviour of steel roof deck diaphragms when subjected to seismic loads. The specific objectives are as follows:

1) Investigate the effect of the longitudinal overlap deck panel joints on diaphragm behaviour and ductility through full-scale testing.
2) Investigate the effect of the non-structural components on diaphragm behaviour and ductility through full-scale testing.
3) Evaluate the inelastic behaviour of the 76 mm deep series steel roof deck through full-scale testing.
4) Evaluate the inelastic behaviour of steel roof deck diaphragms constructed with powder-actuated fasteners from different manufacturers through full-scale testing.
5) Analyse the inelastic seismic response of single storey steel buildings when the roof diaphragm has been designed as the energy dissipating element.
6) Estimate the quantitative change of the in-plane shear properties of diaphragms due to the presence of non-structural components.
7) Analyse the influence of roof flexibility on the seismic torsional behaviour of single storey steel buildings with asymmetric brace stiffness.

The scope of this thesis is limited to light gauge corrugated steel roof deck systems, common roofing materials and single storey steel buildings. A total of 12 full-scale cantilever diaphragm tests are included. The diaphragm specimens were constructed of either welds or powder-actuated fasteners for the deck-to-frame connections, and either button punches or screws for the side lap connections. The steel roof deck panels were either of the 38 or 76 mm deep series with a nominal thickness of either 0.76 or 0.91 mm and a nominal yield strength of 230 MPa. The non-structural roofing materials were selected to represent a typical assembly found in Canada, and hence, were based on the SBS-34 design from the Association des Maîtres Couvreurs du Québec (AMCQ).

In terms of the analysis component of this thesis, a medium size building located in Victoria B.C. was studied. The building was designed according to the proposed

version of the 2005 National Building Code (NRCC 2001), and the Limit States Design of Steel Structures CAN/CSA-S16.1-94 standard (CSA, 1994). The nail/screw connection configuration was used for the design of the diaphragm. The steel deck assembly was specified to act as the energy-dissipating element in the lateral load-resisting path, and two ductility related force modification factors were considered. The hysteretic response obtained from three previous diaphragm tests was utilized, along with three ground motion records. The additional analysis component of the thesis, which addressed the influence of roof flexibility on the torsional response of the building, involved a combination of two roof stiffness cases with eight ground motion records. Finally, for the Finite Element (FEM) analysis, a panel layout similar to that used in the physical diaphragm testing, with and without the non-structural roofing materials, was used.

1.3 METHODOLOGY AND THESIS ORGANISATION

The approach used to complete the research for this thesis included the following steps:

- Literature review;
- Market investigation and selection of roofing components;
- Laboratory testing;
- Inelastic seismic building analyses using RUAUMOKO;
- Static FEM stress roof assembly analyses using SAP2000;
- Building torsion analyses considering roof flexibility using DRAIN-2DX;
- Data processing.

Chapter 2 contains a literature review in which an outline of the current steel deck diaphragm design basis is presented. In addition, a summary of the recent findings by

the research group at École Polytechnique de Montréal on diaphragm behaviour is provided.

Chapter 3, "Roof systems", presents a market study that details the composition of steel deck roof systems and the selection of test models.

Chapter 4, "Diaphragm test analysis", contains the results of the 12 full-scale diaphragm tests.

Chapter 5, "The application of test results", describes the results of the inelastic seismic analyses of single storey buildings using RUAUMOKO. Furthermore, this chapter contains a discussion of the SAP 2000 analyses for the roof assembly.

Chapter 6, "Torsional effect analysis", documents the influence of roof flexibility on the torsional behaviour of a single storey buildings based on DRAIN-2DX analyses.

Chapter 7, "Conclusion and recommendations", summarizes the findings of the research and lists suggestions for topics of future research.

CHAPTER 2 LITERATURE REVIEW

As introduced in Chapter 1, Johnson and Converse (1947) were the first researchers to carry out the testing of light gauge steel diaphragms. Since this initial body of work, many other research projects have been completed at numerous institutions around the world. In this chapter some of these achievements on diaphragm behaviour have been summarized. This includes two early projects on steel diaphragms, two design manuals, two Canadian design codes, and several recent research investigations. Background information on roofing materials will be presented in Chapter 3.

2.1 NILSON

Prior to the investigation undertaken by Nilson, very little information and only a small amount of test data had been published. Nilson's publication "Shear Diaphragms of Light Gage Steel" (1960) provided details on two test approaches (cantilever or simple beam setup) that are still used by researchers today, and are included in ASTM E455 (2002) as the standard test setups.

Based on Nilson's 39 monotonically loaded diaphragm tests, "*it is recognized that the diaphragm strength of floor and roof elements of buildings can be utilized to resist horizontally-applied loads.*" and they "*... will be effective as shear diaphragms*". However, "*the behavior of light gage steel panel diaphragms does not yield nicely to analysis, the large number of relatively small parts involved, with possible individual movement, and the stress concentrations that are present near the welds as horizontal load is applied, prevent the application of the results of analysis with any large degree of confidence*" (Nilson, 1960). Nilson suggested that the cantilever model be

utilized in future tests because, "*a single "end" bay, loaded as a cantilever, that would yield the same strength values as the three-bay frame*" (Nilson, 1960). To this date, full-scale experiments remain the most reliable method in evaluating the behaviour of steel deck diaphragms.

2.2 AMERICAN IRON AND STEEL INSTITUTE

The publication of the manual entitled "Design of Light Gage Steel Diaphragms" by the American Iron and Steel Institute (AISI, 1967) summarized the accomplishments of previous researchers in the area of diaphragm design. It can be seen as the first diaphragm design manual for use in North America, which relied on the allowable stress approach and the results of laboratory testing.

According to the AISI (1967), the allowable in-plane design shear for all diaphragms is given by:

$$S_{des.} = \frac{S_u}{L.F.} \tag{2.1}$$

where:

S_{des} = allowable design shear,

S_u = test ultimate shear strength.

L.F. = load factor, or safety factor.

Even after 40 years, the same design method is still used in current diaphragm design guides. But the meaning and values of the load factors have changed. In the AISI (1967), L.F. was taken as 2.5 for mechanical fasteners, which is higher than that of

welded connections (L.F.=2.4). This is because at that time welded connections were commonly specified in construction, and hence more thoroughly investigated. Additional research later changed this situation, for example in the SDI Manual (1991), L.F. is changed to SF that has a value of 2.35 for mechanical fasteners, which is smaller than that of welded connections (SF=2.75). This change was the result of more thorough investigations of connections, which proved that the quality and performance of mechanical fasteners are more consistent than that of welded connections. For further details refer to the early edition of the SDI Diaphragm Design Manual (1981).

2.3 STEEL DECK INSTITUTE

The "Diaphragm Design Manual – Second Edition" (SDI, 1991), was prepared by Luttrel *et al.*, and published by the Steel Deck Institute (SDI). It can be considered as the most comprehensive reference book on diaphragm design in North America. It contains load tables suitable for use with various deck configurations; it also provides the theories and equations for calculating the in-plane diaphragm strength and stiffness. These design equations can be very helpful when the deck arrangement, i.e. connection type and deck profile, is different from those listed in the load tables.

According to the findings of earlier research investigations, which are documented in the First Edition of the Diaphragm Design Manual (SDI, 1981), three key elements usually determine the overall diaphragm properties; these include the panel type, the connections and the geometry of the roof diaphragm. Most often, failure occurs at the connections in one of three possible locations: along the edge of the diaphragm, at the interior panels, or at the corner of a panel or the diaphragm. The ultimate shear strength, S_u, is limited to the smallest value of these three cases, in addition to the check of overall shear buckling capacity of the roof deck.

Diaphragm connections are divided into deck-to-frame and deck-to-deck types. Welds or powder driven nails are often used in deck-to-frame connections, while welds, screws or button punches are popular in deck-to-deck (side-lap) connections. In some cases, nails and screws are used together to connect the roof deck panels to one another and to the supporting steel frame. The most common connection system found in Canada is the weld and button punch combination.

The diaphragm stiffness G' can be obtained from tests; in addition it may also be determined using elastic theory. The final form of G' in the SDI design method is shown in Equation 2.2 (Refers to Nedisan, 2002):

$$G' = \frac{Et}{2.6(\frac{s}{d}) + \phi D_n + C} \tag{2.2}$$

where:

E	=	modulus of elasticity
t	=	base metal thickness
s	=	girth of corrugation per rib
d	=	corrugation pitch
ϕ	=	purlin effect factor on warping
D_n	=	panel warping constant
C	=	slip relaxation constant

Diaphragms can be defined as rigid or flexible or they can posses an intermediate level of flexibility according to their shear stiffness G' or flexibility F, where, F=1000/G', see Table 2.1.

Table 2.1 Diaphragm flexibility and stiffness (adapted from SDI (1991))

Type	SI unit		U.S. unit	
	F	G'	F	G'
	10^{-6}mm/N	kN/mm	10^{-6}in /lb	Kips/in
Flexible	400 to 855	1.2 to 2.5	70 to 150	14.3 to 6.67
Semi-flexible	57 to 400	2.5 to 17.5	10 to 70	100 to 14.3
Semi-rigid	5.7 to 57	17.5 to 175	1 to 10	1000 to 100
Rigid	<5.7	>175	<1	>1000

2.4 CANADIAN SHEET STEEL BUILDING INSTITUTE

In Canada, a diaphragm design method for steel roof decks has been recommended for use by the Canadian Sheet Steel Building Institute (CSSBI) in "Design of Steel Deck Diaphragms" (CSSBI, 1991), and "Standard for Steel Roof Deck" (CSSBI, 1996). The general design method is based on the Tri-Services Technical Manual published by the Department of Army, Navy and Air Force, U.S. Government Printing Office (Tri-Services, 1982). The method applies primarily to diaphragms welded to structural steel framing since mainly assemblies with this type of connection scenario were tested. The most current Tri-Services Technical Manual recommends that the SDI approach be used in the design of steel roof deck diaphragms (US Army Corps Of Engineers, 1998).

The basic idea of diaphragm design in the Tri-Services Technical Manual (1982) is as outlined below:

The allowable shear strength is taken as lesser of (Nedisan, 2002):

$$q=(q_1+q_2)q_3/q_2, \text{ while } q_3 \leq q_2 \tag{2.3}$$

and the Euler buckling strength, $q = \frac{\pi^2 EI_x}{4L_v^2}$ (2.4)

where:

- q_1 is the contribution of strength from the connection at the ends of the deck sheet;
- q_2 is the contribution of strength from the seam fasteners (side-lap connections);
- q_3 is the limit of shear strength for q_2;
- E is the Young's modulus for sheet steel;
- I_x is the moment of inertia of the fully effective cross-section area of the deck width about its horizontal neutral axis;
- L_v is the joist spacing.

The total flexibility is also composed of three factors, including the steel plate shear deformation, the distortion, and the fastener deformation.

2.5 CONNECTION PERFORMANCE

Since the behaviour of steel roof deck diaphragms is largely controlled by the connection method and their arrangement, knowledge of the load-deformation behaviour of each connection type can be useful in the prediction of overall diaphragm performance. A large number of connection tests having been performed in the past, mainly for static applications, such as Yarnell and Peköz (1973), Fung (1978), and Klingler (1986). The seismic properties of connections were reported by Mazzolani (1994). Recently, Rogers and Tremblay (2000, 2003a,b) carried out a total of 189 connection tests, including 45 side-lap (16 screw, 20 button punch, 9 weld)

and 144 deck-to-frame tests (47 screw, 71 powder actuated fasteners (PAF), 26 weld). Five different loading protocols were used: monotonic, quasi-static, 0.5 Hz cyclic, 3 Hz cyclic and simulated earthquake motion. Seventy-two deck-to-frame weld connected tests were also carried out by Bond *et al.* (2001) to investigate the inelastic cyclic response of the typical fasteners used in roof decks today. A third series of welded deck-to-frame connection tests was completed by Peuler *et al.* (2002a,b) to evaluate the influence of weld washers and welding protocols on cyclic performance. This project involved 235 connections with different sheet thickness, washer types, welding protocols, etc. The results of the above three connection test programs provided an indication of how the large-scale diaphragm test specimens would behave in the inelastic range under seismic excitations. Measurements of connection strength and stiffness were also used with the SDI diaphragm design equations to obtain a more accurate picture of the expected overall response of the large-scale cantilever diaphragm tests.

Some of the general findings of these connection research projects are summarized below:

Side-lap connection tests were composed of two adjacent deck sections. The two most common deck profiles in Canada were utilized, i.e. the 38 mm and 76 mm deep series. The strength from the tests was quite similar to that calculated using the SDI design equations (1991), however, the measured stiffness values did not match those predicted using the SDI method. As an example, the stiffness of test vs. SDI, for the side lap connections of 0.76 mm sheets by Hilti S-MD 12-12x1 HWH #1 screws, is 1.35 vs. 10.1 kN/mm. This "*most likely resulted from the flexible web element of each test specimen*" (Rogers and Tremblay, 2000).

For side-lap connections, it was found that weld connections carried the highest ultimate loads and absorbed the most total energy, which is necessary for the deck

diaphragm to work as a seismic energy dissipation element, although the weld quality is heavily dependent on the ability and experience of the welder and the work conditions. Button-punch side-lap connections yielded the lowest strength and stiffness values. Screwed side-lap connections may become loose at extreme displacements due to hole enlargement and tilting of the fastener. However, the quality of screwed connections exceeds that of the other side-lap fastening methods. In addition, a higher capacity and stiffness for screwed connections can be obtained in comparison with button-punch connections.

The results of deck-to-frame connection tests indicated that the screwed fasteners provided the most consistent results, while nailed (i.e. powder actuated fasteners, PAF) connections could carry higher loads and dissipate greater amounts of energy. Welds fabricated with washers showed much more consistent results in comparison with standard arc-spot weld connections. These reinforced welds could carry higher loads and were more ductile, i.e. the connection could undergo larger deformations without rupture, when proper welding protocols were followed which ensured that adequate penetration of the weld metal into the framing material was obtained.

According to Rogers and Tremblay (2000), the SDI equations for connection strength and stiffness provide the most accurate predictions with the least scatter of data. In addition, "*the shear capacities for PAF connections could be accurately predicted, regardless of the nail type, by using an SDI design equation that was adopted from Hilti ENP2-21-L15 fastener*", (Rogers and Tremblay, 2000).

2.6 ESSA ET AL.

The report, "Inelastic seismic behaviour of steel deck roof diaphragms under quasi-static cyclic loading", prepared by Essa *et al.* (2001) and the associated paper (Essa *et al.*, 2003), are mainly about the experimental investigation of diaphragm behaviour. Since it was the first systemic experimental project at École Polytechnique de Montréal covering a large-scale cantilever deck assembly under reversed cyclic loads; the information concerning the test set-up and the test experience is equally as important as the test results because most of their test arrangements were also used in this study. The overall plan size of the test frame was 20 x 12 ft (6.10 x 3.66 m), which fitted four 3 ft wide or six 2 ft wide deck panels. The three intermediate joists, spaced at 5 ft centre-to-centre, were pinned to the main frame to minimize the influence of the underlying frame on diaphragm shear stiffness and strength. The tests, both monotonic and reversed cyclic quasi-static, carried out by Essa *et al.* are listed in Table 2.2.

Table 2.2 Diaphragm Tests by Essa *et al.* (2001, 2003)

Test	Sidelap [1]	Frame [1]	Deck profile	Loading protocol
38-76-6-WB-M-1	b. p.	welded[2]	P3615 0.76 mm	Monotonic
38-76-6-WB-Q-2	b. p.	welded[2]	P3615 0.76 mm	Quasi-static
38-76-6-SS-M-3	screwed	screwed	P3615 B 0.76 mm	Monotonic
38-76-6-NS-M-4	screwed	nailed (H)	P3615 B 0.76 mm	Monotonic
38-76-6-NS-M-5	screwed	nailed (B)	P3615 B 0.76 mm	Monotonic
38-76-6-SS-Q-6	screwed	screwed	P3615 B 0.76 mm	Quasi-static
38-76-6-NS-Q-7	screwed	nailed (H)	P3615 B 0.76 mm	Quasi-static
38-76-6-NS-Q-8	screwed	nailed (B)	P3615 B 0.76 mm	Quasi-static
38-76-6-WW-M-9	welded[4]	welded[2]	P3615 0.76 mm	Monotonic
38-76-6-W'W-M-10	welded[4]	w. w. washer[3]	P3615 0.76 mm	Monotonic
38-76-6-WS-M-11	screwed	welded[2]	P3615 B 0.76 mm	Monotonic
38-76-6-WW-Q-12	welded[4]	welded[2]	P3615 0.76 mm	Quasi-static
38-76-6-W'W-Q-13	welded[4]	w. w. washer[3]	P3615 0.76 mm	Quasi-static
38-76-6-WS-Q-14	screwed	welded[2]	P3615 B 0.76 mm	Quasi-static
38-76-6-W'S-M-15	screwed	w. w. washer[3]	P3615 B 0.76 mm	Monotonic
38-76-6-W'S-Q-16	screwed	w. w. washer[3]	P3615 B 0.76 mm	Quasi-static
38-91-6-NS-M-17	screwed	nailed (H)	P3615 B 0.91mm	Monotonic
38-91-6-NS-Q-18	screwed	nailed (H)	P3615 B 0.91mm	Quasi-static

Notes:
(1): Nailed connections with Hilti (H) X-EDNK22-THQ12 and Buildex (B) BX-12 fasteners for nailed connections, 12-24x7/8'' fasteners for screwed structural connections, and 12-14x7/8'' fasteners for screwed sidelap connections.
(2): Welded frame connections were made with 19 mm diameter arc spot welds.
(3): Mix of welds and welded with washer frame connections.
(4): Welded sidelap connections were made with 35 mm long welds.

The test designation nomenclature from Table 2.2 were "*designated according to panel depth (mm), sheet thickness (76 = 0.76 mm), diaphragm length (m, to the nearest metre), deck-to-frame (W for welded, W' for welded with washer, N for powder actuated nails, S for screwed) and sidelap (B for button punched (b.p.), S for screwed and W for welded) connection types, loading protocol (M for monotonic, Q for quasi-static) and the test number (sequential). For example, test 38-76-6-WB-Q-2*

denotes 38 mm deep deck, 0.76 mm sheet thickness, 6.1 m long diaphragm, welded structural fasteners, button punched side lap fasteners, quasi-static cyclic loading protocol, and test number 2 in the series" (Essa *et al.*, 2001).

Some of the measured test parameters of the tests by Essa *et al.* have been listed in Table 2.3 such that comparison with the tests documented in this thesis can be carried out.

Table 2.3 Selected test results by Essa *et al.* (2001, 2003)

Test No.	Test designation	Test result		Ratio			
		S_u	G'	S_u	G'	S_u	G'
		KN/m	KN/mm	Test/SDI	Test/SDI	Test/SDI*	Test/SDI*
1	38-76-6-WB-M-1	8.05	2.14	0.87	0.65	0.71	0.78
2	38-76-6-WB-Q-2	7.53	2.14	0.82	0.65	0.66	0.78
4	38-76-6-NS-M-4	12.30	3.12	0.95	0.83	1.11	0.96
7	38-76-6-NS-Q-7	12.19	2.87	0.94	0.77	1.10	0.88
5	38-76-6-NS-M-5(1)	11.48	3.02	0.86	0.81	1.06	0.90
8	38-76-6-NS-Q-8(1)	12.29	2.80	0.92	0.75	1.13	0.84
17	38-91-6-NS-M-17	14.63	4.22	0.94	0.77	1.08	0.93
18	38-91-6-NS-Q-18	15.62	4.76	1.00	0.87	1.16	1.05

Note:
(1) Only test 5 and test8 use ITW Buildex fasteners, others use Hilti fasteners.
(2) For monotonic tests, G' is the secant stiffness at $0.4S_u$; for quasi-static tests, G' is determined for the positive portion of the 7th cycle.
(3) SDI means the strength and stiffness were determined according to the connection properties from SDI equations; SDI* means they are determined according to the connection properties from tests (Rogers and Tremblay, 2000).

The shear load versus distortion hystereses for the above eight tests are shown in Figure 2.1a to Figure 2.1d.

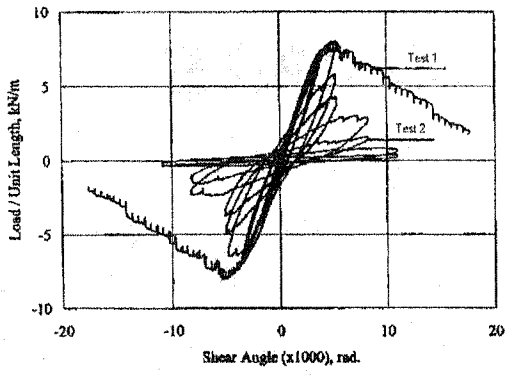

a) Test 1 (M) and Test 2 (Q)

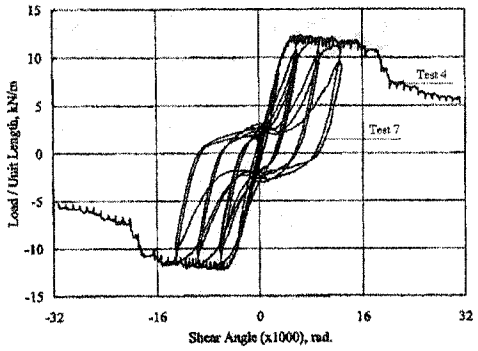

b) Test 4 (M) and Test 7 (Q)

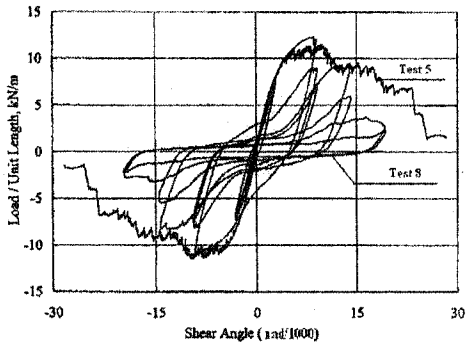

c) Test 5 (M) and Test 8 (Q)

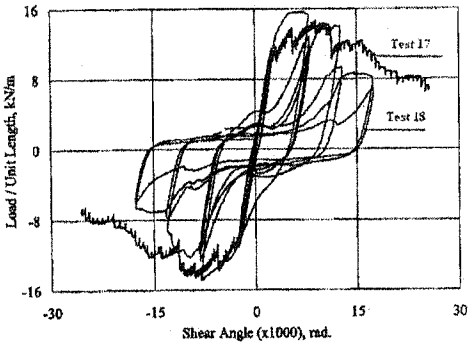

d) Test 17 (M) and Test 18 (Q)

Figure 2.1. Unit shear force /shear angle hystereses (from Essa *et al.*, 2001)

In Figure 2.1, all the test specimens were constructed with 38 mm deep deck panels, i.e. either P3615 or P3615B deck profiles from the Canam Manac Group. Tests 1 and 2 (Figure 2.1a) were weld/button punch connected 0.76 mm specimens. It is noted that for the quasi-static loading protocol, a substantial degradation of strength was observed. On the other hand tests 4 and 7 (Figure 2.1b), constructed with Hilti nail/screw connections and a 0.76 mm sheet thickness, demonstrated a greater level of ductility and a remarkable consistency between the monotonic and cyclic curves. Tests 5 and 8 (Figure 2.1c), also 0.76 mm thick but with ITW Buildex nail/screw

connections, were observed to have less ductility as compared with tests 4 and 7. Figure 2.1d of tests 17 and 18, 0.91 mm thick panels with Hilti nail/screw connections, showed a similar shear/deformation relationship to tests 4 and 7. However, the maximum shear resistance and shear stiffness obtained for test 18 were greater than that of test 17.

Essa *et al.* also provided some useful conclusions on the behaviour and design of steel roof deck diaphragms:

- Screwed side-lap should be used with one of the three deck-to-frame connection types: welded-with-washer, nailed, or screwed. Button punched side-laps are to be avoided when inelastic cyclic loading is anticipated.
- Diaphragms with deck-to-frame welded connections (Test 1 and Test 2) that did not include additional washers exhibited very limited ductility and were not able to sustain a shear resistance under reversed cyclic displacements.
- Diaphragm tests under simulated seismic loading should be carried out to evaluate the influence of strain rate.

2.7 SEISMIC DESIGN CODE PROVISIONS

The seismic design provisions, for Part 4 of the proposed version of 2005 NBCC (NRCC, 2001), and Chapter 27 of CAN/CSA-S16.1, the Limit States Design of Steel Structures (CSA, 2001) are discussed here. The former is for determining the load, and the latter is for the design of structural steel elements.

2.7.1 2005 NBCC

The proposed version of the 2005 National Building Code of Canada (NBCC) (NRCC, 2001) is the design code that forms a basis for this research project. The Canadian Journal of Civil Engineering (CJCE) recently published a special issue in April 2003 (Vol. 30) that contains ten articles covering the proposed earthquake design requirements for the 2005 NBCC, where it is clearly declared that:

"*Structures shall be designed with a clearly defined load path, or paths, to transfer the inertia forces generated in an earthquake to the supporting ground. The structure shall have a clearly defined Seismic Force Resisting System(s) (SFRS), the SFRS shall be designed to resist 100% of the earthquake loads and their effects, other structural framing elements not considered to be part of the SFRS must keep elastic, or have sufficient nonlinear capacity to support both gravity loads and earthquake effects*". (NRCC, 2001)

Both the static and dynamic methods for earthquake design are presented in the 2005 NBCC. For a low-rise building of regular shape, the equivalent static approach is generally appropriate. As a first step in the design of a structure the fundamental lateral period T_a is estimated by one of the following equations:

$T_a=0.085(h_n)^{3/4}$ for steel moment frames (2.5)

$T_a=0.1N$ for other moment frames (2.6)

$T_a=0.075(h_n)^{3/4}$ for concrete moment frames (2.7)

$T_a=0.05(h_n)^{3/4}$ for other structures (2.8)

In the above equations, h_n is the height (in metres) above the base to the roof level, and N in Equation 2.6 is the total number of storeys. Equation 2.8 is used in this case

because the buildings that are the subject of this research are composed of concentrically braced steel frames. If the fundamental period of the structure is determined by other means, e.g. dynamic analyses, then the value used in design must not be greater than 1.5 times that obtained from Equation 2.8.

For design, the minimum lateral earthquake force V is taken as the lesser of:

$$V=S(T_a)M_V I_E W/(R_d R_o) \quad (2.9)$$

$$V \geq S(2.0)M_V I_E W/(R_d R_o) \quad (2.10)$$

If $R_d \geq 1.5$,

$$V \leq 2/3 S(0.2)I_E W/(R_d R_o) \quad (2.11)$$

where:

$S(T_a)$= The ratio of design spectral response acceleration to gravitational acceleration, for a fundamental natural period of T_a (sec.) from one of the equations 2.5 to 2.8. It is determined by linear interpolation between spectral values for sites in Canada. Correction factors F_a and F_v, the acceleration-based site coefficient and the velocity-based site coefficient, respectively, are also incorporated in the calculation as follows:

$$\begin{aligned} S(T) &= F_a S_a(0.2) \text{ when } T<0.2 \text{ sec;} \quad (2.12)\\ &= \text{the less of } F_v S_a(0.5) \text{ or } F_a S_a(0.2) \text{ when } T=0.5 \text{ sec;}\\ &= F_v S_a(1.0) \text{ when } T=1.0 \text{ sec;}\\ &= F_v S_a(2.0) \text{ when } T=2.0 \text{ sec;}\\ &= F_v S_a(2.0)/2 \text{ when } T \geq 4.0 \text{ sec;} \end{aligned}$$

$S_a(T)$= The ratio of 5% damped spectral response acceleration to gravitational acceleration for a natural period of T, using the medium (50%

percentile) values, based on 2% probability of exceedance in 50 years (Adams and Atkinson, 2003).

The values of $S_a(T)$, and S(T) of site class B (Rock) and C (very dense soil and soft rock) in Victoria, B.C. are listed in Table 2.4, where for site class B, F_a=1.0, F_v=0.78; for site class C, F_a=1.0, F_v=1.0.

Table 2.4 $S_a(T)$ and S(T) for site B and C in Victoria, B.C.

T(s)	$S_a(T)$ (g)	S (T) (g)	
		Site Class B	Site Class C
0.2	1.20	1.20	1.20
0.5	0.83	0.65	0.83
1.0	0.38	0.30	0.38
2.0	0.19	0.15	0.19
4.0		0.07	0.095

M_V= Factor to account for higher mode effect on base shear, M_V=1.0 for braced frames when $T_a \leq 1.0$ sec and $S_a(0.2)/S_a(2.0) < 8.0$.

I_E= Importance factor, I_E=1.0 for buildings of normal importance category.

W= Seismic weight, including specified dead load and 25% of the specified snow load.

R_d= Ductility related force modification factor.

R_o= Overstrength related force modification factor

The ductility related force modification factor reflects the capability of a structure to dissipate energy through inelastic behaviour. It is specified as $1.0 \leq R_d \leq 5.0$ in the

2005 NBCC according to the types of seismic force resisting systems (SFRS) being used.

The overstrength related force modification factor has been introduced into the design standard because "*a considerable reserve of strength is not explicitly considered*" in past seismic design calculations (Mitchell *et al.,* 2003). The value assigned to R_o is based on the multiplication of several factors:

$$R_o = R_\phi \cdot R_{yield} \cdot R_{sh} \cdot R_{size} \cdot R_{mech} \qquad (2\text{-}13)$$

where:

$R_\phi = 1 / \phi$; where ϕ is the resistance factor used in design, R_ϕ is included to convert from a factored design to a nominal design.

R_{yield} = ratio of probable yield strength to minimum specified yield strength;

R_{sh} = overstrength due to strain hardening;

R_{size} = overstrength due to restricted choices of member sizes;

R_{mech} = overstrength developed from the point of initial yield until a full collapse mechanism is formed.

It is noted that, when a particular value of R_d is specified, a specific accompanying value of R_o should be utilized in design. However the values of R_d and R_o for steel deck diaphragms are not available in 2005 NBCC since the roof element is not treated as an energy-dissipating element in current design practice. Martin (2002) suggested some R_d and R_o values that could be used in the design of steel roof deck diaphragm and that will be discussed in following sections.

In the 2005 NBCC, a requirement for the torsion analysis of a structure is also presented. The equivalent static approach for seismic design also contains a procedure with which the torsional effects, T_x, are to be calculated:

- $B \leq 1.7$ – by static analysis, with T_x obtained from the following equations:
  - i) $T_x=F_x(e_x+0.1D_{nx})$ (2.14)
  - ii) $T_x=F_x(e_x-0.1D_{nx})$ (2.15)
- $B>1.7$ – by dynamic analysis.

The symbol B refers to the torsional sensitivity of the structure, $B=\delta_{max}/\delta_{ave}$; where δ_{max} is the maximum storey displacement at the extreme points of the structure induced by the equivalent static forces acting at distances $\pm 0.10D_{nx}$ from the centre of mass (CM). δ_{ave} is the average displacement of the extreme points of the structure (Figure 2.2).

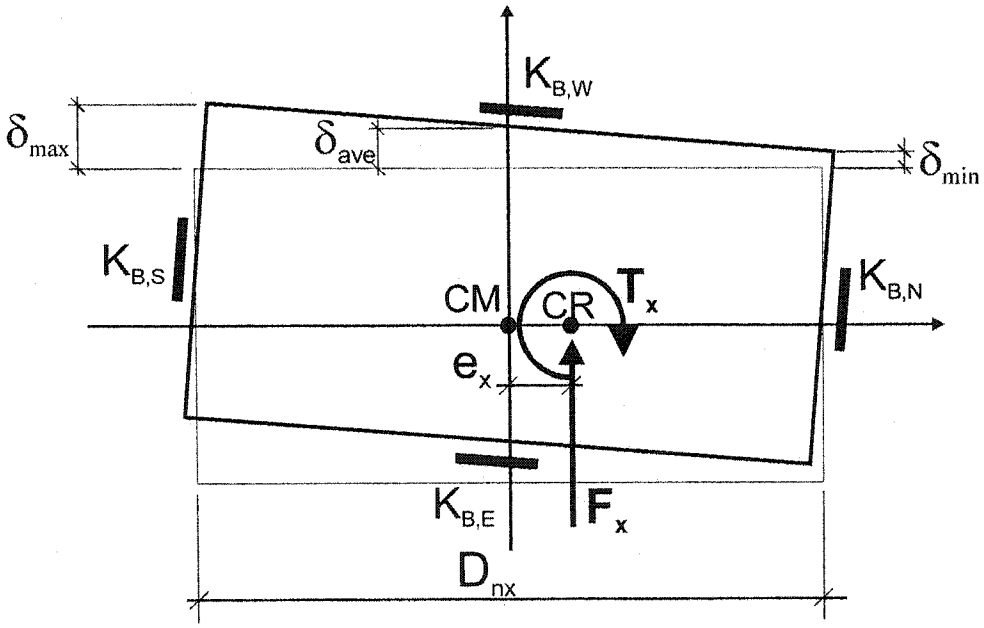

Figure 2.2. Maximum and average storey displacements

T_x= the torsional moment at Level x.

F_x= the lateral force at Level x.

e_x= the eccentricity between centre of rigidity (CR) and the centre of mass (CM) (Figure 2.2).

D_{nx}= the plan dimension of the building at Level x perpendicular to the direction of seismic loading. $0.1D_{nx}$ represents the accidental eccentricity.

The $K_{B,S}$, $K_{B,N}$, $K_{B,E}$, and $K_{B,W}$ in Figure 2.2 represent the brace horizontal stiffness in the south, north, east and west walls respectively, the direction here is only for identification. The eccentricity, e_x results from the difference of the brace horizontal stiffness in opposite walls.

For diaphragms and their connections, the 2005 NBCC will require that they be designed to remain in the elastic range of behaviour. The designer would also need to consider the shape of the diaphragm, the presence of openings, the position of CM, and the additional forces that may result due to the most probable capacity of the fuse element in the SFRS.

2.7.2 CSA-S16

In terms of selecting appropriate sizes for the structural steel elements of the building, Clause 27 of CSA-S16 Limit States Design of Steel Structures (2001) must be followed. This clause contains the seismic design requirements for structural steel members and systems, which are based on the capacity design philosophy.

Clause 27 is mainly for beams, columns and braces and common systems such as moment frames, concentrically braced frames, etc. This clause does not contain any detailed information with respect to diaphragm design, except that it has been made clear that any element in the lateral load-carrying path that is not the fuse member must remain elastic. This is the same requirement as found in the 2005 NBCC.

However, Clause 27 does provide some flexibility with respect to design in that "*Other framing systems and frames that incorporate special bracing, base isolation, or other energy-absorbing devices shall be designed on the basis of published research results, observed performance in past earthquakes, or special investigation*". It can be assumed that the case of roof deck diaphragms that are designed as the weak link in the SFRS falls into this "Other" category. Once the lateral and gravity forces have been determined using the NBCC and the capacity based design approach, other Clauses in the CSA S16 Standard are to be used in determining the sizes of the structural elements.

2.8 MARTIN

The thesis "Inelastic Response of Steel Roof Deck Diaphragms Under Simulated Dynamically Applied Seismic Loading" (Martin, 2002) is comprised of two main parts: analytical and experimental. Since these topics have a very close relationship with the research completed by the author, they will be discussed in detail.

2.8.1 Building analyses

A number of single-storey structures with concentrically braced frames (CBF) and metal roof deck diaphragms were studied to obtain a better knowledge of the anticipated inelastic seismic demand on the diaphragm itself when this portion of the structure is selected as the energy dissipating element in the lateral load carrying path. Considering that the capacity based design approach was followed, the brace elements were expected to remain elastic or at the very most experience limited inelastic deformations. Buildings located in the east and west of the country were

analysed because of the possible change in seismic response for the two geographical areas. The scopes of study for the building analysis portion of the research by Martin included the following:

- Four building sizes: small (15x30 m), medium (30x60 m), large (60x120 m), and double (30x120 m);
- Two main Canadian seismic sites: Victoria, BC, and Quebec, Qc;
- Two ductility related force modification factor values: R_d=3.0, and R_d=2.0;
- Eight ground motions for Victoria, BC, and four ground motions for Quebec, Qc.

The structures were designed according to the proposed 2005 version of the National Building Code of Canada (CANCEE, 2001) and the most current CSA-S16 steel design standard (CSA, 2001). The structures were assumed to be located on Site Class B (rock), a site condition from where most ground motion signals being used in dynamic analysis were collected. The 5% damped spectral response acceleration values, S_a (T), for the reference ground conditions were used to calculate the earthquake forces, where T is the natural period of the designed structure. The overstrength related force modification factor, R_o, is chosen according to Equation (2.13), and simplified as:

$$R_o = R_\phi = 1 / \phi = 1/0.6 \qquad (2.16)$$

Because R_{yield} , R_{sh} , R_{size} , and R_{mech} were all selected as 1.0. In the above equation, ϕ = 0.6 was chosen for mechanically connected roof systems, according to FEMA 302 (BSSC, 1997) and AISI (1997).

Canam Manac's P3615B steel decks, which are manufactured from ASTM A653 SS Grade 230 (2002) sheet steel, were incorporated in the evaluation of the diaphragm properties. The 7500 mm deck sheets spanned over three joists with a spacing of 1875

mm c/c. Deck-to-frame connections were made with Hilti nails (ENP2-21-L15), and the side-lap connections were with #10 screws. The SDI procedure was used to estimate the ultimate strength, S_u, and stiffness, G', of the roof diaphragm.

Based on the tests carried out by Essa *et al.* (2001), it was demonstrated that the nail-screw diaphragm design could exhibit a moderate ductility. Such being the case the building structure was designed with an assumed R_d = 2.0 and 3.0. Martin later evaluated the appropriateness of these values based on the amplitude of the inelastic demand obtained from the analysis and the experimental program.

RUAUMOKO, the Inelastic Dynamic Analysis Computer Program (Carr, 2000), was utilized to carry out a suite of time-history analyses. A Newmark constant average acceleration scheme with a time step of 0.001 seconds was incorporated into the model, and P-delta effects were neglected. Initial stiffness Rayleigh damping equal to 5% of critical damping in the first two modes was assumed. The diaphragm structure for each building was divided into 3 x 3 m spring elements (Figure 2.3) that behaved according to the Wayne Stewart inelastic hysteretic rules (Stewart, 1987).

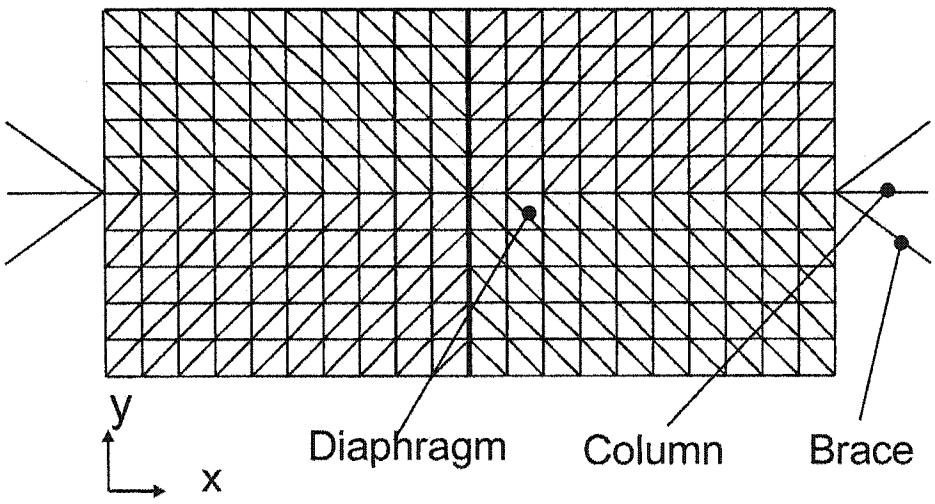

Figure 2.3. Plan view of the building model (from Martin, 2002)

The characteristics of the hysteresis model were based on the results of the reversed cyclic quasi-static nail / screw diaphragm tests (No. 7) by Essa *et al.* An example of the non-linear diaphragm element hysteresis is shown in Figure 2.4. To use the deck diaphragm as a seismic energy dissipating element, it was required that the following characteristics be evident. First, the steel deck panels should demonstrate significant inelastic deformation ability during an earthquake without a brittle failure type or the development of a failure mechanism. If this is the case then the diaphragm can most probably be used as the energy-dissipating element (Figure 2.4 a). Second, the inelastic deformation of the diaphragm, although concentrated at the ends of the roof near the bracing bents, should be able to extend into the central portions of the roof deck (Figure 2.4 b).

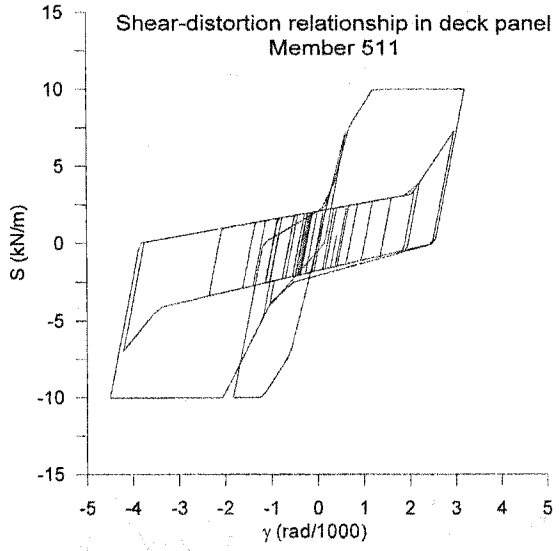

a) Shear-distortion curve in deck element member 511.

Figure 2.4. An example of inelastic deck response (from Martin, 2002)

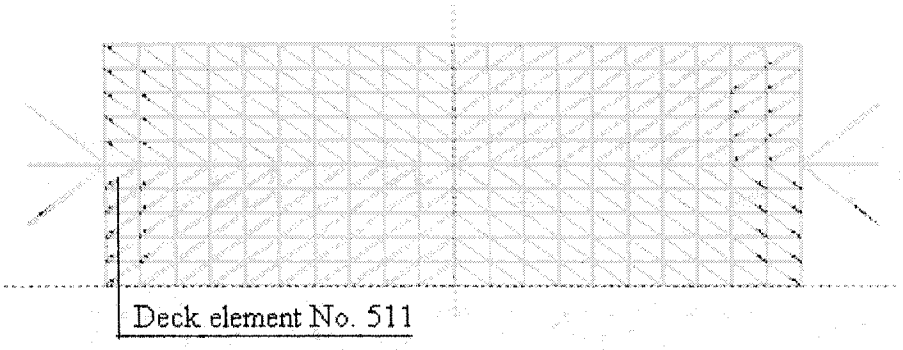

b) Panels that yielded for Victoria medium R_d = 3.0 under ground motion B, where asterisk marks indicate that the elements have yielded.

Figure 2.4 (Continued)

Once the time-history analyses had been run, mid-length storey drift, *i.e.* in-plane displacement at the centre of the roof. The drift prediction was to ensure that the building deflection met the drift limit $0.025h_s$, where h_s is the storey height (NRCC, 2001). The maximum inelastic distortion, γ_p, which equals the total distortion minus elastic distortion γ_u, were also checked. Martin (2002) concluded that the ductility demand, $(\gamma_p + \gamma_u)/\gamma_u$, in the diaphragm increased to a greater extent than expected with the use of a larger force modification factor for ductility. "*It seems that γ_p is not proportional to R_d, as expected (much higher values of γ_p with R_d = 3.0 than with R_d = 2.0). This may be attributed to the hysteretic model involving pinching used with screw-nail designs. The inelastic demand seems to grow very rapidly when R_d increases from 2.0 to 3.0*".

2.8.2 Diaphragm experiments

Martin (2002) also completed a series of full-scale cantilever diaphragm tests using loading protocols that were based on the expected ductility demand obtained from the

non-linear time history analyses. The objectives were to investigate the response of a test diaphragm to the ductility demand obtained from the analytical study and to recommend force modification factors for design. The tests carried out by Martin are listed in Table 2.5.

Table 2.5 Diaphragm Tests by Martin (2002)

Test	Sidelap	Frame	Deck profile	Loading protocol
38-91-6-NS-M-19	Screwed	nailed (H) [1]	P3615B 0.91 mm	Monotonic
38-76-6-WB-SD-20	b. p.	welded [2]	P3615 0.76 mm	Short duration
38-91-6-WB-SD-21	b. p.	welded [2]	P3615 0.91 mm	Short duration
38-91-6-W'W-M-22	w.w.w.[3]	w.w. washer [4]	P3615B 0.91 mm	Monotonic
38-91-6-W'W-SD-23	w.w.w.[3]	w.w. washer [4]	P3615B 0.91 mm	Short duration
38-91-6-W'W-LD-24	w.w.w.[3]	w.w. washer [4]	P3615B 0.91 mm	Long duration
38-91-6-NW-M-25	w.w.w.[3]	nailed (H) [5]	P3615B 0.91 mm	Monotonic
38-91-6-NW-SD-26	w.w.w.[3]	nailed (H) [5]	P3615B 0.91 mm	Short duration
38-91-6-NW-LD-27	w.w.w.[3]	nailed (H) [5]	P3615B 0.91 mm	Long duration
38-76-6-NS-SD-28	Screwed	nailed (H) [1]	P3615B 0.76 mm	Short duration
38-76-6-NS-LD-29	Screwed	nailed (H) [1]	P3615B 0.76 mm	Long duration
38-76-6-NS-M-30[6]	Screwed	nailed (H) [1]	P3615B 0.76 mm	Monotonic
38-76-6-NS-SD-31[6]	Screwed	nailed (H) [1]	P3615B 0.76 mm	Short duration
38-91-6-NS-M-32[6]	Screwed	nailed (H) [1]	P3615B 0.91 mm	Monotonic
38-91-6-NS-SD-33[6]	Screwed	nailed (H) [1]	P3615B 0.91 mm	Short duration
38-91-6-NS-SD-34	Screwed	nailed (H) [1]	P3615B 0.91 mm	Short duration
38-91-6-NS-LD-35	Screwed	nailed (H) [1]	P3615B 0.91 mm	Long duration
38-76-6-WB-SD-36	b. p.	welded [2]	P3615 0.76 mm	Cyclic +Short dur.[7]
38-91-6-WB-M-37	b.p.	welded [2]	P3615 0.91 mm	Monotonic

Notes:
(1): Used Hilti (H) X-EDNK22-THQ12 fastener for nailed frame connections and 12-14x7/8'' fastener for screwed sidelap connections.
(2): Welded frame connections were made with 16 mm diameter arc spot welds.
(3): Welded sidelap connections with washers.
(4): Welded frame connections with washers.
(5): Used Hilti (H) X-EDNK22-THQ12 fastener for nailed frame connections
(6): All fasteners spaced at 152 mm o/c in both directions, spacing in all other tests equal to 305 mm.
(7): 200 cycles at 0.4 γ_u and 2 cycles at 0.6 γ_u prior to short duration loading protocol

The loading protocols were developed such that the diaphragm demand obtained from the analytical investigation for the east and west of the country would be imposed on the deck panel test specimens (Figure 2.5). A short duration protocol for intra-plate earthquakes, along with a long duration protocol for Cascadia subduction type earthquakes (inter-plate) that are anticipated on the west coast were utilized in testing.

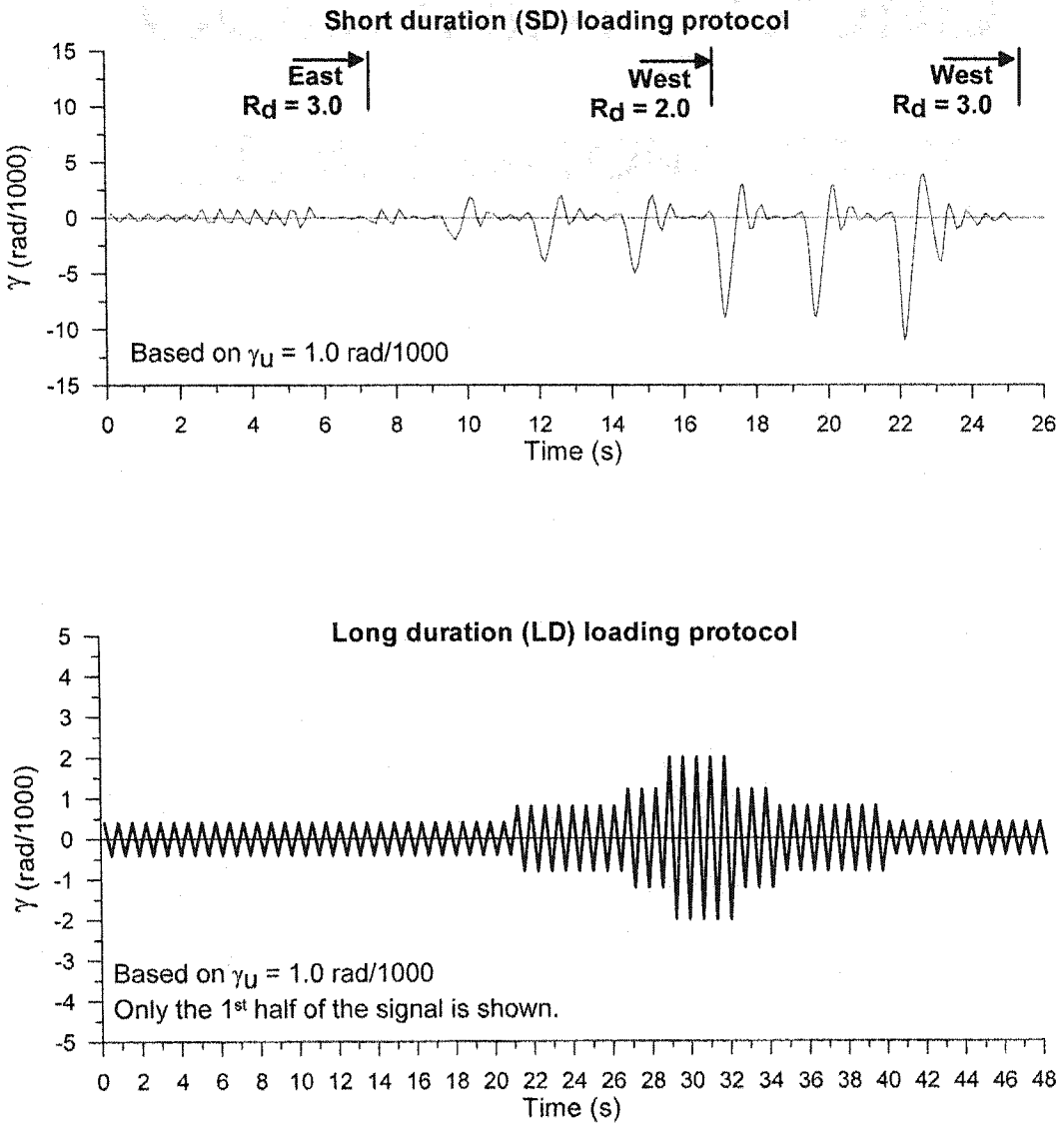

Figure 2.5. SD and LD loading protocols (from Martin, 2002)

Table 2.6 Test results from Martin (2002)

Test	Date of testing	Test values		Test to predicted			
		Su kN/m	G' kN/mm	Su Test/SDI*	Su Test/SDI	G' Test/SDI*	G' Test/SDI
38-91-6-WB-M-37	03/20/2002	12.6	3.32	0.75	1.09	0.80	0.72
38-91-6-WB-SD-21	02/15/2002	13.8	3.16	0.82	1.19	0.76	0.68
38-76-6-WB-SD-20	02/13/2002	9.81	2.44	0.86	1.07	0.88	0.74
38-76-6-WB-SD-36a[1]	03/19/2002	5.80	2.40	0.51	0.63	0.87	0.73
38-76-6-WB-SD-36b[1]		5.69	0.94	0.50	0.62	0.34	0.28
Mean [2]				0.81	1.11	0.81	0.71
C.o.V. [2]				0.07	0.06	0.08	0.04
38-91-6-W'W-M-22	02/20/2002	32.1	4.54	0.88	N/A	0.81	N/A
38-91-6-W'W-SD-23	02/22/2002	34.6	4.60	0.95	N/A	0.82	N/A
38-91-6-W'W-LD-24	02/27/2002	33.2	4.36	0.91	N/A	0.78	N/A
Mean				0.91		0.80	
C.o.V.				0.04		0.03	
38-91-6-NW-M-25	03/01/2002	22.5	4.33	1.06	N/A	0.91	N/A
38-91-6-NW-SD-26	03/04/2002	26.5	4.09	1.25	N/A	0.86	N/A
38-91-6-NW-LD-27	03/18/2002	26.2	3.64	1.24	N/A	0.76	N/A
Mean				1.18		0.84	
C.o.V.				0.09		0.09	
38-91-6-NS-M-19	02/08/2002	16.7	4.13	1.24	1.07	0.91	0.75
38-91-6-NS-SD-34	03/14/2002	17.0	4.01	1.26	1.09	0.89	0.73
38-91-6-NS-LD-35	03/15/2002	17.3	3.90	1.28	1.11	0.86	0.71
38-76-6-NS-SD-28	03/06/2002	14.1	2.45	1.27	1.08	0.87	0.65
38-76-6-NS-LD-29	03/07/2002	13.6	2.39	1.23	1.05	0.85	0.64
Mean				1.25	1.08	0.88	0.70
C.o.V.				0.02	0.02	0.03	0.07
38-91-6-NS-M-32	03/13/2002	34.4	18.3	1.38	1.19	1.27	0.88
38-91-6-NS-SD-33	03/14/2002	35.2	18.4	1.41	1.21	1.28	0.88
38-76-6-NS-M-30	03/08/2002	23.4	13.5	1.16	0.97	1.30	0.84
38-76-6-NS-SD-31	03/12/2002	26.5	15.0	1.31	1.10	1.44	0.93
Mean				1.32	1.12	1.32	0.88
C.o.V.				0.09	0.10	0.06	0.04

(1): Cycles at 0.4 γ_u and 0.6 γ_u were performed prior to the SD loading protocol.
a refers to the cyclic part, b to the SD loading protocol.
(2): Test 36 results are not included in the mean and C.o.V.

The measured acceleration and load cell signals were filtered to remove the possible high frequency motions that may occurred in the frame during the dynamic tests due to the local friction and impact phenomena. In all cases, the chosen low-pass filter was set to 3 Hz for the acceleration and 10 Hz for the load cell recording. A listing of test results carried by Martin is provided in Table 2.6, where SDI means the strength and stiffness were determined according to the connection properties from SDI equations; SDI* means they are determined according to the connection properties from tests (Rogers and Tremblay, 2000).

Martin concluded that "*it was important to use dynamic tests instead of slow cyclic tests since the distribution of forces among fasteners and the strain-rate effects on material properties are influenced by the rate of deformation*". It was also recommended that five sheets instead of four sheets be used in future cantilever diaphragm tests, *i.e.* three regular panels and two half panels at the edges of the test specimen. It was anticipated that the five side laps would have similar stiffness, and hence, each line of connectors would undergo the same amount of slip.

A note was made with respect to the use of the interlocking edge panel type, whereby the quality of welds at side-lap locations was questionable due to the oval shape of the interlock edge. Additionally, button punch side-lap connections were not compatible with welded deck-to-frame connections because the button punches have a much greater flexibility compared with the welds. It was observed that when the welds failed, no increase or maintenance in diaphragm capacity could be expected because the button punched connections also failed immediately.

Based on the ability of the various diaphragm systems to perform during the short duration loading protocols, Martin recommended the following preliminary values for R_d and R_o:

- Weld/Button punch system (WB): R_d=1.0, R_0=1.0;

- Weld with washer/weld system (W'W): R_d=1.5, $R_o = R_\phi$, where $R_\phi = 1 / \phi$;
- Nail/weld (NW) system: same as the Weld with washer/weld system;
- Nail/screw (NS) system, R_d=2.0, $R_o = R_\phi$, where $R_\phi = 1 / \phi$;

Martin also concluded that future research should cover a number of aspects related to diaphragm performance. A partial listing includes: 1) ambient or force vibration tests of real buildings to obtain data on in-situ dynamic properties, 2) improved analytical models that account for the behaviour observed in the short and long duration diaphragm tests, 3) the effect of panel end laps on the behaviour of roof diaphragms, and 4) the effect of non-structural roofing components on diaphragm shear capacity and stiffness.

2.9 TORSION ANALYSIS

2.9.1 Humar *et al.*

Humar and Kumar (1998a) summarized some previous research on the torsional response of buildings under seismic loads: "*A fairly large number of research studies have been carried out on elastic and inelastic torsional responses of buildings. The findings of the various studies are not always consistent with one another. This can be attributed to the complexity of the torsional behaviour and to the large number of governing parameters*".

Humar and Kumar concluded that "*the ratio of the uncoupled torsional and translational frequencies is an important parameter governing the torsional response and it would be a good practice in design to achieve a value greater than 1 for this ratio*".

The ratio of the uncoupled torsional and translational frequencies, Ω, is described as:

$$\Omega=\omega_\theta/\omega_y \tag{2.17}$$

where, ω_y, the translational (in the earthquake direction) frequency, is equal to:

$$\omega_y=(K_y/m)^{1/2} \tag{2.18}$$

ω_θ, the rotational (about the centre of resistance) frequency, is equal to:

$$\omega_\theta=(K_\theta/mr^2)^{1/2} \tag{2.19}$$

Here, K_y is the translational stiffness, K_θ is the rotational stiffness, m is the mass of the floor, r is the radius of gyration of the floor or roof plane.

Humar and Kumar considered the torsional motion of a building during an earthquake for both elastic response (Humar and Kumar, 1998a) and inelastic response (Humar and Kumar, 1998b). The analyses that were carried out included both the static analytical procedure and the dynamic time-history procedure.

According to Humar and Kumar, in the elastic range, the torsional response is governed by ω_y, the uncoupled translational (in the earthquake direction) frequency, e/r, the ratio of eccentricity e to the radius of gyration about the centre of mass of the floor or roof plane, and the ratio of the uncoupled torsional and translational frequencies, Ω. For an inelastic system, the torsional response is governed by a number of additional parameters, such as the yield strength, strength eccentricity, and its post-yield properties.

Humar *et al.* (2003) introduced the background of 2005 NBCC in terms of torsional design aspects, as was presented in Section 2.7.1. They also analysed the effect of asymmetric brace stiffness on the performance of buildings. The studies showed that

the new code requires that "*a dynamic analysis procedure be used for the design of torsional flexible buildings*", and a dynamic analysis procedure is also needed for torsional non-flexible buildings when B is greater than 1.7.

2.9.2 Bruneau *et al.*

As suggested by Humar and Kumar that was discussed in last section, for an inelastic system, the torsional response is governed by a number of additional parameters, such as the yield strength, strength eccentricity, and its post-yield properties. Some of these became the main interests in the "Seismic Response of Symmetric Structures Having Unbalanced Yield Strengths in Plan" (Bruneau *et al.* 1991), where the effect of dissimilarities in yield strength and force-displacement relationships on the torsional response was mainly considered. In addition, the parameters such as the uncoupled period, the ratio of the uncoupled torsional and translational frequencies Ω, and the uncoupled SDOF (single degree of freedom) target ductility levels were also considered.

Bruneau et al. simplified the real structure as having a rigid diaphragm with only two braces equidistant from CM, i.e. 2 DOFs. The following parameters were combined together to see their respective effects:

- Ten values of uncoupled period T_x (0.1, 0.2, 0.3, 0.4, 0.6, 0.8, 1.0, 1.2, 1.6, 2.0 sec);
- Six values of the ratio of the uncoupled torsional and translational frequencies Ω (0.4, 0.8, 1.0, 1.2, 1.6, and 2.0);
- Two target ductility levels μ_T (4.0, 8.0);
- Four combinations of yield strength ratios of weak to strong frames (0.8/1.0, 1.0/1.2, 1.0/1.5, and 1.0/2.0).

One important index that Bruneau et al. introduced was μ/μ_T "the Ductility Amplification Ratio", which is believed to "*provide the best quantitative measure of the damage sensitivity of the structures*". The Ductility Amplification Ratio μ/μ_T is actually the ratio of ductilities, where the ductility demand μ is a ratio of maximum displacement to the yield displacement. It was defined that the $\mu/\mu_T < 1.25$ be of less importance; $\mu/\mu_T = 1.25$ to 1.50 be of moderate importance; $\mu/\mu_T > 1.50$ be of major importance.

According to Bruneau et al, the influence of the structural period T_x and of the target ductility levels μ_T on the Ductility Amplification Ratio μ/μ_T was not significant. Hence, only the ratio of the uncoupled torsional and translational frequencies Ω and the yield strength ratios of weak to strong frames were discussed. In addition, no stiffness eccentricity was considered. Rayleigh type 2% damping ratio for each of the true elastic frequencies was specified. Strain-hardening was chosen as 0.5% of the initial stiffness of the elements. Based on the analysis, Bruneau et al. concluded:

"*The weak element ductility amplification ratios for the strength ratio case 0.8/1.0 are always at least of moderate importance, and often of major importance, ranging from 2 to 4 for the mean response. The strong element ductility amplification ratios are all less than 1.0, except in the case 0.8/1.0, where the lower structures ultimate translational strength make larger inelastic deformation also possible in the stronger element. Weak element ductility amplification ratios tend to increase with Ω, while strong element ductility amplification ratios tend to decrease accordingly.*"

Some design recommendations were suggested by Bruneau et al: when Ω is larger than 1.20, the value of μ/μ_T for weak element is expected to be greater than 1.50, in this case, it was hoped to decrease its target ductility demand to 1/1.50 of the original.

Some limitations could be noted for the analysis by Bruneau et al. Firstly, the target ductility demand μ_T equals to 4.0 and 8.0 may be too high for most limited ductility concentric braced frames that are most popularly used in single storey steel structures, for these structures μ_T equals to 2.0 should be much more appropriate. Secondly, the average of normalized yield strength of weak and strong frames are not 1.0, they are either less than 1.0 (e.g. for yield strength ratios 0.8/1.0 case), or bigger than 1.0 for other cases. The reason for this was the research was mainly about the "*seismic retrofitting of existing structures*" where a partially less strong structure (e.g. 0.8/1.0 case) is to be reinforced. In designing new structures, an average of normalized yield strength of weak and strong frames equalling 1.0 could be expected. Thirdly, the flexible diaphragm is not considered. Fourthly, the eccentricity of braced stiffness was not included in combination with the yield strength eccentricity.

2.9.3 Nedisan

Nedisan (2002) noted the above limitations in the paper by Bruneau et al (1991), and analysed the inelastic dynamic torsion response by using a 30 m x 60 m x 6.6 m single storey steel building in her thesis "Comportement sismique de bâtiments en acier d'un seul étage avec diaphragme de toit flexible" (in French).

Nedisan firstly designed the building by following the equivalent static approach prescribed in the proposed 2005 NBCC (NRCC, 2001). The roof flexibility was estimated based on the SDI procedure. The design conditions, parameters and combinations she considered are summarized hereafter:

- R_d=2.0, R_o=1.2;
- Building is located in a Site Class C in Victoria B.C., critical damping ratio = 4%;

- Two roof rigidities: flexible (G' = 6.486 kN/mm), and rigid (G' = $6x10^6$ kN/mm);
- Three plan layout:
  - Symmetric;
  - brace stiffness asymmetric (the ratio of stiffness is 1.5/1.0);
  - brace stiffness asymmetric plus brace resistance asymmetric, yield strength ratios 0.95/1.05;
- Eight ground motions.

Secondly, she divided the 30 m x 60 m roof diaphragm into 128 discrete plane shell finite elements, see Figure 2.6, all the masses were lumped to the element nodes. By the non-linear time step dynamic analysis in DRAIN-2DX (Prakash *et al.*, 1993), the node response accelerations can be obtained. Thirdly, she calculated the node inertia forces that are equal to the node response accelerations multiplied by the node mass.

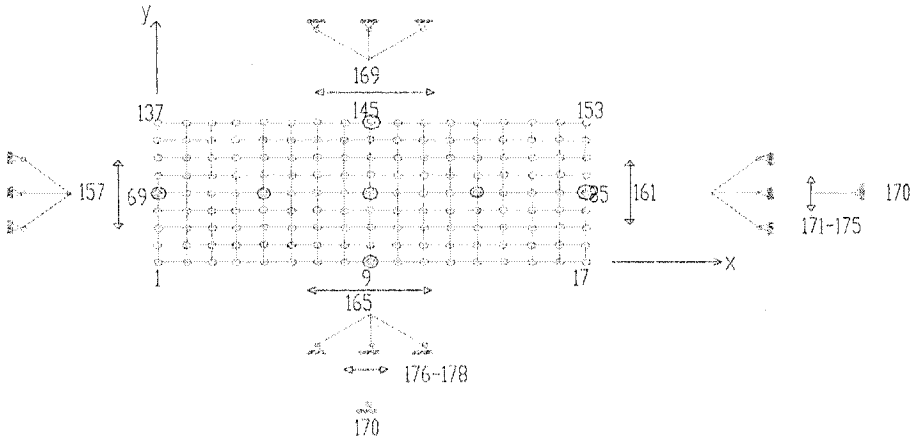

Figure 2.6. Analysis model in DRAIN-2DX (from Nedisan, 2001)

Nedisan further calculated the torsion moment around CM due to these node inertia forces. As was discussed before, the inertia forces caused by ground motion or other dynamic forces must be transferred to the lateral force resisting system (LFRS) such as the vertical braces in Figure 1.1, and finally be transferred to the foundation and ground. So the torsion moment around CM due to inertia forces should be equal to that resisted by the braces. Nedisan compared the above two torsional moments and found that these two results matched quite well (Figure 2.7), even the comparison was shown only for a limited portion of the earthquake duration (up to 10 sec).

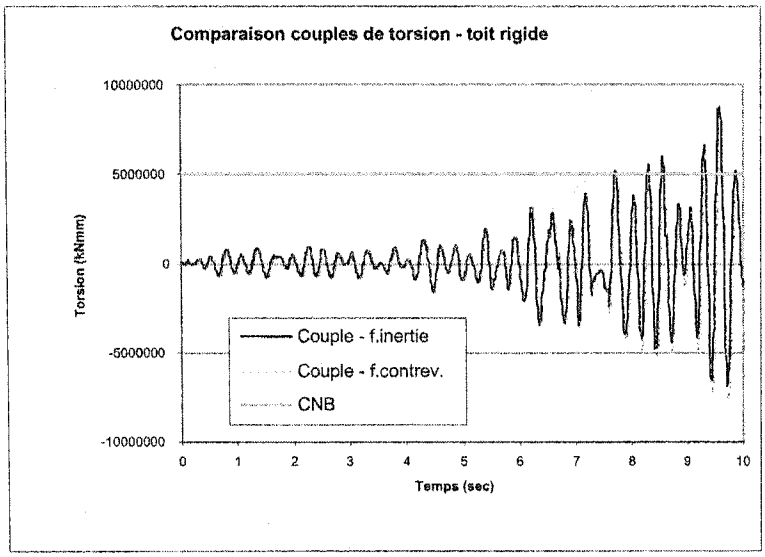

Note: The line that denotes CNB refers to the expected torsion forces based on the equivalent static method seismic design method from the NBCC 2005.

Figure 2.7. History of torsional moment of rigid roof with asymmetric brace stiffness for ground acceleration No.7 (from Nedisan (2002))

Nedisan defined and calculated the position of the resultant inertia forces in the earthquake direction as center of inertia forces (CI), her results of the analyses suggest that considering the stiffness eccentricity by the equivalent static method for seismic design may significantly underestimate the torsional response of the structure. The greater than expected torsional response was attributed to the fact that the centre

of inertia (CI) of the roof does not always maintain the same position as the centre of mass (CM) (see Figure 2.2 in Section 2.7.1) as assumed in static analysis, but oscillate around the CM in dynamic situation.

The study also showed that torsional effects are lower when roof flexibility is considered. But a small difference of yield strength (0.95/1.05) results in large ductility demand amplification in the weak brace elements. It is suggested that roof flexibility and the inherent accidental difference of yield strength be considered in design.

Some limitations could also be noted for the analyses finished by Nedisan. Firstly, the torsional moments are those around the centre of mass (CM), while the torsional moment in the 2005 NBCC is around the centre of rigidity (CR), see Figure 2.2. The comparison of these values is not very reasonable because of the different reference points. It would be more desirable to recalculate these torsional moments around CR such that a comparison with the NBCC results would be possible. Secondly, the examination of the time history of torsional moment in Nedisan's analysis was only for one ground motion and its earthquake duration was only 10 sec. Additional earthquake records over this duration are needed to confirmer the findings of Nedisan. Thirdly, it could be found that, if her analysis model is not adjusted, the torsion moment around CM due to inertia forces and that resisted by the braces does not match well for the response case shown in Figure 2.7 being examined beyond 10 sec.

2.10 CHAPTER SUMMARY

As discussed in this literature review, for the design of single-storey steel buildings seismic lateral loads are applied at the roof level in the form of distributed inertial

loads. These loads produce shear and moment in the diaphragm, which behaves as a deep horizontal girder where the perimeter members resist the bending forces and the deck resists the shear forces. Therefore, one key element in design is the shear behaviour of the roof deck diaphragm.

A large number of static and cyclic tests have been performed on the shear behaviour of the metal roof deck diaphragm specimens, however, cyclic tests on diaphragm specimens that include end lap joints or roofing material have not been reported in the literature. It is quite possible that these two factors pose a significant influence on the inelastic dynamic diaphragm behaviour. Verifying these influences have become two major objectives in the test analysis in the following study.

Based on the hysteresis of unit shear force / distortion of test 7 by Essa et al (2001), Martin (2002) analysed the inelastic dynamic behaviour of single storey buildings and recommended values of R_d and R_o. Since only one test was used, it is quite necessary to verify these values by considering the results of additional tests.

Finite element analysis of deck diaphragm reinforced by non-structural components is required to quantify the influence of roofing materials on both strength and stiffness.

The torsional effect analysis partially finished by Nedisan needs to be continued to give a comprehensive understanding about the dynamic torsional behaviour due to roof flexibility and the inherent variation of brace stiffness.

CHAPTER 3 ROOF SYSTEMS

3.1 INTRODUCTION

As stated in Chapter 1, one major objective of the research documented in this thesis was to study the influence of non-structural components on diaphragm behaviour, or to be more precise, the influence of the roofing materials. This chapter contains an introduction to roof systems, which will complement the following study on the influence of non-structural components. One of the difficulties in carrying out an assessment of non-structural roofing materials is that there are many different types of roof systems with numerous combinations of different components. Therefore, an aim of this chapter is to choose one roof system that is popular in terms of engineering applications, and at the same time, may influence the deck diaphragm behaviour. This was achieved by means of a market survey and through consultation with the Association des Maîtres Couvreurs du Québec, the Ontario Industrial Roofing Contractors Association, the Alberta Building Envelope Council, the Canadian Roofing Contractors' Association, Trow Consulting Engineers Ltd, Plasti-Fab Co, and some internet sources, such as www.roofhelp.com, www.professionalroofing.net, *etc.*

As the most exposed part of any building, the primary function of roofing materials is to deal with and manage weather elements (such as sun, rain, wind, snow, hail, ice), security and energy conservation, etc, thereby protecting the interior environment and structural components. Every year, architects and roof consultants publish many books and articles about roofs. Some helpful references are cited here: ABEC (1985), ASTM Vol. 04.04 (2001), ASTM Vol. 04.06 (2001), Ashby (1999), Baker (1980), Chown (1990), Griffin (1982), NRCC (1989), and Patterson and Mehta (2001).

According to the slope angle, roofs can be classified as low-slope (slope < 3:12) or steep (slope > 3:12). A low-slope roof is generally used for commercial and industrial buildings, where steel deck panels span between framing members. A low-slope roof is also called a *water-resisting roof*, because a waterproof layer is needed. A flat roof is defined when the deck slope is equal to or less than a minimum of ¼ :12 (2%). The market share of low-slope roofs is about 65%, *i.e.* the majority of the roof industry (Patterson and Mehta, 2001). A steep roof is referred to as a water-shedding roof, or pitched roof, which is commonly found in residential buildings. In this thesis the scope of study is restricted to low-slope roofs.

3.2 THE COMPOSITION OF LOW-SLOPE ROOFS

A typical low-slope roof system may have several layers, or components, such as: roof deck, waterproof membrane, insulation, thermal barrier, vapour retarder and flashing. These materials can be classified into two categories:

- Structural components;
- Non-structural components.

Structural components include beams, joists, decks and connections. The most common decks are made of steel, concrete, or wood, where concrete decks provide a stiff diaphragm, while steel and wood decks constitute a relatively flexible one. To be consistent with the objective of this thesis, only steel decks will be considered. Non-structural components are the materials attached to the roof deck, which carry out their own specific functions. A summary of these functions and the required properties of various roof components is listed in Table 3.1.

Table 3.1 Main functions and properties of roof components (NRCC, 1989)

Function of the roof components	Properties required to fulfill the function	Components in the roof that fulfill the function
Attachment of the roof components	Strength Material compatibility Weight (ballast)	Adhesive Mechanical fasteners Ballast
Structural support	Strength Rigidity	Deck and supporting structure
Control of water ingress	Waterproof Ductility Toughness UV resistance	Roofing membrane along with flashing and draining system
Control of air flow Control of heat loss Control of condensation Control wind uplift	Airtightness Continuity Strength Rigidity Toughness	Airtight deck or airtight membranes or underlays fastened to and supported by deck and structure
Control of water vapour diffusion Control of condensation	Low permeance	Vapour retarder in conventional system Roof membranes in PMR[1]
Control of air flow Control of heat loss Control of condensation	Thermal resistance Low permeance in PMR[1]	Thermal insulation
Surface protection	UV resistance Resistance to mechanical damage	Top cover Coatings Covers such as gravel or pavers

[1] *PMR – protected membrane roof system*

Concerning non-structural components, two basic roof systems are commonly used in Canada (NRCC, 1989).

- *The conventional roof system, in which the membrane is outside the insulating layer and essentially exposed to the elements.*
- *The Protected Membrane Roof (PMR) system, in which the membrane is under the insulating layer and protected from the elements.*

It is difficult to say which system dominates the market in Canada; both can give good service and both are susceptible to their own problems. When steel deck is used, a conventional roof system usually has the following basic components, (from top to base, refer to Figure 1.2):

1. top cover;
2. waterproof membrane;
3. thermal insulation;
4. vapour retarder, or air barrier;
5. thermal barrier;
6. steel deck.

"*A top cover protects underlaying roof components from UV radiation and physical wear and tear, and provides ballast for assemblies requiring this function*" (NRCC, 1989).

A protected membrane roof (PMR) system has the following basic components (Figure 3.1):

1. top cover;
2. thermal insulation;
3. waterproof membrane;

4. thermal barrier;
5. steel deck.

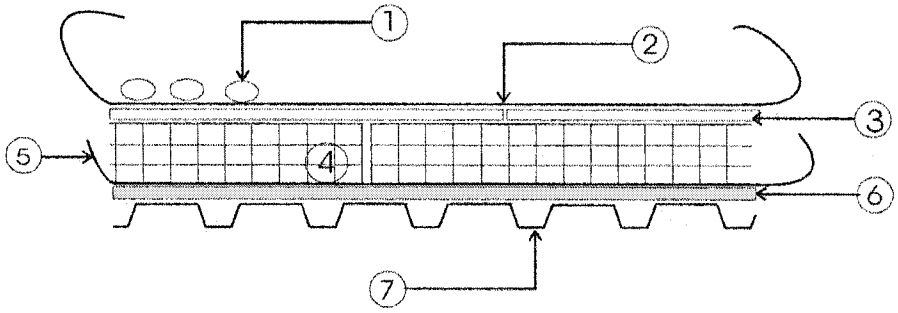

Note:

1. Ballast, round water worn gravel or stone plates, or top pavers;
2. Filter fabric, loose laid, filter fabric is a porous plastic membrane that prevents small debris from penetrating into the insulation layer but permits water to pass through.
3. Top XEPS board, loose laid, XEPS is the acronym of Extruded Expanded Polystyrene, an insulation material specifically suitable to PMR roofing systems;
4. Bottom XEPS board, loose laid;
5. Roof membrane, loose laid, connected in side laps and end laps.
6. Gypsum board, loose laid as a thermal barrier
7. Steel decks

Figure 3.1. One example of protected membrane roof (PMR) roofing system

The common components of the above systems are the steel deck and the thermal barrier. A non-combustible thermal barrier is usually required due to the fireproofing considerations when steel panels are used as deck material. This requirement was reinforced after the disastrous fire in the General Motors plant in Livonia, Michigan, U.S. in 1953, where no thermal barrier was specified, and all of the non-structural components were directly adhered to the steel deck by hot bitumen. "*In this fire, nearly 1.5 million square feet of building was destroyed in little more than one hour.*

The prime cause of the large magnitude of this disaster was the speed at which the flames traveled on the underside of the roof deck. ...molten bitumen from the roof started to drip down through the joints in the roof deck, which further fuelled the fire....After the GM plant fire, ..., it was concluded that there should be non-combustibles between the metal deck and the insulation" (Patterson and Mehta, 2001). The thermal barrier also provides a plane surface for other components to be placed on top of, and hence removes the difficulty of installing these components directly on the corrugated steel deck panels. In addition, the thermal barrier may increase the in-plane shear stiffness of the roof deck diaphragm.

The components differ between these two general roofing categories starting from the vapour retarder layer. A vapour retarder or air barrier layer is needed at the warm side of the roof in order to control condensation and to reduce energy losses. In the case of the PMR system, the waterproof membrane itself could function as the vapour retarder, therefore no extra layer is needed. Steel deck can also function as a vapour retarder, but due to the many attachment holes and side laps, it is not recommended for this use. It should be noted that a vapour retarder is not always needed, according to the "Design Criteria of BUR (Built-Up Roof)" of the Fields Company (www.fieldscorp.com), "*a vapour retarder shall be specified for low-slope roof membranes when both the following conditions exist* (in North America):

1. *The outside average January* (the coldest month) *temperature is below 4° C.*
2. *The expected interior winter relative humidity is 45% or greater."*

In Canada, the first condition always exists, and the second condition usually is met, therefore a vapour retarder is typically specified for buildings constructed in this country.

In a conventional roof system, the insulation is protected against weather attack and mechanical damage, which provides a broad selection of insulating materials for the designer. On the down side, membranes are exposed to extreme weather conditions; and as a result the repair frequency is higher than found for PMR systems. In a PMR system the membrane is protected, however specific insulation is required and ballast is always needed to hold this insulation in place, which adds to the gravity and seismic loads on the roof.

All of the roof components must be held in place to prevent lateral movement and wind uplift. According to the attachment method, there are basically three types of roof system.

- Ballasted roof system;
- Adhered roof system;
- Mechanically-fastened roof system;

The ballasted roof system is applicable to both PMR and conventional roofs, but the other two systems are typically used in conventional roofs. In a ballasted roof system, the entire membrane is loosely laid over the insulation board, and the latter loosely laid over the substrate. Membranes are adhered to themselves at lap seams and attached to the deck at the roof perimeter. On top of the membrane a ballast cover with 56 to 60 kg/m^2 of normally 38 mm rounded gravels or concrete pavers is installed to prevent wind uplift and press the other components into place. The minimum diameter of the gravel ballast is set at 25 mm to reduce the possibility of movement by the wind. The round shape is specified to reduce the possibility of puncturing the membrane. The benefits of a ballasted roof system are: it is often more economical in comparison to other systems, it is easy to install and the membrane is protected. The main drawback is that it significantly increases the weight of the roof assembly and hence, the seismic weight. An example of a ballasted roof system is

shown in Figure 3.2, which is quoted from the "Roofing Insulation Systems" (www.fpcfoam.com).

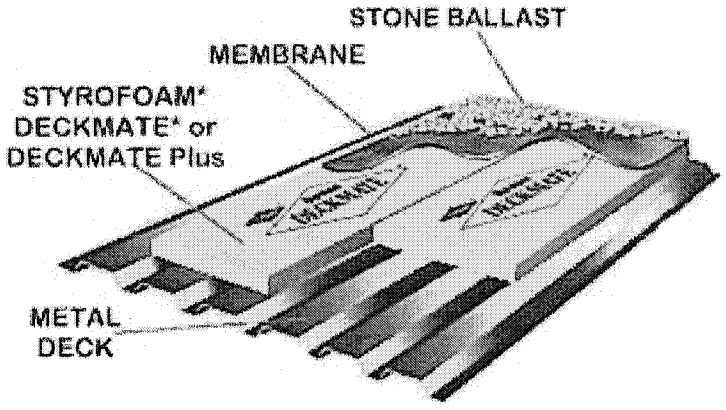

Note: Styrofoam*, Deckmate* and Deckmate Plus are Trademarks of the Dow Chemical Company

Figure 3.2. Ballasted roof system (from Foam Products Corp, www.fpcfoam.com)

A purely adhered roof system is rarely used with a steel deck roof assembly because of the fireproof requirements and the two following reasons:

- The corrugated rib shape decreases the adhered areas;
- The rapid thermal conductivity of the steel decreases the adherence effect.

A substrate such as gypsum board is usually placed between the steel deck and the insulation, which is normally mechanically fastened to the deck panels. An example of an adhered roof system with steel deck is shown in Figure 3.3, where, Figure 3.3 b) is quoted from Plasti-Fab Co. (www.plastifab.com).

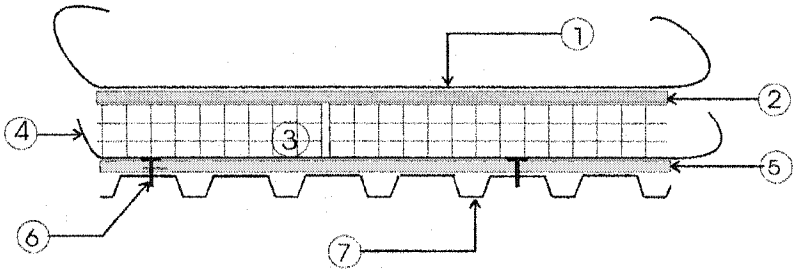

1. Waterproof membrane (any type), adhered;
2. 12.7mm fiberboard as coverboard, adhered;
3. Rigid ISO or EPS board insulation, adhered;
4. Kraft paper as vapour retarder, adhered;
5. Gypsum board as thermal barrier
6. Fasteners between Gypsum board to steel deck;
7. Steel deck.

a) Section view

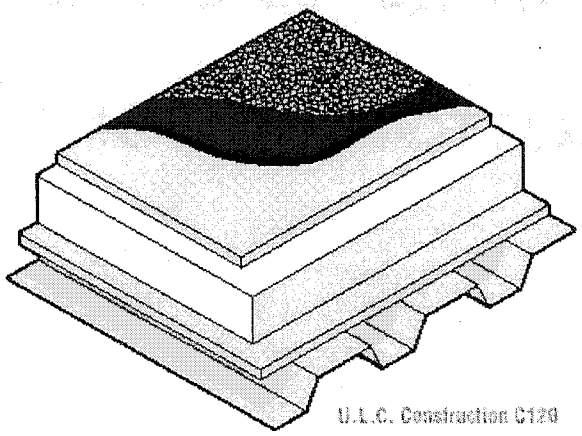

b) 3-D view (from Plasti-Fab Co, www.plastifab.com)

Figure 3.3. Adhered roof system

A mechanically fastened roof system is used mainly when a singly-ply membrane is specified. Here, the membrane is anchored to the deck (through the insulation layer)

by using special fasteners. This fastening method may consist of individual fasteners that are composed of a screw with a plastic disc or washer about 75 mm in diameter. It may also consist of screws with continuous batten bars. The second method is favoured because it will more evenly distribute wind uplift forces on the membrane. In a mechanically fastened roof system the insulation will be anchored to the deck before the membrane connections are installed.

The ballasted roof system will be not considered as a diaphragm test configuration in this study, since all of the layers are loosely laid, and it is doubtful that these roofing materials will substantially influence the in-plane deck diaphragm stiffness and strength. In contrast it is hypothesized that the influence of the non-structural components when other attachment methods are utilized is not negligible. These materials are placed on top of the steel deck in layers, and hence, it is logical to think that the nearest layer will have the greatest effect on the diaphragm performance. Furthermore, it is anticipated that the stiffest material will have the most significant influence on the diaphragm behaviour. From this point of view, the thermal barrier, which is often a quite stiff board, when mechanically connected to the deck may have the most substantial influence on the behaviour of the diaphragm. In contrast, the outermost waterproof membrane layer that is flexible and can carry only tension forces will have the least influence. These relationships will be verified in the test analysis discussion provided in Chapter 4.

3.3 THE STEEL DECKS

Steel decks are fabricated by cold rolling from thin steel sheets. During fabrication the sheet steel is fed continuously through a series of rolls, each of which works the sheet progressively until it reaches the desired shape (Figure 3.4), where Figure 3.4 a)

is quoted from "Cold-Formed Steel Design Gallery" in the American Iron and Steel Institute's Steel Works website (www.steel.org), and Figure 3.4 b) is quoted from the product brochure "Hitachi Cold Forming Roll" published by Hitachi Metals Ltd.

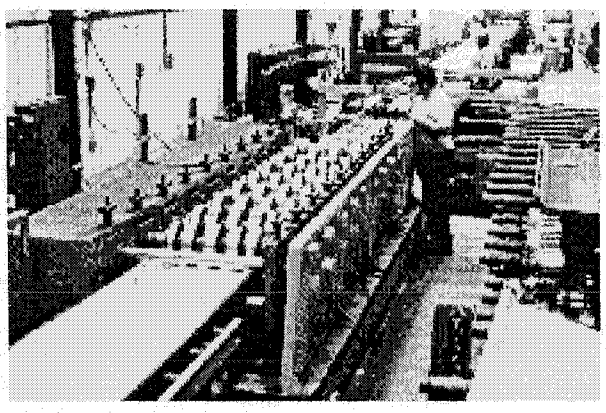

a) Production line of steel deck

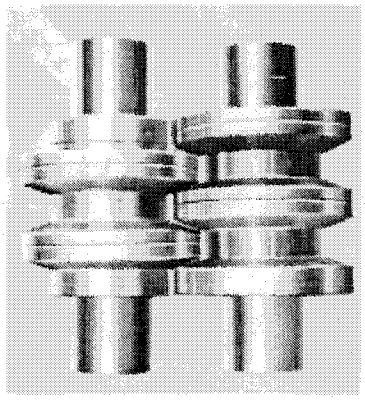

b) Details of Rolls

(Photo Sources: a: from AISI, b: from Hitachi Metals Ltd)

Figure 3.4. Manufacturing of corrugated steel panels

In Canada, two profiled sections are widely used as roof decks, *i.e.* 38 mm series and 76 mm series according to the depth of the deck. In Figure 3.5, three samples of these deck series from the Canam Manac Group Inc. are shown, where the P-3615 is different from P-3615B only in the shape of the side-lap.

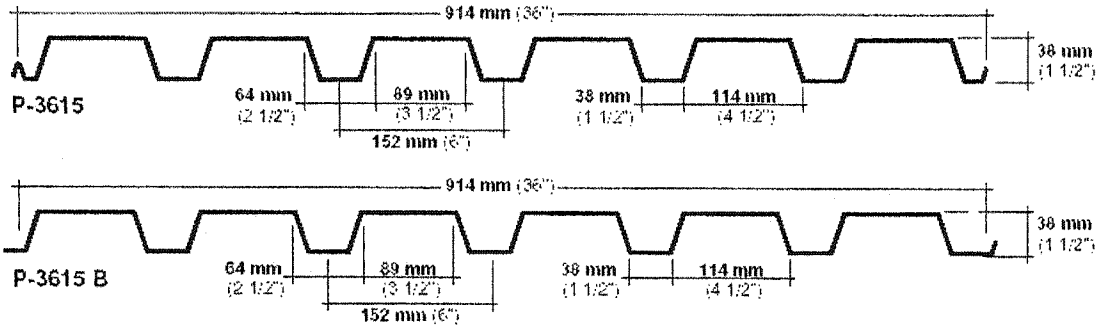

a) 38 mm series profiles (P-3615 & P-3615B)

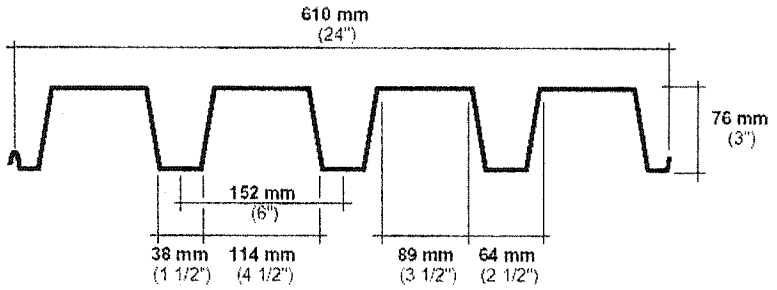

b) 76 mm series profile (P-2436)

Figure 3.5. Common deck profiles available in Canada (Canam Manac, 1999)

Galvanised grade 230 sheet steel conforming to ASTM A653 (2002) is often used for the manufacture of corrugated steel panels. The minimum values of mechanical properties are: F_y = 230 MPa, F_u = 310 MPa, elongation in 50 mm gauge = 20%. The available base sheet thickness ranges from 0.455 mm to 1.214 mm, however, for steel roof deck the design minimum thickness is not less than 0.76 mm (CSSBI, 1996), which is also required by the Factory Mutual (FM) and Underwriters Laboratories (UL) standards. The most common zinc coating is the Z275 (G90), which has a thickness of 0.040 mm.

Deck panels must be connected appropriately to themselves and to the underlying steel joists or frames. Deck-to-frame connection methods often include welds (for steel sheet base thickness > 0.5 mm); welds with washers, screws; and powder actuated nails. Side-lap connections often include welds, screws, button punches and seams.

3.4 ROOF MEMBRANE

A list of common roof membrane types, whose main function is to act as a waterproof layer in PMR or in conventional roofs, is as follows:

- (BUR) Built-up roof membrane
- (MB) Modified bitumen roof membrane
- Single-ply roof membrane

These three membrane types dominate most of the roof membrane market, in the United States the market share of each of these membrane types is approximately the same (Patterson & Mehta, 2001). In Canada, an estimated 90% of all flat roofs are protected by bituminous roofing (Baker, 1980), which includes both built-up roofs and modified bitumen roofs. The personal consultation with the Ontario Industrial Roofing Contractors Association (OIRCA) also confirmed that the most common types of roof in Quebec and British Columbia are 2 ply modified bitumen or built-up roofing. An example of such roof membrane installation on steel deck with other components is shown in Figure 3.6, which is quoted from the flat roofing of the Canada Specialty Product Inc.

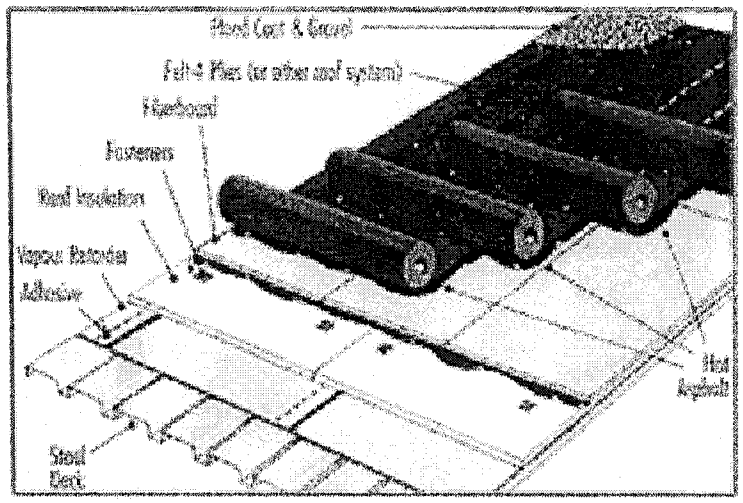

Figure 3.6. An example of a flat roof assembly (Canada Specialty Product Inc., www.canadaspecialty.com)

3.4.1 Built-up roof (BUR)

A built-up roof consists of several plies of roof felts adhered together with bitumen. The roof felts are composed of a mat of organic or inorganic fibres (called dry felt), impregnated or saturated and sometimes coated with bitumen.

Bitumen is a generic term describing any native mixture of heavy hydrocarbons in viscous or solid form. It includes both asphalt and coal-tar pitch. Asphalt has a chain-like molecule structure (C_6H_{14}), while coal tar has a ring-like structure (C_6H_6). Comparatively, coal tar is chemically more stable and more durable to weather than asphalt, it is ideal for flat roofs (slope=0%) where water ponding is probable. The low melting point of coal tar allows it to become fluid in nature during the hot summer season and "self heal". However, since normally a roof has a minimum ¼" per foot slope, and hence the low melting point of coal tar might cause slippage of the membrane. Due to this characteristic, asphalt is more commonly used because it has higher melting point, it is easier and cheaper to obtain; and it is deemed to pose a less

serious health risk to roof workers. In Canada, another reason for the rare use of coal-tar pitch is because it is generally not available unless imported (NRCC, 1989). It should be noted that these two bitumen materials are not chemically compatible.

Baker (1980) discussed the manufacturing of dry felt and the bitumen-saturated felt. In ASTM D226 (2001a), type I Asphalt saturated organic felt is commonly referred to as No. 15 or 15 lb asphalt felt because the earlier types weighed 15 lb/100ft^2. The net mass of type I asphalt felt is now 11.5 lb/100ft^2 (0.56 kg/m^2). The typical felt comes in rolls; its dimension is 36 in (914 mm) wide and 144 ft (43.89 m) long. The thickness is not declared in the ASTM standard or in any of the manufacturers' product catalogues, since the felt is mainly specified by its net mass. A 1 mm thickness relates roughly to an asphalt mass of 1.05 kg/m^2, or coal tar pitch 1.28 kg/m^2 (Baker, 1980). In Canada, two popular organic asphalt saturated felts are No. 15 and No. 25, whose material properties are shown in Table 3.2. Again, the felt thickness is not declared.

Table 3.2 The material properties of No. 15 and No. 25 organic asphalt saturated felt required in CSA A123.3-M (from Baker, 1980)

Type	Minimum mass	Dry felt mass	Pliability at 25°C Radius of bending	Breaking strength at 25°C, kN/m of width	
	kg/m^2	kg/m^2	mm	Along fibre	Across fibre
No. 15	0.598	0.259	12.7	5.25	2.63
No. 25	1.054	0.43	19.1	7.00	3.50

Usually, a built-up roof has a felt base sheet, a felt middle sheet, a felt cap sheet, a gravel or slag surfacing and hot bitumen mopped on each layer to bind them together. The function of the base sheet is to provide a dry moppable surface for felts and bitumen. The most commonly used base sheet is an asphalt-coated glass fibre base sheet that has a minimum mass of 0.68 kg/m^2 and a dry felt mass of 0.04 kg/m^2, as

specified in CSA A123.17 (Baker, 1980). Middle sheets and cap sheet use the same materials, which include fibreglass felts and organic felts; in general, fibreglass felts are stronger than organic felts and are more often used. The fibreglass felts used for the middle sheets and cap sheet have a minimum mass of 0.37 kg/m^2 and the same dry felt mass of 0.04 kg/m^2. There are usually small mineral granules on the top surfaces for weather protection, and fine sand dust on the base surface to avoid adhesion in the roll.

A roof membrane may be composed of up to 2 - 5 felt plies. The number of plies is normally selected by considering the expected weather conditions, the construction budget, and the intended life span of the roofing.

A mineral aggregate surface is often used; which is composed of round shape gravel or slag (about 400 $lb/100ft^2$), mainly due to fireproof considerations. Slag is a residue stony matter from smelting metallic ore.

3.4.2 Modified bitumen roof membrane

Modified bitumen sheet (sometimes called "mod bit", or MB, or MBS) is an asphalt felt that has been modified to obtain plastic or rubber-like properties. Two commonly used modifiers are APP (Atactic Polypropylene) and SBS (Styrene Butadiene Styrene).

APP (Atactic Polypropylene) is a thermoplastic polymer that forms a uniform matrix structure within the asphalt. This improves the bitumen's weather performance including the UV resistance, low temperature flexibility and high temperature softening point. Asphalt modified by APP can be stretched to 1.5 times its original length. APP modified bitumen sheets are generally applied using a propane-fuelled torch.

SBS (Styrene-Butadiene-Styrene) is a synthetic rubber, which forms a polymer network within the bitumen. SBS modifier can significantly increase the elongation behaviour of bitumen. Test data has shown that SBS modified asphalt can be stretched up to six times its original length, and unlike APP modified bitumen, it will return to its original size when allowed to relax. SBS modifier can also improve the bitumen's resistance to aging and weathering. One example of an SBS cap sheet is shown in Figure 3.7, which is quoted from the Technical Information Sheet of Firestone Building Products Company

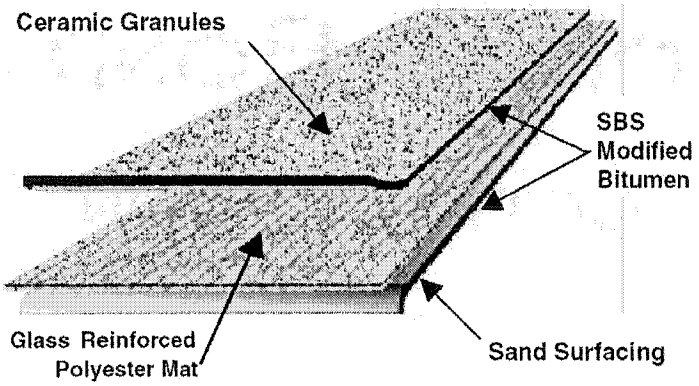

Figure 3.7. Composition of an SBS cap sheet (Firestone Building Products Co.)

Modified bitumen sheets often come with the width 36" or 39" (914 mm or 1000 mm), and the length 10 m, which has a coverage of about 100 ft^2. It is also possible to obtain sheets at 15 m long. The thickness of the base sheet is often 2 mm for mopping hot bitumen, and 3 mm if attached sheets are connected using a torch. The top sheet often has a thickness in the range of 3.3 to 4.0 mm.

SBS modified bitumen sheets are typically installed by mopping hot bitumen; while APP modified sheets are applied by an open-flame-propane-torch, but they are also sometimes adhered with cold-process adhesives. Both APP sheets and SBS sheets can

be combined with a built-up roof membrane to produce a hybrid roof, such as multiple plies of fibreglass felts. A minimum slope of ¼" per 1 foot is recommended.

3.4.3 Single-ply roof membrane

A single-ply membrane is made of a polymeric material; the commonly used polymers are:

- Heat weldable: CPE (Chlorinated polyethylene); CSPE (Chlorosulfonated polyethylene); PVC (Polyvinyl chloride); TPO (Thermoplastic olefin).
- Nonweldable: EPDM (Ethylene propylene diene monomer)

In North America, EPDM has about 75% of the market share for single-ply roof membranes. PVC has about 20% of the market share (Patterson & Mehta, 2001).

EPDM is a synthetic rubber, which can be stretched from 300% to 500% of its original length. Its puncture and tear resistance can be reinforced by embedding polyester materials into two EPDM layers. EPDM is essentially chemically inert, such that it is compatible with most deck and insulation materials, although it is not compatible with bitumen. For very large roofs, the EPDM is often used because it comes in large sheets. One example of product dimensions of the EPDM 45FR (fire rated) is quoted from the Johns Manville Co. as thickness 1.1 mm, width 7' to 50', length 50' to 150'. Single-ply membranes are frequently loose laid with ballast, but can also be mechanically fastened or adhered (partially or fully).

3.5 RIGID INSULATION MATERIALS

Thermal insulation is an important component of a roof system. Modern architectural design calls for materials of high thermal performance, whilst being economic and friendly to the environment. Many different materials are available to make insulation, including mineral fibres, wood fibres, polystyrene, polyurethane, cellar glass, etc. These materials fall into two groups: rigid insulation or flexible insulation. The former is usually used in a low-slope roof, while the later is often used in a steep roof.

The NRCA Roofing and Waterproofing Manual (National Roofing Contractors Association), fourth edition, identifies the following properties for ideal rigid roof insulation (Graham, 1999)

- *Compatibility with bitumen and other adhesives;*
- *Impact resistance;*
- *Fire resistance;*
- *Moisture resistance;*
- *Thermal resistance;*
- *Stable thermal resistance value;*
- *Attachment capability;*
- *Dimensional stability;*
- *Component compatibility.*

In reality, no material can have all these properties together. The choice of insulation material depends on cost, insulation properties, market share, local market

availability, etc. The common rigid insulation materials and their market shares in North America are (Patterson & Mehta, 2001):

- Polyisocyanurate (ISO) board, encompasses Polyurethane (PU) board, 44%;
- Perlite board, 18%;
- Wood fibreboard, 16%;
- Expanded Polystyrene (EPS) board, or called Bead board, 10%;
- Extruded Polystyrene (XEPS) board, called Styrofoam, 3%;
- Fibreglass and cellular boards, 4%.
- Others, 5%

Perlite board and wood fibreboard are often used as a cover-board on top of the insulation layer to provide a torchable substrate. XEPS board is mainly used in protected membrane roof (PMR) roofing system.

The material properties of the various insulation products according to the relative ASTM standards are listed in Table 3.3.

Table 3.3 Insulation material properties from ASTM standards (Graham, 1999)

ASTM material standards for rigid board insulation products					
Insulation type	Water absorption (maximum)	Thermal resistance per 1-inch (25-mm) thickness (minimum)	Compressive strength (minimum)	Flexural strength (minimum)	Dimensional stability (maximum)
Cellular glass [ASTM C 552, Type IV]	0.5 percent volume [ASTM C 240]	2.9 F•h•ft² (0.41 km²/W) [ASTM C 177 or C 518]	65 psi* (448 kPa) [ASTM C 240 and C 165]	60 psi* (414 kPa) [ASTM C 240 and C 203]	Not reported
Glass fiber [ASTM C 612, Type I]	Not reported	3.8 F•h•ft² (0.26 km²/W) [ASTM C 177 or C 518]	25 psi* (1.2 kPa) [ASTM C 165]	Not reported	2 percent [ASTM C 356]
Perlite [ASTM C 728, Type I]	1.5 percent volume [ASTM C 209]	2.7 F•h•ft² (0.48 km²/W) [ASTM C 177 or C 518]	20 psi* (138 kPa) [ASTM C 165]	40 psi* (276 kPa) [ASTM C 203]	Not reported
Polyisocyanurate [ASTM C 1289, Type II]	1.5 percent volume [ASTM C 209]	5.6 F•h•ft² (0.97 km²/W) [ASTM C 177, C 236, C 518, C 976 or C 1114]	16 psi* (110 kPa) [ASTM D 1621]	40 psi* (275 kPa) [ASTM C 203]	4 percent [ASTM D 2126]
Expanded polystyrene [ASTM C 578, Type VIII]	3 percent volume [ASTM C 272]	3.8 F•h•ft² (0.26 km²/W) [ASTM C 177, C 518, C 236, C 976 or C 1114]	13 psi* (90 kPa) [ASTM C 165 or C 1621]	30 psi* (208 kPa) [ASTM C 203]	2 percent [ASTM D 2126]
Extruded polystyrene [ASTM C 578, Type VII]	0.3 percent volume [ASTM C 272]	5 F•h•ft² (0.2 km²/W) [ASTM C 177, C 518, C 236, C 976 or C 1114]	40 psi* (276 kPa) [ASTM C 165 or C 1621]	60 psi* (414 kPa) [ASTM C 203]	2 percent [ASTM D 2126]
Spray polyurethane foam [ASTM C 1029, Type III]	5 percent volume [ASTM D 2842]	6.2 F•h•ft² (1.1 km²/W) [ASTM C 177, C 235 or C 518]	40 psi* (276 kPa) [ASTM C 165 or D 1621]	Not reported	Not reported
Wood fiberboard [ASTM C 208, Type II, Grade I]	10 percent volume [ASTM C 209]	2.63 F•h•ft² (0.38 km²/W) [ASTM C 177, C 518, C 1045 or C 1114]	Not reported	Not reported	0.5 percent [ASTM D 1037]

*pounds per square inch
Note: Applicable ASTM material standards or test methods are designated in brackets.

ISO board was selected in this study due to its higher market share and its high thermal resistance property. ISO boards often come with panel dimensions 1.22 m x 1.22 m (4 x 4 ft) or 1.22 m x 2.44 m (4 x 8 ft), and should be staggered with respect to each other during installation. The thermal resistance specified by the designer determines the panel thickness, which ranges from 25 mm to 102 mm (1" to 4").

3.6 THERMAL BARRIER, COVER BOARD, AND VAPOUR RETARDER

3.6.1 Thermal barrier and cover board

The difference between the thermal barrier and the cover board is that the former is used under the insulation layer, while the latter is used at the top of the insulation layer. Their positions in a roof assembly can be seen in Figure 1.2 of Chapter 1. Because of their physical positions in a roof the thermal barrier is also known as an underlayment, and the cover board as an overlayment or as a fire barrier since it is used with a torchable membrane.

A thermal barrier should be installed on the metal deck due to fireproof considerations. It also provides an ideal flat surface for the insulation board, which can easily be deformed due to the corrugated profile of the deck. An appropriately installed underlayment can also reinforce the in-plane shear stiffness of the deck. A thermal barrier may be omitted only if the insulation board meets the Underwriters Laboratory's fireproof standards and is strong enough itself; for example, the XEPS board, or Styrofoam board from Dow Chemical Co. See Figure 3.2.

Three materials are widely used as thermal barriers or cover boards:

- Gypsum board;
- Wood fibreboard;
- Perlite board.

Gypsum board is the generic name for a family of sheet products consisting of a non-combustible core primarily of gypsum ($CaSO_4 \cdot 2H_2O$) with paper surfacing. It is more

widely used in interior walls, ceilings, or partitions, but also is an ideal material to act as a thermal barrier in a roof assembly where steel deck is present. Type X gypsum board is normally specified because of its special fire-resistance properties.

Gypsum board is usually available in sheets of 1.22 m x 2.44 m (4 x 8 ft). The thickness ranges from 9.5 mm to 15.9 mm, but 12.7 mm (1/2") is often specified when the gypsum board is used as the thermal barrier in roofing. Gypsum board is attached to the steel deck by means of screws (Figure 3.8). The number of connections depends on the wind up-lift loads, where 8 screws per board is minimum, and 12 screws per board is most popular in Canada.

Figure 3.8. Installation of gypsum board on steel deck

Wood fibreboard is made from wood or cane fibres and a binding agent. Perlite board is an insulation board composed of natural perlite ore expanded to form a cellular structure. These two materials are primarily used as the cover boards.

3.6.2 Vapour Retarder

In Canada, a vapour retarder layer is usually recommended due to the low exterior temperatures and high interior humidity levels experienced during winter. The intent is to impede the transmission of water vapour into the insulation layer, thus preventing or reducing the hazard of interstitial or surface condensation.

A 2- or 3-ply built-up roof membrane is the most common available vapour retarder. Such a vapour retarder provides a perm rating that approaches zero. Note that 1 perm in SI units (ng/Pa·s·m2) is equal to one nanogram (10^{-9} gram) of water vapour permeating through a square metre of a component per second under a vapour pressure difference of 1 Pascal. To be a vapour retarder, the perm rating of a material should be smaller than 5.7 (SI) perm. The permeance values of some materials are listed in Table 3.4.

Table 3.4 Material permeance (Chown, 1990)

Material	Thickness (mm)	Permeance (perms)	Permeance (ng/Pa•s•m^2)
Polyethylene	0.15	0.06	3.4
BUR Membrane	9.5	0.01	0.57
Modified Bitumen	3.7	0.06	3.4
EPDM	1.4	0.06	3.4
PVC	1.0	0.09	5.1
Concrete	100.0	0.8	45.6
Metal Sheathing	--	0.0	0.0
Metal Foil (no holes)	--	0.0	0.0
Gypsum Board (plain) Thermal Insulations	9.5	50.0	2860.0
Rigid Glass Fibre	50.0	56.0	3192.0
Extruded Polystyrene	50.0	0.6	34.2
Expanded Poystyrene	50.0	1.0 to 3.0	57 to 171
Cellular Glass	50.0	0.0	0.0

Vapour retarders are prohibited from being installed directly over steel roof decks because the vapour retarder is vulnerable to puncture damage between the ribs of the steel panels. An underlayment, *e.g.* gypsum board, is necessary to provide a plane surface.

Theoretically a steel deck should provide adequate vapour resistance based on the 5.7 (SI) perm definition. However, installation holes and side laps in the deck can allow significant amounts of moisture to diffuse through the air and to eventually contact

cold surfaces in the roof assembly. For this reason a separate and appropriate vapour retarder must be included on the warm side of a conventional roof assembly.

3.7 THE MECHANICAL PROPERTIES OF MATERIALS

The mechanical properties of the various materials that make up the non-structural portion of the roof are important to this study because depending on their relative stiffness and strength to the steel deck they may influence the overall diaphragm behaviour. Each component is placed in the roof due to its ability to perform a certain function (Table 3.1), in light of this, it is expected that not all of the non-structural components will have an effect on the in-plane diaphragm stiffness and strength.

As a further complication, because many of these materials have not been selected for their structural characteristics, it is not always straightforward to obtain their relevant structural mechanical properties, such as shear stiffness, elastic stiffness, yield strength and ultimate strength, without the use of physical tests. It has been shown that the mechanical properties of materials are closely related to their density. In "Materials Selection in Mechanical Design" (Ashby, 1999), two charts for the relationship of Modulus-Density and Strength-Density are provided to evaluate the mechanical properties of engineering materials (Figures 3.9a. and 3.9b.). This information may be of help to determine the mechanical properties of the non-structural components that are utilised in later chapters.

In Figure 3.9a), the Young's modulus E plotted against density ρ, demonstrates that the E for steel is about 200 GPa, for cement or concrete is 20 to 50 GPa, and for rock and stone is 25 to 120 GPa. Wood products have a Young's modulus that ranges from 2 to 5 GPa. In Fig. 3.9a, a lower E limit for true solids is specified as 1.0 GPa, but

also many materials have a modulus lower than that limit, such as elastomers, polymers, or foams. The EPS board (Expanded Polystyrene) has an E value only between 0.00140 and 0.026 GPa and a density between 12 and 48 kg/m^3.

Wood fireboard exhibits a Young's modulus of 2.4 GPa when the density is equal to 770 kg/m^3. Since gypsum board is a material composed of paper and mineral material gypsum, it has a mass of about 8 kg/m^2 at 12.7 mm thickness. The equivalent density is about 630 kg/m^3, and so it is logical to assume a value for Young's modulus in the range of 1.0 to 2.0 GPa.

It is possible that the mechanical properties of gypsum board may be similar to that of concrete, which is also a brittle material. In "Structural Concrete: Theory and Design" (Hassoun, 2002), an equation to calculate Young's modulus is given as follows:

$$E_c = 0.043 w^{1.5} \sqrt{f_c'} \tag{3.1}$$

where:

E_c = the modulus of elasticity for concrete, N/mm^2;
w = density of concrete, kg/m^3;
f_c' = concrete compressive cylinder strength, N/mm^2.

It should be noted that above equation is suitable for w = 1400 to 2500 kg/m^3, and f_c' ranges from 10 to 50 MPa. But here we assume this equation is also suitable for gypsum board. From above, density of gypsum board is about 630 kg/m^3, and the compression strength is about 3.45 MPa (G-P Gypsum Corporation, 2000). Then Young's modulus for gypsum board E_g = 1.26 GPa, which falls into the range previously estimated 1.0 to 2.0 GPa, but conservatively E_g = 1.0 GPa could be used.

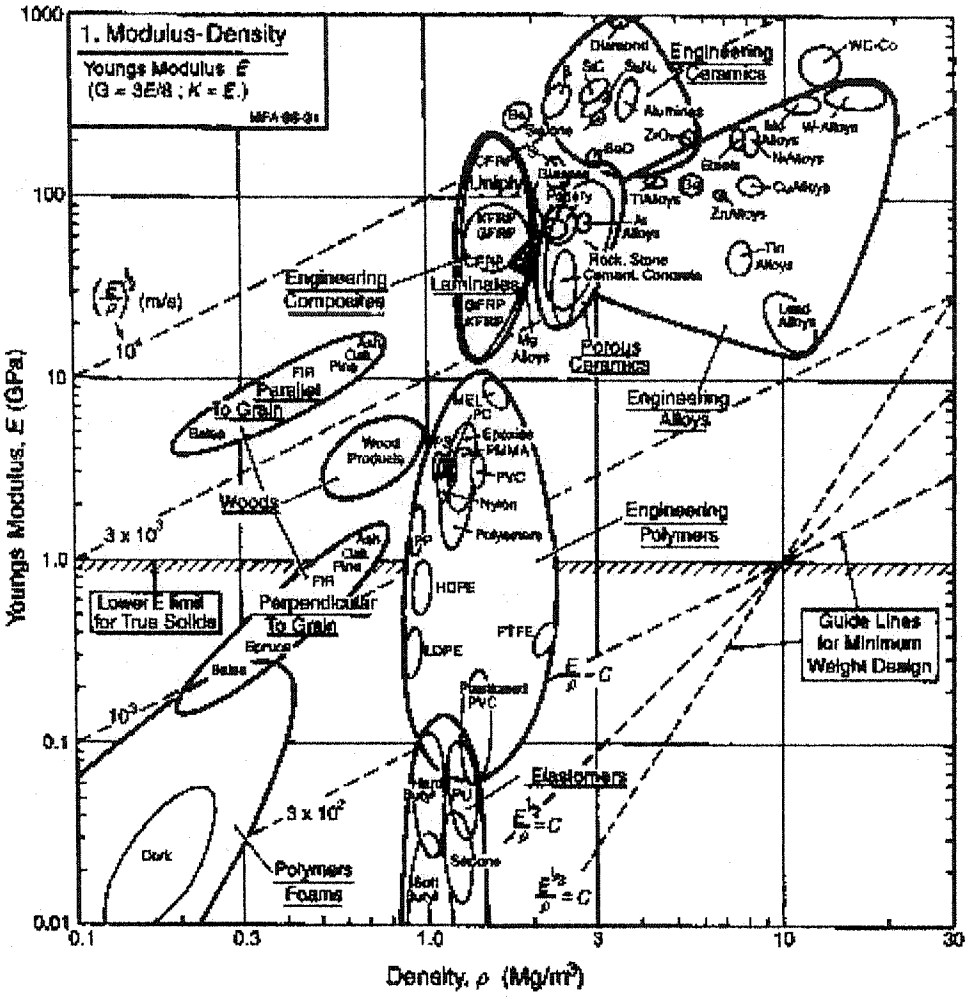

a) Modulus--Density

Figure 3.9. The mechanical properties charts for engineering materials (Ashby, 1999)

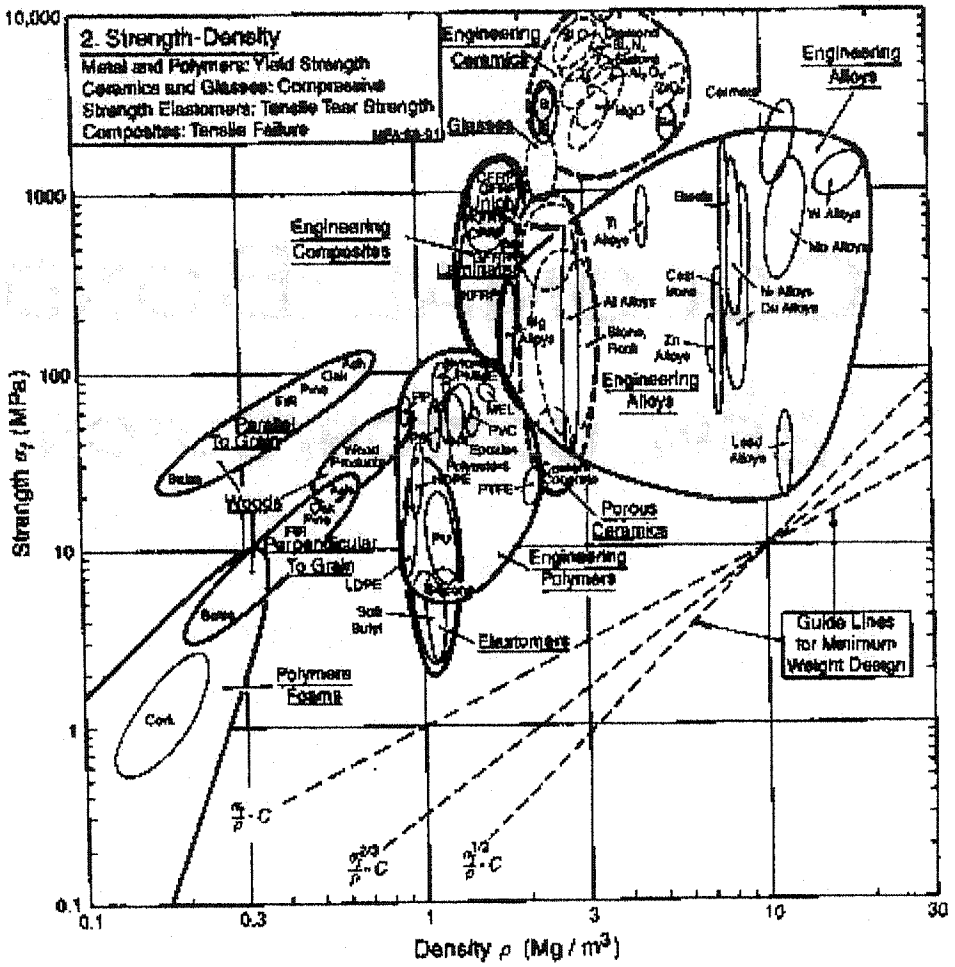

b) Strength--Density

Figure 3.9 (continued)

In Figure 3.9b, the strength refers to the yield strength for metal, compression strength for ceramics and glass, tensile tear strength for elastomers, and tensile failure for composites. The strength for steel is from 200 MPa to 1200 MPa, for cement and concrete is from 20 to 80 MPa, for wood products is 20 to 70 MPa, and for polymers and foams is 0.1 to 10 MPa. Additional data from the ASTM and the CSA regarding the mechanical properties of materials is listed in Table 3.5.

Table 3.5 Mechanical and physical properties of roof materials

a). Steel Deck

Function	Grade or Type	ASTM or CSA Standard	Thickness	Density	Modulus of Elasticity	Modulus of Rigidity	Tensile strength	Tensile yield strength	Shear strength
			mm	kg/m^3	MPa	MPa	MPa	MPa	MPa
Steel Deck	Grade 33 (230)	A 1008/A 1008M	0.76 mm	7850	203 000	77 000	330	230	190.

b). Waterproof membrane

Function	Material	Category	Grade or Type	ASTM or CSA Standard	Thickness	Minimum mass	Modulus of Elasticity	Tensile (or breaking) strength		Elongation, min.
								Length direction	Width direction	
					mm	kg/m^2	MPa	kN/m	kN/m	%
BUR	BUR felts	Asphalt-Coated Organic felt	Type II, or No. 30	D226-97a		1.27	385	7	3.5	
		Coal-tar-saturated Organic felt		D227-97a		0.635	385	5.3	2.6	
	Base sheet	Asphalt-Coated glass fiber bass sheet	I	D4601-98		0.654 (dry)		3.9	3.9	
		Asphalt-saturated and coated organic felt base sheet		D2626-97b		1.806		6.1	3.5	
Modified bitumen roof	SBS (Styrene butadiene styrene), polyester reinforced	Granule surfaced	1	D6164-00	3.3	3.661		50	50	20
		Smooth surfaced	1	D6164-00	2.2	2.636		50	50	20
	APP (Attactic polypropylene), polyester reinforced	Granule surfaced	1	D6222-00	4	0.042		50	50	23
		Smooth surfaced	1	D6222-00	3.5	0.034		50	50	23
Single-ply roof	PVC (Polyvinyl Chloride)	reinforce fiber incorporated	Type II, grade 1	D4434-96	1.14			10.4	10.4	250
	EPDM (Ethylene-propylene-diene terpolymer)	reinforce fiber incorporated	Type II	D4637-96	1.016			0.4 KN	0.4 KN	250

c). Thermal barrier and Insulation boards

Material	Grade or Type	ASTM or CSA Standard	Thick-ness	Density	E	G	Comprs-sion strength	Flex. Streng-th	Tensile streng-th	Shear streng-th
			mm	kg/m3	MPa	MPa	MPa	MPa	MPa	MPa
Gypsum board	Dens-Deck	Georgia-Pacific	12.7				3.45	356 N*		
Wood fibre-board	Fire resistant Midium Density Fiberboard	Canfibre Group Ltd.	13	770	2420	24.2		15.2		
Perlite board	Type 1	C728-97	13	128			0.138	0.276	0.0275	
Cellulosic Fiber Insulating board	Grade 1	C208-95	50		276		0.0012		0.345	
Cellular glass board	Grade 1	C552-00	50	98 to 128			0.689	0.283		
Polyurethane			50	40			0.276		0.212	
XEPS (Extruded expanded polystyrene)			50				0.276			
EPS	By density	Foam Product Co.	50	16 to 32	1.40 to 3.31	2.07 to 4.27	0.083 to 0.200	0.190 to 0.450	0.124 to 0.172	0.152
ISO	By density	C591	50	29 to 96			0.11to 0.862		0.212	
Perlite Faced cellular polyisocyanurate	Type III	C1289	50				0.111	0.275		

Note:

1. The flexural strength for gypsum board is tested in accordance with ASTM C473 (2000). "Standard Test Method for Physical Test of Gypsum Panel Boards", where a specimen of 12"x16"x thickness is placed in a 14" span supports, measure the breaking bending load.
2. The breaking strength of EPDM is tested in accordance with ASTM D751 (2000), "Standard test methods for coated fabrics", where specimen of 100 x 150 mm is grabbed to break.
3. The compression strength of foamed insulation materials are got from 10% compressed deformation.
4. The above values are only for reference, they were quoted from several sources, and may change for specific products.

3.8 SELECTION OF A ROOF SYSTEM FOR THE TEST PROGRAM

As shown in previous sections, roof construction may vary significantly from one project to another, including the type of roof system (PMR or conventional), the type of waterproofing membrane (BUR, Modbit, or Single ply roof membrane), the type of insulation (Rigid or flexible), the need for other layers (thermal barrier, cover boards, and vapour retardant barriers), and the different attachment systems. For this study, it was decided to consider only one roofing system. In order to make the study as useful and effective as possible, the system had to be commonly used in practice for low-rise structures with metal roof deck diaphragms and should include material that had high potential for influencing the stiffness and strength in shear of the diaphragm.

The choice of this roofing system was finally made based on the literature review provided above, on the results of market surveys, on consultation with the Ontario Industrial Roofing Contractors Association (OIRCA), on personal communication with Mr. Claude Jacques of the Association des Maîtres Couvreurs du Québec (AMCQ), and on discussions with various contractors. The following roofing material composition, known as AMCQ SBS-34, was used as the roof assembly in the diaphragm tests that are documented in Chapter 4. This is a common and conventional roof system composed of the following layers (from top to bottom):

- Two layers (4 mm + 2.2 mm) of SBS waterproof membrane;
- One layer of 1" thick non-flammable wood fibre board, hot bitumen adhered;

- One layer of 2.5" thick polyisocyanurate (ISO) insulation, hot bitumen adhered;
- Two layers of paper vapour retarder (No. 15 asphalted felts), hot bitumen adhered;
- One layer of ½" thick gypsum board, 12 screws per panel mechanically fastened.
- Steel deck.

The bitumen used was type 2 asphalt conforming to CSA A123.4 (Baker, 1980).

Above composition is basically same as that shown in Fig. 3.3 but with some component thickness changed or specified, a section view of specimen with roofing material is provided in Fig. 3.10.

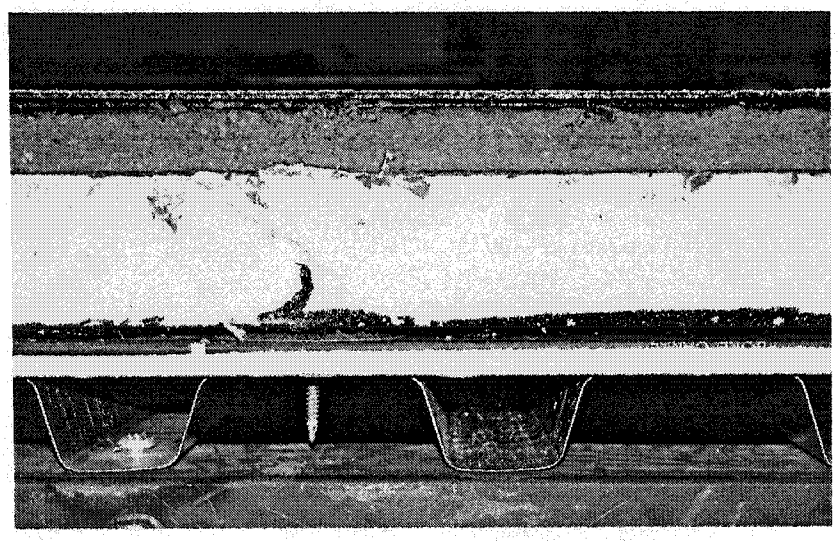

Figure 3.10. Section view of specimen with roofing material

Regarding the anticipated effects on the diaphragm response, the ballasted roofing system (the PMR and the ballasted roof in conventional roofs) was excluded because when all the layers are loosely laid, the influence in terms of shear stiffness and

strength from these roofing materials was not expected to be significant. The selected roof system is of an adhered type (bitumen and mechanical fasteners). The SBS membrane was chosen because it is commonly used in construction. The adhered fastening system is expected to lead to a higher restraint to shear deformations. In the two ply SBS waterproofing layers, the top sheet is 4 mm thick, 1 m (39") wide, side overlap 3", and 8 m long per roll. It is inner reinforced by polyester, the outside is surfaced with mineral granules, and the inside is attached to a plastic film that will be fused by torch during installation. The base sheet is 2.2 mm thick, 1 m (39") wide, side overlap 76 mm (3") and 15 m long per roll. It is inner reinforced by polyester, the outside is attached to a plastic film that will be fused by torch when the top sheets are installed and the inside is surfaced with fine sand to avoid adherence in the roll.

The 1" thick inflammable wood fibreboard (4' x 4' in plane) is required for the fire protection of the insulation board during construction, it also acts as insulation layer. The tensile resistance parallel to the plane is 1.29 MPa (ASTM C-209).

The insulation board was 2.5" thick, 4' x 4' in plane, and had a compression resistance of only 0.14 MPa with 10% consolidation. Since the definition of strength for wood fibreboard and for insulation board is different, the stress in the insulation board should be much smaller than 0.14 MPa if it is expected to deform together with the wood fibreboard. So, one can say that, the insulation board is a soft layer in the roof system. The high stress in the steel deck and perhaps in the gypsum board most likely cannot be transferred efficiently to the wood fibreboard layer because of this soft layer.

The vapour retarder was composed of two layers of No. 15 asphalt felt and bitumen. The product dimension is 36 " wide by 144' long. A specific thickness is not mentioned in the data sheets or in the ASTM or CSA standards, however the author measured a sample from the test specimen that was approximately 0.8 mm per sheet.

The side lap was half width plus 2". The vapour retarder, when fully adhered to the underlying gypsum board, was expected to influence the diaphragm behaviour. Its minimum resistance of rupture, specified in ASTM D146, is 5.25 kN/m along length direction and 2.63 kN/m over the width direction.

The gypsum board, 12.7 mm thick and 4' x 8' in plane, constitutes the stiffest layer of the non-structural roofing components. It was installed directly on top of the steel deck panels using 12 screws (Figure 3.8). The space of these screws is not always uniform, it may change to fit the deck shapes, but an average 18" x 30" spacing could be observed for 12 screws per gypsum board. It is expected that these connections will constrain the deformation between the steel deck and the gypsum board, and thus influence the deck behaviour.

The above arrangement is highly popular in terms of its use in construction, and at the same time it is expected to contribute to the shear response of the overall roof diaphragm. The installation of the above roof assembly is discussed in Chapter 4.

CHAPTER 4 LARGE-SCALE DIAPHRAGM TESTS

In this chapter, the laboratory test program and results of 12 large-scale roof diaphragm tests are described. The scope of testing can be divided into four groups, each of which is related to a specific objective, as follows:

1) To evaluate the inelastic behaviour of steel roof deck diaphragms constructed with powder-actuated fasteners from different manufacturers.
2) To investigate the effect of the longitudinal overlap deck panel joints on diaphragm behaviour and ductility.
3) To investigate the effect of the non-structural components on diaphragm behaviour and ductility.
4) To evaluate the inelastic behaviour of the 76 mm deep steel roof deck series.

This Chapter has been organized into two parts. The first part contains a discussion of the laboratory preparation, which includes the test frame set-up, diaphragm test combinations, load protocols, deck installation and roofing material installation. The second part contains a description of the diaphragm specimens, the details the test results, the failure modes observed as well as the data comparisons.

4.1 PREPARATION

4.1.1 Frame set-up

The diaphragm cantilever test frame set-up was similar to that used by Essa *et al.* (2001) and Martin (2002), hence, only a brief description is provided (Fig. 4.1).

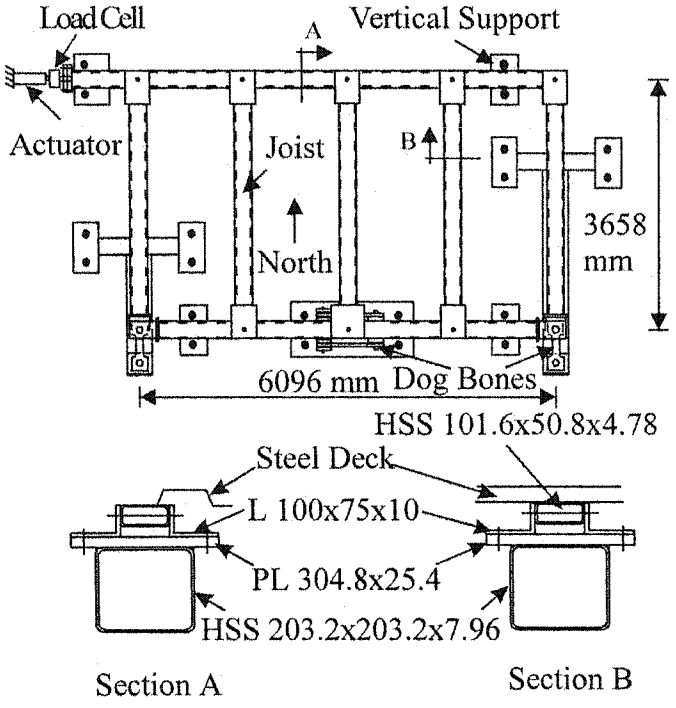

Figure 4.1. Plan view and sections of frame set-up (Essa *et al.*, 2001)

In Figure 4.1, the length of the cantilever (12 ft) was set shorter than its height (20 ft) to minimize the flexural effect, since the shear force between steel decks was of interest. The frame members were made stiff in the lateral direction so as not to influence the diaphragm behaviour. The plan area is 20 x 12 ft (6.096 x 3.658 m), and the frame length is equal to the sheet length L=6.096 m. The width of the frame width

allows for four full size P3615 (4 x 914 = 3656 mm) deck panels or six P2436 (6 x 610 = 3660 mm) deck panels. The spacing of the intermediate beams is 5 ft (1.52 m), which is a representative of a typical joist spacing found in roof structures. The frame members are composed of an HSS (Hollow steel section) 101.6x50.8x4.78; two 100x75x10 angles; one 304x25.4 plate, and one HSS 203.2x203.2x7.96 (see Section A and B in Figure 4.1). The wall thickness of the top frame members (4.78 mm) is representative of the typical thickness of the steel angles used in the top chords of open web steel joists. A view of the test frame prior to the installation of the roof deck is shown in Figure 4.2.

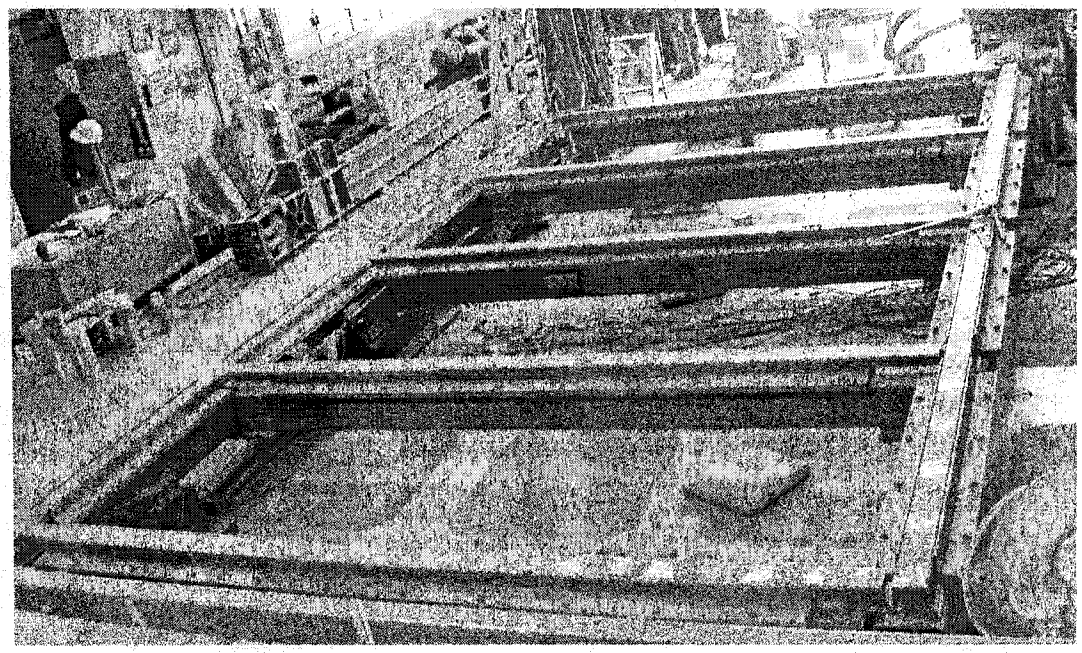

Figure 4.2. Photograph of test frame prior to deck installation

The steel roof deck specimens were connected to the top HSS section (101.6 x 50.8 x 4.78) by welds or nails. After completion of each test, the deck panels were removed and the remnants of the connections were ground flat in preparation for the following test. It is possible to see the marks left from the grinding procedure in Figure 4.2. For welds it was possible to use the same connection location if the grinding was done carefully without removing an excess amount of material from the HSS. However, for the nailed connections it was necessary to leave the shank of the fastener within the HSS, and hence it was not possible to install another nail at the same location. To ensure that there were no coincident nails from one test to the next, the entire diaphragm specimen was moved by 1 inch, either in the longitudinal or transverse directions. This allowed for the HSS 101.6 x 50.8 x 4.78 section to be reused four times in each direction. In addition, the HSS could be inverted and the opposite side used for connections of other tests.

Pins were used to connect the frame at its corners, and to attach the interior joist members to the perimeter frame, in order to limit the shear resistance of the system to that offered by the deck panels and their connections (Figure 4.3). Inter plate contact friction at the pin locations was considerably reduced by installing greased Teflon sheets. The bare frame, without deck panels, was quite easy to move by hand and hence it is believed that the restraining effect of the pin connections was minimal. Essa *et al.* (2001) carried out a bare frame test in order to determine the friction resistance. A force of approximately 1 kN was measured, which was considered to be at such a low level that it could be neglected without a significant loss in accuracy.

Figure 4.3 also shows a dog-bone restraint that was used to limit the movement and to measure force in the North-South direction of the frame. Two LVDTs (Linear Variable Differential Transformer) were placed at the South-East perimeter members' pin location to measure the end displacements and to correct the diaphragm shear

deflection given any movement of the frame (see Section 4.1.5). A similar dog-bone / pin assembly was installed at the south-west corner.

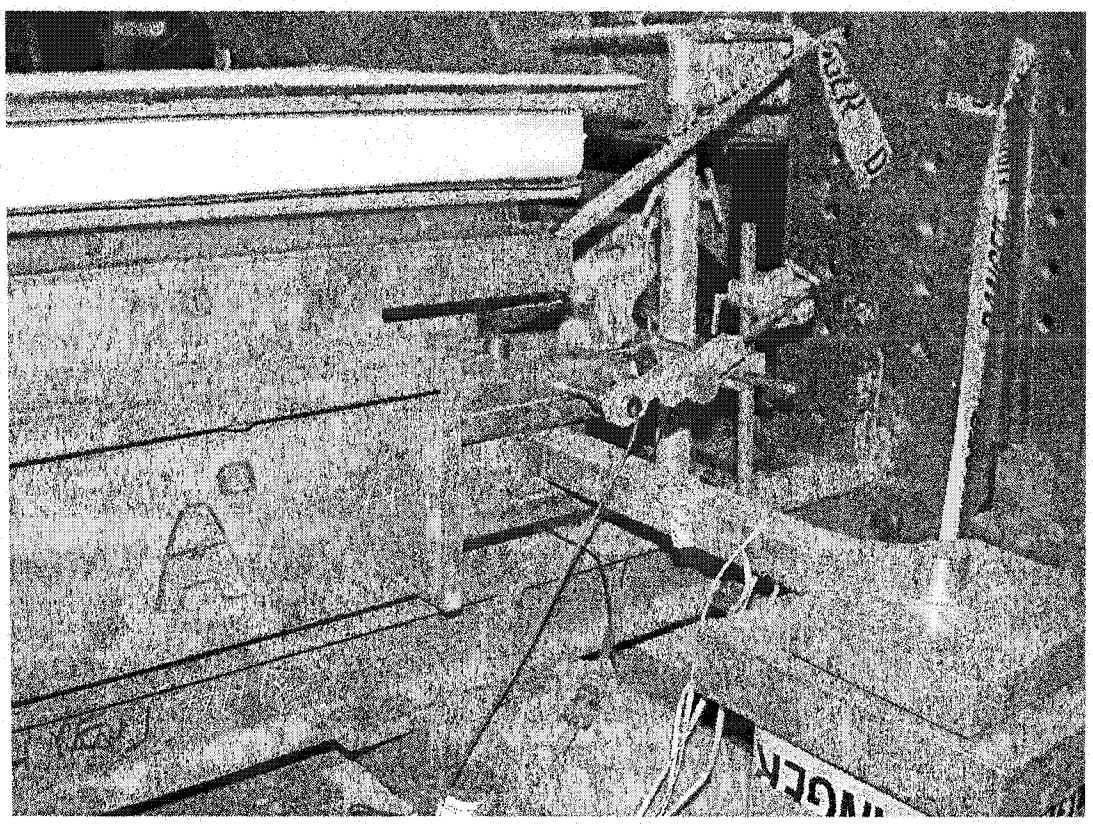

Figure 4.3. The detail of frame corner connection and layout of measurements

Two additional dog-bone measuring cells were placed at the middle of the south frame member, one on each side, to measure the reaction force in the east-west direction (Figure 4.4). The forces measured from these dog-bone load cells were used to check the static equilibrium conditions during testing of the diaphragm specimens.

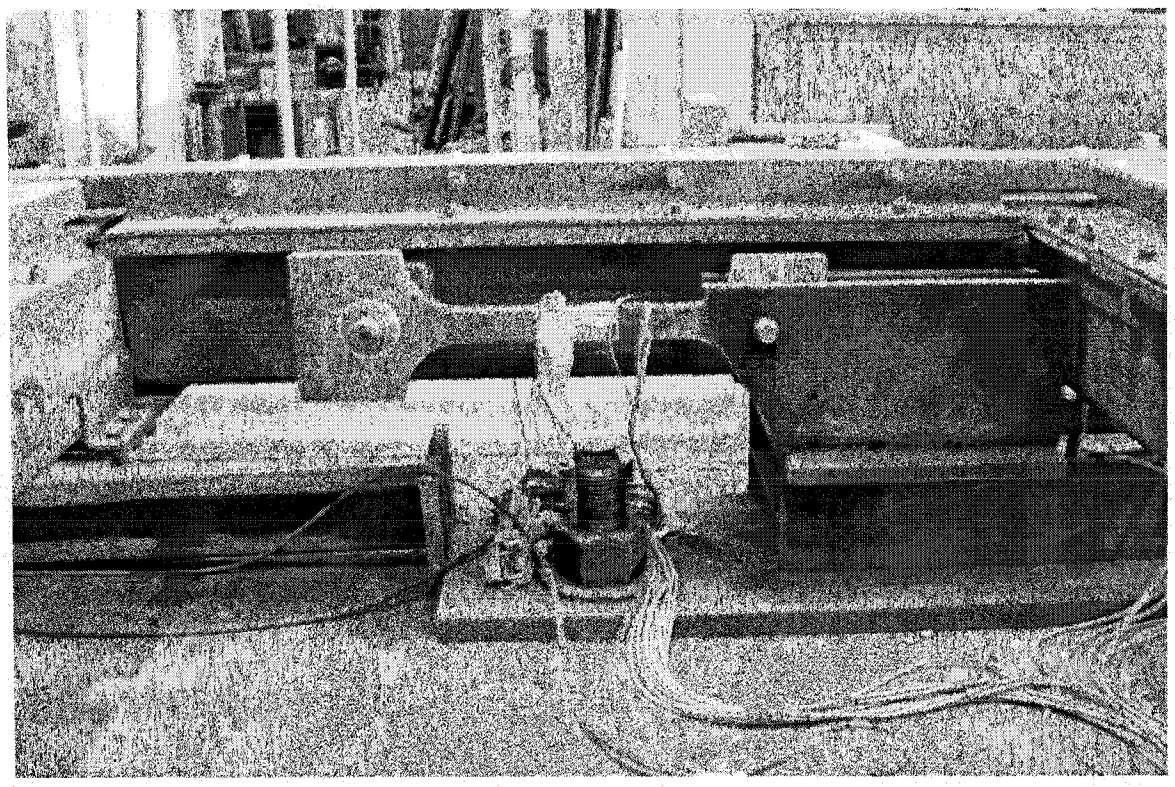

Figure 4.4. East –West oriented dog-bone at the interior of the south frame member

A 1500 kN capacity MDT dynamic actuator was used to apply a given displacement at the north-west corner of the test frame (see Figure 4.1). Based on previous diaphragm tests it was assumed that the shear capacity of the specimens would be in the range of 100 kN, and hence it was necessary to install a 222 kN capacity load cell between the actuator and the test frame to improve the accuracy of the shear resistance measurements.

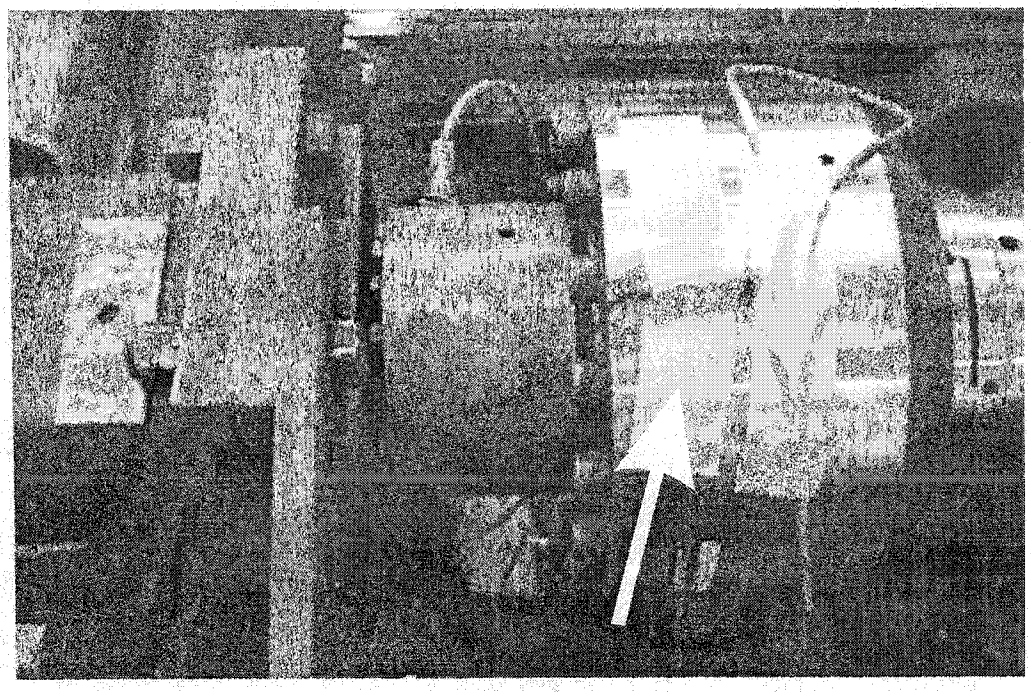

Figure 4.5. Secondary 222 kN load cell with main load cell and attached accelerometer (Martin, 2002)

Due to the dynamic nature of some of the tests a means to determine the forces due to inertial effects was needed. For this reason, an accelerometer (arrowed in Figure 4.5) was attached on the main 1500 kN load cell to record the frame accelerations during testing. This accelerometer was able to measure acceleration accurately up to ± 2 g and frequency from 0 to 100 Hz. Additional frame installation details can be obtained from Essa *et al.* (2001) and Martin (2002). A picture of the test frame with roof deck specimen installed is provided in Figure 4.6.

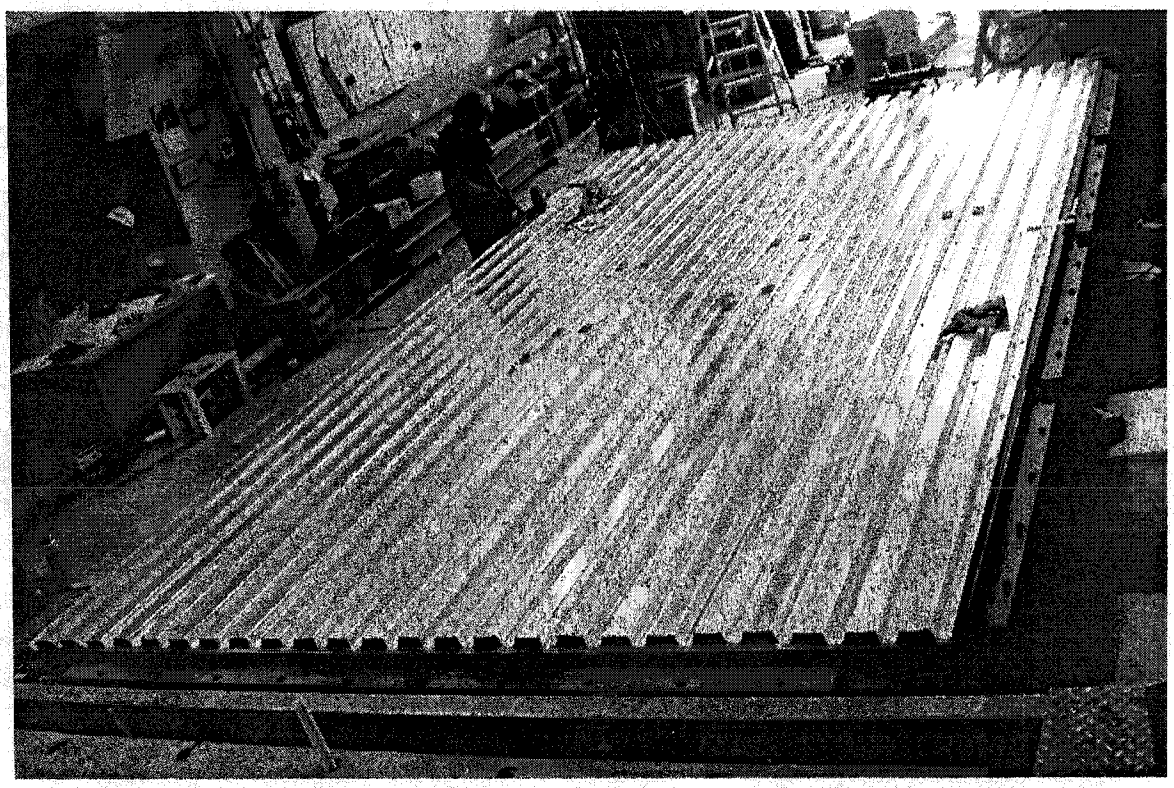

Figure 4.6. The final set-up – with diaphragm installed

4.1.2 Test combinations

A total of 12 large-scale diaphragm tests, which can be divided into four groups, were carried out during the summer of 2002 at École Polytechnique de Montréal (Table 4.1).

Table 4.1. Large-scale diaphragm test series list

GROUP	Description	Test Number	Side-lap	Connection to Frame	Deck type	Load protocal
1	Buildex nail	38-91-6-NS-SD-38	Screwed	Buildex Nailed	P3615 B, 0.91 mm	Seismic SD
2	Longitudinal Overlaped	38-76-3-NS-M-39	Screwed	Hilti Nailed	P3615 B, 0.76 mm	Monotonic
		38-76-3-NS-SD-40	Screwed	Hilti Nailed	P3615 B, 0.76 mm	Seismic SD
		38-76-3-WB-M-41	Button punched	Welded	P3615, 0.76 mm	Monotonic
		38-76-3-WB-SD-42	Button punched	Welded	P3615, 0.76 mm	Seismic SD
3	Bare sheet	38-76-6-NS-M-43	Screwed	Hilti Nailed	P3615 B, 0.76 mm	Monotonic
		38-76-6-NS-C-44	Screwed	Hilti Nailed	P3615 B, 0.76 mm	Cyclic+Monotonic
	With Roofing	38-76-6-NS-M-R-45	Screwed	Hilti Nailed	P3615 B, 0.76 mm	Monotonic
		38-76-6-NS-C-R-46	Screwed	Hilti Nailed	P3615 B, 0.76 mm	Cyclic+Monotonic
4	New Profile	75-76-6-WB-M-47	Button punched	Welded	P2436, 0.76 mm	Monotonic
		75-76-6-WB-SD-48	Button punched	Welded	P2436, 0.76 mm	Seismic SD
		75-91-6-WB-M-49	Button punched	Welded	P2436, 0.91 mm	Monotonic

Note: 1) Test 38 connected with ITW Buildex BX-14 nails and 12-14x1 screws. Other nailed test specimens constructed using Hilti X-EDNK22-THQ12 nails and 12-14x1 screws.
2) Welded frame connections were made with nominal ϕ16 mm arc spot welds;
3) Seismic SD is the Short Duration loading protocol. For cyclic and monotonic loading protocols refer to Section 4.1.7.

The test series nomenclature, developed by Essa *et al.* (2001), was used with only a slight modification. The test name can be read as "deck depth (mm), sheet thickness

(x100 mm), approx. sheet length (m), connection method both to frame and side-lap, load protocol, and the test number". For example, test 38-91-6-NS-SD-38 is composed of a 38 mm deep deck; a nominal sheet thickness of 0.91mm, a sheet length of 6 m (actually 6.20 m); Nailed frame connections and Screwed side-lap connections; a Short Duration seismic load type; and the test number is 38. This number is a continuation from Martin (2002). For the tests with non-structural roofing components, the letter "R" (Roofing) was added between the load properties and the series number, *e.g.* 38-76-6-NS-C-R-46, where "C" means the cyclic load protocol following by monotonic loading. For deck profiles refer to Figure 3.5, where the Canam Manac deck products P3615, P3615B, and P2436 are illustrated. All deck panels were fabricated from Grade 230 sheet steel conforming to ASTM A653 (2002).

4.1.2.1 Group 1

Group 1 comprised only one test specimen (38-91-6-NS-SD-38). This specimen can be considered as being complementary to those diaphragms tested in previous research studies at École Polytechnique. Essa *et al.* (2001) tested two Buildex nailed diaphragms but with 0.76 mm thick steel roof panels. Martin (2002) used 0.91 mm thick decks but with Hilti nails. The layout of decks and fasteners of test 38 is shown in Figure 4.7, where four full-width panel sheets have been used, as in the same pattern used by Essa *et al.* and Martin. The actual sheet length was 20'4" (6200 mm), which was based on the c/c frame spacing, 20 ft, plus two 2 inches at each end. This 2" end lap is recommended in the document "Standard for Steel Roof Deck" (CSSBI, 1996).

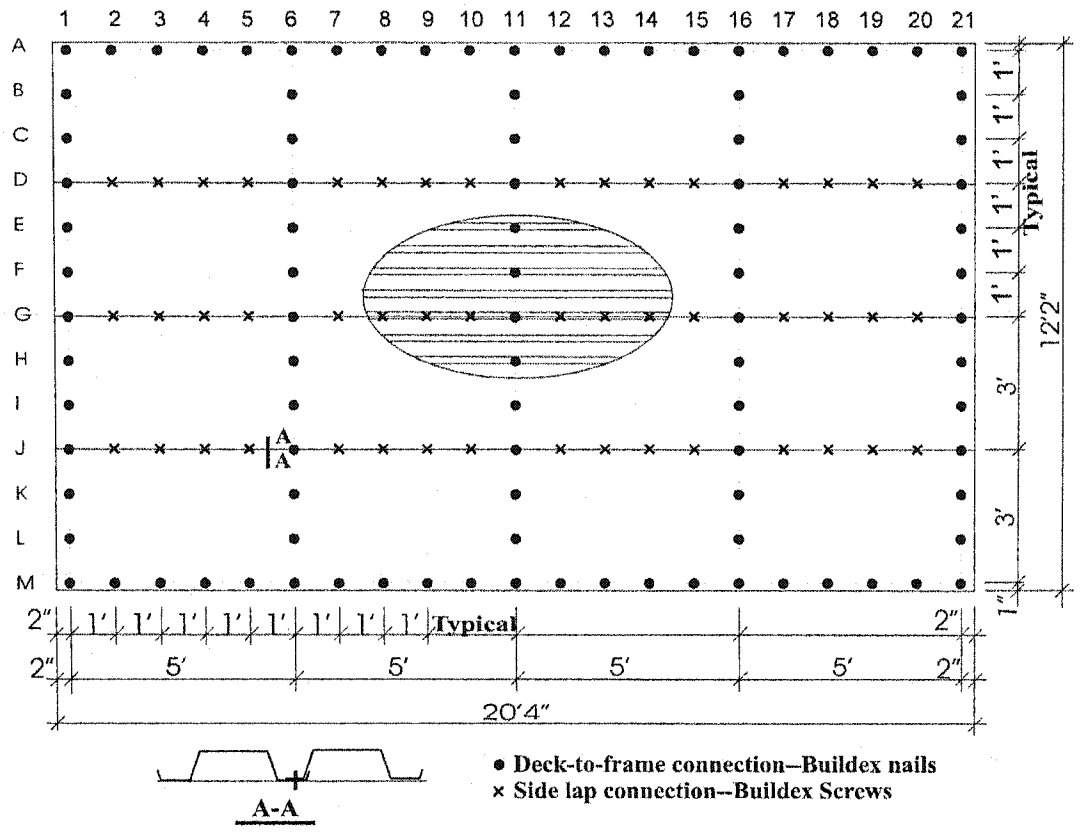

Figure 4.7. Plan layout of test 38-91-6-NS-SD-38

In Test 38, the centre-to-centre spacing of the connections was 1 ft (305 mm). Each connection location was identified with an alphanumeric label that was based on the grid lines shown in Figure 4.7. This labelling scheme was used for all diaphragm tests documented in this thesis. Along the sheet length, 21 deck-to-frame fasteners were used on grid lines A and M, and five deck-to-frame fasteners and 16 side-lap fasteners were installed on grid lines D, G and J.

The fasteners at the deck-to-frame connections were Buildex BX 14 powder actuated pins, which have a length of 1-1/32", a shank diameter of 3/16" (tapered), a head and washer diameter of 9/16", and a yellow electro-zinc finish (Figure 4.8).

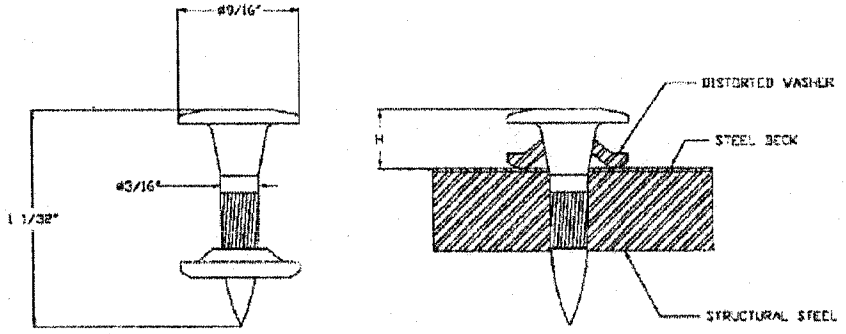

For SI: 1 inch = 25.4 mm.

Note: "H" here is the nail head standoff (also called NHS)

Figure 4.8. ITW Buildex BX-14 nail and connection detail (ICBO, 2003)

These nails were installed as per the manufacturer's instructions with a Buildex Unidek tool (Figure 4.9) and the 0.25" calibre disc loads (Figure 4.10). The power level of the tool was set as level 4 (yellow).

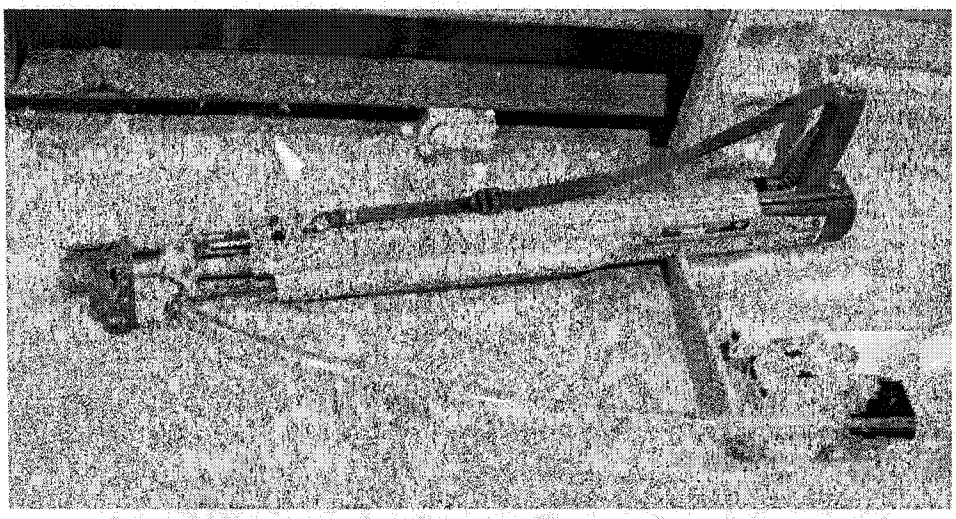

Figure 4.9. Buildex Unidek tool

Figure 4.10. The charges for Buildex nails

The side-lap fasteners consisted of Buildex 12-14x1 HWH TEK/3 CLIMASEAL screws, where "12" is the shank diameter gauge, "14" means 14 threads per inch. "1" is the length (1 inch). "HWT" represents Hexagonal Washer Head. "TEK" is the brand name, "CLIMASEAL" means climate sealed, i.e. corrosion proofed (Fig. 4.11).

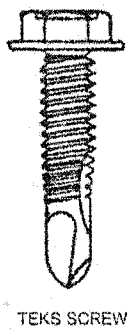

Figure 4.11. ITW Buildex TEK screw (ICBO, 2002)

The seismic short duration (SD) load protocol being used for this test was the same as that implemented for test 34 by Martin (2002).

4.1.2.2 Group 2

Group 2 consisted of four longitudinal overlapped diaphragm specimens:

- 38-76-3-NS-M-39
- 38-76-3-NS-SD-40
- 38-76-3-WB-M-41
- 38-76-3-WB-SD-42

The common characteristics of these tests were: 38 mm series deck panels, 0.76 mm sheet thickness, sheet length was 10'3" (3.12 m), with end lap 2" plus the intermediate overlap 2" that is required by the SDI Design Manual (1987). The characteristics that varied from test to test in this group included the connection method (Nail/Screw *vs.* Weld/Button Punch) and the load type (Monotonic *vs.* Short Duration seismic load).

As recommended by Martin (2002), the specimens were composed of a panel layout that included two half-width sheets along the north and south sides of the diaphragm, and three full width sheets in the interior. The use of two half-width sheets was specified to minimise the influence of the frame on the side-lap slip. The one drawback that existed was that the additional side-lap that existed, in comparison to previous tests, could cause a decrease in shear strength and stiffness of the test specimen. Most of the connections were spaced at 1 ft intervals, except for the half-width sheets, where a spacing of 6" was required at lines 1, 6, 11, 16 and 21 (Figure 4.12).

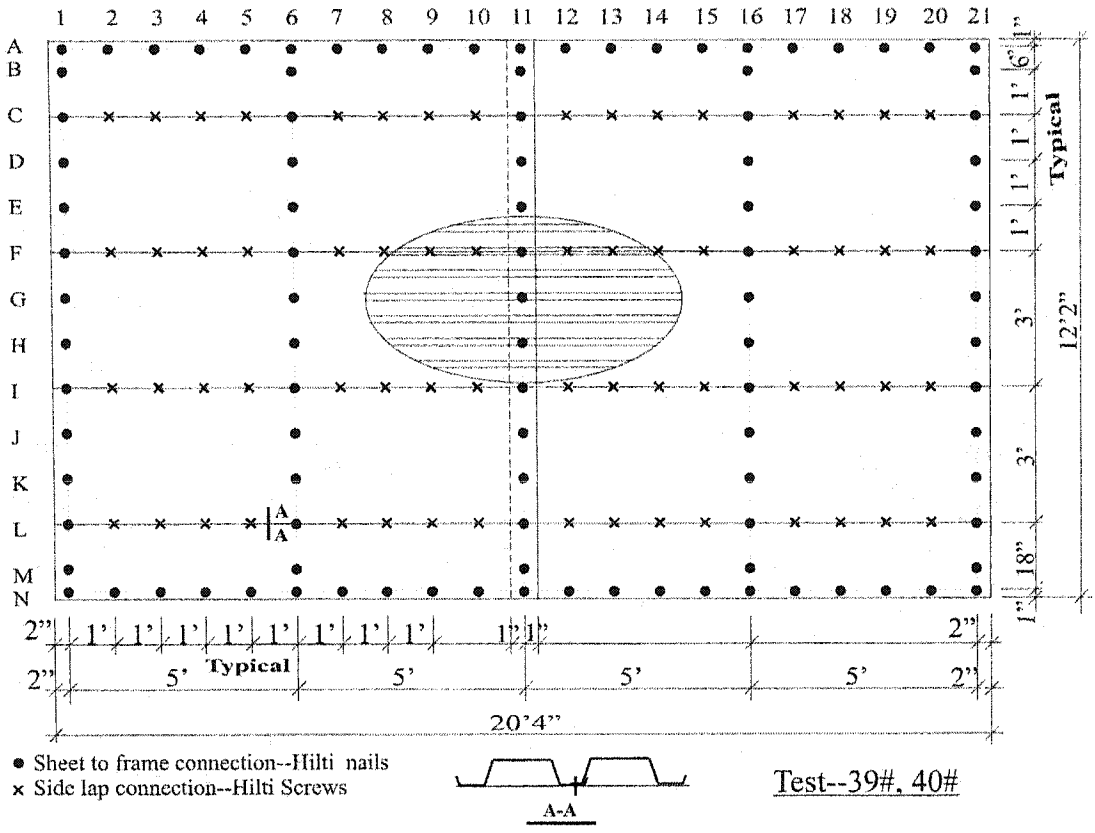

Figure 4.12. Plan layout of Test 38-76-3-NS-M-39 & Test 38-76-3-NS-SD-40

The structural fasteners in test 39 and test 40 were Hilti X-ENDK22-THQ12 nails that had a length of 22 mm and shank diameter of 3.7 mm (tapered, see Figure 4.13). The nails were installed using a Hilti DX A41 SM tool and the 6.8/11M Hilti #5 short red cartridge at a mid-level power setting.

It is important to note that, for the longitudinal overlapped specimens, there were four layers of steel sheets at grid line locations C11, F11, I11, and L11 (Figure 4.12)

instead of the usual two sheet layers at other frame fastener locations along grid line 11.

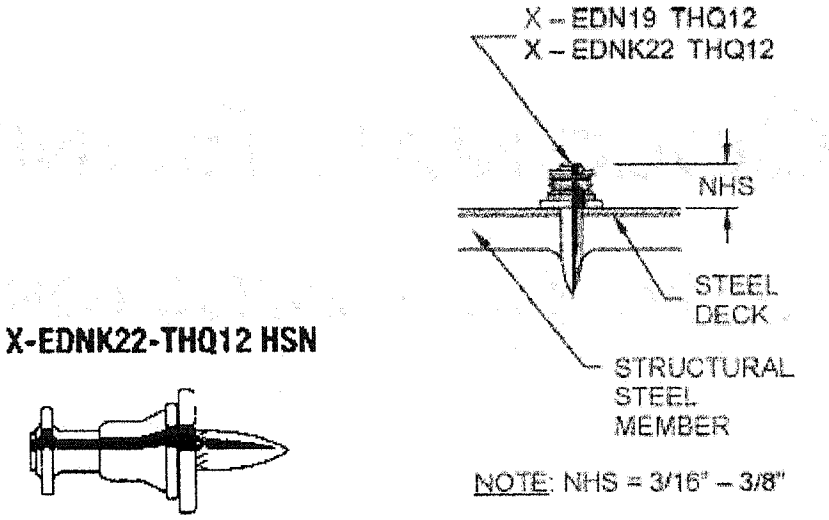

Note: NHS—Nail Head Standoff

Figure 4.13. Hilti X-ENDK22-THQ12 nail and connection detail (ICBO, 2002b)

The side-lap connection for tests 39 and 40 were composed of Hilti S-MD 12-14x1 HWH #1 F.P screws, which were similar in shape and size to that detailed for the Buildex screws (Figure 4.11).

The plan layout of Test 41 and Test 42 is shown in Figure 4.14, where the test specimens consisted of P3615 standard deck panels (with interlocking side-lap edges, see Section A-A in Figure 4.14).

The deck-to-frame connections were made with arc-spot welds and the side-laps were fastened with button punches. The button punch connections were done with a special tool that was provided by Canam Manac Co. Two photographs of both arc-spot weld and button punch installations are given in Figures 4.19 and 4.20 in Section 4.1.3.

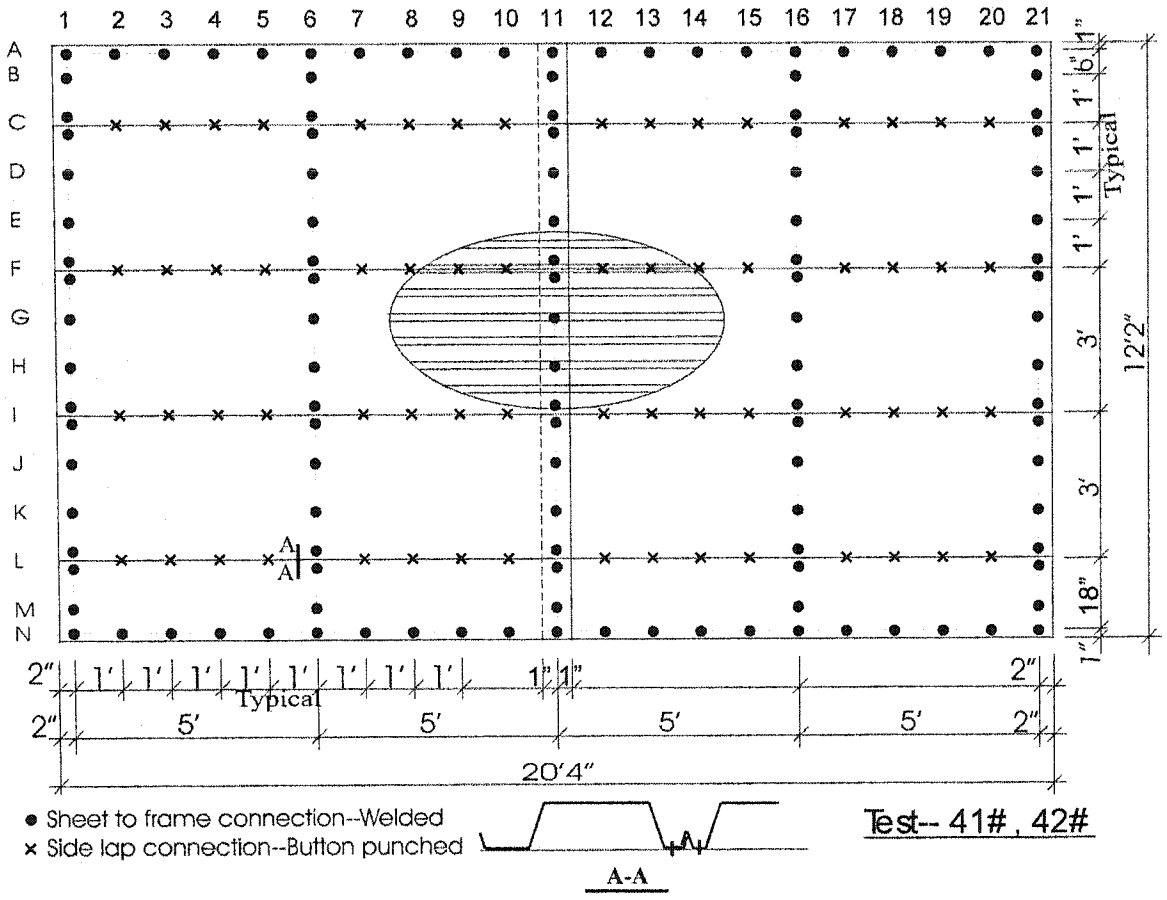

Figure 4.14. Plan layout of Test 38-76-3-WB-M-41 & Test 38-76-3-WB-SD-42

In Figure 4.14, it is noted that, in the east-west direction the spacing of the connections was set at 12" in most situations. However there were two variations to this spacing pattern. In the width direction there were three weld connections in the exterior sheets and four in the interior sheets. Along interior side-lap gridlines C, F, I and L, there were two welds, one on each side of the interlocking panel edge (Section A-A in Figure 4.14). The other change in weld spacing occurred in the half-width panels where a 6" spacing was necessary as shown in Figure 4.14.

Welds were made with a 2.5 mm diameter E6011 electrode following the protocols recommended by Peuler (2002). The weld current was 100 amp and the nominal diameter of deck-to-frame weld was 16 mm. The weld connections were performed by a technician who owned a weld certificate. It took about 10 to 15 seconds to complete each weld connection, which coincided with what was observed by Peuler (2002), where the average welding time for E6011 electrodes was 11.8 sec. The quality of welds largely depends on the welder's skill, the surrounding environment, and the deck profiles. It was found that the weld qualities at non-side-lap positions are usually better than that at side-lap positions, because for interlocking side laps, the space for manufacturing is much more limited, less than half width of the non-side-lap positions (see the common deck profiles available in Canada in Figure 3.5 a). Another reason is that the sheet does not contact closely to the frame members because the curved shape at the interlocking sides (Essa et al 2001). The thin sheet is quite easily penetrated through at these positions. An example photo of this phenomenon from Test 41, taken before the test was carried out, is shown in Figure 4.15. In this case, the thin steel sheet was to some extent burned through around the spot weld.

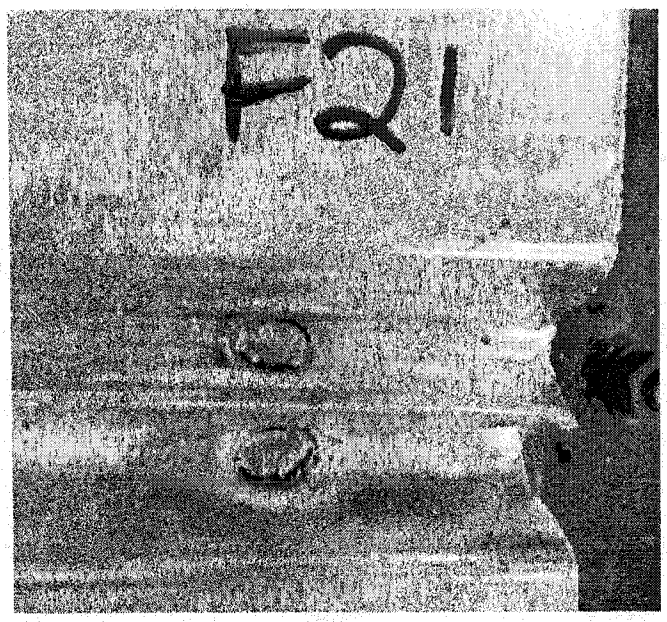

Figure 4.15. An example of weld quality at side lap positions

Two load types were included in test group 2: the monotonic loading and the seismic short duration (SD) loading. Their related load control parameters will be presented in Section 4.1.7.

4.1.2.3 Group 3

Group 3 consisted of four tests; of which two were bare sheet and two were constructed with non-structural roofing components. The listing of test specimens is as follows:

- 38-76-6-NS-M-43
- 38-76-6-NS-C-44
- 38-76-6-NS-M-R-45
- 38-76-6-NS-C-R-46

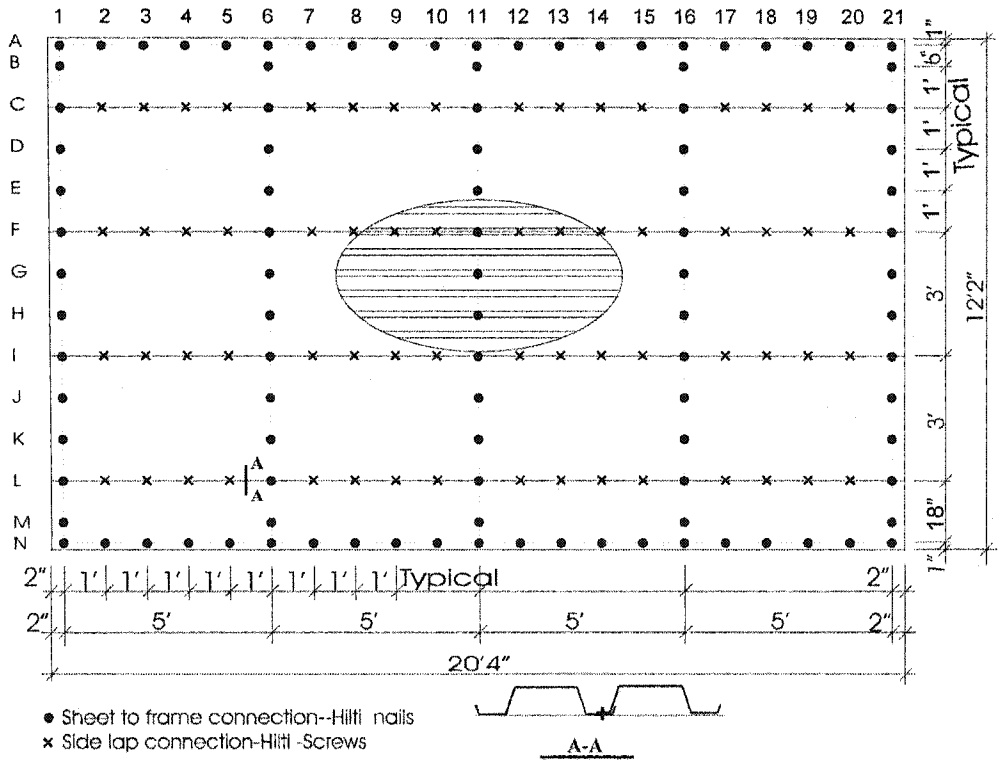

Figure 4.16. Plan layout of Tests 38-76-6-NS-M-43; -C-44; -M-R-45; & -C-R-46

The sheathing and connection layout of tests 43 to 46 (Figure 4.16) were similar to those of tests 39 and 40 (Figure 4.12). The only difference was that tests 43 to 46 consisted of full-length sheets (20' 4"), *i.e.* no longitudinal overlap existed. Along the length direction of test frame there were 21 connections, *i.e.* 5 deck-to-frame fasteners and 16 side-lap fasteners. The spacing was 1' for both directions, except for the half width sheets. The Hilti nails and screws were of the same type as documented for test 39. The testing utilized monotonic and cyclic protocols as described in Section 4.1.7.1 and 4.1.7.3.

4.1.2.4 Group 4

The fourth testing group was composed of three specimens, each constructed with seven P2436, 76 mm deep panels (see Figure 3.5 in Chapter 3).

- 75-76-6-WB-M-47,
- 75-76-6-WB-SD-48,
- 75-91-6-WB-M-49.

The plan layout of the specimens was made up of seven sheets, including 2 half-width sheets and 5 whole-width sheets, as illustrated in Figure 4.17.

The total width of the seven sheets was 3660 mm. Similar to the previous test configurations; the spacing of connections was at 1' centres. However, along the side-lap lines at B, D, F, H, J and L, two welds were needed due to the interlocking panel

profile. The weld installation was the same as that noted for the Group 2 tests. Side-laps were fastened with button punch connections.

Specimens 47 (0.76 mm) and 49 (0.91 mm) were subjected to a monotonic loading protocol, whereas specimen 48 (0.76 mm) was tested with the seismic short duration protocol that will be discussed in Section 4.1.7.

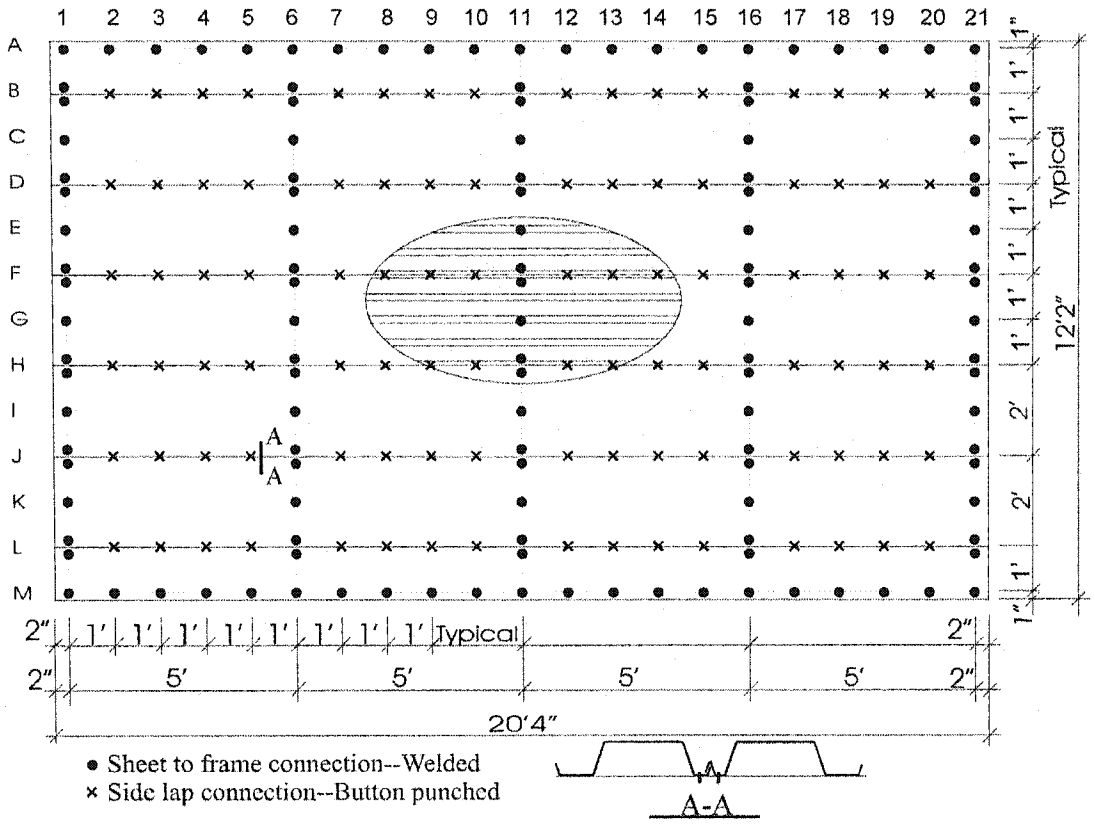

Figure 4.17. Plan layout of Tests 75-76-6-WB-M-47; 75-76-6-WB -SD-48; and 75-91-6-WB-M-49

4.1.3 Specimen installation

The first step was to cut the sheets into proper lengths because the majority of ordered panels were 21'6" (6553 mm) long, which was 1'2" longer than that required. The surplus material was used to fabricate tensile coupons for material testing. For the intermediate overlapped tests (tests 39 to 42) a panel length of 10'3" (3120 mm) was needed. For tests 47 to 49 the ordered sheet length was 20'6". Test 49 was carried out prior to tests 47 and 48, so a panel length of 20'4 was cut. It was noted during testing that only connection failures took place, and hence for tests 47 & 48 the original sheeting of 20'6" was used.

During the installation, all steel sheets were placed and adjusted into position before any connections were made. The connections were installed on one side sheet, e.g. south side, and once this sheet was fixed, the adjacent sheet was connected, etc.

Prior to the installation of any connection on the specimen, numerous practice sessions were held. In the case of the nailed connections these were necessary to obtain the proper tool settings and cartridge type. Practice welds were also fabricated such that the welder could become familiar and proficient with the welding technique. Photographs showing nail, weld and button punch installations are provided in Figures 4.18 to 4.20. A photograph of a diaphragm specimen after deck installation was given in Figure 4.6.

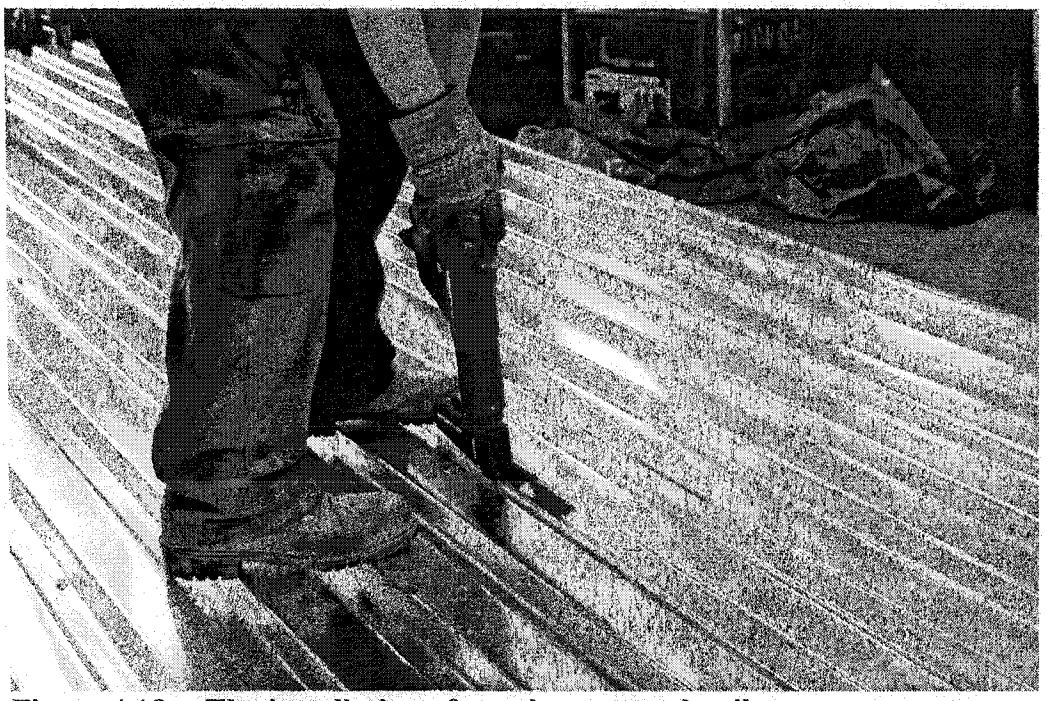

Figure 4.18. The installation of powder actuated nails

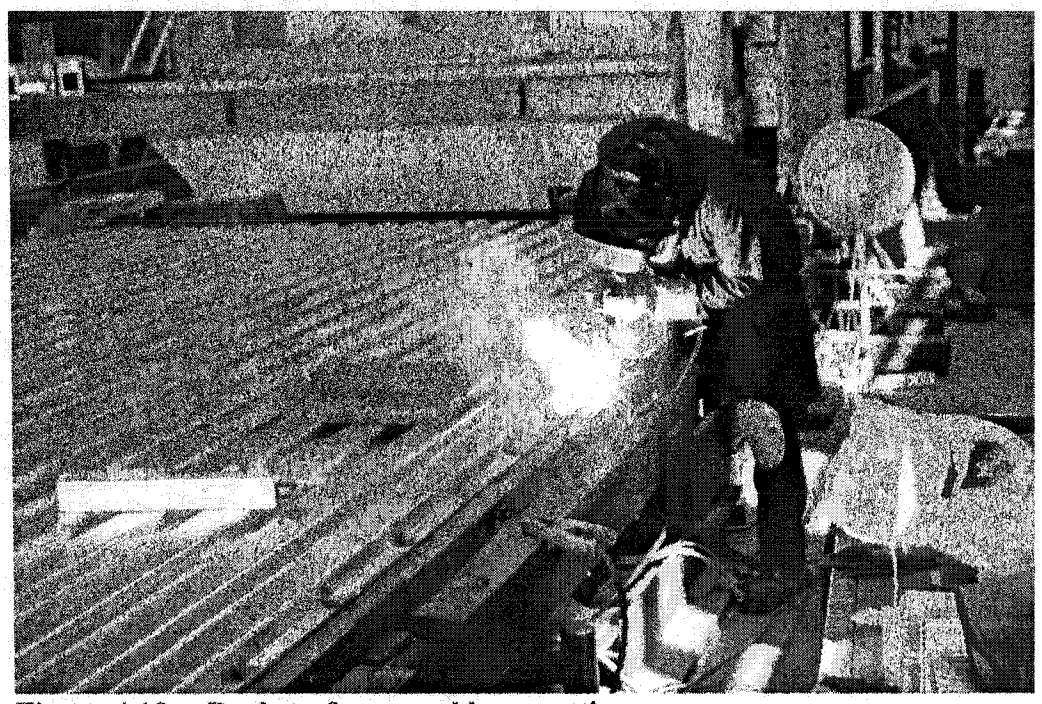

Figure 4.19. Deck-to-frame weld connection

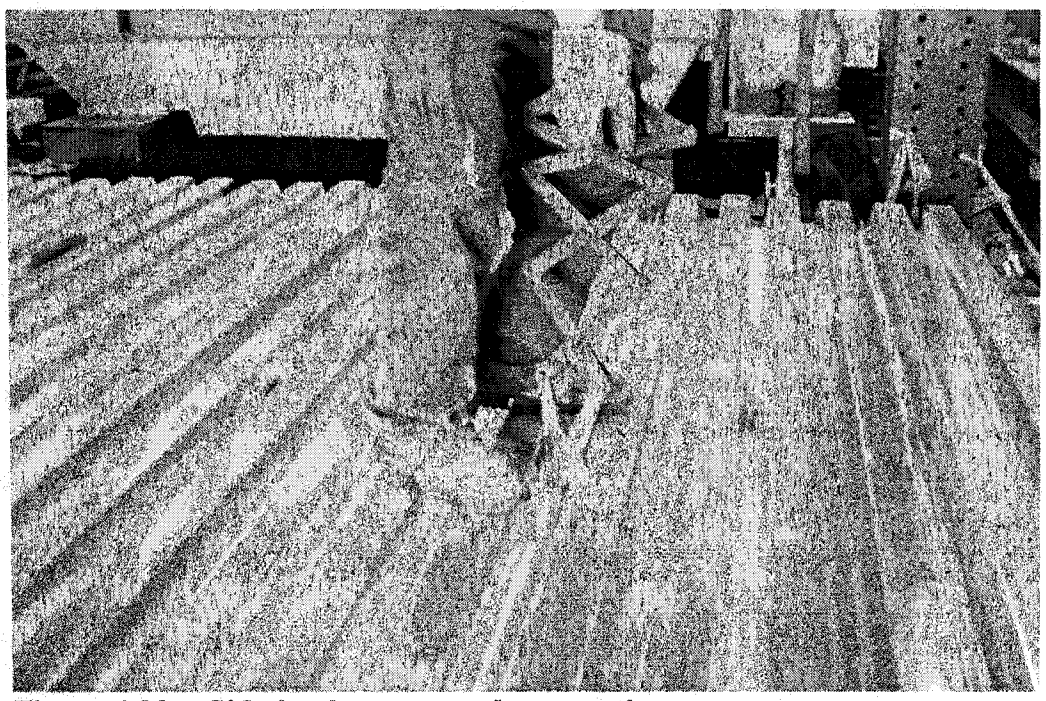

Figure 4.20. Side-lap button punch connection

4.1.4 Roofing material installation (tests 45 & 46)

Prior to this investigation, no diaphragm specimens at École Polytechnique had been constructed with the non-structural roofing components. For this reason the installation procedure is described in detail in this Section. As discussed in Chapter 3, the SBS-34 roofing combination from the Association des Maitres Couvreurs du Quebec (AMCQ) was chosen for these two test specimens.

The steel deck panels were first placed following the procedure documented in the previous Section. The ½" type X gypsum board was then fixed to the steel deck with special screws (Fig 4.21 and 4.22). Its washer is made of a 0.46 mm thick galvanized steel disc with a 76.2 mm (3 in) diameter. The screw itself is 4.76 mm in diameter, 41 mm long, with 16 threads per inch long. The test set-up (12'x20') requires 2.5 pieces of standard gypsum board (4'x8') in the long direction, while 3 pieces in the short direction. For each full size gypsum panel, 12 fasteners were required, whereas for the half size panels 9 fasteners were used. One such example of the fastener layout from test 45 is shown in Figure 4.23.

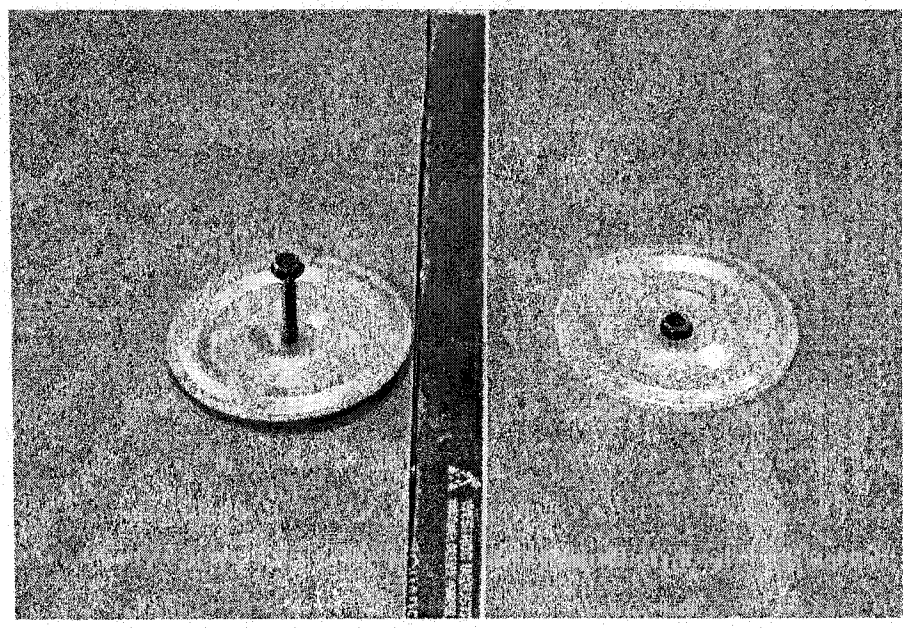

Figure 4.21. Screws used to fix gypsum board to steel deck

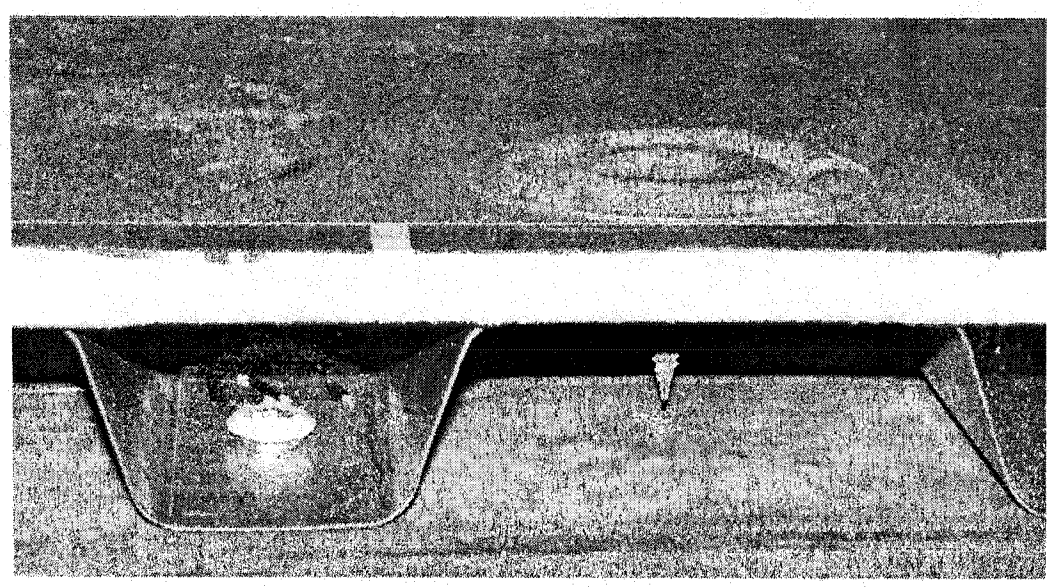

Figure 4.22. Detail of gypsum board to steel deck connection

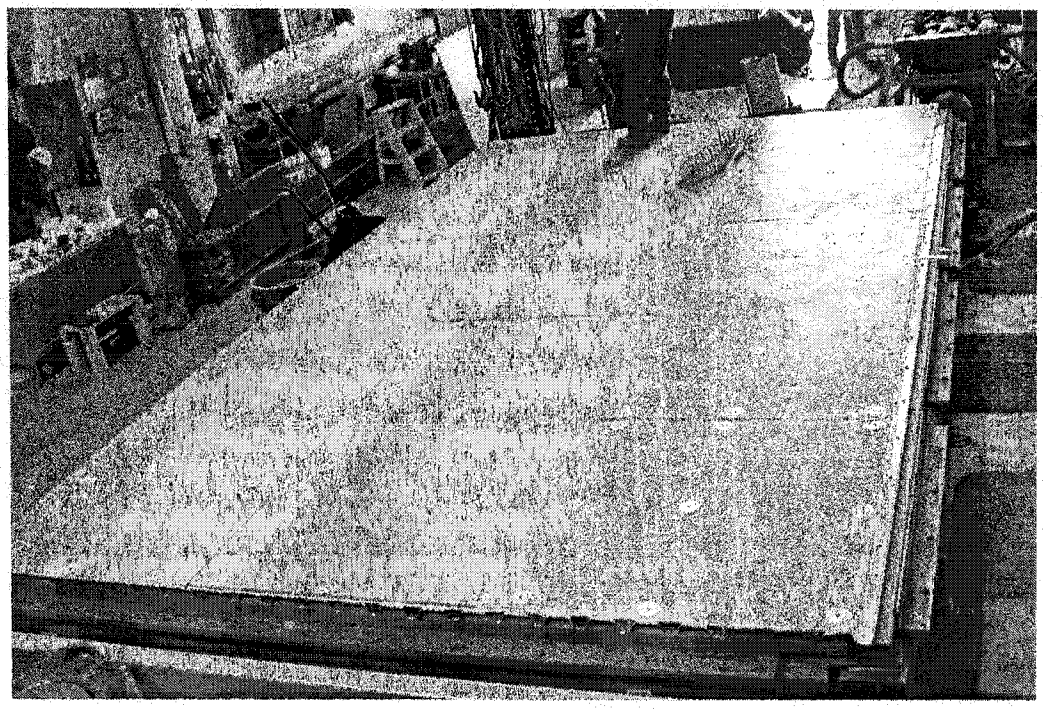

Figure 4.23. Gypsum board-to-deck fasteners' layout

Once the gypsum board had been installed, the vapour retarder was adhered to the gypsum board by mopping hot bitumen (Figure 4.24). The vapour retarder consisted of two layers of 15 lb Kraft paper (perforated asphalt felt No. 15). This was achieved by overlapping each width of paper by a half plus 2".

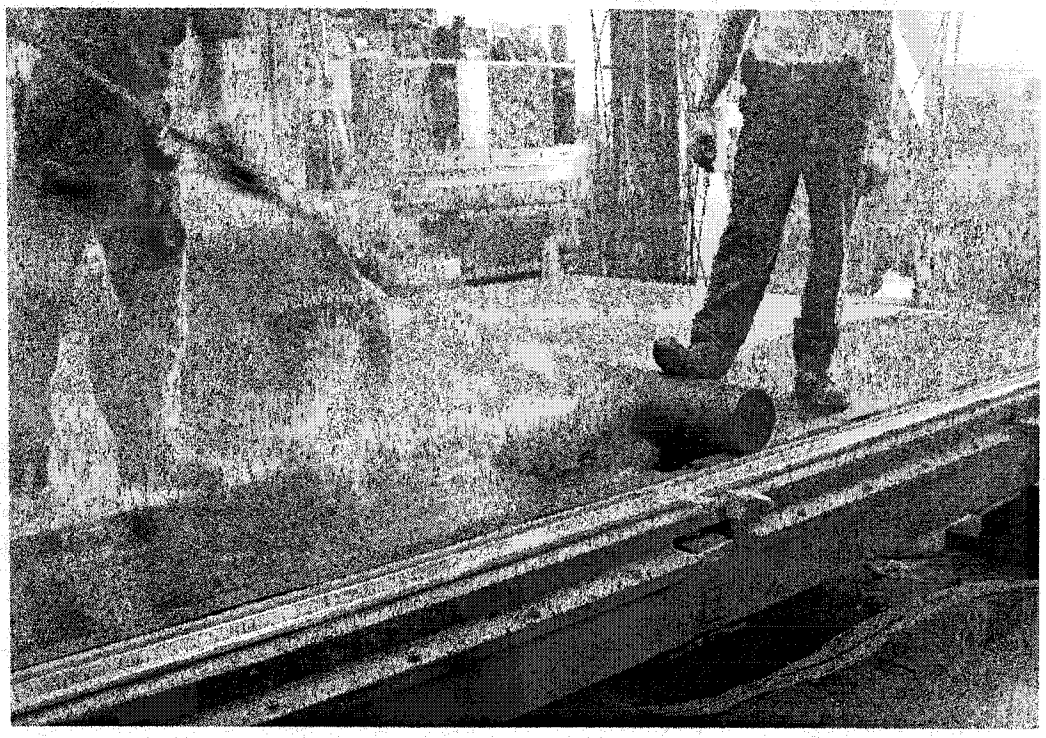

Figure 4.24. Vapour retarder being adhered to gypsum board

After the vapour retarder had been installed, one layer of 2.5" thick Johns Manville E'NRG'Y 3 polyisocyanurate (ISO) insulation board was added. First a layer of hot bitumen was mopped on to the top of the vapour retarder and then the insulation panels were placed (Figure 4.25). The insulation panels were staggered as can be seen in Figure 4.26.

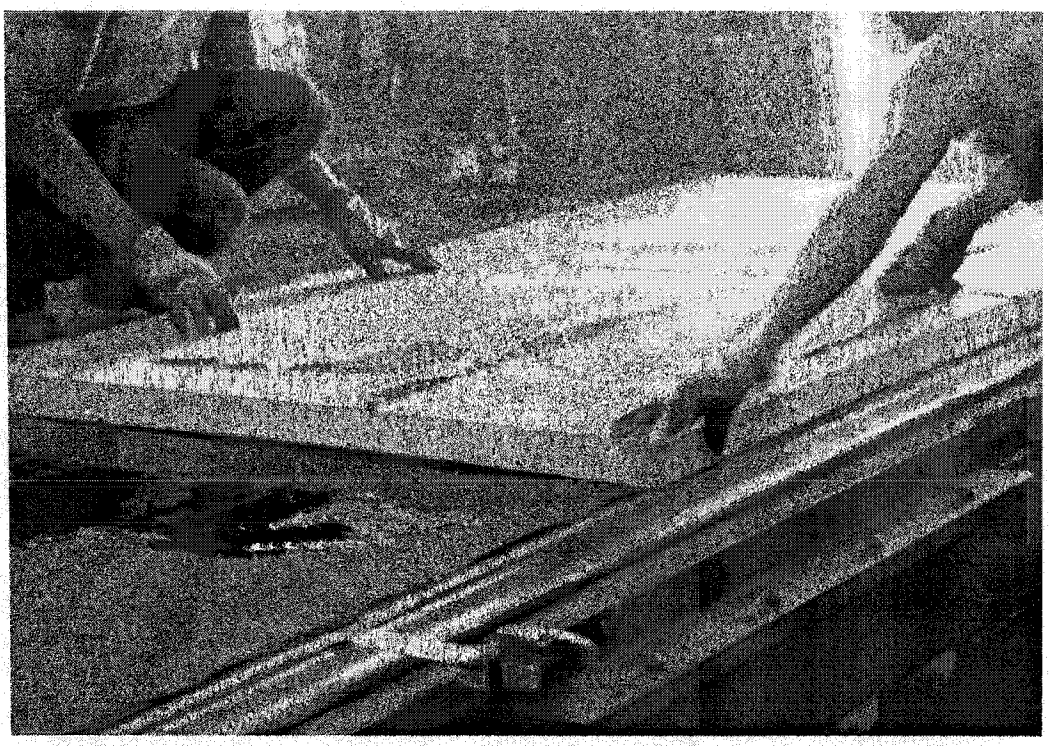

Figure 4.25. Installation of ISO insulation board

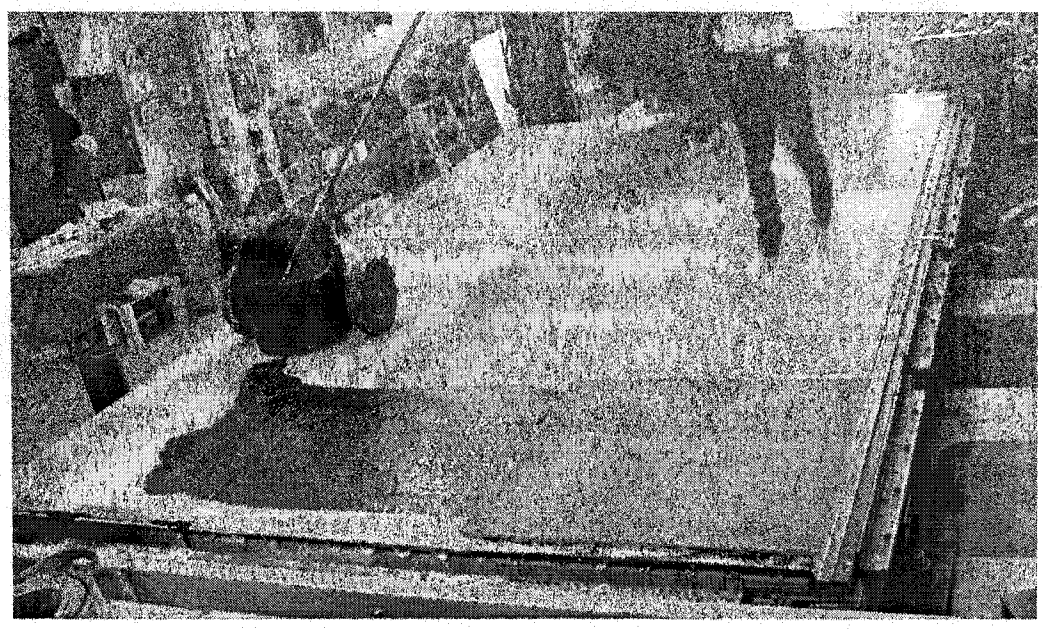

Figure 4.26. Installation of wood fibreboard above ISO insulation layer

On top of the ISO insulation board a single layer of 1" thick SECURPAN fire-resistant wood fibreboard was adhered by mopping hot bitumen on to the ISO insulation layer (Figure 4.26). The fibreboard acted to protect the insulation from being penetrated by any sharp loading and allowed for the waterproof membrane to be adhered with an open flame propane torch (Figure 4.27 & 4.28)

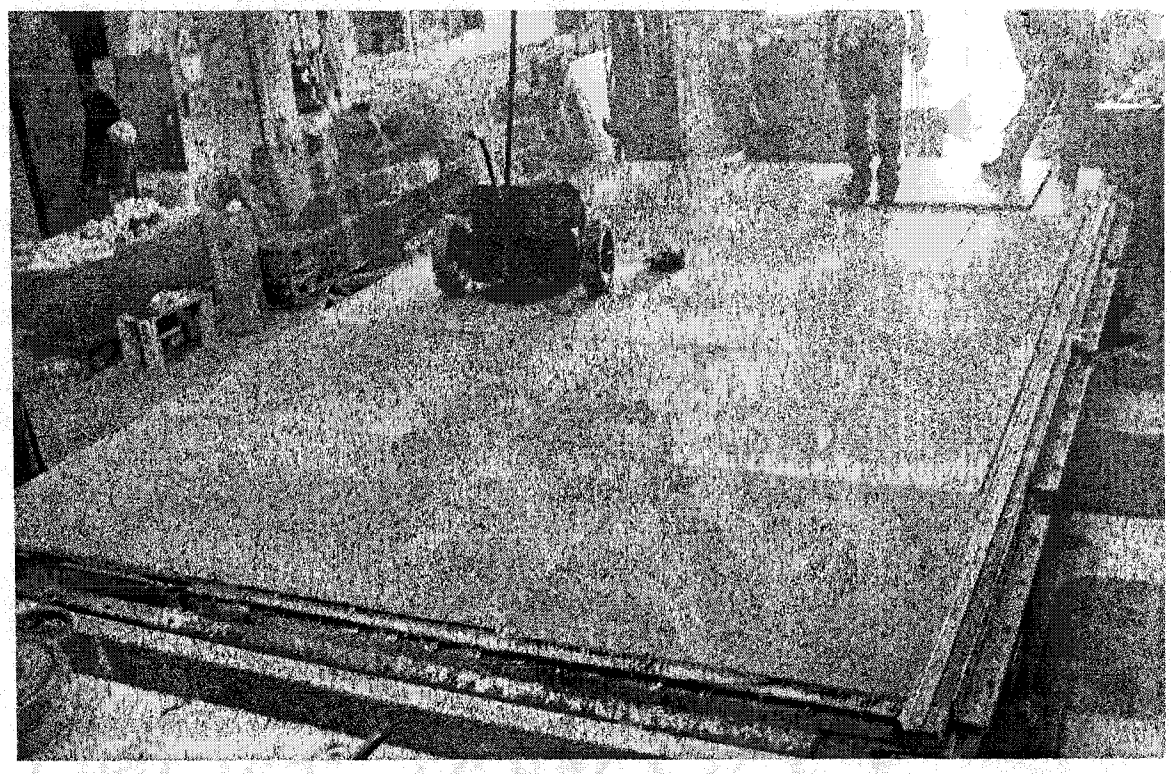

Figure 4.27. Installation of wood fibreboard near completion

Figure 4.28. Installation of SBS base sheet by hot bitumen and flame torch

One layer of 2.2 mm thick ELASTOPHENE 180 PS waterproof membrane base sheet was adhered to the top of the wood fibreboard by melted bitumen and a flame torch (Figure 4.28). The overlap of base sheet was approximately 3". The nearly finished installation of SBS base sheet is shown in Figure 4.29.

Figure 4.29. SBS base sheet after installation

The final layer of the non-structural roofing components was the SBS cap sheet, a 4 mm thick 36" (914 mm) wide SOPRALENE FLAM 250 FR GRANULES sheet with a 3" overlap. The under side of the top sheet was composed of a layer of thermo fusible plastic film, which melted during flaming (Figure 4.30). The top face of the finishing felt was made of a layer of granules that protect the felt from weather attack (Figure 4.31). A section view of the finished test specimen with steel deck and non-structural components can be seen in Figures 4.32.

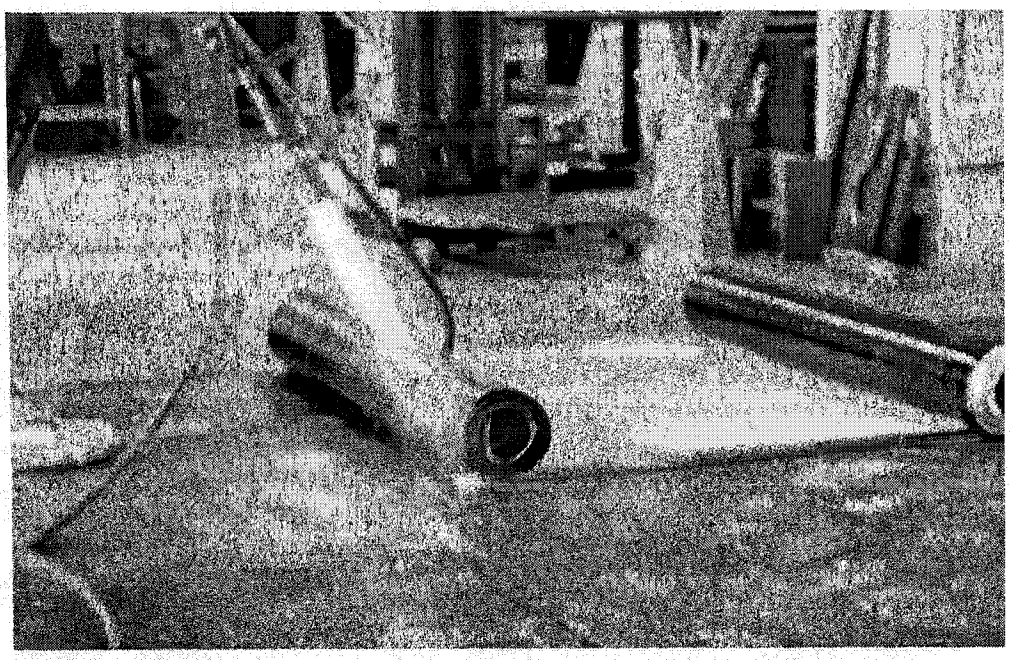

Figure 4.30. Installation of SBS cap sheet by open flame propane torch

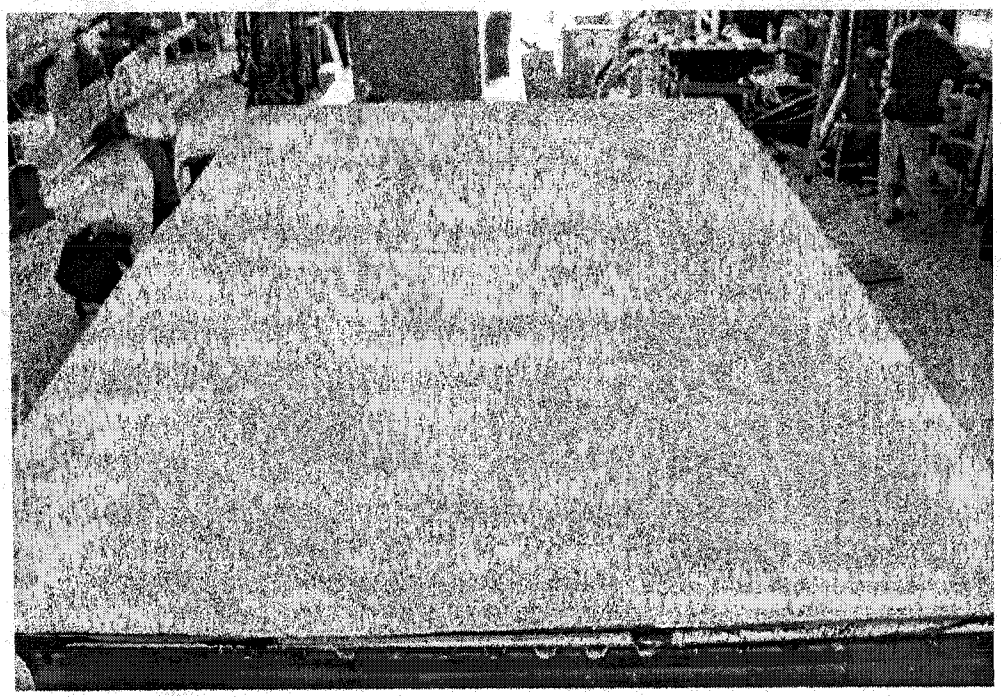

Figure 4.31. Plan view of specimen after roof installation

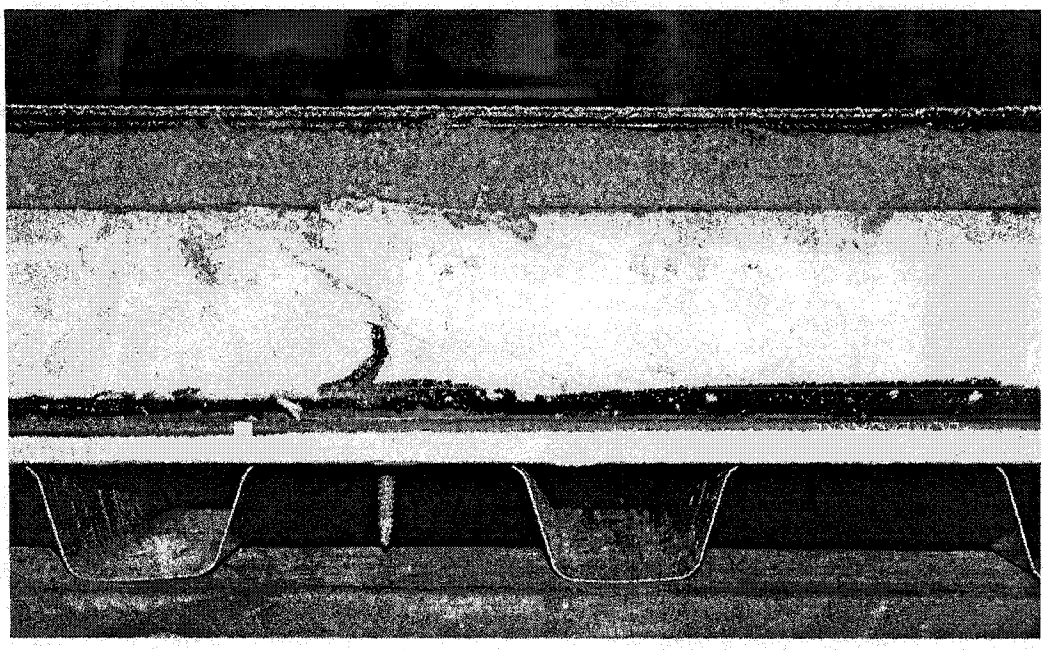

Figure 4.32. Section view of specimen after roof installation

4.1.5 Set-up of measurement instruments

During the running of each test a variety of measurements were taken to evaluate the performance of the diaphragm under shear loading. This included side-lap slip, deck-to-frame slip, frame movement, restraint forces, as well as the applied displacement and force, and for dynamic tests the acceleration. The set-up of the load cell and accelerometer was provided in Section 4.1.

4.1.5.1 Frame movement

The movement of the frame at corner locations was measured to calculate the real diaphragm deflection. This corrected displacement, Δ, can be obtained from equation (4.1), which accounts for any slip of the frame in the direction of loading, as well as the rigid body rotation of the frame. These frame movements were measured with LVDTs (Linear Variable Differential Transformer) located in positions A, B, C, D and E (Fig. 4.33)

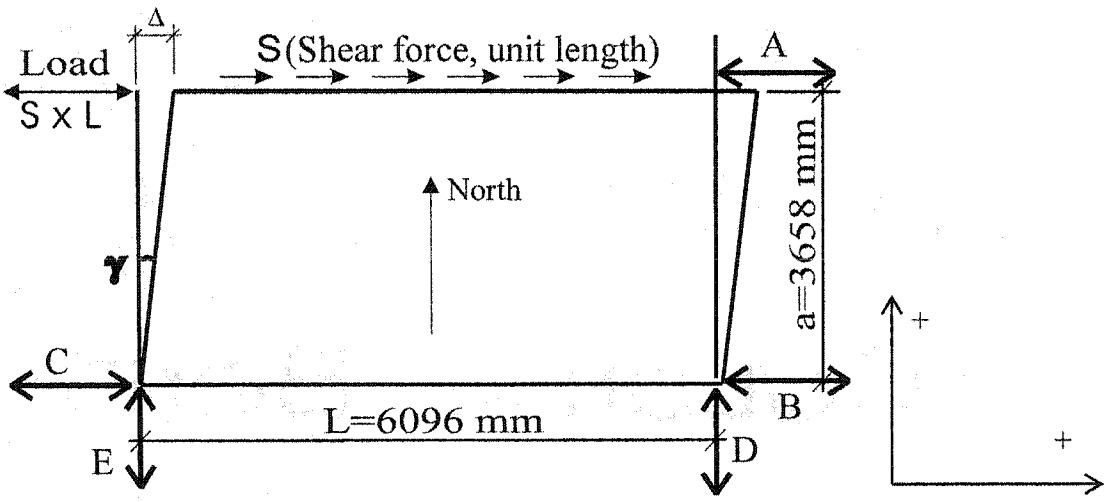

Figure 4.33. Frame movement and LVDT placement

$$\Delta=A-(B+C)/2-(E-D)*a/L \qquad (4.1)$$

where:

Δ----The correct diaphragm displacement

a----Test frame width 3658mm;

L----Test frame length 6096 mm;

A----The displacement measured by the cable transducer at the north-west corner (Figure 4.34), which was considered equivalent to the displacement measured at the north-east corner. Positive direction is shown in Figure 4.33.

B, C, D & E----The displacements measured at the south-east and south-west corners.

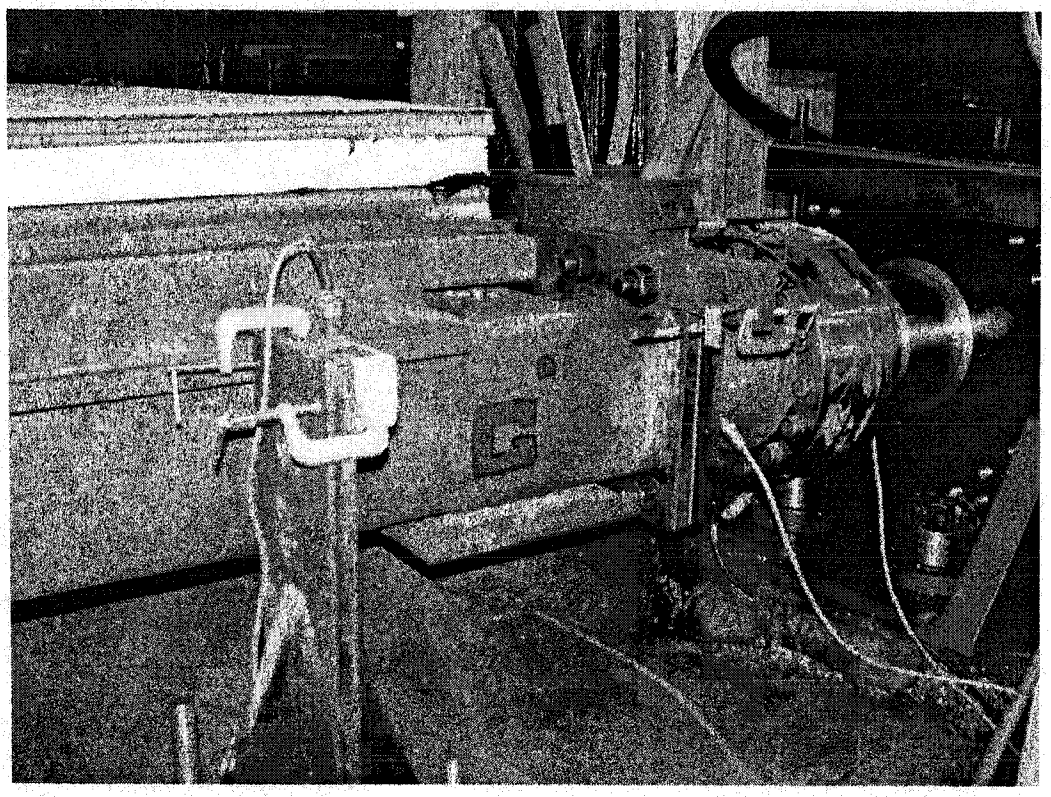

Figure 4.34. North-west corner of frame showing measurement devices

Due to the small dimensions of the test set-up, bending deformation could be ignored. So the shear rotation of the specimen γ could then be presented as:

$$\gamma=\Delta/a \qquad (4.2)$$

4.1.5.2 Restraint forces

Restraint forces were measured through the use of the four dog bone load cells denoted A, B, C, and D in Figure 4.35. These dog bone load cells were also discussed previously in Section 4.1.1 (Figures 4.3 & 4.4). Essa *et al.* (2001) first of all designed, fabricated and calibrated these load cells for a maximum force of 240 kN, and then showed that the forces measured from these load cells could be used to evaluate the overall equilibrium of the test frame.

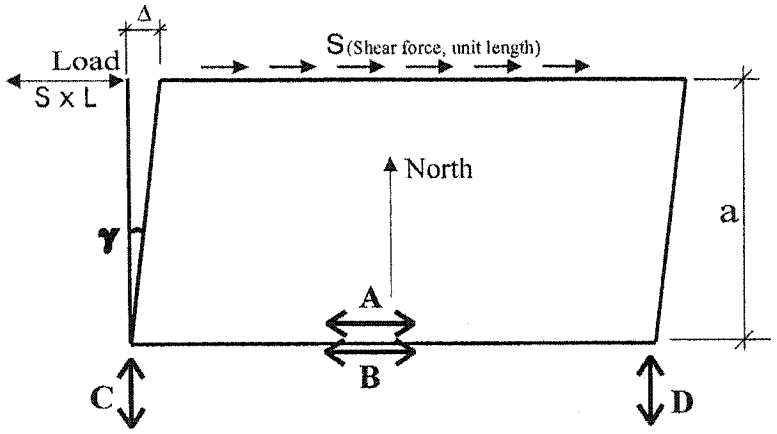

Figure 4.35. Location of dog bone load cells

4.1.5.3 Deck-to-frame slip and deck-to-deck slip

Measurement of the deck-to-frame slip was obtained by placing LVDTs on both side frames and connecting them to the outermost deck panels (Figure 4.36). The arrangements of LVDTs for measuring the side-lap slip was different, in that two instruments were installed below the diaphragm at each side-lap, one on each side (Figure 4.37). The LVDTs were attached to the central joist member and measured the relative slip between a panel and the underlying frame. Given this displacement was obtained on both sides of the side-lap, an overall slip measurement could be calculated.

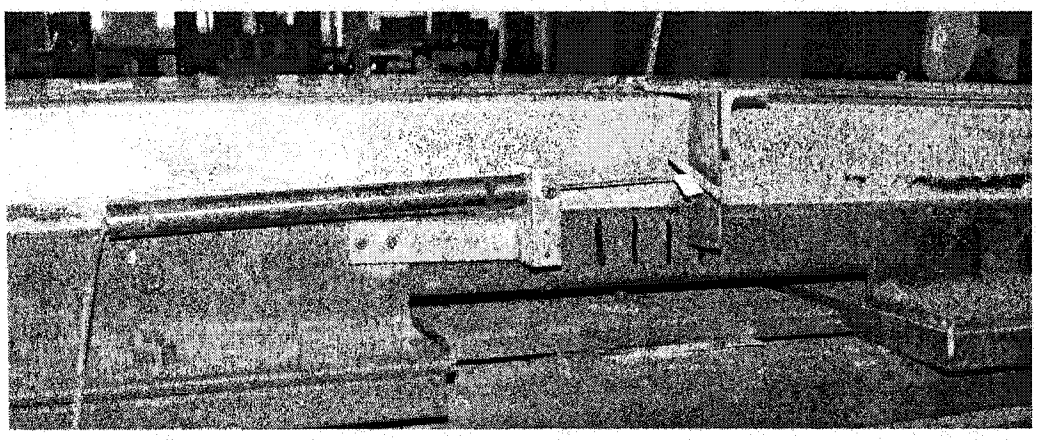

Figure 4.36. LVDT for deck-to-frame slip measurement

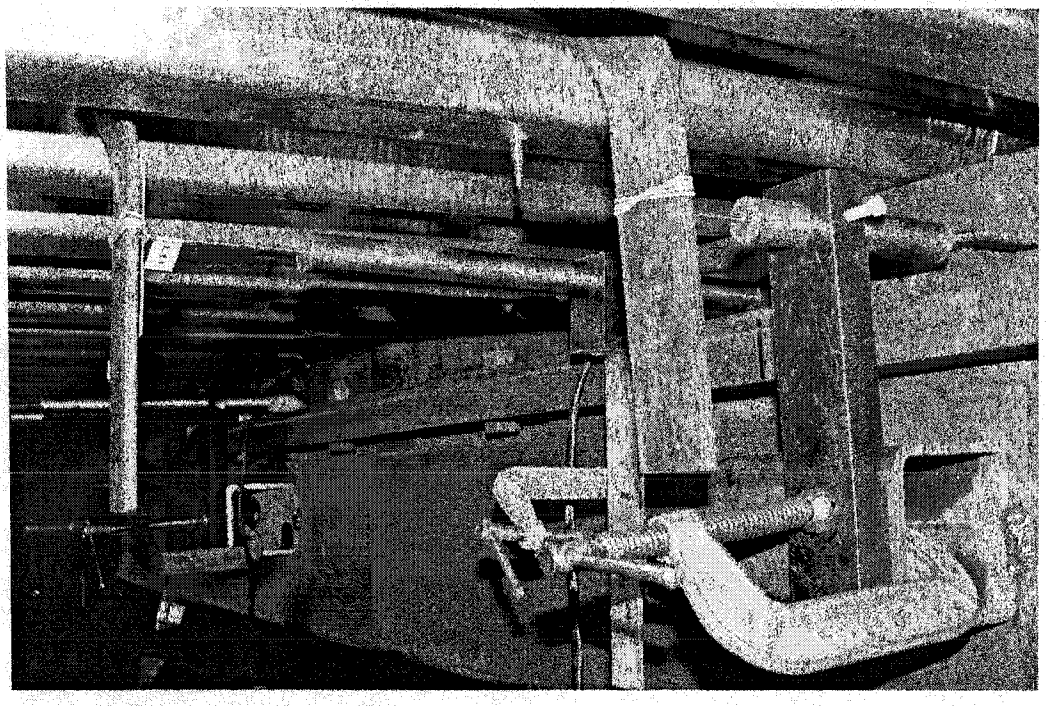

Figure 4.37. LVDTs for side-lap slip measurement

The arrangements of slip measurement are given in Figure 4.38, where the set up for test 38 (Figure 4.38 a) is the same as Essa et al (2001) and Martin (2002). Additional LVDTs were installed for tests 39 to 42 (Figure 4.38 b) because of the additional end lap joint along mid-length, and because of the one more panel used as compared to test 38. The arrangement for tests 43 to 46 is similar to test 38 but one more side lap was included (Figure 4.38 c). For tests 47 to 49, a total of 12 slip measurements were required to calculate the slip in the six side laps (Figure 4.38 d).

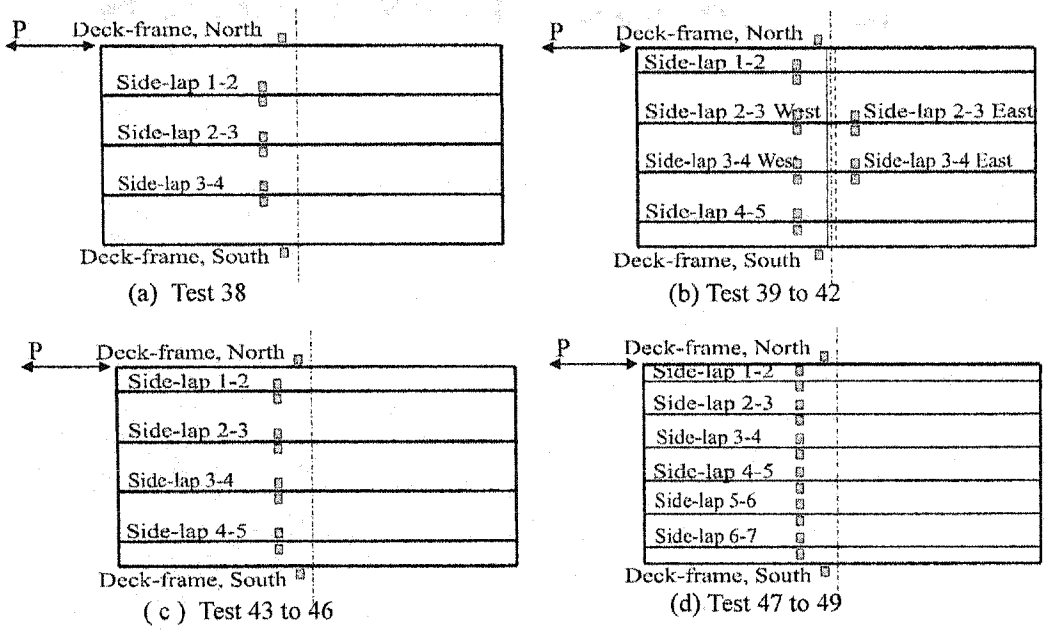

Figure 4.38. The layout of LVDTs for slip measurement

4.1.6 Material properties and connection properties

The deck panels were fabricated from Grade 230 sheet steel conforming to ASTM A653 (2002) with a G275 galvanized coating. Tension coupons cut from the panels were tested to obtain material properties, which include yield strength F_y, ultimate strength F_u, Young's modulus E, and elongation over a 50 mm gauge length, which are from the mean value of three tests. The tension specimens were prepared and tested according to ASTM A370 (2002). Base metal thickness was measured after the galvanized coating had been removed in an acid bath. The sheet steel material properties are listed in Table 4.2 and the material tests are further explained in Appendix 1.

Table 4.2 Material properties

Groups	Sheet type	Base metal thickness (mm)	F_y (MPa)	F_u (MPa)	E (MPa)	50 mm gauge Elongation %
Test 38[1]	P3615 B 0.91mm	0.88	319	394	210000	24
Test 39, 40[1]	P3615 B 0.76 mm	0.70	248	327	204000	32
Test 41, 42[1]	P3615 0.76 mm	0.71	301	373	197000	31
Test 43 to 46	P3615 B 0.76 mm	0.72	317	377	195520	37
Test 47, 48	P2436 0.76 mm	0.74	321	385	184749	29
Test 49	P2436 0.91 mm	0.87	316	378	202282	29

[1] Material properties are from Martin (2002)

In addition to the material properties of the sheet steel, the connection properties are also very important to the diaphragm behaviour. Tables 4.3 and 4.4 list respectively the deck-to-frame and side-lap connection properties related to the diaphragm tests. The values of strength and stiffness in these tables are quoted from Rogers and Tremblay (2000), SDI (1987), Hilti (2001) and ITW Buildex (1993).

Table 4.3 Deck-to-Frame connection properties used in diaphragm tests

Group	Type	Sheet thickness (mm)	Strength (kN)			Stiffness (kN/mm)		
			Test	SDI	Manufacturer	Test	SDI	Manufacturer
Test 38	Buildex BX-14 Nails	0.91	7.66	N/A	7.67	18.7	13.26	N/A
Test 39, 40, 43~46	Hilti X-EDNK22-THQ12 Nails	0.76	6.41	N/A	6.68	23.2	N/A	24.04
Test 41, 42, 47, 48	16 mm dia. Weld	0.76	11	7.84	N/A	25.5	23.4	N/A
Test 49	16 mm dia. Weld	0.91	15	9.29	N/A	31.8	28.82	N/A

Note: 1. No strength values for Buildex BX-14 and Hilti X-EDNK22-THQ12 nails were provided in SDI equations. The values from manufacturer will be used in estimation.

In Table 4.3, the weld strength from tests by Rogers and Tremblay (2000) is higher than that from the SDI (1987), *e.g.* 11 kN vs 7.84 kN for 0.76 mm sheet, 15 kN vs 9.29 kN for 0.91 mm sheet. These differences in the connection strength may result in a range of estimates for the diaphragm strength. As will be discussed later in this Section, the diaphragm test results from this study form a better match with the SDI predictions, which may in part be due to the difference in weld quality of the diaphragm tests compared with the individual connection tests. Based on observations during installation of the deck panels, it was noted that difficulties arose when welding near the side-lap locations. The tests carried out by Rogers and Tremblay (2000) did not consider the effect of the side-lap versus the non side-lap welded connections.

Table 4.4 Side-lap connection properties used in diaphragm tests

Group	Type	Sheet thickness (mm)	Strength (kN)			Stiffness (kN/mm)		
			Test	SDI	Manufacturer	Test	SDI	Manufacturer
Test 38	Buildex 12-14x1 HWH TEK/3 screw	0.91	3.06	3.87	4.53	2.26	11.05	N/A
Test 39, 40, 43~46	Hilti S-MD 12-14x1 HWH #1 screws	0.76	2.37	3.23	N/A	1.35	10.1	N/A
Test 41, 42, 47, 48	Button punch	0.76	0.64	0.83	N/A	0.16	0.98	N/A
Test 49	Button punch	0.91	0.95	1.37	N/A	0.25	1.11	N/A

Note: 1. The test values are actually from 10-14x7/8" screws.

It should also be noted that that values listed Tables 4.3 and 4.4 may be not be exactly as reported by Essa *et al.* (2001) and Martin (2002). The small difference may have arisen because different quotation sources were used. These connection properties will be evaluated in Section 4.2.1, where the SDI estimates of the diaphragm strength and stiffness will be discussed.

4.1.7 Load protocols

Three different load protocols were used in the testing phase of this project: Monotonic load "M", Short Duration seismic load "SD", and Cyclic plus monotonic load "C".

4.1.7.1 Monotonic load

The monotonic tests form the foundation for any dynamic loading protocol. The results from these tests can also be used in a direct comparison with existing diaphragm design methods. There were two main reasons for carrying out this type of test:

- To determine the load parameters for other tests;
- To evaluate the failure modes.

All monotonic tests were run in displacement control with movement of the actuator piston in the east direction at a speed of 1mm/minute until the post peak load reached 80% of P_u. At this point the test speed was increased to 1.5mm/minute. Since the displacements and load increased quite slowly in these monotonic tests, it was

possible to observe the failure modes more clearly and comprehensively. A typical load-to-deformation relationship from test 43 is shown in Fig. 4.39.

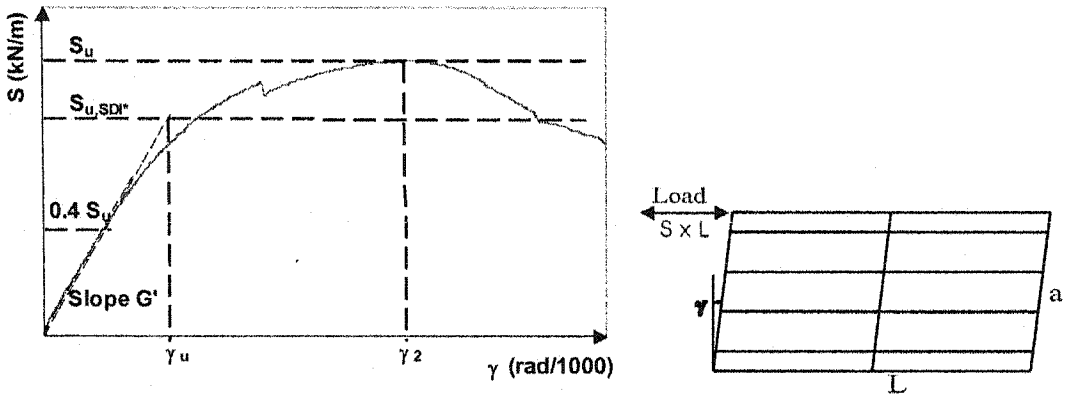

Figure 4.39. A typical load-to-deformation relationship from Test 43

In Figure 4.39:

S----The unit shear along sheet length, S=P/L;

P----The load measured by the load cell;

L----The sheet length;

γ----The shear rotation, γ=Δ/a

Δ----The corrected diaphragm displacement, see Equation 4.1;

a----The frame width;

S_u----The ultimate shear from test. $S_u=P_u/L$.

$S_{U,SDI}^{*}$----The S_u estimated according to the SDI (1987), but the connection properties refer to Rogers & Tremblay (2000).

$G^{'}$----The slope between $0.0S_u$ to $0.4S_u$, in this range the S-γ relationship is assumed to be linear.

γ_2----The shear strain related to S_u of monotonic test.

γ_u----The shear deformation determined by $S_{U,SDI}^{*}/G^{'}$.

4.1.7.2 Short Duration seismic load

As described in Chapter 2 the short duration (SD) loading protocols were first defined by Martin (2002). The intent of using such a protocol is to imitate the inelastic seismic shear deformation demand that would occur in a diaphragm that forms the roof of a single-storey steel building located in the east and west of Canada. Short duration loading is also a displacement controlled test, however the rate of loading is 2 Hz, which is much faster than the quasi-static loading protocol used by Essa et al (2001), and more similar to real seismic load situations. Each SD load protocol includes three sections, called "East R_d=3.0", "West R_d=2.0" and "West R_d=3.0". For further details on the SD loading protocol please refer to Martin (2002).

An example of a SD load protocol (Test 40) is shown in Fig. 4.40, where γ and γ_u represent the specimen's shear rotation and the shear rotation determined by $S_{U,SDI}^{*}/G^{'}$ respectively. The load parameters for all the SD tests are listed in Table 4.5.

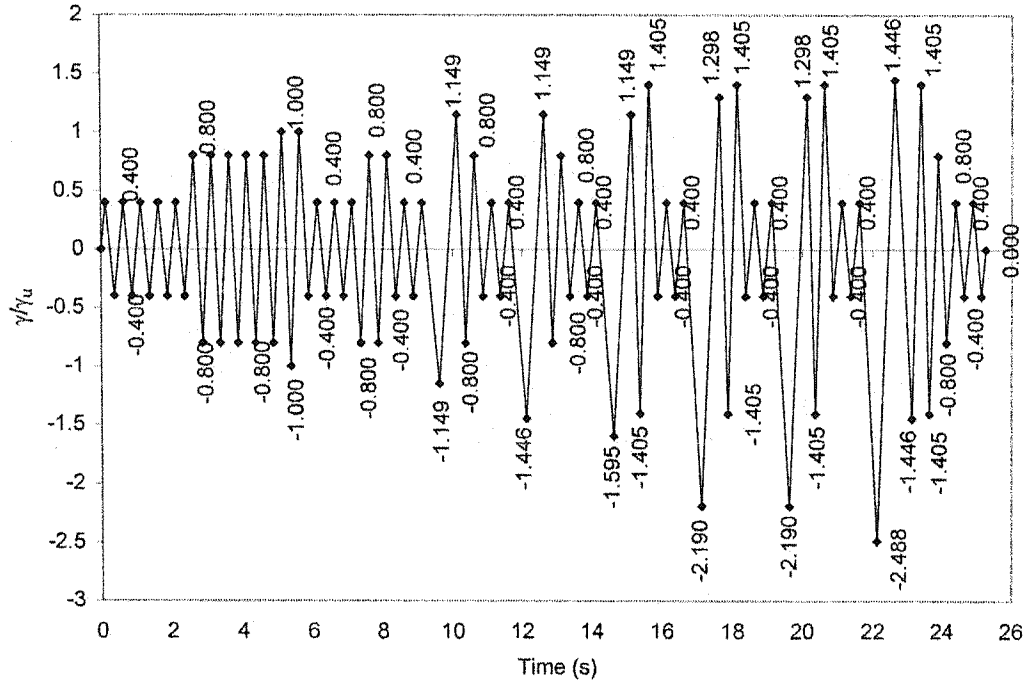

Figure 4.40. SD load protocol (Test 40), sine wave

Table 4.5 Load references used in tests

Test	Parameters in evaluation			Loading references		Time duration
	$S_{U,SDI}^{*}$ (kN/m)	G' (kN/mm)	Ratio γ_2/γ_u	γ_u (rad/1000)	γ_2 (rad/1000)	(s)
38	13.50	4.18	2.04	3.23	6.60	25.25
40	11.65	1.73	1.81	6.72	12.17	504.80
42	12.78	1.65	1.35	7.73	10.46	25.29
48	9.39	0.80	1.01	13.14	13.33	467.80

Note: The value of Test #38 (Buildex connectors) is from Test #34 (Hilti connectors) of Martin (2002).

For test 38 and test 42, the frequency of the load signal was 2 Hz, which results in a time duration of around 25.25 seconds. For tests 40 and 48, the loading equipment was not able to follow the required SD signal at such high frequency cycles. Because of this difficulty with the hydraulic system, it was necessary to adjust the cyclic frequency to 0.1 Hz for test 40, and for this reason the time of testing increased to 504.8 seconds. A similar situation occurred for test 48, which includes two load phases. In the first phase (41.1 sec), the frequency of load signal was 0.2 Hz, and in the second load phase it was changed to 0.1 Hz.

4.1.7.3 Cyclic plus monotonic load

Cyclic testing was included in the program in order to consider the effect of wind induced load and stiffness degradation. An expected wind service load was determined based on the SDI (1987) predictions of strength:

$$P_u=S_u*L \tag{4.3}$$

Based on the SDI calculations, an S_u value of 12.6 kN/m was obtained, which resulted in an expected load P_u=76.81 kN for the specimen length of 6.096 m.

When a safety factor of 2.5 is utilized to obtain the service wind load level, a target shear load of 0.4 P_u = 30.7 kN is obtained. In addition to cycles at this load level, elastic cycles at 0.2 P_u and larger cycles at 0.6 P_u were included in the test protocol, as shown below. The frequency of testing was set at a constant 0.5 Hz.

- 150 cycles $0.2P_u$=15.36 kN
- 50 cycles $0.4P_u$=30.72 kN

- 2 cycles $0.6P_u$=46.08 kN
- 50 cycles $0.4P_u$=30.72 kN
- 2 cycles $0.6P_u$=46.08 kN
- 50 cycles $0.4P_u$=30.72 kN
- 150 cycles $0.2P_u$=15.36 kN
- Monotonic to failure

where:

1. 150 cycles at $0.2P_u$ represent an expected frequent low wind vibration. It is to consider the influence of long time low wind load on the stiffness of structure.
2. $0.4P_u$ represents the service wind load per 30 years.
3. $0.6P_u$ represents the factored wind load per 30 years.
4. After cyclic loading had finished, a monotonic protocol was implemented to complete the test. The cyclic protocol was completed under force control, whereas the monotonic protocol was run under displacement control.

4.2 ANAYLSIS OF TEST RESULTS

4.2.1 Summary of SDI estimation and test results

According to Rogers and Tremblay (2000), the SDI equations for connection strength and stiffness provide the most accurate predictions with the least scatter of data with respect to diaphragm behaviour. The parameters that will be used as part of the SDI estimates of strength and stiffness are listed in Table 4.6.

Table 4.6 Input parameters for SDI equations

Test number		38	39, 40	41, 42	43~ 46	47, 48	49
		P3615	P3615	P3615	P3615	P2436	P2436
Sheet thickness	mm	0.91	0.76	0.76	0.76	0.76	0.91
Yield limit	MPa	230	230	230	230	230	230
Strength limit	MPa	310	310	310	310	310	310
Young's Modules	MPa	203000	203000	203000	203000	203000	203000
Deck							
Depth	mm	38.1	38.1	38.1	38.1	76.2	76.2
Web height (inclined)	mm	40.16	40.16	40.16	40.16	77.25	77.25
Horizontal width of one wave	mm	152.4	152.4	152.4	152.4	152.4	152.4
Half width of base flange	mm	19.05	19.05	19.05	19.05	19.05	19.05
Width of top flange	mm	88.9	88.9	88.9	88.9	88.9	88.9
Horizontal projection of web	mm	12.7	12.7	12.7	12.7	12.7	12.7
Extended width of one wave	mm	207.32	207.32	207.32	207.32	281.50	281.50
Sheet width	mm	914	914	914	914	610	610
Sheet length	mm	6096	3048	3048	6096	6096	6096
Number of Joists		3	1	1	3	3	3
Joist spacing		1524	1524	1524	1524	1524	1524
Effective moment of inertia	mm^4/m	258000	214000	214000	214000	1001000	1189000
Connectors							
Deck-to-frame strength	kN	7.665	6.681	7.84	6.681	7.84	9.29
Deck-to-frame flexibility	mm/kN	0.0754	0.0416	0.038	0.0416	0.0427	0.0347
Side lap strength	kN	4.534	3.23	0.96	3.23	0.83	1.37
Side lap flexibility	mm/kN	0.0905	0.099	0.9903	0.099	1.0204	0.905
No. of ribs between connectors	n_pas	2	2	2	2	2	2
$\Sigma(x_e/w)$ on end joists	α_1	1.333	1.333	1.333	1.333	1	0.5
$\Sigma(x_p/w)$ on intermediate joists	α_2	1.333	1.333	1.333	1.333	1	0.5
$\Sigma(x_e/w)^2$ on end joists	$\Sigma(x_e/w)^2$	0.556	0.556	0.556	0.556	0.5	0.5
$\Sigma(x_p/w)^2$ on intermediate joists	$\Sigma(x_p/w)^2$	0.556	0.556	0.556	0.556	0.5	0.5
Average number of connections over sheet width	n_v	3.25	3	4	3.5	3	3
Number of Connections on end beams except joists	n_e	16	8	8	16	16	16
Number of side lap connections	n_s	16	8	8	16	16	16

In Table 4.6, deck parameters are quoted from product brochures (Canam, 1999). Connection parameters are from Section 4.1.6. Other parameters are obtained from the SDI manual (1987). It is noted that, the nominal material properties were used in the estimation of the strength and stiffness of the diaphragm. This approach was followed such that a comparison with other test investigations such as that carried by Essa et al (2001) and Martin (2002) could be made. It is also because that the connection properties found in the manufacturer's catalogue are given for nominal sheet values.

The results of the SDI predictions are listed in Table 4.7, where S_u is the ultimate shear strength and G' is the diaphragm shear stiffness. The difference between "SDI" and "SDI*" is only in the connection properties, more precisely the connection strength and connection flexibility. For "SDI", the connection properties are obtained from the Diaphragm Design Manual (SDI, 1987). For "SDI*", these properties are from the test results by Rogers and Tremblay (2000).

It should be stated that for nail/screw (NS) connected decks, the S_u and G' for the SDI prediction are larger than that of the SDI* because the connection strength and connection stiffness of SDI are higher. While for the weld/button punch (WB) connected decks, the situation is reversed. The P2436 panels can resist higher vertical loads due to their greater section depth, however they exhibit a smaller in-plane shear strength and stiffness compared with P3615 panels. The longitudinal overlapped diaphragm has similar shear strength but a much smaller shear stiffness as compared to a full-length diaphragm (test 39 *vs.* test 43).

Table 4.7 SDI and SDI* predicted results

Group	Test number	SDI		SDI*	
		S_u	G'	S_u	G'
		kN/m	kN/mm	kN/m	kN/mm
1	38-91-6-NS-SD-38	15.53	5.35	13.15	4.46
2	38-76-3-NS-M-39	12.81	1.70	11.20	1.61
	38-76-3-NS-SD-40	12.81	1.70	11.20	1.61
	38-76-3-WB-M-41	10.17	1.62	12.78	1.60
	38-76-3-WB-SD-42	10.17	1.62	12.78	1.60
3	38-76-6-NS-M-43	12.59	3.65	10.83	3.11
	38-76-6-NS-C-44	12.59	3.65	10.83	3.11
	38-76-6-NS-M-R-45	12.59	3.65	10.83	3.11
	38-76-6-NS-C-R-46	12.59	3.65	10.83	3.11
4	75-76-6-WB-M-47	7.68	1.21	9.39	1.19
	75-76-6-WB-SD-48	7.68	1.21	9.39	1.19
	75-91-6-WB-M-49	10.21	1.58	13.02	1.23

Note: The values listed for tests 45 and 46 are based on a bare sheet diaphragm.

Table 4.8 provides a comparison of the measured to predicted shear stiffness and strength for the test specimens. The measured G' for the short duration tests is from the first cycle ($0.4\gamma_u$). For the cyclic loaded tests, G' was obtained from the monotonic test that was run after the cyclic protocol.

Table 4.8 Test results and comparison with SDI and SDI* predictions

GROUP	Description	Test number	Test result		Ratio			
			Su	G'	Su	G'	Su	G'
			kN/m	kN/mm	Test/SDI	Test/SDI	Test/SDI*	Test/SDI*
1	Buildex nail	38	15.25	3.52	0.98	0.66	1.16	0.79
2	Longitudinal overlapped	39	11.28	1.73	0.88	1.02	1.01	1.08
		40	12.68	1.58	0.99	0.93	1.13	0.98
		41	9.14	1.65	0.90	1.02	0.72	1.03
		42	10.29	1.55	1.01	0.95	0.81	0.97
3	Bare sheet	43	13.40	2.58	1.06	0.71	1.24	0.83
		44	10.47	2.85	0.83	0.78	0.97	0.91
	With roofing	**45**	**15.60**	**4.17**	**1.24**	**1.14**	**1.44**	**1.34**
		46	**15.90**	**3.90**	**1.26**	**1.07**	**1.47**	**1.25**
4	New profile	47	7.27	0.80	0.95	0.66	0.77	0.68
		48	7.02	0.72	0.91	0.60	0.75	0.61
		49	8.58	1.06	0.84	0.67	0.66	0.85
Maximum					1.26	1.14	1.47	1.34
Minimum					0.84	0.60	0.66	0.61
Diaphragm with bare sheets			Mean		0.94	0.80	0.92	0.87
			C.o.V.		0.08	0.21	0.23	0.17
Diaphragm with Nail and Screw connection			Mean		0.95	0.82	1.10	0.92
			C.o.V.		0.10	0.19	0.10	0.13
Diaphragm with Weld and Button punch connection			Mean		0.92	0.78	0.74	0.83
			C.o.V.		0.07	0.25	0.08	0.22

Note: 1) Test 45 and test 46 are not included in the statistical results due to the non-structural roofing components.

2) "Mean" is the average of test results; "C.o.V." is the coefficient of variation, which equals to standard deviation/mean.

In Table 4.8, the maximum test/SDI for S_u is 1.26 and for G' is 1.14; the maximum test/SDI* for S_u is 1.47 and for G' is 1.34. These values are from tests 45 and 46, the specimens that were constructed with roofing materials. The reinforcing effect of the non-structural components is quite remarkable, especially compared to test 43 and 44. For this reason, tests 45 and 46 were not included in the statistical data because of the significant influence of the non-structural components. It seemed that during the loading process, the gypsum board, which is quite rigid in its plane, greatly restrained the warping of the panels. This warping restraint directly increased the shear stiffness, and indirectly reduced the stress in the fasteners, and thus helped to increase the strength at the same time.

The minimum ratio values are from test 48 and test 49. It seems the SDI and SDI* over-estimate the diaphragm capacity for this deck profile P2436. One possible reason is the weld quality, the deeper rib but same flute width made it more difficult to do the welding.

For bare sheet diaphragm tests, the average test/SDI and the average test/SDI* for S_u and G' are higher and more consistent for NS connected diaphragms than WB connected ones, because the installation quality for NS connections is easier to control.

A more detailed discussion about each test is provided in the following sections.

4.2.2 Group 1

4.2.2.1 Test 38

Group 1 consisted of only one short duration test (38) for which the specimen was constructed with Buildex fasteners. No related monotonic test was executed, hence the load protocol was borrowed from Test 34 (Hilti fasteners), an earlier test by Martin (2002). A description of tests 38 & 34, which were constructed with sheet steel panels from the same coil, is found in Table 4.9.

A listing of the connection quality is provided in Appendix 2. The nail head standoff for each fastener was measured, and if found between 5.0 to 9.5 mm the installation was considered as adequate. The nails whose height was out of this range were removed and replaced. Usually, the reason for inadequate nail penetration was because the fastener was placed in the same position as a nail in a previous test. The average nail head standoff was 7.86 mm, with a C.o.V. of 0.12. The installation quality of test 38 was similar to that of test 34.

Table 4.9 Test specimen descriptions (Tests 38 & 34)

Steel properties:	
Supplier and coil number	Canam P-3615 B deck 0.91 mm Coil supplier: Sorevco Coil number: 147624
Base metal thickness (mm)	0.88
F_y measured (MPa)	319
F_u measured (MPa)	394
E measured (MPa)	210000
50 mm gauge length elongation	24 %
Fasteners:	Spacing: 305 mm c/c
Test 38	Nail stand-off: Total Avg.: 7.86 mm C.o.V.: 0.12 At sidelaps Avg.: 8.28mm C.o.V.: 0.12 Except sidelaps Avg.: 7.70 mm C.o.V.: 0.13
	Side-lap fasteners: Buildex Screws 12- 14 x 1 HWH TEK/3
	Deck-to-frame fasteners: Buildex BX-14 nails
Test 34 (Martin, 2002)	Nail stand-off: Total Avg.: 7.0 mm C.o.V.: 0.13 At sidelaps Avg.: 8.1 mm C.o.V.: 0.15 Except sidelaps Avg.: 6.8 mm C.o.V.: 0.10 4 nails (J6, J16, L21 and M1) were not properly installed at first and were replaced.
	Side-lap fasteners: Screws 12- 14 x 1 HWH#1 FP Lot number: 9901-0019
	Deck-to-frame fasteners: Hilti nail X-EDNK-22 THQ 12M Lot number: 413923 (test 19), 413920 (tests 34 and 35)

The time history and shear load *vs.* rotation hysteresis results of Test #38 are shown in Fig. 4.41. The time history of imposed distortions, γ, on the specimen is the same as that of test 34. For the first run, the maximum load reached 92.95 kN, or given as an ultimate load per unit length $S_{u,SD}$=15.25 kN/m. This value is near to the predicted $S_{u,SDI}$ (15.53 kN/m) yet significantly higher than the predicted S_{u,SDI^*} (13.15 kN/m). The ultimate load per unit length $S_{u,SD}$ occurred in the second phase of the protocol, that is West R_d=2.0, at a distortion level, γ, of 5.89 rad/1000. The maximum shear distortion reached during the test was 12.88 rad/1000.

Each short duration test was run for a second time in order to evaluate the post earthquake resistance and stiffness of the diaphragm. During run 2 the shear load reached a maximum of 60.24 kN ($S_{u,SD}$=9.88 kN/m). The residual resistance of this specimen was small, as can be seen in time history of $E_H/S_{u,SD}$, which shows the relative energy dissipated by inelastic deformations. In addition, the $S/S_{u,SD}$ time history shows that during the small amplitude cycles almost no shear capacity was measured, a result of the slotted bearing deformations around the nail and screw fasteners which did not allow for a bearing resistance to develop until large deformations were imposed. Significant pinching of both the Run 1 and 2 hystereses also gives evidence of this bearing slot behaviour at the nailed and screwed connections.

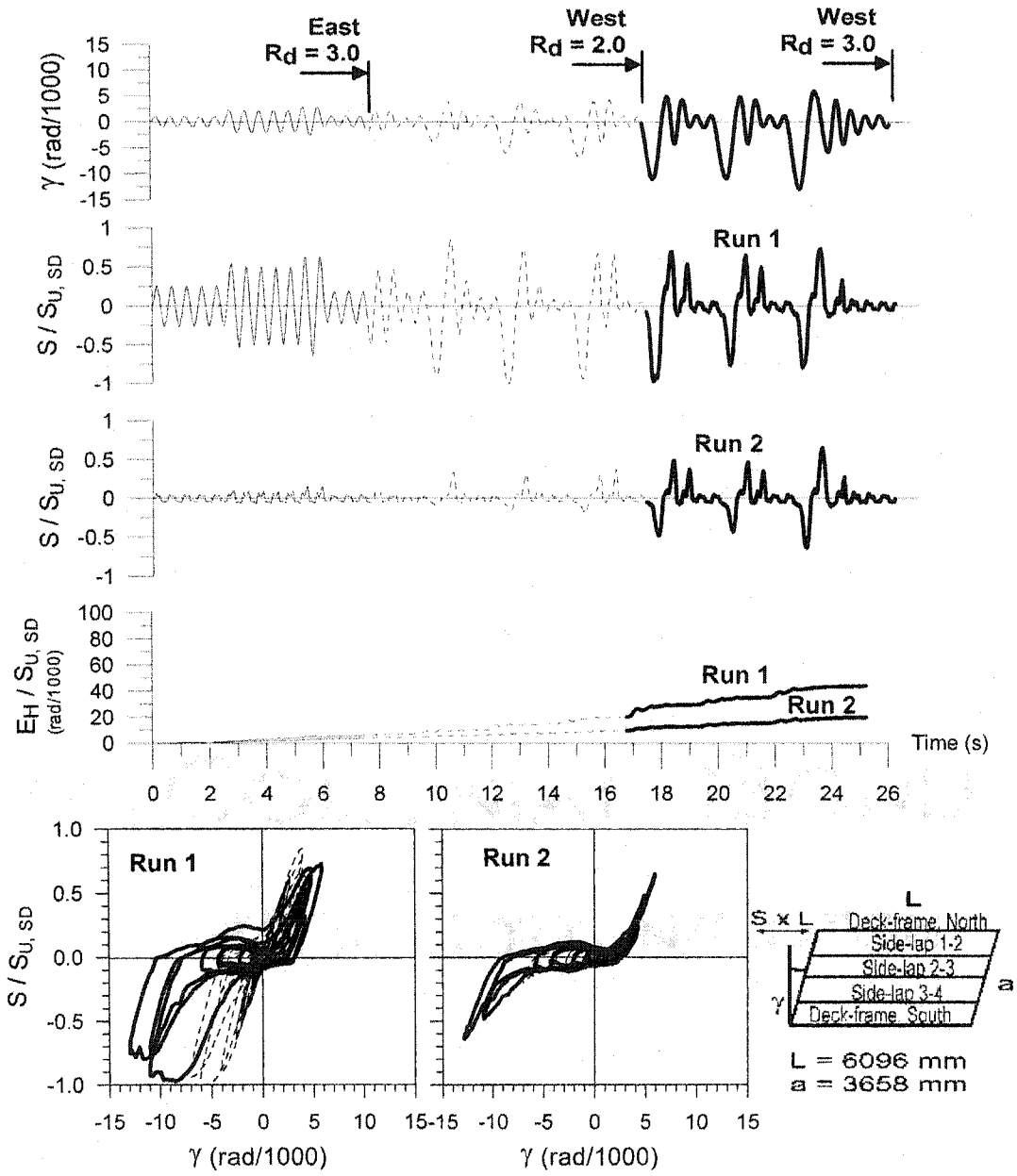

Test No. 38

P3615 - 0.91 mm
Sidelap fasteners : Screws @ 305 Frame fasteners : Buildex nails @ 305
*S_u , SDI * = 13.15 kN/m S_u , SD = 15.25 kN/m*

Figure 4.41. Time history & hysteresis results of Test #38

The three phases of the S *vs.* γ hysteresis of Run 1 for test 38 are shown in Figure 4.42. During the East R_d = 3.0 phase the load-deformation behaviour is almost linear. The shear resistance reached its maximum in the second phase (West R_d=2.0). Pinching of the hysteresis occurred in this phase and became quite evident in phase 3 (West R_d=3.0). "*Pinching is the double change in curvature of the load-deflection curve occurring with half a cycle*" (Essa *et al.*, 2001). As noted above, this pinching behaviour most likely occurred due to the enlargement of the fastener holes during cyclic loading.

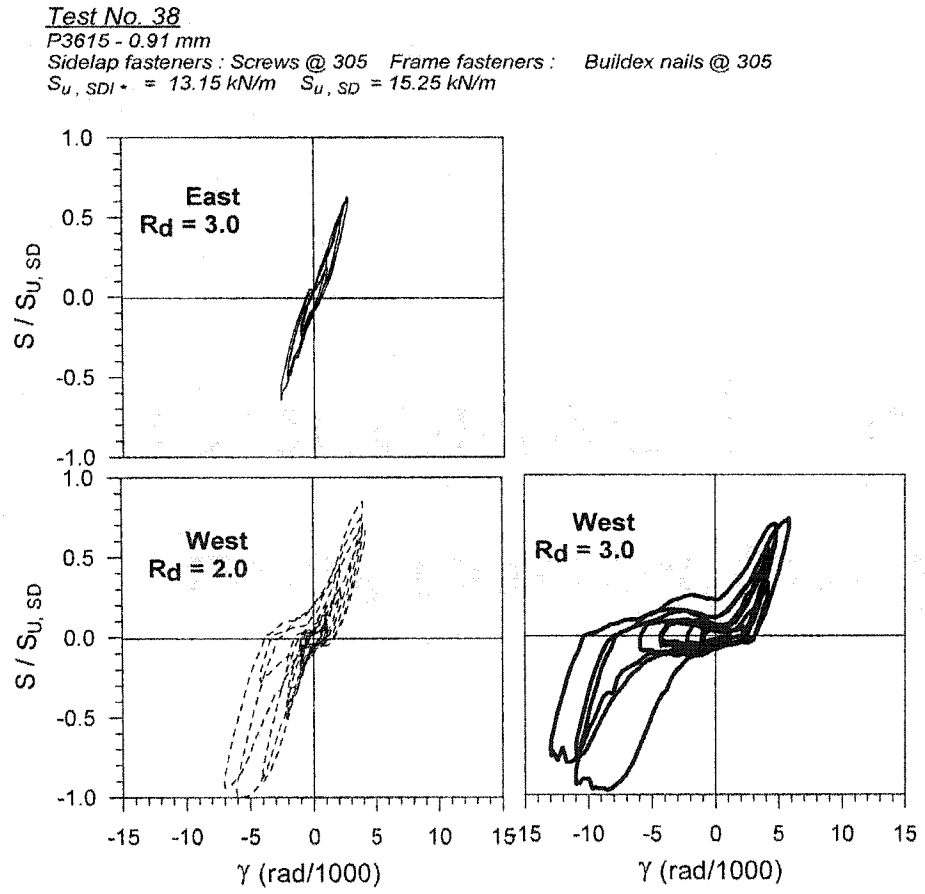

Figure 4.42. Hysteresis results of Test #38 (Run 1)

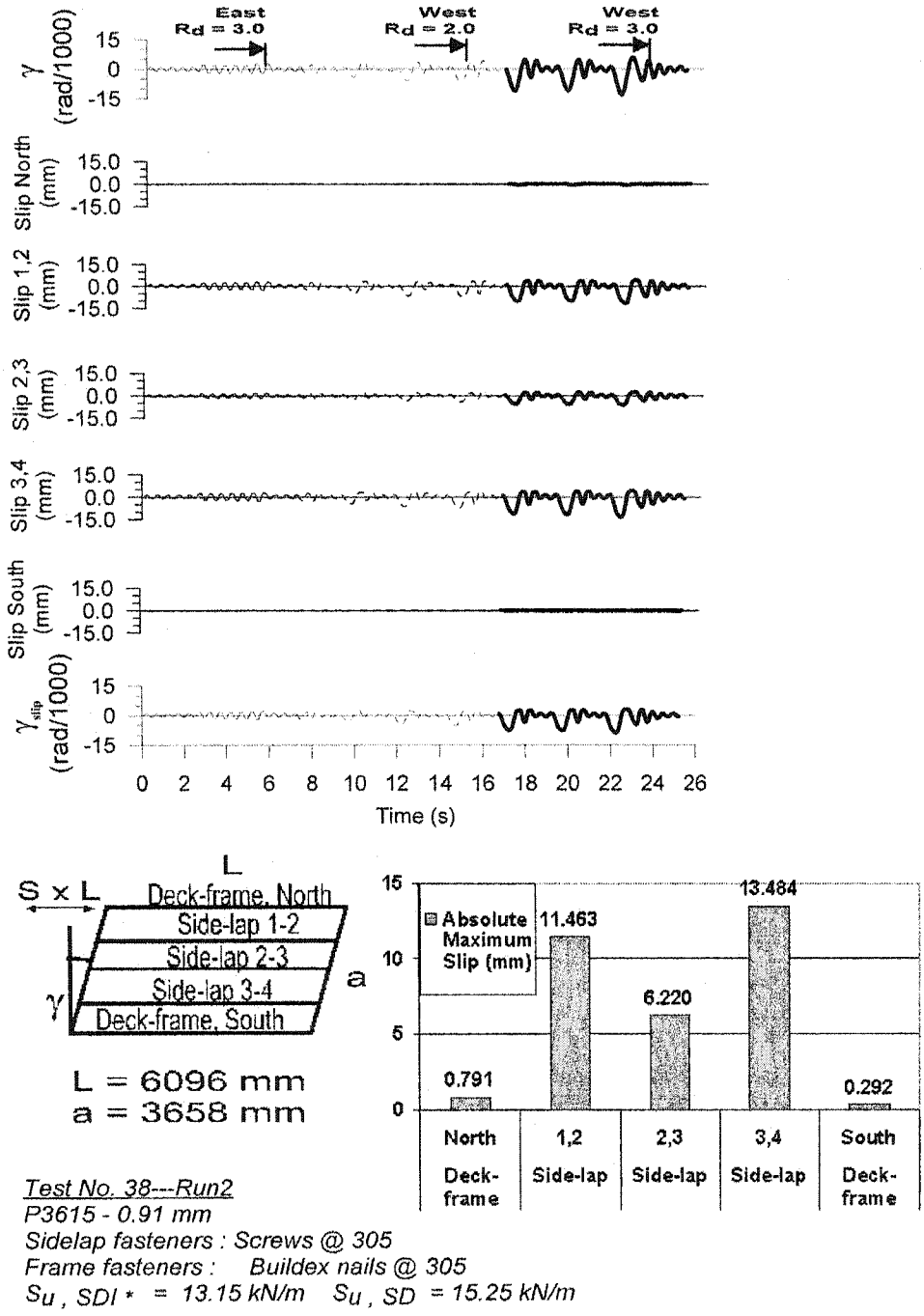

Figure 4.43. Time history slip results of Test #38 (Run 2)

Measurements of the deck-to-frame and deck-to-deck slips for Run 2 are shown in Figure 4.43, since the values for Run 1 are not available due problems experienced with the data acquisition system. It is noted that, the deck-to-frame slip (Slip north and Slip south) are very small, less than 1mm, because all of the connections were nails, which are much stronger and more rigid than screws. The most extensive side-lap slip occurred between sheets 3 and 4, where a value of 13.48 mm was recorded. The γ_{slip} is the distortion due to slip, which equals the total slip deformation divided by the deck width. The maximum slip distortion was calculated to be 8.79 rad/1000, which constitutes approximately 68% of the maximum of total distortion calculated from Δ_{max}/a, which equals to 12.88 rad/1000, and it illustrated that, the distortion from slips between sheets dominates the shear deformations.

Table 4.10: Failure modes of the deck-to-frame connections after Run 1

Position	1		6		11		16		21
B									
C	BE		BE		BE				BE
D	BE+BU		BE		BE		BE		BE+BU
E			BE						
F									
G	BU		BE		BE		BE		BU
H									
I									
J	BE+BU+TE		BE		BE		BE		BU
K	BE		BE		BE		BE		BE
L									

Note:

1. BE--Bearing failure; BU--Buckling failure; TE--Tearing failure
2. The grid lines of D, G, and J are side laps

After the first short duration test was run, a survey of the diaphragm specimen was carried out, with the aim of recording the extent and type of damage (Table 4.10). The observed failure modes around deck-to-frame connections included bearing failures, buckling failures and tearing failures of the sheet steel. Nail shear failure was not observed, which means that the fastener is stronger than the surrounding steel sheets. Photographs of these failure modes can be seen in Figures 4.44 to 4.48, where Figure 4.44 shows a typical bearing failure of steel sheet around a nail that is not at the sheet ends. Figure 4.45 to 4.46 give the both bearing and buckling failure which typically occurred at the sheet ends. It is noted in Figure 4.45 that, the original nail at D1 was removed and re-installed because of inadequate nail penetration.

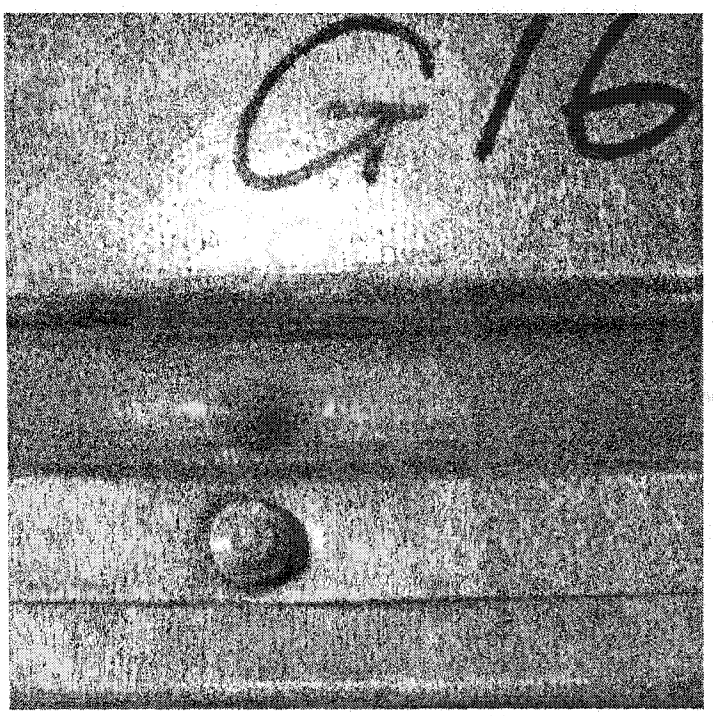

Figure 4.44. Bearing of steel sheet around nail G16

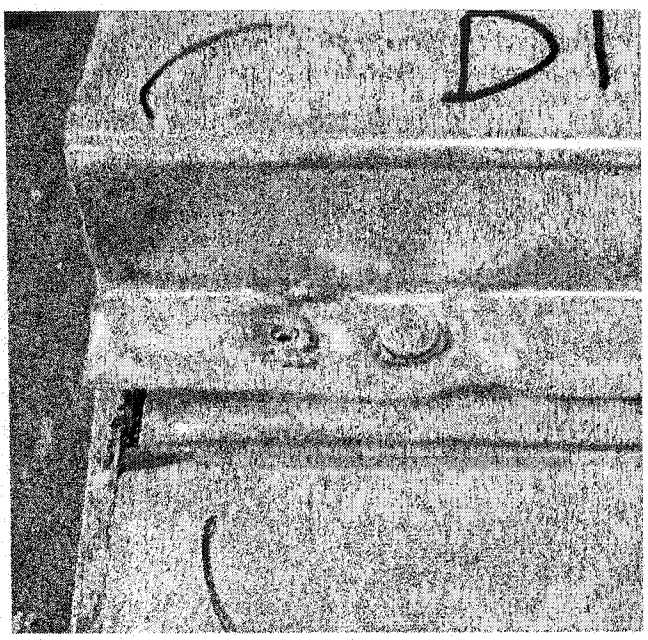

Figure 4.45. Bearing and buckling of steel sheet around nail D1

Figure 4.46. Buckling of steel sheet around nail J21

Under the cyclic load protocol, the extreme result of bearing and buckling is the tearing failure, which is shown in Figure 4.47 and 4.48 for nail position J1.

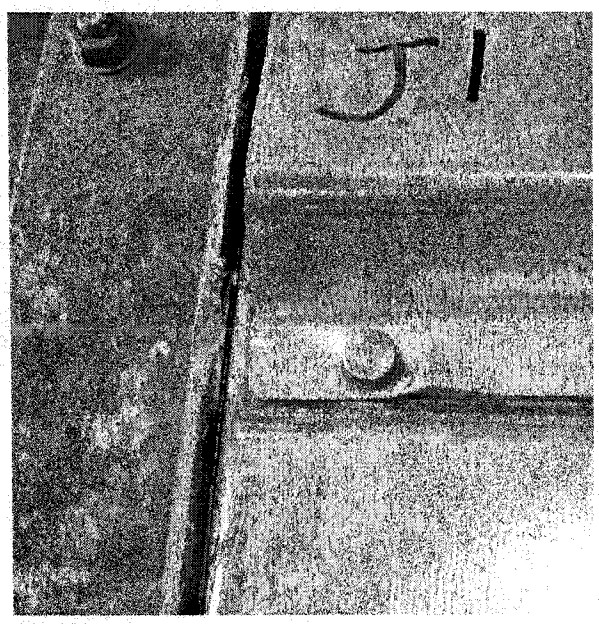

Figure 4.47. Bearing and buckling of steel sheet around nail J1 (during test)

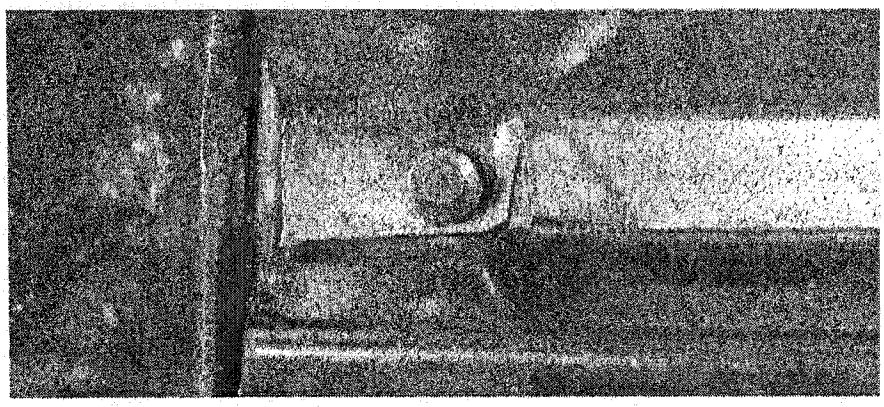

Figure 4.48. Bearing, buckling and tearing of steel sheet around nail J1 (after test).

All of the side-lap screw connections experienced a combination of tilting and bearing failure (Figure 4.49). The screw holes became enlarged (Figure 4.50) during the dynamic test, which resulted in the pinching behaviour noted previously.

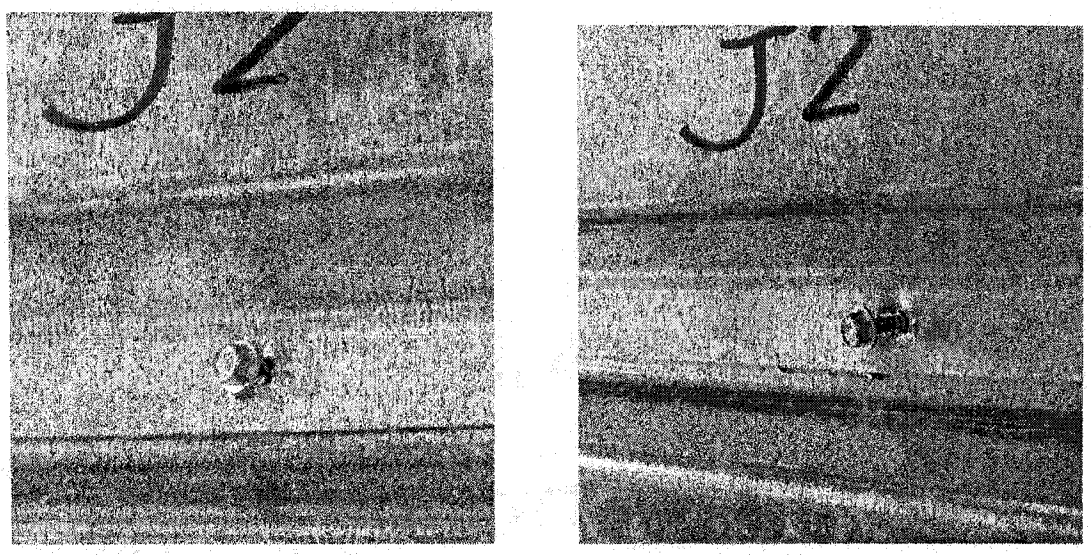

a) During test b) After test

Figure 4.49. Tilting of screw J2

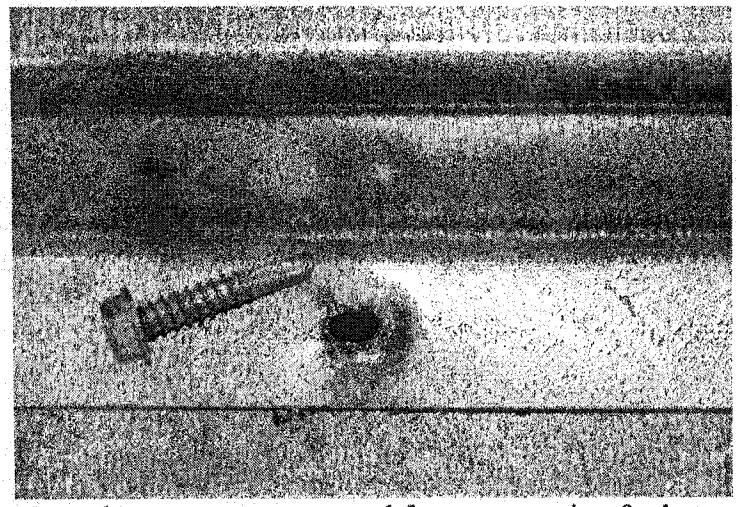

Note: the screw was removed from connection for better observation

Figure 4.50. Hole enlargement at screw J19

4.2.2.2 Comparison of test 38 with previous tests

A comparison of past large-scale test diaphragms constructed with nail-screw connections spaced at 12" and having the same deck panels is presented in this section. The results of tests 17, 18, 19, 34, 35 and 38 are listed in Table 4.11. Tests 17 and 18 were completed by Essa *et al.* (2001), while tests 19, 34 and 35 were carried out by Martin (2002). The only difference in construction lies in the manufacturer of the fasteners, where for test 38 nails and screws from ITW Buildex were used, and in all others tests Hilti products were specified.

Compared with the majority of other diaphragm specimens of similar construction, test 38 has a smaller stiffness but a similar strength. The reason may be that, from connection tests carried by Rogers and Tremblay (2000), the shear stiffness for 0.91 mm deck-to-frame is 18.7 kN/mm for ITW BX-14 nails, but 23.9 kN/mm for Hilti X-EDNK22-THQ12 nails, the former is smaller than the later. It is also noted that the shear strength for these two nails is similar.

In terms of the predictability of strength the SDI method is nearly correct, however the SDI* method seems somewhat conservative. The stiffness predictions are over estimated for both approaches, but that from SDI* appears closer to the test results. In addition, the behaviour of all the nail-screw diaphragm specimens was similar in that it was controlled by bearing strength and stiffness of the deck-to-frame nail connections and the bearing-tilting strength and stiffness of the side-lap screw connections.

Table 4.11: Comparison of test 38 with earlier nail-screw diaphragm specimens

Test number	Test result		Ratio			
	Su	G'	Su	G'	Su	G'
	KN/m	KN/mm	Test/SDI	Test/SDI	Test/SDI*	Test/SDI*
38-91-6-NS-M-17	14.63	4.22	0.91	0.80	1.08	0.96
38-91-6-NS-Q-18	15.62	4.76	0.98	0.90	1.16	1.08
38-91-6-NS-M-19	16.70	4.13	1.07	0.75	1.24	0.91
38-91-6-NS-SD-34	17.00	4.01	1.09	0.73	1.26	0.89
38-91-6-NS-LD-35	17.30	3.90	1.11	0.71	1.28	0.86
Mean 1 (Test 17, 18, 19, 34, 35)	**16.25**	**4.20**	**1.03**	**0.78**	**1.20**	**0.94**
C.o.V. of above tests	0.07	0.08	0.08	0.10	0.07	0.09
38-91-6-NS-SD-38	15.25	3.52	0.98	0.66	1.16	0.79
Test 38 / Mean 1	**0.94**	**0.84**	**0.95**	**0.85**	**0.96**	**0.84**

4.2.3 Group 2

Group 2 consisted of four tests that vary in the connection method (Nail/Screw *vs.* Weld/Button Punch) and the load type (Monotonic *vs.* Short Duration seismic load).

4.2.3.1 Test 39

Specimen 39 comprised a monotonic test of a diaphragm fastened with Hilti nails and screws. The results from this test were also used to prepare the protocol for test 40. The specimen description is shown in Table 4.12.

Table 4.12 Test specimen description (Tests 39 and 40)

Steel properties:	
Supplier and coil number	Canam P-3615 B deck 0.76 mm Coil supplier: Sorevco Coil number: 344057
Base metal thickness (mm)	0.70
F_y measured (MPa)	248
F_u measured (MPa)	327
E measured (MPa)	204000
50 mm gauge length elongation	32 %
Fasteners:	Spacing: 305 mm c/c
	Side-lap fasteners: Screw 12- 14 x 1 HWH#1 FP
	Deck-to-frame fasteners: Hilti nail X-EDNK-22 THQ 12M Four nails were not properly installed at first and were replaced

The slow loading process made it possible to observe the failure modes more closely while the test was in progress. The sequence of failure was as follows: At a shear load equal to 16.5 kN (S=2.7 kN/m) with a corresponding γ = 0.915 rad/1000, the overlapped sheets on gridline 11 began to separate vertically due to the extensive profile warping of the panel ends (Figure 4.51). Panel warping was also evident at the

outside ends of the panels (Figure 4.52). This type of deformation progressed as the applied shear deformation was increased further.

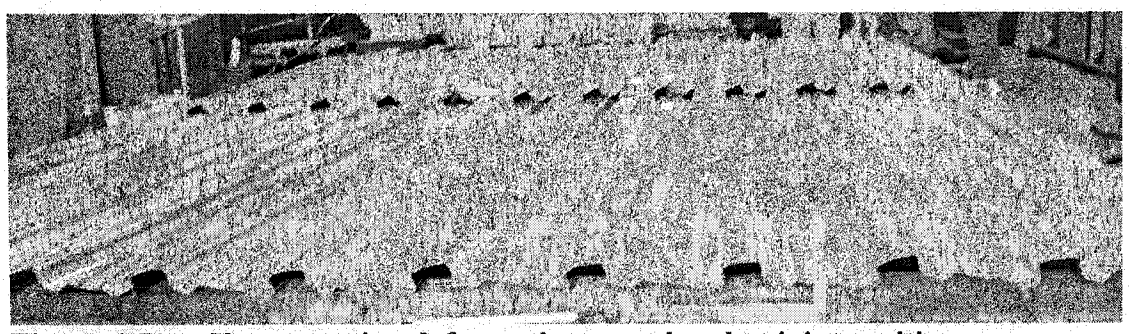

Figure 4.51. Sheet warping deformation at end and at joint position

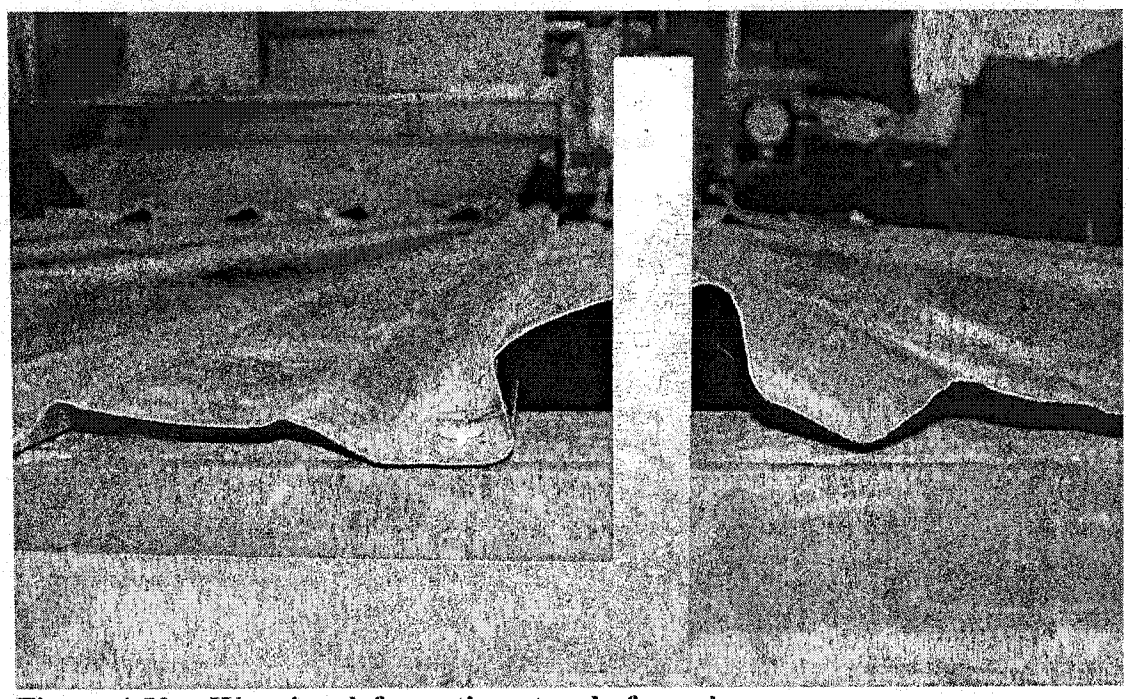

Figure 4.52. Warping deformation at end of panel

Once the applied load was equal to 67 kN (S = 10.99 kN/m) at a shear deformation of γ = 11.033 rad/1000, the side-lap screws began to exhibit a noticeable tilt. At a load of 68.70 kN (S=11.28 kN/m) and a deformation of γ = 12.18 rad/1000, the specimen

achieved its ultimate load, see Figure 4.53. At this peak level the nail at location C1 fractured in shear (Figure 4.54) and the load dropped to 63.55 kN ($S/S_{u,MON}$=0.925 in Figure 4.53).

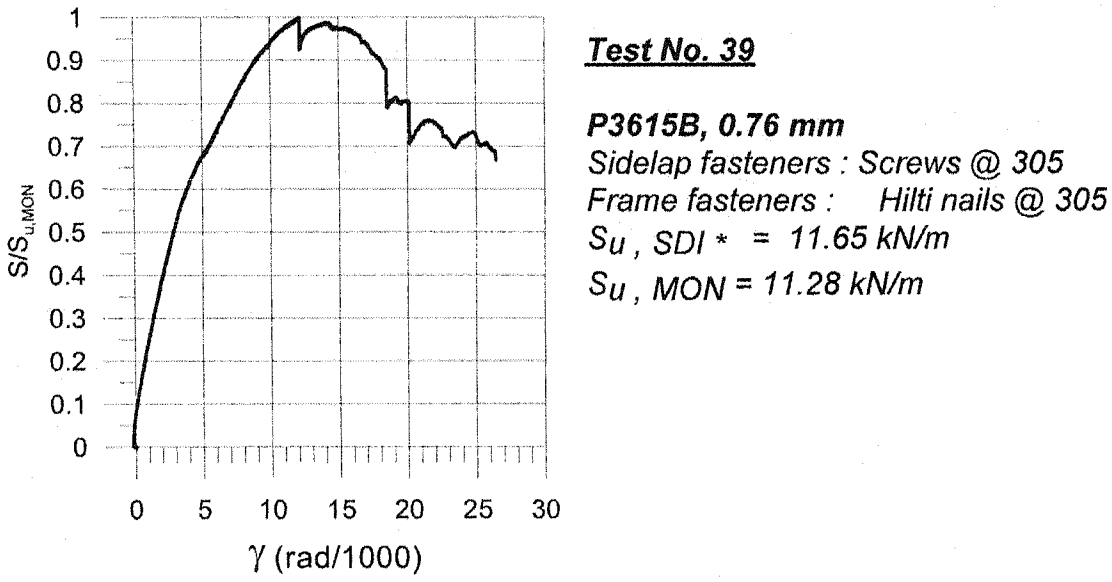

Figure 4.53. S-γ hysteresis for test 39

In Figure 4.53, the graph of the normalized shear load $S/S_{u,MON}$ vs. shear rotation γ shows that the stiffness changes from the range of 0 to 0.6 as compared with the range of 0.6 to 0.9. It is possible that, the east sheets, which are on top of west sheets, provided some restraint to the deformation when the load was less than 0.6Pu. The east sheets would then be stretched over the west sheets when the load exceeded 0.6Pu, as shown in Figure 4.55. As discussed in Section 4.1.7.2, the SD load was determined from the G' of a monotonic test. If this G' is over estimated, it will result

in a γ_u that is smaller than it should be. Hence the load protocol for the short duration (SD) test may be inaccurate, further discussion on this observation is provided for test 40.

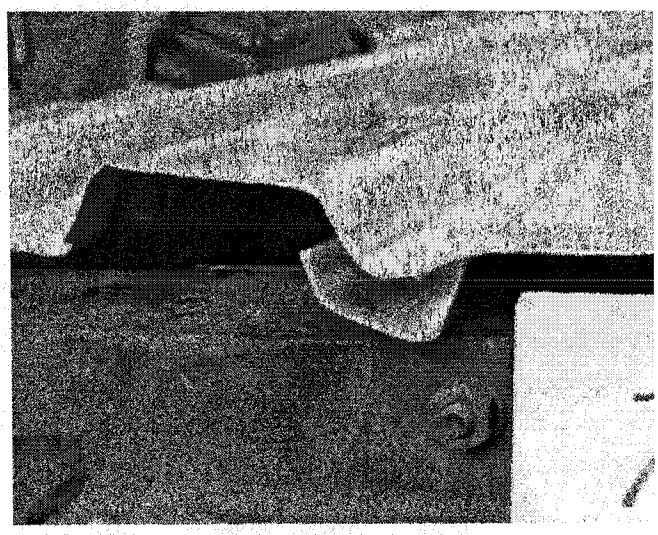

Figure 4.54. Fracture of nail C1 at side-lap C

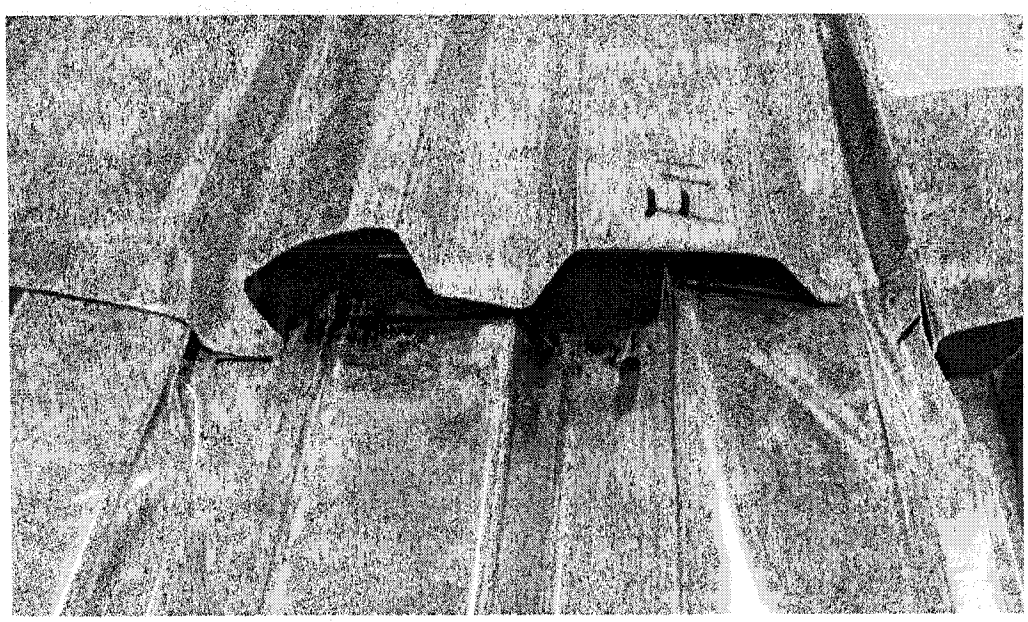

Figure 4.55. Nail shear at F11, and sheet deformation near F11

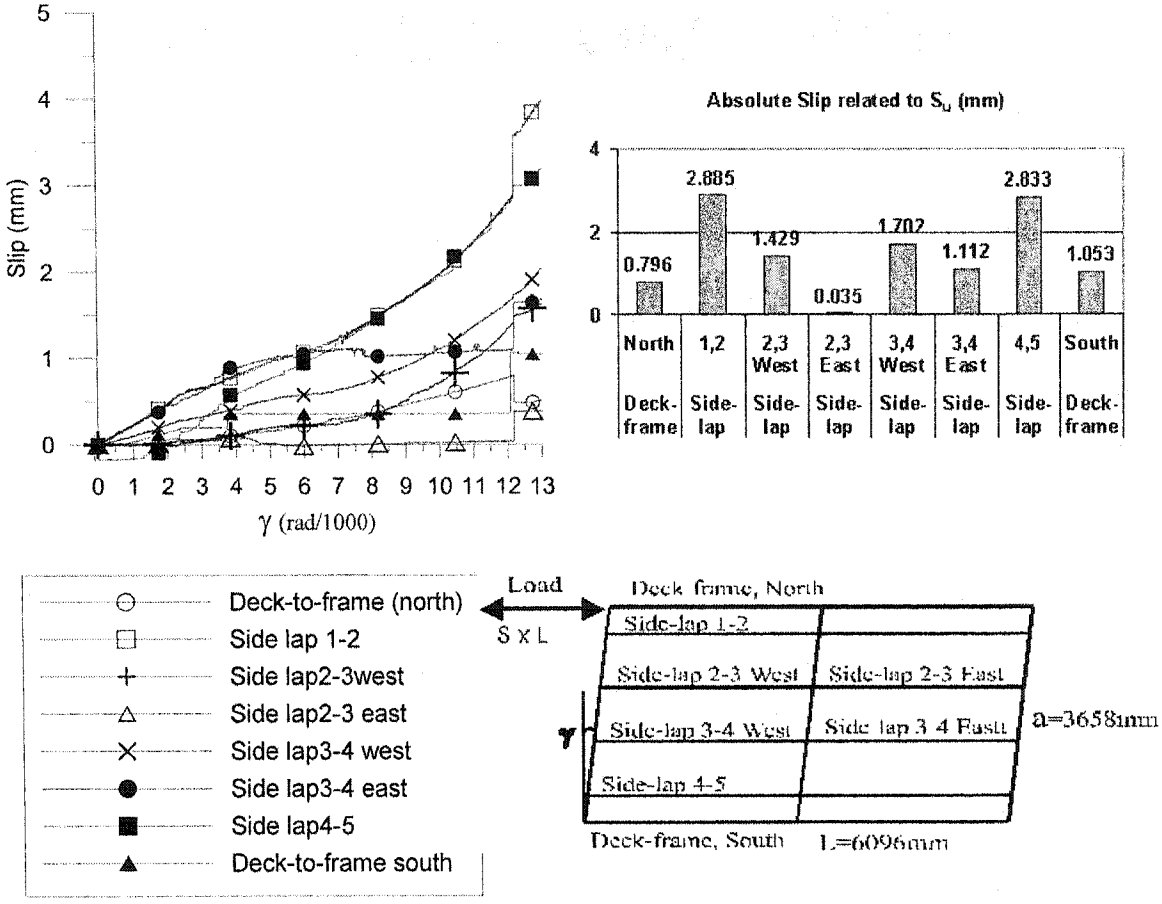

Test No. 39
P3615B, 0.76 mm
Sidelap fasteners : Screws @ 305 Frame fasteners : Hilti nails @ 305
*S_u , SDI * = 11.65 kN/m S_u , MON = 11.28 kN/m*

Figure 4.56. Slips of side laps and deck-to-frame connections for test 39

Figure 4.56 illustrates the slips at side laps and deck-to frame connections. It can be seen from this Figure that the slip measured along gridline C, *i.e.* the side-lap 1-2,

experienced a jump at γ_2=12.18 rad/1000 due to the loss of this nail fastener. In the Figure 4.56, the distribution of slips for each side laps at S_u was also given. The results showed that the deck-to-frame slips are smaller than the interior slips at side laps. The interior side lap slips are not uniform, even in the same side lap position, the slips have large differences in east and west sheets. For example, the slips at S_u for side-lap 3-4 west is 1.70 mm, while for side-lap 3-4 east is 1.11 mm, for side-lap 4-5 is 2.83 mm. The slip value at side lap 2-3 east is not correct due to the disorder of the instrument.

After the peak load was reached, the specimen then stabilized and was able to pick up shear capacity to 67.9 kN (S = 11.14 kN/m) with increasing displacement. During this rebound in shear resistance, more and more failures occurred, including sheet material damage and connection damage. A listing of the deck-to-frame failure modes is provided in Table 4.13. In total 5 nail shear failures were recorded, three of them were at the end lap and side-lap joist locations, *i.e.* at F11, I11 and L11. This may be due to the inferior connection quality because of 4 sheets overlapping together. This failure mode was not observed for the non-overlapped diaphragm tests, simply because there were no locations with four sheet steel layers (see Figure 4.55). It should be noted that significant deformation occurred in the sheet steel prior to shearing of the nails. Figures 4.57 & 4.58 show that steel sheets near the connections at both east and west ends of the specimen experienced substantial bearing and buckling distortion.

Table 4.13: The failure modes of Deck-to-Frame connections of test 39

Position	1		6		11		16		21
B	BE		BE		BE		BE		BE
C	**SH**		**BE**		**BE+BU**		**BE**		**BE+BU**
D									
E	BE		BE		BE		BE		BE
F	**BE+BU**		**SH**		**SH**		**BE+BU**		**BE**
G	BE		BE						
H	BE						BE		BE
I	**BE+BU**		**BE+BU**		**SH**		**BE**		**BE+BU**
J					BE+BU		BE		BE
K	BE				BE+BU		BE		BE
L	**BE+BU**		**BE**		**SH**				**BE+BU**
M	BE				BE				BE

BE--Bearing failure; BU--Buckling failure; TE--Tearing failure; SH--Nail shear

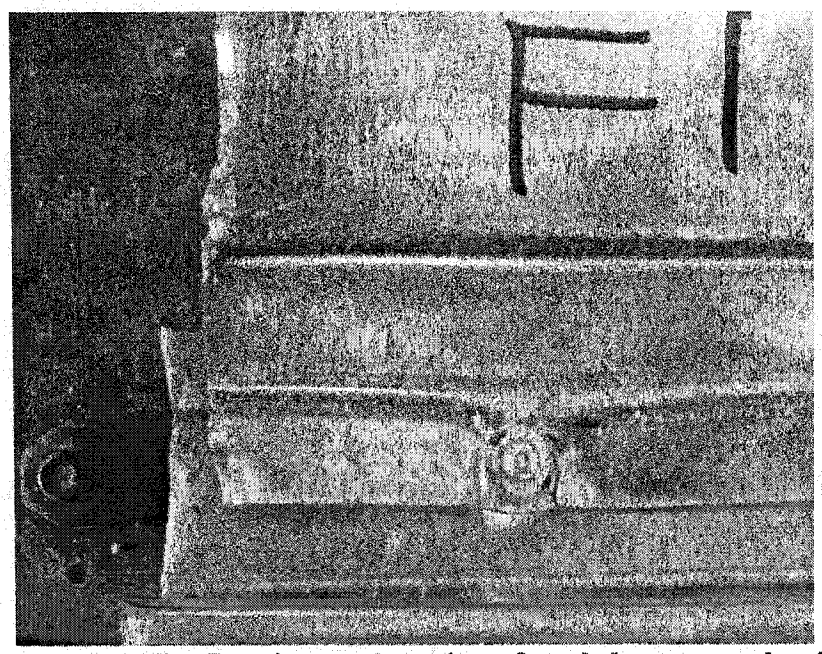

Figure 4.57. Bearing, and tearing of steel sheet around nail F1

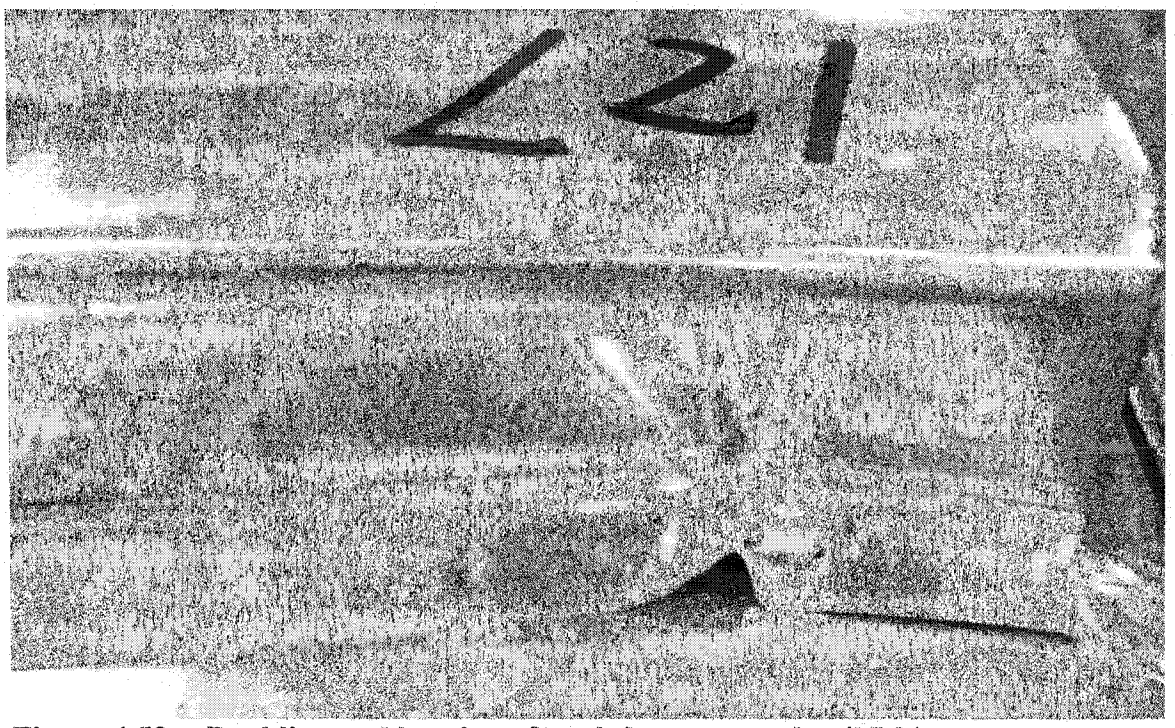

Figure 4.58. Buckling and bearing of steel sheets around nail L21

All side-lap screw connections experienced some degree of tilting failure and in a number of cases the screw itself had pulled out of the sheet steel because of the large deformations, e.g. the screws at C3, C4, C19, C20, and L12 (Figure 4.59 & 4.60). The extensive side-lap deformation may have been caused by shear failure of the deck-to-frame connection at location C1, after that the force was transferred to other connectors along the joint, including side-lap connections. Obvious screw hole enlargements can be viewed in Figures 4.59 and 4.60.

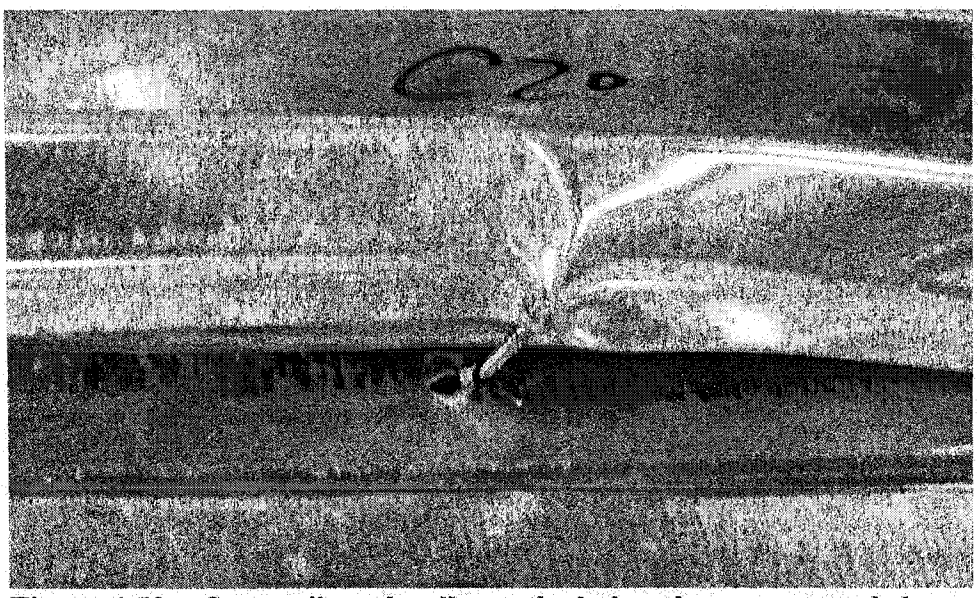

Figure 4.59. Screw tilt and pull out, the hole enlargement, and sheet deformation at C20

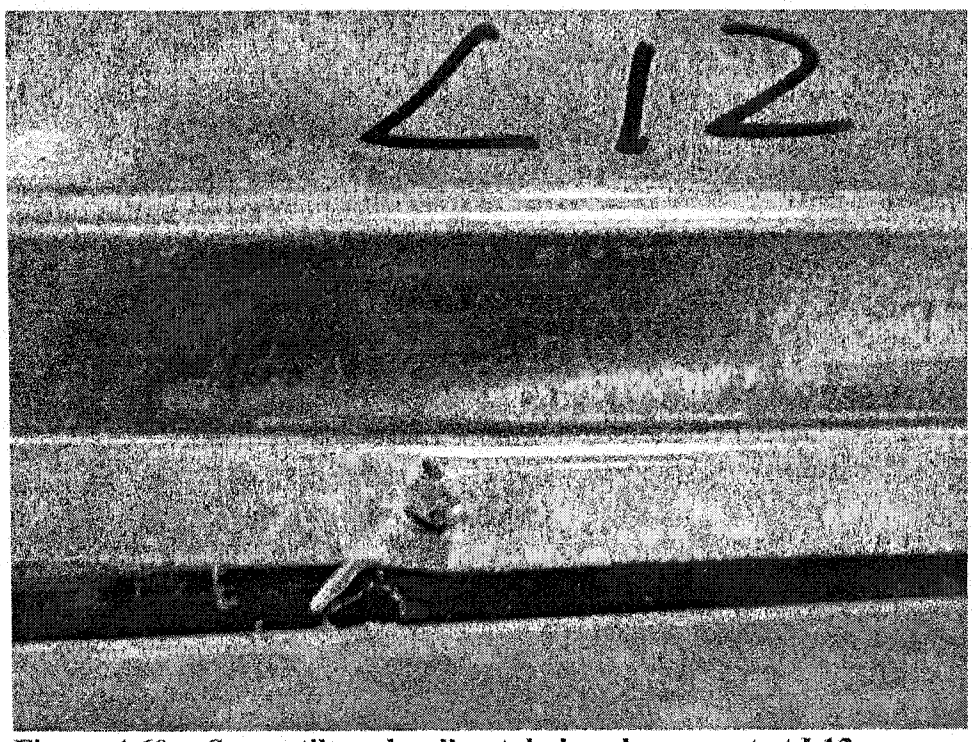

Figure 4.60. Screw tilt and pull out, hole enlargement at L12

4.2.3.2 Test 40

Test specimen 40, which had the same configuration as test 39, was subjected to a short duration (SD) loading protocol. The time history and hysteresis results have been provided in Figure. 4.61. The normalized shear force vs. shear rotation hysteresis is quite slim, which indicates that extensive plastic and non-linear deformations of the diaphragm did not take place. In addition, the normalized shear and energy time history plots for run 1 and 2 are similar. Furthermore, even after Run 2, most of the connectors had not been damaged.

Figure 4.62 shows the hysteresis of $S/S_{U,SD}$ to γ. The maximum unit shear force S_u was recorded in the third load phase (West R_d=3.0) instead of in the second load phase as in test 38. For the second load phase (West R_d=2.0) of Run 1, the relationship of $S/S_{U,SD}$ to γ is almost linear. It is surmised that the control parameters γ_2 and γ_u obtained from test 39 were of such a low value that test 40 was not forced to enter into the inelastic zone of behaviour. This is likely because the initial stiffness of the monotonic test 39 was used in the calculation of the cyclic amplitudes in test 40. In the case of overlap tests where two distinct stiffness are evident in the monotonic shear load vs. rotation graph, it is recommended that in future tests the second stiffness be accounted for in order to evaluate the inelastic performance of the diaphragm during a short duration test.

Figure 4.63 gives the time history of slips for load Run 1. One LVDT for slip measurement at side lap 3-4 went out of order during testing, causing the slip value become erroneous.

Prior to running the short duration protocol for a second time, all the LVDTs were inspected and adjusted when necessary, so the slip measurement in load Run 2 seems more logical (Figure 4.64). Similar to test 39, the exterior slips are quite small, the interior slips are not uniform (Figure 4.65), the slip at side lap 4-5 is remarkably larger than the other ones. This may be due to the installation qualities of the connections. In this test, the slips at east and west sheets of the same side lap positions appeared relatively uniform. The values of run 1 were omitted because the data is not correct.

The time history of the distortion contribution from the side-lap slips is also shown in Figure 4.65, which shows that this distortion does not dominate the total distortion as shown in test 38. For the end lapped specimen, the main distortion may come from the warping of the profiles.

The failure modes of Test #40 after Run 1 and Run 2 are shown in Table 4.14. Most failures are of the BU (buckling) mode, which involves only the failures of the sheet materials, not the fasteners. Unlike the monotonic test 39, no shear failures of the nails were observed. For this test specimen all of the damage occurred along side-lap lines C, F, I and L, this is due to the weaker resistance along these gridlines because the resistance is made up of a combination of a few nails and many screws. On the sides of the specimen the stronger nail connections exist. Some screws at side-laps such C and L tilted, but did not pull out as in test 39. It seems that the small cycles in the initial phase of the protocol allow for a redistribution of connector forces so that the overlap nails are not as highly loaded.

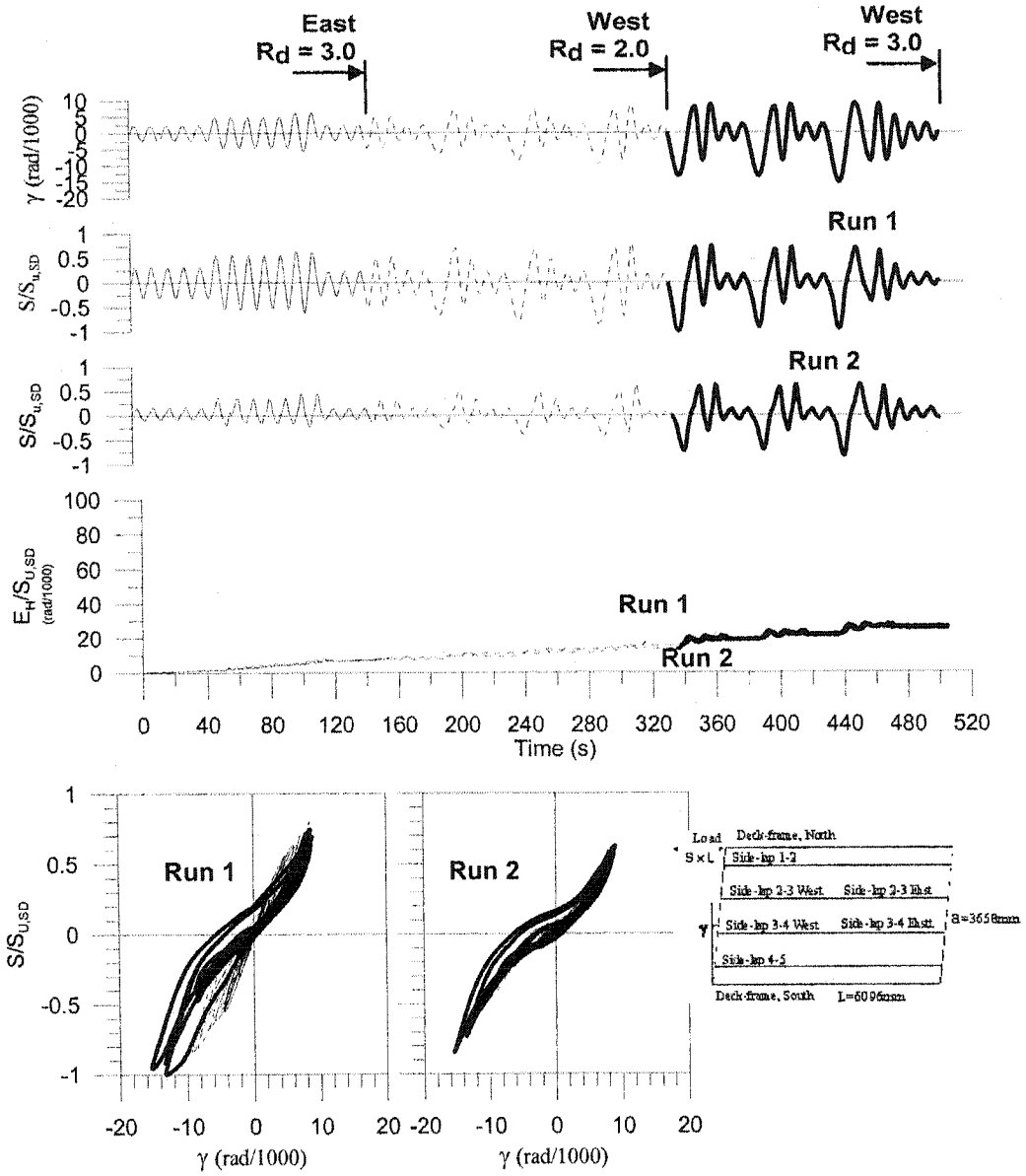

Test No. 40

P3615B, 0.76 mm

Sidelap fasteners : Screws @ 305 Frame fasteners : Hilti nails @ 305

$S_{u,SDI}$ = 11.20 kN/m $S_{u,SD}$=13.03 kN/m $S_{u,MON}$ = 11.28 kN/m

Figure 4.61. Time history & hysteresis results of Test 40

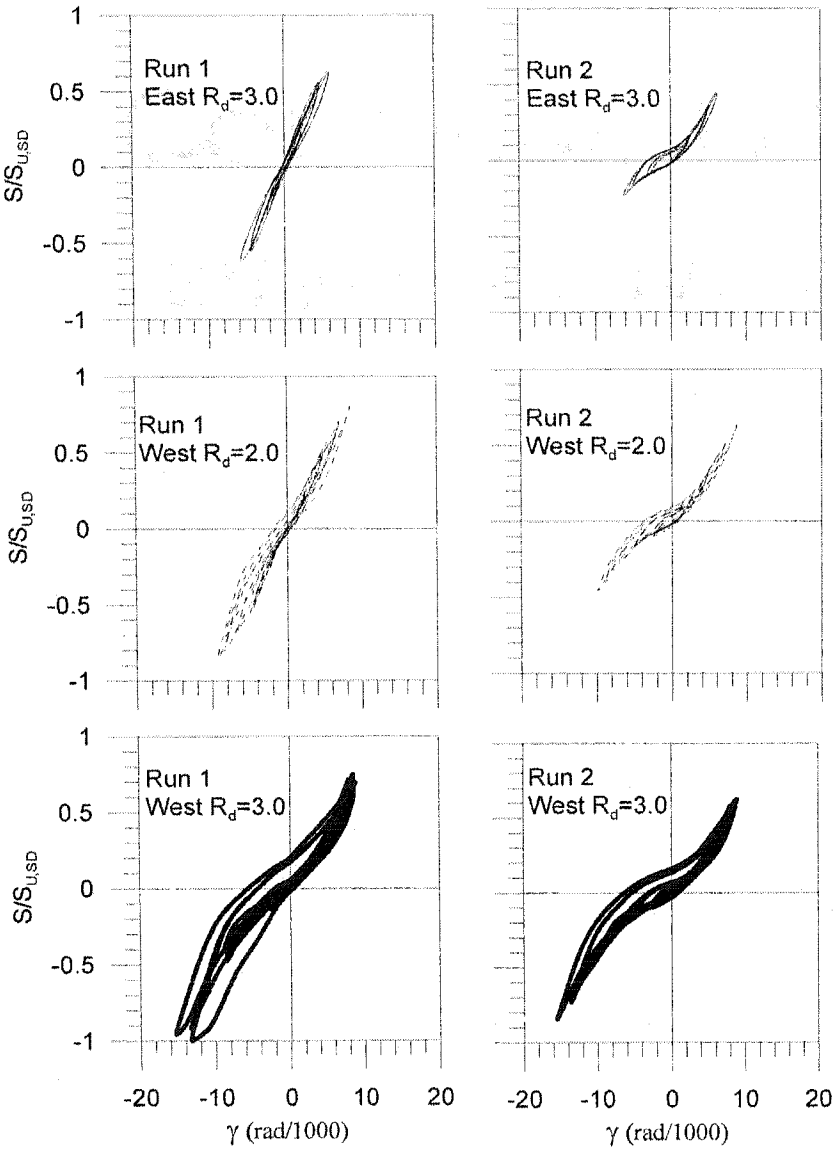

Test No. 40

P3615B, 0.76 mm

Sidelap fasteners : Screws @ 305 Frame fasteners : Hilti nails @ 305

$S_{u,SDI*}$ = 11.20 kN/m $S_{u,SD}$=13.03 kN/m $S_{u,MON}$ = 11.28 kN/m

Figure 4.62. Hysteresis results of Test 40

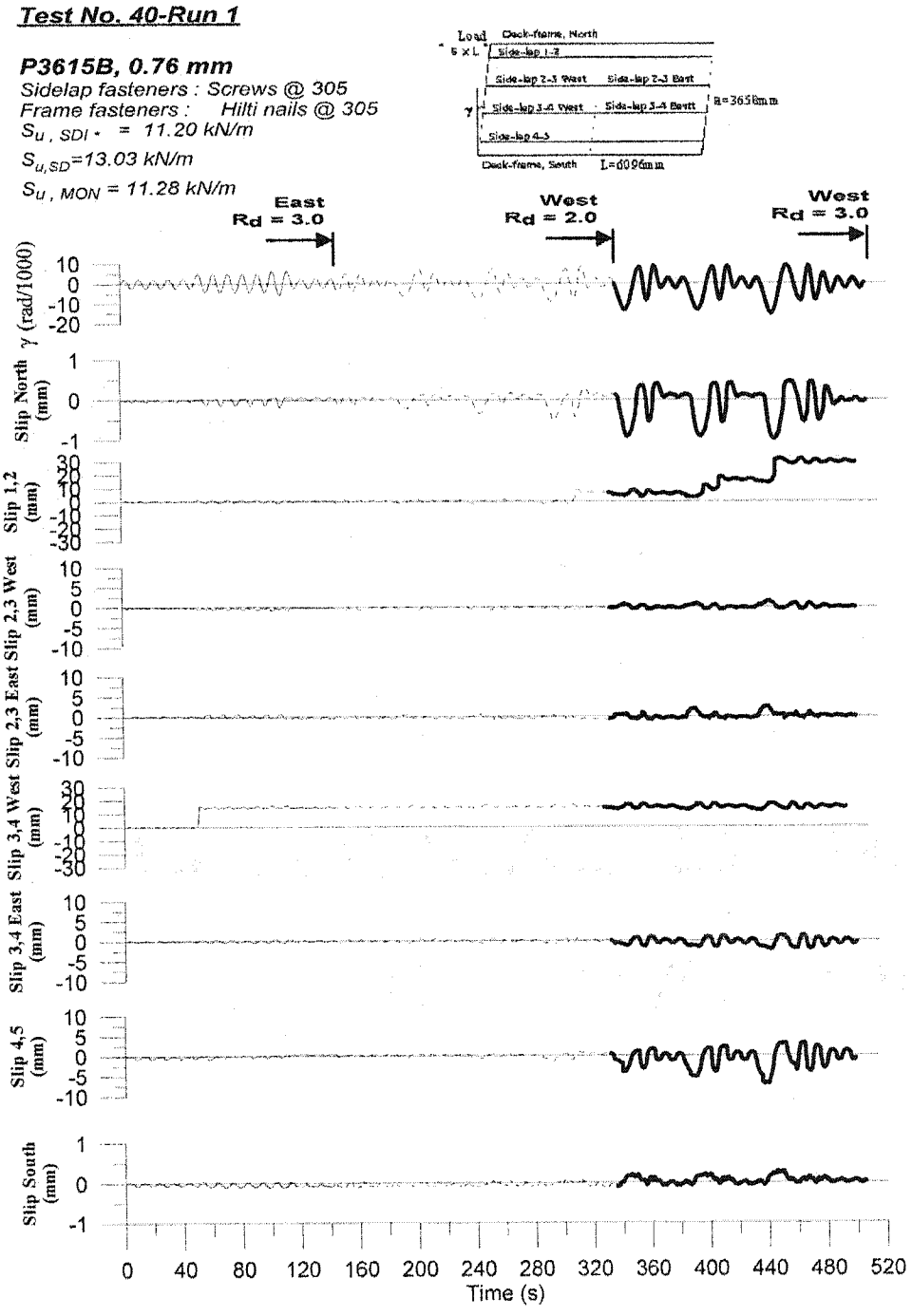

Figure 4.63. Slip time history results of Test #40 (Run 1)

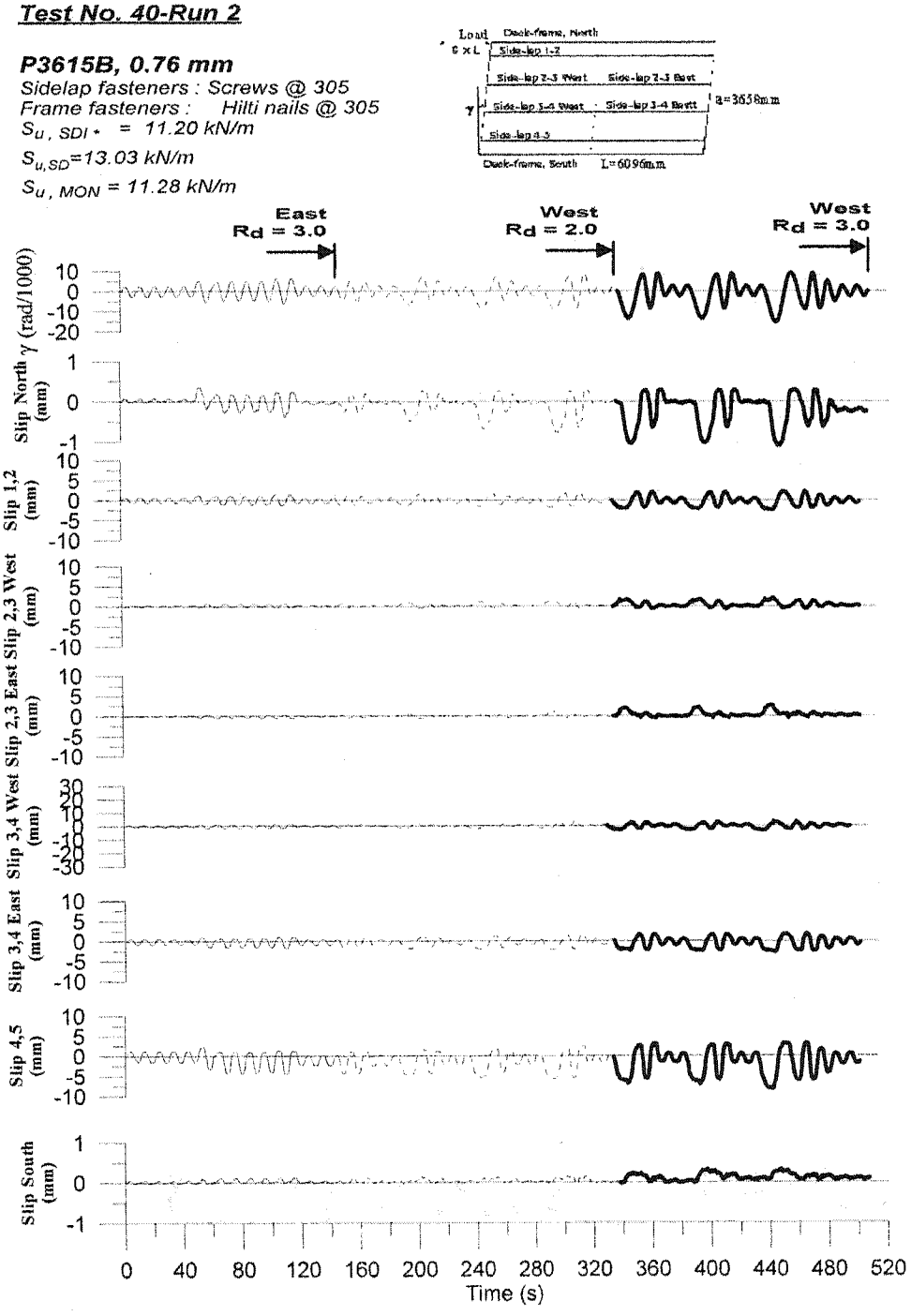

Figure 4.64. Slip time history results of Test #40 (Run 2)

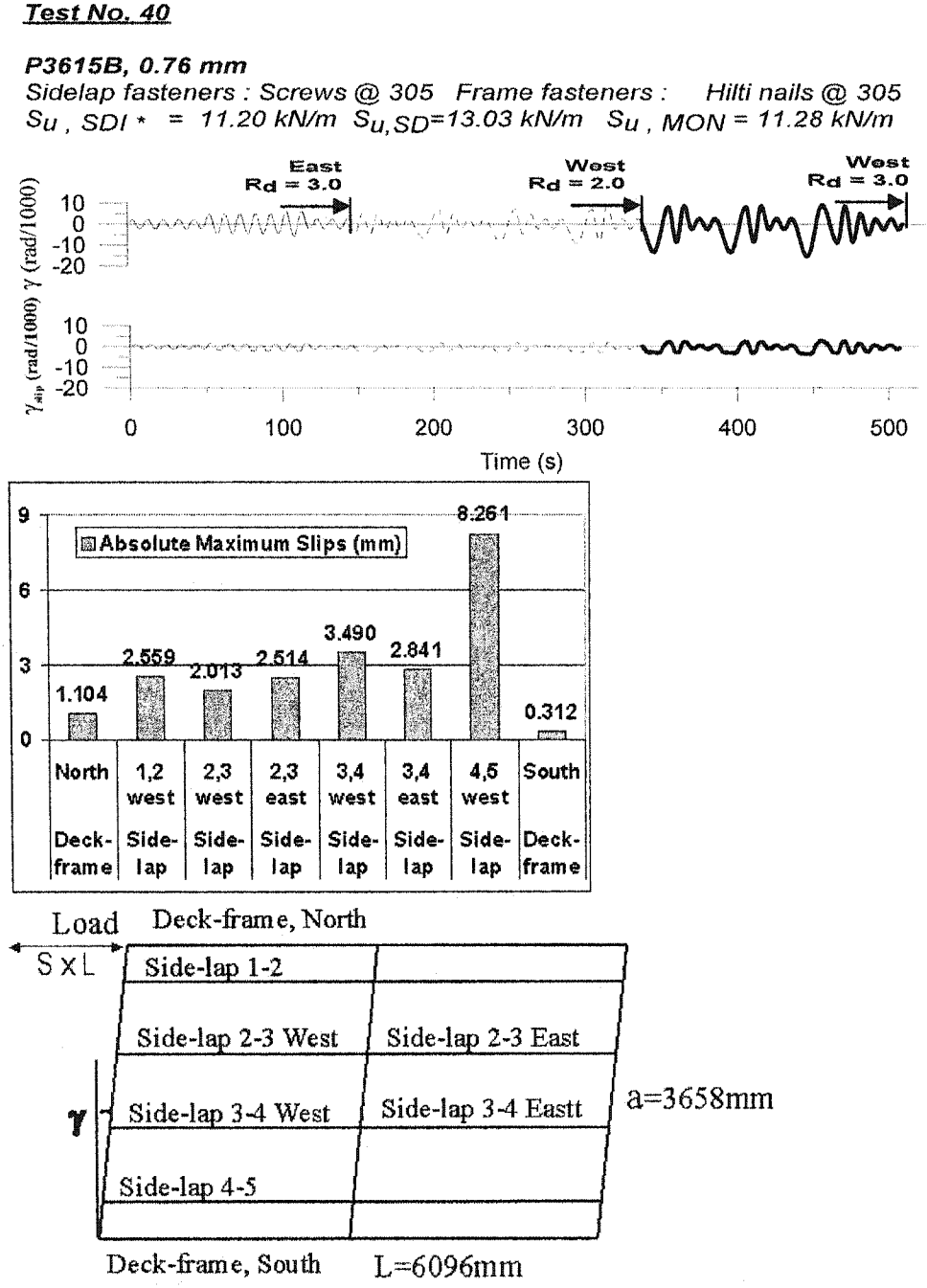

Figure 4.65. Distortion contribution from the side-lap slips and the slips related to S_u of Test 40 (Run 2)

Table 4.14: The failure modes of Deck-to-Frame connections of Test 40

Position	1		6		11		16		21
B									
C	**BU**				**BU**		**BU**		**BU**
D									
E									
F	**BU**				**BU**				**BU**
G									
H									
I	**BU**						**BU**		**BU**
J									
K									
L	**BU**				**TE+BU**				**BU**
M									

BU--Buckling failure; TE--Tearing failure

Related to Table 4.14, Figure 4.66 shows a typical buckling failure at L1. Figure 4.67 shows the tearing failure at L11, the only one that was observed in this test. That failure may be due to the large warping deformation that occurred at the end laps. Very obviously, the nail is stronger than its surrounding steel sheets, even though there are 4 sheets overlapped together at this location. Figure 4.68 gives an example of the development from bearing to buckling of the steel sheet around the screw connection at C20.

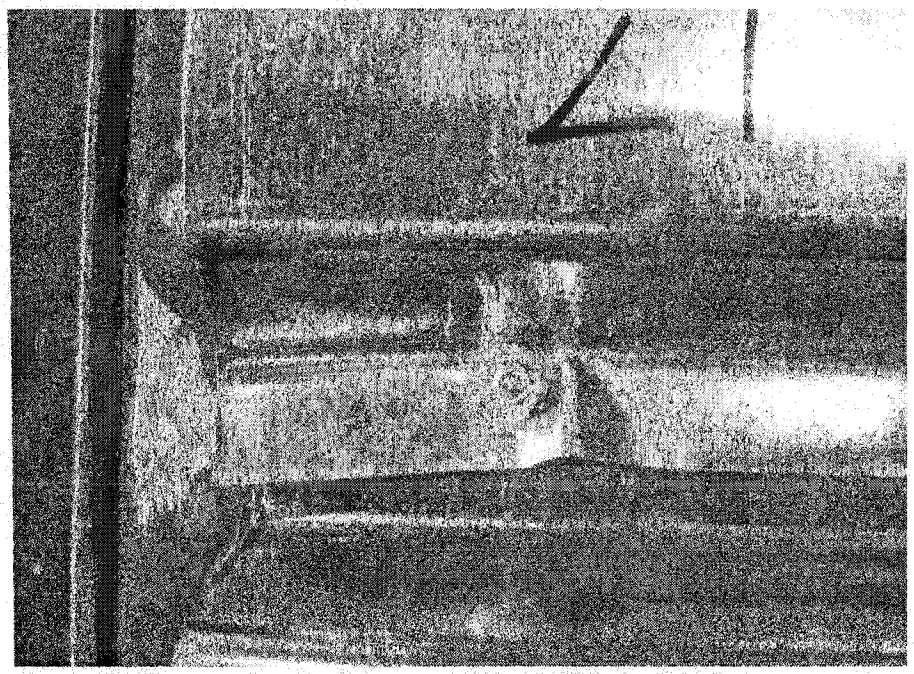

Figure 4.66. Buckling of steel sheet around nail L1

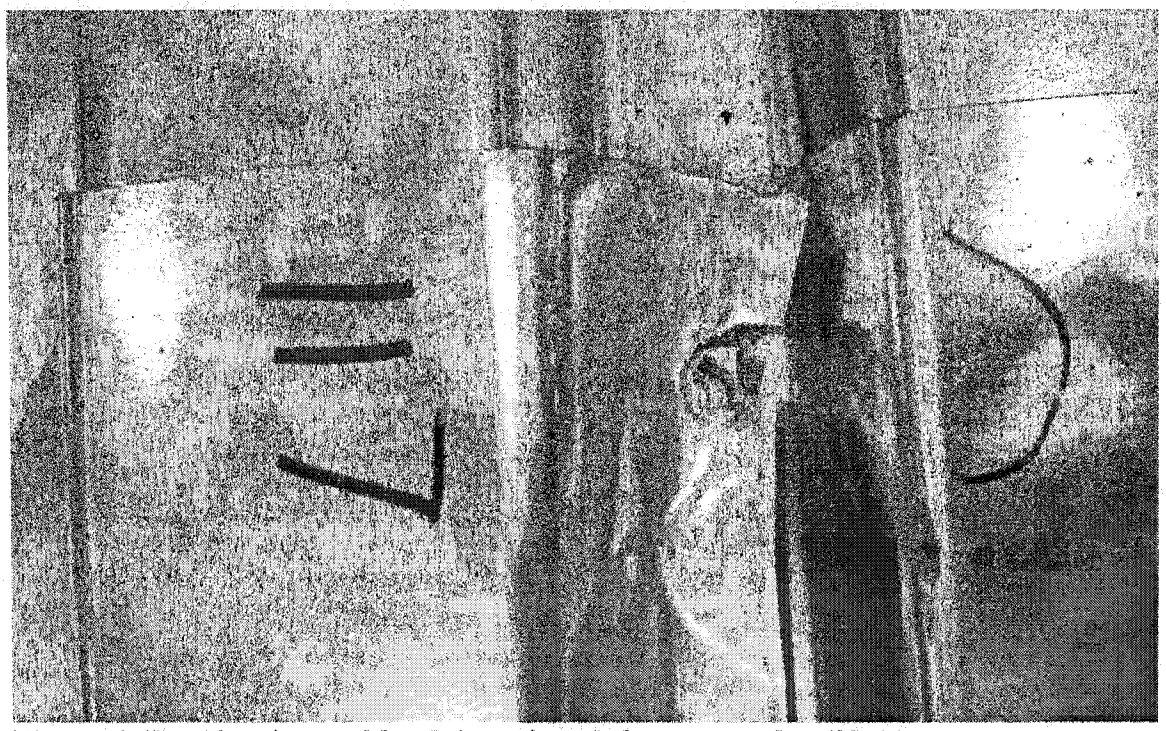

Figure 4.67. Tearing and buckling of steel sheet around nail L11

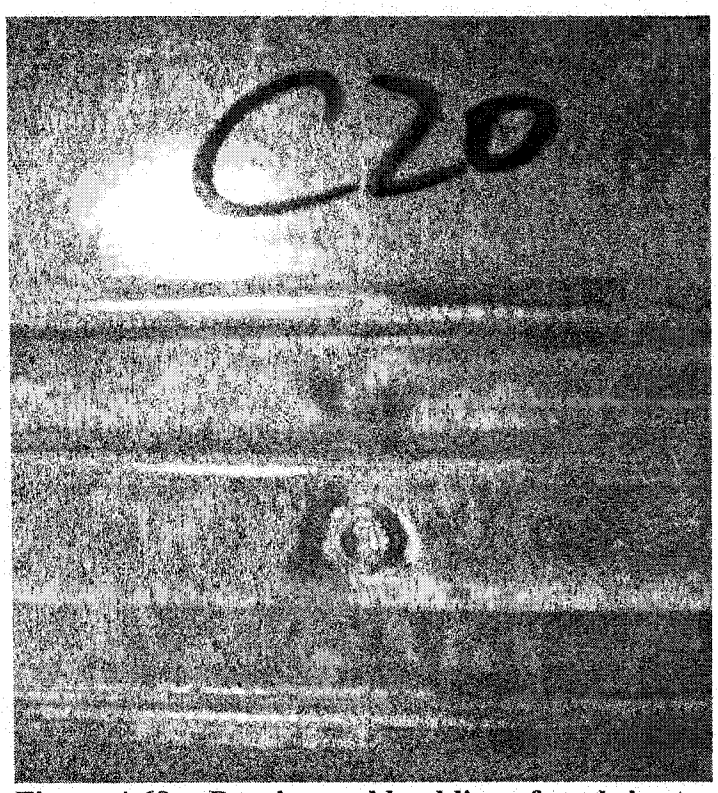

Figure 4.68. Bearing and buckling of steel sheet around screw C20

4.2.3.3 Test 41

Monotonic test #41 was of the overlap configuration, however the P-3615 panel profile with interlocking edges, along with welded and button punch connections, were used. The results from this test were also used to prepare the protocol for test 42. The test specimen description is listed in Table 4.15.

Table 4.15 Test specimen description (Tests 41 and 42)

Steel properties:	
Supplier and coil number	Canam P-3615 deck 0.76 mm Coil supplier: Sorevco Coil number: 344056,
Base metal thickness (mm)	0.71
F_y measured (MPa)	301
F_u measured (MPa)	373
E measured (MPa)	197000
50 mm gauge % elongation	31 %
Fasteners:	Spacing: 305 mm c/c
	Side-lap fasteners: Button punch
	Deck-to-frame fasteners: Diameter 16 mm weld

A detailed listing of the observed weld quality is provided in Appendix 2. In general, along the side-laps, the average equivalent weld diameter on the north side of the gridline (D_{eq}=14.8 mm) was smaller than that of the south side (D_{eq}=17.0 mm). This may be because the north sheet was laid over the south sheet, and hence its contact to the steel frame may not be as good as the south side, and hence it was more difficult to obtain a weld of equal size.

During the execution of monotonic test 41 the following observations were recorded: at a load level of 15 kN (S = 2.46 kN/m), and a γ = 1.09 rad/1000, the overlapped sheets on gridline 11 began to exhibit noticeable vertical separation due to the

warping distortion of the panel profile (Figure 4.69). As the load continued to increase this distortion became more evident. When a load of 49.25 kN (S = 8.08 kN/m) was reached at γ = 7.11 rad/1000, the weld connection at C1 (north) (Figure 4.70) broke suddenly, followed immediately by the weld connection at L1 (north) (Figure 4.71). The failure of these welded connections caused a sudden jump in the extent of side-lap slip.

Figure 4.69. Sheet deformation at overlapped joint (Gridline 11)

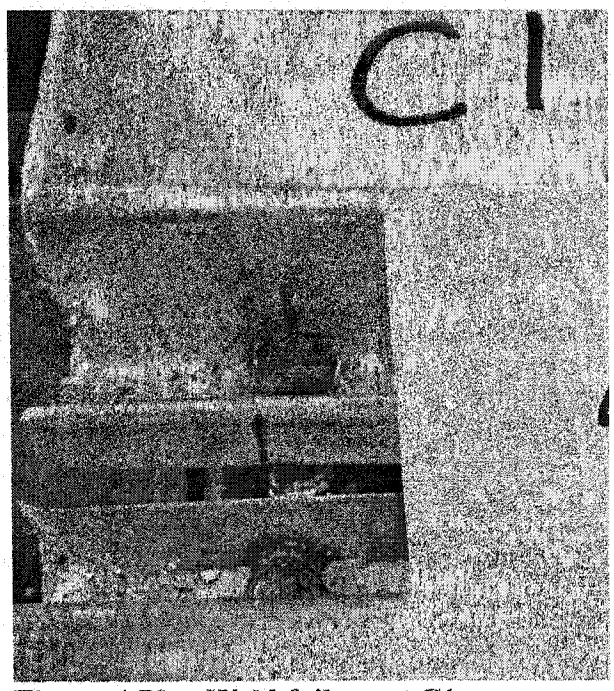

Figure 4.70. Weld failure at C1

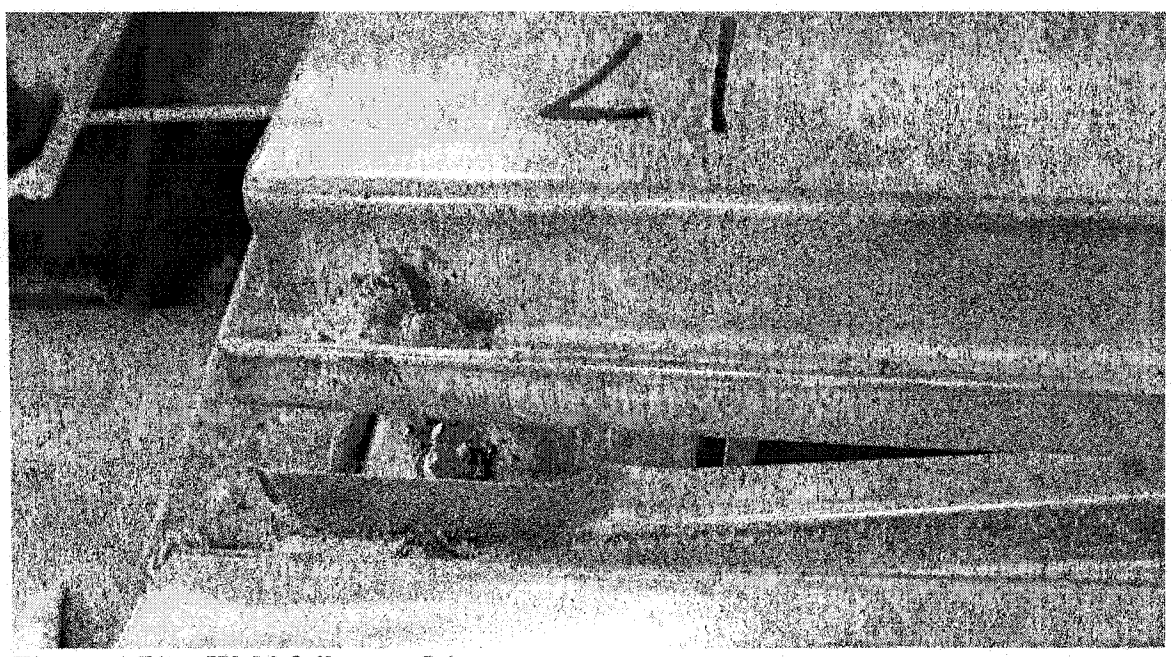

Figure 4.71. Weld failure at L1

Even though these two welds had failed, the applied load continued to increase up to 53.9 kN (S = 8.84 kN/m). At this point the third welded connection I1 (north) failed.

This was followed by the failure of a fourth welded connection L6 (north) when the load equalled 54.0 kN (S = 8.86 kN/m). Shortly after that, the maximum load 55.73 kN (Su=9.14 kN/m) was reached at a shear rotation of γ_2 = 10.463 rad/1000.

As compared to the deck-to-frame weld connection, the side lap button punch connections are much weaker and more flexible. They cannot provide much help when the weld connection fails. The main failure of these side lap connections is the sheet separation and sheet sliding. Since the shape of punches did not change much even when the sheets separated or slipped during the tests, their failure modes could

not be easily observed. The separation of a typical button punch connection is shown in Figure 4.72.

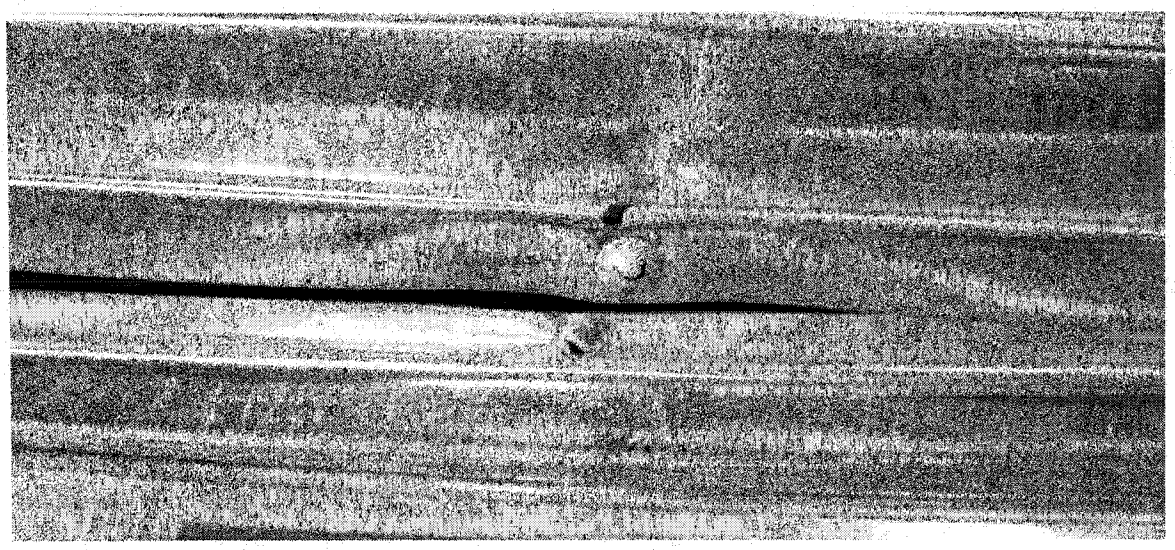

Figure 4.72. Separation of button punch connection at F10 (after test)

The normalized shear force and slip *vs.* shear rotation graphs are shown in Figure 4.73. Three drops in load that correspond to the weld damage at C1, L1 and I1 can be observed. The two-stiffness behaviour that was observed for the NS specimen was not found here. The softening of the diaphragm is gradual until final failure occurred.

The slip/distortion relation from γ=0.0 to 10.46 rad/1000, the γ_2, i.e. the distortion relating to S_u, was given in Figure 4.74, where the measured side-lap slips along the north side and south side were minimal. The interior slips were not uniform. The slips at gridlines C and L (side lap 1-2 and 4-5) seems larger than that in side lap 2-3 and 3-4. This may relate to the early damage of the connection at C1 and L1 as discussed before. The slip value measured for side-lap 2-3 East was not included, because the LVDT was out of order.

Test No. 41

P3615, 0.76 mm
Sidelap fasteners : Button punched @ 305
Frame fasteners : Welds 16mm @ 305
S_u , *SDI* * = 12.78 kN/m
S_u , *MON* = 9.14 kN/m

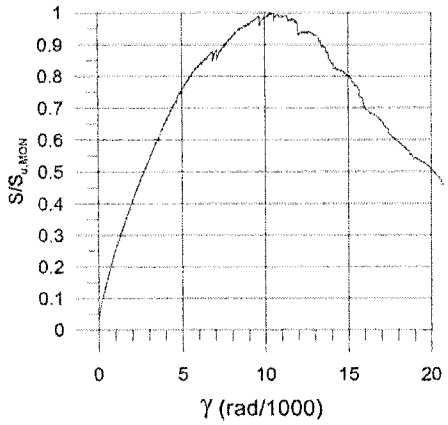

Figure 4.73. Shear load vs. rotation graphs for Test 41

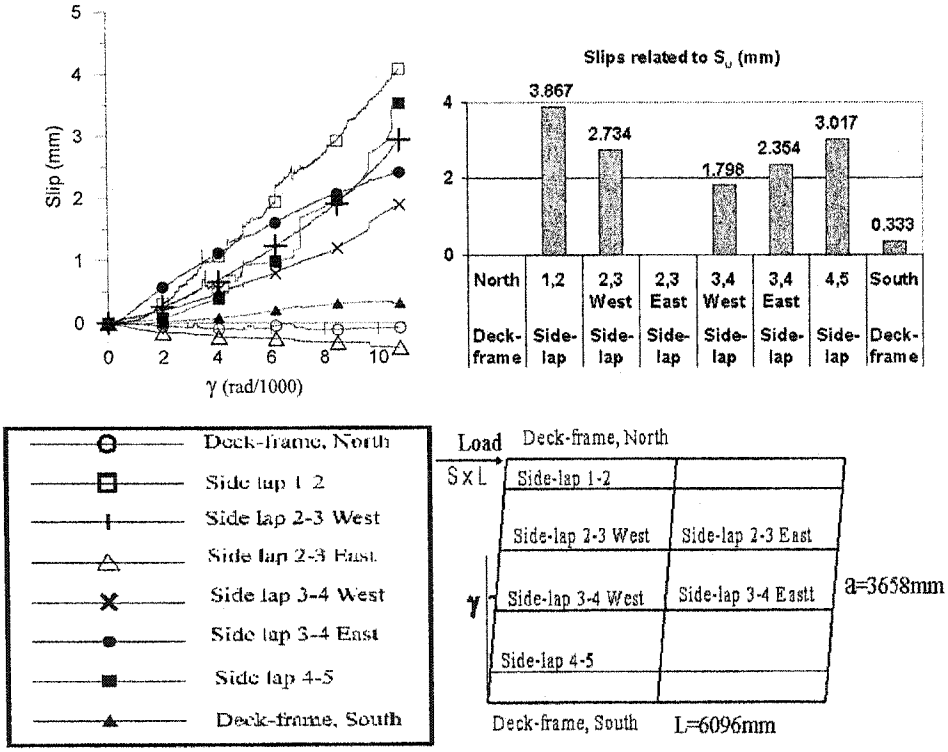

Test No. 41
P3615, 0.76 mm
Sidelap fasteners : Button punched @ 305, Frame fasteners : Welds 16mm @ 305
$S_{u,SDI}$ * = 12.78 kN/m $S_{u,MON}$ = 9.14 kN/m

Figure 4.74. Slip vs. rotation and the slips related to S_u

The failure modes for deck-to-frame connections are shown in Table 4.16, where both connection damage and sheet damage existed. Some of them were presented before, other pictures of these failure modes can be found in Figures 4.75 to 4.76.

In Table 4.16, more failures on the north side of the side laps were observed than on the south side. This may be due to the inferior weld quality on the north side because it overlapped the south side. Another phenomenon is that the strength of the weld connections was not always higher than the surrounding steel sheets.

Table 4.16. The failure modes of Deck-to-Frame connections of Test 41

Position	1		6		11		16		21
B	BE								
C (north)	**WE**		**BE**		**WE**		**BE**		**BE**
C (South)			**BE**				**BE**		**BE**
D									
E	WE		BU		BU		BU		BU
F (north)	**WE**		**WE**		**WE**		**BE**		**WE**
F (South)					**BU**		**BE**		
G									
H							BU		BU
I (north)	**WE**		**WE**		**BU**		**BE**		**WE**
I (South)					**BU**		**BE**		
J									
K	BE		BE		BE		BE		
L (north)	**WE**		**WE**		**BU+BE**		**BE**		**BU+BE**
L (South)							**BE**		**BE**
M	BU		BU		BU				BE

BE--Bearing failure; BU--Buckling failure; WE--Weld failure

Figure 4.75. Tearing damage of steel sheet at H11

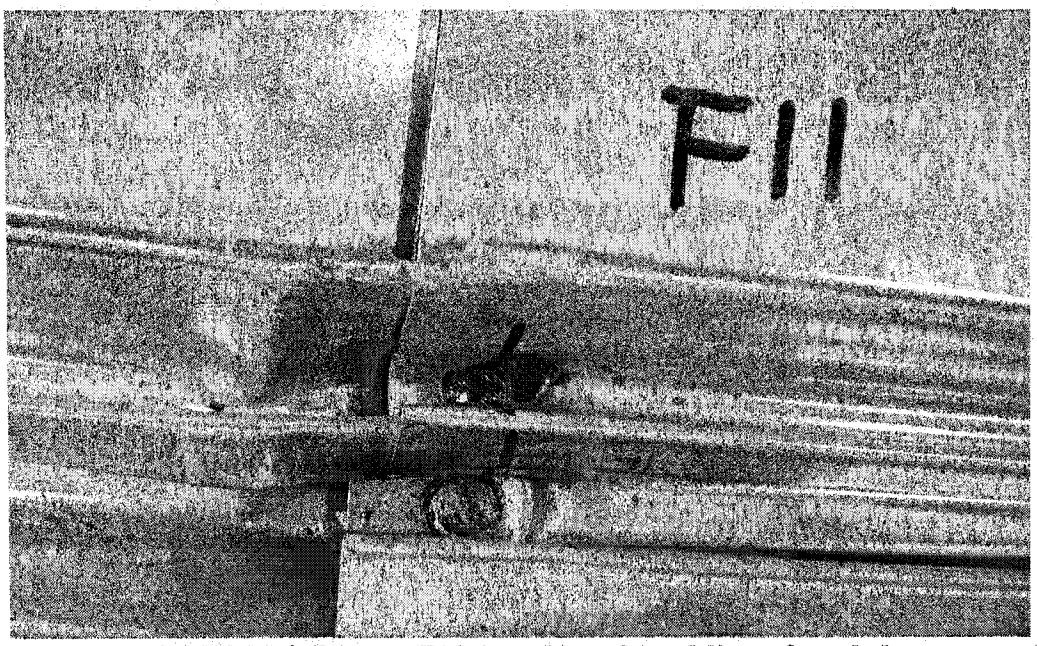

Figure 4.76. Weld failure at F11 (north) and buckling of steel sheet around F11

4.2.3.4 Test 42

Test 42 was a short duration seismic loaded test with time duration of 25.2 sec. The test specimen description is the same as for Test 41 (Table 4.15). The time history and hysteresis plots for shear force and distortion are given in Figure 4.77 and 4.78.

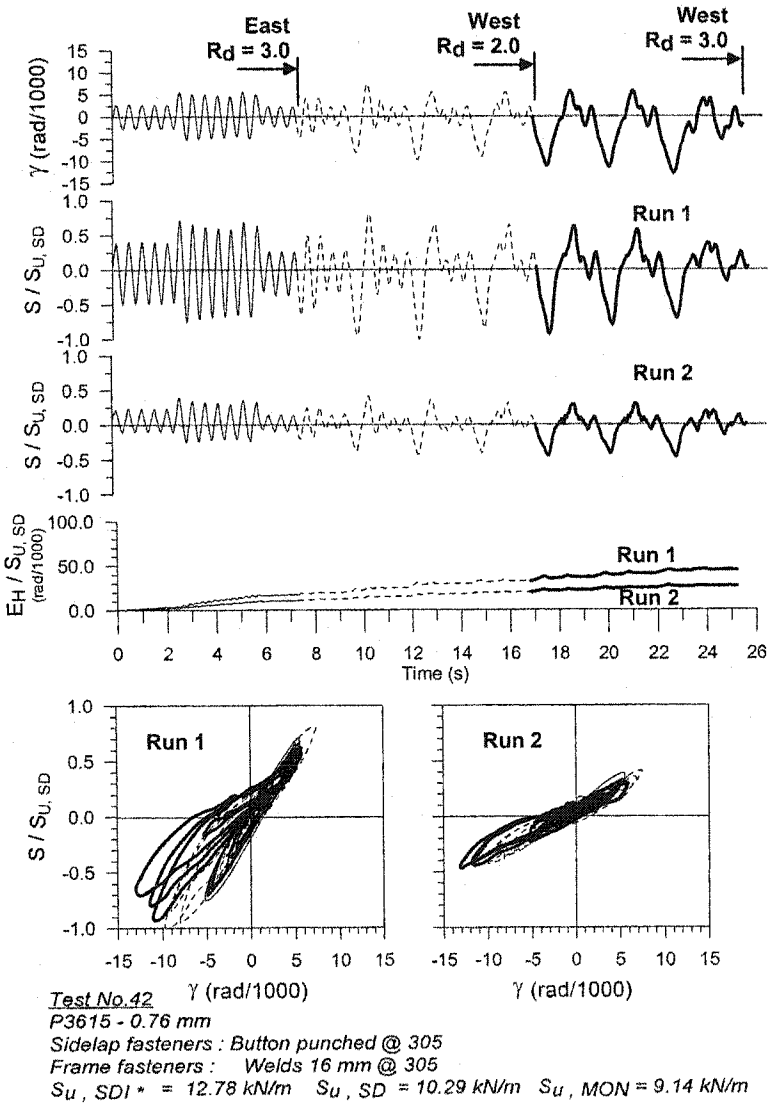

Figure 4.77. Time history & hysteresis results of Test 42

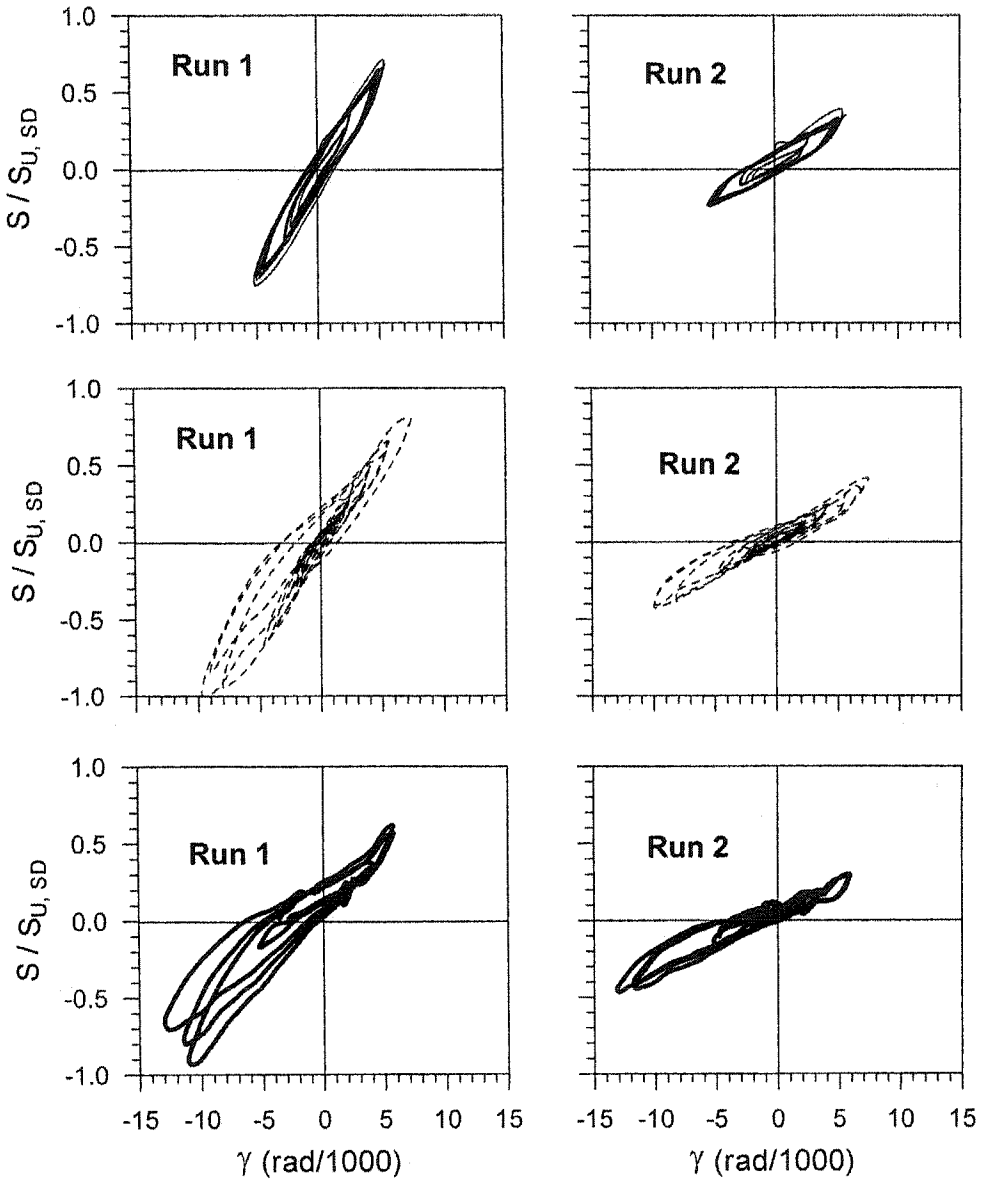

Test No.42
P3615 - 0.76 mm
Sidelap fasteners : Button punched @ 305
Frame fasteners : Welds 16 mm @ 305
$S_{u,\ SDI}$ * = 12.78 kN/m $S_{u,\ SD}$ = 10.29 kN/m $S_{u,\ MON}$ = 9.14 kN/m

Figure 4.78. Hysteresis Results of Test 42

The maximum shear value recorded during the protocol, S_u = 10.29 kN/m, was obtained during the second load phase (West R_d=2.0) of Run 1 (Figure 4.78). Normally the welds or button punches failed and then had no residual capacity, according to the observation recorded by Martin (2002). During this test, a malfunction of the hydraulic system occurred, and hence the time history of the γ curves became not smooth sine shapes for the phases 2 and 3, and the displacements were smaller than that expected in the protocol (Figure 4.79). For example, the greatest distortion input into the control program was –17.734 rad/1000, but the maximum realistic distortion was –12.983 rad/1000. The smaller deformation allowed the specimen to retain some residual capacity (Figure 4.78).

Another feature of Figure 4.78 is that, the pinching, which very often occurs in nailed diaphragms, is not obvious for welded diaphragm, because the slotted holes in the deck did not develop.

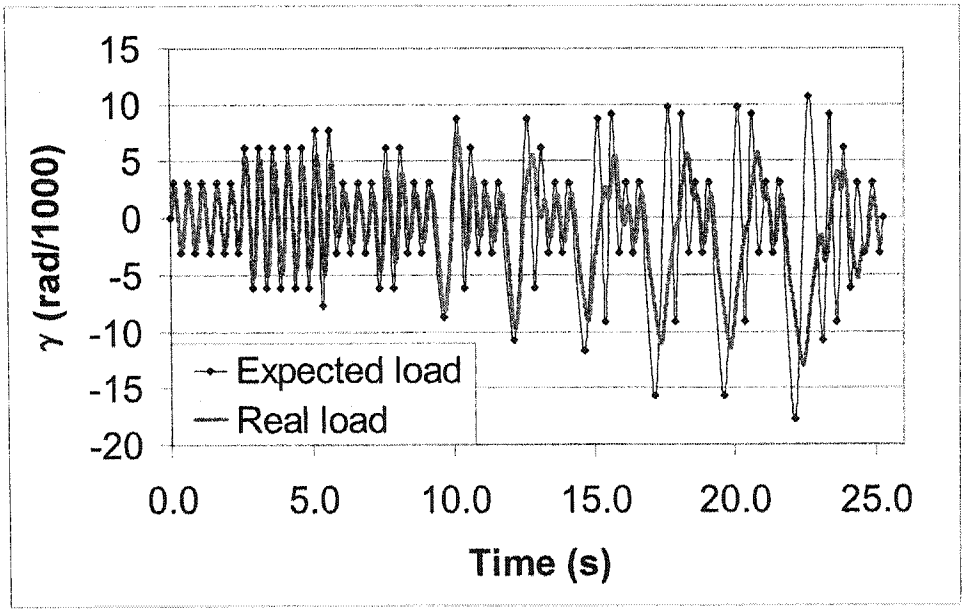

Figure 4.79. Comparison of real load to expected load

During test Run 1 many weld failures occurred along gridlines F and L, see Table 4.17. For this reason the damage modes for Run 2 were not recorded. The damage modes and positions were largely influenced by the connection quality. For example, the equivalent diameter of the arc-spot weld at L21 was only about 4.3 mm, which is much smaller than the nearby weld diameters. Hence, this weld failed first (Figure 4.80), followed by a redistribution of force to the other connections along gridline L. The remaining connections along this side-lap line then had to endure higher shear forces than the other connections in other grid lines in the diaphragm, and failed soon afterward (the L16 in Figure 4.81).

Table 4.17. The failure mode of Deck-to-Frame connections of Test 42 after Run 1

Position	1		6		11		16		21
B									
C (north)	**WE**		**WE**						
C (South)			**WE**						
D									
E	WE								
F (north)	**WE**		**WE**		**WE**		**WE**		**WE**
F (South)	**WE**		**WE**				**WE**		
G	WE								
H	WE								WE
I (north)									**WE**
I (South)									
J									WE
K	WE		WE						WE
L (north)	**WE**		**WE**				**WE**		**WE**
L (South)	**WE**		**WE**				**WE**		**WE**
M							WE		WE

BE--Bearing failure; BU--Buckling failure; WE--Weld failure

In Table 4.17, the weld connections here in non-sidelap positions failed too, one such typical damage at H21 is shown in Figure 4.82. This may be due to the redistribution of force when some connections at side lap positions failed.

It is interesting to note that, at the end lap position (gridline 11 in Table 4.17), only one connection (F11) failed, which was shown in Figure 4.83. It is possible that the sheet warping here were restrained by profiles.

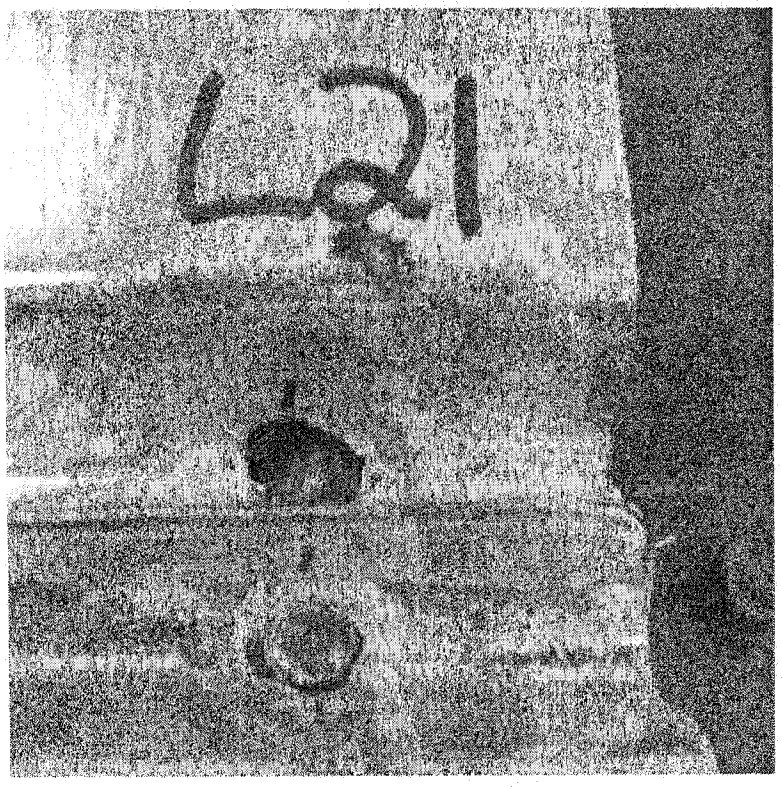

Figure 4.80. Weld failure at L21

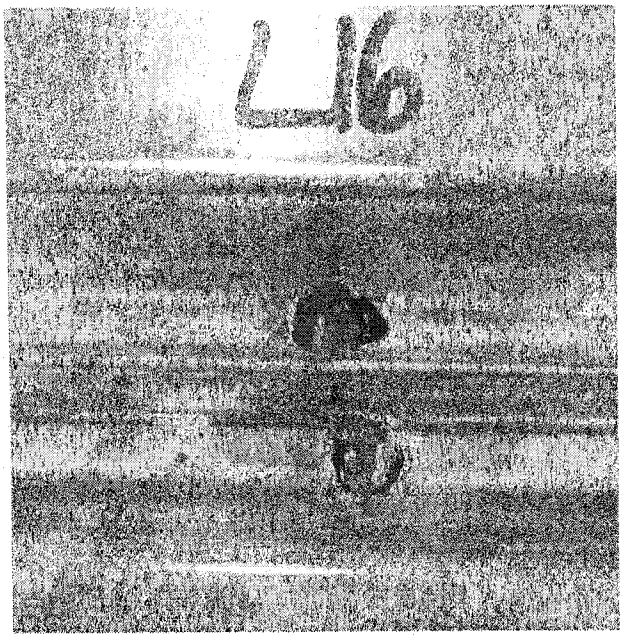

Figure 4.81. Weld failure at L16

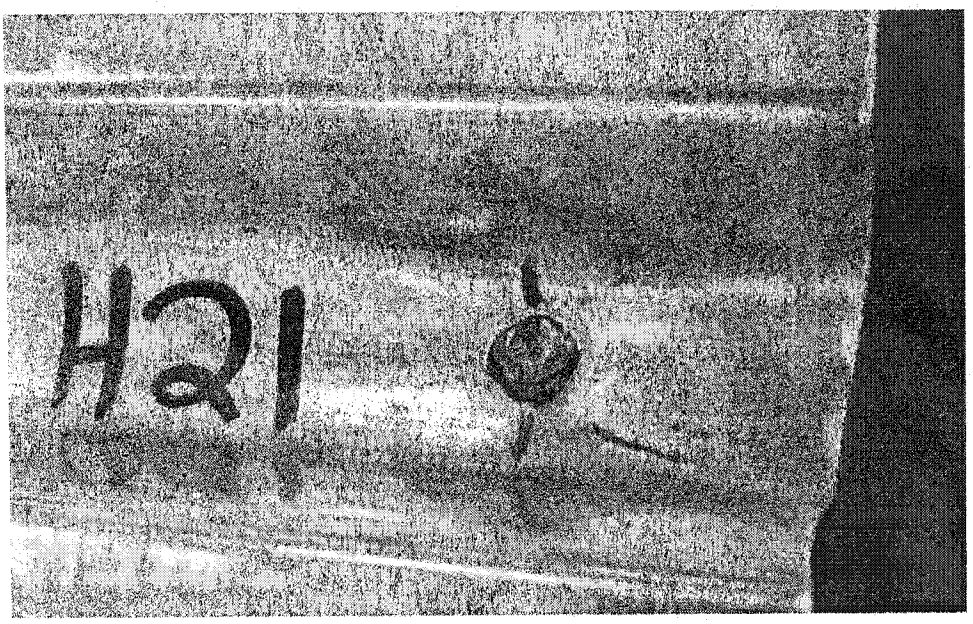

Figure 4.82. Weld failure at non-sidelap connections

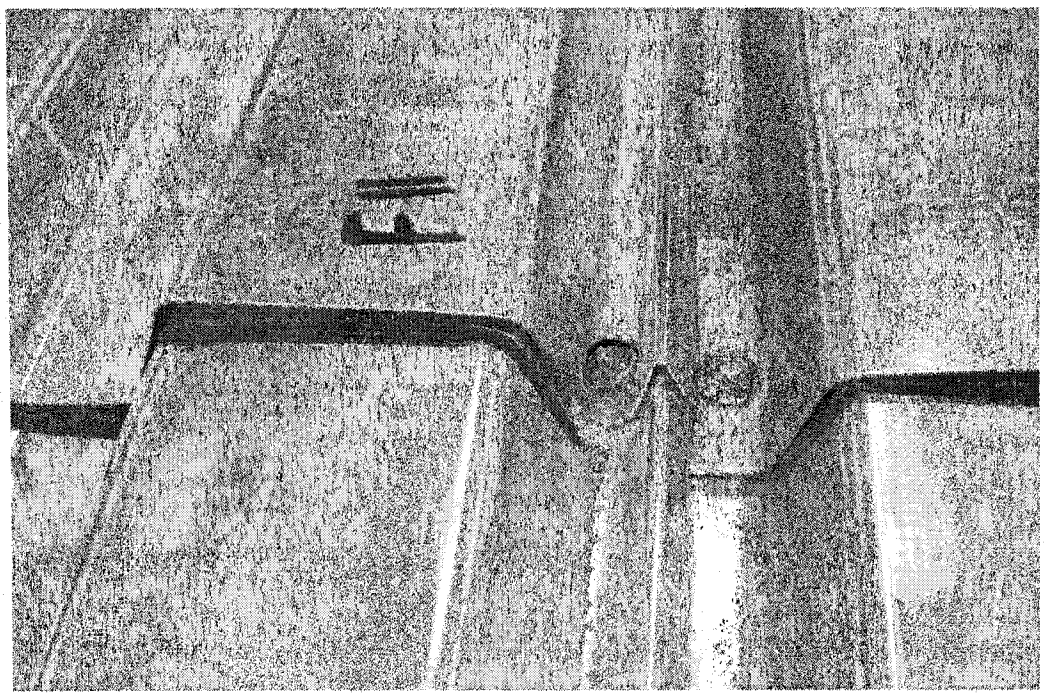

Figure 4.83. Weld failure at end lap (F11) and adjacent sheet deformation

Figure 4.84 contains the time histories of slips for load Run 1. For this test specimen the interior side-lap slips were quite uniform, while the slips at both north and south sides were insignificant. The distortion due to slips did not dominate the total distortion that is similar to other end lapped specimen. A similar slip performance was noted for Run 2 (Figure 4.85). The largest slips recorded from Run 1 and Run 2 are shown in Figures 4.86 and 4.87 respectively.

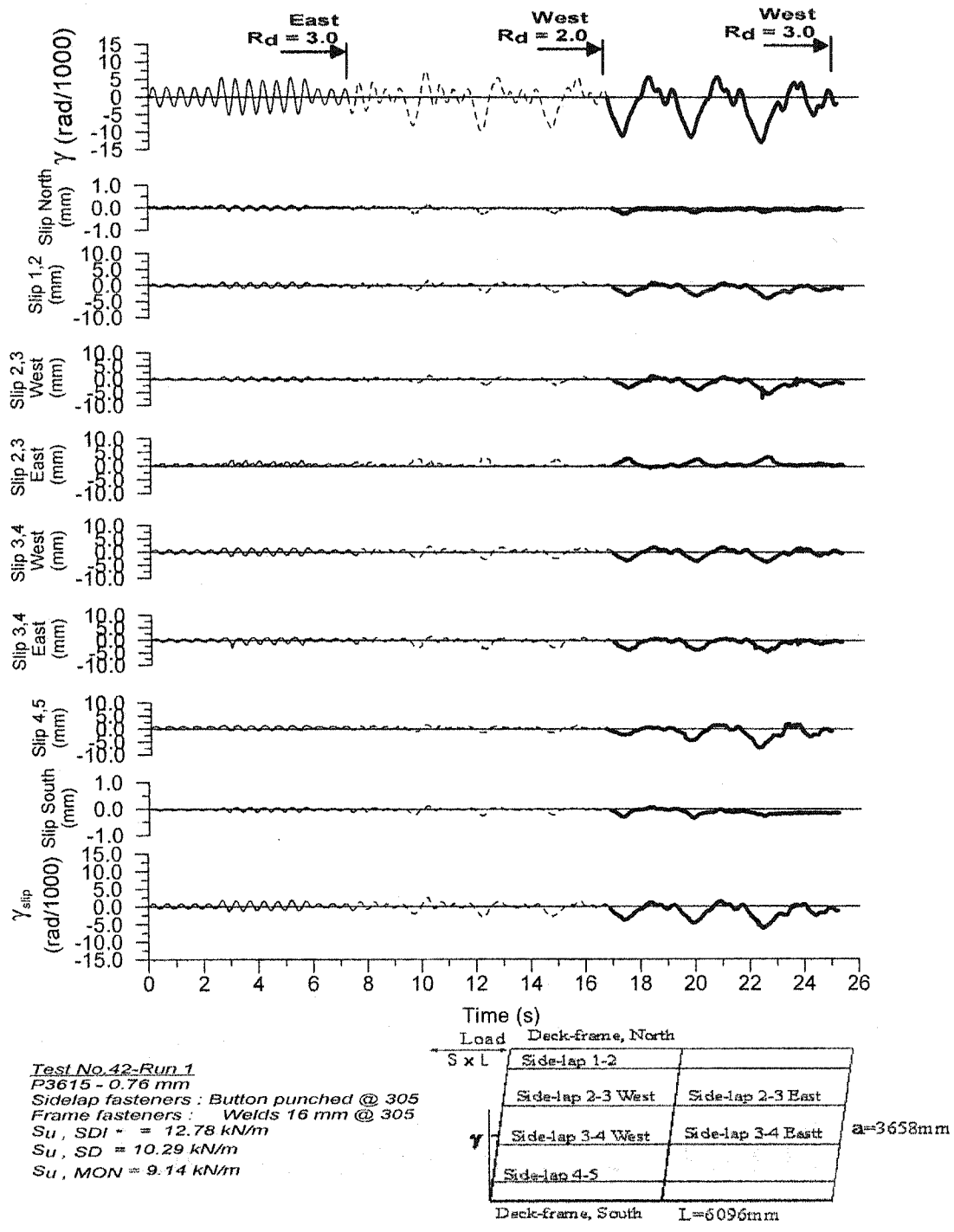

Figure 4.84. Time history of side lap slip of Test 42 Run 1

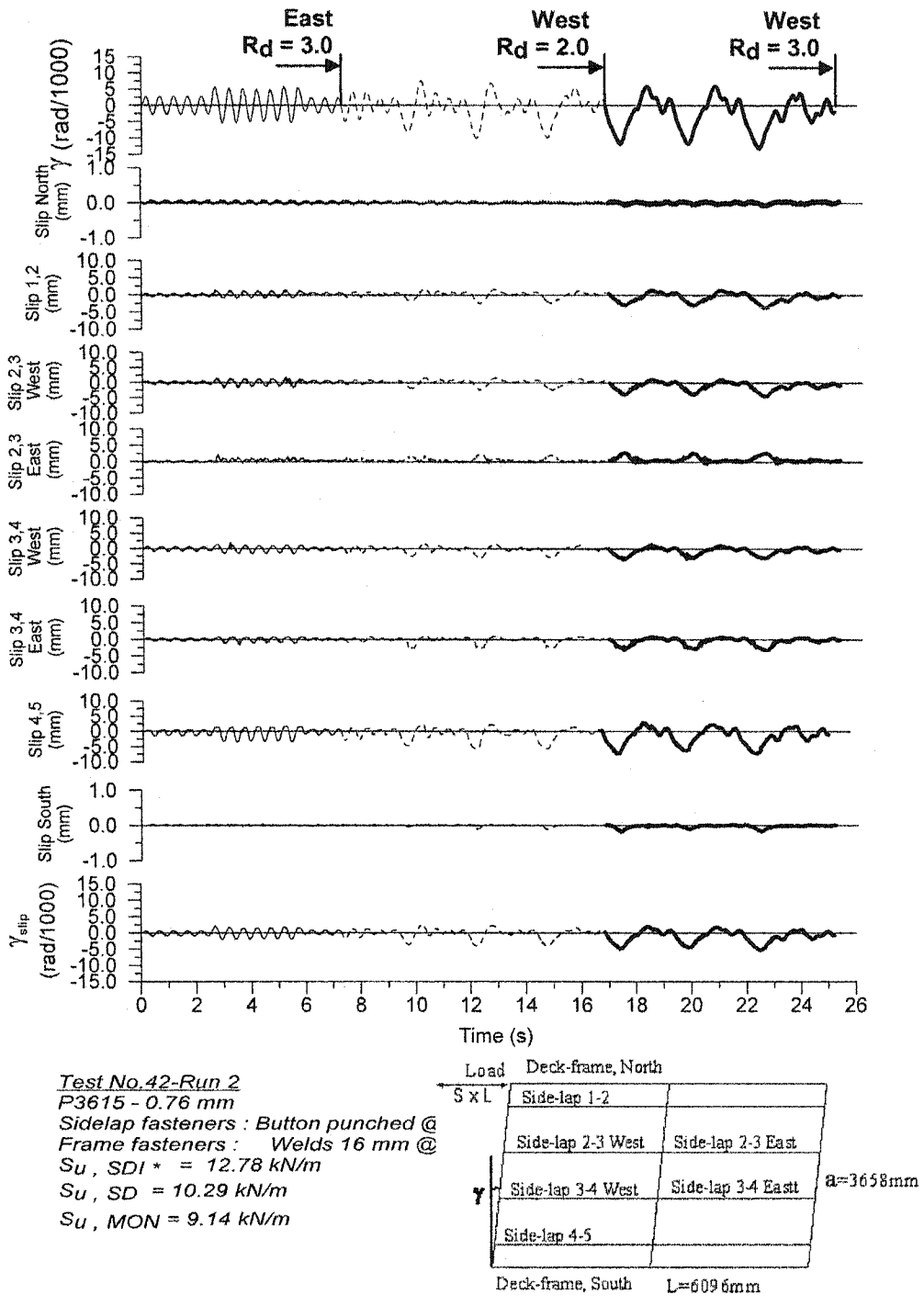

Figure 4.85. Time history of side lap slip of Test 42 Run 2

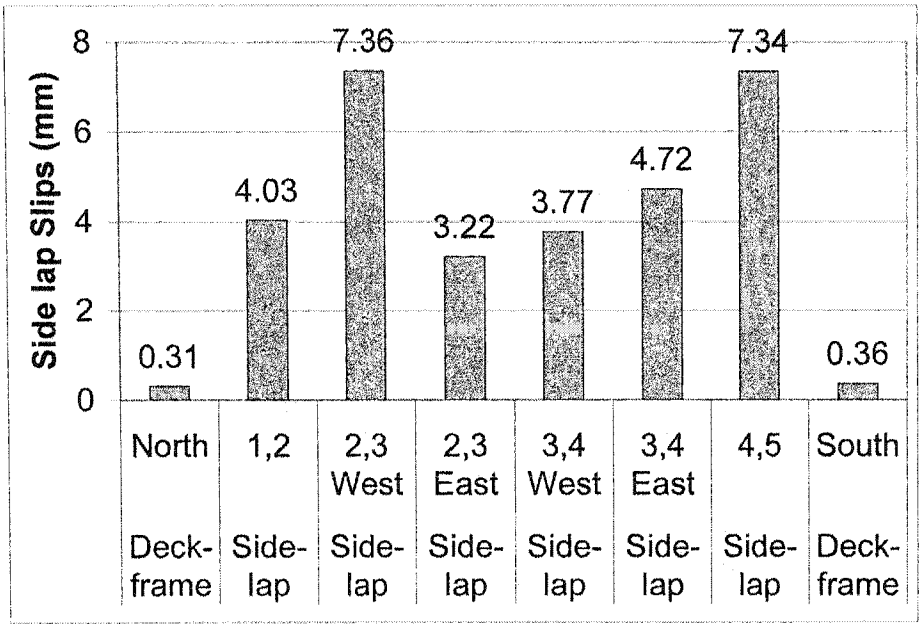

Figure 4.86. Maximum side lap slips from Run 1

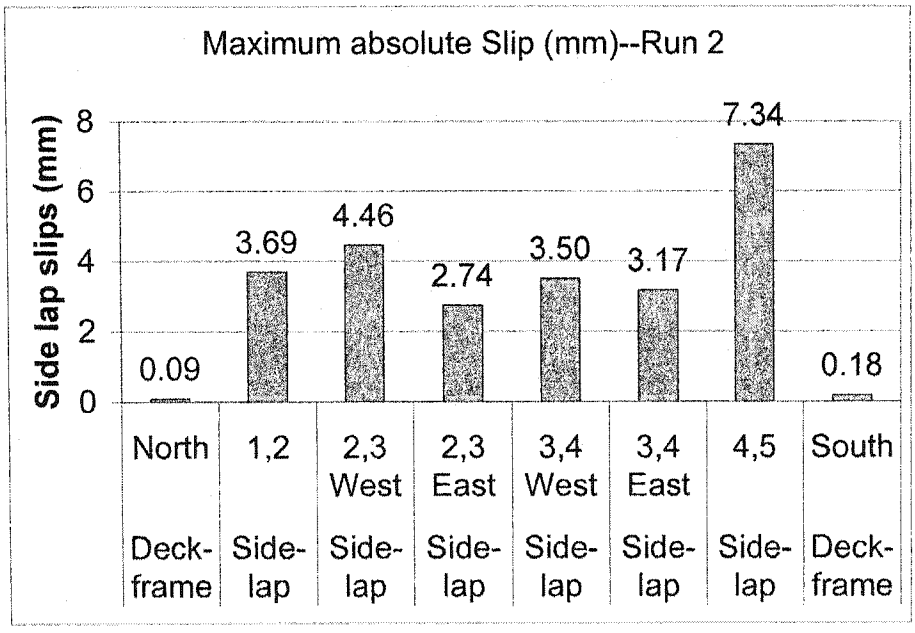

Figure 4.87. Maximum side lap slips from Run 2

4.2.3.5 Comparison with non-overlapped deck test results

4.2.3.5.1 Nail/screw connected diaphragm

The measured shear strength and stiffness results of tests 4 and 7 by Essa *et al.* (2001) and tests 28 and 29 (Martin, 2002) are compared with tests 39 and 40 in Table 4.18. The differences between these specimens are: tests 4, 7, 28 and 29 are 6 m long, while tests 39, 40 were 3 m long, and furthermore the loading protocols were not the same. These tests were, however, constructed with the same deck profile and the same fasteners. Based on the information listed it is apparent that the presence of the longitudinal overlap did not influence the ultimate shear strength of the specimen, however there was a marked decrease in the stiffness of both the monotonic and short duration tests. It is noted in Table 4.18 that the SDI estimation of strength and stiffness coincides with that from tests 39 and 40 when panel length was specified.

Table 4.18: Comparison of shear and stiffness results for tests 39 and 40 with other tests

Test number	Test result		Ratio			
	Su	G'	Su	G'	Su	G'
	KN/m	KN/mm	Test/SDI	Test/SDI	Test/SDI*	Test/SDI*
38-76-6-NS-M-4	12.30	3.12	0.92	0.84	1.11	0.96
38-76-6-NS-Q-7	12.19	2.87	0.91	0.77	1.10	0.89
38-76-6-NS-SD-28	14.10	2.45	1.08	0.65	1.27	0.87
38-76-6-NS-LD-29	13.60	2.39	1.05	0.64	1.23	0.85
Mean 1 (Test 4,7,28, and 29)	13.05	2.71	0.99	0.73	1.18	0.89
38-76-3-NS-M-39	11.28	1.73	0.88	1.02	1.01	1.08
38-76-3-NS-SD-40	12.68	1.58	0.99	0.93	1.13	0.98
Mean 2 (Test 39, 40)	11.98	1.66	0.94	0.98	1.07	1.03
Ratio of mean2 to mean1	0.92	0.61	0.94	1.34	0.91	1.15

4.2.3.5.2 Weld/button punch connected diaphragm

The results of tests 1 and 2 by Essa *et al.*(2001) and test 20 by Martin (2002) are compared with tests 41 and 42 in Table 4.19. The differences of these specimens are: the panel length of tests 1, 2, and 20 are 6 m long, while for tests 41, 42 are 3 m long, and the loading protocols were not the same. These tests were however, constructed with the same deck profile and the same fasteners. Similar to the conclusion reached for the nail/screw connected diaphragms, the longitudinal overlap did not have a significant influence on the shear strength, but caused a substantial loss of shear stiffness. The higher strength of tests 20 and 42 may be due to the dynamic load properties, but the reason the test 42 has the highest strength may be due to the weld quality. The average weld diameter for test 41 is 15.74 mm, for test 42 is 16.62 mm, and the C.o.V. of these two tests are same, 0.13 (see Appendix 2). Again the SDI approach provided good estimates of the diaphragm strength and stiffness for the end lapped tests.

Table 4.19: Comparison of tests 41 and 42 with other tests

Test number	Test result		Ratio			
	Su	G'	Su	G'	Su	G'
	KN/m	KN/mm	Test/SDI	Test/SDI	Test/SDI*	Test/SDI*
38-76-6-WB-M-1	8.05	2.14	0.83	0.77	0.71	0.78
38-76-6-WB-Q-2	7.53	2.15	0.78	0.78	0.66	0.78
38-76-6-WB-SD-20	9.81	2.44	1.07	0.74	0.86	0.88
Mean 1 (Test 1,2 and 20)	8.46	2.24	0.89	0.76	0.74	0.81
38-76-3-WB-M-41	9.14	1.65	0.9	1.02	0.72	1.03
38-76-3-WB-SD-42	10.29	1.55	1.01	0.95	0.81	0.97
Mean 2 (Test 41, 42)	9.72	1.60	0.96	0.99	0.77	1.00
Ratio of mean2 to mean1	1.15	0.71	1.07	1.29	1.03	1.23

4.2.4 Group 3

In this section, the results of two bare steel and two fully cladded diaphragm tests are discussed. Since the objective was to understand the influence on diaphragm behaviour from the non-structural roofing components, the basic specimen configuration was the same for all specimens except, of course, for the additional gypsum, insulation, fibreboard, etc. The nail and screw connection configuration was selected because this type of diaphragm has previously exhibited the most consistent results during testing. The test specimen descriptions are given in Table 4.20 and a full description of the composition of the non-structural components can be found in Section 4.1.4.

Table 4.20 Test specimen description (Tests 43 to 46)

Steel properties:	
Supplier and coil number	Canam P-3615 B deck 0.76 mm Coil supplier: Sorevco Coil number: 358365
Base metal thickness (mm)	0.72
Fy measured (MPa)	317
Fu measured (MPa)	377
E measured (MPa)	195520
50 mm gauge % elongation	37 %
Fasteners:	Spacing: 305 mm c/c
	Side-lap fasteners: Screw 12- 14 x 1 HWH#1 FP
	Deck-to-frame fasteners: Hilti nail X-EDNK-22 THQ 12M

4.2.4.1 Test 43

The intent of carrying out bare sheet monotonic test #43 was to provide a specimen that could be directly compared with the fully cladded specimen #45 in order to evaluate the influence of non-structural components. During the nail installation, fasteners at positions K1, I11, K16, L16, M16, G21 and I21 were replaced because the first installation did not provide the necessary nail penetration into the frame. The quality index, the nail head standoff after final installation, is provided in Appendix 2.

As per previous monotonic tests, the progression of shear behaviour and connection failure throughout the experiment is documented as follows: as the load increased, the warping deformation of the panel profile became more and more extensive (Figure 4.88). The load vs. deflection graph was shown in Figure 4.89. When the load reached 75.4 kN (S = 12.37 kN/m, or $S/S_{u,MON}$=0.92 approximately) at a shear deformation of γ = 7 rad/1000, the nail at I21 sheared (Figure 4.90). At this point a sudden drop in the resistance occurred (Figure 4.89). In addition, the early breakage of this fastener caused other connections failures along gridline I before ultimate load reached, and also resulted in a sudden increase in the side-lap slip (3,4 side-lap).

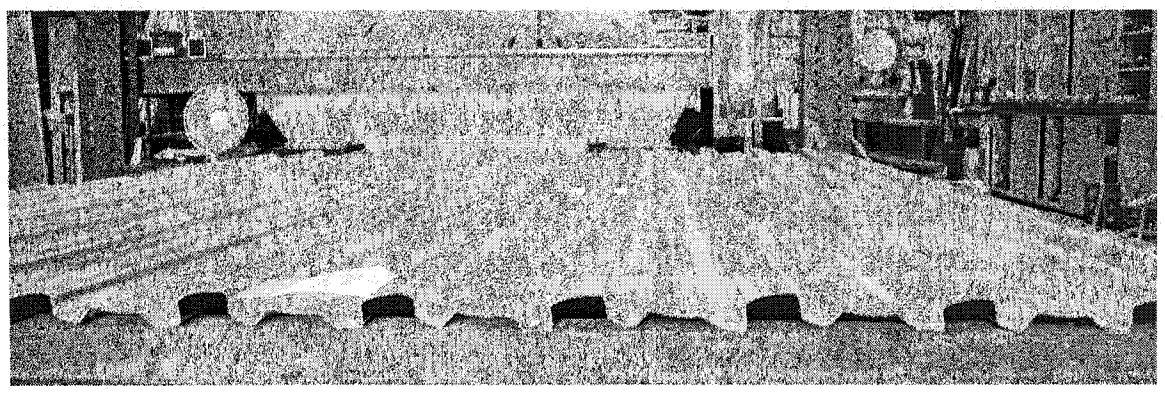

Figure 4.88. Warping deformation of the panels

Test No.43
P3615B - 0.76 mm
Sidelap fasteners : screwed @ 305
Frame fasteners : Hilti nailed @ 305
*Su , SDI * = 10.83 kN/m*
Su , MON Test 44 = 10.47 kN/m
Su , MON Test 43 = 13.40 kN/m

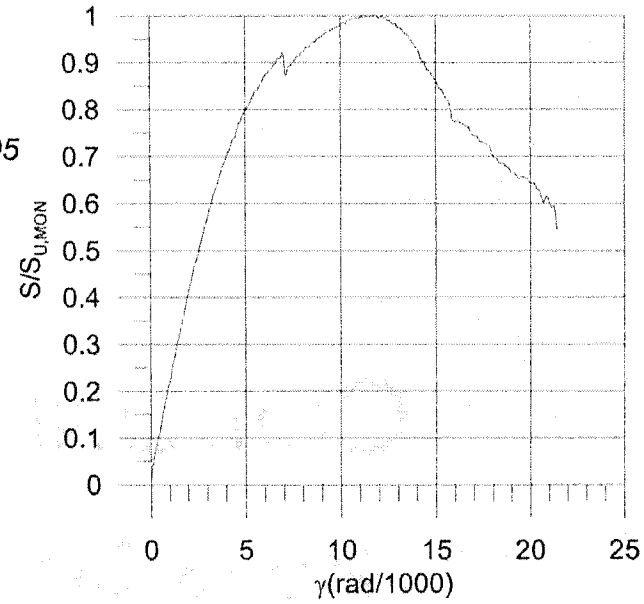

Figure 4.89. Shear load vs. rotation graphs for test 43

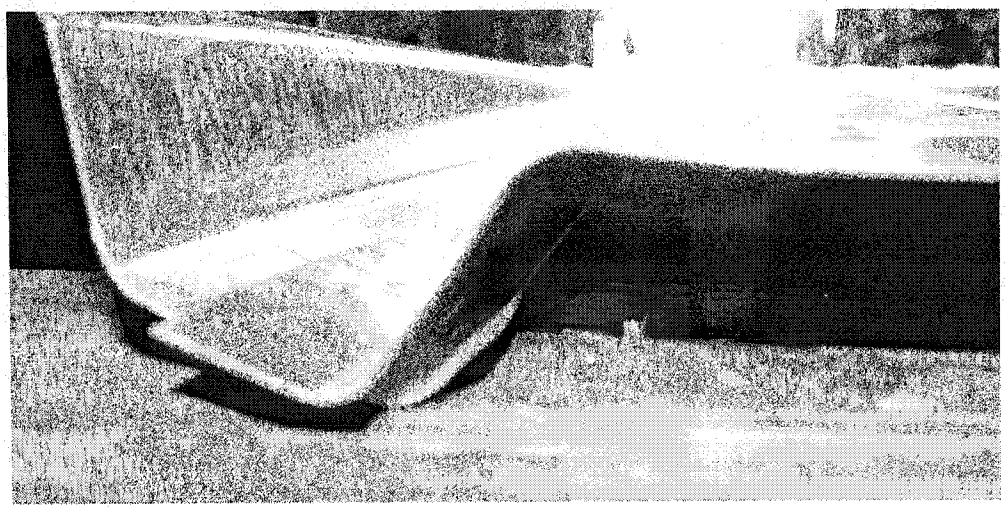

Figure 4.90. Nail shear at I21 when load reached 75.4 kN

Forces in the diaphragm were redistributed to other fasteners and the load continued to increase until a maximum of 81.71 kN (S_u=13.40 kN/m) was obtained at a shear deformation of γ = 11.86 rad/1000. From this point on, the shear resistance of the diaphragm decreased until the test was stopped.

Table 4.21 The failure modes of Deck-to-Frame connections of test 43

Position	1		6		11		16		21
B									
C	**BE+TE**		**BE**		**BE**				**BE**
D			BE		BE				
E									
F	**BE+TE**		**BE**		**BE**				**BE+BU**
G									
H			BE						
I	**BE+TE**		**BE**		**BE+TE+BU**		**BE+BU**		**SH**
J			BE						
K									
L	**BE**		**BE**		**BE**		**BU+BE**		**BE+BU**
M					BE				

BE--Bearing failure; BU--Buckling failure; TE--Tearing failure; SH--Nail shear

The failure modes of the deck-to-frame connections after completion of the test are listed in Table 4.21. The majority of failures consisted of tearing, bearing, or buckling of the steel sheet near the connections (Figure 4.91 & 4.92). Only one case (I21 in Figure 4.90) of shear failure at the fastener occurred. The early shearing of this nail may be due to two reasons:

1) The shear force distributed to each connection was not uniform, and hence this particular joint might had a higher stress concentration than any others;

2) The installation quality of this nail did not meet the manufacturer's requirements.

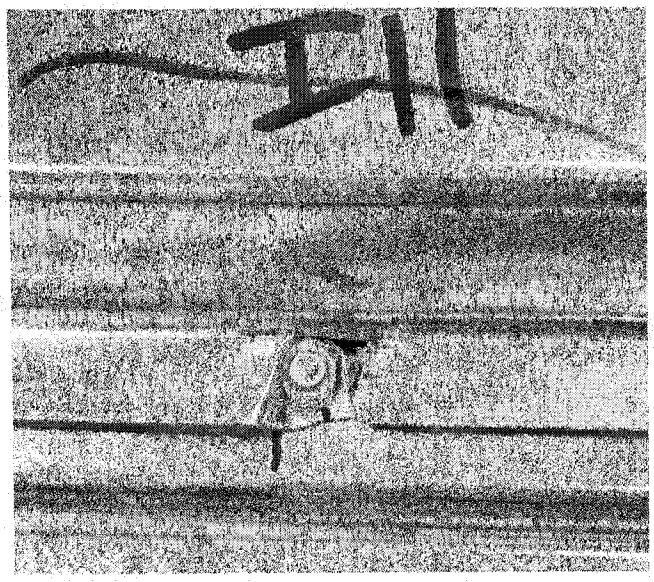

Figure 4.91. Side-lap slip and bearing, tearing damage of steel sheet at I11

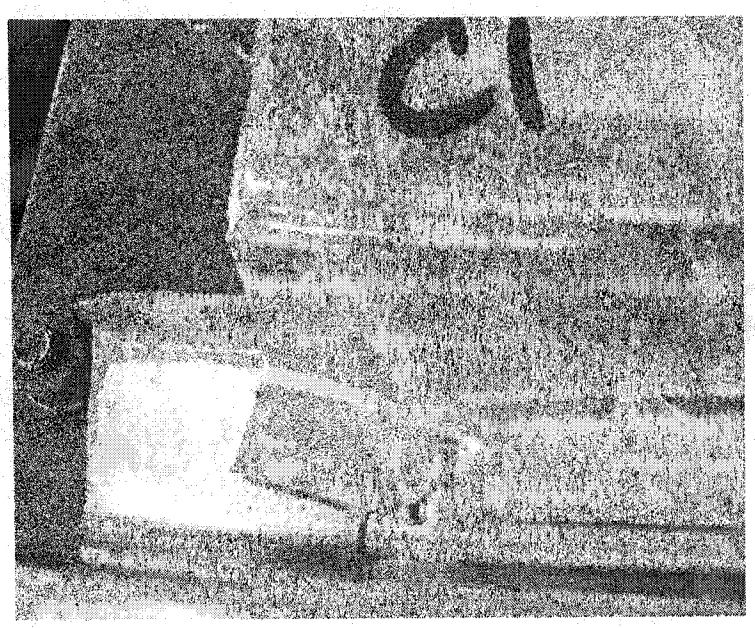

Figure 4.92. Side-lap slip and bearing, tearing damage of steel sheet at C1

An ink line was marked at the locations along the side-laps as a visual reference used to evaluate the extent of slip. This line extended from one sheet to the other making possible to see the deformation along the side-laps, as can be seen in Figures 4.91 and 4.92.

All the screws tilted to some degree under loading, and only the screws at C20 and at F20 were pulled out (the screw at C20 in Figure 4.93). Substantial sheet buckling near the screw connections was also observed (Figures 4.93 & 4.94).

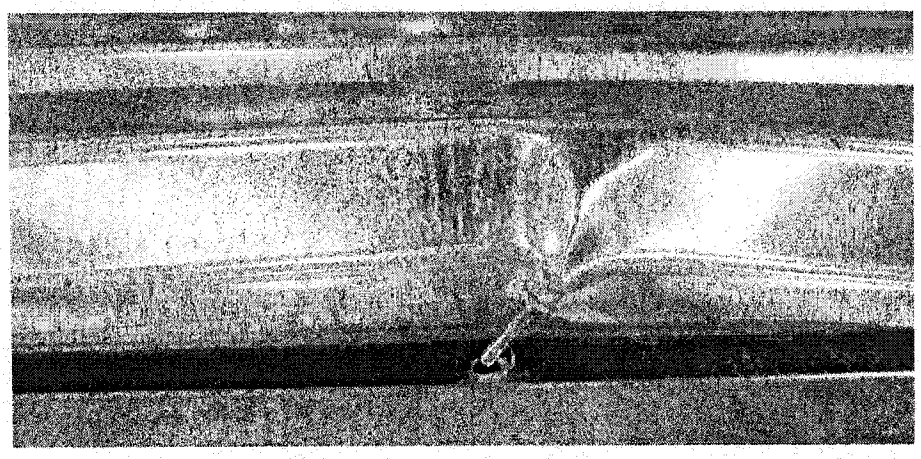

Figure 4.93. Sheet buckling, screw tilt and pull out at C20

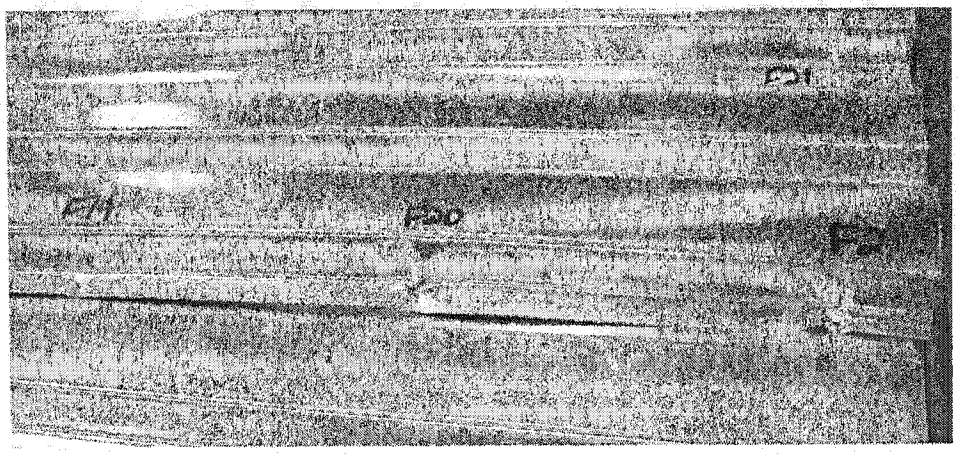

Figure 4.94. Sheet buckling, screw tilt and pull out at F20

The slips related to rotation γ from 0.00 to 12.00 rad/1000 (slightly larger than the γ_2=11.86 rad/1000) are shown in Figure 4.95. The slips at the south side and north side were very small, whereas the interior side-lap slip constituted the majority of the diaphragm shear distortion. The biggest slip at side lap 3-4 may be related to the nail shear failure at I 21.

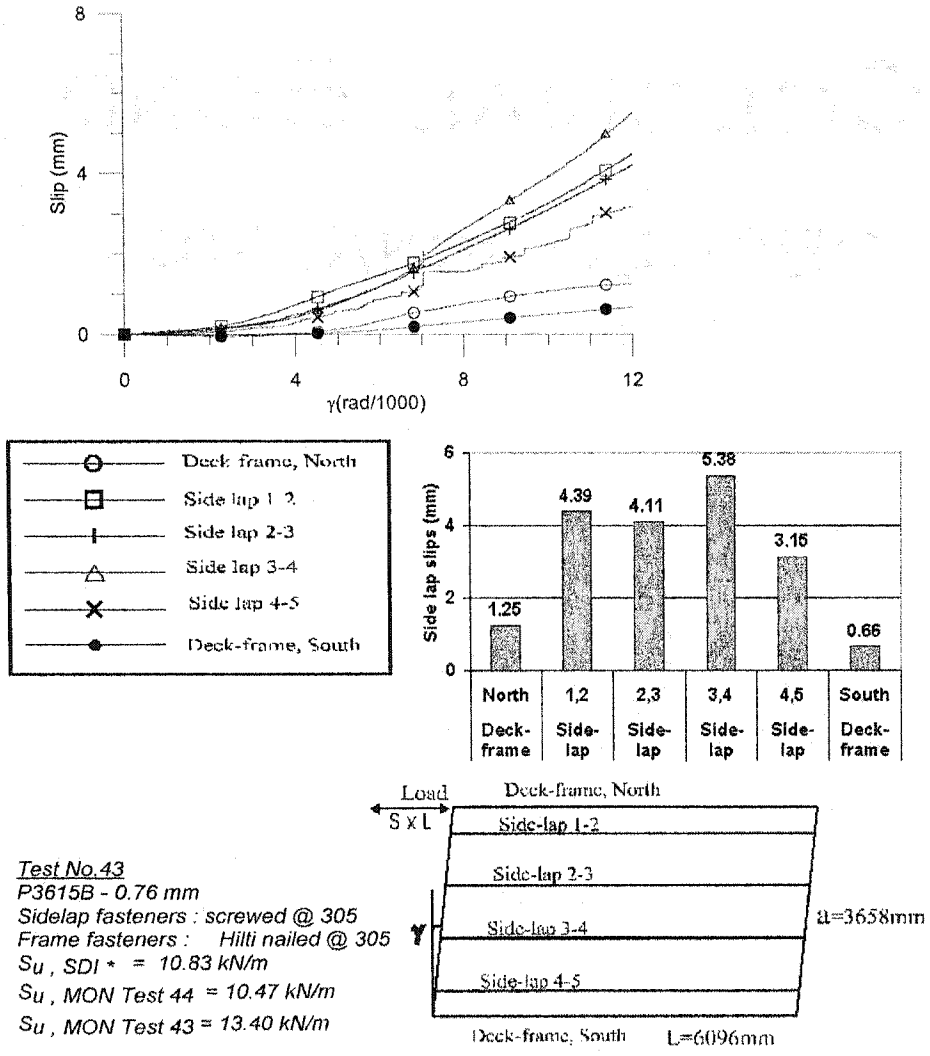

Figure 4.95. Slip deformation vs. rotation (0.0 to γ_2) graphs for test 43

4.2.4.2 Test 44

The testing of specimen 44 was divided into two phases: cyclic load and monotonic load. The cyclic load phase was under load control. Its frequency was 0.5 Hz. It is noted that the real cyclic load did not reach the target load because the actuator did not function properly (see Figure 4.96 and the ratio of test/target load approximately equals to 0.8 in Table 4.22). In the target cyclic load protocol, the unit shear force S was expected to reach about 60% of the ultimate shear strength S_u, which was estimated based on the SDI approach (Section 4.1.7.3).

In Figure 4.97, the cyclic results of test 44, it is noted the unit shear force S reached approximately 60% of the $S_{u,MON\ Test44}$., the hysteresis of S/ $S_{u,MON\ Test44}$ to γ is almost linear, which is shown in Figure 4.98 in seven loading segments. Figure 4.99 shows that, the slips were quite small during the cyclic loading phase.

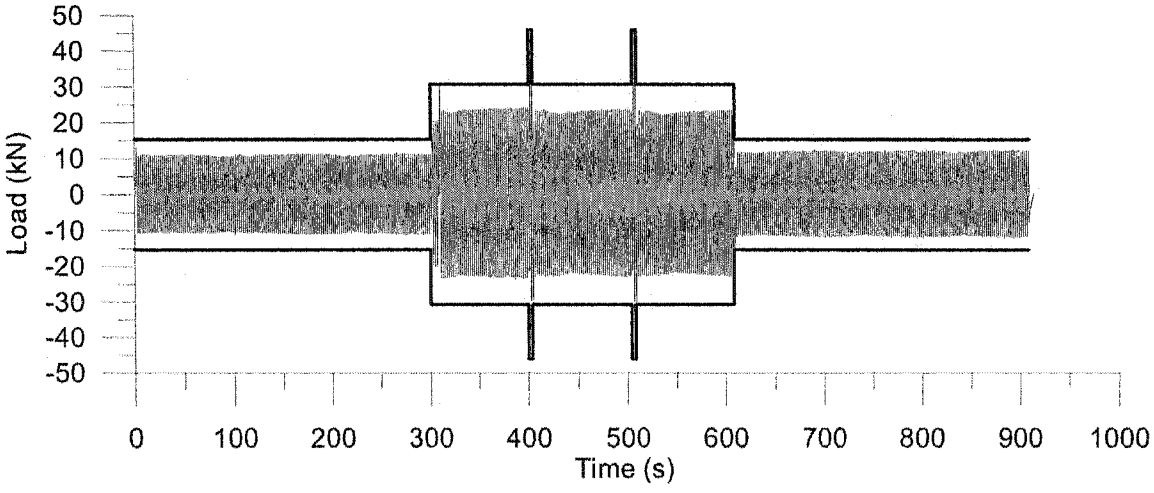

Figure 4.96. The comparison of target load to test load protocol for test 44

Table 4.22. The comparison of target load to test load protocol of Test 44

Segment		1	2	3	4	5	6	7
Target Load	KN	15.36	30.72	46.08	30.72	46.08	30.72	15.36
Test load	kN	11.40	24.11	36.78	23.73	38.21	23.42	12.17
Test / Target Load		0.74	0.78	0.80	0.77	0.83	0.76	0.79

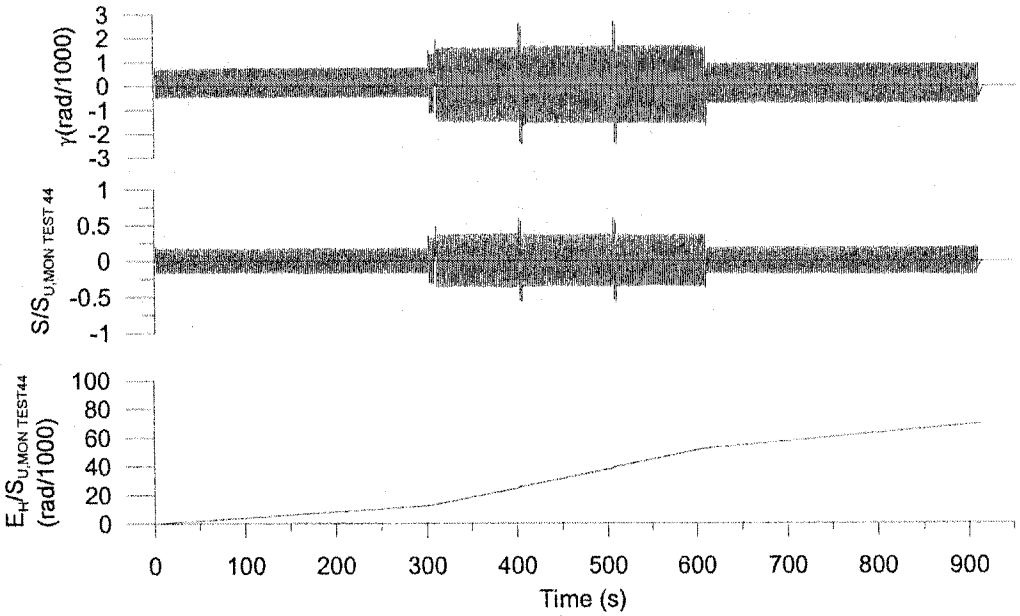

Test No.44-Cycles prior to monotonic load
P3615B bare sheet- 0.76 mm
Sidelap fasteners : screwed @ 305
Frame fasteners : Hilti nailed @ 305
*Su , SDI * = 10.83 kN/m*
Su , MON Test 44 = 10.47 kN/m
Su , MON Test 43 = 13.40 kN/m

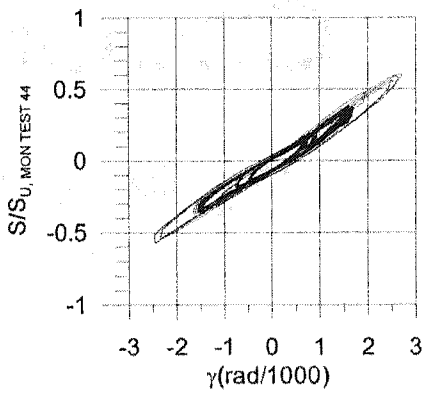

Figure 4.97. Time history of test 44 for the cyclic load phase

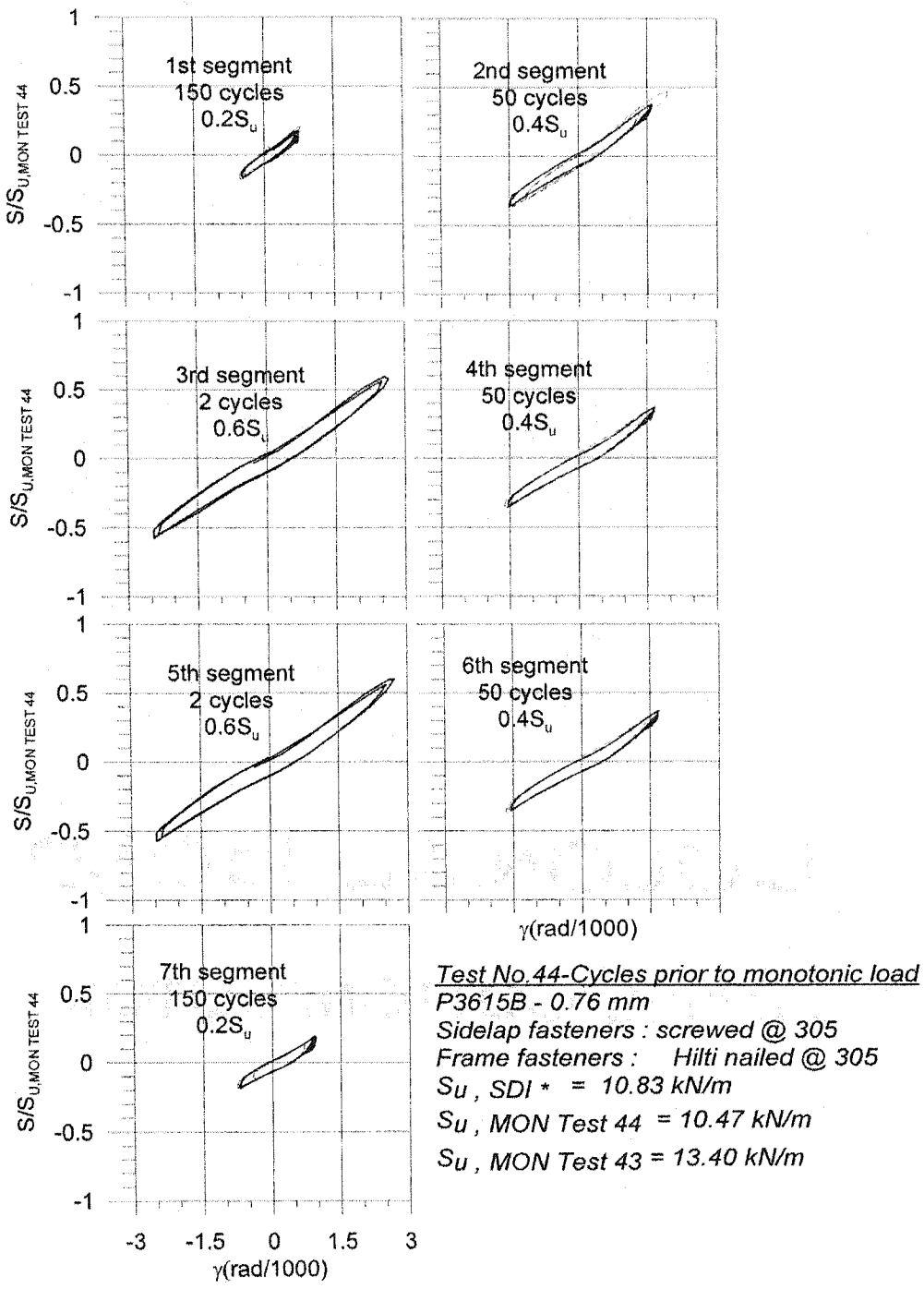

Figure 4.98. Force-deformation hysteresis of test 44 for the cyclic load phase

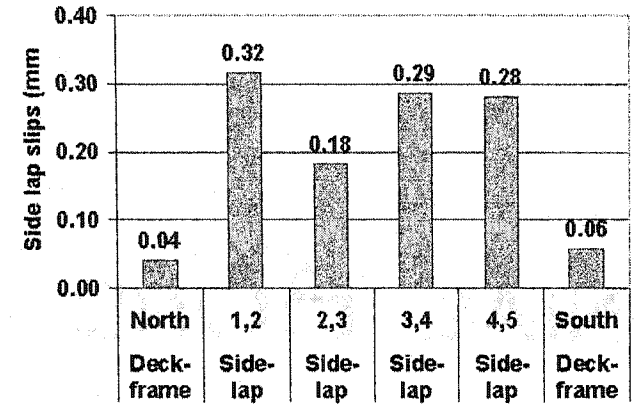

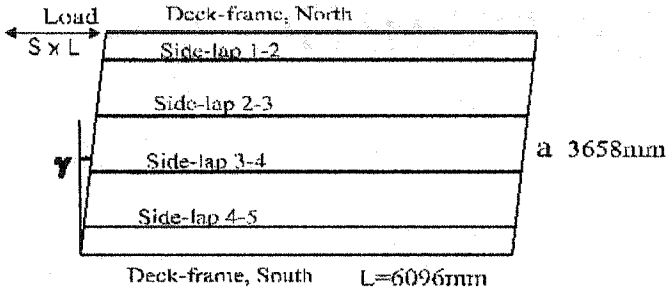

Test No.44-Cycles prior to monotonic load
P3615B bare sheet- 0.76 mm
Sidelap fasteners : screwed @ 305 Frame fasteners : Hilti nailed @ 305
*Su , SDI * = 10.83 kN/m*
Su , MON Test 44 = 10.47 kN/m; Su , MON Test 43 = 13.40 kN/m

Figure 4.99. Maximum side lap slips at cyclic load phase

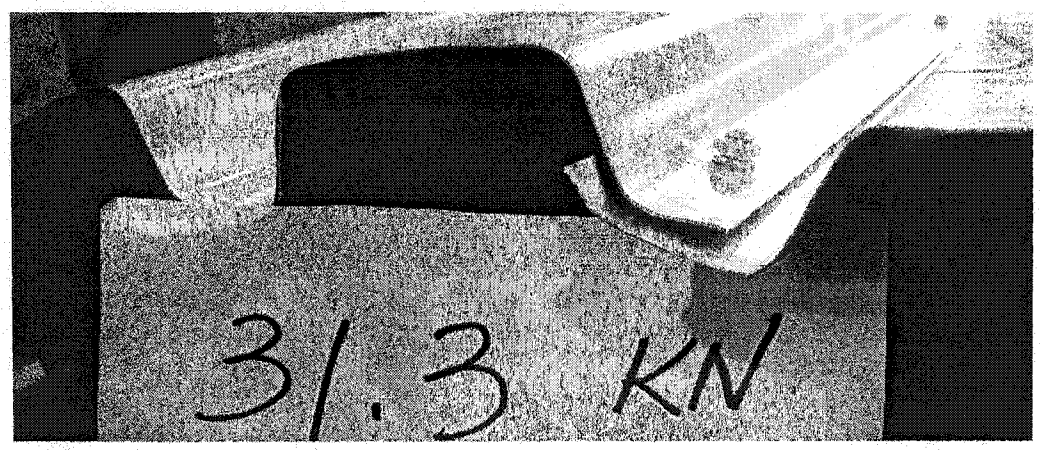

Figure 4.100. Nail shear at L21 when loaded at 31.3 kN in cyclic load phase

The mostly linear force-deformation relationship in Figure 4.98 gives an impression that the diaphragm seemed in the elastic range under cyclic loading. Actually, the nail at L21 sheared at a relatively low load of 31.3 kN (S=5.13 kN/m), during the cyclic load phase, see Figure 4.100. The early damage of this nail may be due to the non-uniform force distribution and the low installation quality for this specific fastener. The head standoff of nail L21 was 8.75 mm, which is among the largest measured, while the average head standoff was 6.87mm.

This early damage of nail L21 also caused the ultimate resistance $S_{u,\ MON\ Test\ 44}$=10.47 kN/m, which is much lower than $S_{u,\ MON\ Test\ 43}$ (13.40 kN/m), see Figure 4.101. The force measured during the monotonic phase was filtered at a frequency 0.02 Hz because it was initially found that the loading was not stable. The high frequency signals were filtered so that the normalized shear vs. rotation curve in Figure 4.101a became smooth. The values for slips were not filtered, and hence the curves in Figure 4.101b exhibit some high frequency noises. As found from previous monotonic tests, the interior side-lap slips constitute a significant portion of the overall shear deformation of the diaphragm specimen, see Figure 4.101c. The interior slips here are quite uniform. The exterior slips at the south and north sides are once again so small that they can be considered as non-existent.

As discussed, during the cyclic loading phase, the nail at L21 failed in shear. The progression of failures in the monotonic loading phase was not recorded. The final failure modes were recorded in Table 4.23, where both connection damage and steel sheet damage existed. In Test 43, only one nail failed in shear. In contrast, for this specimen four nails failed in shear. Hence it is possible that the early cyclic loading history did influence the monotonic diaphragm response. The details of the observed failure modes can be seen in Figures 4.102 to 4.105.

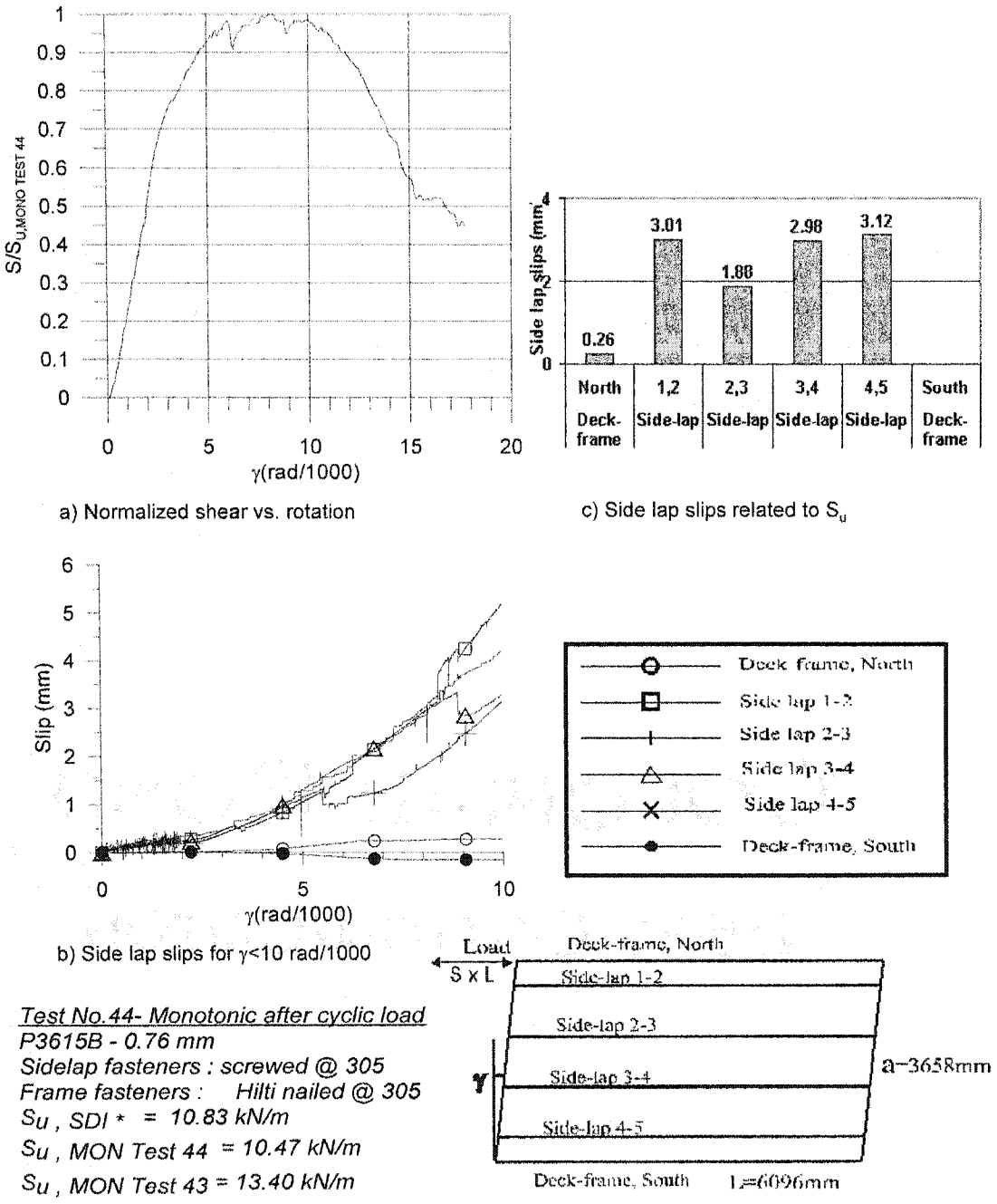

Figure 4.101. Results of test 44 for the monotonic load phase

Table 4.23 Failure modes after both cyclic and monotonic phases of Test 44

Position	1		6		11		16		21
B									
C	**BU**								**SH**
D									
E									
F	**BU**		**SH**						**TE+BE**
G									
H									
I	**BE+BU**				**BU**				**SH**
J									
K									
L	**BU**								**SH**
M									

BE--Bearing failure; BU--Buckling failure; TE--Tearing failure; SH--Nail shear failure

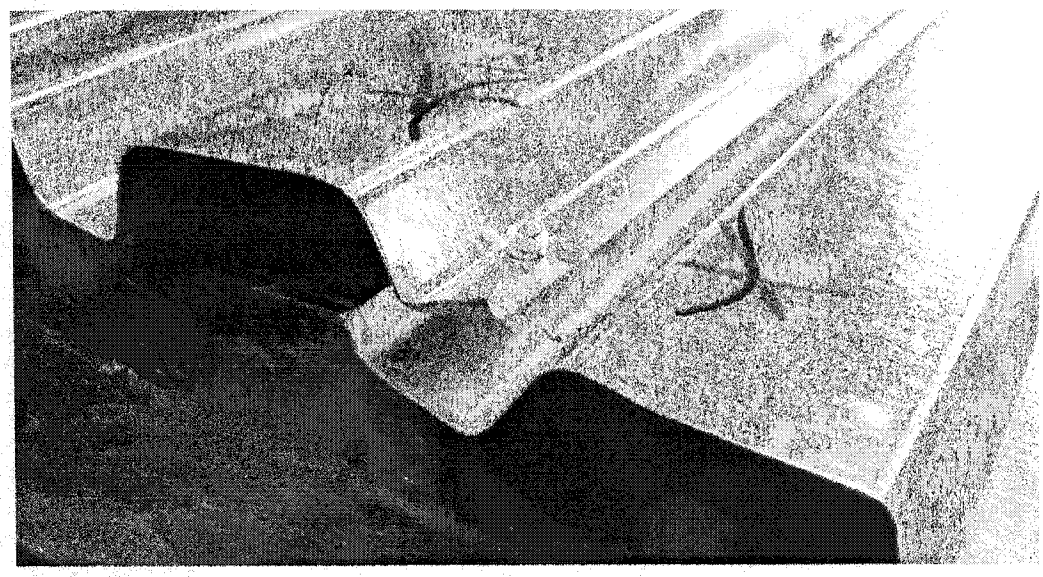

Figure 4.102. Nail shear failure at I21

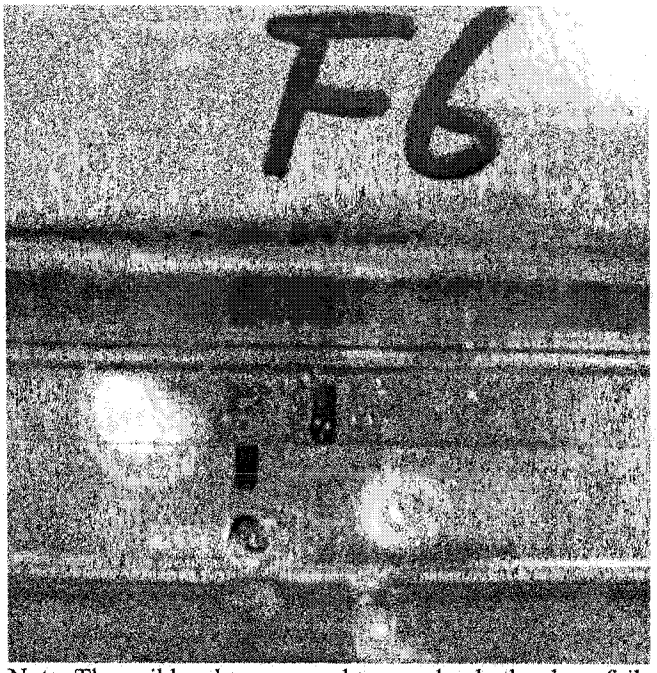

Note: The nail head was moved to see clearly the shear failure.

Figure 4.103. Side-lap slip and nail shear failure at F6

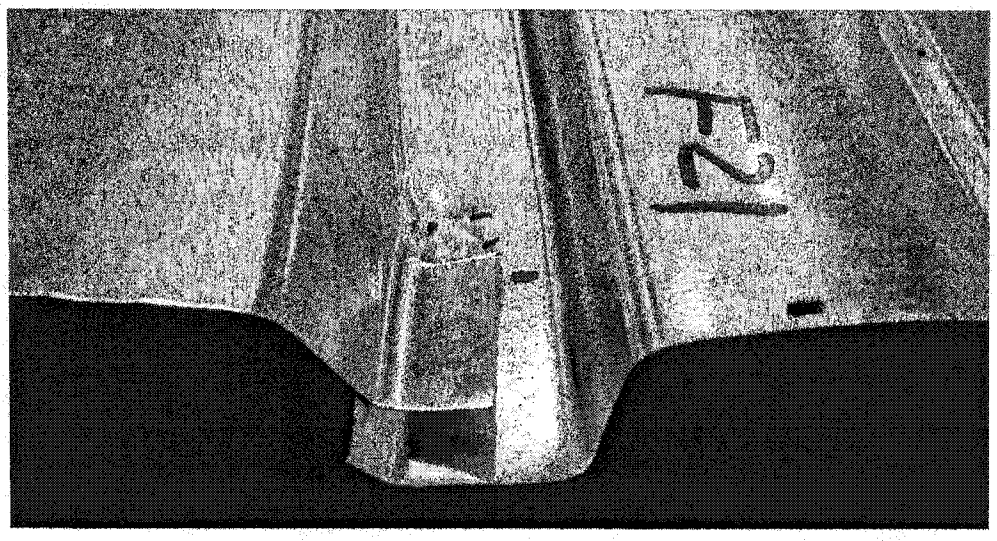

Figure 4.104. Tearing, bearing, and buckling of steel sheet near F21

Figure 4.105. Screw tilt, sheet tearing and buckling, and slip at L3

4.2.4.3 Test 45

Specimen #45 was a monotonically tested diaphragm constructed with non-structural components. The installation of the roofing material was presented in Section 4.1.4. Detail of the nail installation quality is provided in Appendix 2. The general failure modes observed were the deformation of the steel sheet, the cracking of the gypsum board, as well as the buckling and tearing of the steel sheet around nails (Figure 4.106 to 4.111). Because the roofing materials covered the deck, it was not possible to establish the failure situations of interior connections thoroughly, however, all of the

previously tested bare sheet diaphragms demonstrated that the connections at the both ends are damaged in advance of the interior connections. Since no shearing of nails was observed along the two ends, one can say that nails did not shear for this specimen. In addition, it was not possible to inspect the failure modes after the non-structural components were removed because tools or sometimes machines were required in the removal. Thus, all the compositions were damaged, including the structural components.

During the loading, the decks experienced significant warping deformations between two deck-to-frame fasteners, one flute width enlarged and another one diminished (Figures 4.106 & 4.107).

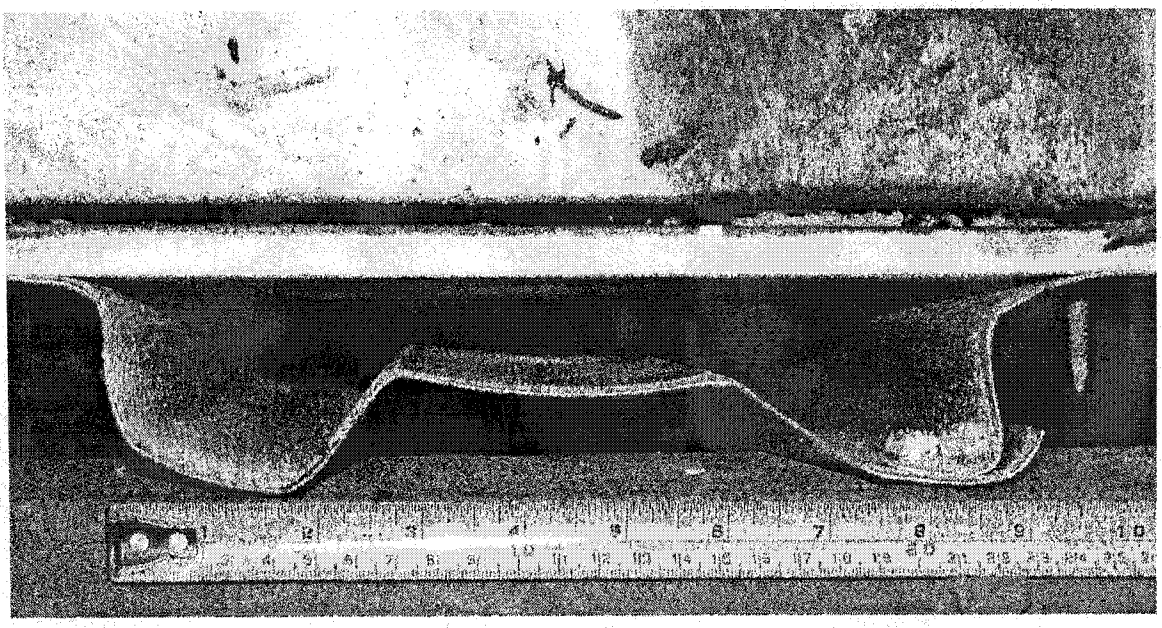

Figure 4.106. Steel sheet deformation during loading, flute width enlarged

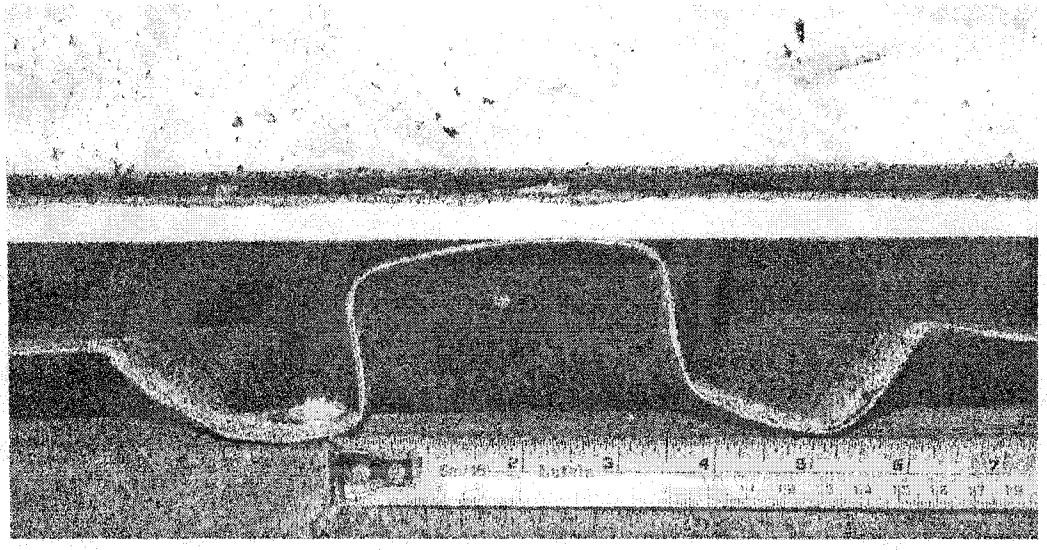

Figure 4.107. Steel sheet deformation during loading, flute width diminished

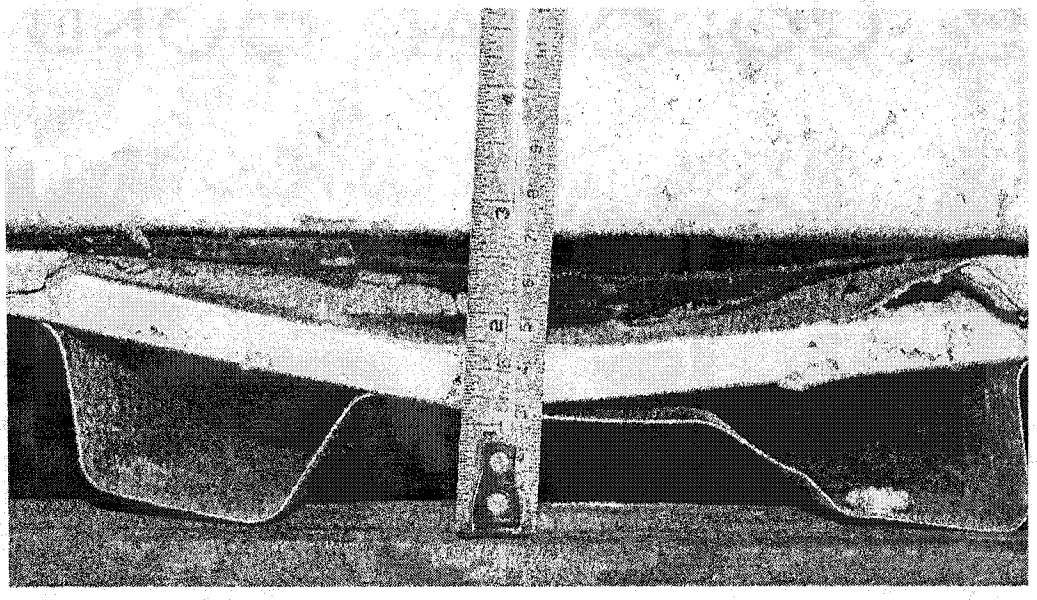

Figure 4.108. Steel deck flute height diminished, gypsum board cracked

The gypsum board in Figure 4.108 cracked because the screw that connects it to the top sheet of the steel deck pulled the gypsum board down. The gypsum board at the frame corner was damaged due to bearing and tearing from the fastener (Figure 4.109).

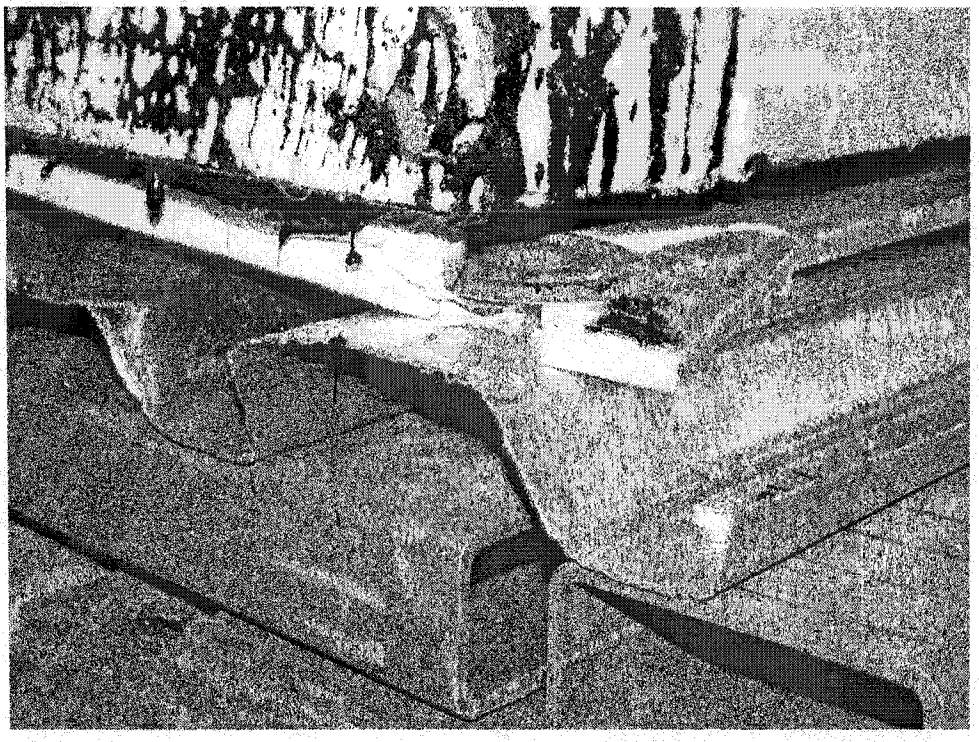

Figure 4.109. Cracking of gypsum board at the frame corner

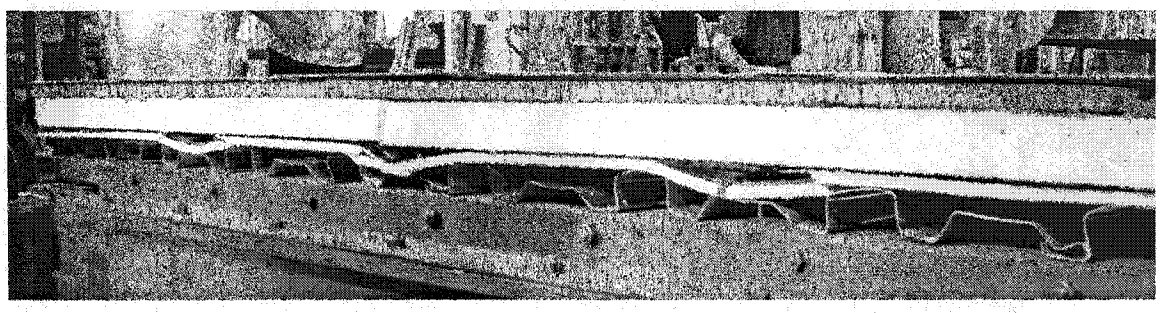

Figure 4.110. Warping deformation of steel deck and cracking of gypsum board

The roofing materials, except the gypsum board, exhibited no detectable deformations (Figure 4.110), the reason may be that the stress and strain in the non-structural components other than gypsum board was very small. The ISO insulation layer was too flexible to transfer any loads through it, so whatever is located above it did not experience significant deformations.

The steel sheet may experience bearing and tearing failure together with the cracking of the gypsum board (Figure 4.111). However no nail failure was observed along the sheet ends.

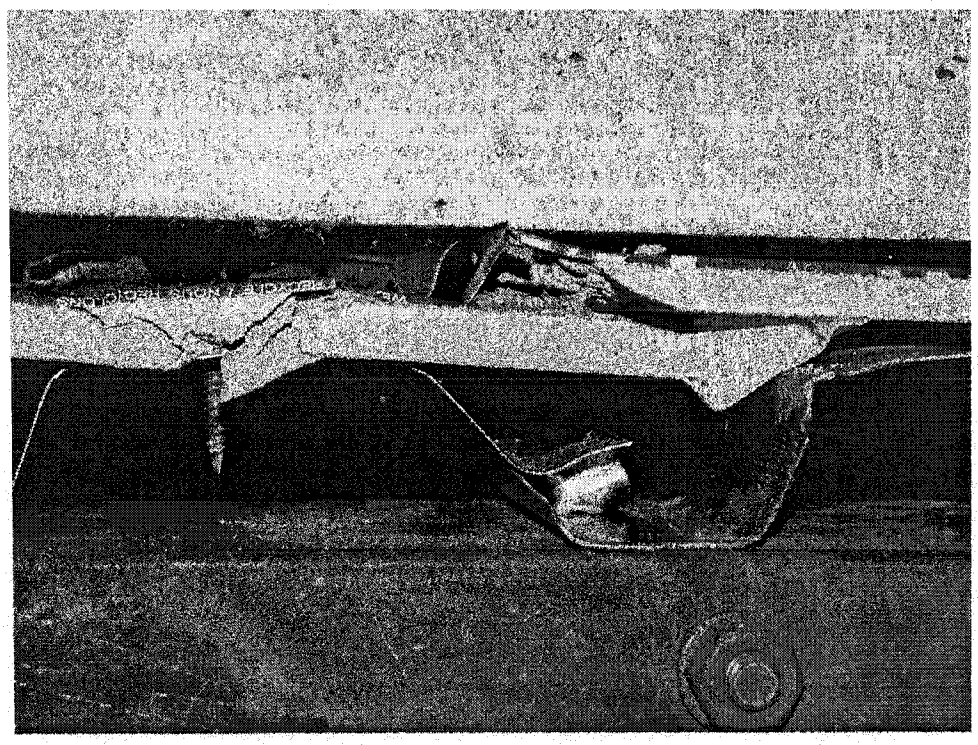

Figure 4.111. Tearing of steel sheet and cracking of gypsum board

The force-deformation relationship is shown in Figure 4.112. It is found that the measured strength was much higher than $S_{u,SDI*}$ that was estimated from bare sheet diaphragm. The strength increased about 44% here as compared to $S_{u,SDI*}$. The stiffness measured is 4.17 kN/mm, which is also higher than that estimated from the bare sheet specimen. A more detailed result comparison will be presented in Section 4.2.4.5.

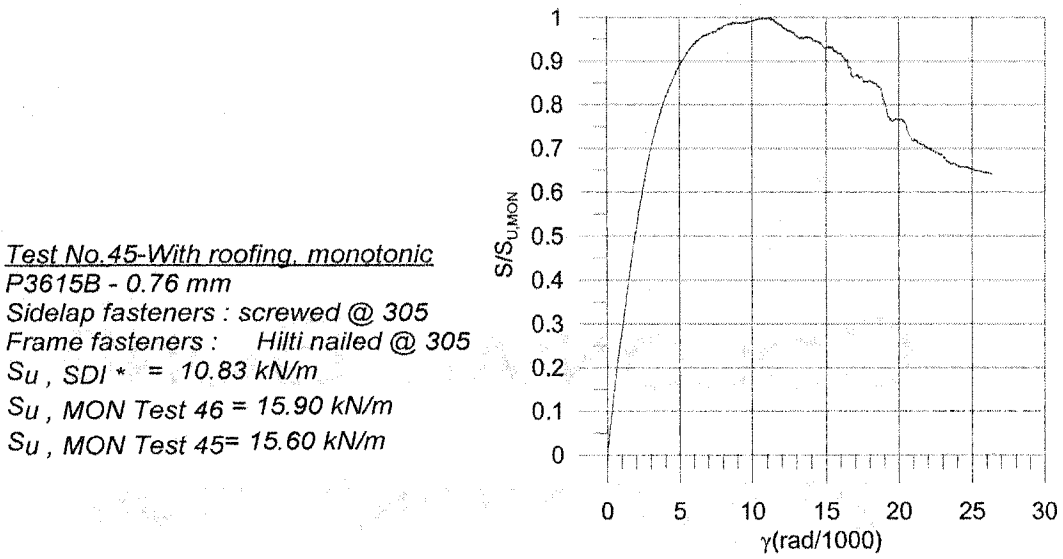

Figure 4.112. Normalized shear vs. rotation curve of test 45

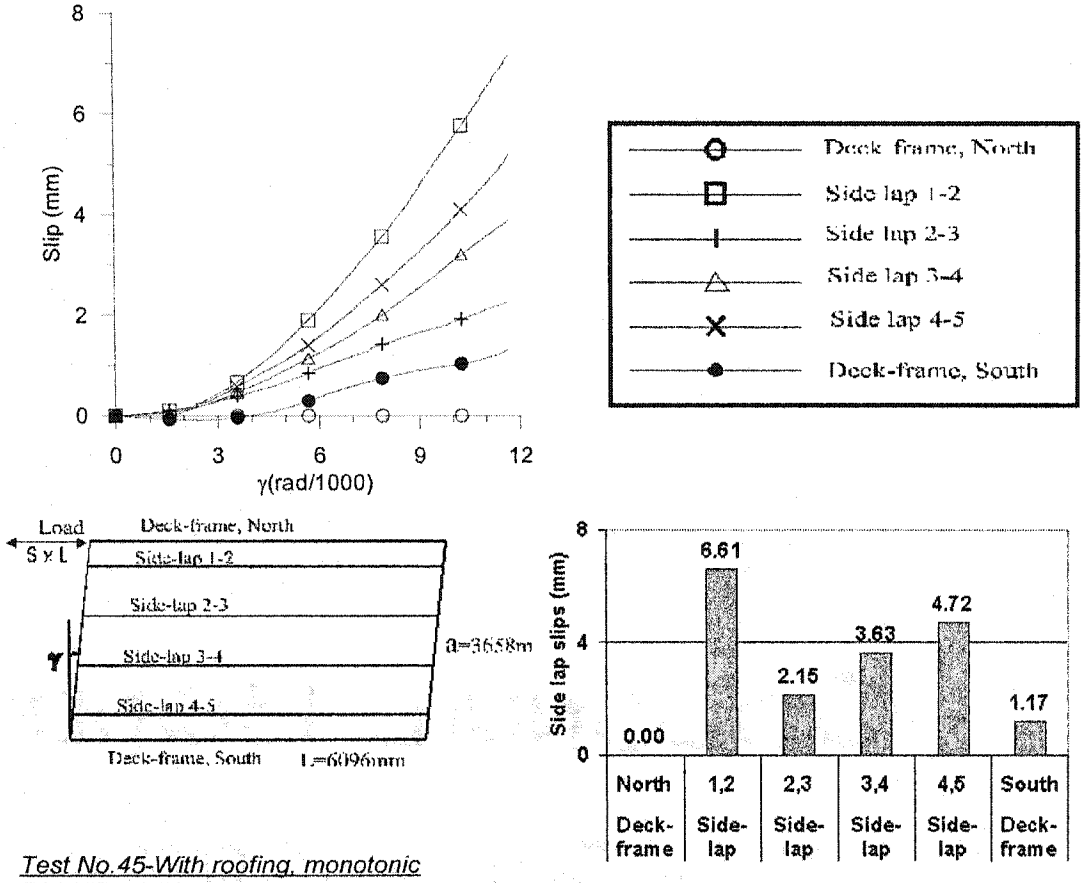

Test No.45-With roofing, monotonic
P3615B - 0.76 mm
Sidelap fasteners : screwed @ 305 Frame fasteners : Hilti nailed @ 305
*Su , SDI * = 10.83 kN/m Su , MON Test 46 = 15.90 kN/m Su , MON Test 45= 15.60 kN/m*

Figure 4.113. Slip deformation vs. rotation (0.0 to γ_2) graphs for test 45

During testing, when load reached its peak, the related rotation γ_2 was equal to 11.13 rad/1000. The relationship of slips vs. rotation is given in Figure 4.113 for the deformation range 0.0 to γ_2. The slip measurement on the north side is not correct because the LVDT was out of order. It is expected to be very small based on the measured slips in previous tests. The slips for the interior side-laps were not uniform

as compared to that observed for the bare sheet diaphragms. This characteristic may be due to the influence of the arrangement of the gypsum board panels, which were not continuous, nor connected with one another as the steel deck panels were. The middle steel panel, which was covered by a whole gypsum board (the middle gypsum board in Figure 4.23), experienced less slips at the side-laps 2-3 and 3-4 than at the side-laps 1-2 and 4-5. This is most likely because the stiff gypsum board acted as a reinforcement.

4.2.4.4 Test 46

Test Specimen 46 was constructed in a similar manner to #45 in order to evaluate the effect of pre cyclic loading on the monotonic shear performance of a diaphragm with non-structural components. It was necessary to re-install some nails at D16, I16, J16, K16, F21, G21, and K21, where the initial nail penetration was not adequate. This most likely happened when these nails were located at the same positions used by previous tests. After re-installation, all nails were qualified. See Appendix 2.

Similar to test specimen 44, diaphragm Test 46 was subjected to two load phases: cyclic load and monotonic load. Again, the measured load did not reach the target load values (Figure 4.114) due to a technical problem with the load actuator. It was found that the ratios of test/target loads are approximately the same as for Test 44.

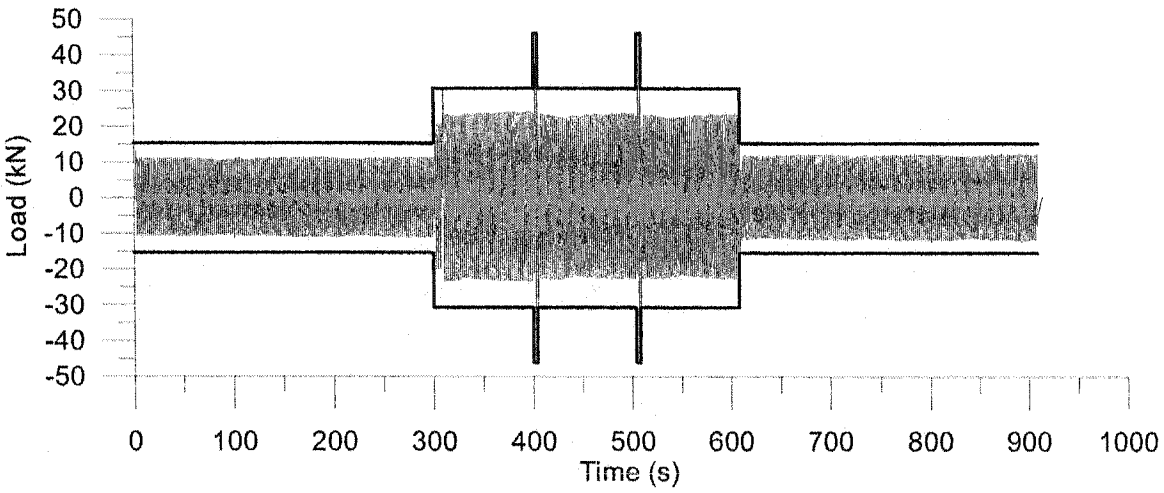

Figure 4.114. The comparison of target load protocol to test load protocol

After the cyclic load phase had been completed, a survey of the diaphragm specimen revealed that no damage occurred to any of the material layers. This should have been expected because the shear load imposed on the diaphragm during cycling was only 48% of the ultimate capacity of the specimen because the target maximum load was $0.6P_u$, where P_u is estimated from the bare sheet diaphragm. The actual test maximum load was only about 80% of the target maximum load due to a malfunction of the actuator. Hence the actual load for the cyclic load phase was about 48% (0.6 x 80%) of the ultimate load capacity of the bare sheet diaphragm. It should be noted that the maximum resistance capacity for roofed diaphragm should be even stronger. The test result for this cyclic loaded phase is shown in Figure. 4.115, where the maximum $S/S_{U,MON\ TEST\ 46}$ is 0.39, which is smaller than 0.48 as was expected.

During the cyclic loading phase, the slips were very small; the maximum value was of only 0.12 mm (Figure 4.115). The detailed hysteresis of $S/S_{U,MON\ TEST\ 46}$ to γ for each load segment is shown in Figure 4.116. The stiffness that was obtained from the average of the 2nd segment (0.4 S_u) was 4.02 kN/mm. This value is larger than that

estimated from the bare sheet diaphragm by using the SDI approach (Table 4.7), but it is smaller than that measured in test 45 (4.17 kN/mm).

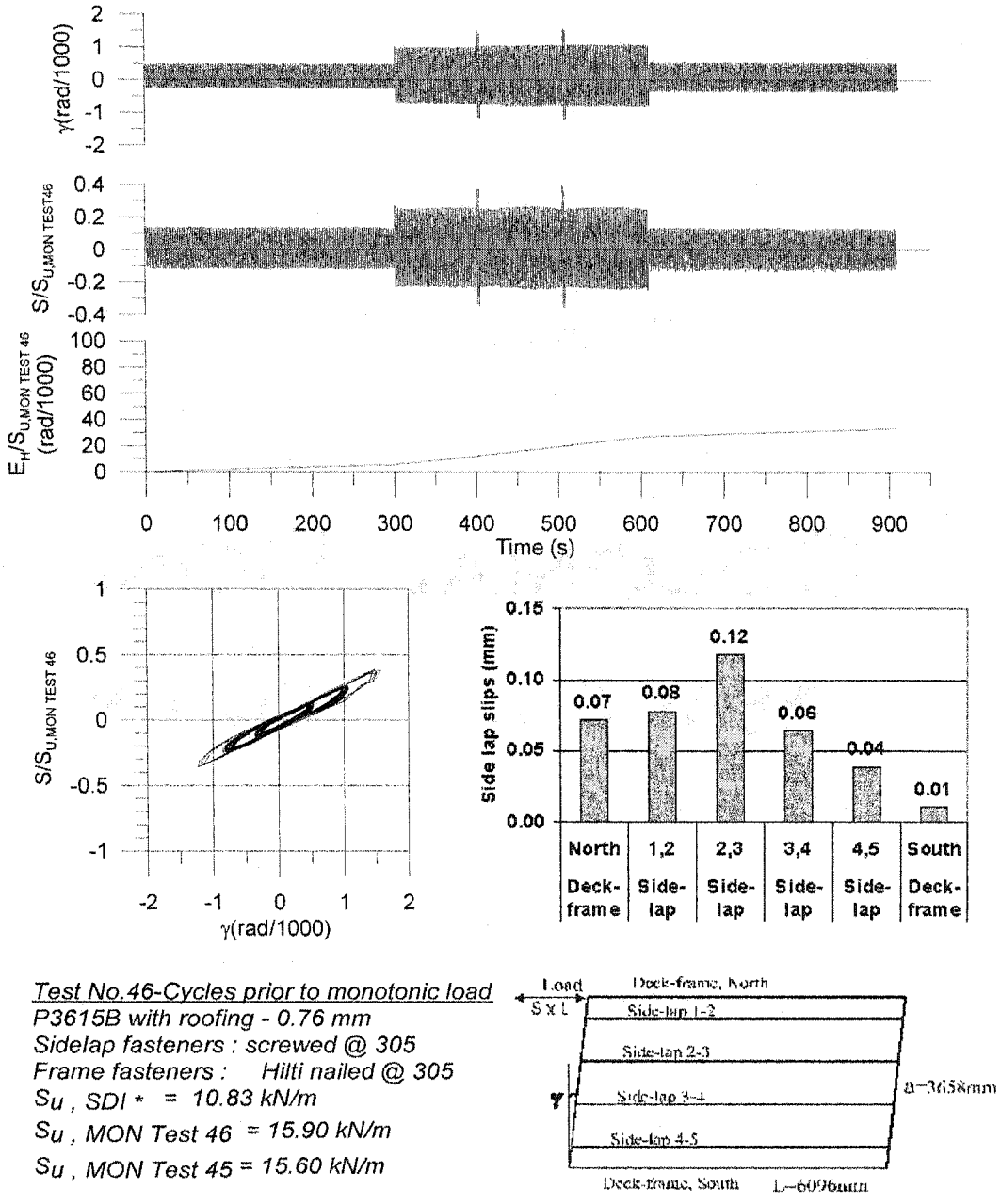

Figure 4.115. Results of Test 46 at cyclic loading phase

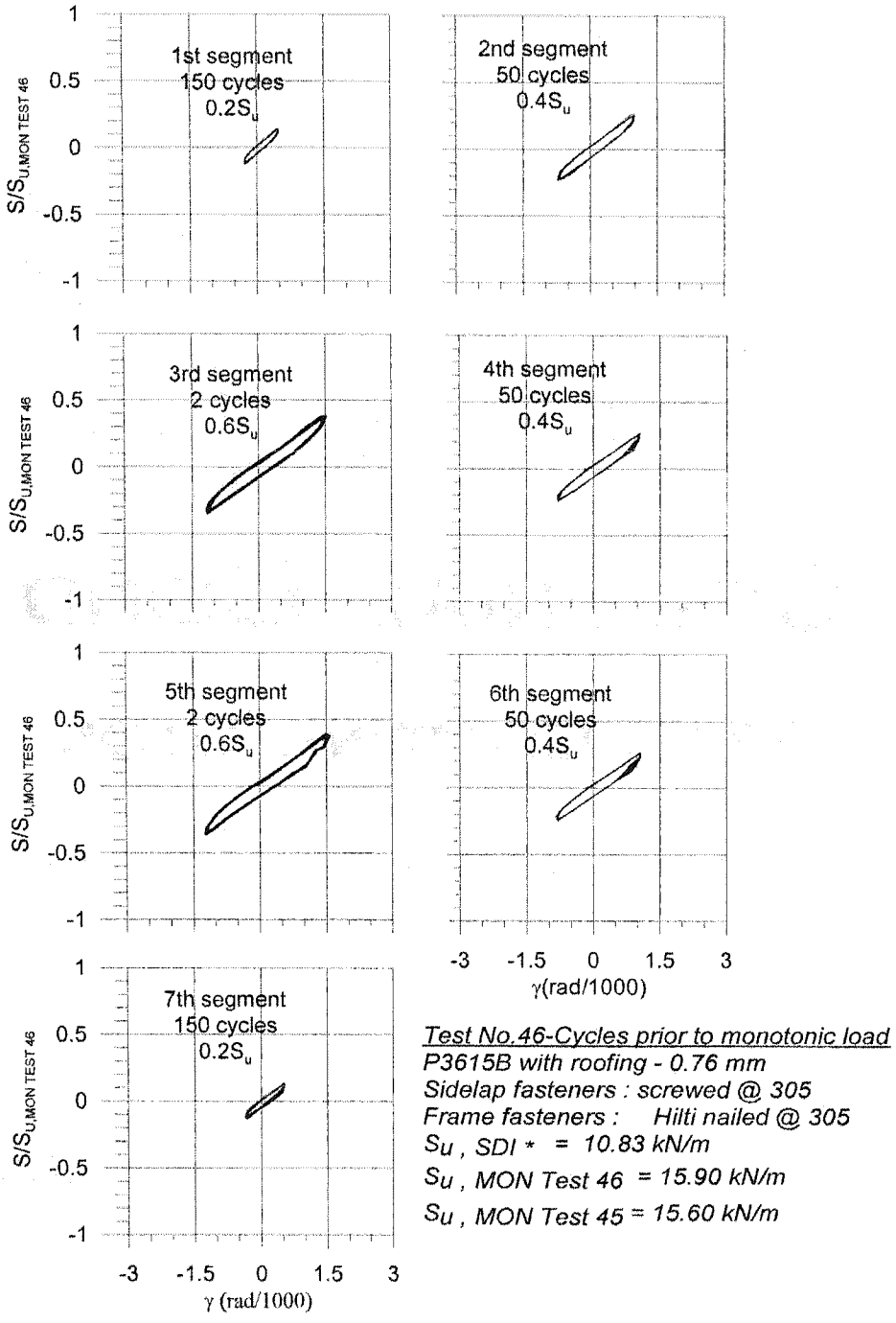

Figure 4.116. Detailed hysteresis of $S/S_{U,MON\ TEST\ 46}$ to γ at cyclic loading phase

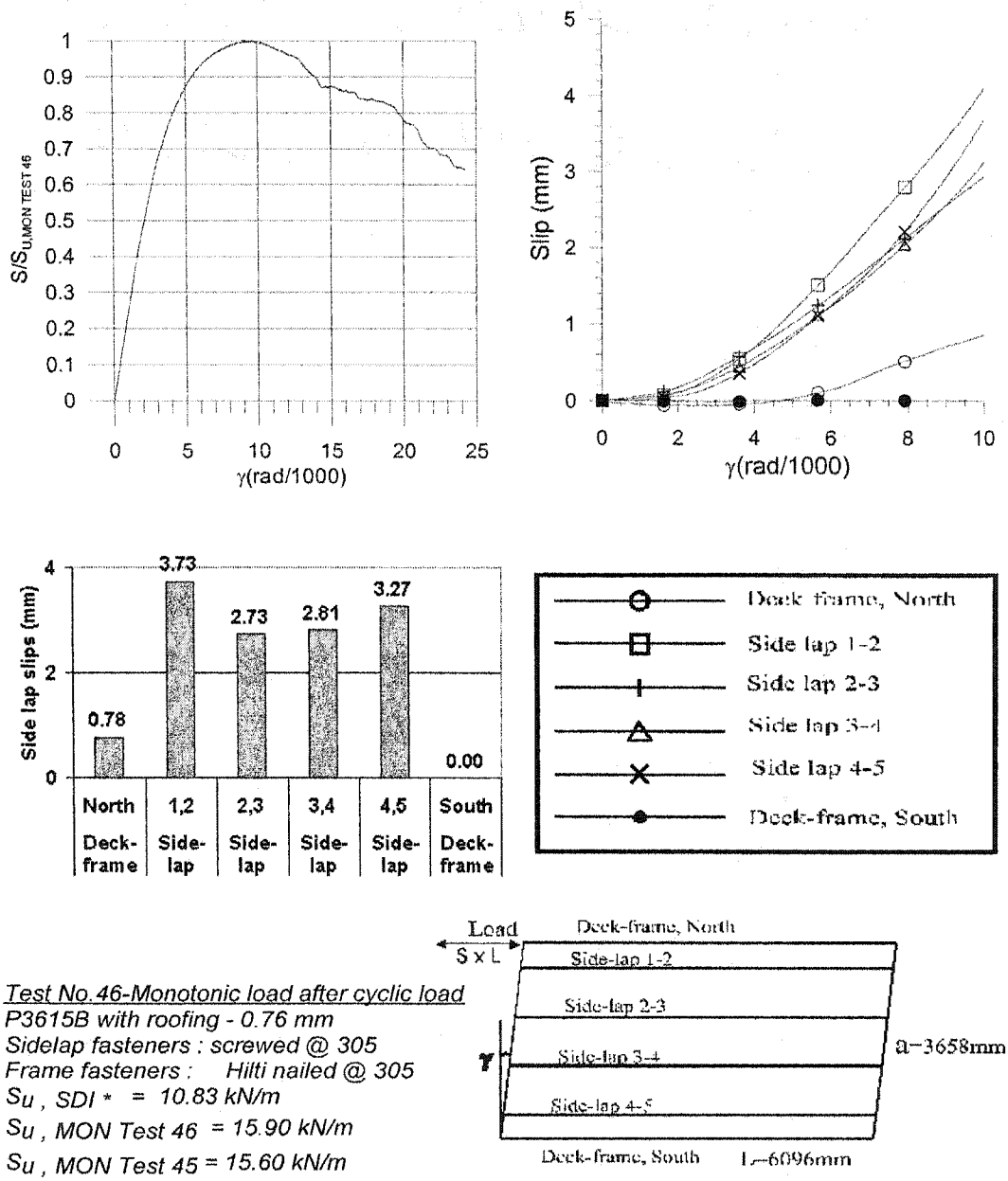

Test No.46-Monotonic load after cyclic load
P3615B with roofing - 0.76 mm
Sidelap fasteners : screwed @ 305
Frame fasteners : Hilti nailed @ 305
*Su , SDI * = 10.83 kN/m*
Su , MON Test 46 = 15.90 kN/m
Su , MON Test 45 = 15.60 kN/m

Figure 4.117. The results of Test 46 at monotonic loading phase

After the cyclic protocol was run, the diaphragm specimen was tested monotonically, which provided the normalized shear and slip vs. shear rotation results given in

Figure 4.117. The ultimate shear $S_{u,MON\ Test\ 46}$ was 15.90 kN/m, which is similar to test 45 (15.60 kN/m), and much larger than $S_{u,SDI*}$ that was estimated from the bare sheet specimen. The similarity of strength for these two specimens showed that the cyclic load did not decrease the strength. The stiffness G' of the diaphragm specimen determined for the monotonic loaded period for test 45 is 4.17 kN/mm. For test 46, it is 3.90 kN/mm. The difference is not very large. Hence, it could be concluded that, the low value cyclic loading protocol, which was composed of loads less than 48% of the capacity of the bare sheet diaphragm, had no remarkable influence on the diaphragm resistance and stiffness when the test specimen was reinforced with non-structural roofing components.

Similar to test 45, slips at side-lap 1-2 and side-lap 4-5 were greater than those measured at side-lap 2-3 and side-lap 3-4. Since the placement of the gypsum panels was the same as for Test 45, it is possible that the non-structural panels and their screw fasteners had stiffened certain areas of the test specimen more than others. Given this finding, in general, it can be said that the gypsum panels do have an influence on the overall diaphragm performance. The same phenomenon means that the screw connections between the gypsum board and steel sheet do influence their nearby slip deformation.

As discussed before, no damage was observed after the cyclic load phase. The failure modes shown in Figures 4.118 to 4.123 were recorded after the monotonic loading had been completed. The major damage was limited to the cracking of gypsum board, as well as the deformation, tearing, bearing, and buckling of the steel sheet around the nail connections. It is assumed that the screw side-lap connections suffered from the typical bearing-tilting failure mode because of the side-lap slips recorded, even though it was not possible to confirm visually because of the roofing material. Shearing of the nails at both ends was not observed at the visible ends of the

specimen. It can be presumed that no nail damage occurred for the interior connections even though they could not be inspected due to the covering roof material. In addition, no detectable deformation was observed for the roofing materials, except for the gypsum board, because the stress should have been very small. It is thus possible to conclude that the roofing material placed above the gypsum board had a negligible effect on the overall diaphragm behaviour.

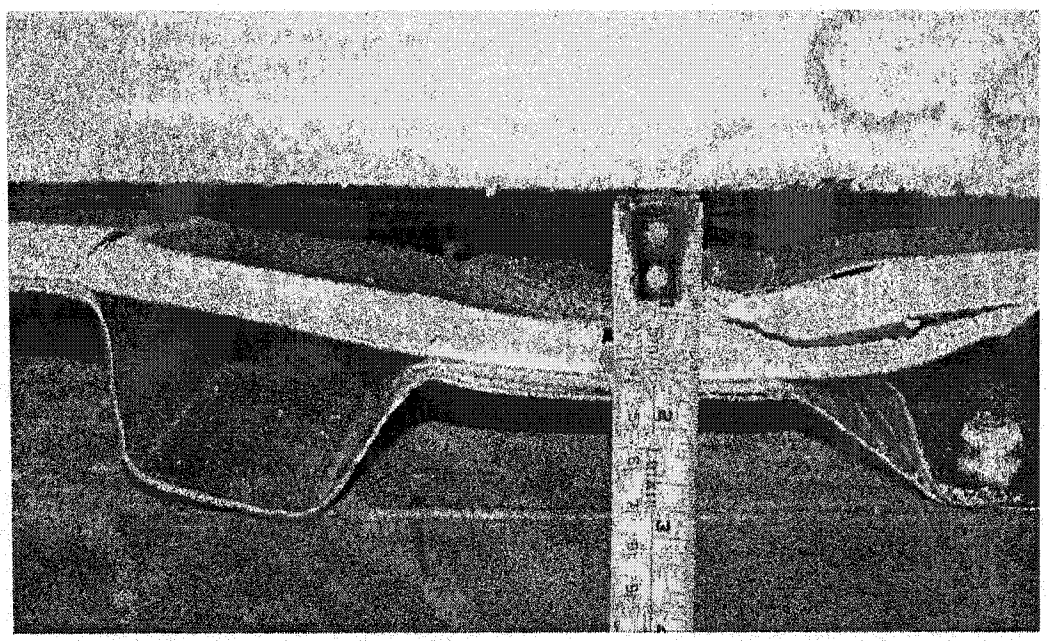

Figure 4.118. Deformation of steel deck profile (the height decrease), and cracking of gypsum board due to screw pulling.

Figure 4.119. Tearing of steel sheet at D1

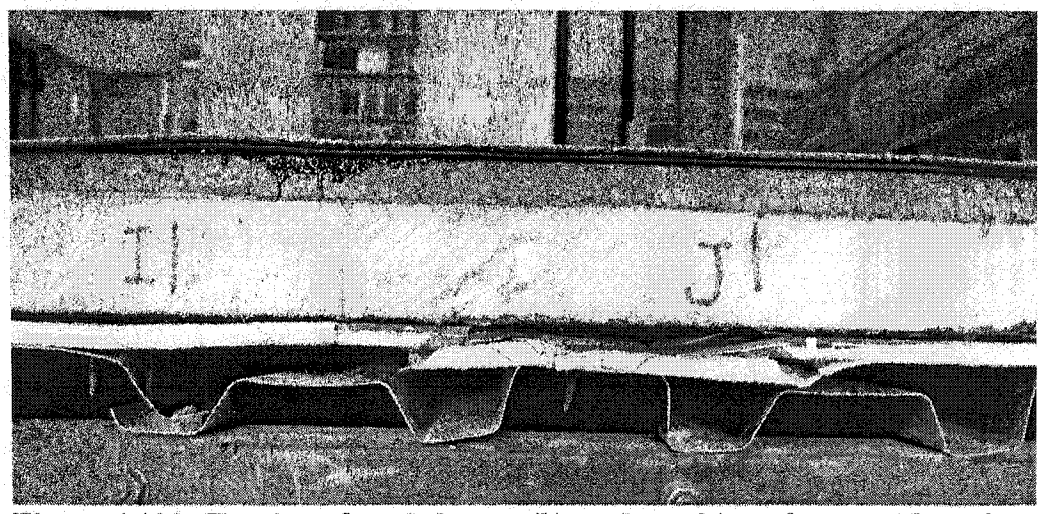

Figure 4.120. Tearing of steel sheet at I1, and cracking of gypsum board near J1

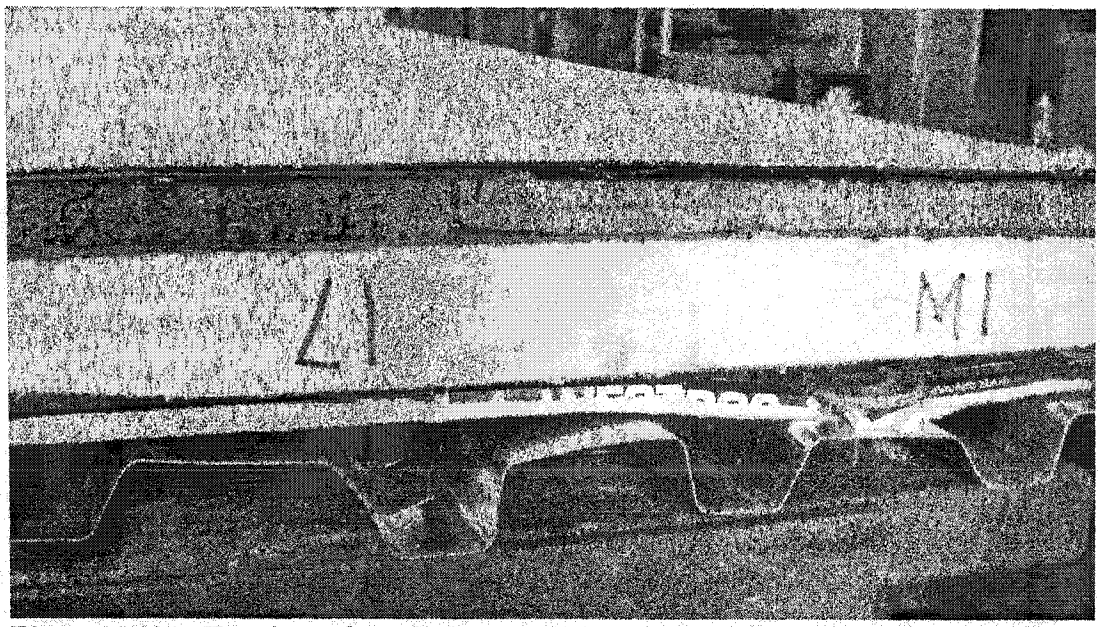

Figure 4.121. Tearing of steel sheet at L1, and cracking of gypsum board near M1

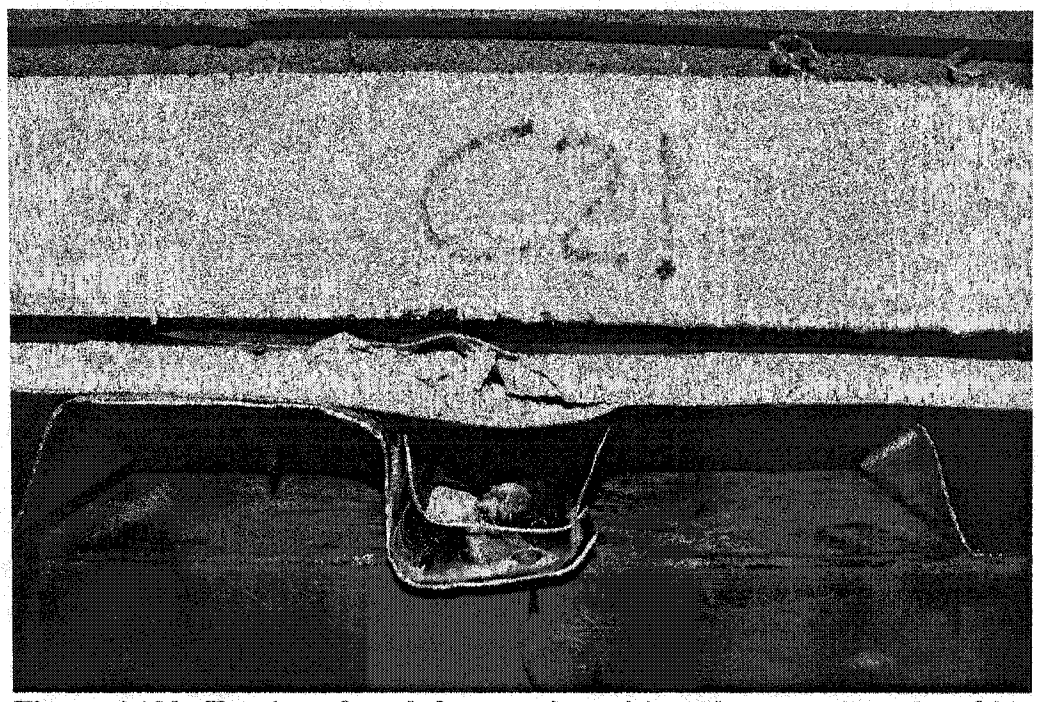

Figure 4.122. Tearing of steel sheet, and cracking of gypsum board at C21

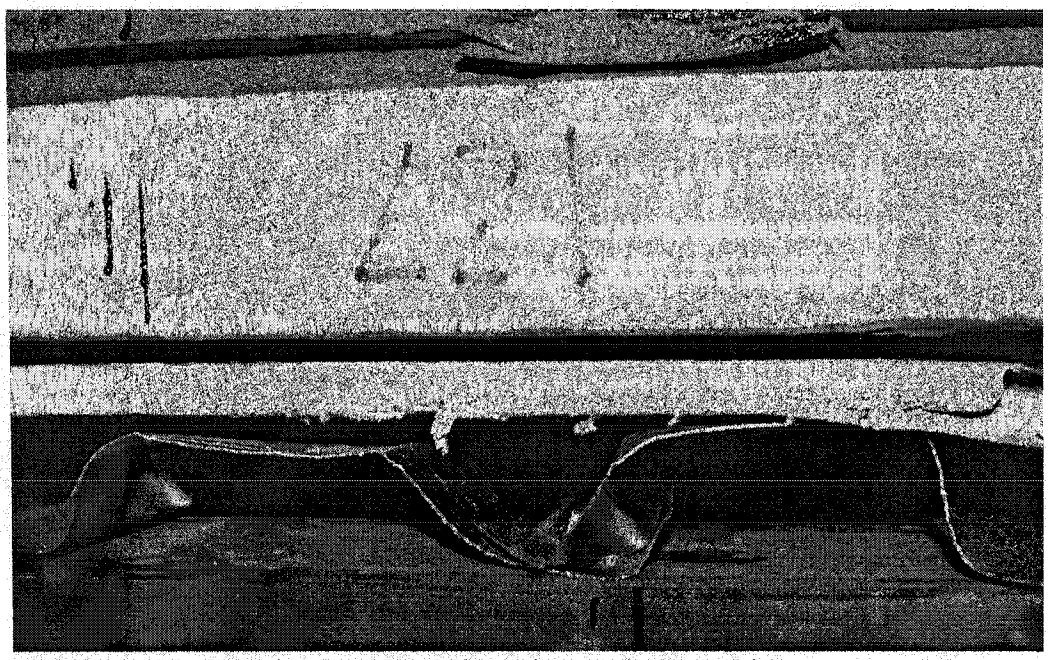

Figure 4.123. Tearing and buckling of steel sheet at L21

4.2.4.5 Comparison of the test results

A comparison of the uncladded versus cladded performance of the roof diaphragm specimens is presented in Table 4.24. This includes only tests that were constructed with the nail-screw pattern and 0.76 mm P3615B deck panels, *i.e.* tests 4, 7, 5, 8, 28, 29, 43, 44, 45, and 46.

Table 4.24 Comparison of tests 4, 7, 5, 8, 28, 29,43, 44, 45, and 46

Test number	Test result		Ratio			
	Su	G'	Su	G'	Su	G'
	KN/m	KN/mm	Test/SDI	Test/SDI	Test/SDI*	Test/SDI*
38-76-6-NS-M-4	12.30	3.12	0.92	0.84	1.11	0.96
38-76-6-NS-Q-7	12.19	2.87	0.91	0.77	1.10	0.89
38-76-6-NS-M-5*	11.48	3.02	0.86	0.81	1.06	0.90
38-76-6-NS-Q-8*	12.29	2.80	0.92	0.75	1.13	0.84
38-76-6-NS-SD-28	14.10	2.45	1.08	0.65	1.27	0.87
38-76-6-NS-LD-29	13.60	2.39	1.05	0.64	1.23	0.85
38-76-6-NS-M-43	13.40	2.58	1.06	0.71	1.24	0.83
38-76-6-NS-C-44	10.47	2.85	0.83	0.78	0.97	0.91
Mean 1 (Tests 4, 5, 7, 8, 28, 29, 43, and 44)	**12.53**	**2.76**	**0.95**	**0.74**	**1.14**	**0.88**
C.o.V. of above specimens	0.09	0.10	0.10	0.10	0.09	0.05
38-76-6-NS-M-R-45	15.60	4.17	1.24	1.14	1.44	1.34
38-76-6-NS-C-R-46	15.90	3.90	1.26	1.07	1.47	1.25
Mean 2 (Tests 45, 46)	**15.75**	**4.03**	**1.25**	**1.11**	**1.46**	**1.30**
Ratio of mean2 to mean1	**1.26**	**1.46**	**1.31**	**1.49**	**1.28**	**1.47**

Note:

1) Tests 4, 5, 8, and test 7 by Essa *et al.* (2001), Test 28 and test 29 by Martin (2002). Only test 5 and test 8 use ITW Buildex fasteners, others use Hilti fasteners.
2) Mean 1 is the average of tests with bare sheets, Mean 2 is the average of tests with roofing material.

In Table 4.24, the value of S_u for test 44, which was obtained from the monotonic load phase after the cyclic load protocol, was much smaller than that of the other bare sheet tests. Hence, the earlier cyclic loading does have an influence on the mean value used for the bare sheet specimens even when the maximum cyclic load is only about

60% of the ultimate load. This also suggests that the forces in each connection may be quite different due to the high degree of static indeterminacy. However, it seems that there is no effect of this cycling on the measured stiffness for the same group of tests. As a general observation, the roofing material reinforces the diaphragm strength and stiffness. An increase of the mean strength of approximately 26% was realised, in addition to a mean stiffness increase of near 46% for the tested diaphragms.

Since no other information about the reinforcement effects of roofing materials on the steel deck diaphragm was found, the SDI estimates are all based on bare sheet configurations. The SDI and SDI* values for test 45 and 46 are for reference only. The mean 1 of G' in Table 4.24, which is based on eight bare sheet tests, equals to 0.77 from SDI, and 0.88 from SDI*. It seems that the SDI approach over-estimated the stiffness of the NS connected bare sheet diaphragms. By comparing the mean 1 of test/SDI and test/SDI*, it seems that the former provided a better estimate of the strength, but the latter provided for a better value of the stiffness.

4.2.5 Group 4

Group 4 contains three P2436 deck diaphragm tests. This roof deck panel, because of its deeper profile, is often used to span larger distances and/or to sustain larger vertical loads. The deck-to-frame connections were composed of arc-spot welds with a nominal diameter of 16 mm. The welds were fabricated using a Φ3.2 mm E6011 electrode and a 100 Amp electric DC current. All of the side-laps away from joist locations were connected with button punches.

4.2.5.1 Test 47

A description of the specimen 47, a monotonic test, is provided in Table 4.25. The composition of this specimen is similar to its matching short duration specimen 48. A survey of the weld quality is provided in Appendix 2.

During the test, the welded connections at D21 south (Figure 4.124) and C21 (Figure 4.125) were damaged at a load of 45 kN (S = 7.27 kN/m). That corresponded to a shear rotation of γ_2 = 12.63 rad/1000 (Figure 4.126). The onset of this initial damage also signalled the ultimate shear capacity of the diaphragm specimen. After this point, the load began to descend. It is noted that the ductility of this specimen is very limited. With increasing shear deformations, many other welded connections became damaged one after the other. The final failure modes are shown in Table 4.26, most of them were of the weld failure type. Photographs of the profile warping deformation and the failure modes at connections are shown in Figures 4.127 to 4.131. Figure 4.127 illustrates the profile deformations; it has the similar deformed shapes as the former tests of P3615 panels with one flute width enlarged and the next flute width diminished, even though the deformation of P2436 seems larger. Figure 4.128 is the weld failure at D1 (north), and sheet buckling at D2. It is noted that significant deformations in the steel sheet took place before the deck-to-frame connections were damaged. Figures 4.129 and 4.130 show two weld failures at side lap gridlines. The shape deformation of the button punch side laps was not remarkable, even after the test is finished (Figure 4.131).

Table 4.25 Test specimen description (Tests 47 and 48)

Steel properties:	
Supplier and coil number	Canam P-2436 deck 0.76 mm Coil supplier: Sorevco Coil number: 287982
Base metal thickness (mm)	0.74
F_y measured (MPa)	321
F_u measured (MPa)	385
E measured (MPa)	185000
50 mm gauge % elongation	29 %
Fasteners:	Spacing: 305 mm c/c
	Side-lap fasteners: Button punch
	Deck-to-frame fasteners: Welded with nominal diameter 16 mm

Figure 4.124. Weld failure at D21

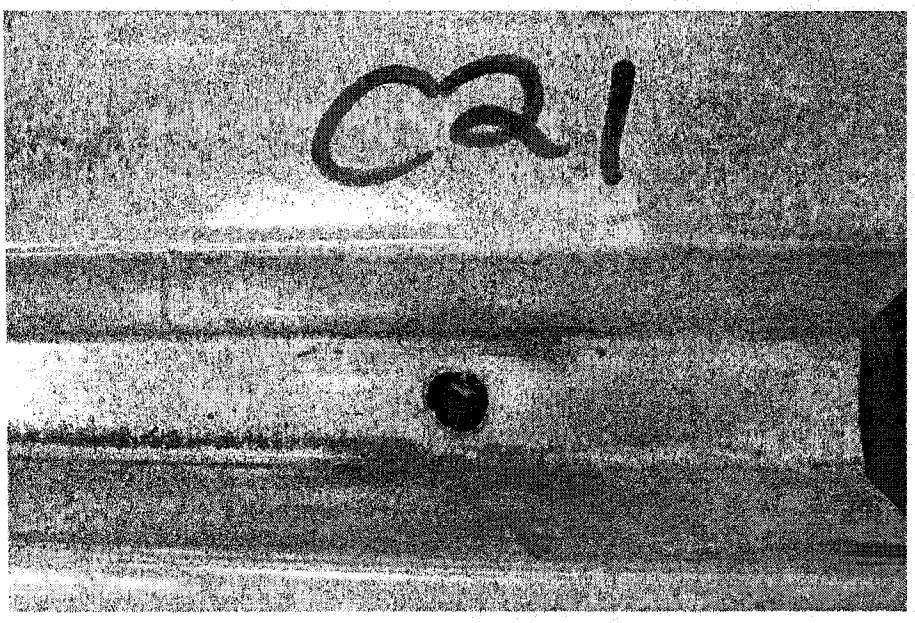

Figure 4.125. Weld failure at C21

Test No. 47

P2436, 0.76 mm
Sidelap fasteners : Button punched @ 305
Frame fasteners : Welds 16 mm @ 305
*S_u , SDI * = 9.39 kN/m*
S_u , MON = 7.27 kN/m

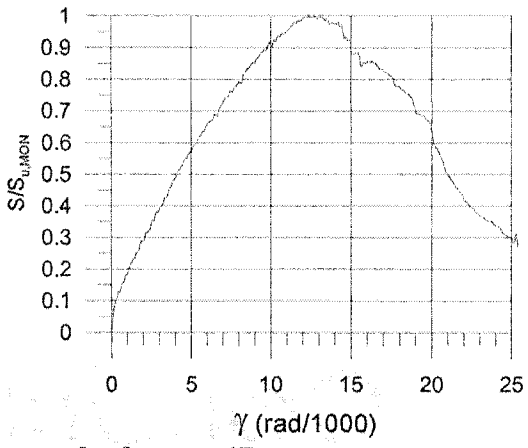

Figure 4.126. Shear load vs. rotation graphs for test 47

Table 4.26 Failure modes of deck-to-frame connections of Test 47

Position	1		6		11		16		21
B (north)	**WE**		**WE**		**WE**				**WE**
B (south)	**WE**		**WE**		**WE**				**WE**
C									WE
D (north)	**WE**		**WE**		**WE**		**WE**		
D (south)			**WE**		**WE**		**WE**		**WE**
E	WE								WE+BE
F (north)	**WE**		**WE**		**WE**		**WE**		
F (south)			**WE**		**WE**		**WE**		**WE**
G	WE								WE
H (north)	**WE**		**WE**		**WE**		**WE**		
H (South)	**WE**		**WE**		**WE**		**WE**		**WE**
I									BE+WE
J (north)	**WE**		**WE**		**WE**		**WE**		
J (south)	**WE**		**WE**		**WE**		**WE**		**WE**
K									BE
L (north)	**WE**		**WE**		**WE**		**WE**		**WE**
L (south)									**WE**

BE--Bearing failure; BU--Buckling failure; WE--Weld failure

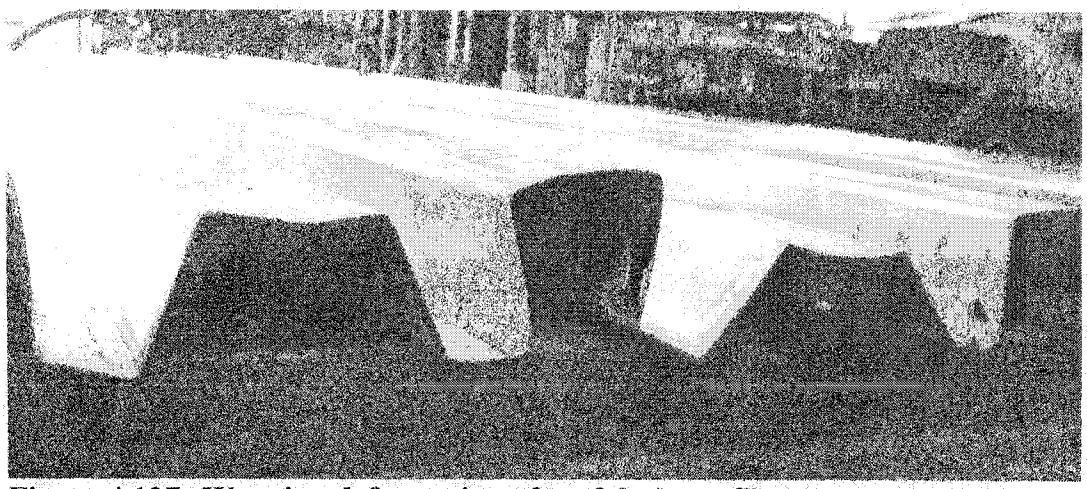

Figure 4.127. Warping deformation of roof deck profile

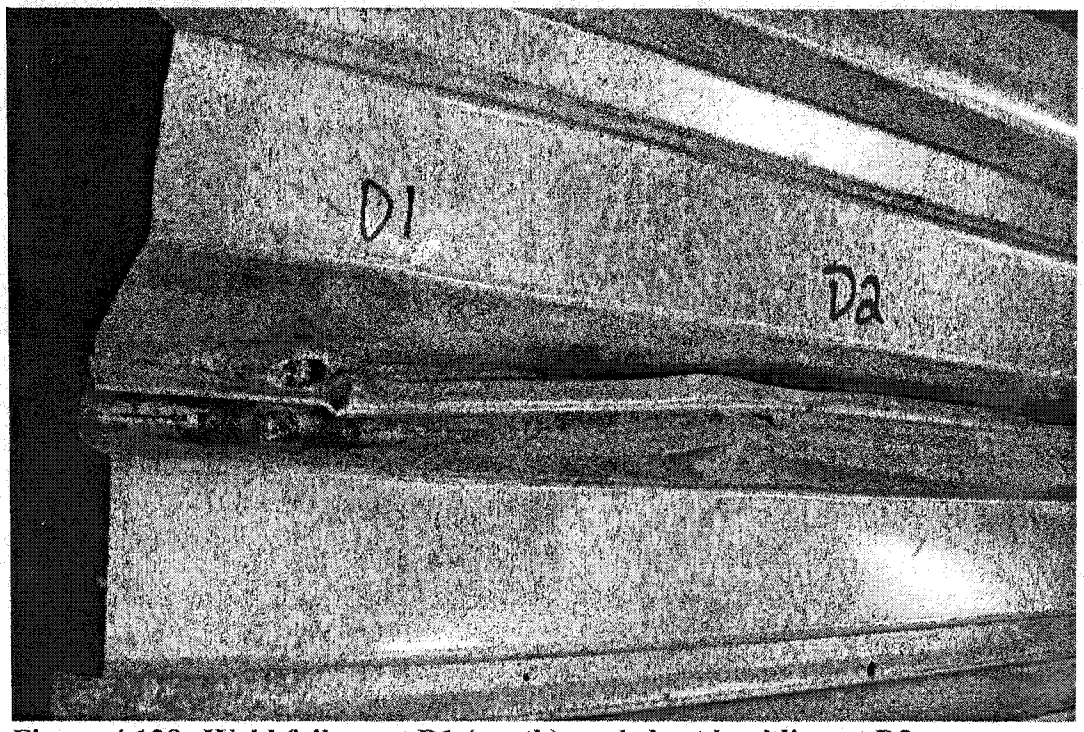

Figure 4.128. Weld failure at D1 (north), and sheet buckling at D2

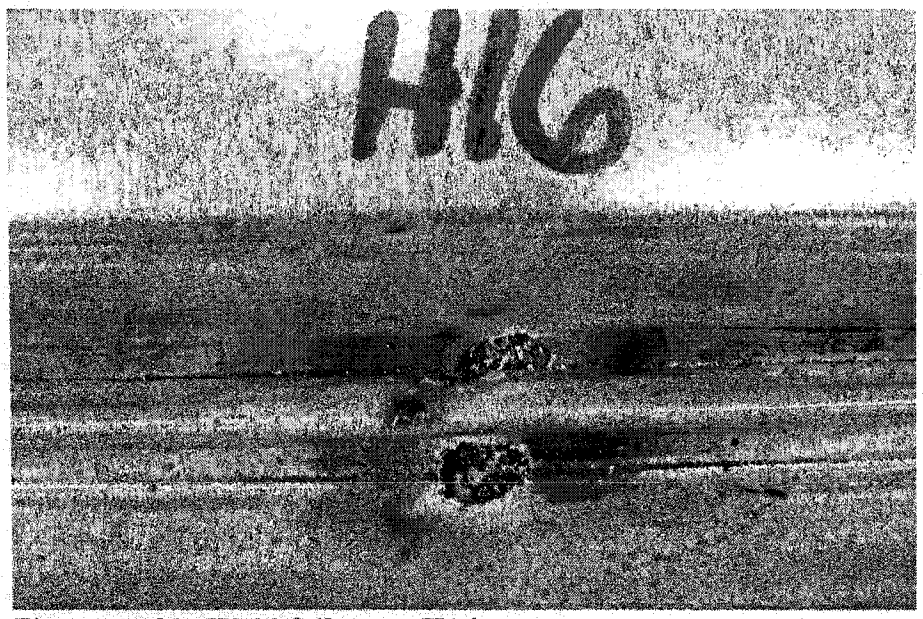

Figure 4.129. Weld failure at H16

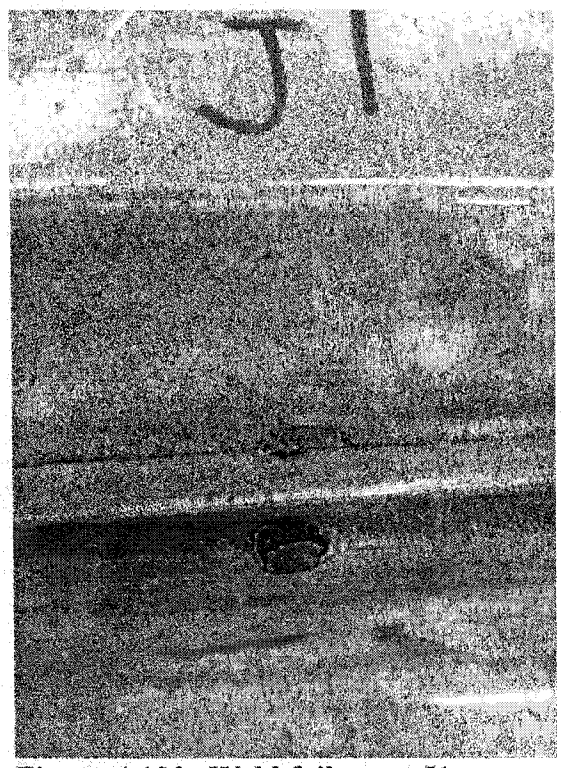

Figure 4.130. Weld failure at J1

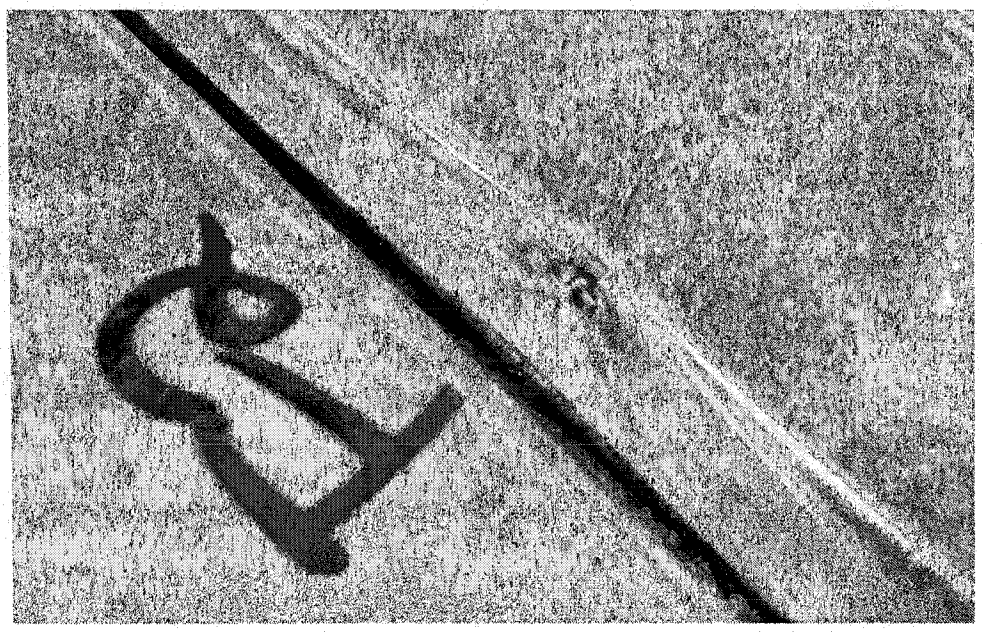

Figure 4.131. Button punch shape did not change even when test finished

Figure 4.132 shows the slip values for the range of rotation from 0.0 to γ_2 (12.63 rad/1000). The bar graph related to γ_2 shows that the interior slips are not uniform. The slips of side lap 1-2 and 2-3 are higher because the welded connection at D21 and C21 failed prior to those on other gridlines. The values of slip measurement along deck-frame north, deck-frame south, and side-lap 6-7 are not shown in the bar graph in Figure 4.132 since those values seemed not reasonable. It is possible that the LVDTs on these gridlines did not function properly.

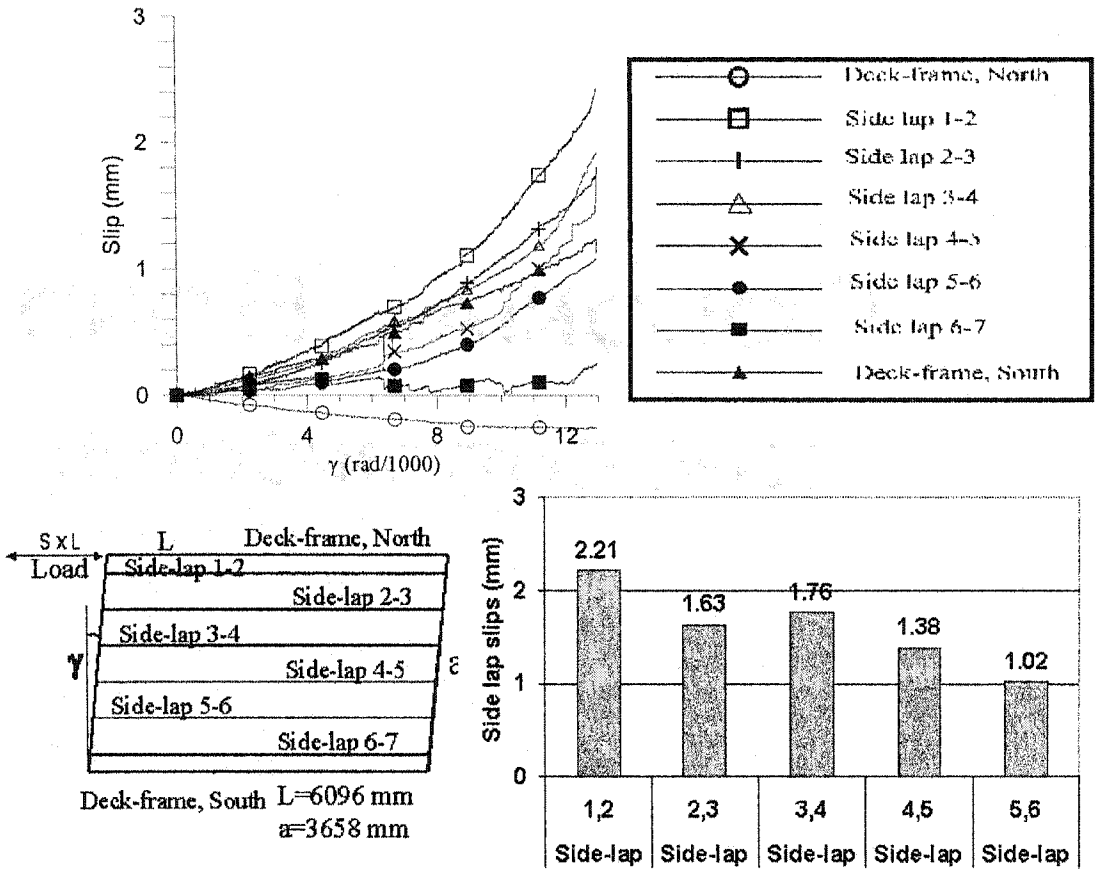

Test No. 47

P2436, 0.76 mm

Sidelap fasteners : Button punched @ 305 Frame fasteners : Welds 16 mm @ 305

*S_u , SDI * = 9.39 kN/m S_u , MON = 7.27 kN/m*

Figure 4.132. Slip deformation vs. rotation graphs for test 47

4.2.5.2 Test 48

A description of the short duration test specimen 48 is provided in Table 4.25 in Section 4.2.5.1. The loading protocol was based on the performance of the previously tested monotonic specimen 47. A listing of the weld quality is given in Appendix 2. It is important to note that the weld quality at non-side-lap connections was much better than at side-lap locations. The weld at non-side-lap connections was nearly a perfect circle (Figure 4.133), whereas at side-lap connections a flat ellipse profile typically existed (Figure 4.134). The difficulty in welding at these side-lap locations occurred because the flute bottom at the interlocking side-lap locations actually had a curved shape, which created only a minimal contact area between the deck and frame. At the edges of this contact surface it is very easy for the welder to burn through the sheet steel because the frame cannot act as a heat sink during the welding process. Similar problems also existed in test 47 and test 49, but seemed more pronounced in test 48. As compared to 38 mm deep decks, the higher flute in P2436 panels also made the weld operation more difficult, thus the quality seemed poorer.

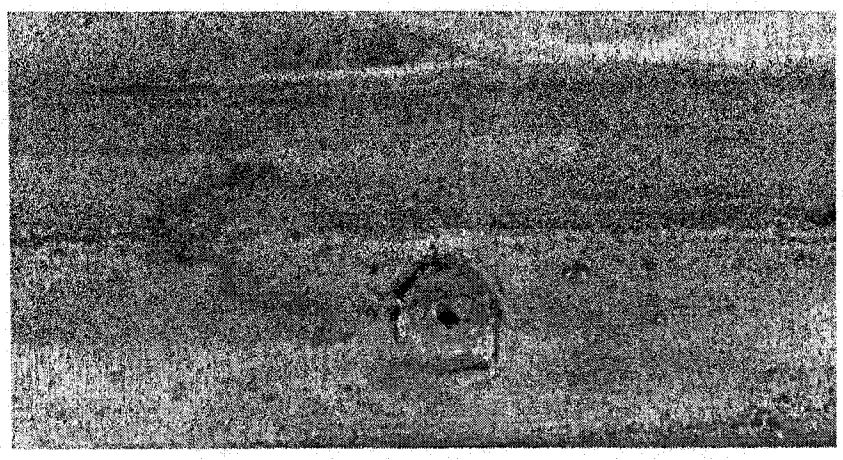

Figure 4.133. Example of weld quality at non-side-lap connections (G21)

Figure 4.134. Example of weld quality at side-lap connections (D11)

This dynamic loading test started with a cyclic frequency 0.2 Hz (total of 467.8 sec for protocol), but stopped after 41.1 seconds, because some slip measuring instruments were discovered to be out of service. This 41.1 sec loading is called the first load segment. During this period, the maximum shear rotation reached was γ_{max} = 10.51 rad/1000, which represents approximately $0.8\gamma_u$, where γ_u is from test 47, equalling to 13.14 rad/1000, see Table 4.5. However, it was during these initial loading cycles that the maximum load was reached, S_u=7.02 kN/m. Extensive weld damage was observed after the first load segment, especially on the south side of the side-lap connections because the quality there was poorer, but no weld damage was recorded at non-sidelap connections. The failure modes after the first load phase are shown in Table 4.27, where damage consisted of weld failure only. Photographs of

representative failed welds are shown in Figures 4.135 to 4.136. The situation of button punches is similar to test 47 (see Figure 4.131).

Table 4.27. Failure modes after 41.1 sec dynamic loading

Position	1		6		11		16		21
B (north)	**WE**		**WE**						
B (south)	**WE**		**WE**		**WE**		**WE**		**WE**
C									
D (north)			**WE**						
D (south)			**WE**		**WE**				
E									
F (north)	**WE**		**WE**						
F (south)	**WE**		**WE**		**WE**		**WE**		**WE**
G									
H (north)					**WE**				
H (South)			**WE**		**WE**		**WE**		
I									
J (north)									
J (south)	**WE**		**WE**		**WE**		**WE**		
K									
L (north)			**WE**				**WE**		**WE**
L (south)	**WE**		**WE**		**WE**		**WE**		**WE**

WE--Weld failure

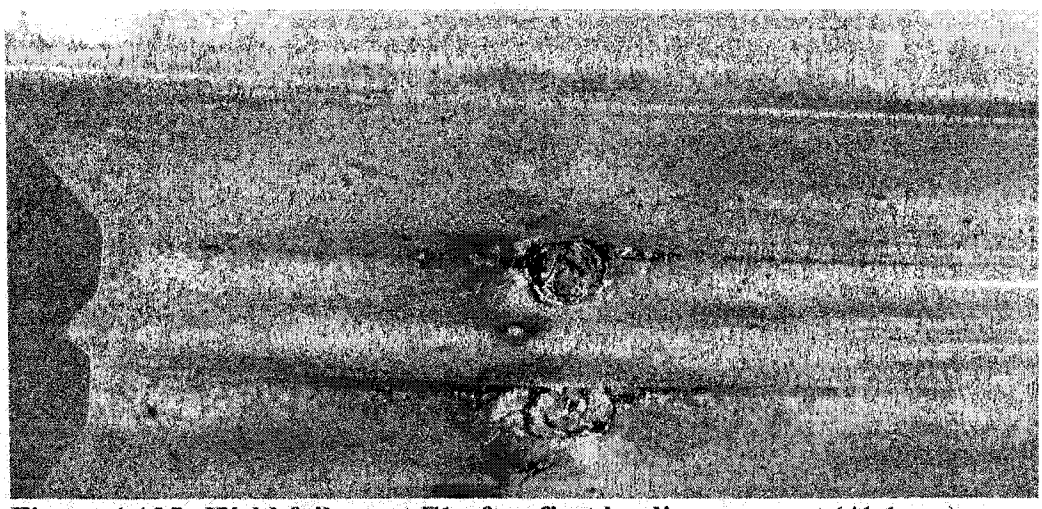

Figure 4.135. Weld failure at F1 after first loading segment (41.1 sec)

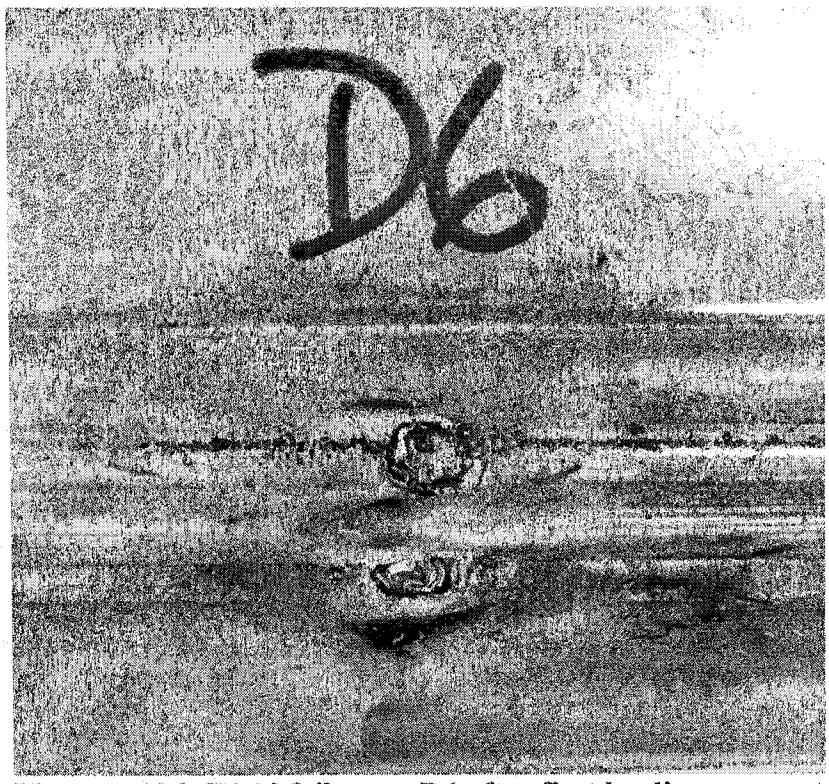

Figure 4.136. Weld failure at D6 after first loading segment (41.1 sec.)

The test was restarted the next day after all the measuring instruments had been inspected and adjusted. The frequency of loading was changed to 0.1 Hz to ensure that the correct load protocol would be applied. In the second loading segment, only the unfinished part of the load protocol was executed. Soon after loading had been restarted nearly all of the welded and button punch connections were damaged. Essentially zero shear resistance remained at the end of Run 1. The failure modes recorded at the end of the second loading segment are shown in Table 4.28.

Table 4.28. Failure modes after Run 1

Position	1		6		11		16		21
B (north)	**WE**		**WE**		**WE**		**WE**		**WE**
B (south)	**WE**		**WE**		**WE**		**WE**		**WE**
C	WE		WE		WE		WE		WE
D (north)			**WE**				**WE**		**WE**
D (south)	**WE**		**WE**		**WE**		**WE**		**WE**
E	WE		WE		WE		WE		WE
F (north)	**WE**		**WE**						
F (south)	**WE**		**WE**		**WE**		**WE**		**WE**
G	WE								
H (north)	**WE**		**WE**		**WE**		**WE**		**WE**
H (South)	**WE**		**WE**		**WE**		**WE**		**WE**
I	WE		WE		WE		WE		WE
J (north)			**WE**						**WE**
J (south)	**WE**		**WE**		**WE**		**WE**		**WE**
K	WE								WE
L (north)	**WE**		**WE**				**WE**		**WE**
L (south)	**WE**		**WE**		**WE**		**WE**		**WE**

WE--Weld failure

The time histories of test results showing applied shear deformation, normalized shear force and normalized energy, are provided in Figure 4.137. The structure reached its ultimate shear capacity of S_u=7.02 kN/m at only 29.20 sec during the loading phase (East R_d=3.0), which relates to a shear deformation of γ = 7.11 rad/1000. The shear capacity of the specimen deteriorated rapidly after this point to such an extent that almost no shear resistance was available during the West segments of the SD protocol.

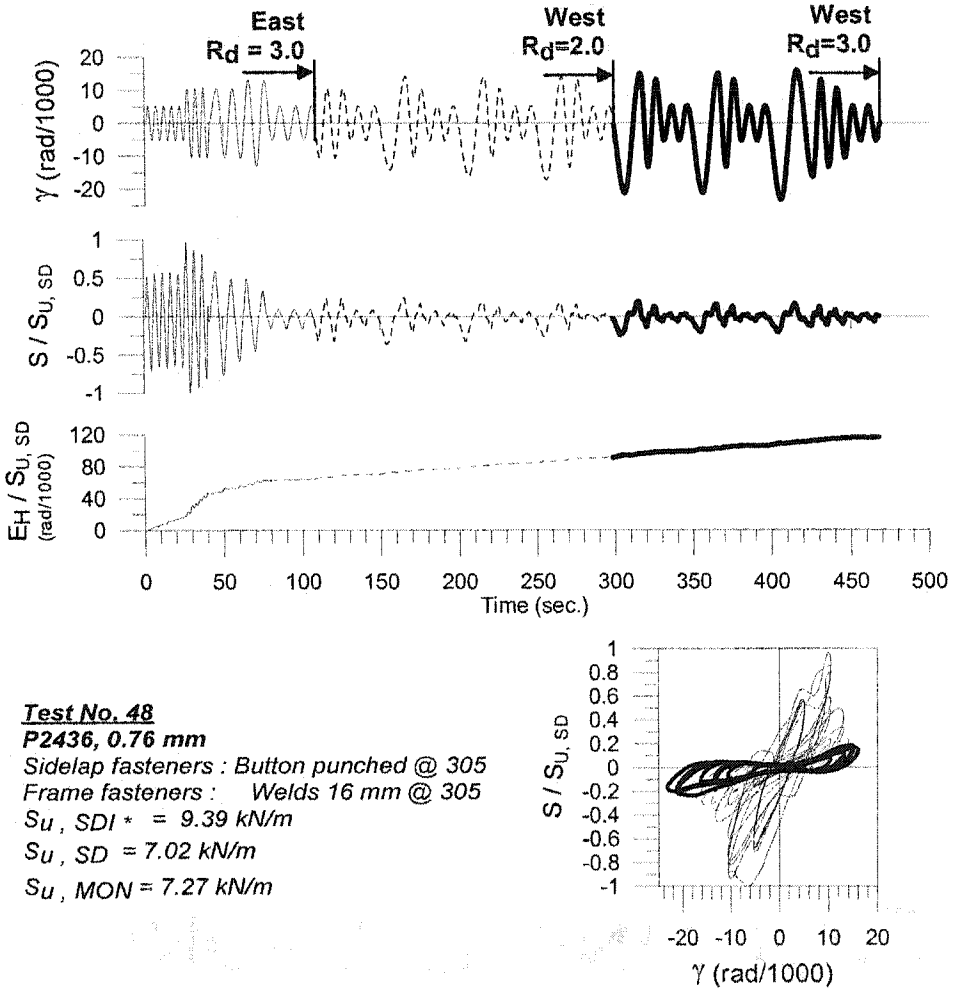

Figure 4.137. Time history & hysteresis of test 48

The details of $S/S_{U,SD}$ vs. γ hystereses for the East and West segments of the protocol are shown in Figure 4.138. Run 2 was deemed not necessary since no resistance remained after Run 1.

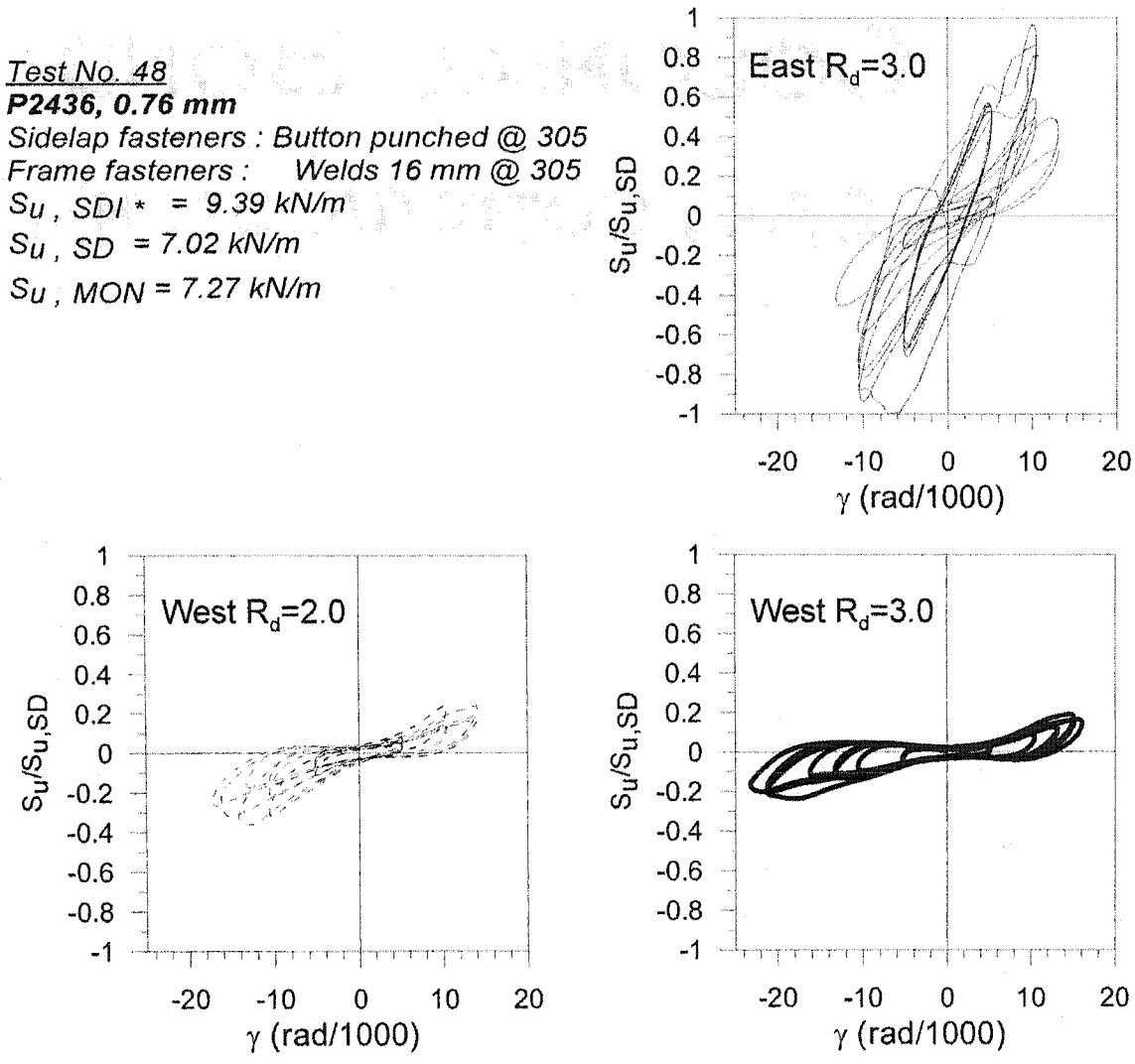

Figure 4.138. Normalized shear force vs. deformation for East and West segments of SD protocol.

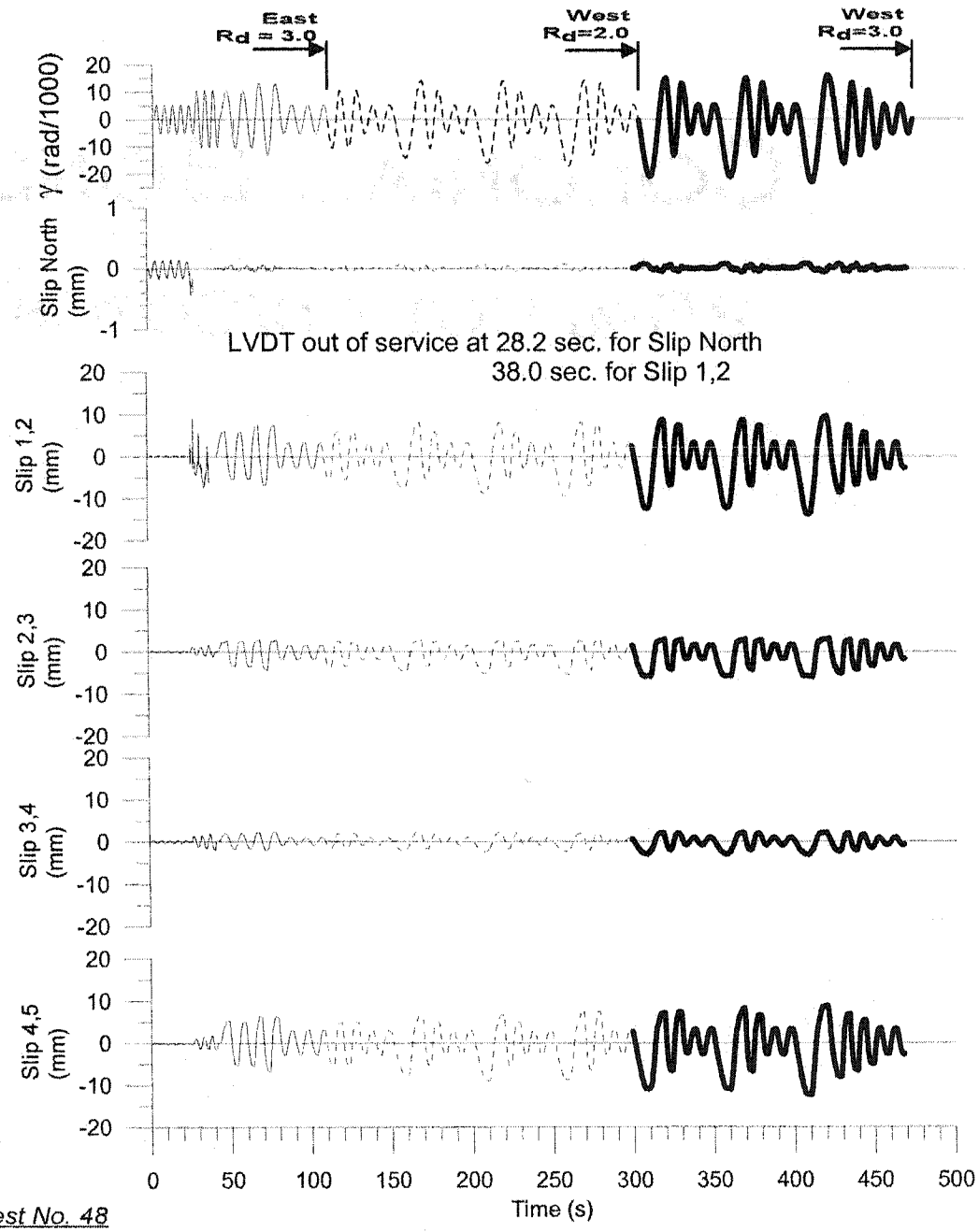

Test No. 48
P2436, 0.76 mm
Sidelap fasteners : Button punched @ 305 Frame fasteners : Welds 16 mm @ 305
*S_u , SDI * = 9.39 kN/m S_u , SD = 7.02 kN/m S_u , MON = 7.38 kN/m*

Figure 4.139. Time history of side-lap slips

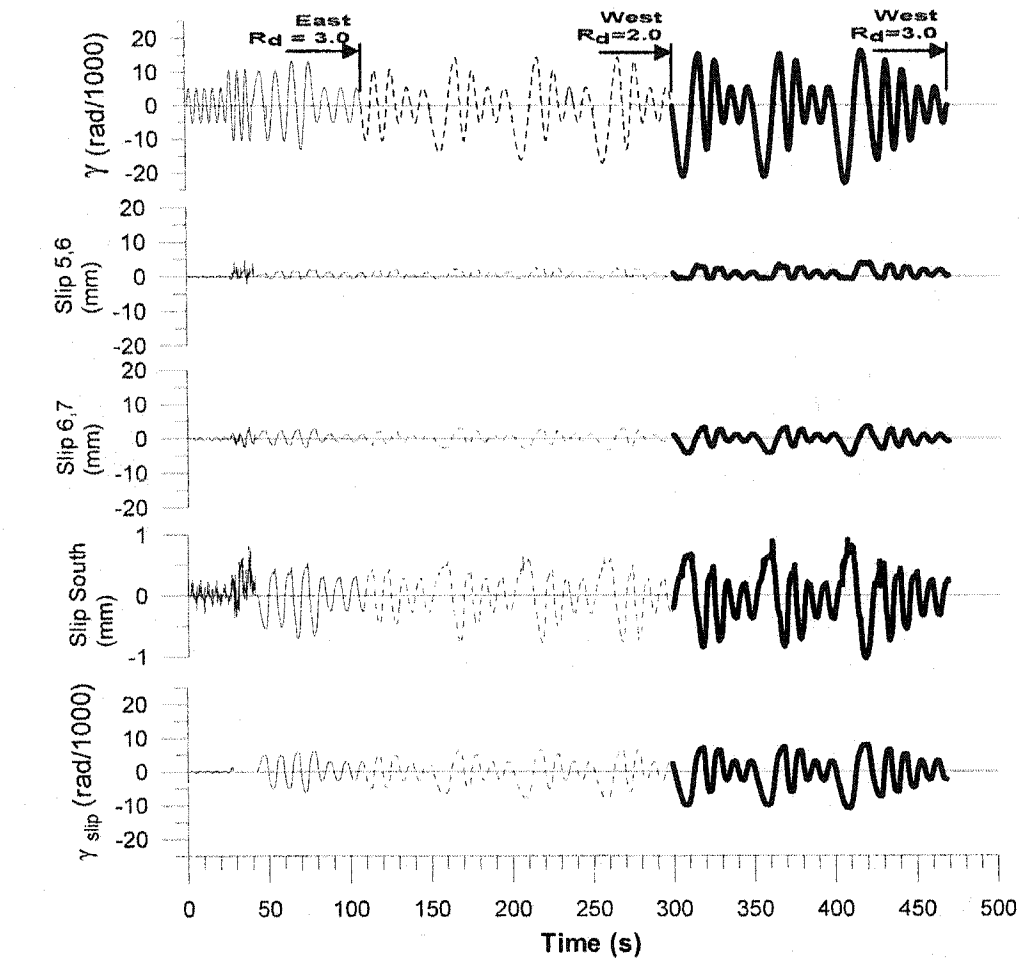

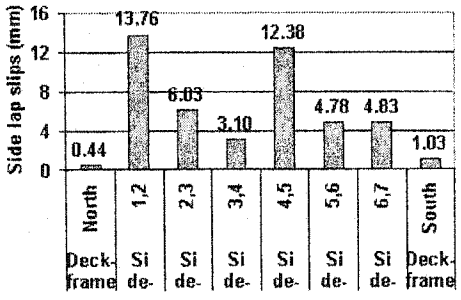

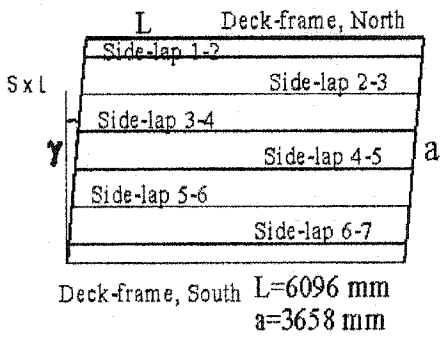

Test No. 48
P2436, 0.76 mm
Sidelap fasteners : Button punched @ 305 Frame fasteners : Welds 16 mm @ 305
*S_u , SDI * = 9.39 kN/m S_u , SD = 7.02 kN/m S_u , MON = 7.27 kN/m*

Figure 4.140. Time history of side-lap slip

The time history of the side-lap slips for Run 1 is shown in Figures 4.139 and 4.140, where the abnormally large slip at side-lap 1-2 and at side-lap 4-5 is related to the extensive weld connection damage along gridline B and gridline H (both south and north), see Table 4.28. When compared to the P3615 deck panels, the proportion of distortion due to slips in the deeper profiled decks becomes less, but that due to warping becomes larger.

When the side-lap weld connections failed, the button punches were not able to resist the applied shear on their own and hence complete failure of the sidelap took place. With almost no shear resistance available along the length of the side-lap, extensive slip was measured. The diaphragm then transferred the shear force to adjacent side-lap lines through regular deck-to-frame connections. These connections were not able to provide sufficient resistance and became damaged. An example of weld damage in a non-sidelap connection is shown in Figure 4.141.

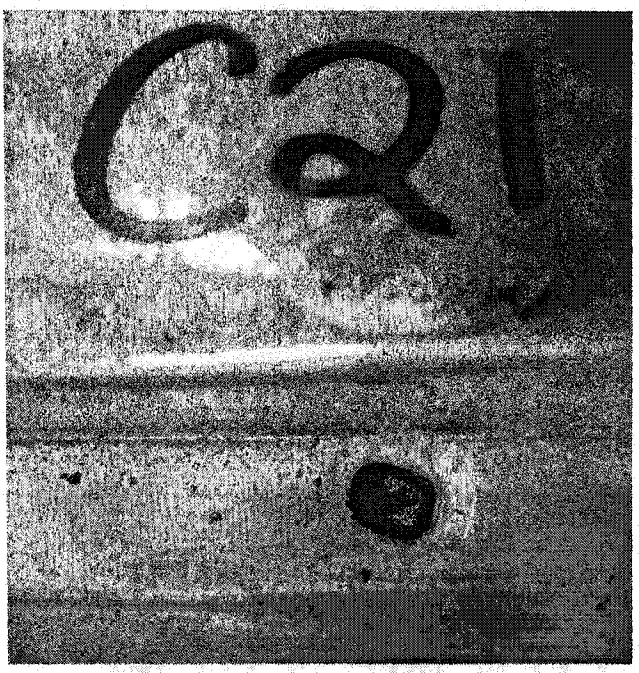

Figure 4.141. Weld failure at C21 after load Run 1.

4.2.5.3 Test 49

The final diaphragm specimen tested for this research project (# 49) was constructed of 0.91 P-2436 panels as noted in Table 4.29. As for the two preceding diaphragms with this panel type, a weld / button punch connection pattern was used. In this case, however, only the monotonic test was run due to the inability of specimen 48 to resist significant shear forces under inelastic cyclic loading.

Table 4.29 Test specimen description (Tests 49)

Steel properties:	
Supplier and coil number	Canam P-2436 deck 0.91 mm Coil supplier: Sorevco Coil number: 287982
Base metal thickness (mm)	0.87
F_y measured (MPa)	316
F_u measured (MPa)	378
E measured (MPa)	202282
50 mm gauge % elongation	29 %
Fasteners:	Spacing: 305 mm c/c
	Side-lap fasteners: Button punch
	Deck-to-frame fasteners: Diameter 16 mm weld

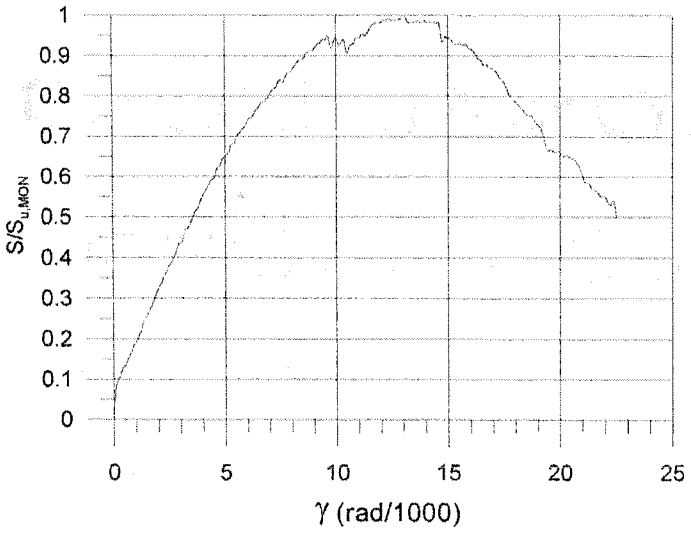

Test No. 49

P2436, 0.91 mm
Sidelap fasteners : Button punched @ 305 Frame fasteners : Welds 16 mm @ 305
$S_{u,SDI}$ = 13.17 kN/m $S_{u,MON}$ = 8.58 kN/m

Figure 4.142. Shear load vs. rotation graphs for test 49

A plot of the normalized shear force vs. shear rotation is provided in Figure 4.142. Prior to reaching the ultimate load, three sudden drops in load occurred as a result of welded connection failures. The following observations were made during testing:

- Weld E21 failed at a load of 50.28 kN (S = 8.25 kN/m), and γ = 9.71 rad/1000 (Figure 4.143);
- Weld H1 failed at a load of 49.75 kN (S = 8.16 kN/m) , and γ = 10.07 rad/1000 (Figure 4.144);
- Welds D1 and I1 failed at a load of 48.57 kN (S = 7.97 kN/m) , and γ=10.43 rad/1000 (Figure 4.145).

Although these four welded connections failed, the load continued to increase, until it reached P_u=52.33 kN (S_u = 8.58 kN/m) at γ_2 = 13.03 rad/1000.

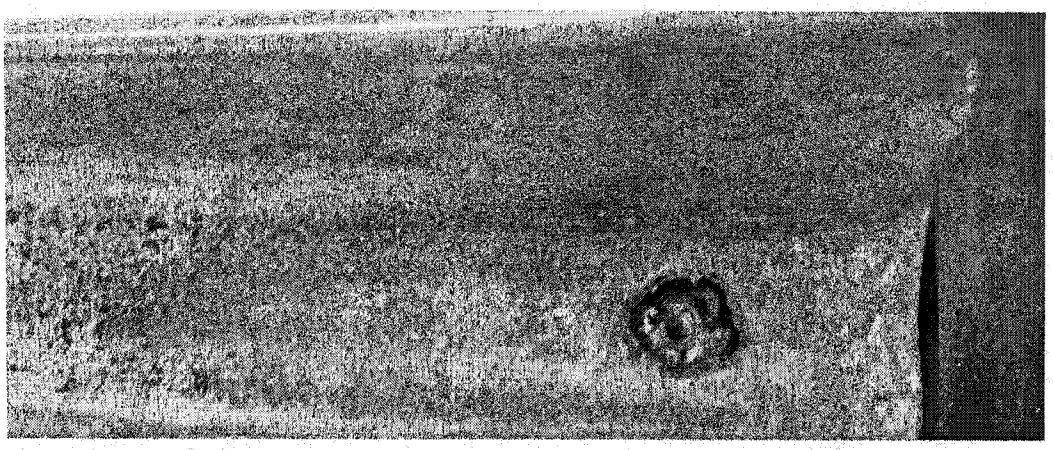

Figure 4.143. Weld failure at E21 at γ=9.71 rad/1000

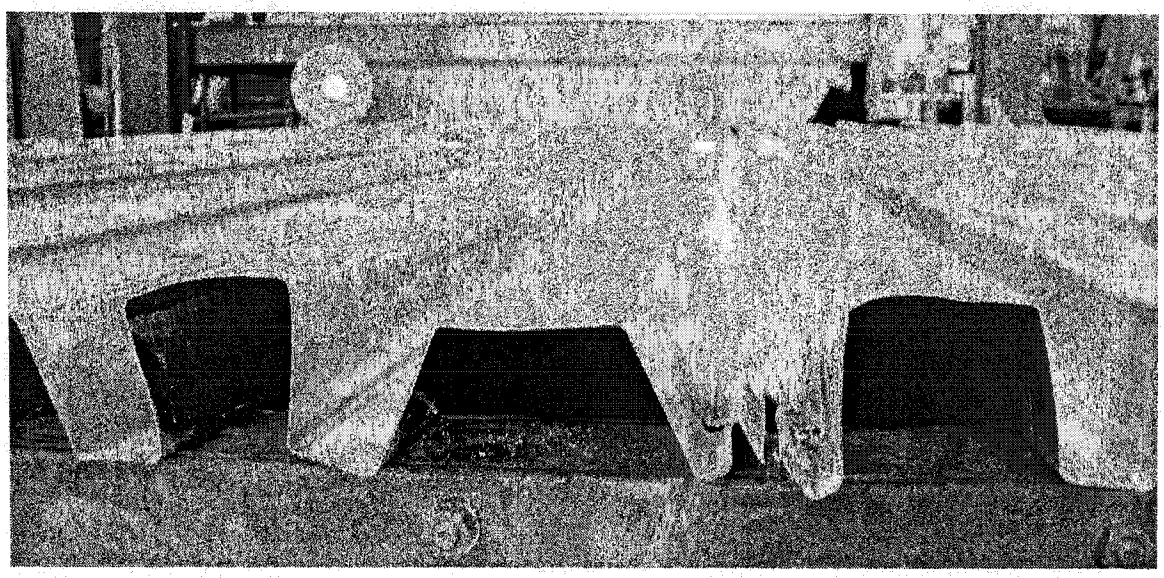

Figure 4.144. Weld failure at H1 and warping of the deck profile at γ=10.07 rad/1000

Figure 4.145. Weld failure at D1 at γ=10.43 rad/1000

The failure modes recorded after the test had been completed are listed in Table 4.30. It should be pointed out that all of the failures were at the welds without extensive bearing or buckling deformation of the adjacent sheet steel. Similar to the other two P2436 tests, the button punches did not provide significant assistance to the strength when the weld connections failed. Three typical weld failures are given in Figures 4.146 to 4.148.

Table 4.30 Failure modes of deck-to-frame connection of test 49

Position	1		6		11		16		21
B (north)	**WE**		**WE**				**WE**		
B (south)	**WE**		**WE**		**WE**		**WE**		**WE**
C									
D (north)			**WE**		**WE**		**WE**		**WE**
D (south)					**WE**		**WE**		**WE**
E									
F (north)	**WE**		**WE**		**WE**		**WE**		**WE**
F (south)	**WE**		**WE**		**WE**		**WE**		**WE**
G									
H (north)	**WE**		**WE**		**WE**		**WE**		**WE**
H (South)	**WE**		**WE**		**WE**		**WE**		
I	WE								
J (north)	**WE**		**WE**		**WE**		**WE**		
J (south)			**WE**		**WE**		**WE**		**WE**
K	WE								
L (north)	**WE**		**WE**		**WE**		**WE**		**WE**
L (south)	**WE**		**WE**		**WE**		**WE**		**WE**

WE--Weld failure

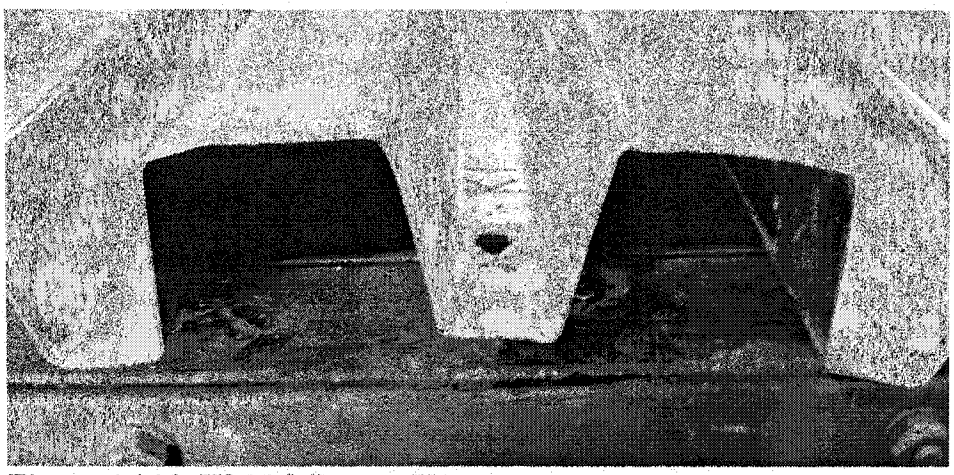

Figure 4.146. Weld failure at K1

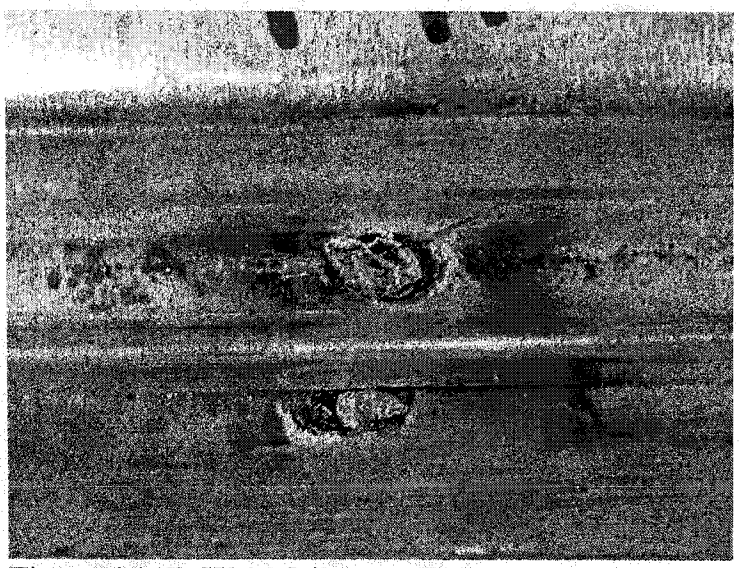

Figure 4.147. Weld failure at F11

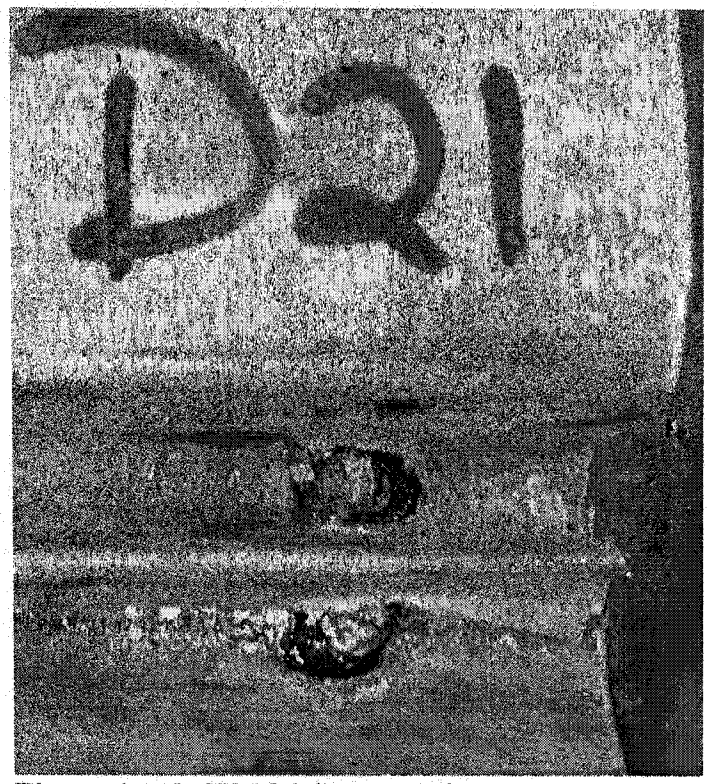

Figure 4.148. Weld failure at D21

4.2.5.4 Comparison of P-2436 test results

In Table 4.31, the test results of the P-2436 panels are compared with those of the P-3615 panels tested by Essa *et al.* (2001) and Martin (2002). For both panel types the weld / button punch connection pattern was specified. As a diaphragm resisting in-plane shear forces, the P2436 deck does not provide the resistance offered by the P3615 deck (decreases 16% for 0.76 mm deck, decreases 35% for 0.91 mm deck).

Table 4.31 Comparison of test results

Test Number	Test result		Ratio			
	Su	G'	Su	G'	Su	G'
	kN/m	kN/mm	Test/SDI	Test/SDI	Test/SDI*	Test/SDI*
t=0.76 mm						
38-76-6-WB-M-1	8.05	2.14	0.83	0.77	0.71	0.78
38-76-6-WB-Q-2	7.53	2.15	0.78	0.78	0.66	0.78
38-76-6-WB-SD-20	9.81	2.44	1.07	0.74	0.86	0.88
Mean 1 (Test 1, 2, 20)	**8.46**	**2.24**	**0.89**	**0.76**	**0.74**	**0.81**
75-76-6-WB-M-47	7.27	0.80	0.95	0.66	0.77	0.68
75-76-6-WB-SD-48	7.02	0.72	0.91	0.60	0.75	0.61
Mean 2 (Test 47, 48)	**7.15**	**0.76**	**0.93**	**0.63**	**0.76**	**0.65**
Mean 2 / Mean 1	**0.84**	**0.34**	**1.04**	**0.83**	**1.02**	**0.79**
t=0.91 mm						
38-91-6-WB-M-37	12.60	3.32	1.09	0.72	0.75	0.80
38-91-6-WB-SD-21	13.80	3.16	1.19	0.68	0.82	0.76
Mean 3 (Test 37, 21)	**13.20**	**3.24**	**1.14**	**0.70**	**0.79**	**0.78**
75-91-6-WB-M-49	8.58	1.06	0.84	0.67	0.66	0.85
Test 49 / Mean 3	**0.65**	**0.33**	**0.74**	**0.96**	**0.84**	**1.09**

Note:
Tests 1 and 2 by Essa *et al.* (2001)

Tests 20, 21 & 37 by Martin (2002)

In Table 4.31, the in-plane shear stiffness of the diaphragm specimens constructed with the 76 mm deep P-2436 panels is significantly below that of the 38 mm P-3615 panels (decrease approximately 66% for both 0.76mm and 0.91 mm deck). This loss in stiffness is mainly due to the reduction in the warping stiffness of the deeper panel type. It is noted that, the S_u values estimated using the SDI method are more accurate than those from SDI* method. The G' values from both the SDI and SDI* methods are larger than the test values, but relatively the SDI* provides a better estimate.

The diaphragm properties are greatly influenced by the weld quality, which is quite inconsistent itself. As compared to P3615 panels, the P2436 deck is more difficult to properly weld due to the more limited space between webs and the depth of the flutes. This may also be one reason for its lower strength and stiffness. According to the P2436 and P3615 tests, the weld / button punches connection is quite brittle, the diaphragm with this connection system has very limited ductility, no surplus shear capacity was maintained when undergoing inelastic deformations.

4.3 CHAPTER CONCLUSION

Based on the above discussions of the four groups of diaphragm tests, the following conclusions can be made:

1. The diaphragm fastened with Buildex BX-14 nails has an ultimate shear strength, S_u, similar to that measured for the Hilti X-EDNK22-THQ 12 nail diaphragms. However, the former seems to be more flexible than the latter (G' is approximately 16% less).
2. The longitudinal overlapping seems to have no significant influence on the shear strength of the diaphragm, although there is an associated decrease in the

shear stiffness mainly due to the shorter panel length and hence, greater possibility for panel warping (G' is averagely 35% less).

3. The non-structural roofing materials increase the strength and stiffness of the diaphragm. The increase in strength was in the range of 26%, and the increase in stiffness was near 46% for the specified test composition.
4. As a diaphragm resisting in-plane shear forces, the P-2436 deck is weaker than the P-3615 deck. In addition, it is significantly more flexible with respect to in-plane shear. In tests, the strength decreased 16% for the 0.76 mm deck and 35% for the 0.91 mm deck. However the stiffness decreased nearly 66% as compared with the P3615 decks.
5. For nailed and screwed decks, the majority of failures were in the sheet steel. This included bearing, buckling, and tearing of the sheet steel near the connections. Moderate ductility could be observed. In contrast for welded and button punched decks nearly all the failures were in the welds, which caused sudden button punch failure. Failure appeared to be brittle, and the resistance descended quickly after the ultimate load was reached.
6. The installation quality of weld is more difficult to control than that of nail and screw.
7. The measured diaphragm strength, S_u, is more closely estimated by use of the SDI approach, whereas the shear stiffness, G', was better predicted using the SDI* method.
8. The ratio, γ_2/γ_u provides a good evaluation of the ductility. The ratios for tests 38 and 40 are 2.04 and 1.81 respectively, which coincide the R_d=2.0 as recommended by Martin (2002) for NS connected diaphragm. The ratios for tests 42 and 48 are 1.35 and 1.01 respectively, which are near to R_d=1.0 for WB connected diaphragm.

CHAPTER 5 COMPUTER ANALYSES & APPLICATION OF TEST RESULTS

5.1 INTRODUCTION

According to previous research investigations, a steel roof deck diaphragm can transmit horizontal forces and act as an energy-dissipating element during severe earthquakes (Essa et al, 2001; and Martin, 2002). There are however, factors that have not been fully investigated, such as the type of attachment, sheet length, profile shape and roofing materials, which may influence the diaphragm's inelastic behaviour. In this Chapter, the main objective is to describe this effect through analytical methods, where the behaviour of the computer models is based on the results of previous diaphragm tests.

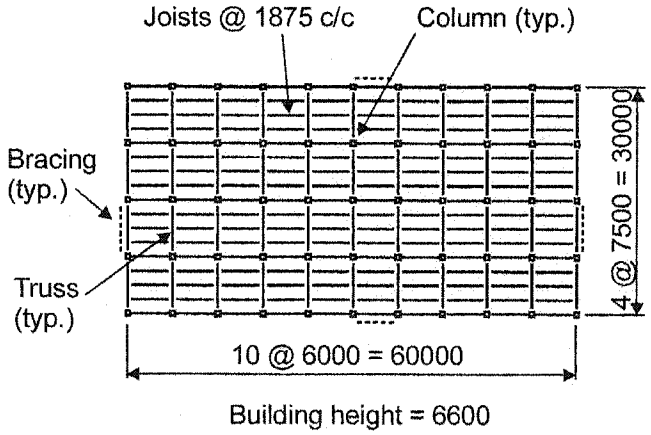

Figure 5.1. Plan view of the medium size building to be analysed (Martin, 2002)

A medium sized single-storey steel building is considered as the model building (Fig. 5.1). Earthquake is assumed to be in the short dimension direction. The structure of this building was designed in compliance with the draft 2005 NBCC (NRCC, 2001) and the current CSA-S16 steel design standard (2001). In the 2005 NBCC, one very important parameter is the ductility related force modification factor, R_d, which ranges from 1.0 to 5.0 for various types of seismic force resisting systems (SFRS) based on their capability to deform in a ductile manner (Mitchell et al, 2003). Due to a lack of information on the performance of the roof deck diaphragm as the energy-dissipating element in the SFRS, an R_d value has not yet been approved for use in design. The selection of an appropriate R_d value for the inelastic deck diaphragm has been the subject of earlier research projects. Martin (2002) suggested values for several connection configurations, which include R_d=2.0 for the nail/screw connected deck diaphragm. Since Martin's research did not consider the influence of the longitudinal overlap of the panels nor the non-structural roofing components, the objective of this Chapter is to include these situations in the building analyses and to verify the applicability of the previously proposed R_d values.

In addition, Section 5.3 has been included in order to present the results of a finite element method (FEM) study of P3615B steel deck panels. The intent of carrying out these analyses was to better explain the influence of the non-structural roofing materials on the diaphragm shear stiffness.

5.2 DYNAMIC ANALYSES OF A MEDIUM SIZE BUILDING

5.2.1 Analysis scenarios

The analyses that are discussed in this section involved a number of different scenarios for which combinations of the following factors were utilized:

- Two R_d values: R_d=3.0 and R_d=2.0;
- Three roof assembly types:
  1) Roof type 1: bare sheet, no overlap, sheet length 7500 mm;
  2) Roof type2: bare sheet, with overlap, sheet length 5625 mm;
  3) Roof type 3: with roofing, no overlap, sheet length 7500 mm.
- Three ground motions: A, B, G (See Section 5.2.3.6).

The alphanumeric title for each scenario, e.g. 3-1-A, can be described as follows: R_d=3.0, roof type 1, and ground motion A. In some cases only the model type is referred to, e.g. 2-2 means R_d=2.0 with roof type 2.

Based on the results of the building analyses, Martin (2002) recommended two R_d values, which are associated with the intermediate to low ductility range of an SFRS.

The roof types were chosen from the test configurations described in Chapter 4. It should be noted that there are some differences between the diaphragm in the model building shown in Figure 5.1 and that constructed for the test specimens. The first difference is the sheet length. It is 7500 mm for roof type 1 and type 3, but about 6100 mm in the full length tests; it is 5625 mm for roof type 2, but 3050 mm in the end lapped tests. The second difference is the joist spacing. It is 1875 mm wide in Figure 5.1, but 1520 mm in tests. As will be discussed, the model building was designed based on the SDI approach that has been verified by numerous tests to

provide an appropriate evaluation of the strength and stiffness of diaphragms of various configurations. Factors such as sheet length and joist spacing are considered in the SDI design approach.

The ground motions were chosen because it was anticipated that they would cause the most extensive inelastic deformations in the roof diaphragm, based on the results by Martin (2002).

5.2.2 Building design

5.2.2.1 Design conditions

The 30x60x6.6m single-storey steel building that was designed (Figure 5.1), with an assumed location in Victoria, B.C, had a horizontal bracing bent length of D_s=7.5 m. A unit dead load of DL=1.0 kPa and a unit design snow load of LL=1.0 kPa were assumed. According to the 2005 NBCC the seismic weight on the roof is the dead load plus 25% of the snow load, which results in W=2250 kN. The building is of normal importance and in a class B (rock) site condition. The storey drift limit, Δ_{limit}, is set as 2.5%h, where in this case h is the height of the building.

As discussed in Chapter 2, the natural period of vibration, T_a, used in the base shear evaluation for braced frames, was assumed not to exceed $T=1.5x0.05(h_n)^{3/4}=0.309$ sec, where h_n=6.6 m, the height of the building. The minimum lateral earthquake force V was taken as the lesser of Equations 2.9 to 2.11, where S(T), the ratio of design spectral response acceleration to gravitational acceleration, is shown in Table 2.4; M_V, the factor to account for higher mode effect on base shear, was chosen as 1.0; I_E, the importance factor, is equal to 1.0 for normal importance buildings; R_d=3.0

or 2.0, and will be verified by the following dynamic analysis; and R_o, the overstrength related force modification factor, is set as the inverse of the resistance factor ϕ (Martin, 2002). For diaphragm design under earthquake loads, FEMA 302 (BSSC, 1997) and AISI (1997) prescribe a ϕ value equal to 0.60 for mechanically connected roof systems, hence,

$$R_o = 1/\phi = 1/0.6 = 1.67. \qquad (5.1)$$

In the design of this building, the steel roof deck diaphragm was chosen as the weak link in the SFRS. The P3615B roof deck profile from the Canam Manac Group was specified for use. The sheet is made of Grade 230 steel conforming ASTM A653 (2002) with a minimum nominal yield strength F_y=230 MPa, an ultimate strength F_u=310 MPa, and a Young's modulus E =203000 MPa. The base metal sheet thickness is either 0.76mm or 0.91mm depending on the level of shear force in the diaphragm or the required stiffness. The sheet length was set at either 7500mm or 5625 mm, which corresponds to 4 or 3 spans, respectively, over a joist spacing of 1875mm. Hilti nails (ENP2-21-L15) were selected for the deck-to-frame connections, along with sidelap connections made with Hilti #10 screws for Roof type 1 and type 3, and Hilti #12 screws for Roof type2.

The bracing system consisted of tension only flat steel bar conforming to CSA G40.21- 300W grade material (CSA, 1992), with F_y=300 MPa and E =200000 MPa. The braces were designed with a factored tension capacity, T_r, which is larger than or equal to 1.1 times the deck shear capacity, i.e. a capacity based design philosophy that is now explicitly required by the S16 Standard (2001), as shown by the following equation:

$$T_r = \phi A_g F_y \geq 1.1 S_u B / \cos\theta \qquad (5.2)$$

where:

ϕ : resistance factor for CBFs = 0.90

A_g: total gross area of the brace element (mm^2)

F_y: specified minimum yield stress for the steel flat bar (MPa)

θ: slope angle of the brace with respect to horizontal

S_u: deck ultimate nominal shear strength (kN/m)

B: width of the building (m)

If we define $T_{deck} = S_u B / \cos\theta$ as the deck shear capacity in the direction of the brace elements, and $T_y = A_g F_y$ as the axial yield capacity of the braces themselves, then:

$$T_y = 1.1 T_{deck}/\phi = 1.22 T_{deck} \quad (5.3)$$

This indicates that the expected tensile yield capacity of a brace member is 1.22 times the shear capacity of the diaphragm. In effect, this 22% higher capacity provides a margin that ensures that the braces remain elastic, or at most experience only limited inelastic deformation, while the diaphragm is subject to significant inelastic demand.

The perimeter beams at the roof level and the columns in the bracing bents were also designed according to the capacity based design requirements. The other beams and columns were designed according to the estimated gravity loading.

5.2.2.2 Building Design with $R_d = 3.0$

The design base shear force was equal to V_f=360 kN based on the 2005 NBCC, which is in the direction of the short dimension of the building. The maximum unit shear force along the edge of the diaphragm, from a static analysis, is:

$S_f=V_f/2B=360/(2*30)=6.00$ kN/m (5.4)

The required factored strength of the diaphragm, S_r, equals to ϕS_u, should be no less than the S_f shown in Equation 5.4, where S_u is the ultimate strength of diaphragm evaluated by the SDI approach or other methods. This results in:

$S_u \geq S_f/\phi=6.00/0.6=10.00$ kN/m (5.5)

A summary of the final building design for $R_d=3.0$ is shown in Table 5.1,where the deck type reads: "sheet thickness - nail spacing along sheet length - stitched screw spacing along sheet length - nail distribution along sheet width". The nail spacing along sheet length is only at the two ends of the building (Figure 5.1). Similar deck-to-frame connected situations were specified in tests along the south and north sides. For example, 0.76-625-625-7/7 means 0.76 base sheet thickness, 625 mm spacing for deck-to-frame nails along sheet length (building sides), 625 mm spacing for side lap stitched screws along sheet length, and 7 nails along 7 flutes (sheet width).

Table 5.1 Summary of building design for R_d=3.0

Roof type	1	2	3
Diaphragm			
Properties	Bare sheet, no overlap	Bare sheet, longitudinal overlap	With roofing, no overlap
Sheet length (mm)	7500	5625	7500
Deck type	0.76-625-625-7/7	0.91-937-625-4/7	0.76-625-625-7/7
Su (designed) (kN/m)	10.1	10.1	11.9
G' (kN/mm)	11.9	4.31	13.4
γ_u (rad/1000)	0.848	2.35	0.889
Braces			
T_f diag (kN)	442	445	522
A_g diag (mm^2)	1636	1648	1932
K_B (kN/mm)	36.9	37.2	43.6
Perimeter beam			
Ag (mm^2)	2850	4590	2850
EI (kN-mm^2)	2.57E+14	4.13E+14	2.57E+14
Deflection			
Δ_B (mm)	9.75	9.68	8.26
Δ_F (mm)	3.95	2.45	3.95
Δ_W (mm)	7.59	20.9	6.74
$R_d R_0 \Delta_{TOT}$ (mm)	107	165.0	94.7
Δ_{limit} (mm)	165	165	165
K_D (kN/mm)	38.9	19.1	42.0
Period T (sec.)	0.69	0.85	0.65

In Table 5.1, S_u (designed) and G' are the ultimate diaphragm shear strength and in-plane stiffness based on the SDI design method (1987), which must exceed the minimum capacity of the diaphragm S_u shown in Equation 5.5. The shear angle, γ_u, an index to describe the start of inelastic of inelastic deformation, is defined as S_u/G'.

The goal of the design is to obtain an S_u (design) that is only slightly greater than S_u, while ensuring that the maximum lateral deflection of the building $R_dR_o\Delta_{TOT}$ does not exceed Δ_{limit}. Note: Δ_{TOT} is the overall elastic building deflection at the mid-length of the diaphragm, which includes the bracing bent horizontal displacement in addition to the in-plane diaphragm displacement. The overall deflection is comprised of three components:

$$\Delta_{TOT}=\Delta_B+\Delta_F+\Delta_W \qquad (5.6)$$

where:

$\Delta_B=V/K_B$, the horizontal deflection of the brace members, where V, the design base shear force, equals to 360 kN as discussed before, K_B is the sum of stiffness of brace members in the horizontal direction, and is calculated as following:

$$K_B=2EA_g\cos^3\theta/D_s \qquad (5.7)$$

where, E = 200 kN/mm^2; A_g and θ were defined in Equation 5.2, D_s is horizontal length of the bracing bent (7.5 m) as assumed in design conditions.

$\Delta_F=\frac{5wL^4}{384EI}$, the deflection due to diaphragm flexure (based on the moment of inertia of the perimeter beams), w is the uniform lateral load, w=V/L; and

$EI=2EA_g*(B/2)^2$, where A_g is the section area of the perimeter beams shown in Table 5.1, B is the building width (30 m) , L the building length (60 m long).

$\Delta_W = \frac{wL^2}{8BG'}$, the deflection due to diaphragm shear, where w, L, B are same as defined above, G' is the stiffness of the steel deck diaphragm as given in Table 5.1.

The period of the building was estimated based on a calculation that included the effect of the flexible diaphragm (Medhekar, 1997, and Tremblay et al, 2000).

$$T = 2\pi\sqrt{\frac{(K_B + K_D)}{K_B K_D}\frac{W}{g}} \tag{5.8}$$

where:

$$K_D = \frac{\pi^2}{\frac{L^3}{\pi^2 EI} + \frac{L}{G'B}} \tag{5.9}$$

K_D here represents the total stiffness of the diaphragm (decks and perimeter beams). K_B was defined in Equation 5.7; W/g is the total seismic mass of the building.

The perimeter beams (Steel Grade 300W) were designed such that they remained elastic under the design base shear force V. For the roof type 2, the beam size was adjusted to meet the displacement limits Δ_{limit} since the G' of decks for roof type 2 is much smaller than other roof types. Also due to the displacement limits, 0.91 mm thick steel sheets were used for roof type 2.

The roof type 3 is different from roof type 1 in that it has roofing materials. Therefore S_u (designed) and G' are equal to the values of roof type 1, plus the estimated

contribution of non-structural components, i.e. the difference between test 28, and test 46, see following equations and the Table 5.2:

$$S_{u,type3}=S_{u,type1}+(S_{u,test46}-S_{u,test28}) \quad (5.10)$$

$$G'_{type3}=G'_{type1}+(G'_{test46}-G'_{test28}) \quad (5.11)$$

Test 28 and test 46 were chosen because they have the same test composition, the only difference is test 28 used a short duration (SD) load protocol, while test 46 used a cyclic plus monotonic load protocol. Test 43 is exempted from consideration because it is a monotonic test. Test 44 is excluded because its S_u was substantially lower than other diaphragm tests of the same compositions, since some connections were damaged during its cyclic load period.

Table 5.2 Strength and rigidity of Roof type 3 for R_d=3.0

Type or Test No.	S_u (kN/m)	G' (kN/mm)	γ_u (rad/1000)
Roof type 1	10.1	11.9	0.848
Test 28	14.1	2.45	5.76
Test 46	15.9	3.94	4.04
Difference (Test 46 – Test 28)	1.82	1.50	
Roof type 3	11.9	13.4	0.889

5.2.2.3 Building Design with R_d=2.0

A similar procedure to that used for the R_d = 3.0 design was followed for the situation with R_d=2.0. In this case the design base shear force was V_f=540 kN, which resulted in a maximum shear force along the edge of the diaphragm, S_{max}:

$$S_f=V_f/2B=540/(2*30)=9.00 \text{ kN/m} \quad (5.12)$$

The required capacity of diaphragm will be:

$$S_u \geq S_f/\phi=9.00/0.6=15.00 \text{ kN/m}. \quad (5.13)$$

An explanation of the remaining calculations and assumptions is given in Section 5.2.2.2, with a final summary of the building design for R_d=2.0 shown in Table 5.3.

By comparing Table 5.1 with Table 5.3, it can be found that different deck configurations result in significant changes in the diaphragm properties. For example, roof type 1 with R_d=3.0, the deck type in Table 5.1 is 0.76-625-625-7/7, with S_u is 10.05 kN/m, and G'=11.854 kN/mm; but for R_d=2.0, the deck type in Table 5.3 is 0.76-208-208-4/7, with a S_u of 15.29 kN/m, and G'=4.573 kN/mm. It seems that the spacing of the connections along the sheet length significantly influences the strength, while the spacing of connections along sheet width has more of an influence on the stiffness.

In Table 5.3, the section areas of braces were adjusted due to different forces, but those of the perimeter beams were the same as those in Table 5.2 because they were assumed to remain elastic.

Table 5.3 Summary of building design for R_d=2.0

Roof type	1	2	3
Diaphragm			
Properties	Bare sheet, no overlap	Bare sheet, longitudinal overlap	With roofing, no overlap
Sheet length (mm)	7500	5625	7500
Deck type	0.76-208-208-4/7	0.91-625-313-4/7	0.76-208-208-4/7
Su (designed) (kN/m)	15.3	15.4	17.1
G' (kN/mm)	4.57	4.70	6.07
γ_u (rad/1000)	3.34	3.27	2.82
Braces			
T_f diag (kN)	672	675	752
A_g diag (mm^2)	2489	2499	2784
K_B (kN/mm)	56.2	56.4	62.8
Perimeter beam			
Ag (mm^2)	2850	4590	2850
EI (kN-mm^2)	2.57E+14	4.13E+14	2.57E+14
Deflection			
Δ_B (mm)	9.62	9.58	8.60
Δ_F (mm)	5.92	3.68	5.92
Δ_W (mm)	29.5	28.8	22.2
$R_dR_0\Delta_{TOT}$ (mm)	150	140	123
Δ_{limit} (mm)	165	165	165
K_D (kN/mm)	18.9	20.6	23.8
Period T (sec.)	0.80	0.77	0.72

5.2.3 Dynamic analyses and data preparation

5.2.3.1 Introduction of the analysis program

The non-linear dynamic analysis program RUAUMOKO (Carr, 2000) was used to perform the time history response analyses for the various buildings that were designed. One of the advantages of this program is that it provides a wide selection of inelastic force-deformation relationship rules. Among them, the Wayne Stewart degrading stiffness hysteresis (Stewart, 1987) provides a good representation of the behaviour observed in diaphragm tests.

In the dynamic analysis, a Newmark constant average acceleration method is used in the time history analysis with a time step of 0.001 sec. Rayleigh or a proportional damping model is used with a critical damping ratio of 5% for the first two modes of vibration. A two-dimension analysis model was used to simulate the real 3-D structure, in a similar fashion as successfully implemented by Bérair (1999), Nedisan (2002) and Martin (2002). An illustration of the analysis model is shown in Figure 5.2, which was initially developed by Martin (2002).

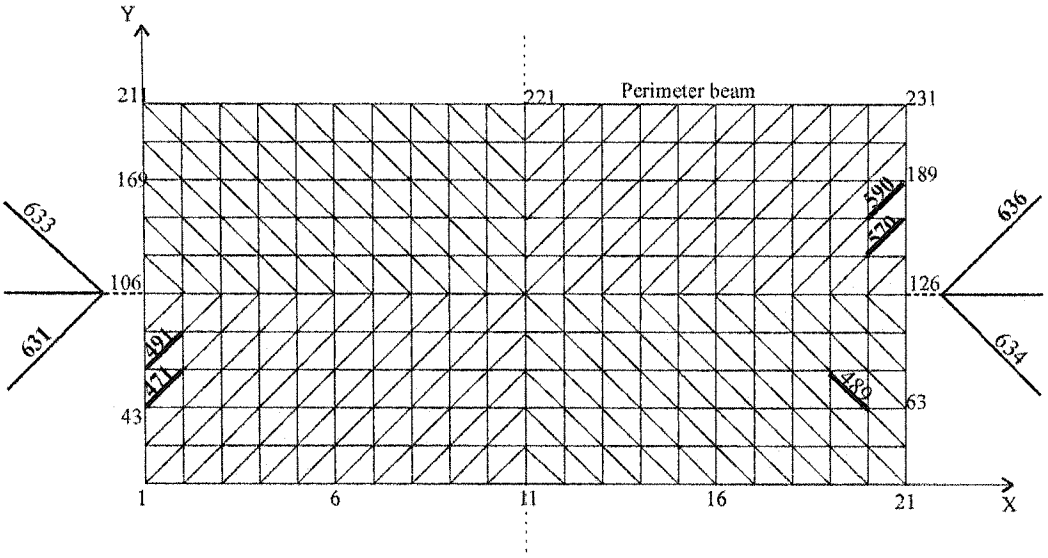

Figure 5.2. RUAUMOKO analysis model

In Figure 5.2, the highlighted deck spring elements will be used in the results discussion since they exhibited the largest deformations during the dynamic analyses. The ductility demand on the brace elements was also evaluated. Nodes 106 and 221 will be used to verify the storey drifts at the building side and at mid-length. The origin of the coordinates is at node 1, the bottom-left corner.

In this model, the roof deck elements, braces, perimeter beams and columns are all defined as spring type members (Carr, 2000). The roof deck and brace elements have been selected such that they are able to undergo inelastic non-linear deformations, whereas the perimeter beams and column elements are elastic in nature.

5.2.3.2 Roof deck and interior member elements

The roof of the building was partitioned into 3x3 m truss elements (Figure 5.3) where the deck is represented by the diagonal spring element with a length L_D=4.243 m. The

interior members (vertical and horizontal) in the truss model to provide stability to the spring deck element.

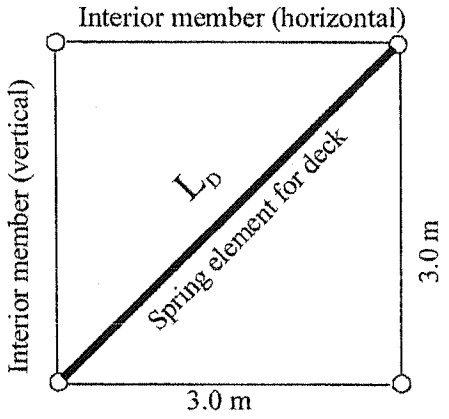

Figure 5.3. Roof deck spring element

A detailed discussion of the roof deck spring elements is contained in the following section. The longitudinal stiffness of the interior members was chosen in order to maintain the accuracy of the analysis, *i.e.* not too large to avoid influencing the deck stiffness, and not too small to cause the instability of the model. Martin (2002), based on an error analysis, suggested that axial spring stiffness values of KX=235000 kN/m for R_d=3.0 and KX=90000 kN/m for R_d=2.0 be incorporated in the model, and hence these values were also specified for the models detailed in this thesis.

5.2.3.3 Hysteresis study and Wayne Stewart parameters

In using the RUAUMOKO inelastic dynamic analysis program, an important step is to choose a suitable hysteresis rule for stiffness degradation, and to determine the necessary parameters. There are approximately 37 stiffness degradation hysteresis

models listed in the RUAUMOKO manual. The objective of the hysteresis study was to select an appropriate rule, as well as to adjust the related parameters, to best imitate the real diaphragm behaviour observed in the laboratory. Based on research by Martin (2002) and Essa *et al.* (2001), the best hysteresis rule available in that program for the analysis of diaphragms is the Wayne Stewart degrading stiffness hysteresis (Stewart, 1987). "*This very general rule was initially developed by Wayne Stewart for the representation of timber framed structural walls sheathed in plywood nailed to the framework. This model allows for initial slackness as well as subsequent degradation of the stiffness as the nails enlarged the holes and withdraw themselves from the framework*" (Carr, 1998). The behaviour described in this quotation is quite similar to that observed in the steel roof deck diaphragm assemblies that were subjected to reverse cyclic loading.

Another reason for using this hysteretic model is that it considers both the yield strength and the ultimate strength of the diaphragm assembly. This is very important, since a steel deck diaphragm with many fasteners distributed over its area, constitutes a system with a very high degree of static indeterminacy for which the forces at inner joints, panels and fasteners may not be accurately represented by average values. Hence the yield strength of a diaphragm may be much lower than its ultimate strength. The Wayne Stewart hysteresis rule is shown in Figure 5.4a and Figure 5.4b, for which the physical explanation of all symbols is given in Table 5.4.

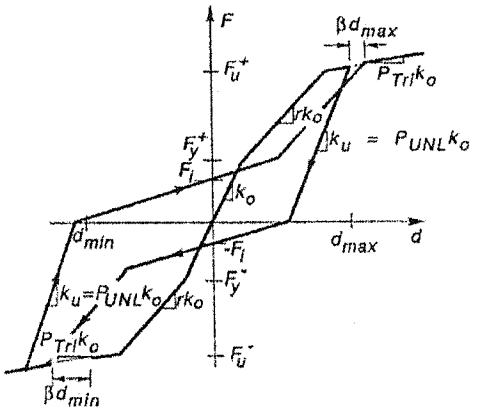

Wayne Stewart Degrading Hysteresis

a) Parameters: β, F_i, F_u, P_{tri}, and P_{UNL}

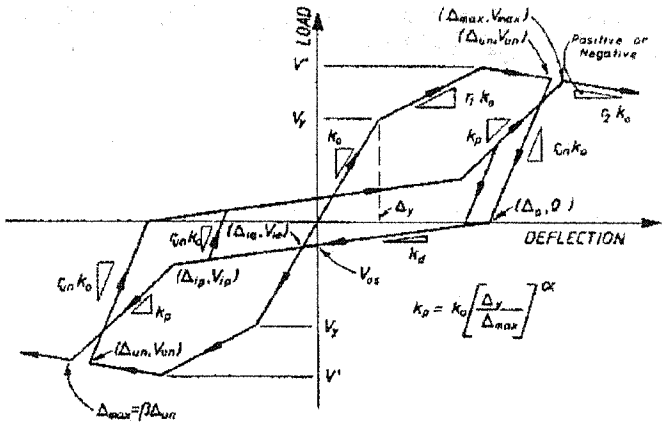

b) Parameters: α

Note: the βd_{max} and βd_{min} in the Figure a) may be in error, because $\beta >= 1.0$ in the software. The real meaning may be $(\beta-1)d_{max}$ and $(\beta-1)d_{min}$. See Figure b).

Figure 5.4. Physical definitions of the parameters in Wayne Stewart hysteresis rule (from Carr, 2002)

Table 5.4 Wayne Stewart hysteresis parameters

Parameter	Figure 5.4.a)	Figure 5.4.b)	Physical meaning
FU	F_u	V'	Ultimate force or moment
FX	F_y	V_y	Yield force or moment
FI	F_i	V_{os}	Intercept force or moment
	d_{min}	Δ_{un}-	Maximum negative displacement in unloading
	d_{max}	Δ_{un}+	Maximum positive displacement in unloading
KX	k_0	k_0	Elastic stiffness
RF	r	r_1	Bi-linear factor, ratio of stiffness between Fy and Fu
BETA	β	β	Softening factor
PTRI	P_{tri}	r_2	Tri-linear factor beyond ultimate force or moment
PUNL	P_{unl}	r_{un}	Unloading stiffness factor
	k_u	$r_{un}k_o$	Unloading stiffness
ALPHA	α	α	Reloading or pinch power factor

Martin (2002) showed that it was possible to match the test measured shear deformation vs. force hysteresis with that predicted by the Wayne Stewart model (Figure 5.5). The specified parameters used to obtain the behaviour illustrated in this Figure are listed in Table 5.5, together with upper and low bound limits that were suggested.

Table 5.5 Wayne Stewart hysteresis parameters (from Martin, 2002)

	RF	FX/FU	FI/FU	PUNL	BETA	ALPHA
Suggested	0.32 ~0.62	0.70 ~0.75	0.17 ~0.28	1.20 ~1.41	N/A	N/A
Test 7	0.40	0.72	0.20	1.30	1.12	0.55

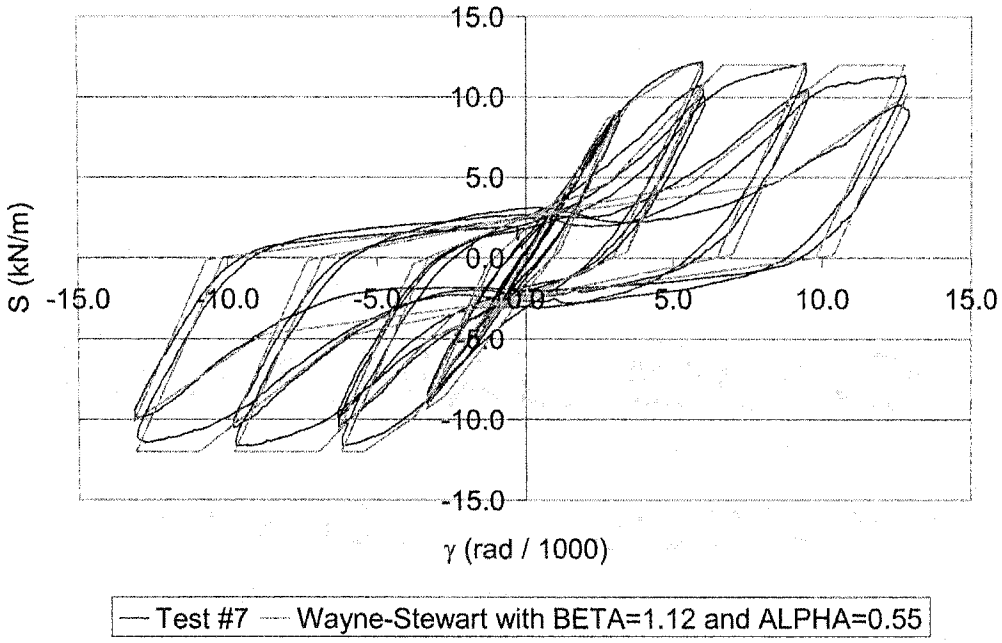

Figure 5.5. Wayne-Stewart hysteresis compared to test 7 (Martin, 2002)

In Table 5.5, the suggested limits are intended for use with a P3615B deck with nail (deck-to-frame) and screw (side lap) connection system. Test 7 was a quasi-static reversed cyclic test composed of roof decks 0.76 mm in thickness and 6 m in length connected with Hilti nails and screws. It is noted that not all of the nine parameters that are required in Table 5.4 are listed in Table 5.5, because KX=G' and FU=S_u

(Figure 5.5), can be determined directly from test results. In addition PTRI=0.0 is always used for diaphragm analyses to keep same the practice of Martin.

As discussed above, the initial attempt was based on a quasi-static test when the seismic loading protocol was not yet developed for flexible diaphragms. Martin (2002) developed a more appropriate loading protocol, the short duration (SD) cyclic loading protocol, and the tests were carried out. A SD load condition better represents the earthquake condition when compared to the quasi-static load condition used by Essa et al. For this reason is was felt necessary to improve the hysteresis rules so that a more accurate prediction of how a diaphragm would behave under seismic loading could be realised. Another reason for revisiting the hysteresis study was to verify whether the parameters determined by Martin needed to be modified or if they could be used directly with other diaphragm configurations.

The results from the hysteresis loop time history analyses, which can be determined using the Hysteresis module in Ruaumoko, were compared with the various diaphragm shear load versus deformation test results. The parameters listed in Figure 5.4 were varied until an acceptable match was obtained between the predicted hysteresis and that recorded during a test. Visual inspection and the value of the energy dissipated were employed to evaluate the analysis accuracy for all the tests unless specified. A total of nine tests, which are discussed in more detail in the following sections, all with P3615B roof deck panels, were included in the hysteresis comparison. A listing of the different roof types is as shown below:

- Roof Type 1: bare sheet, no overlap;
- Roof Type2: bare sheet, with overlap;
- Roof Type 3: with roofing, no overlap.

5.2.3.3.1 Roof type 1

The roof type 1 is made of 7500 mm long bare sheets without overlap, and supported by joists spaced at 1875 mm. The deck type for R_d=3.0 is 0.76-625-625-7/7, and for R_d=2.0 is 0.76-208-208-4/7. The fasteners are Hilti ENP2-21-L15 nails and Hilti #10 screws.

Five tests were selected in order to determine the Wayne Stewart hysteresis parameters. They are tests 28, 31, 33, and 34 from Martin (2002), and test 38 from this study. The common characteristics of these tests with the designed roof type 1 are: bare sheet, no overlap, P3615B panel, nail/screw connection, and the simulated seismic Short Duration load protocol. However the test sheet length is 6 m long, with a joist spacing of 1524 mm. The fasteners are Hilti X-EDNK22-THQ12 nails and Hilti 12-14x7/8'' screws for tests 28, 31, 33, and 34; but Buildex BX-14 nails and Buildex Screws 12- 14 x 1 HWH TEK/3 for test 38. As discussed previously, the objective of this hysteresis study is to improve the Wayne Stewart hysteresis rules and to determine the parameters listed in Table 5.4. The ultimate shear strength S_u and stiffness G' were determined by the SDI method. Therefore the differences between the test specimen and the roof type 1 will not affect the S_u and G' of the model buildings to be analysed.

The deck types of these five tests were summarized as following:

- Test 28, 0.76-305-305-4/7, Hilti nails and screws;
- Test 34, 0.91-305-305-4/7, Hilti nails and screws;
- Test 38, 0.91-305-305-4/7, Buildex nails and screws;
- Test 31, 0.76-153-153-7/7, Hilti nails and screws;
- Test 33, 0.91-153-153-7/7, Hilti nails and screws.

It is proposed to use the hysteresis rule of test 31 for R_d=3.0 of the roof type 1 because test 31 has the same sheet thickness and the 7/7 fastener configuration. For R_d=2.0, test 28 is used because of the same sheet thickness and 4/7 fastener configuration, if the hysteresis results can be verified.

5.2.3.3.1.1 Test 28, 0.76-305-305-4/7, Hilti nails and screws:

Initially the same parameters as recommended by Martin (2002) were tried (see Table 5.5). The predicted hysteresis curve was compared with the test curve (shear load versus rotation) in Figure 5.6. This first trial prediction, using KX=G'=2.445 kN/mm and FU=S_u=14.088 kN/m, provided a reasonable facsimile of the recorded test results.

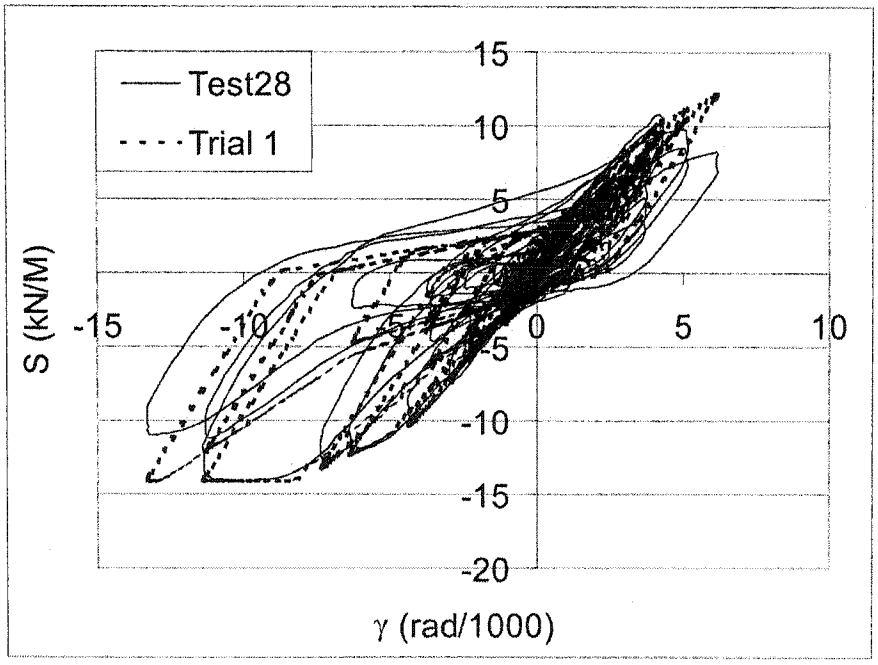

Figure 5.6. Comparison of predicted and test hystereses for Test 28

It is noted that the force-deformation relationship in Figure 5.6 is not symmetrical about the two axes. This is due to the asymmetry of the SD loading protocol (refer to Section 4.1.7.2). In addition, there are some imperfections in the predicted response that may be the result of limitations in the model itself. Firstly, the test hysteresis is composed of curves, while the Wayne Stewart hysteresis is composed of straight lines. Secondly, there are two interception points (FI) along the vertical axis, positive and negative, which may differ in the test, although for the computer analysis, only one FI can be specified (Figure 5.7). The third imperfection is the inability to consider the strength degradation after the ultimate capacity is reached when using the Wayne Stewart hysteresis. In RUAUMOKO, the strength degradation functions well with the elasto-plastic hysteresis, it made the strength decrease when deformation (or ductility) exceeds a specified value as shown in Figure 5.8, however after several trials this proved not to be the case for the Wayne Stewart hysteresis. Therefore, strength degradation was not considered in this study.

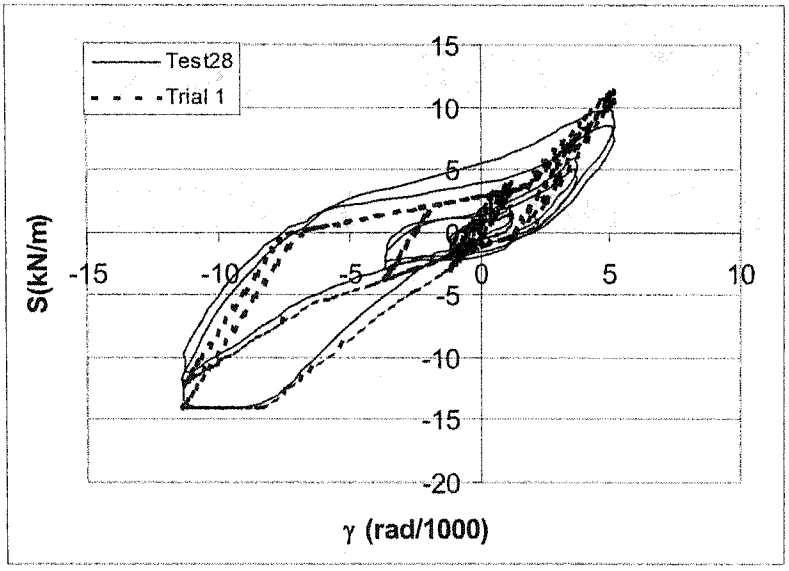

Figure 5.7. Details of comparison about Wayne Stewart hystereses to test result in cycles of S_u (=14.088 kN/m) for Test 28

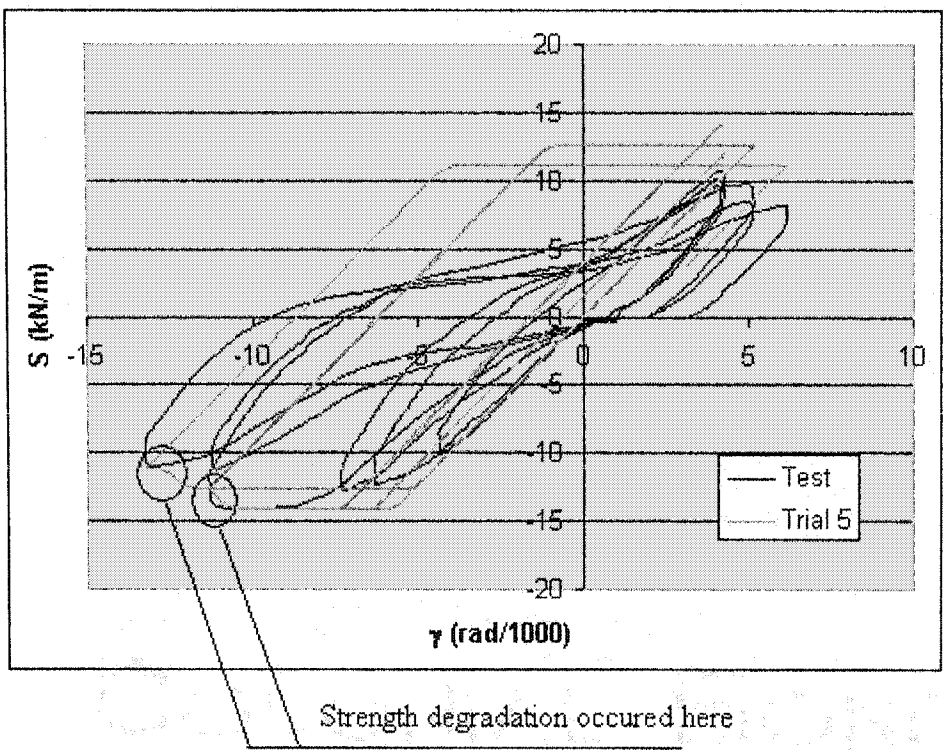

Figure 5.8. Strength degradation of test 28 by elasto-plastic hysteresis

These three limitations indicate that it is nearly impossible to create a hysteresis model that precisely duplicates all of the test data. Hence, it was considered most important to be able to predict the hysteretic behaviour around the cycles in which the load reached S_u. Figure 5.7 shows that the Wayne Stewart hysteresis matches quite well the load vs. shear rotation curve of test 28 in the cycles where S_u is reached. The hysteresis model was considered to be acceptable because it could be used to represent the most important part of the test behaviour.

It is to be noted that in Fig. 5.8, not all the cycles were illustrated, only six cycles with high unit shear forces (>10.14 kN/m, the yield S value) were shown to see more clearly the match details. For these six cycles, it was realized that the energy

dissipated by inelastic deformation E_d, which is equal to the area enveloped by the hysteresis curves, could be relied on to obtain the best combination of the Wayne Stewart hysteresis parameters. In Table 5.6, the E_d value of the six cycles of the Trial 1 is 348 (kN/m)*rad/1000, when compared with other trials, it is closer to that from test 28 (= 447 (kN/m)*rad/1000).

Table 5.6 Parameters of Wayne Stewart hysteresis for test 28

	KX=G'	RF	FX+	FX-	FU=Su	FI	PTRI	PUNL	BETA	ALPHA	E_d
	kN/mm		kN/m	kN/m	kN/m	kN/m					(kN/m)* rad/1000
Trial 1	2.45	0.40	10.14	-10.14	14.09	2.82	0.00	1.30	1.12	0.55	348
Trial 2						1.41		1.30		0.55	302
Trial 3						1.41		1.40		0.55	319
Trial 4						1.41		1.40		0.45	299

Note: Blank cells in the Table indicate that the same values as Trial 1 were considered. Only the values different from Trial 1 are shown to highlight the change of parameters.

5.2.3.3.1.2 Test 34 0.91-305-305-4/7, Hilti nails and screws:

Shear stiffness and strength values were obtained from the results of test 34: KX=G'=4.014 kN/mm and FU=S_u=17.025 kN/m. Once again the parameters suggested by Martin were first tried. Afterwards, a second trial was done with some of the parameters being adjusted, as shown in Table 5.7, to arrive at a visually satisfactory hysteresis. The two trials are shown in Figure 5.9.

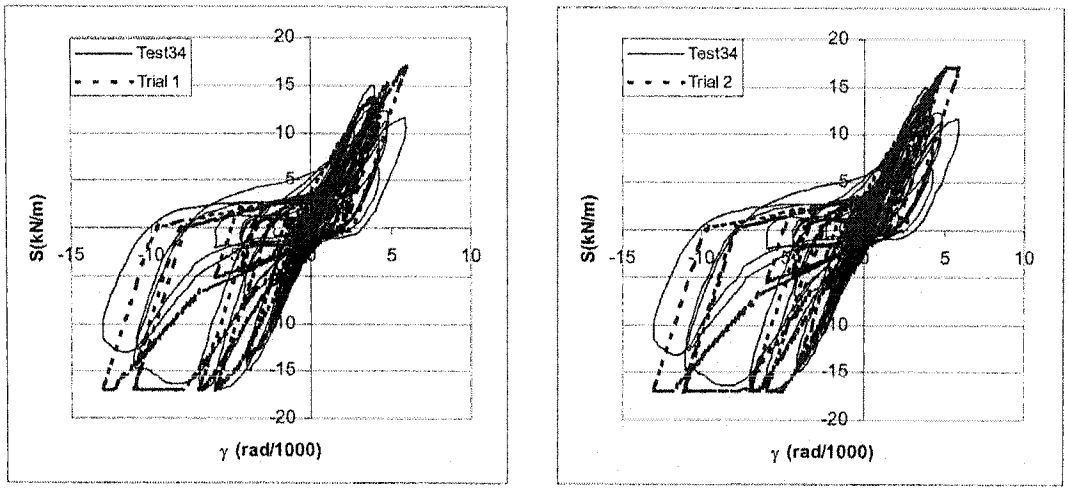

a) Trial 1 b)Trial 2

Figure 5.9. Comparison of predicted and test hystereses: Test 34

Table 5.7 Wayne Stewart hysteresis parameters for test 34: Trials 1 & 2

	RF	FX/FU	FI/FU	PUNL	BETA	ALPHA	E_d
Trial 1	0.40	0.72	0.20	1.30	1.12	0.55	744
Trial 2	0.60	0.72	0.20	1.30	1.06	0.55	759

It is noted that the results of Trial 2 (Figure 5.9.b) provide a better match to the test results than what was obtained for Trial 1 (Figure 5.9.a). The energy dissipated by the hysteresis cycles also showed that E_d of trial 2 (=759 kN/m*rad/1000) is closer to that from test 34 (=829 kN/m*rad/1000). The effect of adjusting parameters RF and BETA (Table 5.7) is significant, as is illustrated in the detailed comparison of the six cycles before and after S_u (Figure 5.10). It must be noted that the Trial 2 described

here is actually the result of numerous attempts to improve the hysteretic model by adjusting the various parameters.

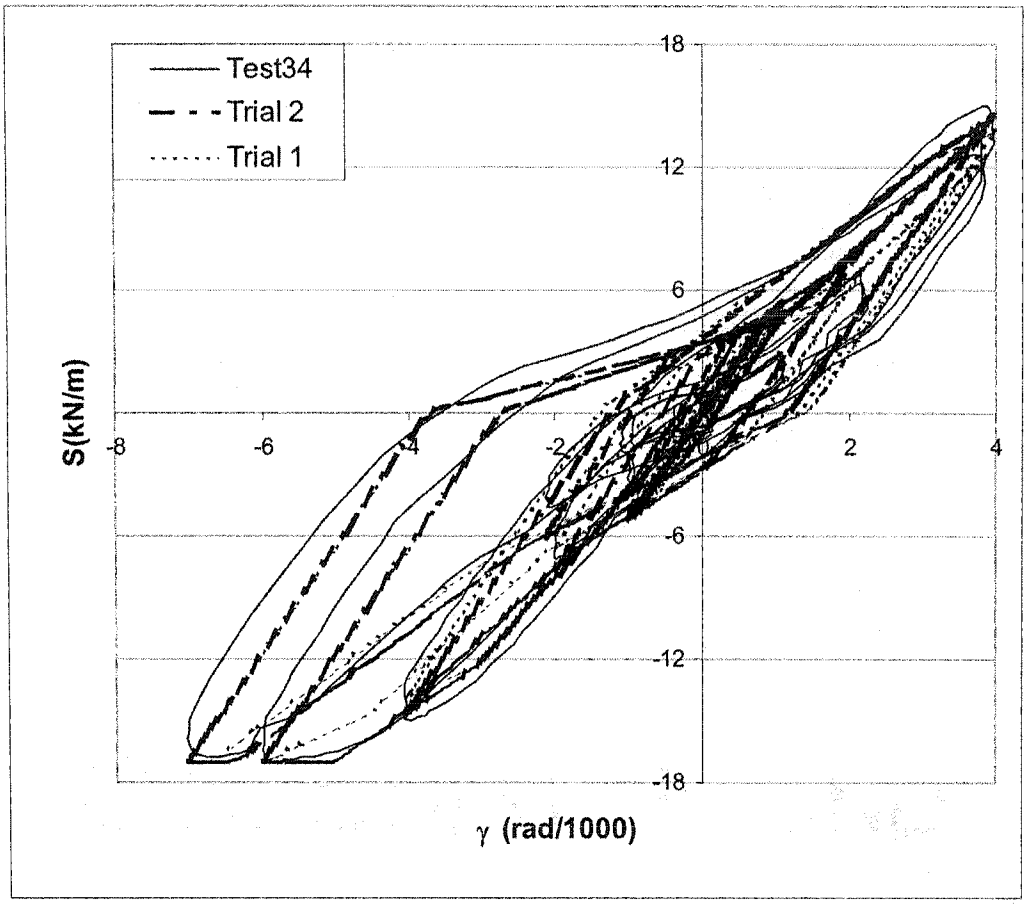

Figure 5.10. Detailed comparison of predicted and test hystereses: Test 34

5.2.3.3.1.3 Test 38, 0.91-305-305-4/7, Buildex nails and screws:

Similar interpretation of the results for test 38 was carried out resulting in stiffness and strength values of KX=G'=3.518 kN/mm and FU=S_u=15.247 kN/m, respectively.

An initial trial was based on Martin's recommended parameters (Trial 1). Subsequent modification of the Wayne Stewart parameters, by adopting the same values as the Trial 2 in test 34 discussed in last Section, led to the Trial 2 values that were used in the building analyses (Table 5.8). The effect of modifying RF and BETA is shown in Figure 5.11, where the Trial 2 enveloped the test curves better than the Trial 1. This is more clearly illustrated in the cycles when S_u is reached (Figure 5.12), and the energy dissipated E_d of test 38 = 668 KN/m*rad/1000, which is very close to that of Trial 2.

Table 5.8 Wayne Stewart hystereses parameters for test 38:Trials 1 & 2

	RF	FX/FU	FI/FU	PUNL	BETA	ALPHA	Ed
Trial 1	0.40	0.72	0.20	1.30	1.12	0.55	652
Trial 2	0.60	0.72	0.20	1.30	1.06	0.55	665

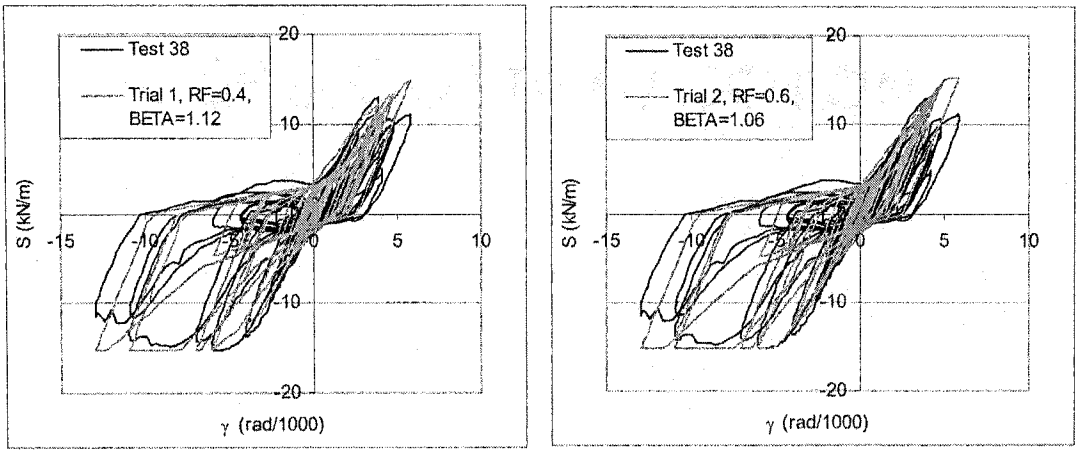

a) Trial 1 b) Trial 2

Figure 5.11. Comparison of predicted and test hystereses: Test 38

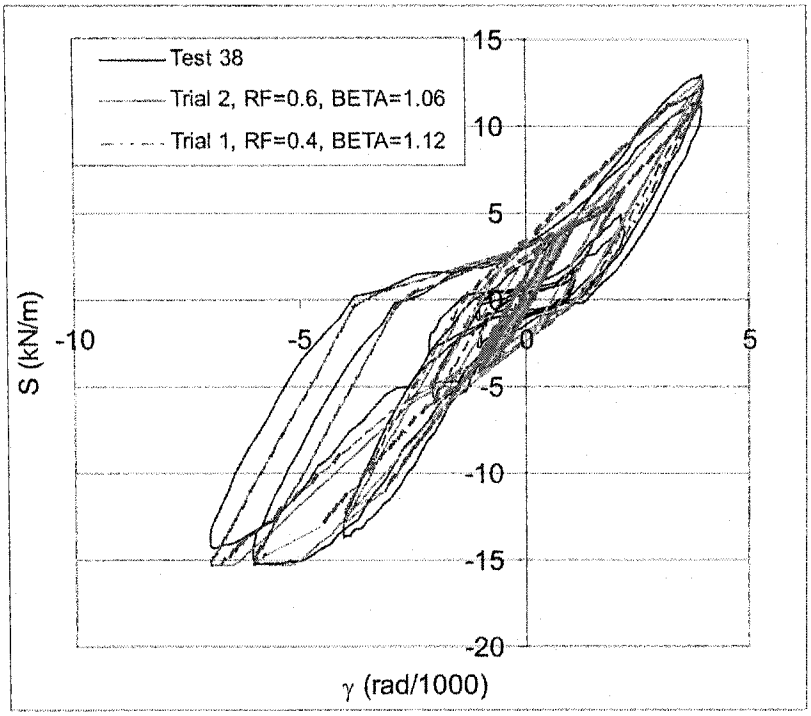

Figure 5.12. Detailed comparison of predicted and test hystereses: Test 38

5.2.3.3.1.4 Test 31, 0.76-153-153-7/7, Hilti nails and screws

Again, similar procedures for test 31 were carried out, where stiffness and strength values of KX=G'=14.952 kN/mm and FU=S_u=26.545 kN/m, respectively. Trial 1 was based on Martin's recommended parameters. In the subsequent Trial 2, parameter FI/FU was changed from 0.2 to 0.3 (Table 5.9). The results reveal that the parameters in Trial 1 match better the test hysteresis as shown in Figure 5.13. The energy dissipated E_d in Table 5.9 also shows that Trial 1 is better (E_d of test 31 = 998 KN/m*rad/1000, which is very close to that of Trial 1). Therefore Trial 1 is retained for that roof system.

Table 5.9 Wayne Stewart hystereses parameters for test 31:Trials 1 & 2

	RF	FX/FU	FI/FU	PUNL	BETA	ALPHA	E_d
Trial 1	0.40	0.72	0.20	1.30	1.12	0.55	973
Trial 2			0.30				1151

Note: The values not illustrated in Trial 2 are same as those in Trial 1.

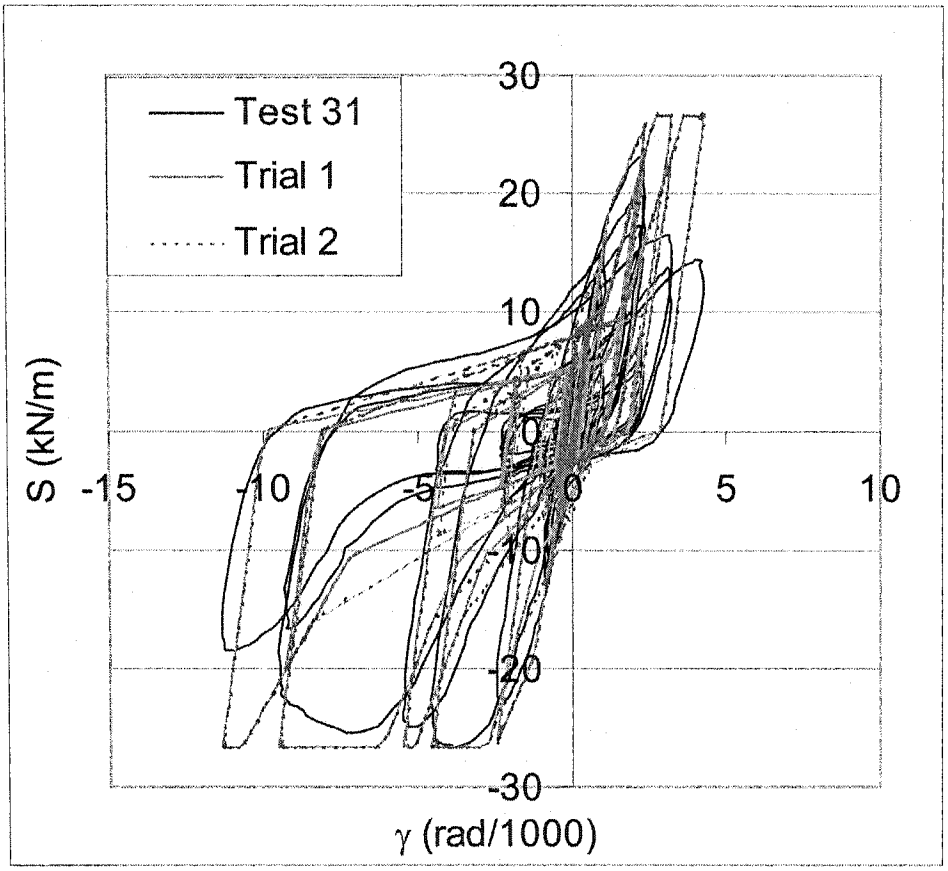

Figure 5.13. Comparison of predicted and test hystereses: Test 31

5.2.3.3.1.5 Test 33, 0.91-153-153-7/7, Hilti nails and screws

For test 33, stiffness and strength values equal to KX=G'=18.418 kN/mm and FU=S_u=35.229 kN/m are specified. The parameters of two trials are shown in Table 5.10, where Trial 1 is based on Martin's recommended values, and Trial 2 is based on that of test 34. It is found that Trial 1 gives a better result that trial 2, the dissipated energy by inelastic deformations, E_d, (= 1122 kN/m*rad/1000), is very close to that of Trial 1. A comparison of these trials with test curves is shown in Figure 5.14.

Table 5.10 Wayne Stewart hystereses parameters for test 33:Trials 1 & 2

	RF	FX/FU	FI/FU	PUNL	BETA	ALPHA	Ed
Trial 1	0.40	0.72	0.20	1.30	1.12	0.55	1161
Trial 2	0.60	0.72	0.20	1.30	1.06	0.55	1207

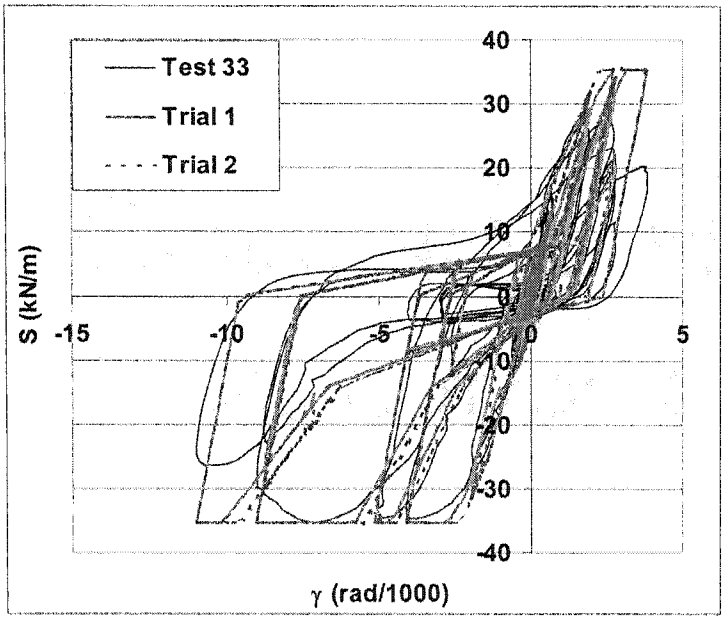

Figure 5.14. Comparison of predicted and test hystereses: Test 33

To summarize, based on the findings of this study, Table 5.11 lists the parameters of the Wayne Stewart hysteresis that were used for all the roof type 1 building analyses. It was found that the parameters are the same as those recommended by Martin (2002). It should be noted that for R_d=3.0, the parameters were actually obtained from Test 31; while for R_d=2.0, the parameters were based on the results of Test 28. In summary, two different deck diaphragms can be modelled with the same parameters, except for S_u and G', which can be evaluated by the SDI or other approaches.

However, it was also found that, for 0.91 mm thick decks, some changes of the parameters are recommended to better match the test results, as shown in Table 5.11. The parameters can be used whether the fasteners are Hilti type or ITW Buildex types.

Table 5.11 Wayne Stewart hysteresis parameters for roof type 1

R_d	Deck type	RF	FX/FU	FI/FU	PUNL	BETA	ALPHA
3.0	0.76-625-625-7/7	0.40	0.72	0.20	1.30	1.12	0.55
2.0	0.76-208-208-4/7	0.40	0.72	0.20	1.30	1.12	0.55
Test	0.91-153-153-7/7	0.40	0.72	0.20	1.30	1.12	0.55
Test	0.91-305-305-4/7	0.60	0.72	0.20	1.30	1.06	0.55

5.2.3.3.2 Roof type 2

Roof type 2 includes bare sheets, end panel overlaps, sheet length of 5625 mm, and joist spacing of 1875 mm. The deck type for R_d=3.0 is 0.91-937-625-4/7, for R_d=2.0, the deck type is 0.91-625-313-4/7.

The following two tests were selected for the Wayne Stewart hysteresis parameters to be specified. They were chosen because they are the only end-lapped tests carried out:

- Test 38-76-3-NS-M-39, with deck type 0.76-305-305-4/7;
- Test 38-76-3-NS-SD-40, with same deck type as test 39.

In these two tests, the sheets were 3 m long with longitudinal overlap, and were made of bare sheet P3615B panels, the joist spacing was 1524 mm, and Hilti nail/screw connections were used. However, test 39 involved monotonic loading, while specimen 40 was a Short Duration (SD) test.

The common characteristics between roof type 2 and these tests are that they have end-lap effects, they use 4/7 deck-to-frame connection spacing along the sheet width, and they are under simulated seismic loaded conditions. The composition difference between roof type 2 and these tests are: sheet length of 5625 mm vs. 3050 mm; joist spacing of 1875 mm vs. 1524 mm; sheet thickness of 0.91 mm vs. 0.76 mm. From the hysteresis study results of roof type 1, it was found that the same parameters could be used for very different diaphragm systems. Based on this observation and because of the lack of test data for a diaphragm corresponding exactly to roof type 2, the parameters from test 39 and 40 are to be used for the roof type 2 system.

The monotonic test (test 39) could only provide information for RF and FX, therefore it was mainly used to check the result from the dynamic test. For test 40, Trial 1 was again based on the recommendations of Martin (see Table 5.12), and Figure 5.15 a), where the match between the predicted and tested hystereses is not ideal, that is the envelop of predicted hysteresis exceeds that of the measured. The final result of Trial 2 is shown in Figure 5.15 b). Only two parameters were adjusted, *i.e.* FX/FU and

BETA as shown in Table 5.12. Based on visual appearance, Trial 2 is more accurate than what was obtained for Trial 1, which is more clearly shown in Figure 5.16, where three hystereses were drawn together.

These two trials are also compared to test 39 (Figure 5.17). The parameters in Trial 2 are observed to be more accurate. For the non-linear time history analyses of roof type 2, the parameters of Trial 2 are therefore specified for the roof diaphragm panel elements.

Table 5.12 Wayne Stewart hysteresis parameters for test 40

	RF	FX/FU	FI/FU	PUNL	BETA	ALPHA
Trial 1	0.40	0.72	0.20	1.30	1.12	0.55
Trial 2	0.40	0.66	0.20	1.30	1.14	0.55

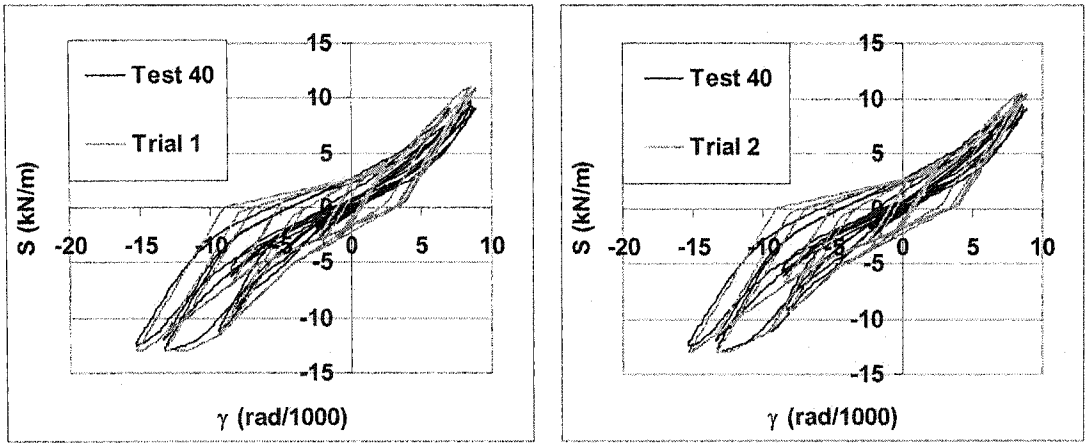

a) Trial 1 b) Trial 2

Figure 5.15. Comparison of predicted and test hystereses: Test 40

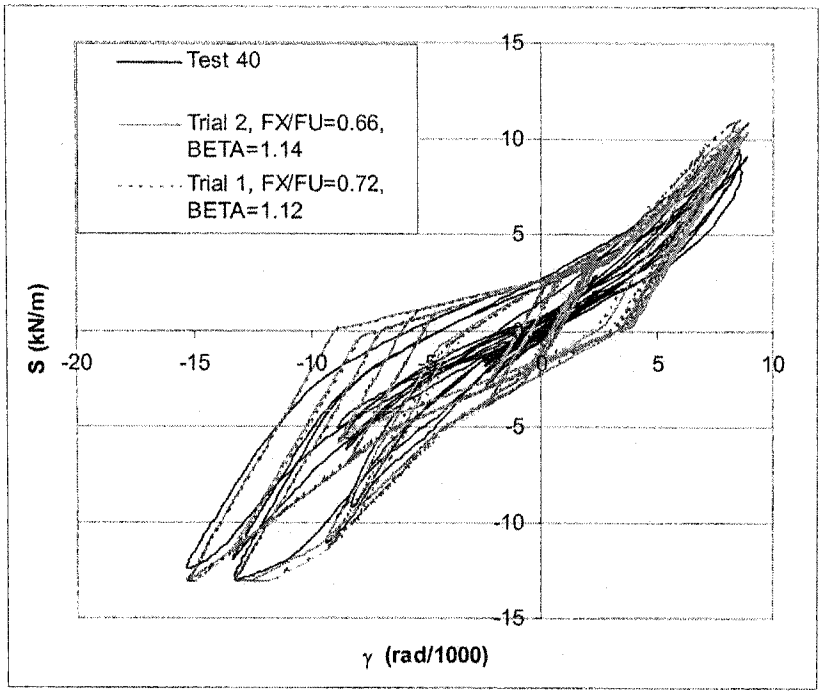

Figure 5.16. Detailed comparison of predicted and test hystereses: Test 40

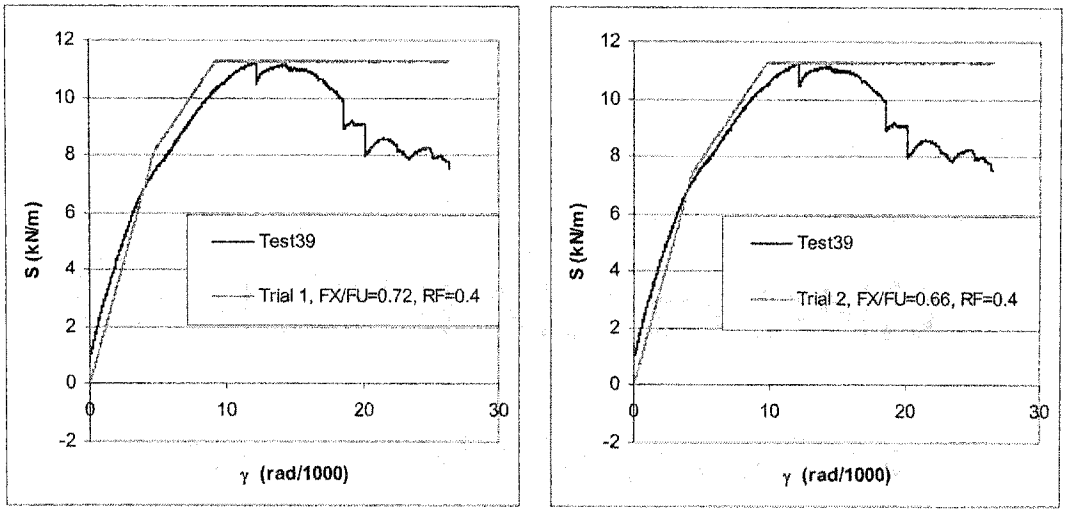

a)Trial 1 b)Trial 2

Figure 5.17. Comparison of predicted and test hystereses: Test 39

5.2.3.3.3 Roof type 3

Roof type 3 is the same as roof type 1, but it includes the non-structural roofing material. Two tests were selected such that the Wayne Stewart hysteresis parameters could be specified:

- Test 45, or 38-76-3-NS-M-R-45
- Test 46, or 38-76-3-NS-C-R-46

These tests have some common characteristics: 6 m long, with roofing materials, without overlap, P3615B panel, and Hilti nail/screw connections. Test 45 was subjected to a monotonically increasing load, while specimen 46 was tested with a reversed cyclic load at $0.6S_u$, and the S_u was estimated from the results of the bare sheet deck assembly. Given this, the roofed specimen experienced a cyclic load well below the yield level, and the load-deformation relationship mostly remains elastic, therefore it was felt not necessary to carry out the hysteresis study for the cyclic loaded period, but that for the monotonic loading period is analysed

The results of hysteresis analyses for the monotonic loaded period of test 45 and test 46 are shown in Table 5.13 and Figure 5.18.

Table 5.13 Wayne Stewart hysteresis parameters for tests 45 & 46

	KX	RF	FX/FU	FU	FI/FU	PTRI	PUNL	BETA	ALPHA
Test45	4.167	0.4	0.68	15.6	0.20	0	1.30	1.12	0.55
Test46	3.941	0.4	0.68	15.9	0.20	0	1.30	1.12	0.55

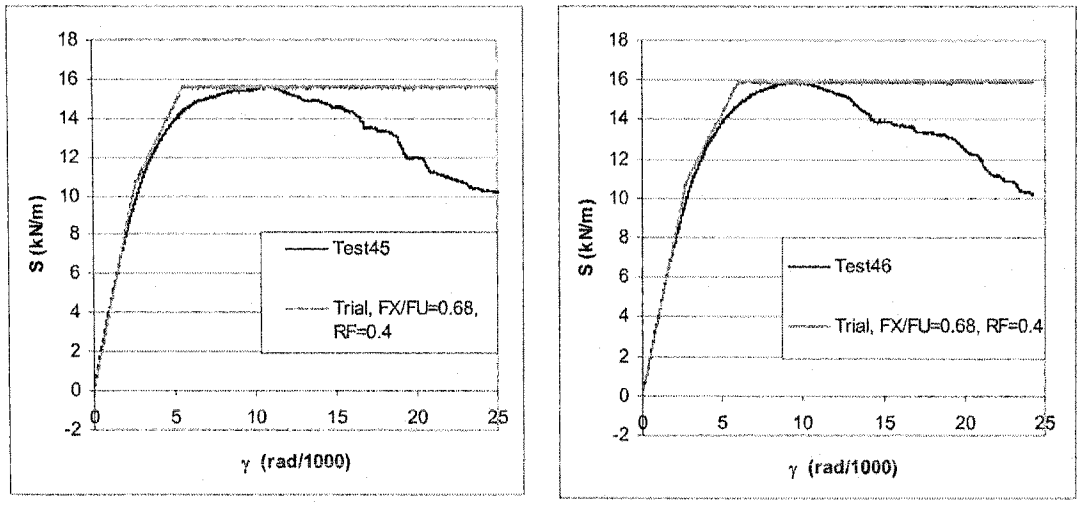

a) Test 45 b) Test 46

Figure 5.18. Comparison of predicted and test hystereses: Tests 45 & 46

In Table 5.13, only RF and FX could be evaluated because only the monotonic parts were studied. For roof type 3, RF was set at 0.4 and FX/FU at 0.68. For the other remaining parameters, the same values as for the 0.76 mm roof type 1 case (as recommended by Martin) were used, since the bare sheet deck composition of roof type 3 is same as that of roof type 1.

Figure 5.18 showed that, the predicted hysteresis in both cases was similar to the initial shear load versus rotation measured in the initial phases of the two monotonic tests, and hence, these Wayne-Stewart parameters in Table 5.13 were incorporated into the building models with non-structural roofing components.

5.2.3.4 Other members

5.2.3.4.1 Brace members

The brace members are those shown in Figure 5.2 as the side truss element No. 631, 633, 634, and 636. Since they are tension-only braces, a bi-linear with slackness model (IHYST = 5) spring element in RUAUMOKO was used, whose hysteresis rule is shown in Figure 5.19.

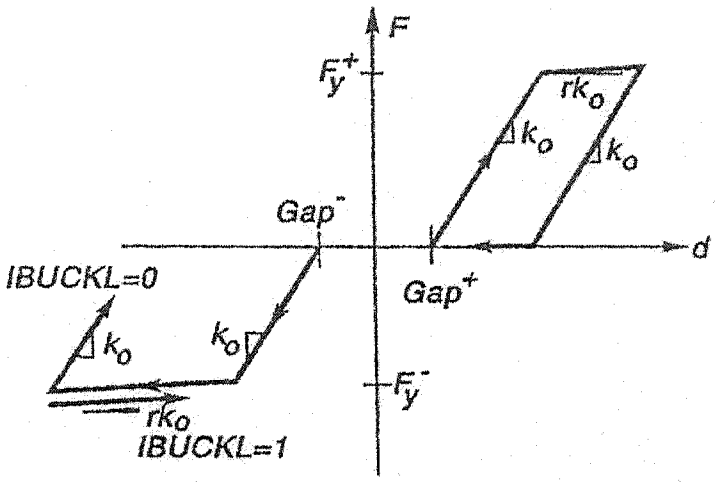

Figure 5.19. Bi-linear with slackness hysteresis (from Carr, 2000)

The symbols in Figure 5.19 are defined as follows:

k_0 = EA_g/L, the axial stiffness of the brace element, where E=200 GPa; A_g is the gross cross-section area (see Tables 5.1 & 5.3), L the brace member length, L=9.99 m;

r = 0.001 or 0.1%, the Bi-linear factor;

F_y^+ = $A_g \sigma_y$, the positive spring yield force in the axial direction, where σ_y the specified minimum yield stress of steel, σ_y=0.300 kN/mm^2 for CSA G40.21-300W grade steel (CSA, 1992).

F_y^- = -0.001 kN, the negative spring yield force in the axial direction. It represents a negligible resistance of the bracing member in compression.

Gap+ and Gap- are the Initial slackness, they were assumed to be zero.

5.2.3.4.2 Perimeter beams

Considering that the perimeter beams were designed to remain elastic, only the axial stiffness was required as input. This is represented by K_0=EA_g/L, where E is Young's modulus, A_g is the gross cross-section area of the beam (Tables 5.1 & 5.3), and L is the member length.

5.2.3.4.3 Columns

The columns were also designed to remain elastic. In this case a fictitious axial stiffness was assumed in the model so that the lateral deflection of the CBFs due to column axial deformations was negligible (K_0 = 10^6 kN/m).

5.2.3.4.4 Joists

Joists in Figure 5.1 were placed to support decks at a spacing 1875 mm c/c. Joist top chords were made of two angles L51x51x4.8 back-to-back with a 20 mm spacing. Local bending of the top chords about the weak axis was expected due to the difference of shear forces along the long direction of the building. Therefore, frame elements were used to represent the joists in the roof system. The parameters in Table 5.14 were specified to define the behaviour of these elements, particularly the section area, A, and the moment of inertia, I.

Table 5.14. Frame member parameters

ITYPE =1	One component beam member
IPIN =1 or 2	=1 End 1 pinned (internally) to the joint =2 End 2 pinned (internally) to the joint
ICOND = 0	No initial loads
IHYST =0	Elastic
E	Young's modulus, E=200 GPa.
G	Shear modulus, G=77 GPa.
A	Cross-sectional area of the member section
AS = 0	Effective shear area of the member section
I	Moment of inertia of section
WGT = 0	No weight considered

Figure 5.20 shows two typical frame elements of joists and their bending deformations. In this building, a total of 15 rows of joists are needed over the building

width, plus two rows of perimeter beams. These 15 rows of joists are lumped into the frame members along the building centreline. The section area of the two angles L51x51x4.8 is 922 mm^2, therefore the cross-sectional area of the member section, A, is 13830 mm^2. The moment of inertia for these two angles is 780 759 mm^4, but the total moment of inertia of the frame member sections should also include that of the two perimeter beams, in addition to the 15 joists. The perimeter beam is made of W150x22 sections, with a weak axis moment of inertia of $3.87x10^6$ mm^4. The total moment of inertia for the frame member sections was equal to $1.945x10^7$ mm^4.

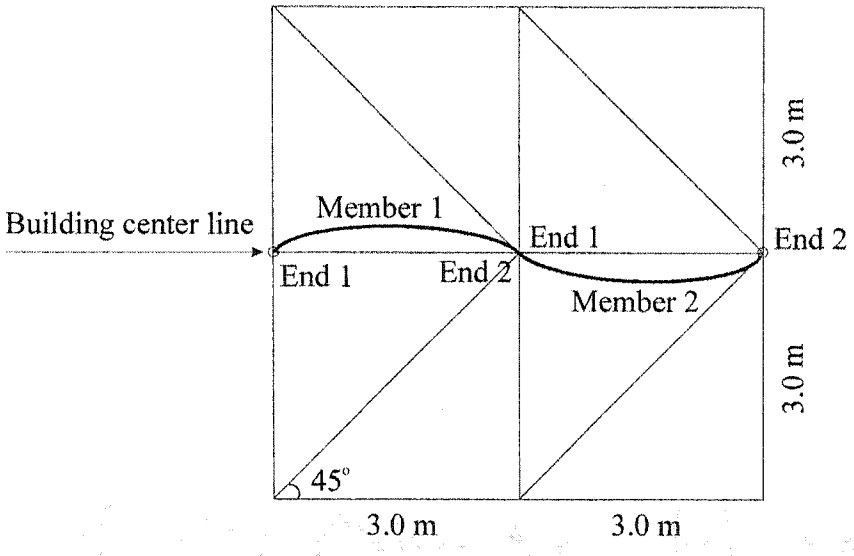

Note: The sloped lines represent the spring elements of decks (see Figure 5.3). The horizontal and vertical grid lines are the interior elements of decks.

Figure 5.20. Joist element and its position

As shown in Figure 5.1, the joists and perimeter beams are 6.0 m long in the building structure. In the model (Figure 5.20), the frame members are 3.0 m long to fit the diagonal member pattern adopted to reproduce the diaphragm. Two 3.0 m long frame members were therefore used to model the 6 m long joists and perimeter beams, as

shown in Figure 5.20. Member 1 is pinned at End 1, but is rigidly connected at the node End 2. Member 2 is rigidly connected at the node End 1, but is pinned at End 2.

5.2.3.5 Summary of data preparation

A summary of the input data for the RUAUMOKO analyses is listed in Table 5.15.

Table 5.15 Summary of model properties

		R_d=3.0			R_d=2.0		
Roof type		1	2	3	1	2	3
Deck elements—Spring members with Wayne Stewart hysteresis							
G'	kN/mm	11.9	4.31	13.4	4.57	4.70	6.07
KX	(kN/m)	23708	8628	26700	9146	9392	12138
RF		0.400	0.400	0.400	0.400	0.400	0.400
S_u	kN/m	10.1	10.1	11.9	15.3	15.4	17.1
FU	(kN)	42.6	42.9	50.4	64.9	65.1	72.6
FX/FU		0.72	0.66	0.68	0.72	0.66	0.68
FX	(kN)	30.7	28.4	34.2	46.7	43.0	49.3
FI/FU		0.20	0.20	0.20	0.20	0.20	0.20
FI	(kN)	8.53	8.59	10.1	13.0	13.0	14.5
PRTI		0.00	0.00	0.00	0.00	0.00	0.00
PUNL		1.30	1.30	1.30	1.30	1.30	1.30
BETA		1.12	1.14	1.12	1.12	1.14	1.12
ALPHA		0.55	0.55	0.55	0.55	0.55	0.55
Brace elements---Spring members of bi-linear with slackness hysteresis							
A_g	mm^2	1636	1648	1932	2489	2499	2784
FX+	kN	491	494	580	747	750	835
KX	kN/m	32751	32991	38677	49821	50020	55740
Perimeter beams---Elastic spring members							
A_g	mm^2	2850	4590	2850	2850	4590	2850
KX	kN/m	190000	306000	190000	190000	306000	190000
Period T_1	Sec.	0.664	0.832	0.623	0.795	0.773	0.720
Period T_2	Sec.	0.190	0.264	0.179	0.251	0.247	0.224

In Table 5.15, KX is the rigidity of the spring element of the diaphragm. It is derived from the geometry relationship between the distortion of the deck element and the axial deformation of the spring element as shown in Figure 5.21.

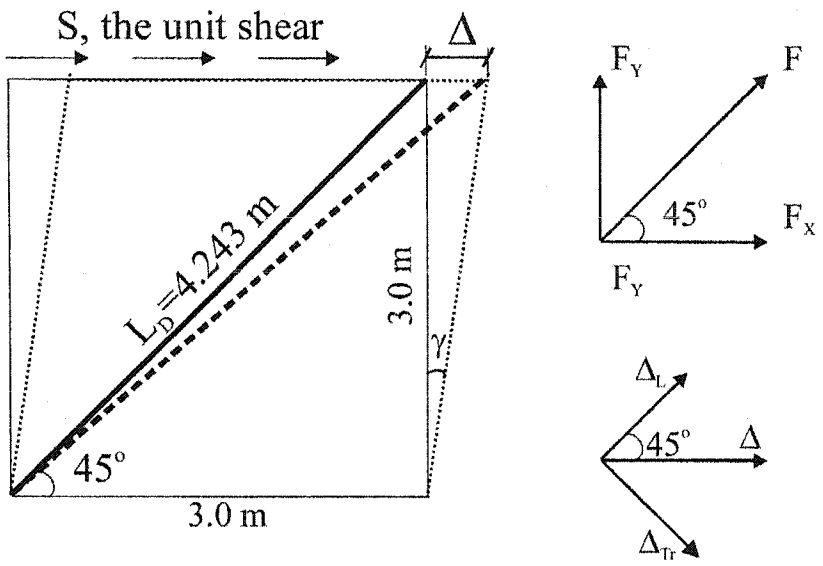

Figure 5.21. The geometry relationship between deck distortion and the axial deformation of the spring element

Each deck element is 3x3 m in plane, so the length of the spring element is 4.243 m. S is the unit shear, Δ is the displacement due to shear deformation, and γ is the distortion angle. F is the axial force in the spring, and F_X and F_Y are its x-component and y-component respectively. Δ_L and Δ_{Tr} are respectively the spring's axial deformation and its transverse displacement. From the above geometry relationships, the rigidity of the spring element is:

$$KX = F/\Delta_L \tag{5.14}$$

$$\text{where: } F = F_X/\cos(45°) = 3S/\cos(45°) \tag{5.15}$$

and, $\Delta_L=\Delta * \cos(45^o)=3\gamma * \cos(45^o)=3\ (S/G') * \cos(45^o)$ (5.16)

Hence, the rigidity of the spring element can be expressed by:

$KX = G'/\cos^2(45^o) = 2G'$ (5.17)

Also from Equation 5.12, the following expression for FU can be obtained:

$FU = 3S_u/\cos(45^o)$ (5.18)

The other parameters for the deck elements were derived from Section 5.2.3.3. The length of each element is: Deck panel spring element 4.243 m; Perimeter beams, interior members and joists 3.00 m; Braces 9.990 m; and Columns: 6.6 m.

The seismic weight of the different structures was distributed over the roof plane as lumped masses at each of the deck nodes. The intent of the analysis was to produce a symmetric movement of the structure, hence all elements on either side of the building were identical and ground motions were applied in the vertical direction.

5.2.3.6 Ground motions

Three ground motions, which were intended to match the expected seismic activity in Victoria, B.C., were selected (Table 5.16 / Figure 5.22) based on their tendency to cause significant inelastic distortion in the designed structures (Martin, 2002). The analysis time duration was chosen as 25 sec and the ground motions were scaled to match the 2005 NBCC design spectra over the applicable period ranges, which are compared in Figure 5.23.

Table 5.16 Selected ground motions for Victoria, B.C.

	Event	Magn.	R (km)	Station	Comp	PHA (g)	PHV (m/s)	S_F
A	Apr. 24, 1984 Morgan Hill	M_S 6.1	38	San Ysidro, Gilroy #6	90°	0.29	0.37	1.00
B	Jan. 17, 1994 Northridge	M_W 6.7	44	Castaic, Old Ridge Rd	90°	0.57	0.52	0.70
G	Jan. 17, 1994 Northridge	M_W 6.7	44	Castaic, Old Ridge Rd	0°	0.51	0.53	0.60

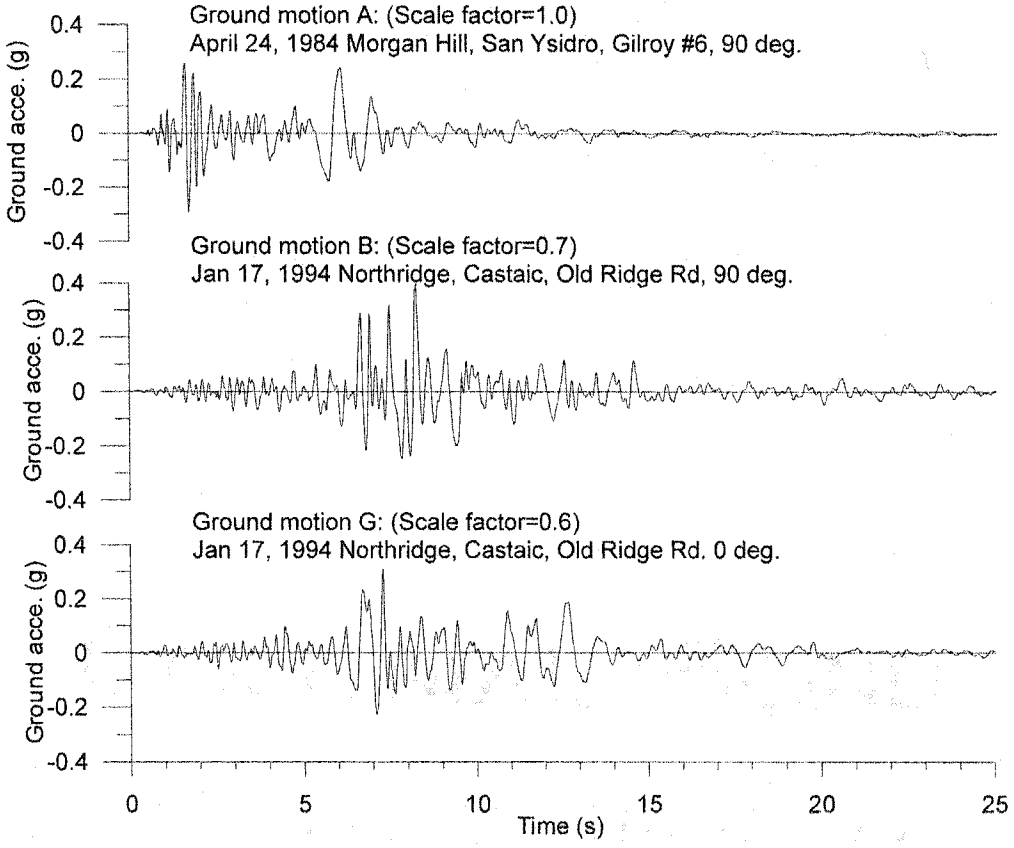

Figure 5.22. Time history of the selected scaled ground motions

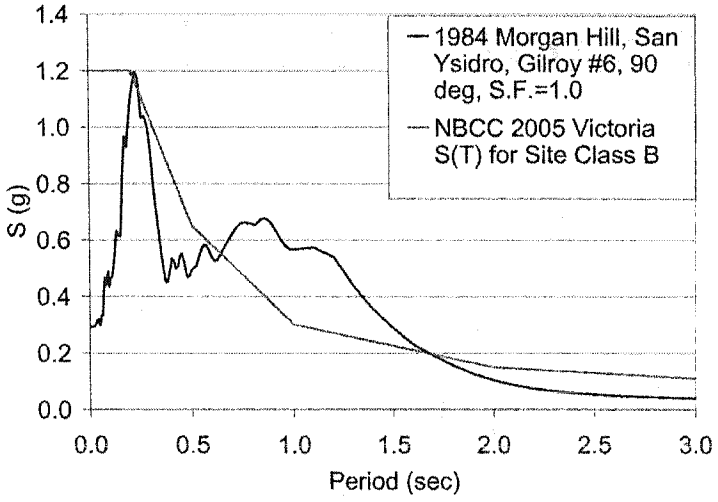

a) Ground motion A

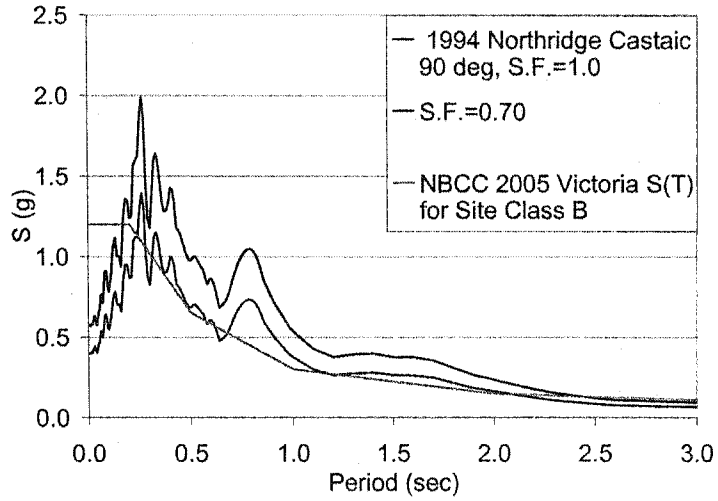

b) Ground motion B

Figure 5.23. Design and ground motion response spectra for Victoria B.C.

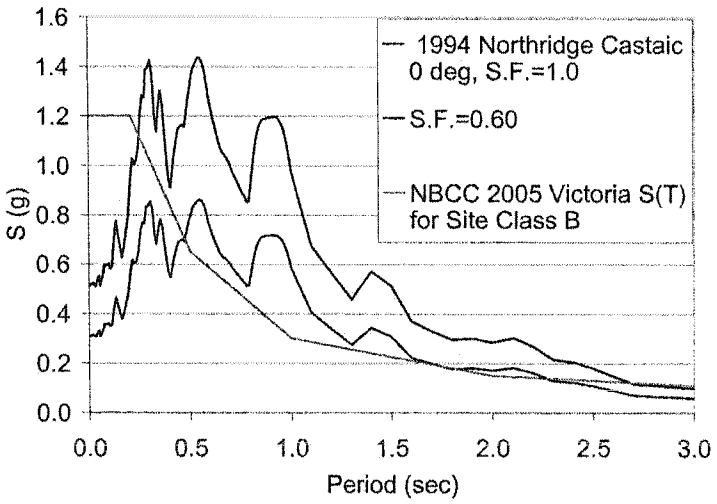

c) Ground motion G

Figure 5.23. Design and ground motion response spectra (continued)

5.2.4 Result Analysis

5.2.4.1 Shear distortion and S-γ hysteresis

At first, some background information about inelastic distortion γ_p and ductility demand in deck panels, μ_D, is presented. Figure 5.24 shows the S-γ relationship and the parameters adopted to represent the response of diaphragms under monotonic loading up to failure. The vertical axis is the unit shear force in the diaphragm, S, where S_1 is the strength limit of linear response, and S_u is the ultimate shear strength. The horizontal axis is the shear distortion γ. The definition of γ_1 is the deformation limit of linear response, γ_u is the beginning of inelastic deformation that equals to S_u/G', where G' is the linear stiffness of the S-γ curve, and γ_2 is the shear distortion

related to S_u. An additional parameter to show the extent of inelastic distortion, γ_p, is equal to $\gamma_{total} - \gamma_u$, the total shear distortion minus the start limit of inelastic deformation (Figure 5.24).

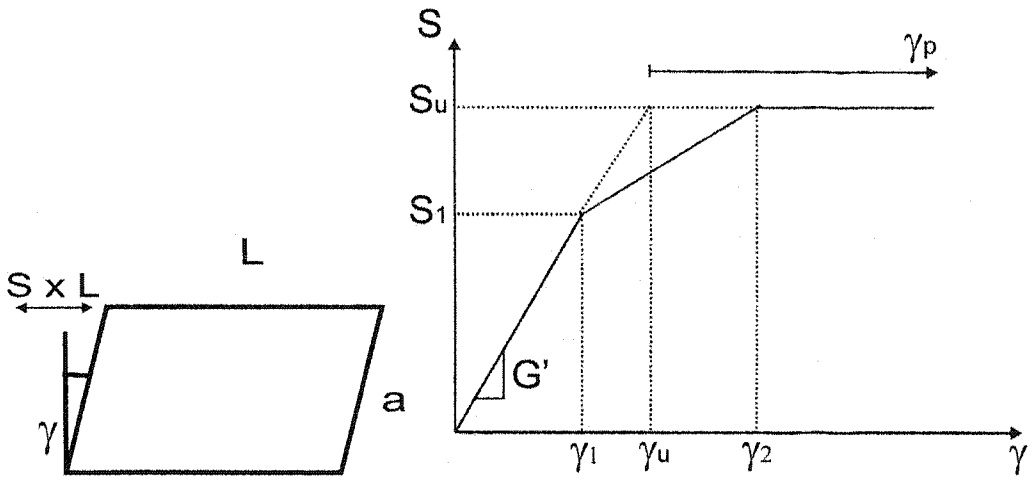

Figure 5.24. Distortion parameters (from Martin, 2002)

Figure 5.25 shows the relationship of the anticipated inelastic distortions γ_p with γ_u for R_d= 2.0 and 3.0, where V is the shear force, V_e the elastic shear force. Since $\gamma_{total}=\gamma_u+\gamma_p$, and we define the ductility demand in deck panels μ_D as:

$$\mu_D = \gamma_{total}/\gamma_u \tag{5.19}$$

According to the equal displacement principle, it would be suggested that:

$$\gamma_{total}=2.0\gamma_u, \text{ i.e. } \mu_D = 2.0 \text{ for } R_d=2.0 \tag{5.20}$$

$$\gamma_{total}=3.0\gamma_u, \text{ i.e. } \mu_D = 3.0 \text{ for } R_d=3.0 \tag{5.21}$$

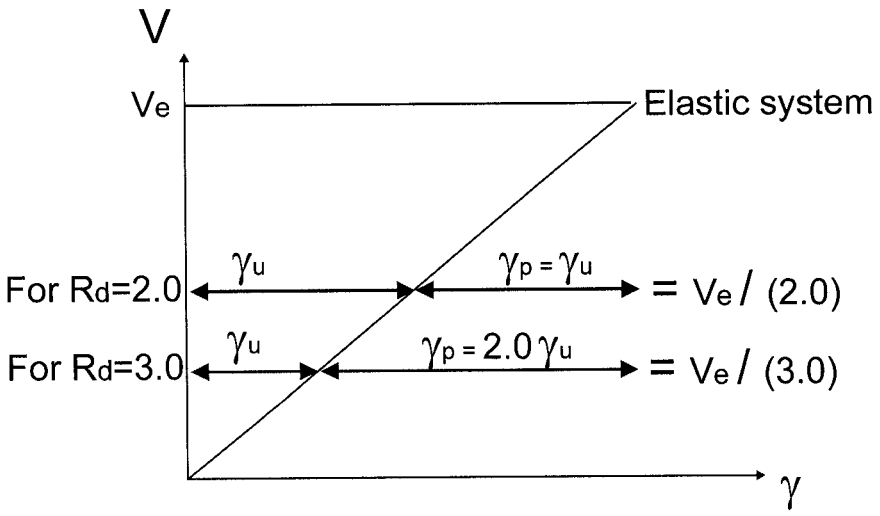

Figure 5.25. Anticipated inelastic distortions for R_d= 2.0 and 3.0 (Martin, 2002)

The shear distortion time history and S-γ hysteresis from the various analyses are shown in Figures 5.26 to 5.31. The deck distortions and S-γ hysteresis presented in these figures are representative of the deck elements that experienced the largest deformations in each analysis. The element numbers are shown in Table 5.17 (refer to Figure 5.2 for the element positions). It is noted that for analysis case 2-2-B, the deck element that experienced the largest inelastic deformation is No. 489, the element not at the end of the building. This may be due to the influence of higher mode of vibration for this specific case. For all other cases, the elements are on the end of the building.

Table 5.17. Deck elements that experienced the largest inelastic deformations

Acce.	Roof type	R_d=3.0			R_d=2.0		
		1	2	3	1	2	3
A		491	491	491	491	471	491
B		491	570	491	471	489	590
G		491	491	491	471	471	471

Note: refer to Figure 5.2 for the element positions

5.2.4.1.1 R_d=3.0 (Figures 5.26 to 5.28):

Compare the roof type 1 with roof type 2, the former has a significantly higher diaphragm rigidity, G'=11.854 kN/mm *vs.* 4.314 kN/mm, but they have similar shear capacity S_u=10.05 kN/m vs. 10.12 kN/m. Their maximum distortions are 9.85 rad/1000 vs. 11.98 rad/1000 due to ground motions A; 4.74 rad/1000 vs. 7.43 rad/1000 due to ground motions B; 11.54 rad/1000 vs. 11.34 rad/1000 due to ground motions G. A better index of distortion considering the design differences is the inelastic distortion, γ_p, and ductility demand in deck panels, μ_D, that will be discussed in Section 5.2.4.1.3.

Roof type 3 exhibited the smallest shear distortions. As anticipated, the non-structural components, when appropriately attached, can reinforce the diaphragm in terms of shear strength and stiffness.

In the figures, the positive and negative limit of γ_u, the upper and lower horizontal lines, were placed to help the reader appreciate the extent of inelastic distortion.

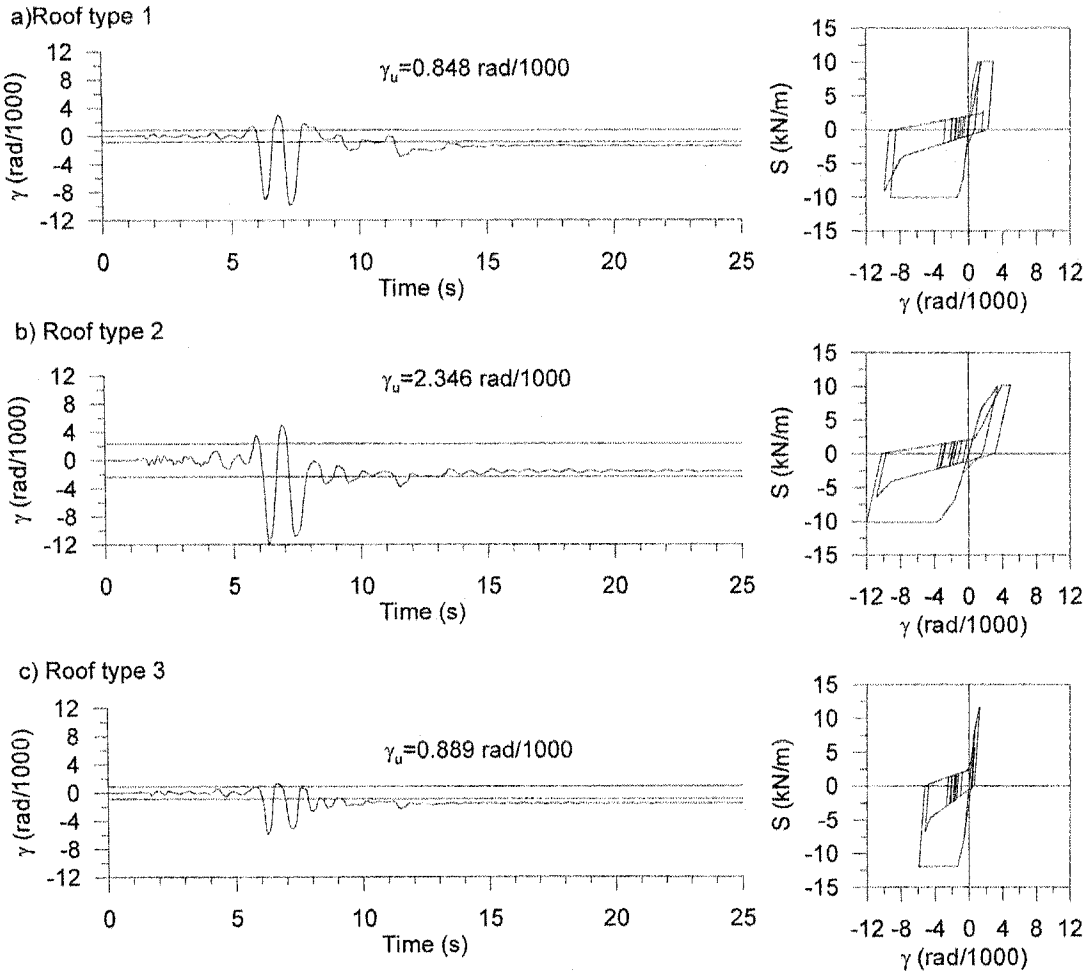

Deck panel distortion time history and S-γ hysteresis for Victoria Medium building (30x60x6.6m), Ground motion No.A, Rd=3.0

Figure 5.26. Results for R_d=3.0 and ground motion A

a) Roof type 1 (γ_u=0.848 rad/1000)

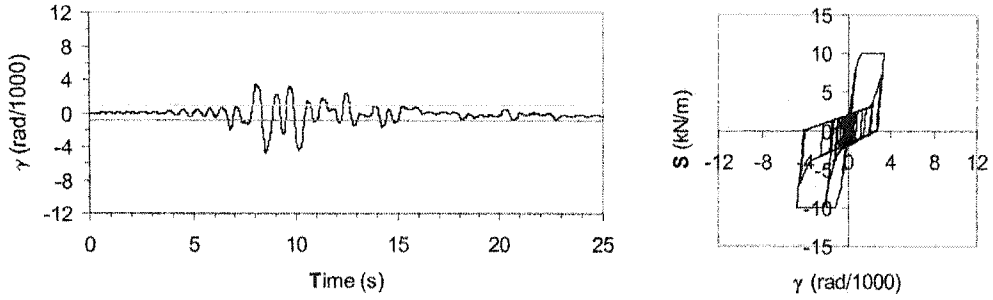

b) Roof type 2 (γ_u=2.346 rad/1000)

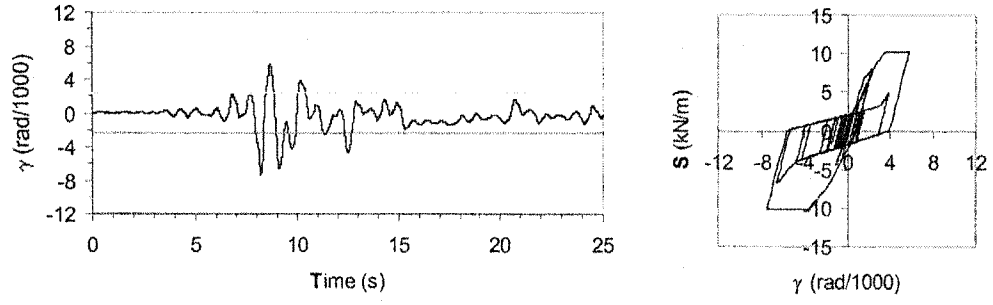

c) Roof type 3 (γ_u=0.889 rad/1000)

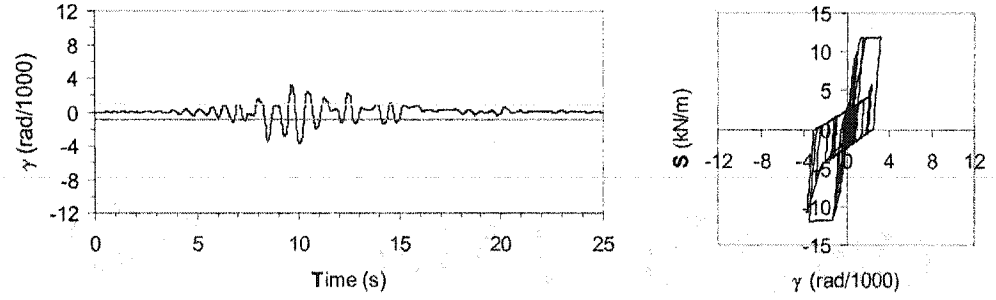

Deck panel distortion time history and S-γ hysteresis for Victoria. Medium building (30x60x6.6m), Ground motion No.B, Rd=3.0

Figure 5.27. Results for R_d=3.0 and ground motion B

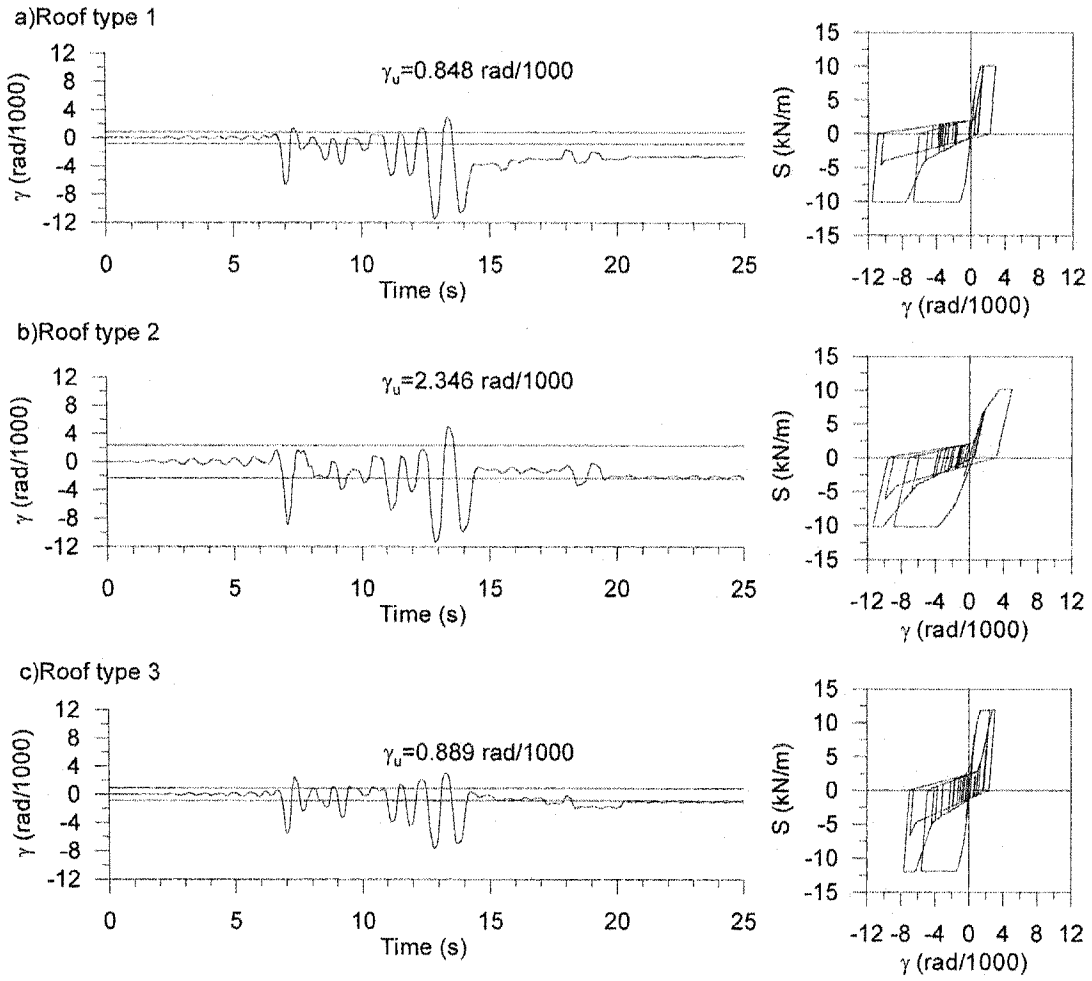

Deck panel distortion time history and S-γ hysteresis for Victoria Medium building (30x60x6.6m), Ground motion No.G, Rd=3.0

Figure 5.28. Results for R_d=3.0 and ground motion G

5.2.4.1.2 R_d=2.0 (Figures 5.27 to 5.29):

Roof type 1 and 2 showed very similar responses since their design properties were almost identical (S_u: 15.3 kN/m vs. 15.4 kN/m; G': 4.57 kN/mm vs. 4.70 kN/mm, and the brace K_B: 56.2 kN/m vs. 56.4 kN/m), their maximum distortions are 9.18 rad/1000 vs. 8.77 rad/1000 due to ground motions A, 4.80 rad/1000 vs. 4.30 rad/1000 due to ground motions B, 5.64 rad/1000 vs. 5.19 rad/1000 due to ground motions G. Therefore, for the same base shear force, it is possible to design two buildings that behave in a similar fashion even though some parameters are different, e.g. the sheet length.

Roof type 3, again because of the roofing materials, displayed a greater stiffness and strength than the other roof types.

It is noted that ground motions significantly influence the structural response, e.g. the distortions due to ground motion B is much smaller than that due to ground motion A. In dynamic analysis, it is important to use at least three ground motions and to consider the maximum, average and deviation of the resulting data. The three ground motions were selected from the eight ground accelerations used by Martin (2002).

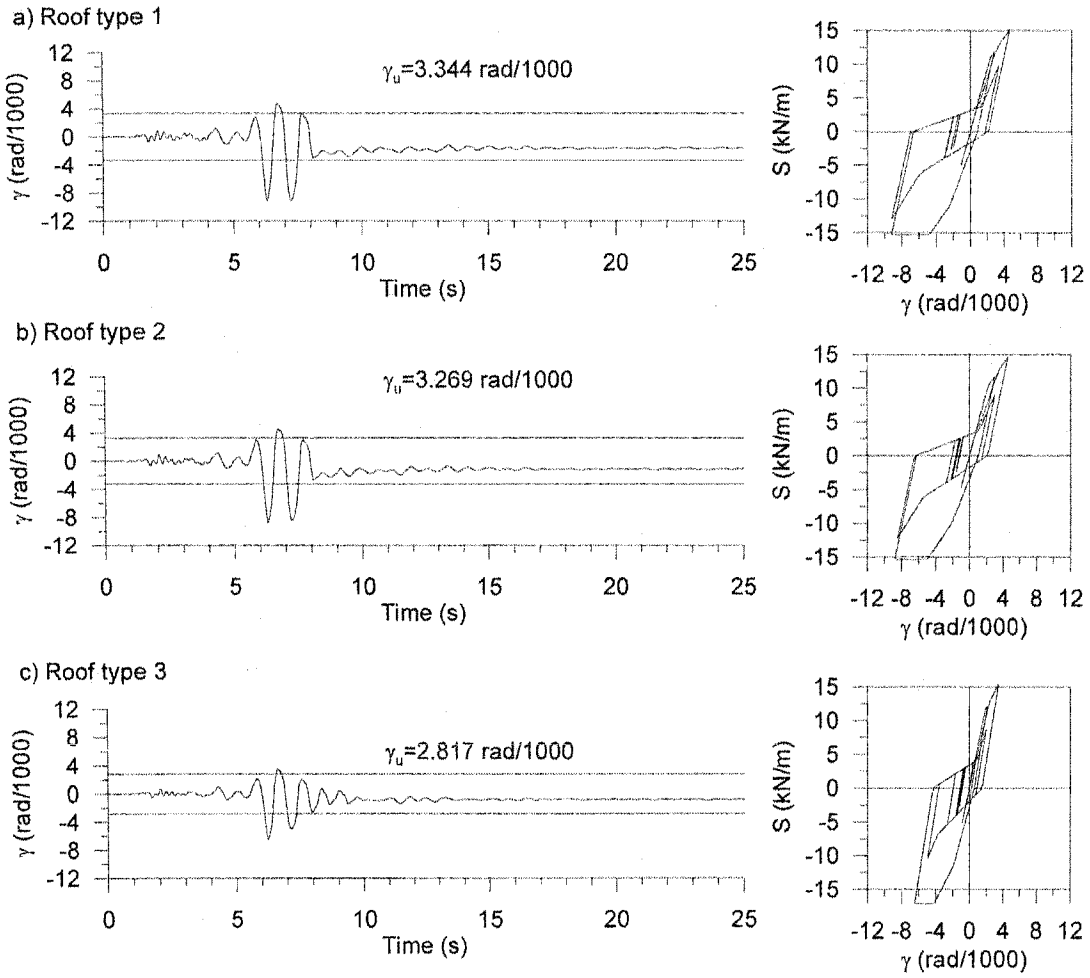

Deck panel distortion time history and S-γ hysteresis for Victoria Medium building (30x60x6.6m), Ground motion No.A, Rd=2.0

Figure 5.29. Results for R_d=2.0 and ground motion A

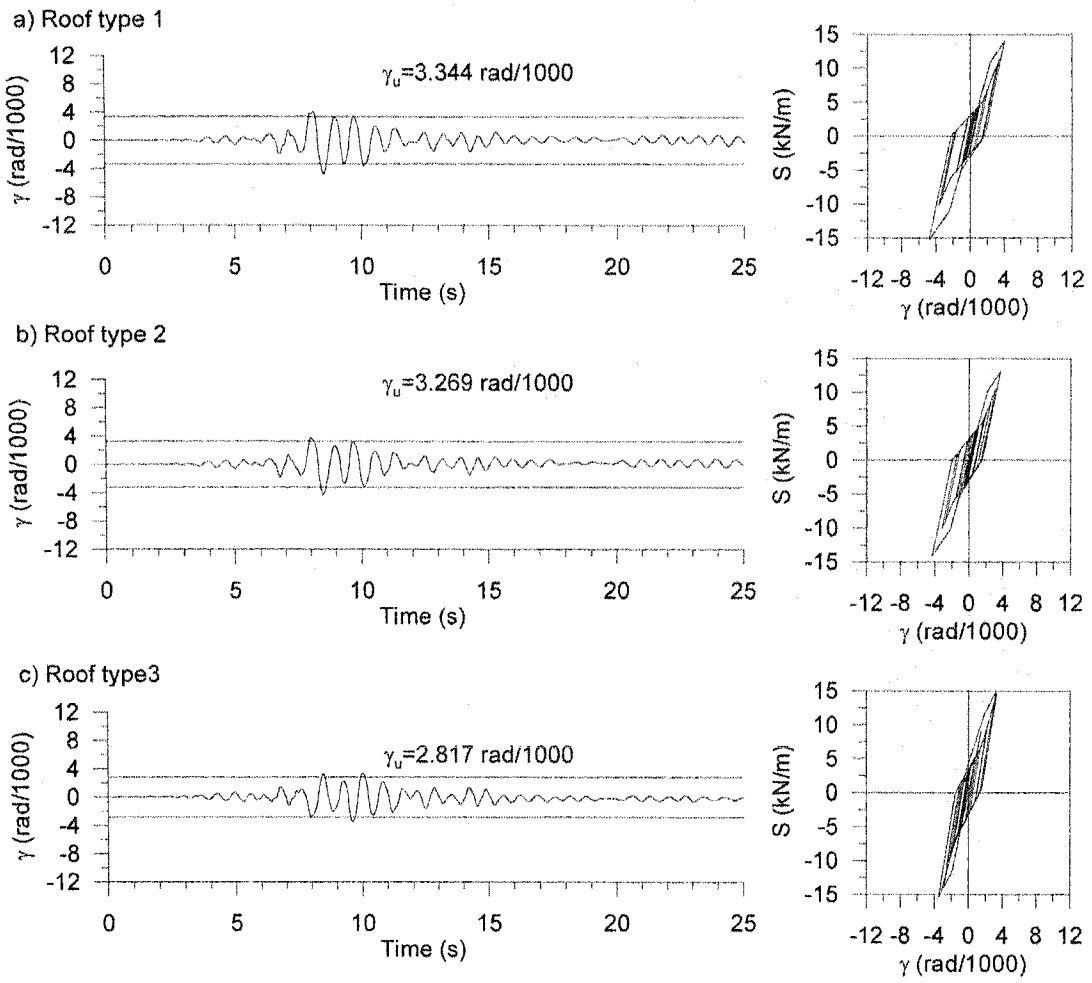

Deck panel distortion time history and S-γ hysteresis for Victoria Medium building (30x60x6.6m), Ground motion No.B, Rd=2.0

Figure 5.30. Results for R_d=2.0 and ground motion B

a) Roof type 1 (γ_u=3.344 rad/1000)

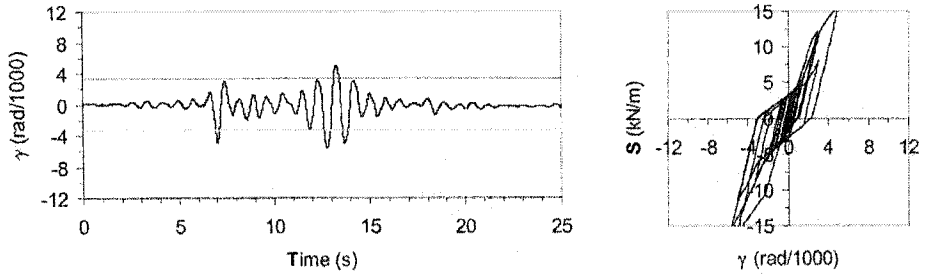

b) Roof type 2 (γ_u=3.269 rad/1000)

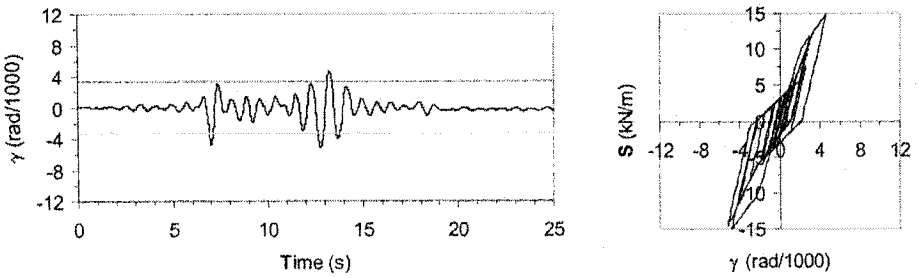

c) Roof type 3 (γ_u=2.817 rad/1000)

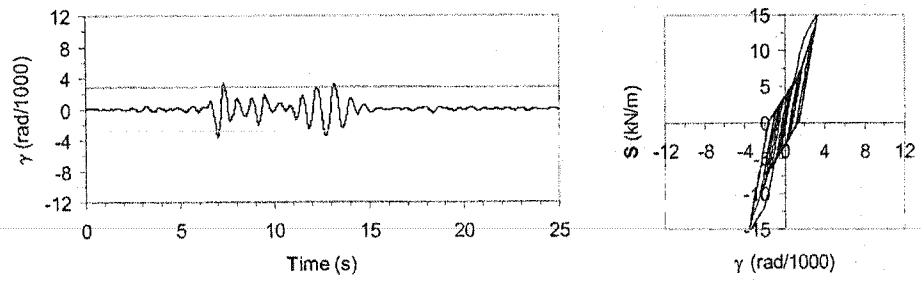

Deck panel distortion time history and S-γ hysteresis for Victoria. Medium building (30x60x6.6m), Ground motion No.G, Rd=2.0

Figure 5.31. Results for R_d=2.0 and ground motion G

5.2.4.1.3 Inelastic distortion γ_p and ductility demand in deck panels μ_D

The maximum deck panel inelastic distortions resulting from the dynamic response analyses are listed in Table 5.18. In terms of the analyses that were carried out, the real γ_p does not always coincide with the expected values. For R_d=3.0, the inelastic distortions γ_p listed in Table 5.17 due to ground motion A, B and G are all relatively higher than the expected values, and the values of γ_p are not uniform. For R_d=2.0, these values are not uniform either, but the mean values are smaller than what was expected. It seems that for R_d=2.0, the γ_p can be controlled, but for R_d=3.0, the inelastic distortion is quite variable and much higher.

Table 5.18 Maximum inelastic distortion γ_p (x 10^{-3} rad) in deck panels

R_d value	R_d=3.0			R_d=2.0		
Roof type	1	2	3	1	2	3
γ_u	0.848	2.346	0.889	3.344	3.269	2.817
γ_p, expected	1.696	4.692	1.778	3.344	3.269	2.817
Ground motion						
A	9.01	9.64	4.99	5.84	5.50	3.64
B	3.89	5.09	2.80	1.46	1.03	0.68
G	10.70	9.00	6.77	2.30	1.93	0.80
Mean	7.87	7.91	4.85	3.20	2.82	1.71
Maximum	10.70	9.64	6.77	5.84	5.50	3.64

Concerning the allowable value of γ_p, Essa *et al.* (2001) suggested to use 10 rad/1000 for nail/screw diaphragm construction, which was defined as the shear distortion related to a load equalling to 80% of the peak load on the descending branch of the S-

γ diagram, $\gamma_{0.8Su}$. By using this criterion, the maximum inelastic distortion for test 43 is 10.57 rad/1000, which is approximately equal to 10 rad/1000, the allowable inelastic distortion set by Essa *et al.* but a little bit smaller than, The maximum value for roof type 1 in Table 5.18 is 10.70 rad/1000, slightly exceeds the 10 rad/1000. Since, for roof type 1, R_d=3.0 may result in the deck inelastic distortion exceeding its limitation, therefore R_d=3.0 is not recommended in design practice for this roof type.

For roof type 2, the maximum allowable γ_p from test 39 is 11.97 rad/1000, which is a higher than 10 rad/1000, and also higher than 9.64 rad/1000 of roof type 2 in Table 5.18. For roof type 3, the maximum allowable γ_p from test 45 is 15.76 rad/1000, much higher than 10 rad/1000, and 6.77 rad/1000, the maximum value for roof type 3 in Table 5.18. It is thus possible that R_d=3.0 be used for roof type 2 and roof type 3.

Another index that can also be used to explain the higher extent of inelastic deformation in the roof diaphragm is the ductility demand, μ_D, in the deck panels (Table 5.19).

Table 5.19. The ductility demand μ_D in deck panels

R_d value	R_d=3.0			R_d=2.0		
Roof type	1	2	3	1	2	3
Ground motion						
A	11.63	5.11	6.61	2.75	2.68	2.29
B	5.59	3.17	4.15	1.44	1.32	1.24
G	13.62	4.84	8.62	1.69	1.59	1.28
Mean	10.28	4.37	6.46	1.96	1.86	1.61
Maximum	13.62	5.11	8.62	2.75	2.68	2.29

In Table 5.19, it is found that the real values of ductility demand for the R_d=3.0 buildings is substantially higher than that expected (around 3.0 for R_d=3.0 case), it is

apparent that the equal displacement principle did not hold true in this case. Additionally, these values varied with the type of roof. In contrast, for the R_d=2.0 buildings the average ductility demand of the deck elements was found to be in the anticipated range of 2.0, and furthermore the results were consistent for the different roof types. The results again verify what Martin (2002) suggested, that is, R_d=2.0 could be used in the design of weak diaphragm systems when connected with the nail/screw configuration.

In Table 5.19 it is also found that, for R_d=3.0, the ductility demand μ_D in deck panels for the roof type 1 is significantly higher than for other roof types. Martin explained that, "*the γ_u was very small for the medium building (0.84 rad/1000) in comparison to other designs and it is possible that this explains the higher ratios* (μ_D)" (Martin, 2002). The roof type 3 was modified from roof type 1 by including roofing materials; the reinforcement effect is limited based on the test results, so its μ_D is also quite high.

Roof type 2 was quite flexible, with $R_d R_0 \Delta_{TOT}$ from static procedure reaching the limit 165 mm. The mean value of μ_D is 4.37, which is still higher than the expected value (=3.0).

It is possible that, buildings designed with R_d=3.0 experience large inelastic deformations, the strength degradation will become significant, force distribution may change, and lead to higher μ_D than expected.

5.2.4.2 Deflections

The maximum lateral deflections obtained from the dynamic analysis and from the static procedure are listed and compared in Table 5.20.

Table 5.20 Maximum values of the horizontal deflections (mm)

	Analysis Case	Δ_{106}	$R_dR_o\Delta_B$	Δ_{221}	$R_dR_o\Delta_{TOT}$	$\Delta_{221}/\Delta_{106}$
Rd=3.0	3-1-A	26.0	48.8	86.4	107	3.33
	3-1-B	20.0	48.8	65.3	107	3.27
	3-1-G	22.2	48.8	92.8	107	4.19
	Average	22.7		81.5		3.60
	3-2-A	19.7	48.4	124	165	6.31
	3-2-B	18.6	48.4	89.7	165	4.84
	3-2-G	19.1	48.4	121	165	6.33
	Average	19.1		111.7		5.83
	3-3-A	20.0	41.3	64.9	95	3.24
	3-3-B	19.0	41.3	58.4	95	3.08
	3-3-G	19.9	41.3	74.6	95	3.75
	Average	19.6		65.9		3.36
Rd=2.0	2-1-A	18.1	32.1	125	150	6.87
	2-1-B	16.3	32.1	112	150	6.85
	2-1-G	17.0	32.1	108	150	6.37
	Average	17.2		115		6.70
	2-2-A	18.2	32.0	118	140	6.48
	2-2-B	15.0	32.0	102	140	6.79
	2-2-G	16.3	32.0	97.3	140	5.97
	Average	16.5		105.6		6.41
	2-3-A	17.8	28.7	103	123	5.77
	2-3-B	13.9	28.7	82.3	123	5.92
	2-3-G	15.2	28.7	79.0	123	5.21
	Average	15.6		88.1		5.63

Note: the analysis case is read as the R_d-roof type-ground motion.

In Table 5.20, Δ_{106} and Δ_{221} are the Y-direction deflections at end walls and mid-length respectively, which were obtained from dynamic procedure. $R_dR_0\Delta_B$, and $R_dR_0\Delta_{TOT}$ are the deflections at end wall and at mid-length respectively, but from static method (refer to Tables 5.1 and 5.3).

It is noted that the deflection at mid length of the roof includes both the lateral movement of the walls as well as the diaphragm. The deflections at wall sides are mainly affected by the brace stiffness, but may also be influenced indirectly by other factors, such as the damping forces and the shear forces in the joists.

5.2.4.2.1 R_d=3.0

The structure of roof type 2 was more flexible due to the shorter deck panel length (G'=4.314 kN/mm) in comparison to the other roof types; its maximum mid-length deflection Δ_{221} is much larger than that of other roof types. Roof type 2 also shows the highest ratios of mid-length deflection (of the building) to end wall deflection, $\Delta_{221}/\Delta_{106}$.

In Table 5.20, the roof type 3, reinforced by the non-structural components, demonstrated the smallest mid-length deflection and the smallest ratios of mid-length deflection to end wall deflection.

Each mid-length deflection Δ_{221} from dynamic analysis is smaller than its related $R_dR_0\Delta_{TOT}$, the value obtained from the static procedure during building design. So, the static procedure provided a safe estimate of deflection.

Comparing the deflection at the node on the wall side, Δ_{106} (Table 5.20), it was found that the roof type 2, the most flexible roof type, has the smallest deflections, although

the stiffness of its braces (K_B=37.2 kN/mm) was smaller than that of roof type 3 (K_B=43.6 kN/mm), and was similar to that in roof type 1 (K_B=36.9 kN/mm). So, it seems that flexible roof tends to transfer lower forces to the braces that are in the building sides. Another reason may be that the longer period decreased the response.

5.2.4.2.2 R_d=2.0

For R_d=2.0, the shear stiffness of the three roof diaphragms G' (kN/mm) was equal to: 4.573<4.696<6.070 for roof type 1, 2, and 3 respectively. Roof type 2 was stiffer than roof type 1 but more flexible than roof type 3. This relationship can also be seen in the mid-length deflection results, Δ_{221}, and the ratios of mid-length deflection to end wall deflection, $\Delta_{221}/\Delta_{106}$ that are given in Table 5.20. As noted in the previous section, buildings with roof type 3 that are reinforced with non-structural materials always displayed the smallest mid-length deflections and the smallest ratios of mid-length deflection to end wall deflection when compared within each earthquake record group.

5.2.4.3 Ductility demand for brace elements μ_B

The braces used in the building are tension only braces. Hence, the ductility demand for these elements, μ_B, is defined as the ratio of total extension to yield extension. This parameter is used to present the extent of plasticity in the structural element.

$$\mu_B=\Delta/\Delta_y \qquad (5.22)$$

where: $\Delta_y=F_yL/E$ (5.23)

In the above equations, Δ is the axial extension obtained from an analysis; Δ_y is the yield extension; F_y is the minimum nominal yield strength for the brace element, which is equal to 300 MPa for steel material conforming CSA G40.21- 300W grade (CSA, 1992); L is the axial length of the brace element (= 9990 mm); E=200 000 MPa.

The values of the ductility demand in the different buildings were checked. Only the braces in the models 3-1-A and 3-1-G showed a limited extent of inelasticity, i.e. the ductility demand is greater than 1.0 (Table 5.21). Martin (2002) suspected that the ground motions A and G are higher than the 2005 NBCC design spectrum, but this may be not true. The real reason may be due to the frame members (Figure 5.20 in Section 5.2.3.4.4) that represent 15 joists in the roof (Figure 5.1 in Section 5.1). When the deck diaphragm experiences large deformations, it results in additional forces in the end 1 of frame member 1 (Figure 5.20) to accommodate the same deformations, and this additional force is transferred to the brace elements by the connections and cause larger demand in the braces. In all the other analysis cases, the braces remained elastic, which is in line with the modified capacity based design approach whereby the roof deck diaphragm is to act as the seismic energy dissipation element in the SFRS. The force in the brace elements may also be influenced by the damping forces and the shear forces in the joists.

Table 5.21 Ductility demand for brace elements

Analysis Case	Brace Element No.			
	631	633	634	636
3-1-A	0.914	1.286	0.915	1.283
3-1-G	0.925	1.095	0.925	1.094

Note: Brace Elements No. 631 and 633 are in left end wall, while No. 634 and 636 are in right end wall, see Figure 5.2. A ductility demand smaller than 1.00 means the element remains elastic. The values smaller than 1.0 from other analyses are not listed.

5.3 STATIC ANALYSES OF A STEEL DECK PANEL

In this section a description of the analyses carried out on a 3048 mm long portion of a single P3615B steel deck panel, with the same connection configuration as test 39, is provided. The analyses involved the use of the SAP2000 3-dimension FEM software (Computers And Structures, Inc. 2002). Three general cases were considered:

- Bare sheet
- With roofing layout 1
- With roofing layout 2

The objective of this section of the research project was to develop a better understanding and a quantitative evaluation of the effects of the non-structural components on the roof deck diaphragm behaviour. Because not every configuration

can be studied by physical tests, the FEM could provide an economical and efficient procedure if its results are comparable to those from tests. The analysis is static and linear, and only the shear stiffness and the force distribution in connections were examined. The former is to quantify the stiffening effects of the roofing materials. The latter is to explain the non-uniform force distribution in connections due to the high degree of static indeterminacy, which could help to explain the early yield and the significant redundancy after yield.

The laboratory test specimens 45 and 46 were constructed with the following roofing material composition (from top to bottom):

- Two layers of SBS waterproof membrane;
- One layer of 1" thick non-flammable wood fibre plate, hot bitumen adhered;
- One layer of 2.5" thick polyisocyanurate (ISO) insulation, hot bitumen adhered;
- Two layers of paper vapour retarder, hot bitumen adhered;
- One layer of ½" thick gypsum board, mechanically fastened.

Theoretically, each and every layer contributes to the stiffening and strengthening of the roof diaphragm, however the use of all the layers in a numerical model would cause the analysis to become overly complex. Furthermore, not all of the layers in the roof possess similar material characteristics and, hence, do not provide an equal amount of influence on the overall diaphragm behaviour. As an example, the Young's modulus for steel is 200 GPa, whereas a value of approximately 0.002 GPa is common for the ISO insulation layer. In light of this, it seems reasonable to ignore the influence of the insulation and any of the materials that are placed above this layer. As a verification of this assumption, the test results documented in Chapter 4 showed

that there were no visibly detectable deformations in the insulation layer and the layers above during shear deformation of the diaphragm. For these reasons, only the gypsum board was included as a non-structural component in the static SAP 2000 analyses.

5.3.1 SDI estimate of shear strength and stiffness

Prior to describing the analysis model, the SDI manual (1987) was used to estimate the bare steel diaphragm stiffness and strength. The deck and fastener (nail/screw) layout was the same as that used for test 39: 0.76-305-305-4/7, the sheet length and width were L=3048 mm and W=914.4 mm, and in addition only one intermediate joist was located at 1524 mm spacing from the panel ends.

Based on the equations in the SDI manual, one obtains:

- Shear stiffness of the bare sheet diaphragm: G'_b =1.70 kN/mm;
- Shear stiffness of the roofed diaphragm: G'_r=3.29 kN/mm, see explanations below.

Since the SDI estimate of stiffness for a deck diaphragm with roofing is not available, it was necessary to estimate values based on the results of monotonic tests No. 43 and No. 45. The relevant shear stiffness values are G'_{Test43}=2.58 kN/mm and G'_{Test45}=4.17kN/mm, which result in a stiffening of 1.59 kN/mm. The SDI based stiffness for a deck diaphragm with roofing may be estimated by:

$$G'_r = 1.70 + 1.59 = 3.29 \text{ kN/mm} \quad (5.24)$$

It must be noted that these two tests comprised of 6 m long sheets, while the SAP 2000 analysis included sheets of only 3 m in length. For this reason the G'_r in Equation 5.24 is for reference only.

5.3.2 Analysis model

In the diaphragm tests, a cantilever frame set-up was used (Figure 4.1), where deck panels were attached to the perimeter frames and joists that were pin-jointed together. The same configuration was used in the cantilever analysis model shown in Figure 5.32.

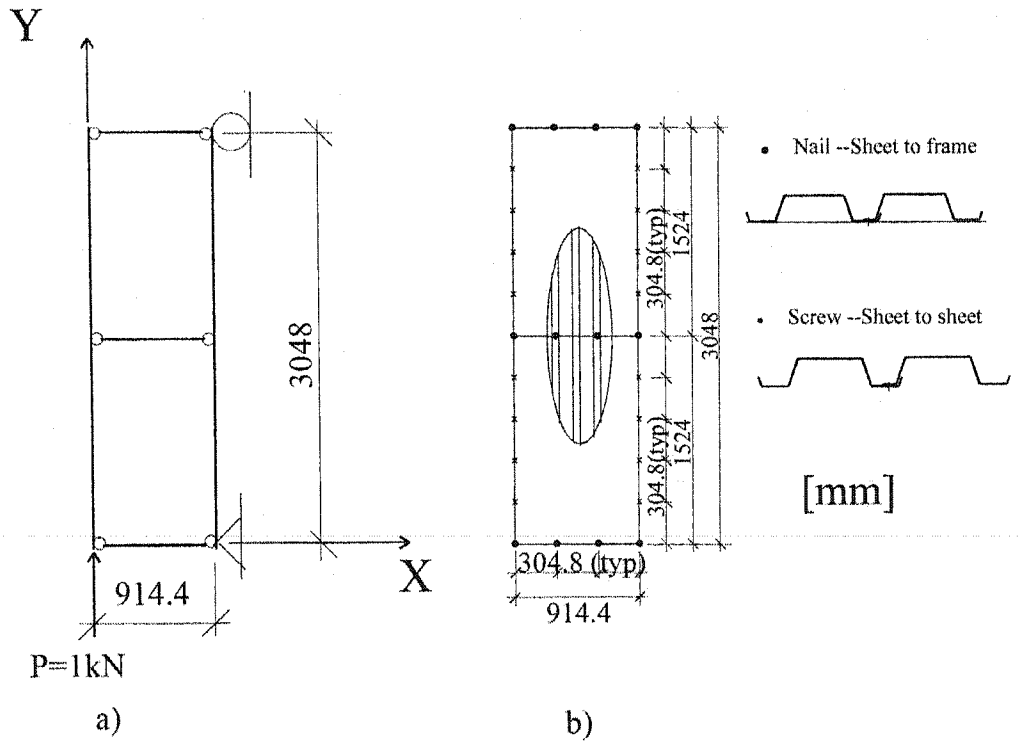

Figure 5.32. Cantilever analysis model, a) Frame & joists; b) Sheet layout

In Figure 5.32, P is the static load (1 kN) acting on the frame corner. Some useful parameters are defined as follows:

- L, the sheet length, L=3.048m=10 ft;
- S, the unit shear force, S=P/L=1/3.048 kN/m;
- Δ, the Y-direction deflection due to P: mm;
- A, the sheet width (also called W), A=914.4 mm;
- γ, the shear distortion, $\gamma=\Delta/A=\Delta/0.9144$ (rad/1000);
- G', the shear stiffness, $G'=S/\gamma=/\gamma=(1/3.048)/(\Delta/0.9144)=0.3/\Delta$.

5.3.3 Frame elements

Figure 5.32 shows the perimeter frames and an intermediate joist, which are all pinned together to support the deck panel. The frame elements were given large values for their area and moment of inertia such that their deformations did not have a significant influence on the roof deck behaviour.

- Steel material properties: Young's modulus E=203 GPa, Poisson's ratio υ=0.3.
- Section properties: the section area $A=10^7$ mm^2; and the section moment of inertia $I=10^{10}$ mm^4.

5.3.4 Panel shell elements----Bare sheet

5.3.4.1 500 shell element case

As a first trial, the 3048 mm long steel deck panel was divided into 500 shell elements, i.e. 25 elements over the width and 20 elements along the length. Therefore 26 nodes in the X direction, 21 nodes in the Y direction, for a total of 546 nodes were needed to define these 4-node shell element models, see Figure 5.33. These nodes were defined in a three-dimensional, right-hand Cartesian coordinate system (X-Y-Z), with the origin sets at node 1, the bottom-left corner (Figure 5.33 a). The Y direction dimension of each shell element is 152.4 mm, which is one half of the connection spacing used in tests (=304.8 mm). This value was selected for convenience in defining the link elements between the sheet-to-frame and sheet-to-sheet. The X direction dimension is the width of each deck flat segment.

For steel sheets, E = 203 GPa and υ=0.3 were used as in the SDI estimation. For most elements, the thickness was 0.76 mm, but 7.6 mm was assumed along the two longer sides (X=0 and X=914.4 mm in Figure 5.33), where the shell elements were reinforced by connections and surface contacts. In an initial trial, 0.76 mm thick shell elements were used along the edge, but this resulted in too flexible a response because the gap elements used along the edge were spaced too far apart to prevent the deck from penetrating into the supporting members. From former tests, no obvious bending or distortion was observed in the steel sheets along the two longer sides. As discussed later, this 10 times thickness level lacked a physical basis and was discarded when a finer mesh was used.

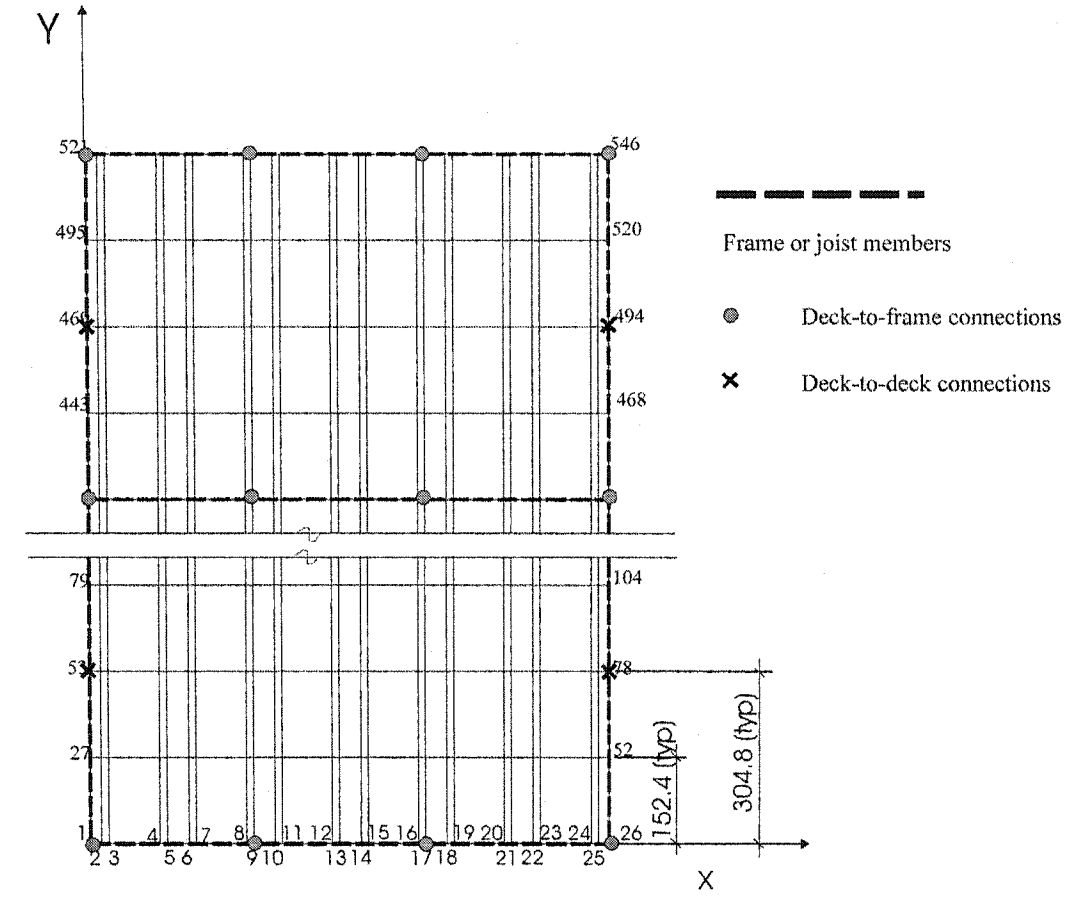

a) Plan view

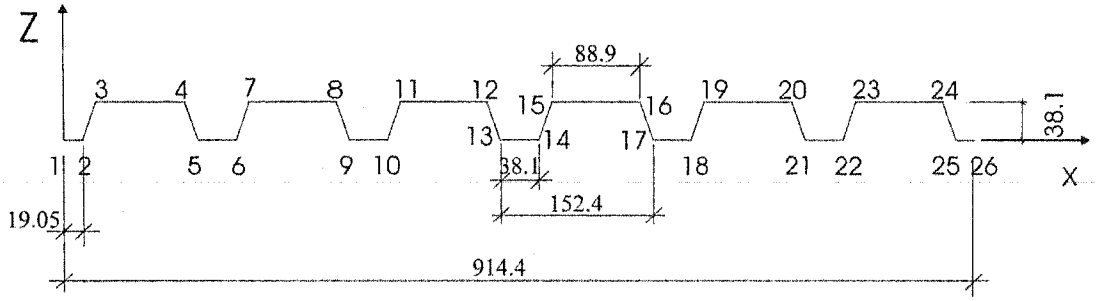

b) Section view

Figure 5.33. Shell elements and node numbers of 500 shell element case

In the tests, each roof deck panel was connected across its width to the underlying frame by four nails, which were placed at the mid position of the flutes (Figure 5.34 a). Due to the assignment of shell elements in the analytical model, it was more convenient to assume that these fasteners were located at a node, i.e. at ends of the bottom flange elements (Figure 5.34 b). The link elements were then used to represent the connections, which are discussed in greater detail in Section 5.3.6. An isolator1 type link element was used to represent the deck-to-frame or deck-to-deck connections; and a gap type link element was used to prevent the deck from penetrating into the frame, while at the same time allowing it to move freely in the upward direction. For side lap connections, similar link elements were used.

This simplification in the modelling of the connections did not precisely represent the actual construction conditions. This also motivated the development of a more refined model discussed next.

a) Real deck-to-frame connection layout

b) The link elements in SAP analysis

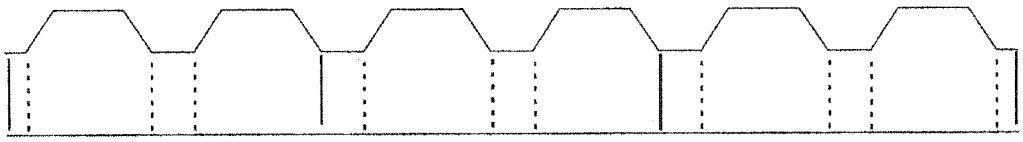

Link element type 1: ISOLATOR

Link element type 2: GAP

Figure 5.34. Test connections and their simplification in SAP analysis

5.3.4.2 1596 shell element case

In this case, the 3048 mm long steel deck panel was divided into 1596 shell elements, i.e. 38 elements over the width and 42 elements along the length. This required 39 nodes in the X direction, 43 nodes in the Y direction, for a total of 1677 nodes to define the diaphragm specimen, see Figure 5.35.

The Y direction dimension of each shell element is 76.2 mm, which is 1/4 of the connection spacing used in tests (=304.8 mm). The X direction dimension is ½ of the width of each deck segment. In this way, the connections could be exactly at the same position as in the tests.

All shell elements were defined as 0.76 mm in thickness, and thus the problem of locally increasing sheet thickness as done for the 500-shell element case was solved. More gap type link elements were used to prevent the deck from penetrating into the frames; hence the diaphragm was stiffer than in the previous case.

It is also noted that the sheet dimension was 952.5 x 3200.4 mm, which was larger than the 914.4 x 3048 mm case in the previous Section. In the tests, the sheet length was at least 100 mm longer than the centre-to-centre frame length. The real sheet width was also wider than its effective length (=914.4 mm). Based on these considerations, the analysis using this model was to be closer to the test situation or to the SDI evaluations.

The plane dimension of the frame was kept the same, i.e. 914.4 x 3048 mm. Its relationship with the deck shell elements is shown in Figure 5.35.

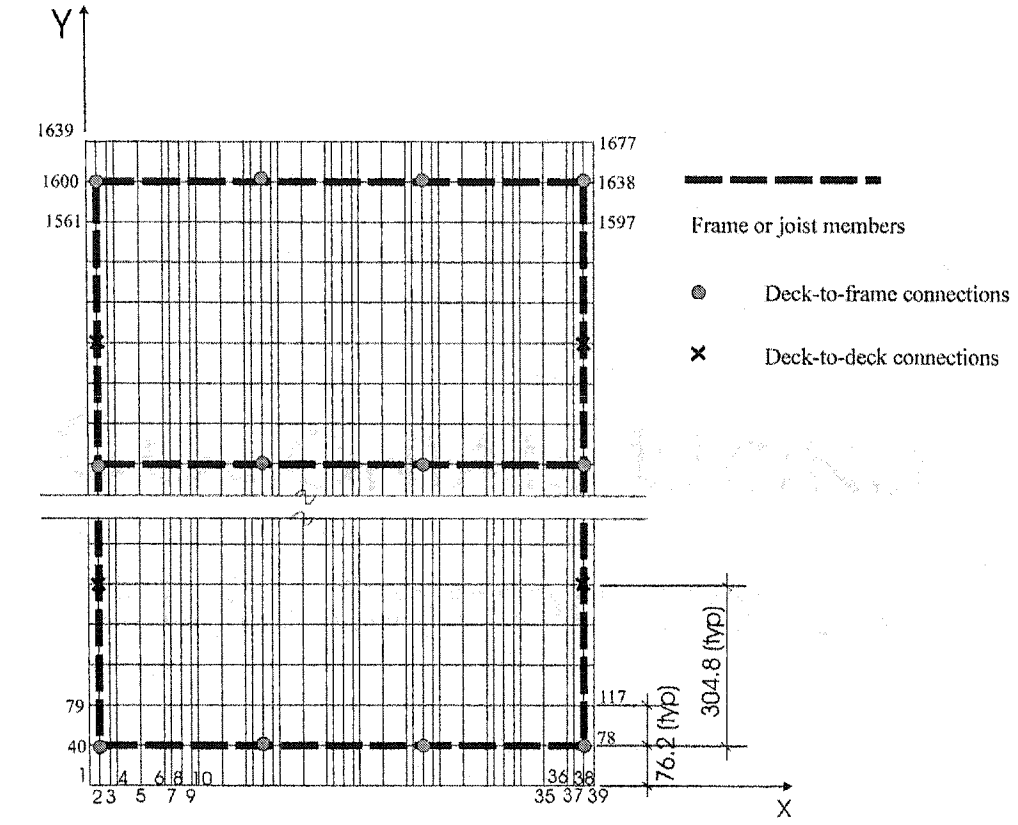

a) Plan view

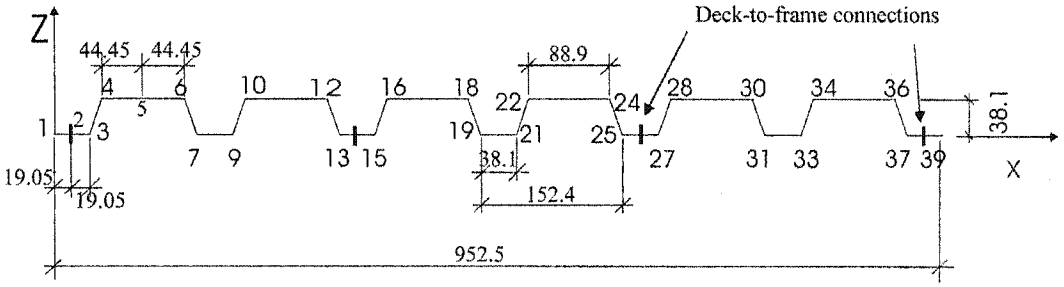

b) Section view

Figure 5.35. Node numbers of 1596 shell elements, frames, joists and connections

5.3.4.3 3192 shell element case

In order to check the accuracy of the analysis with 1596 shell elements, an even finer mesh was also used. In this case, the 3048 mm long steel deck panel was divided into 3192 shell elements, with 38 elements along the width direction and 84 elements in the length direction. The Y direction dimension of each shell element was 38.2 mm, which is 1/8 of the connection spacing used in tests (=304.8 mm), i.e., ½ of the 1596 sheet element case. The X direction dimensions and the other conditions remained the same. Figure 5.35 can be used as a reference for the node numbers, shell elements, frame elements and the connections because these two cases are very similar.

5.3.5 Gypsum board shell elements

5.3.5.1 40 shell element case

As discussed before, the only non-structural component that was considered to influence the diaphragm behaviour was the gypsum board. Shell elements 12.7 mm (1/2 in.) in thickness were implemented in the SAP 2000 model for this component. In defining the material properties it was not possible to obtain a documented measure of the shear or Young's modulus. Hence, a value was estimated based on the ratio of compression strength of gypsum to steel. The ultimate strength for 230 grade steel is in the range of 330 MPa based on coupon tests, while for gypsum board, it is about 3.45 MPa (Chapter 3). This results in a ratio of roughly 1/100 or an equivalent E_g = 2 GPa for gypsum. Poisson's ratio υ=0.3 was also incorporated for the gypsum board. Gypsum seems to be anisotropic in nature, e.g. the paper mainly reinforces the

tension behaviour, but no relevant document on the material properties was available, and therefore an isotropic shell element was utilized.

The plan dimensions of the steel roof deck panel and the gypsum board are not consistent, e.g. 1220x2440mm (4x8 ft) for the gypsum and 914.4x3048mm (3x10 ft) for the deck. Hence, two sections of gypsum board had to be used to cover the deck. A number of possible configurations exist, however, only two were considered to investigate the effect of the gypsum board arrangement (Figure 5.36):

- Layout 1, (Figure 5.36 a), 914.4 x 2438.4 mm and 914.4 x 607.6 mm.
- Layout 2, (Figure 5.36 b), 914.4 x 1676.4 mm and 914.4 x 1369.6 mm.

For the combination with the first 500 steel sheet shell element case, the gypsum board was divided into 40 shell elements (Figures 5.36a and 5.36b), which included 5 elements along the X direction and 8 elements along the Y direction.

These two layouts provided for a comparison of the effects of the arrangement of the gypsum boards on diaphragm response. In layout 1, one 8' length board with a 2' length board were used, which corresponds to the arrangement in test 45 and test 46. In layout 2, two gypsum boards with approximately the same length were used, which is more representative of the conditions likely to exist in practice. Integrating the small difference in the length is for convenience of the shell element numbering. Between the two gypsum sections, a gap of 2 mm exists, which is to consider the non-overlap condition of the gypsum boards.

To prevent wind uplift, 12 special screws were required to attach each 1220x2440mm gypsum board to the underlying steel deck (see Figure 4.23 in Section 4.1.4). In this case, because the model did not extend over the full area of one standard sheet of gypsum, 8 screws were placed for the 914.4x2438.4 mm area, and 4 screws for the

914.4x607.6mm area (see Figure 5.36a). For Layout 2, 6 screws were installed in each of the sheets (see Figure 5.36b). The spacing and distribution of screws are the same as in the tests.

Similar to the deck-to-frame connections that were shown in Figure 5.34, the real screw connectors for deck-to-gypsum board are positioned near or at the mid-width of the deck top flanges (see Figure 5.36c). In the 500 shell element SAP 2000 model, these connections were moved to one edge of the top flange, at the node location (Figure 5.36d). One link element (Isolator1 type) was used to represent the deck-to-gypsum board connection; and another link element (Gap type) was used to prevent the gypsum board from penetrating into the steel deck (Figure 5.36e).

The results obtained with 40 gypsum board shell elements appeared not to be very good, as will be discussed in Section 5.3.7.1. A finer mesh was therefore used as presented in the following Section.

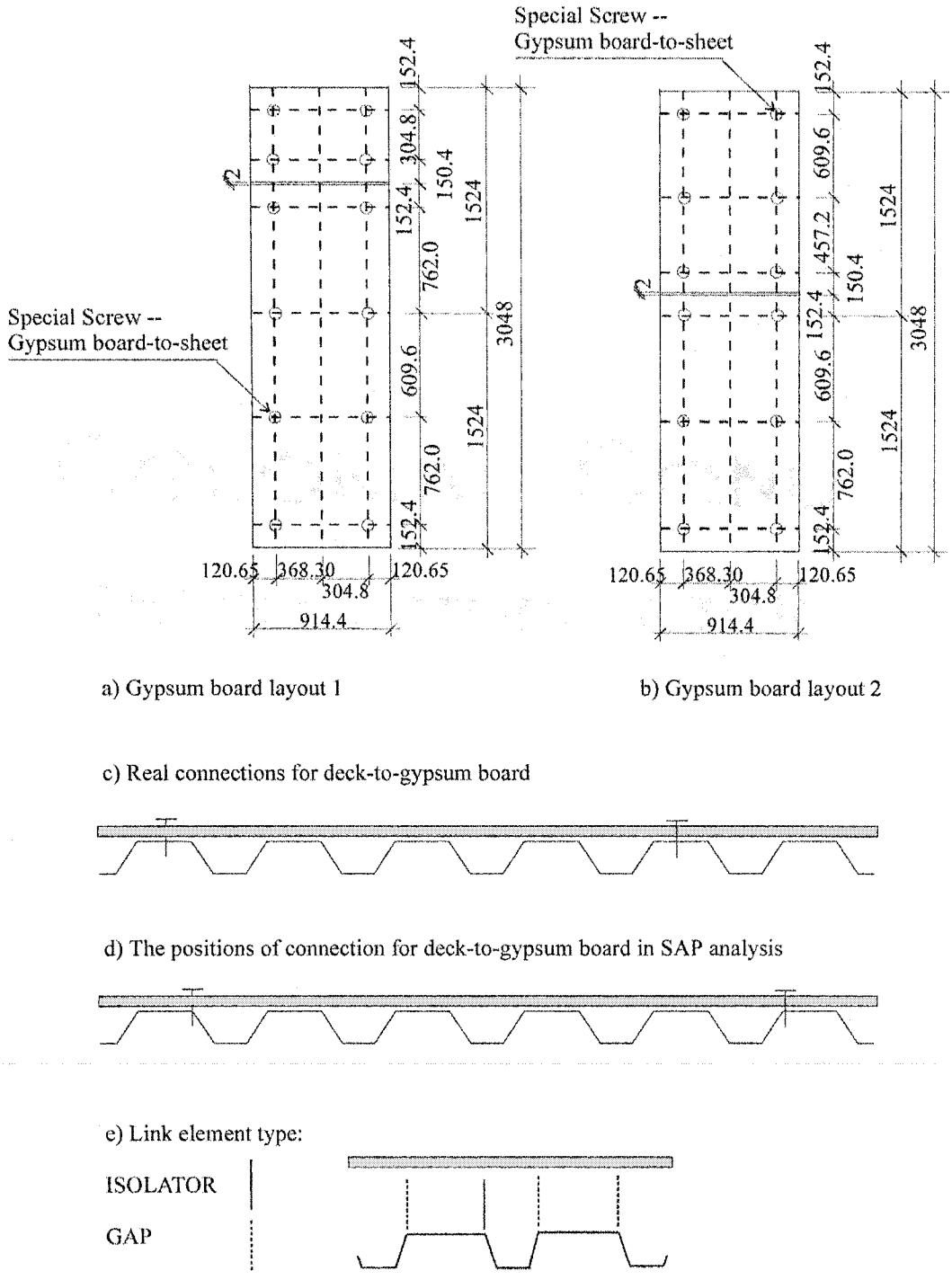

Figure 5.36. Gypsum board layout and connection positions

5.3.5.2 1596 shell element case

To be compatible with the 1596 shell element case of the steel deck, the same amount of shell elements was used for the gypsum board, but only the Layout 1 was studied. In this case, moving the deck-to-gypsum board connection positions as shown in Figure 5.36d was no longer necessary. The finer mesh resulted in a larger number of nodes, more Gap type link elements, and finally made the diaphragm stiffer.

In the analysis, two values were considered for the Young's modulus of the gypsum board:

- E_g = 1.0 GPa;
- E_g = 0.293 GPa.

The first value E_g = 1.0 GPa was selected to represent the similarity of gypsum board with low density concrete, both being of fragile materials. In Chapter 3, an E_g value of 1.26 GPa was reached by using the equation of Young's modulus available for concrete. In order to be conservative, E_g = 1.0 GPa was chosen. Poisson's ratio υ is changed to be same as that of concrete, i.e., 1/6 (or = 0.167).

The second value E_g = 0.293 GPa is estimated from the shear modulus G of gypsum board that was discussed in the "Racking Tests of High-Rise Building Partitions" (Freeman, 1977). Freeman tested several partitions made of gypsum boards, where for 15.9 mm thick gypsum board, a shear stiffness G'=1.10 kN/mm, and a shear modulus G = G'/t =69 MPa were recorded. Assuming υ=0.16, together with the G' and t from test 43 and 45, then E_g is equal to 0.293 GPa.

5.3.6 Link elements

Two SAP 2000 (CSI, 2002) link elements are designed to represent the connection properties between two different materials. This connection between the two materials may be made of two nodes that have the same coordinates, *i.e.* the element has zero length. These two link element types are:

- Isolator 1;
- Gap

5.3.6.1 Isolator 1 element

The Isolator1 was used in order to account for the shear deformation between the different layers in the model. In Figure 5.37, I and J are the nodes in each of the two materials to be connected by the element, e.g. J is in the steel sheet and I is in the steel frame; or I is in the steel sheet and J is in the gypsum board. The local coordinate system 1-2-3 is used to define the link properties; including f_{u2} and f_{u3} which are the shear forces in directions 2 and 3 respectively, as well as d_{u2} and d_{u3} which are the shear deformations in directions 2 and 3 respectively.

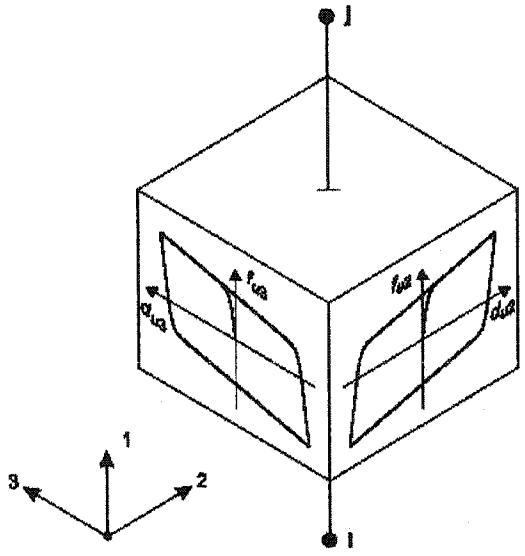

Figure 5.37. Link element--- Isolator1 Property for Biaxial Shear Deformation (from CSI, 2002)

The following parameters for Isolator1 type link elements are required to carry out a SAP 2000 analysis (see Section 5.3.1 and Table 4.3 and Table 4.4):

- Deck-to-frame: Hilti X-EDNK22-THQ12 nails

  NAME=NL1 TYPE=ISOLATOR1
  DOF=U1 KE=100 kN/mm
  DOF=U2 KE=24.04 kN/mm
  DOF=U3 KE=24.04 kN/mm

- Side-lap connection: Hilti 12-14x1 screws

  NAME=NL2 TYPE=ISOLATOR1
  DOF=U1 KE=100 kN/mm
  DOF=U2 KE=10.10 kN/mm

DOF=U3 KE=10.10 kN/mm

- Deck-to-gypsum board: special screws

  NAME=NL4 TYPE=ISOLATOR1

  DOF=U1 KE=100 kN/mm

  DOF=U2 KE=1.0 kN/mm

  DOF=U3 KE=1.0 kN/mm

The identification "NAME" of the link element is for quotation in the computer program, "DOF" is for the deformation directions, where U1 refers to the axial properties, U2 refers to the shear properties in the direction 2, and U3 refers to the shear properties in the direction 3. The parameter "KE" is the linear effective stiffness. For U1, a value of 100 kN/mm was assumed, this value being only for tension. The compression stiffness is defined in the Gap element that will be discussed in next Section. The shear stiffness for U2 and U3 directions are assumed to have the same value because they all refer to the shear plane although in different directions. KE=24.04 kN/mm and 10.10 kN/mm are quoted from SDI method (Table 4.3 and 4.4) respectively. In the case of U2 and U3 of the deck-to-gypsum board connections, a 1/10 of the values of deck-to-frame connections were assumed due to lack of documented information.

Side lap properties are assigned to the locations along the two edges to simulate the side lap connection in tests, except the locations having joists.

5.3.6.2 Gap element

A Gap type link element allows one to simulate the contact conditions between different materials where no connection exists. This element can be compressed at a

very high axial stiffness without deformation, yet pulled apart with little effort. In Figure 5.38, I and J are the nodes in the two different materials to be linked. The variable "open" refers to the initial gap opening, which can be defined as zero. The axial stiffness, "k", is required for the compression properties of the element.

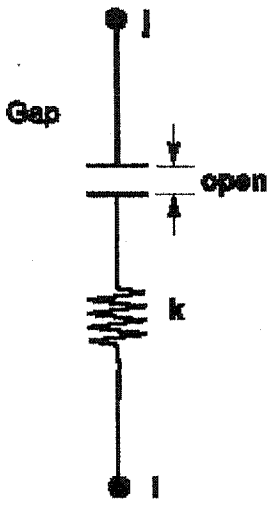

Figure 5.38. Link element--- Gap Property Types, Shown for Axial Deformations (from CSI, 2002)

For gap link element, following parameters are to be defined:

- Deck-to-frame:

  NAME=NL3 TYPE=GAP
  DOF=U1 KE=10^9

- Deck-to-gypsum board:

NAME=NL5 TYPE=GAP

DOF=U1 KE=10^8

The identification "NAME" (NL3 or NL5) is for element quotation in the computer program. The parameter "DOF=U1" means axial direction and "KE" is the axial stiffness. A 10^9 kN/mm level stiffness value was assumed in order to prevent the steel deck from penetrating into the supporting steel frame. A 10^8 kN/mm level stiffness values was assumed in order to limit the penetration of the steel deck into gypsum layer, which is consistent to the 1/10 assumption for the Isolator 1 element.

5.3.7 Result Analysis

5.3.7.1 Shear stiffness

The resulting stiffness values are listed in Table 5.22.

Table 5.22 Shear Stiffness: Measured and Analytical

	G' (kN/mm)
Bare sheet	
SDI	1.70
500 shell element case (sheet thickness 0.76 mm and 7.6 mm*)	1.52
1596 shell element case (sheet thickness 0.76 mm)	2.31
3192 shell element case (sheet thickness 0.76 mm)	2.24
With roofing (with 12.7 mm thick Gypsum board)	
SDI + (Test 45 – Test 43)	3.29
Gypsum board 40 shell element case: Layout 1, E_g=2.0 GPa	1.96
Gypsum board 40 shell element case: Layout 2, E_g=2.0 GPa	1.92
Gypsum board 1596 shell element case: Layout 1, E_g=1.0 GPa	4.13
Gypsum board 1596 shell element case: Layout 1, E_g=0.293 GPa	3.31
Stiffening (ΔG')	
(Test 45 – Test 43)	**1.59**
Gypsum board 40 shell elements, Layout 1	**0.44**
Gypsum board 1596 shell elements Layout 1, E_g=1.0 GPa	**1.82**
1596 shell element case: Layout 1, E_g=0.293 GPa	**1.00**

Note:

* 7.6 mm thick elements along the edges.

For Bare sheet diaphragm, the shear stiffness obtained from the 500 shell element case (G'=1.52 kN/mm) is nearer to SDI's evaluation (G'=1.70 kN/mm). However, it must be noted that the shell elements along the two frame sides were assumed to be

10 times thicker than the non-side elements. This assumption lacks an accurate and convincing physical explanation. The results from the 1596 shell element case (G'=2.31 kN/mm) and the 3192 shell element case (G'=2.24 kN/mm) are comparable, which suggests that 1596 shell element is enough to give a consistent result. These two finer meshes give stiffer diaphragm responses than predicted by the SDI.

For with roofing diaphragm, the result of stiffening related to the gypsum board for the 1596 shell element case ($\Delta G'$=1.00 to 1.82 kN/mm) matches better with that estimated from SDI plus tests. The stiffening due to non-structural components with E_g=1.0 GPa seems too large, but that with E_g=0.293 GPa seems too small. A more accurate estimate of E_g based on experiments is required, as well as the connections between the gypsum board and the deck.

The division of 40 shell elements seems too coarse to capture the interaction between the two materials. However, the results from these analyses indicate that the layout of gypsum board does not have a significant influence on the structural response.

5.3.7.2 The deformed shapes

The undeformed and deformed shapes of the bare sheet steel deck diaphragm are shown in Figure 5.39. The deformed shape in Figure 5.39b is very similar to the warping deformation of the panels as observed in test 43 (see Figure 4.88).

The undeformed shape and deformed shape of the deck panel with the gypsum board is shown in Figure 5.40. Again the deformed shape in Figure 5.40b is close to that of test 45 (Figure 4.110).

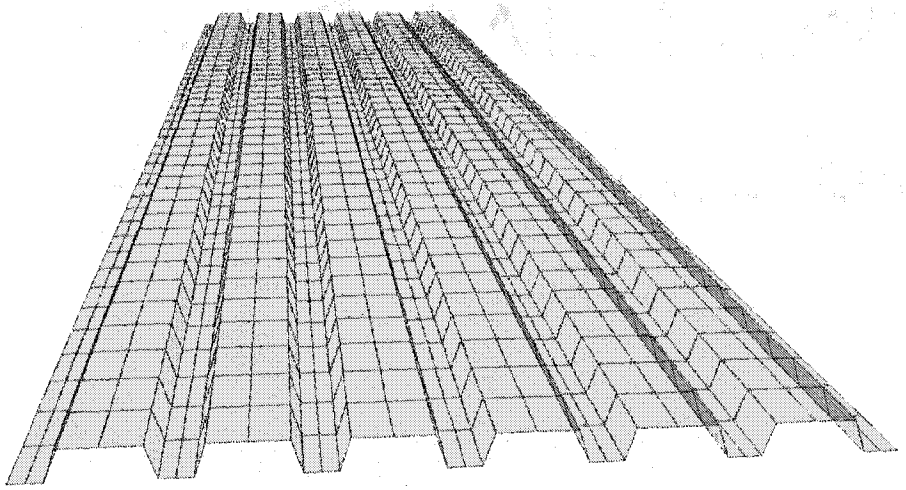

a) Undeformed shape of bare sheet deck

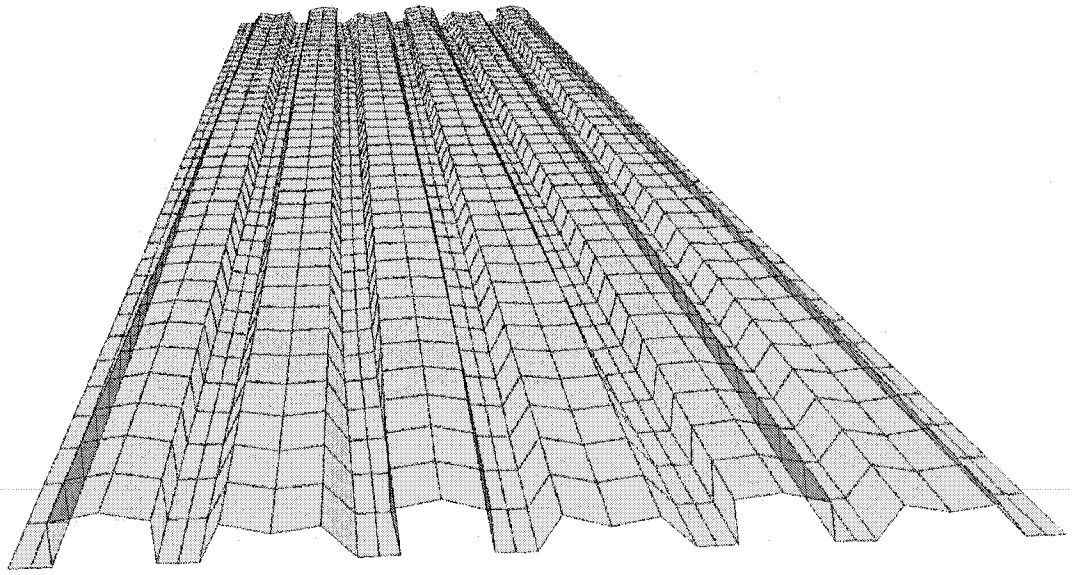

b) Deformed shape of bare sheet deck

Figure 5.39. Undeformed and deformed shapes of the bare sheet steel deck (1596 shell elements)

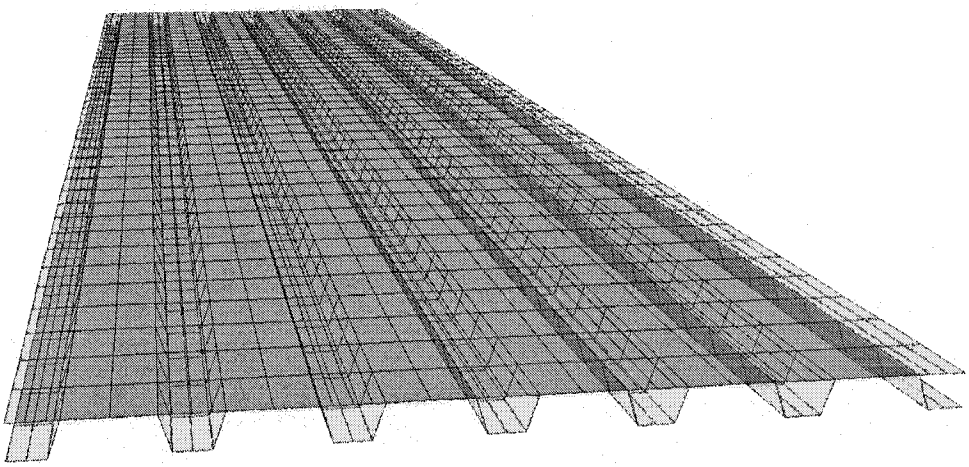

a) Undeformed shape of deck with gypsum board

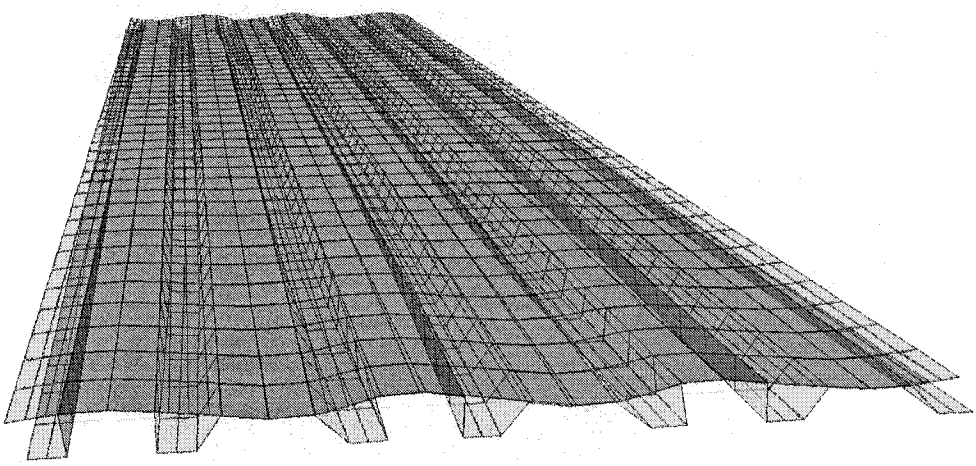

b) Deformed shape of deck with gypsum board

Figure 5.40. Deformed shape of the deck with the gypsum board (1596 shell deck elements, 1596 shell gypsum board elements, Layout 1, E_g=1.0 GPa)

5.3.7.3 The shear force distribution in fasteners

For bare sheet diaphragm, the distribution of shear forces in the deck-to-deck and sidelap connections is presented in Figure 5.41, which is obtained from SAP analysis and from SDI approach. The following observations are recorded:

1). The equilibrium condition is met, i.e. the sum of all forces in both directions is zero. For the vertical forces in one side, the sum is equal to 0.999 kN, no virtual difference with 1.0 kN, the loading applied at the bottom-left corner.

2). The shear forces in the load direction are usually larger than those perpendicular to the load direction, except at the sheet ends, where the horizontal forces are larger than those in the vertical direction. The shear forces in the load direction are not uniform, with the greatest force located at the intermediate joist, V_3=0.185 kN.

3). As expected, the shear force in a connector is closely related to the stiffness of the connection. For example, the shear forces in deck-to-frame connections are larger than in deck-to-deck connections.

4). The connection forces from FEM analysis are comparable with that from SDI (1991). In the vertical direction, the largest shear force at the intermediate joist is 0.185 kN vs. 0.146 kN; at the corner is 0.0970 kN vs. 0.120 kN. For the side lap connections, the mean value of shear forces from SAP is 0.0775 kN, while from SDI is 0.0707 kN. The assumption of linear force distribution along deck width from SDI may be not accurate. E.g., the V_3 at non-side position have large differences (0.0009 or 0.0024 kN vs. 0.0487 kN). This may be due to the non-linearly distributed shear deformation.

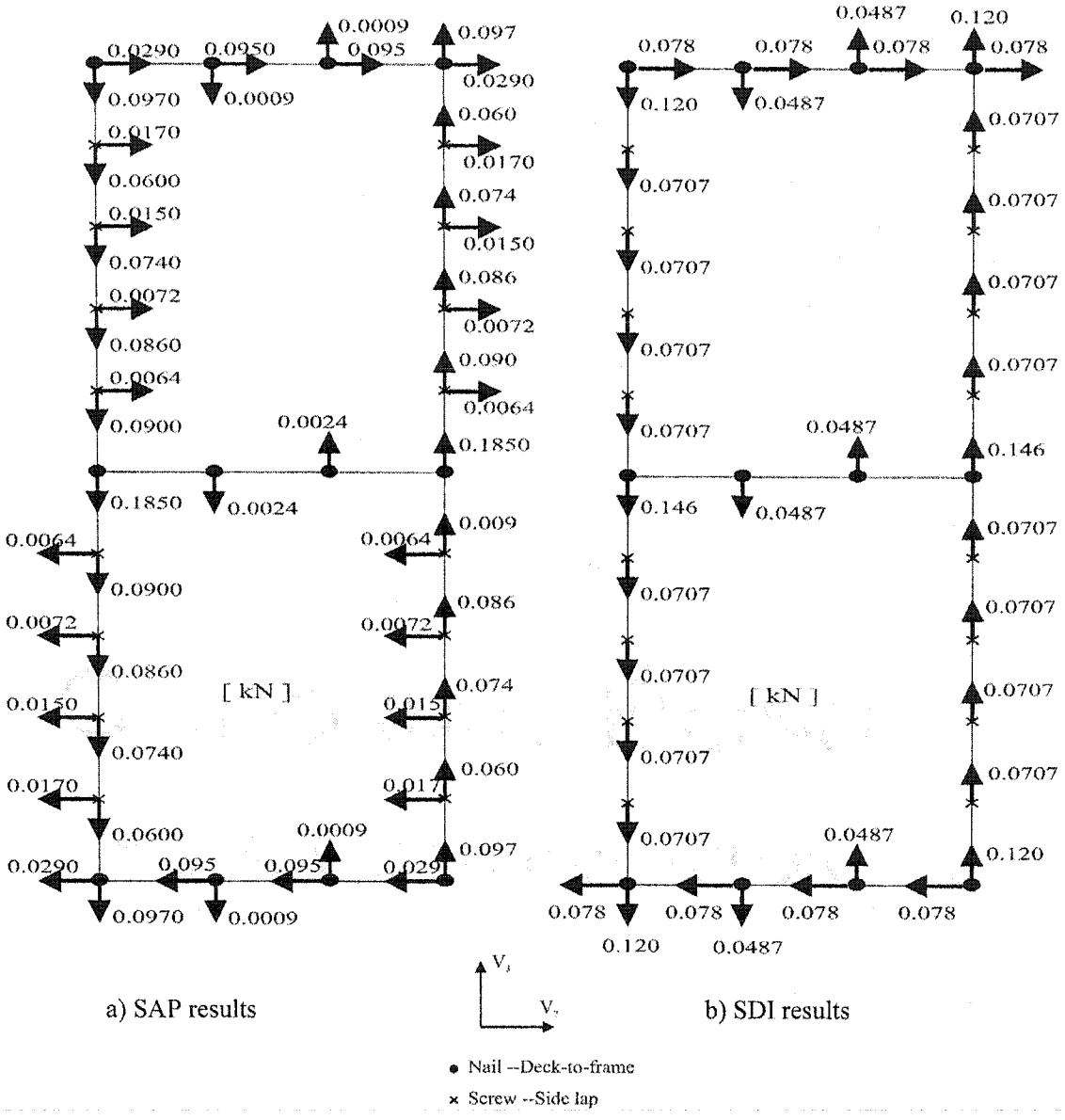

Figure 5.41. Shear force distribution in connections for bare sheet diaphragm (a: SAP, b: SDI)

The shear force distribution in the connection for the diaphragm with roofing is shown in Figure 5.42. If compare it with Figure 5.41a, no significant change was

found. This may be because only one deck panel was used, the in-plane forces were more efficient to be transferred in the deck instead of through the gypsum board. A future analysis of two or three deck panels is recommended.

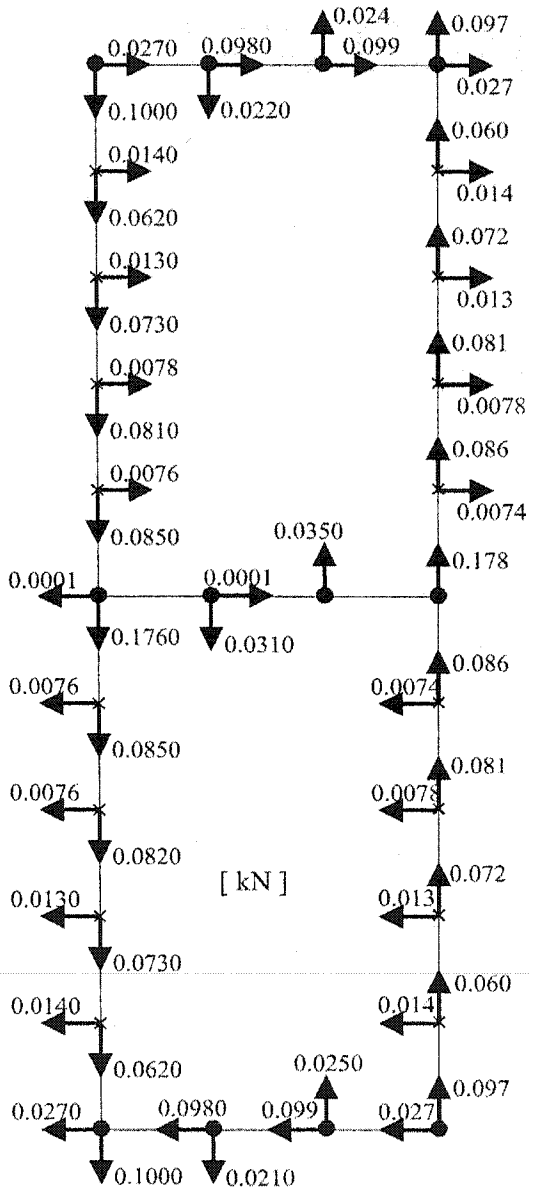

Figure 5.42. Connection shear force distributions for diaphragm with roofing

Using the case with 1596 roofing shell elements (Layout 1, E_g=1.0 GPa), the fastener's shear force distribution for the deck-to-gypsum board connections is shown in Figure 5.43, where the equilibrium condition is also met. It is noted that the shear forces are quite small, and the force directions are not always consistent due to the relative deformations of the steel sheets.

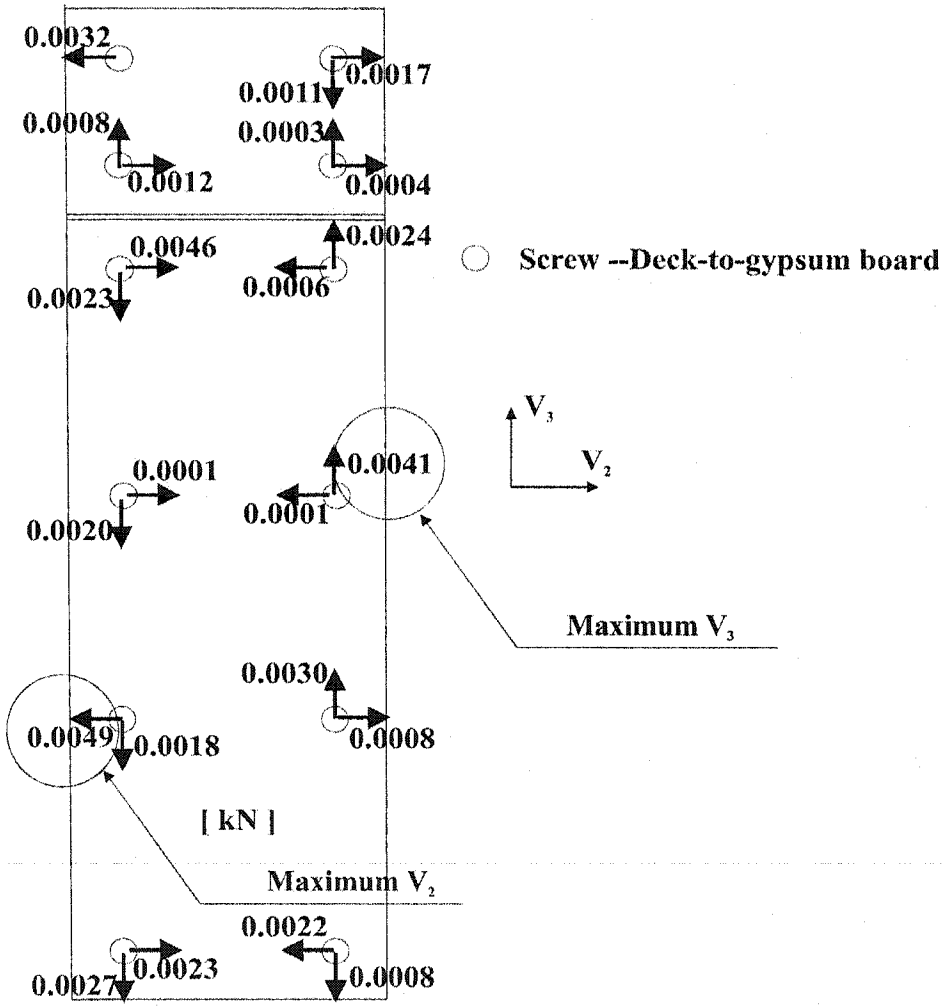

Figure 5.43. Shear force distribution in deck-to-gypsum board connections

5.4 CHAPTER SUMMARY

In this Chapter, two series of analyses were carried out: inelastic dynamic analysis of buildings with roof deck diaphragm acting as the energy-dissipating element in the seismic force resisting system (SFRS), and elastic static analysis of deck panels with or without roofing materials.

5.4.1 Inelastic dynamic analysis of buildings

A medium size (30x60x6.6 m) single-storey steel building was analysed by a non-linear dynamic analysis program RUAUMOKO (Carr, 2000). The force-deformation hysteresis rules were modified according to the test results to describe the influence from the type of attachment, sheet length, profile shape, and roofing materials. The following aspects were summarized and discussed:

1). Short sheet length makes the deck more flexible. Non-structural components, when appropriately attached, make the deck stiffer.

2). The ductility related force modification factor, R_d=2.0, suggested by Martin (2002) for the nail/screw connected deck diaphragm, was also verified by the analyses detailed in this Chapter.

3). In describing the inelastic behaviour of steel deck diaphragms, two important parameters were introduced: the inelastic distortion γ_p and the ductility demand, μ_D, the former describes an absolute magnitude, while the later provides a relative one.

Essa *et al.* (2001) recommended an ultimate value of γ_p = 10 rad/1000 for nail/screw diaphragm construction. This value was defined as the inelastic shear distortion related to a load equalling to 80% of the peak load on the descending branch of the S-γ diagram, $\gamma_{0.8Su}$. By using this criterion, the maximum inelastic distortion for test 43 was 10.57 rad/1000, which is quite similar to the value from Essa et al. From this point of view, it seems that R_d=3.0 cannot be used for the roof type 1 (bare sheet, without end laps) because the maximum response exceeds that of the limiting γ_p = 10 rad/1000. In contrast, R_d=3.0 could be used for the roof type 2 and roof type 3 that are described in this Chapter.

Concerning the deck element ductility demand, μ_D, the results of the analyses indicate that it is approximately equal to R_d when R_d=2.0, but it varies significantly when R_d=3.0. The mean values of μ_D obtained from several dynamic analyses are $3.43R_d$; $1.46R_d$; and $2.15R_d$ for roof type 1, 2, and 3 respectively. This shows that the μ_D value for roof type 1 is much larger than expected, i.e. the use of R_d=3.0 for roof type 1 can too large deck element ductility demand, that may lead to significant strength degradation. The μ_D values for roof type 2 and roof type 3 were also not consistent, but their inelastic distortions remain in the allowable range, hence R_d=3.0 can be used for these two roof types.

5.4.2 Elastic static analysis of deck panels

In the second analysis, a 3048 mm long portion of a single P3615B steel deck panel was analysed with the SAP2000 3-dimension FEM software (CSI, 2002). The following results were discussed:

1). Non-structural components limit the relative in plane deformations between adjacent flutes; they also limit the vertical deformations of the panel by compression between materials or by tension due to the deck-to-gypsum board screws. These effects result in a much stiffer roof deck diaphragm. The main deformation of the gypsum board is the bending caused by the tension of the deck-to-gypsum board screws. The increase of G' due to the gypsum board is between 1.0~1.82 kN/mm, which is comparable to the test result ($G'_{Test45} - G'_{Test43} = 1.59$ kN/mm). Further research about the properties of the non-structural components and the connections is recommended. This information is required to provide more accurate material parameters that can be used to improve the results of the FEM analyses.

2). The fastener forces were not distributed evenly over the diaphragm panel that was modeled. This is due in-part to the differences in their positions and stiffness, and may be the cause of the early yield load level. The fastener force distribution was found to conform to that described in the SDI manual.

3). The layout of gypsum board does not significantly change the stiffening effect.

4). Consistent results were obtained using the 1596 shell element FEM model.

CHAPTER 6 ANALYSIS OF TORSIONAL EFFECTS

In this chapter, the torsional effect and the influence of the flexibility of the steel roof deck diaphragm on the seismic response of a single-storey steel building with asymmetric brace stiffness is studied using both a static method and a non-linear dynamic analysis method. The objective is to obtain a comprehensive understanding of the dynamic torsional behaviour combined with roof flexibility effects. As discussed in Chapter 2, Nedisan (2002) carried out similar analyses to calculate the torsional moment about the centre of mass (CM) with one specific ground motion. The work presented here is a continuation of her work. A total of eight ground motions are considered, in order to provide more conclusive statistics of response data. In addition, the torsional moment is computed about the centre of rigidity (CR) instead of the center of mass, which is consistent with the equivalent static approach proposed in the 2005 NBCC.

6.1 BUILDING DESCRIPTION

The single-storey building documented in this Chapter is located in Victoria, B.C. and it is very similar to the building studied in Chapter 5 (see Figure 5.1). There were however, important differences between the two buildings; namely the building in Chapter 5 was designed with the roof diaphragm as the seismic energy-dissipating element, whereas the building described in this Chapter was designed with a weak brace and strong diaphragm philosophy, reflecting current design practice.

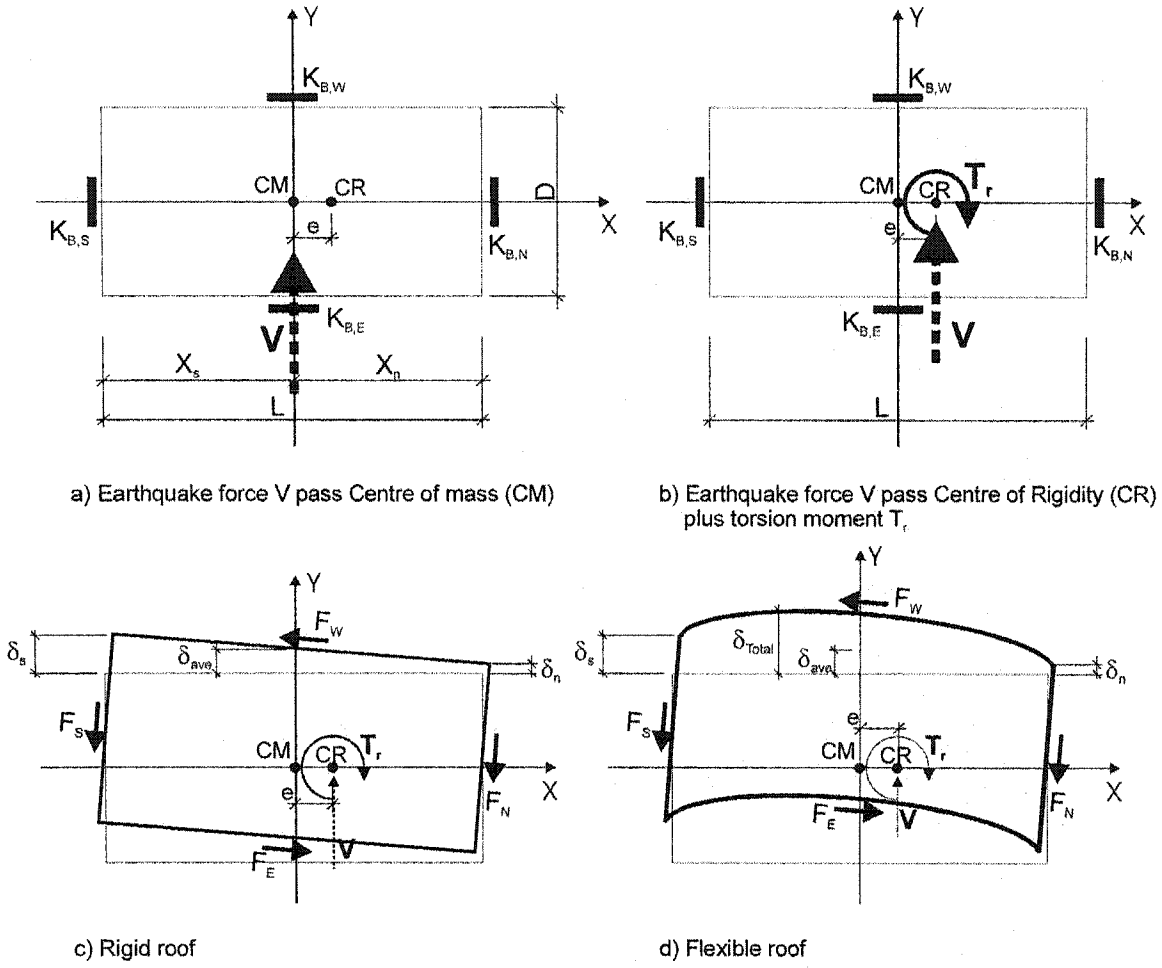

a) Earthquake force V pass Centre of mass (CM)

b) Earthquake force V pass Centre of Rigidity (CR) plus torsion moment T_r

c) Rigid roof

d) Flexible roof

Figure 6.1. The structure, forces, and deflections

According to the 2005 NBCC (NRCC 2001) the equivalent static load procedure is applicable for the analysis of a regular structure. The building in Figure 5.1 has been redrawn in the form of a simple plan view (Figure 6.1a), where only 4 braces and the forces are shown to highlight the asymmetric brace stiffness. A static horizontal load V that passes through the centre of mass (CM) represents the inertia induced seismic forces applied at the roof level acting in the Y direction. The parameters $K_{B,S}$, $K_{B,N}$, $K_{B,E}$, and $K_{B,W}$ represent the brace horizontal stiffness in the south, north, east and

west walls, respectively. All braces are tension-only braces, and the stiffness $K_{B,E}$, and $K_{B,W}$ are assumed to have the same value. An eccentricity is introduced in the building by defining different horizontal stiffness values for the South and North walls. Thus, the centre of mass does not coincide with the centre of rigidity, resulting in an eccentricity "e" of the lateral earthquake design force, V.

Figure 6.1b is equivalent to Figure 6.1a, however the lateral earthquake design force, V, is moved from the CM to the CR position, and the corresponding torsional moment in the roof deck plane, $T_r = V*e$, is applied. Figures 6.1c and 6.1d are the expected roof deformation shapes produced by the force and the torsion moment shown in Figure 6.1a or 6.1b for both the rigid roof and flexible roof cases, where F_S, F_N, F_E, and F_W represent the brace horizontal forces in the walls. The adequacy of the response illustrated in Figure 6.1d is to be verified in this study.

The additional symbols found in Figure 6.1 are explained below:

L = the building length, L=60 m is assumed;

D = the building width, D=30 m in this study;

X_s = the distance from south wall to CM;

X_n = the distance from north wall to CM;

e = the distance measured perpendicular to the earthquake force direction between the CM and the CR;

δ_s = the south wall roof displacement;

δ_n = the north wall roof displacement;

δ_{ave} = the average roof displacement; δ_{ave}=(δ_s+ δ_n)/2

δ_{Total} = the total roof drift at the building mid-length.

6.1.1 Building Design (Nedisan, 2002)

A building with a strong diaphragm was first designed according to the proposed 2005 NBCC (NRCC, 2001) and the existing CAN/CSA S16 Steel Design Standard (CSA, 2001). From Chapter 5, the seismic weight for that structure is W = 2250 kN and the fundamental lateral period T_a = 0.31 sec. A ductility related force modification factor R_d of 2.0 was chosen for the tension-only braced frame, and the overstrength related force modification factor R_o = 1.2. It is noted these two factors are different from those in Chapter 5, due to the difference in design philosophy.

From the equivalent static load procedure, the lateral earthquake design force at the base of the structure for design V = 750 kN. For analysis, the brace elements must be able to develop yielding in tension, and the yield capacity of the system $V_{max} = V / \phi$, where $\phi = 0.90$ is the resistance factor for steel braces (CSA 2001).

V_{max} =750/0.9=833.33 kN (6.1)

Using the static horizontal load, a symmetric structure was first designed, where the braces were sized based on the distribution of brace forces obtained from a linear analysis and a rigid diaphragm. The lateral stiffness along each wall is equal to 20.87 kN/mm. Thereafter, the height of the structure and the inclination of the braces in the North and South walls were modified such that the horizontal stiffness along the north wall, $K_{B,N}$, became 1.5 times that of the south wall brace, $K_{B,S}$. Thereby, the

desired eccentricity between the CM and CR positions was introduced into the building model. The stiffness along the other two building sides remained unchanged, resulting in the brace properties listed in Table 6.1.

Table 6.1 Summary of brace properties

Location	Vertical height	Horizontal distance	Brace length	Slope angle	Section area	Horizontal stiffness K_B
	m	m	m		mm^2	kN/mm
South	7.5	5.263	9.162	54.94	2318	16.69
North	5.7	4.841	7.478	49.66	2234	25.04
East	6.6	7.5	9.990	41.35	1850	20.87
West	6.6	7.5	9.990	41.35	1850	20.87

The dimensions of the other structural members were:

- Perimeter Beams: W 250 x 39 (A=4920 mm^2);
- Columns: HSS 152 x 152 x 6.6 (A=3610 mm^2);

Two roof deck cases were considered:

- Flexible roof: the diaphragm shear stiffness G' is 6.486 kN/mm, ultimate deck nominal shear strength S_u is 18.01 kN/m. These values were obtained from the SDI manual (SDI, 1987) assuming P3615B 0.91 mm steel deck panels, 7500 mm long; joists c/c spacing of 1875 mm (= 7500/4), see Figure 5.1; deck-to-frame connections: Hilti ENP2-21-L15 powder driven fasteners on a 36/4 layout pattern; and side lap connections: No. 14 self-drilling screws.
- Rigid roof: G' = 6.4 x 10^6 kN/mm.

6.1.2 Eccentricity and torsional moment

The eccentricity, e, between the centre of rigidity and the centre of mass was calculated as follows (see Figure 6.1a):

$$e = [K_{B,S} (-X_s)+K_{B,N} (X_n)]/(K_{B,S}+ K_{B,N}) = 6 \text{ m} \quad (6.2)$$

The torsional moment T_r was calculated as follows (see Figure 6.1b):

i) $T_r=V_{max} (e+0.1L)$ (6.3)

ii) $T_r=V_{max} (e-0.1L)$ (6.4)

The parameter 0.1L represents the accidental eccentricity, which considers the possible variation of stiffness, weights, or the addition and removal of partition walls, etc. This accidental eccentricity was neglected in this analysis. From Equation 6.1 and Equation 6.2:

$$T_r=V_{max} * e = 5 \text{ MNm} \quad (6.5)$$

The above static procedure can be used only when the torsional sensitivity ratio B < 1.7, where (see Figure 6.1 c)):

$$B = \delta_{max}/\delta_{ave} \quad (6.6)$$

If B > 1.7, a dynamic analysis procedure is to be specified. This ratio was verified once the analyses were completed (See Section 6.22).

6.2 LINEAR AND NON-LINEAR STATIC ANALYSIS

The DRAIN-2DX (Prakash and Powell 1993) computer software was used for the static numerical analysis discussed in this section. The analysis model was initially developed by Nedisan (2002) and is shown in Figure 6.2.

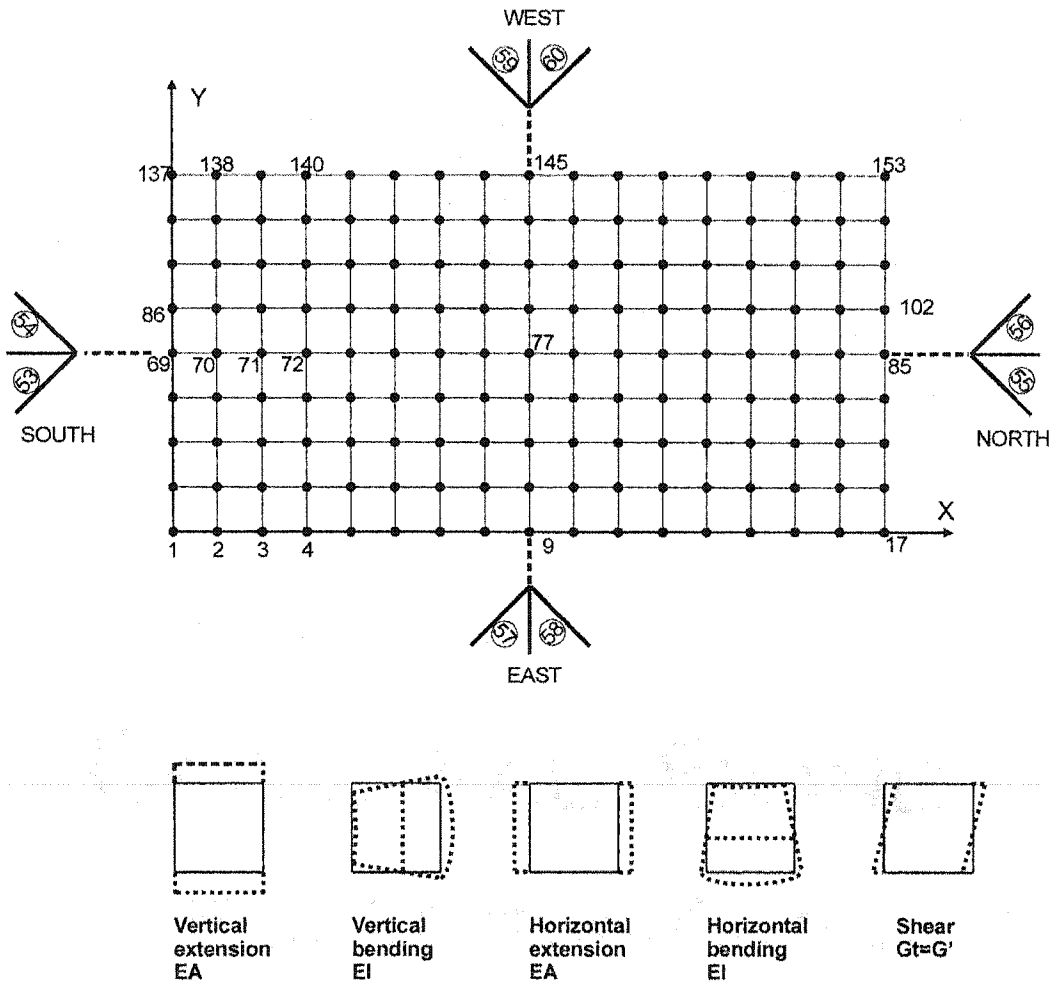

Figure 6.2. DRAIN-2DX model for static and dynamic numerical analysis

Two static numerical analyses were carried out; the first being a linear analysis that corresponds to the equivalent static force procedure in the 2005 NBCC, where the lateral force V_{max} = 833.33 kN was transferred into uniformly distributed node forces over the building width. In this analysis, all elements were assumed to remain elastic (by raising the yield strength). The second analysis was a non-linear analysis (pushover analysis, or incremental loading analysis), where the same load was used, however the braces were allowed to yield under the force V_{max}.

A two-dimension coordinate system (X-Y) was used, *i.e.* the 3D problem was simplified into a 2D model. Berair (1999) and Nedisan (2002) have shown this method to be effective. In Figure 6.2, the 60 x 30 m roof deck was divided into 3.75 x 3.75 m rectangular panel elements that are connected to the bracing bents. The structure is connected to the ground by the columns and braces along the four sides. Five deformation shapes of the rectangular panel elements (Prakash and Powell 1993) and their related parameters are also shown.

6.2.1 Element information

6.2.1.1 Deck diaphragm

The simple elastic (linear) 3.75 x 3.75 m rectangular panel element was used to represent the deck diaphragm (Figure 6.2). The following parameters (Table 6.2) are required:

- Effective vertical extension stiffness, EA, where E is the Young's modulus, and A is the deck panel cross-section area over a 3.75 m width;

- Effective vertical bending stiffness, EI, where I is the moment of inertia for the deck panel over a 3.75 m width;
- Effective horizontal extension stiffness, EA, where A is the cross-section area of the joists and interior beams over the 3.75 m distance;
- Effective horizontal bending stiffness, EI, where I is the moment of inertia for the joists and interior beams in the 3.75 m range;
- Effective Gt for shear racking, where G is the shear modulus, t is the thickness of the panel (Gt was set equal to G' of the deck diaphragm).

Table 6.2 Rectangular panel parameters for deck diaphragm (Nedisan, 2002)

Roof type	Vertical		Horizontal		Gt = G'
	EA	EI	EA	EI	
	kN	$kNmm^2$	kN	$kNmm^2$	kN/mm
Rigid	$9x10^{11}$	$1.07x10^{18}$	$8.0x10^{11}$	$1.0x10^{15}$	$6.4x10^6$
Flexible	$9x10^5$	$1.07x10^{12}$	$8.0x10^5$	$1.0x10^9$	6.486

Note: The parameters for the rigid roof were assumed to be 10^6 times those of the flexible roof.

6.2.1.2 Columns, perimeter beams, interior beams, braces, and P-Δ columns

Columns, perimeter beams, interior beams and braces were all defined as truss elements, which have only axial forces and deformations. For the linear static analysis, all the structural components were expected to behave elastically, whereas for the non-linear analysis, only the braces were expected to undergo tension yielding and compression buckling, while all other structural components would remain elastic.

The following parameters were defined:

- Young's modulus, E, which is assumed to be 200 kN/mm^2 for steel;
- Strain hardening ratio, E_h/E, is assumed to be 0.00;
- Cross section area, A, (Table 6.3);
- Yield stress in tension, S_{yt}, equals to 3.5 kN/mm^2 for linear analysis, but 0.30 kN/mm^2 or 0.35 kN/mm^2 according to the material grade (Table 6.3) for non-linear analysis, yield force equals to S_{yt}*A. For P-Δ column, it equals to 1.0 kN/mm^2.
- Yield stress or buckling stress in compression, S_{yc}. For the tension-only steel bar braces, it was assumed to be very small in compression and to correspond to the Euler critical buckling stress about the weak axis. For the other members, it was assumed equal to S_{yt} (Table 6.3).

Table 6.3 Element geometry and properties

Structural members		A	Linear static		Nonlinear static	
			S_{yt}	S_{yc}	S_{yt}	S_{yc}
		mm^2	kN/mm^2	kN/mm^2	kN/mm^2	kN/mm^2
Column		10^9	3.50	3.50	0.35	0.35
Perimeter beam		4920	3.50	3.50	0.35	0.35
Interior beam		1536	3.50	3.50	0.35	0.35
P-Δ column		10^9	1.00	1.00	1.00	1.00
Steel bar Brace	South	2318	3.50	0.00078	0.30	0.00078
	North	2234	3.50	0.00117	0.30	0.00117
	East	1850	3.50	0.0006	0.30	0.0006
	West	1850	3.50	0.0006	0.30	0.0006
Horizontal yield force in Brace bents	South	kN	4660		399	
	North	kN	5062		434	
	East	kN	4861		417	
	West	kN	4861		417	

6.2.2 Static numerical analysis results

The results from the linear and non-linear static numerical analyses, under $V = V_{max} = 833.33$ kN uniformly distributed over the building width, are listed in Table 6.4 for both the rigid and the flexible roof cases. A more detailed discussion is given in Section 6.5.

Table 6.4 Static numerical analysis results ($V_{max} = 833.33$ kN)

Item		Unit	Linear		Non-linear	
			Rigid Roof	Flexible roof	Rigid Roof	Flexible roof
G' = Diaphragm shear stiffness		kN/mm	6400000	6.486	6400000	6.486
Storey drifts	δ_s (137 Y-direc)	mm	24.06	25.83	24.06	25.83
	δ_n (153 Y-direc)	mm	17.41	18.41	17.41	18.41
	δ_{ave}: $(\delta_s+\delta_n)/2$	mm	20.74	22.12	20.74	22.12
	δ_w (145 X-direc)	mm	1.66	0.966	1.66	0.966
	Δ_{total}: (145 Y-direc)	mm	20.73	57.83	20.73	57.83
	$R_0R_d\Delta_{Total}$	mm	49.8	138.8	49.8	138.8
	Δ_{Limit}= Drift limit	mm	165	165	165	165
B = The torsional sensitivity ratio			1.16	1.17	1.16	1.17
F_S		kN	402	413	399	399
F_N		kN	436	433	434	433
F_W		kN	34.7	20.2	34.7	20.2
S = unit shear force along north wall		kN/m	14.53	14.42	14.46	14.42
T = the fundamental lateral period		Sec.	0.477	0.721	0.477	0.721

Note:

The positions of node 137, 153, 145 and their directions refer to Figure 6.2.

In Table 6.4, the deflections δ_s, δ_n, δ_{ave}, and Δ_{Total} are shown in Figure 6.1. They represent the roof displacements at the south wall and at the north wall, the average roof displacement at the north and south walls, and the total roof displacement at mid-length of the roof. The parameter $R_0R_d\Delta_{Total}$ represents the equivalent inelastic total roof drift at mid-length. This value is used to compare with Δ_{Limit}, the drift limit specified in the 2005 NBCC (2.5% of the storey height). The forces F_S, F_N, F_E, and F_W are illustrated in Figure 6.1. They represent the brace horizontal forces in each of the four exterior walls. The deflection δ_w is for the west side.

In the non-linear static numerical analysis it was also found that the south or north wall brace members yielded. This is because the earthquake force V was modified by the material resistance factor ϕ, see Equation 6.1, so that the tension yield strength in the brace elements was just reached. The maximum ductility demand for the rigid roof case was 1.005), and for the flexible roof case 1.034, hence the storey drifts were of similar values. Comparing the results of the linear analysis with those of the non-linear analysis in Table 6.4, it is noted that differences exist only for F_S and F_N, the two braces that yielded, and their related unit shear S, while all other results remained the same.

The comparison of the rigid roof and flexible roof response parameters in Table 6.4 shows that δ_s, δ_n, and δ_{ave} are similar in value since they are mainly dependent on the brace stiffness. However, the deformation Δ_{Total} becomes much larger for the flexible diaphragm case, due the in-plane shear flexibility of the roof, even though the $R_0R_d\Delta_{Total}$ did not exceed Δ_{Limit}.

The torsional sensitivity ratio "B" was only 1.16 for the rigid roof, a small value when compared to the limit 1.70 in Equation 6.6. This indicates that the equivalent static load procedure is applicable for the torsional analysis of this structure,

according to the 2005 NBCC requirements. For the torsional analysis of a structure with a flexible roof diaphragm, no provisions concerning the equivalent static procedure are provided in the NBCC, and it is deemed that a dynamic analysis is required.

It is interesting to note that, for the rigid roof, F_E and F_W are much larger than found for the flexible roof, which indicates that the torsional restraint created by the East and West braces is more effective for the rigid roof than for the flexible roof. Furthermore, the deflection δ_w at the west side, which is larger for the rigid roof than for the flexible roof, shows the effect of the east and west braces. Therefore, the increase in roof flexibility tends to decrease the torsional effect.

6.3 LINEAR DYNAMIC ANALYSIS (SPECTRUM METHOD)

A linear spectrum analysis was performed to better assess the influence of the roof diaphragm flexibility on the building response and the distribution of the seismic forces in the bracing members, as suggested by the 2005 NBCC. The DRAIN-2DX software was used along with the analysis model for the static case, except that the following additional parameters were required: a design response spectrum and mass. The seismic mass was assumed uniformly distributed over the roof plane. The ratio of design spectral response acceleration to gravitational acceleration, $S(T_a)$, for a fundamental natural period of T_a assuming a site class C was used (Table 2.4).

One modification that had to be made was the brace cross-section area. In the nonlinear static pushover analysis, the compression brace element could buckle at very small forces, however for the spectrum analysis, this assumption was no longer

available as the analysis is linear elastic. In such an analysis, the two braces would be fully effective and the lateral stiffness would have been nearly two times larger than that used in Section 6.2. To maintain the same stiffness level as in these two previous analyses, and also to be consistent with the actual brace response and the nonlinear dynamic analysis to be discussed next, the brace cross-section areas were chosen as half of the brace values in Table 6.3.

The spectrum analysis results and the SRSS combinations are listed in Table 6.5. According to the 2005 NBCC, these results should be modified by V_d/V_e to determine their static equivalent values, where V_d is the larger of V_e/R_dR_o or V_{max} that is determined by the static method. The elastic base shear V_e is obtained from the spectrum analysis. The modified results are also shown in Table 6.5. They will be compared with the results from other methods at the end of this Chapter.

Table 6.5 Linear spectrum analysis results

Mode Number			**1st**	**2nd**	**3rd**	**4th**	**SRSS**
Rigid Roof	Period (sec)		0.477	0.268			
	Disp. (mm)	137-Y	58.6	4.14			58.8
		145-X	5.6	2.301			6.0
		145-Y	47.4	-0.458			47.4
		153-Y	36.3	-5.06			36.6
	Brace axial force (kN)	53 or 54	852	60.22			854
		55 or 56	701	97.83			708
		57 to 60	77.7	32.0			84.04
Flexible Roof	Period (sec)		0.721	0.359	0.226	0.222	
	Disp. (mm)	137-Y	-23.0	0.219	3.20	0.119	23.3
		145-X	-0.688	0.0482	0.68	0.711	1.200
		145-Y	-90.3	-0.0306	-4.36	0.251	90.4
		153-Y	-15.9	-0.160	2.09	-0.354	16.1
	Brace axial force (kN)	53 or 54	613	5.82	85.2	3.64	619
		55 or 56	542	5.44	70.0	12.6	546
		57 to 60	19.1	1.34	18.9	19.8	33.4

Result modification		Before Modification		After Modification	
		Rigid	Flexible	Rigid	Flexible
Disp. (mm)	δ_s	58.8	23.3	25.8	13.7
	δ_w	6.05	1.20	2.65	0.70
	Δ_{Total}	47.4	90.4	20.8	53.1
	δ_n	36.6	16.1	16.1	9.44
Brace axial force (kN)	South	854	619	375	364
	North	708	546	311	321
	East	84.0	33.4	36.9	19.6
Shear force (kN)	F_S	981	711	431	418
	F_N	917	707	402	415
	F_E	126	50.1	55.4	29.4
Base shear V_e (kN)		1898	1419	833	833
V_e/R_dR_o (kN)		791	591		
V (kN)		833	833		
V_d (kN)		833	833		
V_d/V_e		0.439	0.587		

6.4 NON-LINEAR DYNAMIC ANALYSIS (TIME HISTORY)

A suite of non-linear time-history dynamic analyses of the structure was performed with the DRAIN-2DX software. The analysis model was the same as for the previous analyses, except that ground motion time histories were added. A time step of 0.001 sec was considered in the analyses, together with the 4% Rayleigh damping presented earlier. The Rayleigh damping model is described as follows:

$$\mathbf{C}=\alpha\mathbf{M}+\beta\mathbf{K} \qquad (6.7)$$

where:

C= the damping matrix of the whole structure;

M= the mass matrix;

K= the stiffness matrix of the whole structure;

α= the damping coefficient for mass matrix;

β= the damping coefficient for stiffness matrix.

In the RUAUMOKO program, the parameters α and β are calculated automatically. In DRAIN-2DX, these coefficients should be prepared beforehand in order to run a modal analysis. For the vibration modes in Y-direction of the rigid roof, the fundamental periods were T_1= 0.477 sec and T_2 = 0.268 sec. It is found that these two modes include 100% of the effective modal mass in the Y-direction. So only these two modes were needed. With the 4% equivalent proportional critical damping ratio, the values of α and β can be determined: α=0.671998, β=0.002193;

For the flexible roof, four Y-direction vibration modes were needed to obtain an appropriate spectrum result, because these four modes constitute 98.63% of the

effective modal mass in the Y-direction. The fundamental periods were T_1= 0.721 sec, T_2 = 0.359 sec, T_3= 0.226 sec, and T_4 = 0.222 sec, respectively. The values of α and β were as: α=0.462041, β=0.003066.

6.4.1 Ground motions

A total of eight ground motion records were considered for the dynamic analyses: four simulated signals and four historical earthquake recordings from the west coast of North America. These seismic ground motions represent two dominant magnitude-distance scenarios for Victoria, B.C.: M6.5-30 km and M7.2-70 km (Tremblay and Atkinson 2001). All of the ground motions were scaled to match the 2005 NBCC Uniform Hazard Spectra (UHS) over the applicable period range for a 2% possibility of exceedance over 50 years (Adams and Atkinson, 2003), see Table 6.6. Time histories of scaled ground accelerations are shown in Figure 6.3, response spectra in Figure 6.4 and 6.5.

Table 6.6 Ground motion time history characteristics (Nedisan, 2002)

Event	Magn.	R (km)	Station	Comp.	PHA (g)	t_D (s)	S_F
1. Simulated (Trial #1)	M_W 6.5	30	-	-	0.53	4.7	1.0
2. Simulated (Trial #4)	M_W 6.5	30	-	-	0.39	5.7	1.0
3. Simulated (Trial #1)	M_W 7.2	70	-	-	0.25	12.5	1.0
4. Simulated (Trial #2)	M_W 7.2	70	-	-	0.26	13.1	1.0
5. Apr. 24, 1984 Morgan Hill	M_S 6.1	38	San Ysidro, Gilroy #6	90°	0.29	6.5	1.0
6. Jan. 17, 1994 Northridge	M_W 6.7	44	Castaic, Old Ridge Rd	90°	0.57	9.1	0.8
7. Apr. 4, 1965 Puget Sound	M_W 6.7	87	Olympia, Test Lab	266°	0.20	20.8	2.0
8. Apr. 13, 1949 West.Wash.	M_W 7.1	76	Olympia, Test Lab	86°	0.28	18.1	1.4

Note: t_D= the Trifunac duration (Trifunac and Brady, 1975), which means the time duration of strong shaking that has 5~95% of the total ground shaking energy.

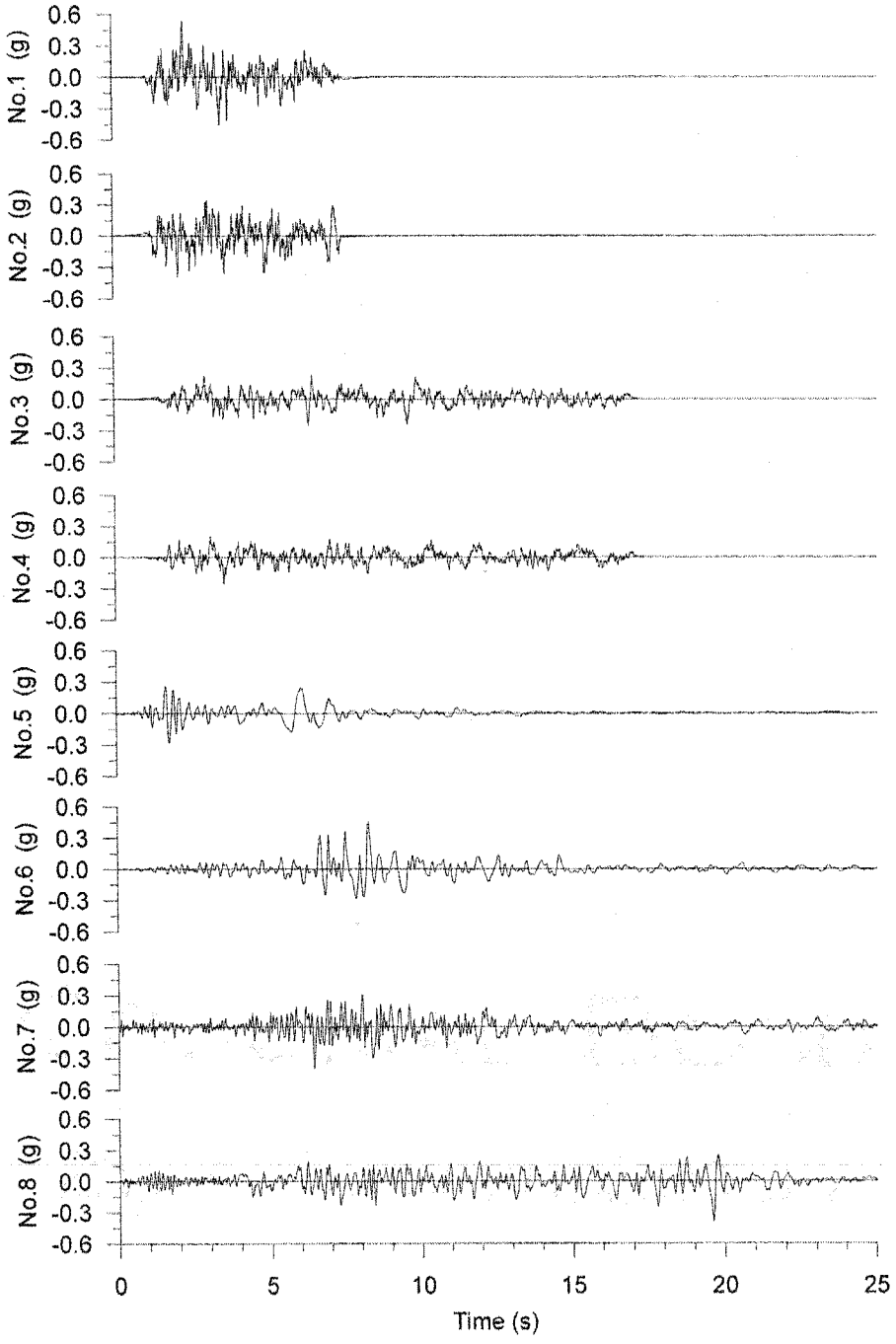

Figure 6.3. Scaled ground motion time histories

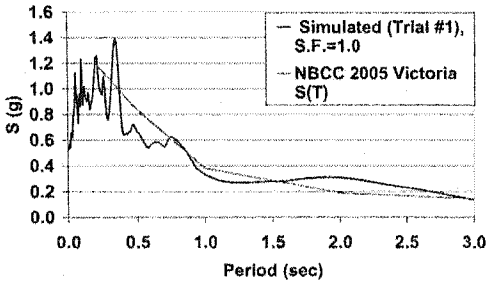

a) No. 1

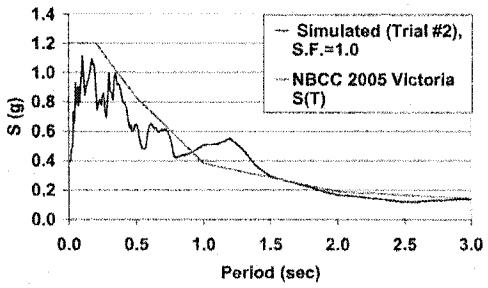

b) No. 2

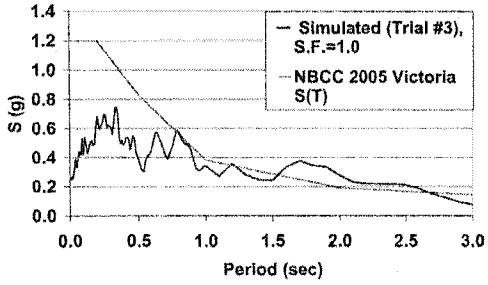

c) No. 3

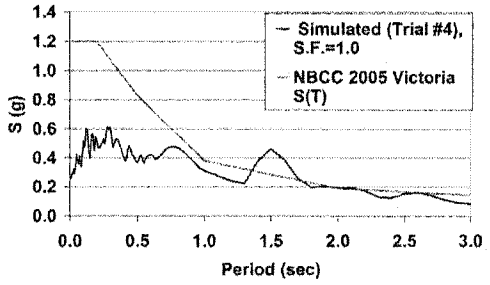

d) No. 4

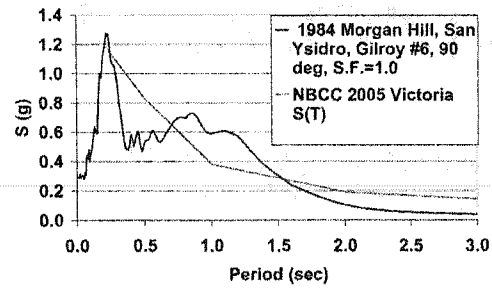

e) No. 5

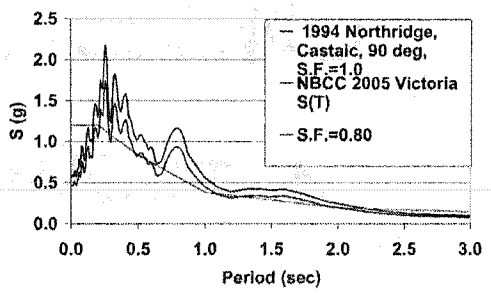

f) No. 6

Figure 6.4. Design and ground motion response spectra (No. 1 to No. 6)

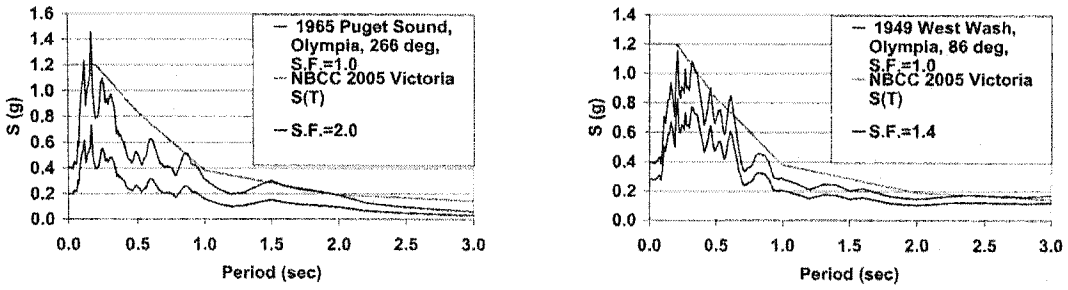

Figure 6.5. Design and ground motion response spectra (No. 7 and No. 8)

6.4.2 Calculation of torsional moments

One of objectives in this Chapter was to verify the torsional moment for the two roof cases and the eight ground motions. To identify each analysis case, the following nomenclature was used:

"2----roof type----ground acceleration No."

In this example:

"2" refers to the model of the structure, which has a stiffness eccentricity. Model 1 and 3 refer to the symmetric and stiffness & strength eccentricities considered by Nedisan (2002) and Tremblay *et al.* (2003).

Roof type is either rigid "R" or flexible "F".

The ground acceleration number varies from No. 1 to No. 8 (Table 6.6).

For example, Model "2-R-1" is a building with an asymmetric brace stiffness and a rigid roof, which was subjected to ground motion acceleration record No. 1.

6.4.2.1 The distribution of nodal accelerations

Once a non-linear dynamic time history analysis had been run, the nodal response accelerations were obtained. Figure 6.6 shows node numbers that will be quoted later in the thesis and the direction of acceleration for node i (i=1 to 153), a_{xi} and a_{yi}.

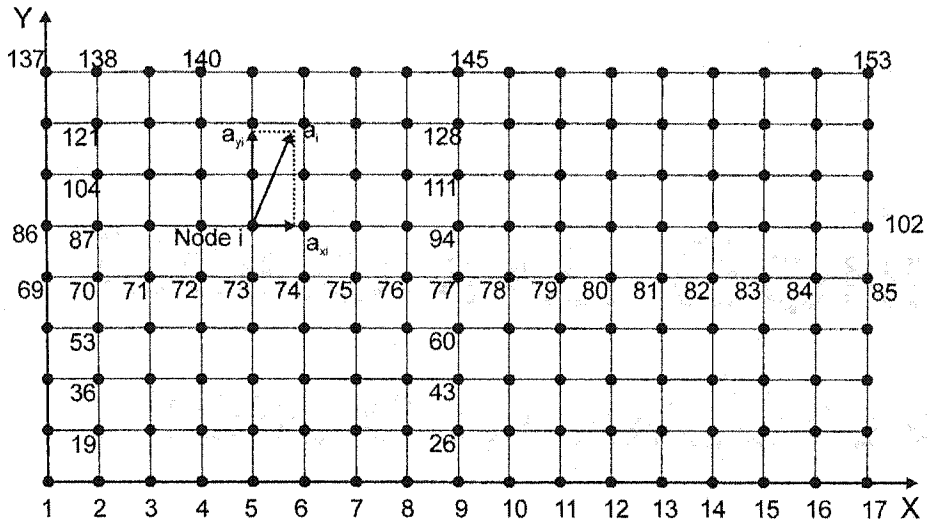

Figure 6.6. Node numbers and node acceleration direction

Two characteristics of the distribution of nodal acceleration are summarized below:

First, the distribution of nodal acceleration is linear for the rigid roof case, but may become non-linear for the flexible roof. Figure 6.7 shows two such representative examples (rigid vs. flexible roof) of the Y-direction nodal acceleration distributions a_y over the building mid-width (node 69 to 85 in Figure 6.6). These nodal accelerations are those when the maximum torsional moment about the centre of mass is achieved.

Since the maximum torsional moment corresponds to the extreme situation for torsion, some structural members may have yielded at that time. However, even if yielding takes place, the linear variation of the acceleration will remain for the rigid roof case (Figure 6.5a) when the torsional moment is smaller. For the flexible roof case, the shape of the nodal acceleration distribution in Figure 6.5b is transient and the values and the shape can change totally from time to time during an earthquake.

The second characteristic of the distribution of nodal accelerations is that, for either rigid roof or flexible roof, the X or Y direction component of the nodal acceleration a_{xi} and a_{yi} (Figure 6.4) can be approximately (with acceptable accuracy) represented by the nodal accelerations of the nodes located along the mid-length or the mid-width axes. For instance, Figure 6.8 compares the acceleration computed in the Y direction at node 70 to the mean value of the acceleration determined in the same direction at nodes 2, 19, 36, 53, 70, 87, 104, 121 and 138 (refer to Figure 6.4 for position). These two curves match very well. Similar correlation was also observed for other nodes along the two principal axes, for both directions, and for both the rigid and flexible roof cases. Therefore, in the calculation of the torsional moments, only the accelerations of the nodes located along the principal axes of the roof were considered, which significantly simplified the calculations.

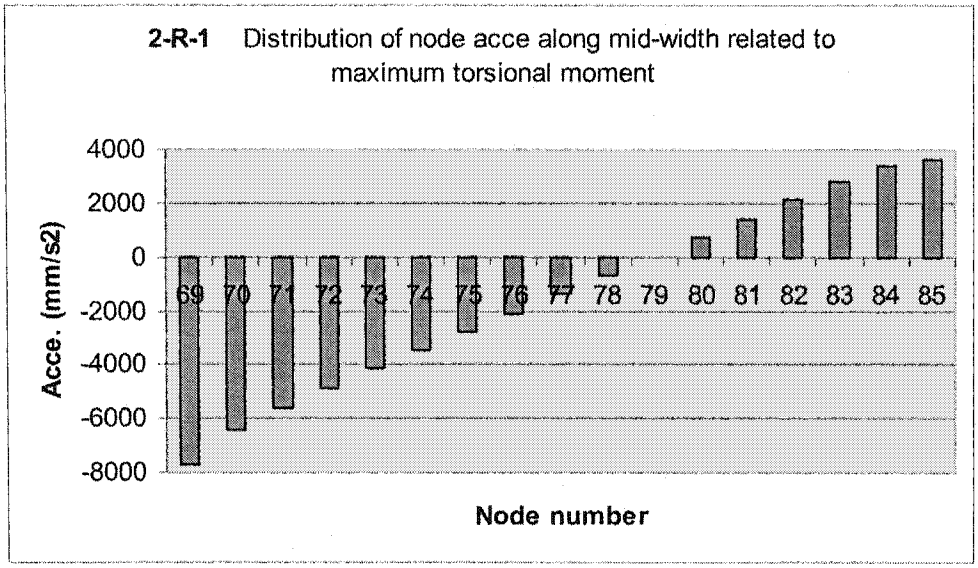

a) Rigid roof (t=3.68 sec. and T_{CM}=16.33 MN-m)

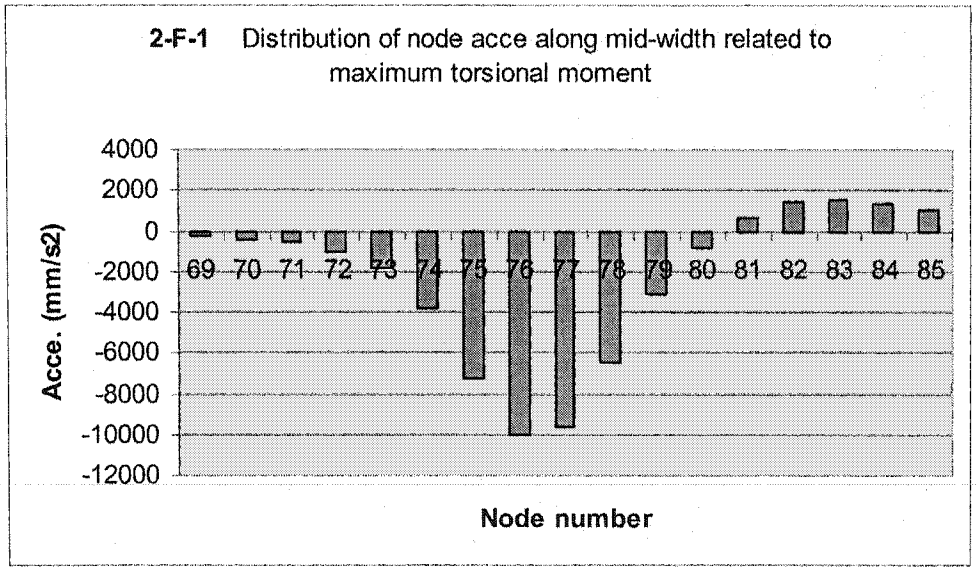

b) Flexible roof (t=4.57 sec. and T_{CM}=4.26 MN-m)

Note: See Figure 6.6 for the node positions.

Figure 6.7. Examples of nodal acceleration distribution

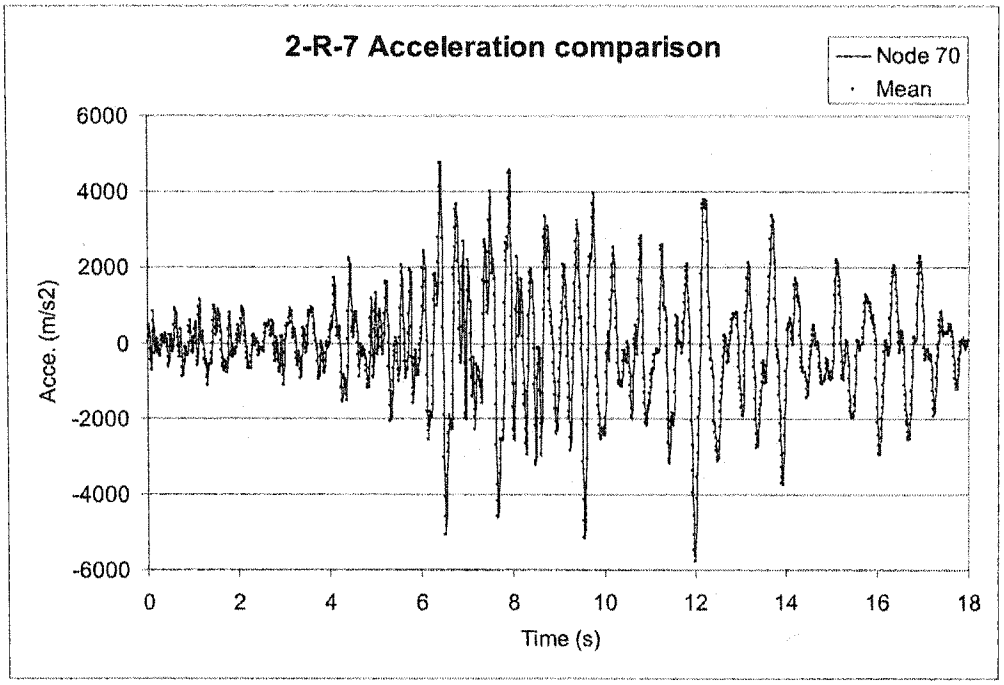

Figure 6.8. Example of node acceleration similarity

6.4.2.2 Calculation of torsional moment around CM

The overall torsion moment about the centre of mass, $T_{CM,D}$ due to the deck inertial forces was obtained by summing all the nodal moments (Figure 6.9):

$$T_{CM,D}=\Sigma F_{xi}Y_i +\Sigma F_{yi}X_i \quad (i=1 \text{ to } 153 \text{ in this building}) \qquad (6.8)$$

where F_{xi}, F_{yi} are the X and Y direction components of nodal inertial force at node i, which are assumed as positive in the X and Y direction. The inertial force at each node was determined by multiplying the lumped node mass and the nodal acceleration:

$$F_{xi}=m_{xi}a_{xi} \tag{6.9}$$

$$F_{yi}=m_{yi}a_{yi} \tag{6.10}$$

where m_{xi} and m_{yi} are respectively the lumped masses of node i in the X and Y directions, and X_i and Y_i are the rectangular X and Y coordinates of node i. For simplicity, the origin of the coordinate system is located at the CM, i.e. the centre of building model.

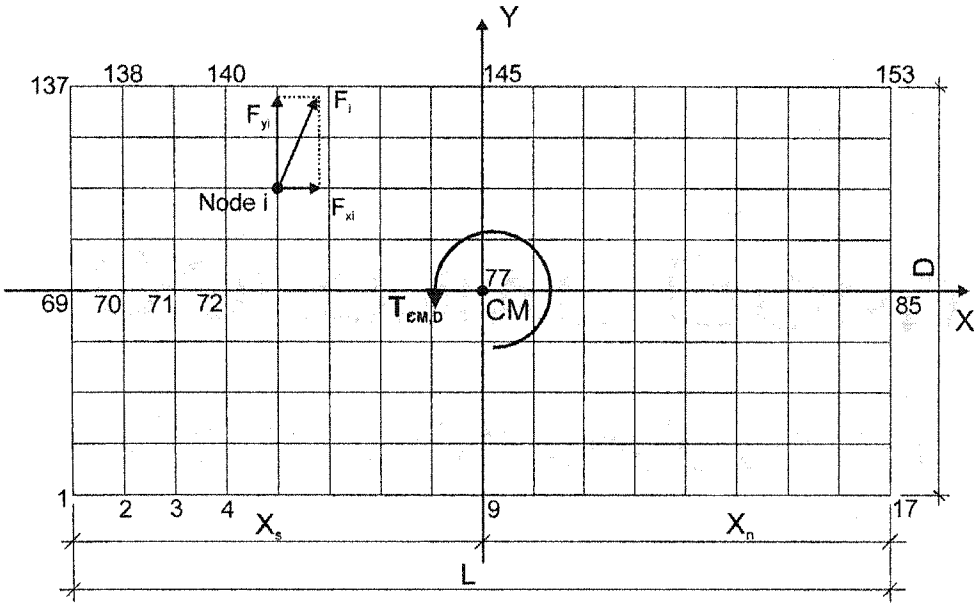

Figure 6.9. Nodal inertial force and its components

It is important to note that, the torsion moment, $T_{CM,D}$ in Figure 6.9, is that about the CM, which is not the same as T_r around the point CR as shown in Figure 6.2. The moment $T_{CM,D}$ is used to introduce the concept of calculating torsion moments based on nodal accelerations of the roof. Later, the torsion moment around CR, $T_{CR,D}$, will be presented.

Equation 6.8 could be simplified based on the similarity of nodal accelerations in the same direction and the same axis as was illustrated in Figure 6.8. As indicated, only the node accelerations along the axes passing CM could be included in the calculations. For the X direction components, these will be nodes 9, 26, 43, 60, 77, 94, 111, 128, 145. For the Y-direction components, accelerations at nodes 69 through 85 were included. Details of this simplification are given in Figure 6.10. In this way, only 17 X-direction and 9 Y-direction component values of the nodal accelerations were needed. To verify the accuracy of this method, the torsional moment $T_{CM,D}$ will be checked later with the torsional moment from brace forces, $T_{CM,B}$, as described in Section 6.3.3.4.

In Figure 6.10, the overall torsional moment around the centre of mass, $T_{CM,D}$, in Equation 6.8 was divided into two parts: that from Y-direction inertia forces and that from X-direction inertia forces, i.e.:

$$T_{CM,D} = T_{CM,DY} + T_{CM,DX} \qquad (6.11)$$

These two parts of the overall torsional moment are defined as follows:

$$T_{CM,DY} = \Sigma F_{yi} X_i \qquad (i=69 \text{ to } 85, \text{ see Figure 6.8 a}) \qquad (6.12)$$

$$T_{CM,DX} = \Sigma F_{xi} Y_i \qquad (i= 9, 26, 43, 60, 77, 94, 111, 128, 145, \text{see Figure 6.8 b}) \qquad (6.13)$$

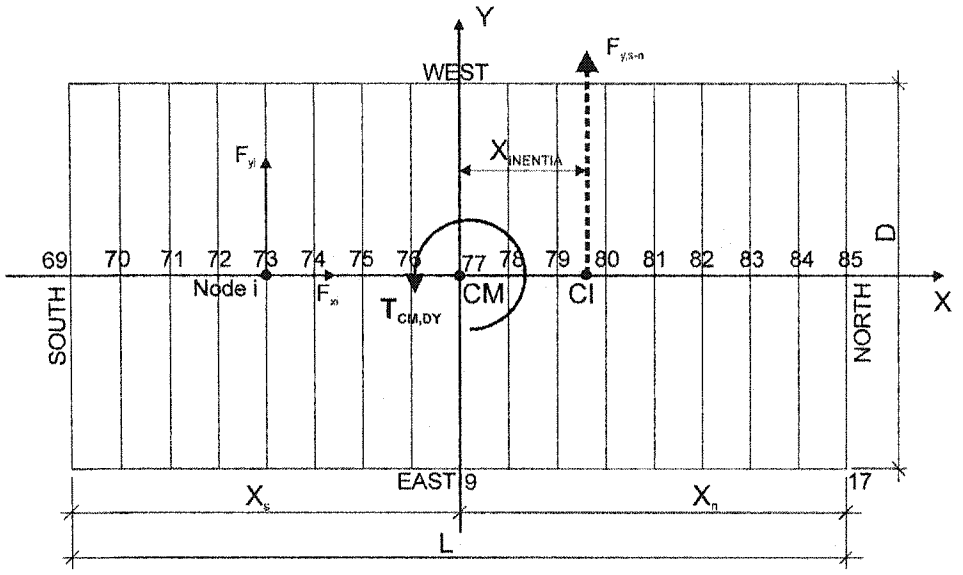

a) The calculation of $F_{y,s-n}$, $T_{CM,DY}$, and $X_{INERTIA}$

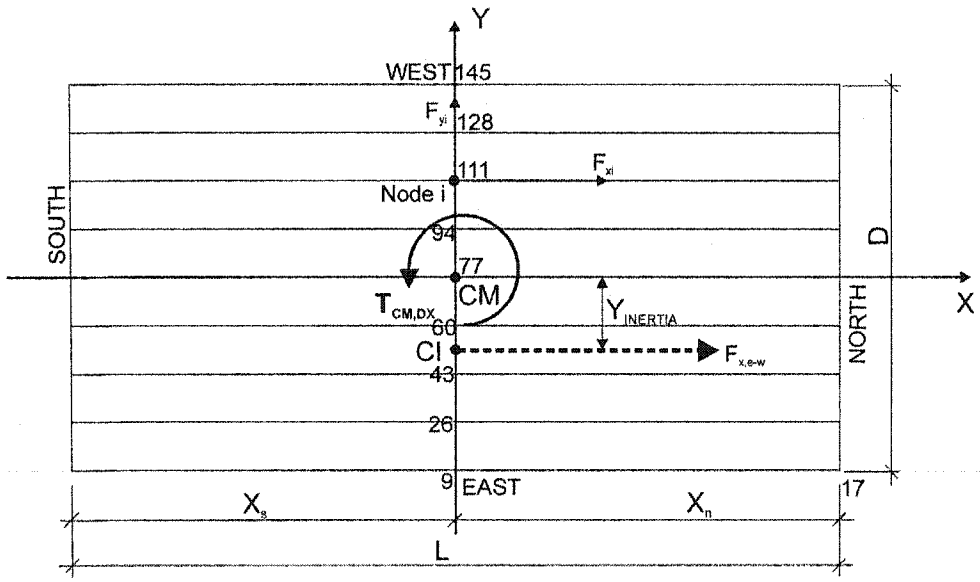

b) The calculation of $F_{x,e-w}$, $T_{CM,DX}$, and $Y_{INERTIA}$

Figure 6.10. Calculation of torsion moment $T_{CM,D}$, ($T_{CM,D}$= $T_{CM,DY}$+ $T_{CM,DX}$)

Following the above steps, the overall torsional moment around CM could be obtained, and the results will be discussed in Section 6.5.

6.4.2.3 Centre of Inertia (CI) Calculation

The position of the centre of inertia (CI) is defined as the point through which the resultant force passes. It can be explained by dividing the resultant force into its two components, $F_{y,s\text{-}n}$ and $F_{x,e\text{-}w}$, where y and x are the force directions, s-n means south and north sides, and e-w means the east and west sides (see Figure 6.10).

From earlier studies (Nedisan, 2002) it is noted that $T_{CM,D}$ does not always match T_r calculated from static methods (Equation 6.5). The reason is that the position of the centre of inertia is transient, i.e. it does not always coincide with the centre of mass during an earthquake. The offset distance $X_{INERTIA}$ (see Figure 6.10a) for the summed inertia force $F_{y,s\text{-}n}$ in the Y-direction, and $Y_{INERTIA}$ (see Figure 6.10b) for the summed inertia force $F_{x,e\text{-}w}$ in the X-direction can be calculated as follows:

$$X_{INERTIA} = T_{CM,DY} / F_{y,s\text{-}n} \tag{6.14}$$

$$Y_{INERTIA} = T_{CM,DX} / F_{x,e\text{-}w} \tag{6.15}$$

where:

$$F_{y,s\text{-}n} = \Sigma F_{yi} \qquad (i=69 \text{ to } 85) \tag{6.16}$$

$$F_{x,e\text{-}w} = \Sigma F_{xi} \qquad (i= 9, 26, 43, 60, 77, 94, 111, 128, 145) \tag{6.17}$$

The buildings were only subjected to earthquake records acting along the east-west direction. For this reason, the summed force in the X-direction, $F_{x,e\text{-}w}$, must be zero, that is, a pure force couple exists. In this case, it is possible that $Y_{INERTIA}$ (see Figure 6.10b) becomes infinite. Hence, only the offset distance $X_{INERTIA}$ (Figure 6.10 a) based on the Y-direction force, $F_{y,s\text{-}n}$, is considered of interest. Typically, a relative offset value is used to represent the torsional effects, which can be evaluated by $X_{INERTIA}/L$. It is noted that $F_{y,s\text{-}n}$, may also become very small, which will cause $X_{INERTIA}$ to become excessively large, even when the torsion $T_{CM,DY}$ is small in value. Because only the position of the CI when significant forces are acting on the structure is of interest, the calculation of CI was carried out only when $F_{y,s\text{-}n} > 180$ kN (about 22% of the yield base shear V = 833.33 kN); a value arbitrarily chosen and suggested by Nedisan (2002). Further work is recommended to choose a value that has a clearer physical meaning.

6.4.2.4 Torsional moment about CM from brace forces

As indicated previously, the accuracy of the calculated torsion moment, $T_{CM,D}$, was checked by determining the torsional moment from the brace forces, $T_{CM,B}$, which was calculated as follows:

$$T_{CM,B}=(F_s-F_n)L/2+(-F_e+F_w)D/2 \qquad (6.18)$$

where F_s, Fn, Fe, and Fw are respectively the storey shears calculated from the brace member forces along the south, north, east and west walls. They are assumed to be positive in the Y or X positive directions, see Figure 6.11. L and D are the building length and width respectively. $T_{CM,B}$ is assumed to be positive when it is in the clockwise direction, which is opposite to that for $T_{CM,DY}$ to keep them in balance.

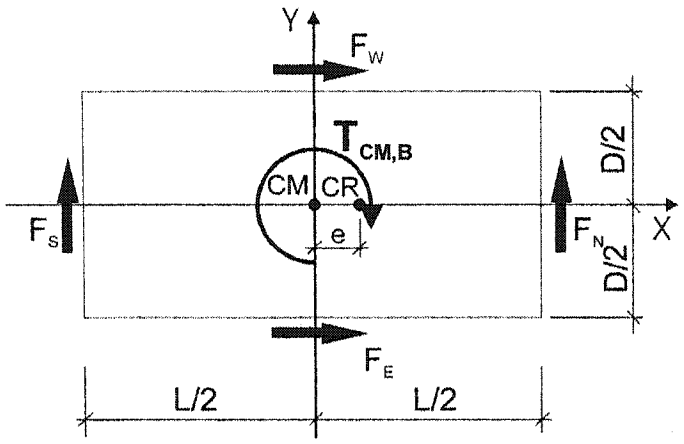

Figure 6.11. Calculation of $T_{CM,B}$

6.4.2.5 Torsional moment about centre of rigidity (CR)

To compare the torsional moment with those calculated from static approaches, T_r (Figure 6.1 b), the moment $T_{CM,D}$ had to be changed to a moment about centre of rigidity, i.e. $T_{CR,D}$. The transferring process is shown in Figure 6.12.

In Figure 6.12a and Figure 6.12b, the torsional moment about CR from the deck inertia forces, $T_{CR,D}$ is as follows:

$$T_{CR,D} = T_{CM,D} - F_{y,s\text{-}n}e \qquad (6.19)$$

where e is the eccentricity between CM and CR (Equation 6.2), $T_{CM,D}$ is from Equation 6.11, and $F_{y,s\text{-}n}$ is from Equation 6.16. Similarly, the torsional moment about CR from the brace forces, $T_{CR,B}$, shown in Figure 6.12c and Figure 6.12d, is calculated from:

$$T_{CR,B} = T_{CM,B} + (F_S + F_N)e \qquad (6.20)$$

$T_{CM,B}$ is from Equation 6.18 and F_S and F_N are the storey shear calculated from the brace members along the south wall and along the north wall, respectively. As noted above, $T_{CR,D}$ is positive in the counter clockwise direction, while $T_{CR,B}$ is positive in the clockwise direction.

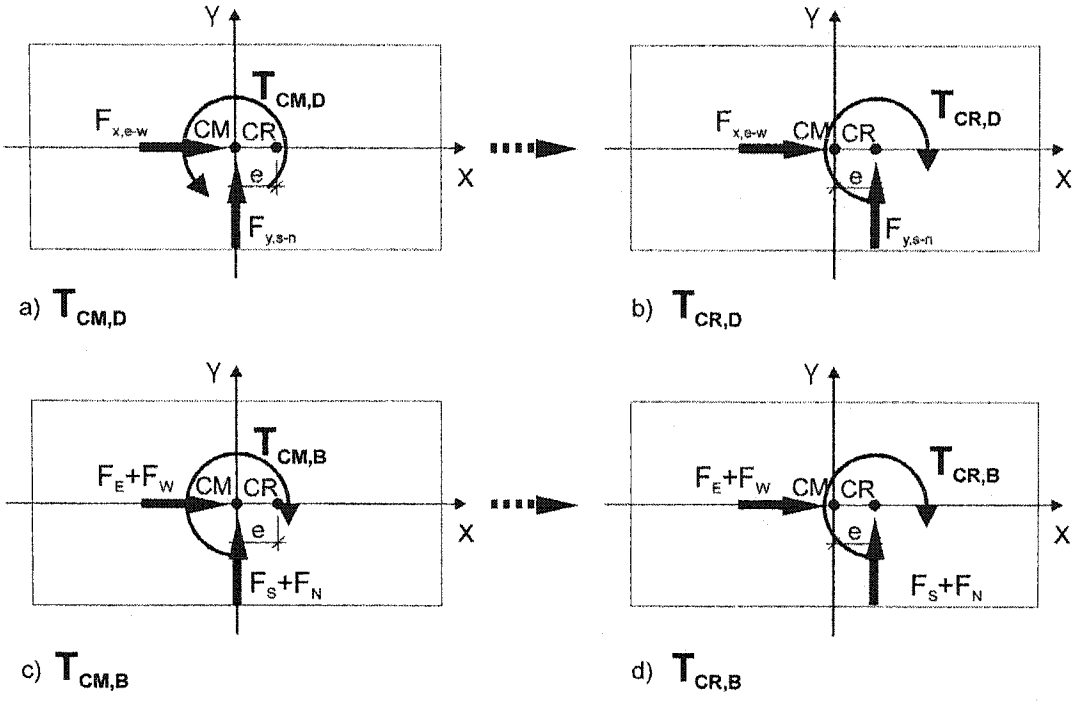

Figure 6.12. Calculation of $T_{CR,D}$ and $T_{CR,B}$

6.4.3 Non-linear Dynamic analysis results

The results obtained from the static analysis and the dynamic time history analyses are discussed in this section. Only two cases are illustrated here and other analysis results are given in Appendix 4.

6.4.3.1 The results of 2-R-1 and 2-F-1

As presented before, the model "2-R-1" is a building with an asymmetric brace stiffness and a rigid roof subjected to ground motion acceleration record No. 1. The building "2-F-1" means a flexible roof. The responses of these two structures are compared to see the influence of the roof flexibility.

Figure 6.13 and Figure 6.14 show the response time history results for buildings 2-R-1 and 2-F-1, respectively. The response parameters shown are:

a) The storey drifts Δ_{centre}, which is the Y-direction displacement of node 145 (Figure 6.6).
b) The relative displacement (Δ_s-Δ_n), which is the difference between the Y-direction displacements of nodes 137 and 153 (Figure 6.6).
c) The sum of inertia forces in the Y-direction $F_{y,s-n}$, see Figure 6.10 and Equation 6.16.
d) The storey shear along the east wall braces F_e, see Figure 6.11.
e) The torsional moments around the CM due to the Y-direction inertia forces (or the N-S forces), and that due to the X-direction inertia forces (or the E-W forces). Refer to Figure 6.10 and Equations 6.12 and 6.13.
f) The total torsion moment $T_{CM,D}$ due to the inertia forces, as shown in Figure 6.9 and corresponding to the sum of the two torsional moments $T_{CM,DY}$ and $T_{CM,DX}$. The moment $T_{CM,D}$ is checked with the torsion moment $T_{CM,B}$ due to the brace forces.
g) The relative offset of CI ($X_{INERTIA}/L$), see Figure 6.10a.
h) The ground motion acceleration used in the analysis.

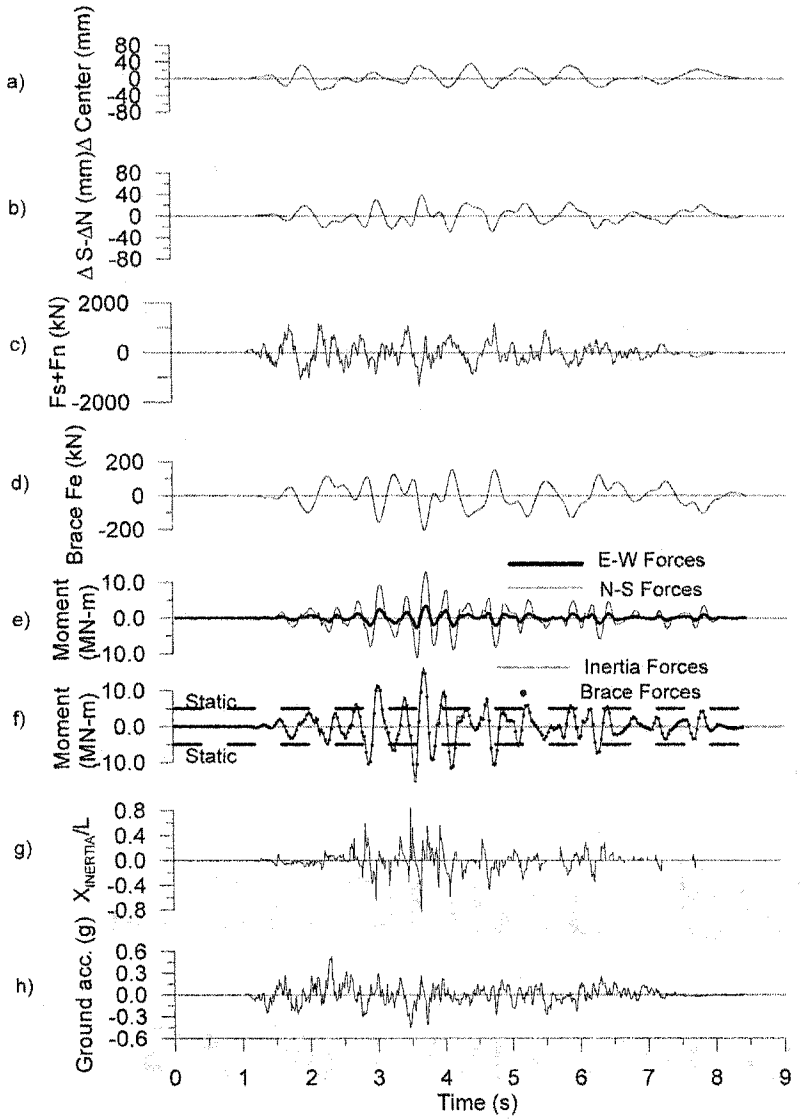

Response of 2-R-1 (Model 2-R to Seismic event No.1)
a) Storey drift at mid-length of the building;
b)Difference between storey drifts at South and North walls;
c) Sum of inertia forces in E-W direction;
d) Sum of brace force horizontal components in East wall;
e) Torsional moments due to E-W and N-S inertia forces;
f) Torsional moments due to total inertia forces and brace forces;
g) Location of E-W inertia center (CI);
h) Selected ground motion

Figure 6.13. Result for case 2-R-1

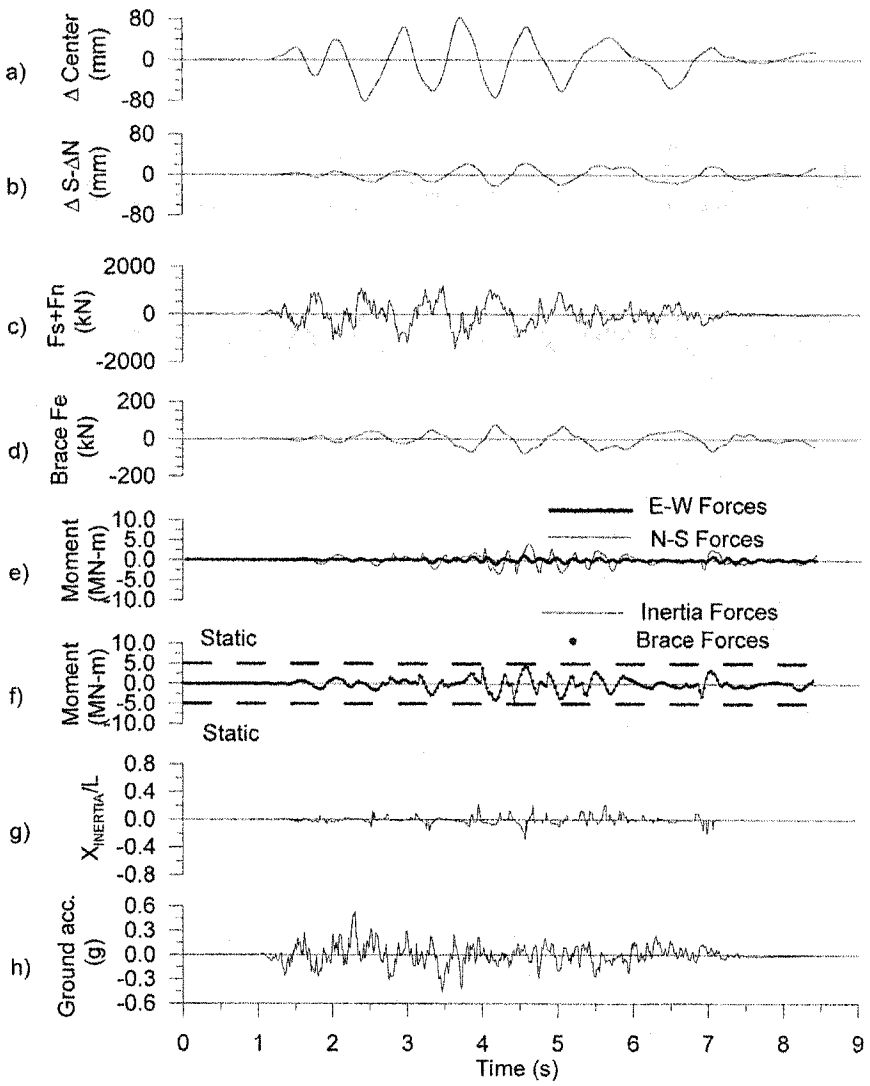

Response of 2-F-1 (Model 2-F to Seismic event No.1)

a) Storey drift at mid-length of the building;
b)Difference between storey drifts at South and North walls;
c) Sum of inertia forces in E-W direction;
d) Sum of brace force horizontal components in East wall;
e) Torsional moments due to E-W and N-S inertia forces;
f) Torsional moments due to total inertia forces and brace forces;
g) Location of E-W inertia center (CI);
h) Selected ground motion

Figure 6.14. Result for case 2-F-1

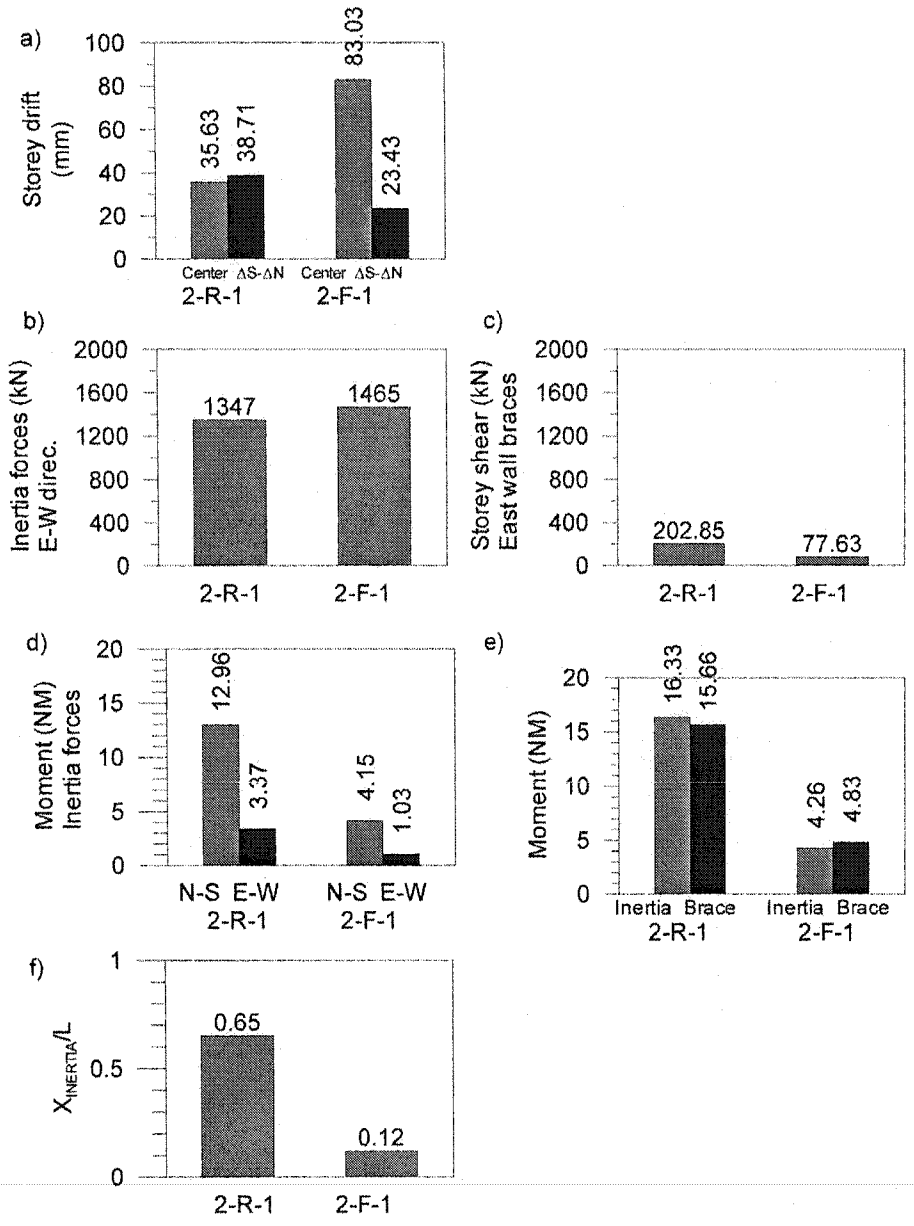

Maximum Response of 2-R-1 & 2-F-1 (Absolute value)

a) Storey drifts (at mid-length; Difference between South and North walls);
b)Sum of E-W direc. inertia forces; c) Storey shear by East wall braces;
d) Torsional moments due to inertia forces (North-South; East-West);
e)Torsional moments due to inertia forces and due to brace forces;
f) Location of E-W inertia center (CI) at maximum inertia torsion moment

Figure 6.15. Comparison of 2-R-1 to 2-F-1

A direct comparison of the maximum value of response parameters is provided in Figure 6.15. Since we are more interested in these peak values, Figure 6.15 will be explained in greater detail, while Figure 6.13 and Figure 6.14 are used for additional remarks.

Figure 6.15d shows that the torsional moments about the CM due to theY-direction inertia forces are much larger than that due to the X-direction forces, i.e. Y-direction force dominated the torsional moment. Figure 6.13 e) compares the total torsion moment $T_{CM,D}$ due to the inertia forces with the total torsion moment $T_{CM,B}$ due to the brace forces. The two values match very well, which confirms the accuracy of the calculation of $T_{CM,D}$ presented in Section 6.3.3.2. Much higher values of torsional moments took place for the rigid roof than for flexible roof. Therefore, the flexible roof tends to lessen the torsional effects.

Similar effects occurred for the storey shear along east wall braces F_e, as shown in 6.15c. It is much higher for the rigid roof case than for the flexible roof case, which coincides with the above statement, i.e. the torsion response for rigid roofs is more severe than for flexible roofs. In Figure 6.15f, the relative offset of CI ($X_{INERTIA}/L$) to CM, is another index to show that torsional effects are greater for the rigid roof case than for the flexible roof case.

In Figure 6.15a, the storey drifts at mid-length Δ_{centre} for the rigid roof case is much smaller than that of flexible roof case. This has also been observed in the static analysis results (the $R_0R_d\Delta_{Total}$ in Table 6.4) and all other dynamic analysis cases, even though the values may have been different. The relative displacement (Δ_s-Δ_n) in the model 2-R-1 is larger than in the model 2-F-1.

The values of the total inertia forces in y-direction, $F_{y,s\text{-}n}$, shown in 6.15b are consistent for these two roof cases.

6.4.3.2 Torsional moment about CR

As discussed before, the torsional moment about CM can be translated into the torsional moment about CR. The two moments are illustrated for the model 2-R-1 in Figure 6.16. Figure 6.16a shows the results of the overall torsional moment about the centre of mass, $T_{CM,D}$, due to the deck inertial forces, and that due to the brace forces, $T_{CM,B}$. Figure 6.16b shows the results of the overall torsional moment about the centre of rigidity, $T_{CR,D}$ due to the deck inertial forces and that due to the brace forces $T_{CR,B}$. In both cases, the torsional moment calculated from the deck inertia forces agrees with the moment calculated from the brace forces.

It appears that the torsional moment about CR (maximum at 18.98 MNm) is larger than that about CM (maximum at 16.33 MNm). They are both much larger than the value calculated from the static method (T_r=5 MNmm). This illustrates that the asymmetric brace stiffness makes the structural torsional analysis more complex. Hence, a number of analyses with several ground motions were undertaken as presented in the following Section.

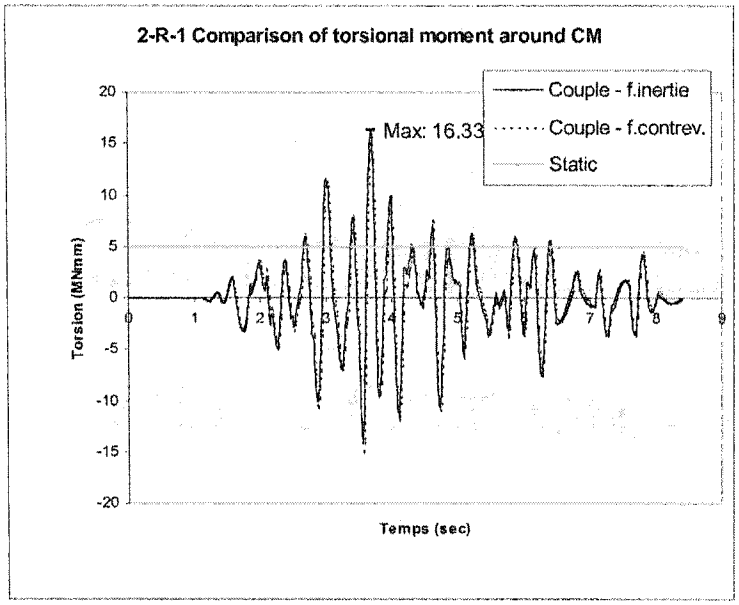

a) The torsional moment about CM

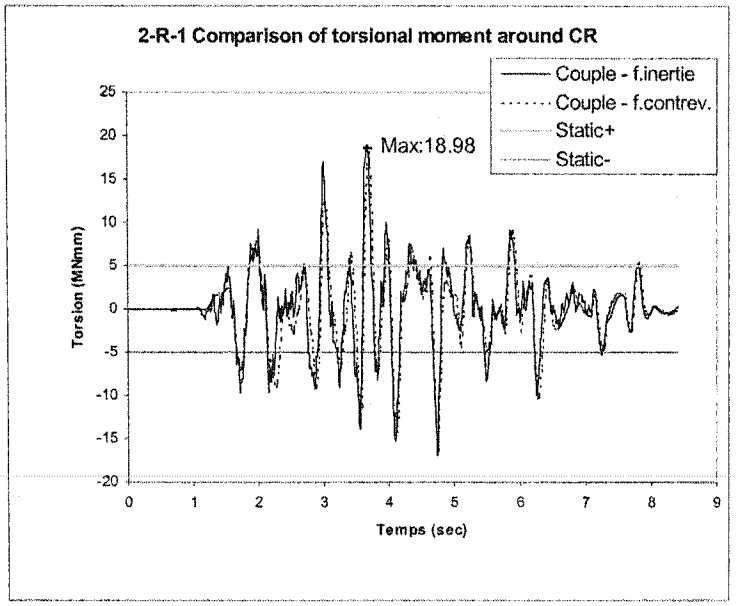

b) The torsional moment about CR

Figure 6.16. The comparison of torsional moment about CM to about CR

6.5 SUMMARY OF STATIC, SPECTRUM AND DYNAMIC ANALYSIS RESULTS

The results of the peak horizontal shear resisted by the braces, the peak ductility demand in the brace elements, the peak storey drifts, and the statistics of the peak response parameters for all design scenarios and earthquake records are shown in Table 6.7 to 6.10. From Table 6.7, it is found that, the structural responses are greatly influenced by each earthquake record as the values vary significantly from one record to the next. This confirms that in dynamic analyses, several ground motions must be included, and the statistics of the data need to be utilized. The "mean" values of the peak horizontal shear in the vertical bracing bents show that torsional effects are more obvious in the rigid roof model than in the flexible roof model. As an example, the peak horizontal shear in the east wall for the rigid roof model is larger than for the flexible roof model, and so is the situation for all dynamic analyses, except under seismic events No.4 and 5.

For the linear static analyses, the resultant horizontal shear force calculated from south and north braces seems larger than the maximum load V_{max}=833 kN, because the high capacity limits were never reached. For the other analyses, this value does not exceed V_{max}. The spectrum analyses result in a shear force at the south wall larger than at the north wall, which is quite abnormal in comparison to the other results. This discrepancy places doubt in the accuracy of the spectrum analyses that were completed.

Table 6.7 Peak horizontal shears in the vertical bracing bents (kN)

Model	Location	Static		Spectrum	Seismic event No.										
		Linear	Non-linear		1	2	3	4	5	6	7	8	Mean	Mean+SD	Max
2-R	South	402	399	431	399	399	399	399	399	399	399	399	399	399	399
	North	436	434	402	434	434	409	389	434	434	434	434	425	442	434
	East	34.7	34.7	55.4	202.1	175.9	76.4	47.0	70.5	230.1	93.5	229.9	140.7	217.2	230.1
2-F	South	413	399	418	399	399	399	399	399	399	399	358	394	409	399
	North	433	433	415	434	434	416	434	434	434	416	349	419	448	434
	East	20.2	20.2	29.4	76.8	92.1	33.9	49.9	92.7	119.0	26.0	23.2	64.2	100.1	119.0

Note: The values for the west bracing bents are same as the east one, and are not illustrated. The statistic values were obtained from the seismic events (No.1 to No. 8). The designed yield forces of the horizontal shear are: South 399 kN, North 434 kN. East 417 kN. The comparison of the results obtained from the static, spectrum, and dynamic (mean value) analysis is also shown in Figure 6.17. For the dynamic analysis (Figure 6.17c and d), the mean values of the brace forces are used instead of the mean + SD because the later may exceed the yield capacity of the element, which is not realistic. In Figure 6.17a and b, the sum of shear forces calculated from the south and north braces in the Y-direction is larger than the designed V_{max} = 833 kN because of P-Δ effect. The results for the non-linear static analyses are similar to Tremblay et. al (2003), therefore it is not illustrated in the Figure.

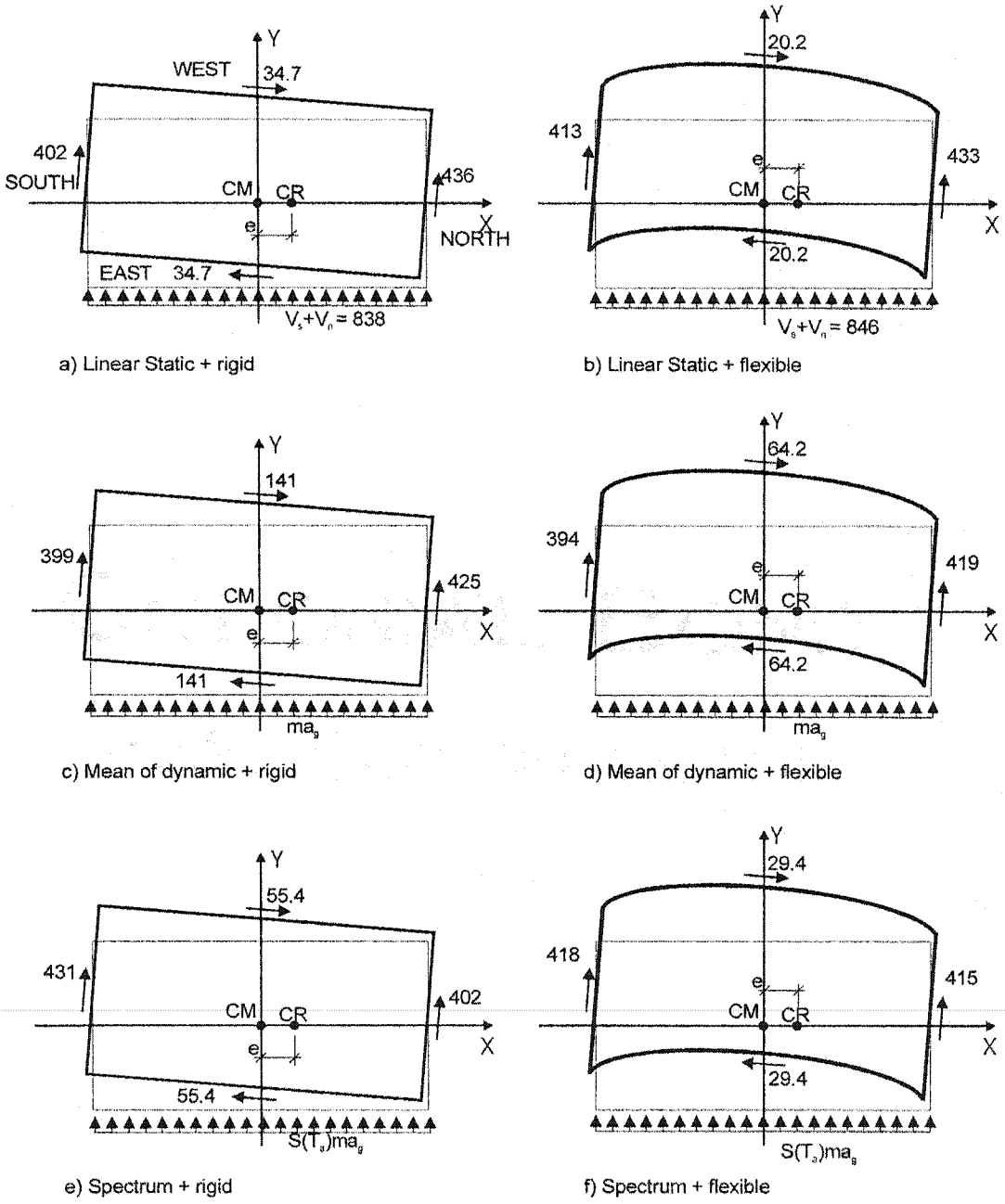

Figure 6.17. Comparison of shear forces in brace bents

Table 6.8 shows the ductility demand determined from the static and dynamic analyses. This parameter could not be evaluated from the spectrum analysis because it is a linear elastic analysis. The values from static analysis are slightly higher than 1.0 because the load acting on the building was expected to make the braces to yield in tension. The mean values of the dynamic analyses are smaller than the expected ductility value R_d=2.0, however, the values of "mean + SD" are greater than R_d=2.0. For the rigid roof, the difference is not significant, but for the flexible roof, the difference should be considered in design practice. Therefore, a group of dynamic analyses is recommended when studying the performance of buildings with flexible roof diaphragms.

Table 6.8 Peak ductility demand in the bracing bents

Model	Location	Static	Seismic event No.								Mean	Mean+ SD	Max
		Non-linear	1	2	3	4	5	6	7	8			
2-R	South	1.01	2.06	1.93	1.10	1.01	1.36	2.69	1.45	2.13	1.71	2.30	2.69
	North	1.01	1.50	1.07	1.00	1.00	1.16	1.95	1.04	1.31	1.25	1.58	1.95
2-F	South	1.03	1.96	2.14	1.19	1.47	3.88	2.61	1.01	1.00	1.91	2.89	3.88
	North	1.00	1.60	1.63	1.00	1.24	3.84	2.18	1.00	1.00	1.69	2.65	3.84

Note: the peak ductility demand for the east and west bracing bents is not listed since the braces remained elastic. The statistic values are from the seismic events (No.1 to No. 8).

In Table 6.8 it was found that the structural response for each earthquake event is not consistent, however, some trends can still be summarized. For example, the less stiff brace elements (south side) tend to have higher ductility demand and the roof flexibility seems to make the brace ductility demand more uniform, although the values are usually higher.

Table 6.9 lists the peak storey drifts from the static, spectrum and dynamic analyses. The mean values from the dynamic analyses, of the storey drifts in the south wall, in the north wall, and in the centre, are larger in the 2-F model, which is the result of lower horizontal stiffness. In the south and north walls, the brace stiffness is the same for both model 2-R and model 2-F, but the displacements in these locations are affected by the roof flexibility. The mean values of the storey drifts in the west wall, the torsional sensitivity ratio B, and the relative displacement (Δ_s-Δ_n), are larger for the 2-R model, which indicates higher effects of torsion. In Table 6.9 (continued), the ratios of the above parameters between flexible and rigid roofs are given. These ratios also show these relationships.

It is noted that the torsional sensitivity ratio B for the static analyses is quite small, around 1.16, which is much lower than 1.7, the limit up to which dynamic analysis is not required in the proposed 2005 NBCC. However, in the dynamic analyses, this parameter changed significantly, the highest value being 1.53 for the case 2-R-2, and the average value of B from dynamic analysis being 1.34. So, the value of B calculated from static procedure may not be representative of reality.

It was also observed that the maximum storey drifts Δ from the spectrum and the mean + SD of dynamic analysis did not exceed $R_0R_d\Delta e$ determined by the static procedure and of course less than the Δ_{limit}=165 mm. So, the check of storey drifts in the static procedure seems to be conservative.

Figure 6.10 shows visually the deformed shapes of the rigid and flexible roof diaphragms by using the static, spectrum, and time history methods.

Table 6.9 Peak storey drifts (absolute values: mm)

Model	Location	Node No.	Static		Spectrum		Seismic event No.								Mean	Mean+SD	Max
			Δ_{st}	$R_0R_d\Delta_{st}$	$\Delta_{sp}*V_d/V_e$	Δ_{sp}	1	2	3	4	5	6	7	8			
Rigid	δ_s	137-Y	24.1	57.7	25.8	58.8	49.3	46.1	26.2	24.2	32.5	64.3	34.7	50.9	41.0	54.9	64.3
	δ_n	153-Y	17.4	41.8	16.1	36.6	26.0	18.5	16.3	15.6	20.1	33.7	18.0	22.6	21.4	27.4	33.7
	δ_w	145-X	1.66	3.98	2.65	6.05	9.68	8.43	3.66	2.25	3.37	11.02	4.48	11.02	6.74	10.41	11.02
	Δ_{Total}	145-Y	20.7	49.8	20.8	47.4	35.7	30.1	21.1	19.9	27.0	49.0	26.2	34.8	30.5	39.9	49.0
	$B=\delta_{max}/\delta_{ave}$		1.16	1.16	1.24	1.24	1.38	1.53	1.24	1.22	1.20	1.31	1.32	1.46	1.34	1.45	1.53
	δs-δn	137-153	6.65	15.96	9.70	22.20	38.71	33.68	14.63	9.00	13.50	44.03	17.91	44.06	26.94	41.60	44.06
Flexible	δ_s	137-Y	24.7	59.4	13.7	23.3	48.1	52.3	29.7	36.4	94.0	63.5	25.3	22.5	46.5	70.4	94.0
	δ_n	153-Y	17.3	41.5	9.44	16.1	26.5	29.5	17.8	22.6	67.8	38.9	17.8	14.9	29.5	46.8	67.8
	δ_w	145-X	0.97	2.33	0.7	1.2	3.68	4.41	1.62	2.39	4.44	5.70	1.24	1.11	3.07	4.79	5.70
	Δ_{Total}	145-Y	57.8	138.8	53.1	90.4	83.1	84.6	62.2	72.4	130.7	98.1	62.5	56.4	81.2	105.6	130.7
	$B=\delta_{max}/\delta_{ave}$		1.18	1.18	1.18	1.18	1.29	1.28	1.25	1.23	1.16	1.24	1.18	1.20	1.23	1.28	1.29
	δs-δn	137-153	7.45	17.88	4.26	7.20	23.43	26.95	12.54	14.68	29.26	32.61	8.29	7.58	19.42	29.26	32.61

Note:

1. Node number refers to Figure 6.4. East location is neglected since it is same as the west location.
2. The statistic values are got from the seismic events (No.1 to No. 8).
3. The non-linear static results are same as the linear static results, so they are shown together.

Table 6.9 (continued)

Ratio			Static	Spectrum	Dynamic		
			Δ_{st}	Δ_{sp}	Mean	Mean+SD	Max
Flexible/Rigid	South	137-Y	1.028	0.531	1.133	1.281	1.462
	North	153-Y	0.993	0.586	1.380	1.707	2.011
	West	145-X	0.584	0.264	0.456	0.461	0.517
	Centre	145-Y	2.790	2.553	2.667	2.649	2.667
	$B=\delta_{max}/\delta_{ave}$		1.014	0.955	0.920	0.877	0.841
	$\Delta_s-\Delta_n$	137-153	1.120	0.439	0.721	0.703	0.740

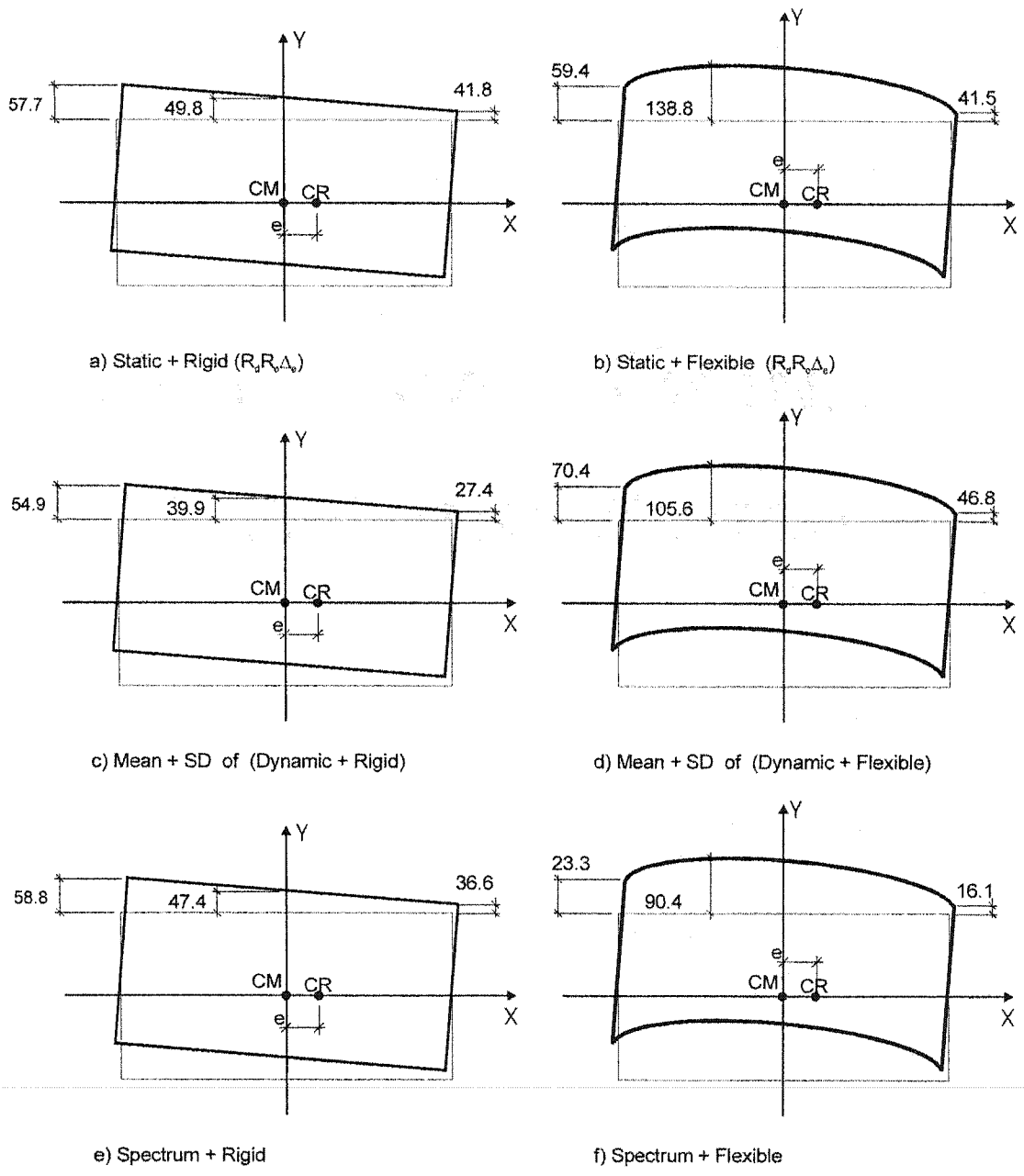

Figure 6.18. Comparison of peak story drifts from static, spectrum and dynamic analysis

In Table 6.10, the statistics of several peak response parameters reflecting the torsional behaviour are listed. It is found that the values of the sum of inertia forces in the y-direction, $F_{y,s-n}$, are usually consistent for either the 2-R model or the 2-F model since this force is limited by the capacity of the east and west braces and is not influenced much by torsional effects. It must be noted that the $F_{y,s-n}$ does not equal to the sum of horizontal shear forces calculated from braces in the south and north walls, F_s+F_n. The former is equivalent to a loading acting on the diaphragm due to ground motion, while the later is the resistance of the structure, which cannot exceed 833 kN as per their capacity.

The storey shear for the east wall braces, F_e, is much larger in the rigid roof case than in the flexible roof case, which confirms that the braces perpendicular to the loading are more effective in resisting torsion effects with a rigid roof diaphragm than with a flexible roof. The four torsional moments around CM, $T_{CM,DY}$ due to Y-direction inertia forces, $T_{CM,DX}$ due to X-direction inertia forces, the total torsion moment $T_{CM,D}$ due to total inertia forces, and the total torsion moment $T_{CM,B}$ due to brace forces, all illustrated higher torsional effects in the rigid roof model. The relative offset of the centre of inertia ($X_{INERTIA}/L$) to the centre of mass, showed the same rule about the torsional effect. These effects can be more clearly observed from Table 6.11, the ratio of peak responses that were listed in Table 6.10.

Spectrum analysis results are not illustrated in these two Tables because the results in the peak horizontal shears in the vertical bracing bents in Table 6.7 are quite different from the other analysis methods. In addition, the spectrum analysis provides only the peak response for each node, for which the calculated torsional moment calculated does not promise to be the largest that can be obtained.

Table 6.10 Statistics of Peak Response

Model	Item	static	Seismic event No.										
			1	2	3	4	5	6	7	8	Mean	Mean+SD	Max
2-R	Sum inertia forces $F_{y,s-n}$ (kN)	833	1347	1446	1147	753	1078	1206	1044	1177	1150	1358	1446
	East Storey shear Fe (kN)	34.7	202.9	176.6	77.2	47.8	71.3	230.6	94.3	230.7	141.4	217.9	230.7
	Torsion N-S forces $T_{CM,DY}$ (MN-m)		12.96	7.65	5.25	2.44	5.52	10.32	6.95	13.01	8.01	11.81	13.01
	Torsion E-W forces $T_{CM,DX}$ (MN-m)		3.37	1.88	1.13	0.61	1.42	2.43	1.74	3.45	2.00	3.02	3.45
	Torsion inertia forces $T_{CM,D}$ (MN-m)	5.00	16.33	9.44	6.38	3.05	6.94	12.76	8.66	16.46	10.00	14.82	16.46
	Torsion brace force $T_{CM,B}$ (MN-m)	5.00	15.66	9.62	5.60	2.90	6.94	13.14	7.98	17.19	9.88	14.90	17.19
	XINERTIA/L to maximum $T_{CM,D}$	0.10	0.65	0.42	0.15	0.78	1.18	0.25	0.21	0.26	0.49	0.85	1.18
2-F	Sum inertia forces $F_{y,s-n}$ (kN)	832	1465	1384	1022	948	835	1187	1124	984	1119	1336	1465
	East Storey shear Fe (kN)	20.2	77.6	92.8	34.7	50.6	93.4	119.7	26.8	24.1	64.9	100.8	119.7
	Torsion N-S forces $T_{CM,DY}$ (MN-m)		4.15	5.51	1.81	3.21	4.98	8.11	1.33	1.57	3.83	6.18	8.11
	Torsion E-W forces $T_{CM,DX}$ (MN-m)		1.03	1.30	0.41	0.94	1.21	2.21	0.27	0.40	0.97	1.61	2.21
	Torsion inertia forces $T_{CM,D}$ (MN-m)	5.00	4.26	6.30	2.07	3.86	5.31	9.36	1.55	1.89	4.33	6.97	9.36
	Torsion brace force $T_{CM,B}$ (MN-m)	5.00	4.83	6.31	2.31	4.31	5.91	10.06	1.57	1.90	4.65	7.49	10.06
	XINERTIA/L to maximum $T_{CM,D}$	0.10	0.12	0.13	0.13	0.28	1.06	0.22	0.04	0.04	0.25	0.59	1.06

Note: the unit of torsion MN-m equals to 10^3 KN-m. West storey shear F_w is same as the East Storey shear F_e, so it is not listed.

Table 6.11 Ratio of Peak Response

Ratio	Item	Static	Dynamic		
			Mean	Mean +SD	Max
Flexible /Rigid	Sum inertia forces $F_{y,s-n}$ (kN)	0.998	0.973	0.984	1.013
	East Storey shear Fe (kN)	0.581	0.459	0.463	0.519
	Torsion N-S forces $T_{CM,DY}$ (MN-m)		0.478	0.523	0.623
	Torsion E-W forces $T_{CM,DX}$ (MN-m)		0.485	0.532	0.641
	Torsion inertia forces $T_{CM,D}$ (MN-m)	1.000	0.432	0.471	0.569
	Torsion brace force $T_{CM,B}$ (MN-m)	1.000	0.471	0.502	0.585
	XINERTIA/L to maximum $T_{CM,D}$	1.000	0.518	0.697	0.898

To summarise, for the torsion analysis of a regular building with a rigid roof such as that described in this Chapter, the equivalent static force procedure proposed by the 2005 NBCC seems appropriate. This can be verified by the following aspects:

1). The braces yielded as expected, but the "mean" value of peak ductility demand that was obtained from the eight ground motions was less than R_d=2.0, while the "mean+SD" value was around 2.0. Hence, the brace response was controlled.

2). The largest "mean+SD" peak storey drift (54.9 mm) is lower than $R_0R_d\Delta e$ (57.7 mm), and well below the Δ_{limit}=165 mm. Therefore, the check of storey drifts in the static procedure is adequate.

3). The torsional sensitivity ratio $B=\delta_{max}/\delta_{ave}$, by any of the methods, is smaller than 1.70, the upper limit given for use of the equivalent static method. It should also be noted that almost all the B values calculated by the dynamic methods were larger than

from the static analyses. It is quite possible that when the B value calculated from the static procedure is slightly lower than 1.70, say 1.50, it may be larger than 1.70 based on a dynamic analyses.

For a building with flexible roof diaphragm, it was found that the torsional effects will generally be reduced, including the torsional moment, the relative storey drifts, the brace forces perpendicular to the earthquake direction, and the offset of the centre of inertia from the centre of mass. However, the flexibility of the roof deck diaphragm will increase the maximum storey drift at mid-length of the building. It can also increase (not always) the ductility demand of the braces acting in the earthquake direction, although the mean values were still slightly smaller than R_d=2.0.

In current design practice, roof diaphragms are typically assumed as rigid, even if flexible roofs are used. In general, this practice is adequate, because the torsion effect with flexible roof becomes less. However, it is important to verify the maximum storey drift with a flexible roof, which can be done using a static or spectrum method.

The ductility demand for the braces on the less stiff side (south) is higher than on the stiffer side (north) of the building. The forces in the braces perpendicular to the earthquake obtained from the dynamic analysis method are much higher than those obtained from the static and spectrum analyses.

Comparing the linear static, non-linear static, spectrum, and dynamic methods mentioned above, the linear static method is very simple, and can even be done by hand calculations, although it cannot provide the real force distribution for some structural members. A non-linear static method improved such situations, but the torsion effect considered was not adequate, e.g. B and T_r values were too small. The

spectrum method is one kind of dynamic analysis that does not require significant computation time, however the resulting information should be limited to the elastic range. Furthermore, the force distribution calculated from the spectrum method is not consistent to that obtained for other analysis methods. The time-history dynamic method is the most comprehensive, however, it requires the longest computation time and in addition, a time step. Moreover, appropriate ground motions need to be selected and correctly scaled for the building period. In any structural analysis, the linear static or non-linear static method should be included, together with one or two dynamic methods.

CHAPTER 7

CONCLUSIONS AND RECOMMENDATIONS

7.1 GENERAL

In this study, the inelastic seismic behaviour of steel roof deck diaphragms under dynamic load conditions was researched using both experimental and analytical methods. The results of this investigation, together with former studies, have revealed that an appropriately connected steel roof deck diaphragm can act as an efficient energy-dissipating element during severe earthquakes. The inelastic capacity γ_p, and ductility demand μ_D on deck diaphragms, are influenced by many factors, including the deck profile shape, sheet length, sheet thickness, connection distribution, connection method and quality of installation, and the effects of non-structural components.

In the experimental component of this research, a total of 12 large-scale cantilever diaphragm tests were carried out. These tests allowed for a better understanding of the dynamic behaviour of steel roof deck diaphragms; provided new information with respect to actual roof diaphragm composition; and validated or improved the knowledge of the diaphragm properties and response.

In the analytical phase, which contains three separate sections, the structural dynamic response of a medium sized single-storey steel building was analysed with regard to the inelastic deck performance as well as the torsion effect due to a flexible roof. In

addition, the effects of non-structural components on deck stiffness and deck deformations was investigated using both non-linear and elastic approaches. The non-linear time history analyses were carried out using the Ruaumoko software program, whereas the torsion analyses relied on the DRAIN 2DX software, and the elastic non-structural component analyses incorporated the SAP 2000 program.

7.2 CONCLUSIONS

7.2.1 Experimental Studies

1) Effects of longitudinal overlapping

The longitudinal overlapping did not influence the shear strength to any significant extent, as indicated by the similar measured shear capacity for the 2 x 3 m and 6 m long specimens. In contrast, the shorter sheet length used with the overlap specimens significantly decreased the stiffness of the test diaphragms due to the panel warping. The load-deformation response exhibited more pronounced non-linear behaviour between 0.0 to maximum load. As compared to 6 m long specimen, for nail/screw connected deck, G' was approximately 39% smaller; for weld/button punch connected deck, it was reduced by nearly 29%.

For the nail/screw connected deck diaphragm tests, damage was typically limited to bearing, tearing and buckling of the sheet steel adjacent to frame fasteners. No nail shearing was observed for the Short Duration dynamic test, and only 5 nail failures were recorded for the monotonic tests. It was possible for the screw fasteners at side laps to cause bearing distortion in the sheet steel, and as well the fasteners would tilt to the extent that for some monotonically loaded specimens they were pulled out of

the steel panel. Both the deck-to-frame and side lap connection holes could be substantially elongated due to bearing stress from the fastener, which constitutes the main reason for the pinching phenomenon recorded for the reversed cyclic force-deformation hystereses.

For the weld/button punch connected diaphragm tests, the weld connections typically failed in a brittle fashion with minimal distortion of the surrounding sheet steel. Button punch connections were not able to provide a supplementary shear resistance once the welds had failed; a characteristic that was evident during the late phases of loading when the entire side lap lines had disconnected.

In general, most damage occurred along the side lap lines where the material is discontinuous. Along the longitudinal overlapping joint, where four sheets are interconnected, it was expected that the connection quality may not have been as good as at other positions. However, this phenomenon occurred only in one test. In the other three tests, the four sheet overlapping did not decrease the test diaphragm strength.

Based on the tests of P3615 panels with either the nail/screw or the weld/button punch connection scenario, the evaluation for the deck diaphragm strength and stiffness using the SDI (1987) procedure is appropriate. The SDI approach does not specifically consider the longitudinal overlap of panels; rather the effect of these overlaps is accounted for in the panel length term of the design method. Two approaches were utilized: 1) "SDI" for which the connection properties were obtained from the Diaphragm Design Manual SDI (1987), and 2) "SDI*" for which the connection properties were from the test results documented by Rogers and Tremblay (2000). It seems that the SDI* method overestimates the shear strength, S_u, for the

weld/button punch connected diaphragm, were the average ratio of test/SDI*for S_u is about 75%.

2) Effects of non-structural roofing materials

Testing of similar diaphragm specimens, two without roofing and two with roofing was carried out. The non-structural roofing materials in roof type SBS-34 (from AMCQ) that were attached to the deck panels by screws reinforce the diaphragm. This resulted in a 24% strength increase and a 49% stiffness increase compared with the test results of nominally identical bare steel specimens. Considering these bare steel diaphragms, the test results for strength were nearer to the SDI prediction, with the average ratio of test/SDI for S_u equal to 98%, while for test/SDI* ratio was about 116%. The test results for the stiffness were closer to that predicted using the SDI* method (89%), whereas the ratio of test to predicted SDI value was only 73%.

Repeated service level cyclic loading, whose maximum was about 48% of the ultimate capacity, P_u, evaluated using the SDI method, decreased the final strength (about -22%) but did not influence the stiffness of the bare sheet steel test diaphragm. Cyclic loading at the same force level as the bare steel diaphragm specimen exhibited no significant influence on the deck properties for the tests with non-structural components, because the ultimate shear strength of the diaphragm was measurably greater than the service level cyclic loads.

In the case of the roofed specimens, the failure modes for the deck panel and nails at the sheet ends were observed to be similar to that noted in the bare sheet diaphragm tests. No nail failure was inspected at the sheet ends.

For the roofing materials, except for the gypsum board, no detectable deformation was observed. For this reason it is was assumed that the other non-structural roofing materials had a negligible effect on the diaphragm performance.

Due to the strengthening effect of the non-structural components, most notably the gypsum layer, particular attention must be paid to the anticipated forces in the seismic force resisting system (SFRS) if the steel deck diaphragm is chosen as a weak link. The remaining structural members in the SFRS are designed to remain elastic, and hence should be stronger than the diaphragm. At this time, designers may encounter a problem concerning the strengthening and stiffening effect of the roofing components on the diaphragm, since these non-structural components have not been thoroughly studied. If the influence of the roofing material is not considered then the possibility exists that the diaphragm will not yield and dissipate dynamic energy as expected, rather other structural members in the SFRS may fail first. Therefore, the practical application of the steel deck diaphragm as the weak link in the SFRS still requires basic and quantifiable information on the effect of typical roofing components.

The roof strengthening characteristic could also be incorporated into the seismic design method for buildings designed with the lateral braces as the weak link in the seismic force resisting system. Instead of adjusting the diaphragm thickness or connector pattern to accommodate for the actual brace strength, the non-structural roofing components could be relied on to provide a greater diaphragm capacity. But this practice is still not recommended at the time being because the strengthening effect due to roofing materials is not thoroughly investigated.

3) Effect of different nail/screw manufacturers

Hilti Corp. and ITW Buildex Inc. provided the fasteners for the nail/screw diaphragm tests. The test results showed that strength levels were similar for the diaphragms, although the diaphragm using ITW Buildex fasteners appeared more flexible having a rigidity 16 % lower than the Hilti fastened specimen. This is in line with the results of connection tests carried out by Rogers and Tremblay (2000), where the shear stiffness for 0.91 mm deck-to-frame connections was 18.7 kN/mm for the ITW BX-14 nails, compared with 23.9 kN/mm for the Hilti X-EDNK22-THQ12 nails. It should also be noted that the measured shear strength for these two nails in the deck-to-frame connections was similar.

A comparison of the nail/screw diaphragm test results to the SDI designs shows similar situations to those discussed above.

4) Effects of 76 mm series panels

In terms of in-plane diaphragm shear properties the 76 mm series panel deck, connected with welds and button punches, was weaker than the 38 mm series panel deck. A 15% decrease in capacity was measured for the 0.76 mm thick sheets and a 35% decrease for the 0.91 mm thick sheets. The stiffness of the 76 mm series panel deck was also much lower than the 38 mm series panel deck. For both the 0.76 and 0.91 mm thick panels, a decrease of nearly 66% was recorded. The decrease in strength may have resulted from the weld quality, because the deeper flutes made the

welding operation more difficult than for the 38 mm series decks. The lower stiffness is mainly due to the increased warping deformation of the taller profile deck panel.

The test results for strength were closer to the evaluation provided using the SDI design method. For the 0.76 mm sheets the average ratio of test/SDI for S_u was about 91%, while the ratio of test/SDI* was close to 75%. In terms of the 0.91 mm sheets the average ratio of test/SDI for S_u was 104%, while for test/SDI* a value of 74% was obtained.

The stiffness determined using the SDI procedures over-estimated the measured test values. Concerning the 0.76 mm sheets, the average ratio of test/SDI for G' was 71%, while for the test/SDI* ratio was 75%. Similarly for the 0.91 mm sheets, ratios of 69% and 80% were obtained for the SDI and SDI* methods, respectively.

Most of the failure modes that were observed fell in the category of brittle weld fracture. As well, the button punch side lap connections disconnected soon after the welds at frame locations failed. As with the 38 mm deep welded diaphragms, this led to the sudden and complete separation of the side lap lines, and hence almost no residual shear capacity. For this reason it is suggested that the 76 mm series panels with welded/button punch connections be designed to remain elastic during seismic loading.

7.2.2 Analytical Studies

1) Inelastic Deck Response

A 30x60x6.6 m medium sized single-storey steel building located in Victoria, B.C. was designed following the CSA-S16 Limit States Design of Steel Structures Standard (2001) and the 2005 NBCC. A nail/screw connected steel roof deck diaphragm was specified and designed to be the weak link in SFRS, considering two R_d values (2.0 and 3.0). A study of the performance of this building when subjected to three different earthquake records, which were anticipated to cause the most extensive inelastic deformation of the roof diaphragm, was completed.

According to the studies, with respect to the buildings designed with an R_d=3.0, the ductility demand on deck elements exceeded the anticipated value of 3.0. The ductility demand ranged from 3.17 to 13.6, which is significant considering the level expected. For roof type 1 (no end lap, no roofing), the maximum inelastic distortion exceeded the allowable inelastic distortion (γ_p=10 rad/1000), while for roof type 2 (with end lap, no roofing) and roof type 3 (no end lap, with roofing), the computered maximum inelastic distortions were below the limitation. From this information, it seems that the use of R_d=3.0 is not advised for roof type 1, but may be used for the design in the future for the other two roof types,

It was also revealed, through the analyses results, that for the R_d=3.0 case with roof type 1, a structure which is designed with the deck diaphragm as the seismic energy dissipating element, may also experience a limited inelastic response in the brace members. This result might be obtained because of damping effect and the shear

forces in the joists. It also suggests that the margin 10% for the designed capacity of braces higher than decks may be not enough to keep the braces elastic.

For the R_d=2.0 designed structure, the ductility demand on the deck elements ranged from 1.24 to 2.75 with an average value of 1.81. Although these results are not fully consistent in an overall sense, they were near the anticipated value of 2.0; and furthermore exhibited a greater degree of consistency if only one roof type was considered. These analytical findings provide additional evidence that an R_d=2.0 can be used for the inelastic design of 38 mm series deck panel with nail/screw connections as was proposed by Martin (2002).

2) Torsion Effect for Buildings with Flexible Roof Diaphragm

The torsion effect was studied using another 30x60x6.6 m medium sized single-storey steel building located in Victoria, B.C. The same design codes as in the former inelastic deck analysis were utilized, however the deck was chosen to be stronger than the vertical braces and hence remain elastic. Two roof cases: (rigid roof with in-plane shear stiffness G'=6.4 x 10^6 kN/mm and flexible roof with G'=6.4 kN/mm), three analysis methods: (static, spectrum and dynamic time-history analysis), and eight ground motions were considered. The stiffness eccentricity was introduced into the model by specifying that the brace stiffness along one of the building sides was 1.5 times greater than that along the opposing side.

The study showed that a flexible roof diaphragm usually decreases the torsion effect. For example, the mean value of the torsional moment, $T_{CM,D}$, due to the eight ground motions reduced from 10.0 MN*m to 4.33 MN*m; and the difference of storey drifts in the two walls changed from 26.9 mm to 19.4 mm. Furthermore, the average force

in the braces perpendicular to the earthquake direction decreased by 54%, and the relative offset of the centre of inertia force from the centre of mass changed from 0.49 to 0.25.

In contrast, the flexible roof diaphragm caused an increase in the storey drift; the mid-length storey drifts were 2 to 4 times higher than found for the rigid diaphragm case. The deck diaphragm was also largely distorted in the flexible roof building. The roof flexibility may also have increased the ductility demand on the braces, the mean values ranged from 1.69 to 1.91 in the flexible roofed building and from 1.25 to 1.71 in the rigid roofed building.

In current design practice, roof diaphragms are typically assumed as rigid, even if flexible roofs are used. In general, this practice is adequate, because the torsion effect becomes less, however, it is important to verify the maximum storey drift and the ductility demand for the braces. It is recommended that, for any building analysis, either with rigid roof or flexible roof, the linear static or non-linear static method should be included, but one or two dynamic methods should also be carried out at the same time.

3) Effects of non-structural components

A simple static and linear FEM analysis of a diaphragm with roofing components was carried out as a first step to economically and efficiently analyse the force distribution in the connections between different materials under in-plane shear forces, and to simulate the reinforcement from non-structural materials. The study suggests that the non-structural components in a AMCQ SBS-34 roofing configuration with 12 fasteners per gypsum board can increase the shear stiffness of the diaphragm by 1.0 to

1.8 kN/mm. The stiffening effect can mainly be attributed to the gypsum board. The non-uniform force distribution in connections due to the connection positions and stiffness helps to explain the progressive yielding in resistance.

7.3 LIMITATIONS AND RECOMMENDATIONS

1) Test investigation

The mechanical shear and bending properties for the roofing materials should be identified through testing, especially for the gypsum board and its connections. It is suggested that a large-scale diaphragm test with only gypsum board above the steel panels be carried out. This would provide information to compare with the results described in this thesis to see if the effects from other roofing materials could be ignored. Measure shear deformations in roofing materials to determine whether they are involved or not. A series of tests comprising the 3 m long overlap specimen with 0.91 mm steel sheet thickness is also suggested to verify the roof type 2 configuration in the inelastic diaphragm analysis segment.

On-site measurements are recommended to investigate the overall dynamic properties of a typical single-storey building, which include the natural period, the response forces in structural members, the storey drifts, the diaphragm distortion, etc. This information could then be compared with the results of the non-linear time history results, and improvements to the modeling techniques could be forthcoming.

2) Structural analysis

The Wayne Stewart degrading stiffness hysteresis used in the inelastic analysis of the steel deck diaphragm should be improved to better reflect the real force-displacement relationships. The inelastic dynamic analysis for non-rectangular deck diaphragms should also be considered.

The 3D FEM elastic analysis finished by the author is an elementary step. It needs to be improved with the inclusion of accurate values for the mechanical shear parameters of the non-structural components.

A study of the torsional effect caused by strength asymmetry in a building, combined with the stiffness/strength asymmetry should also be carried out.

REFERENCES

ABEC, (1985). Building Envelope Failures: Causes and Remedial Measures, Seminar No. 2 – Roofs. Alberta Building Envelope Council (ABEC), Calgary, Alberta, Canada.

ADAMS, J., W EICHERT, D., AND HALCHUK, S. (1999). Trial Seismic Hazard Maps of Canada – 1999: 2%/50 Year Values for Selected Canadian Cities. Geological Survey of Canada Open File 3274, National Earthquake Hazards Program, Geological Survey of Canada, Natural Resources Canada, Ottawa, Ont.

ADAMS, J. AND ATKINSON, G. (2003). Development of seismic hazard maps for the proposed edition of the National Building Code of Canada. Can. J. Civ. Eng. 30: 255-271.

AISI, (1967). American Iron and Steel Institute. Design of Light Gage Steel Diaphragm. New York, N.Y. USA.

AMERICAN IRON AND STEEL INSTITUTE (1997). 1996 Edition of the Specification for the Design of Cold-Formed Steel Structural Members. Washington, DC, USA.

AMERICAN SOCIETY FOR TESTING AND MATERIALS, A370. (2002). Standard Test Methods and Definitions for Mechanical Testing of Steel Products. Philadelphia, PA, USA.

AMERICAN SOCIETY FOR TESTING AND MATERIALS, A653. (2002). Standard Specifications for Steel Sheet, Zinc-Coated (Galvanized) or Zinc-Iron Alloy-Coated (Galvannealed) by the Hot-Dip Process. Philadelphia, PA, USA.

AMERICAN SOCIETY FOR TESTING AND MATERIALS, E455. (2002). Standard Test Method for Static Load Testing of Framed Floor or Roof Diaphragm Construction for Buildings. West Conshohocken, PA, USA.

AMERICAN SOCIETY FOR TESTING AND MATERIALS, Vol. 04.04, (2001a). Annual Book of ASTM Standards - Roofing, Waterproofing and Bituminous Materials. West Conshohocken, PA, USA.

AMERICAN SOCIETY FOR TESTING AND MATERIALS, Vol. 04.06, (2001b) Annual Book of ASTM Standards - Thermal Insulation, Environmental Acoustics. West Conshohocken, PA, USA.

ASHBY, Michael F. (1999). Materials Selection in Mechanical Design. Second edition. Butterworth-Heinemann, Oxford, England.

BAKER, M. C. (1980). Roofs----Design, Application and Maintenance. Sponsored by the National Research Council of Canada, Montréal, QC, Canada

BÉRAIR, T. (1999). Étude expérimentale sur le comportement sismique de bâtiments d'un seul étage en acier avec diaphragme de toit flexible. École Polytechnique de Montréal, Montréal, QC, Canada.

BOND, W.F., ROGERS, C.A., TREMBLAY, R., (2001). Seismic Performance of Arc-Spot Weld Deck-to-Frame Connections. 3rd International Conference on Thin-Walled Structures, Kraków, Poland, 357-364.

BRUNEAU, M., MAHIN, S.A. (1991) Seismic Response of Symmetric Structures Having Unbalanced Yield Strength in Plan. 6th Canadian Conference on Earthquake Engineering, (1991) Toronto, ON, Canada. P109-116.

BRYAN, E.R. (1972). The Stressed Skin Design of Steel Building. Constrado Monographs, Crosby Lockwood Staples, London, England.

BSSC (1997). NEHRP Recommended Provisions for Seismic Regulations for New Buildings and Other Structures. Federal Emergency Management Agency Report FEMA 302, Building Seismic Safety Council, Washington, DC, USA.

CANAM (1999). Steel deck. Canam Manac Gr, www.canammanac.com.

CANADIAN STANDARDS ASSOCIATION, CSA (1992). CAN/CSA-G40.20/G40.21-92. General Requirements for Rolled or Welded Structural Quality Steel/Structural Quality Steels. Etobicoke, Ont., Canada.

CANADIAN STANDARDS ASSOCIATION, CSA (1994). CAN/CSA-S136. Cold Formed Steel Structural Members. Etobicoke, Ont., Canada.

CANADIAN STANDARDS ASSOCIATION, CSA (1994). CAN/CSA-S16. Limit States Design of Steel Structures. Etobicoke, Ont., Canada.

CANADIAN STANDARDS ASSOCIATION, CSA (2001). CAN/CSA-S16. Limit States Design of Steel Structures. Etobicoke, Ont., Canada

CANADIAN SHEET STEEL BUILDING INSTITUTE, CSSBI (1991). Design of Steel Deck Diaphragms. B13-91, Cambridge, Ont., Canada.

CANADIAN SHEET STEEL BUILDING INSTITUTE, CSSBI (1996). Standard for Steel Roof Deck. CSSBI 10M-96, Cambridge, Ont., Canada.

CARR, A.J. (2000). RUAUMOKO – Inelastic Dynamic Analysis. Version March 15th 2000. Dept. of Civil Eng., University of Canterbury, Christchurch, New Zealand.

CHOCKALINGAM, C., FAZIO, P., HA, K., (1978). Strength of Cold Formed Steel Shear Diaphragms. Recent Research and Developments in Cold-Formed Steel Structures, the Fourth International Speciality Conferences on Cold-Formed Steel Structures, 1978, Vol. II. Univ. of Missouri-Rolla, MO, USA.

CHOPRA, A.K. (2001). Dynamics Of Structures: Theory And Applications To Earthquake Engineering. Prentice-Hall Inc., Upper Saddle River, NJ, USA.

CHOWN, G.A. (1990). Roof Function, Requirement, and Components. Construction Canada 32(1), p6-10, 13-14. National Research Council Canada, Ottawa, Ontario, Canada.

COMPUTERS AND STRUCTURES, INC. (2002). SAP2000 Version 8.0, Integrated Finite Element Analysis and Design of Structures. Berkeley, CA, USA.

DAVIES, J.M., BRYAN, E.R. (1982). Manual of Stressed Skin Diaphragm Design. John Wiley and Sons Inc., New York, NY, USA.

ESSA, H.S., TREMBLAY, R., ROGERS, C.A. (2001). Inelastic seismic behaviour of steel deck roof diaphragms under quasi-static cyclic loading. Report no. EPM/CGS-2001-11. Department of Civil, Geological and Mining Engineering, École Polytechnique de Montréal, Montréal, QC, Canada.

ESSA, H.S., TREMBLAY, R., ROGERS, C.A., (2003). Behavior of Roof Deck Diaphragms Under Quasi-Static Cyclic Loading. *Journal of Structural Engineering, ASCE, Vol. 129 No. 12, 1658-1666.*

FLEISCHMAN, R.B., FARROW, K.T. (2001). Dynamic behavior of perimeter lateral-system structures with flexible diaphragms. Earthquake engineering and structural dynamics, **30**: 745-763.

FORD W.H. AND. TOPP, W.R.(1998). Introduction to Computing with C++ and Object Technology. Prentice Hall, Upper Saddle River, NJ, USA

FREEMAN S .A. (1977). Racking Tests of High-Rise Building Partitions. J. of the Structural Division, ASCE (103) (ST8): 1673-1685.

FUNG, C., (1978). Shear Strength of Puddle Welds in Gauge Metal Construction. Final Report on Project 373 for the Canadian Steel Industries Construction Council, Westeel-Rosco Limited.

GOEL, R.K., CHOPRA, A.K., (1990) Inelastic Seismic Response of One-Story, Asymmetric-Plan Systems. Report No. UCB/EERC-90/14. Earthquake Engineering

Research Center, College of Engineering, University of California at Berkeley, Berkeley, CA, USA.

GRAHAM M. S. (1999). Technology Today --- Properties of Rigid Roof Insulation. Professional Roofing, published by National Roofing Contractors Assoc. (NRCA), May 1999. www.professionalroofing.net.

GRIFFIN C. W. (1982). Manual of Built-up Roof Systems. Second Edition. McGraw-Hill ltd. New York, NY USA.

G-P GYPSUM CORPORATION (2000). Gypsum Product Catalog. www.gp.com

HILTI (2001). Hilti North America. Product Technical Guide-2001 Edition. Hilti Corporation, Schaan, Principality of Liechstenstein.

ICBO (2002a). Steel Deck Diaphragms Attached with TEKS and I.C.H. Traxx Screws (ER-3056). ICBO Evaluation Service Inc. Whittier, CA, USA.

ICBO (2002b). Roof Decks---Diaphragm Shear Values (ER-2078P). ICBO Evaluation Service Inc. Whittier, CA, USA.

ICBO (2003). Steel Deck Diaphragms Attached with Buildex BX14 or BX12 Fasteners and Traxx or I.C.H. Traxx Screws (ER-4254). ICBO Evaluation Service Inc. Whittier, CA, USA.

ITWBuildex (1993). Building Ideas That Work----BX 12TM and BX 14TM. www.itwbuildex.com/BX12and14.htm,

JAIN, S.K., JENNINGS, P.C. (1985). Analytical Models for Low-Rise Buildings with Flexible Floor Diaphragms. Earthquake Engineering and Structural Dynamics, Vol. 13, 225-241 (1985).

JU, S.H., LIN, M.C. (1999). Comparison of Building Analyses Assuming Rigid or Flexible Floors. Journal of Structural Engineering, ASCE, **125:** P.25-31.

KLINGLER, C.J., (1986). The Strength and Flexibility of Mechanical Connectors in Steel Shear Diaphragms. M.Sc. Thesis West Viginia Univ. Morgantown, WV, USA.

MARTIN, E. (2002). Inelastic Response of Steel Roof Deck Diaphragms Under Simulated Dynamically Applied Seismic Loading. Masters Thesis, Dept. of Civil, Geological and Mining Engineering, École Polytechnique, Montreal, Canada.

MAZZOLANI, F.M., LABINI, F.S. (1983). Skin-Frame Interaction In Seismic Resistant Steel Structures. Costruzioni Metalliche, 4, pp.212-225.

MAZZOLANI, F.M. (1994). Thin-Walled Metal Construction: Research, Design and Codification. Proc. of the 1994 SSRC Conf., Structural Stability Research Council, Bethlehem, PA, USA.

MAZZOLANI, F.M., DE MATTEIS, G., LANDOLFO, R. (1997). Dynamic behaviour of sandwich diaphragms in simple pin-jointed steel frames. Proceedings, Behaviour of Steel Structures in Seismic Areas, STESSA 1997, Kyoto, Japan.

MCGUIRE, W., GALLAGHER, R.H., (1979). Matrix Structural Analysis. John Wiley & Sons, Inc. New York, NY, USA.

MEDHEKAR, M.S. (1997). Seismic Evaluation of Steel Buildings with Concentrically Braced Frames. Ph.D. Thesis, Dept. of Civil and Environmental Engineering, Univ. of Alberta, Edmonton, Alberta, Canada.

MEDHEKAR, M.S., KENNEDY, D.J.L. (1999a). Seismic Evaluation of Single-storey Steel Buildings. Canadian Journal of Civil Engineering, **26** P.379- 394.

MEDHEKAR, M.S., KENNEDY, D.J.L. (1999b). Seismic Response of Two-Storey Buildings with Concentrically Braced Steel Frames. Canadian Journal of Civil Engineering, **26** P.497- 509.

MITCHELL, D. et al (2003). Seismic force modification factors for the proposed 2005 edition of the National Building Code of Canada. Can. J. Civ. Eng. 30: 308-327.

NEDISAN, C. (2002). Comportement sismique de bâtiments en acier d'un seul étage avec diaphragme de toit flexible. Masters Thesis, Dept. of Civil, Geological and Mining Engineering, École Polytechnique de Montréal, Montréal, QC, Canada.

NEWMAN, Alexander, (1997). Metal Building System. McGraw-Hill, New York, N.Y. USA.

NILSON, A.H. (1960). Shear Diaphragm of Light Gage Steel. Journal of the Structural Division, Proceedings of the American Society of Civil Engineers, Vol.86, No. ST 11, P111-139.

NRCC (1989) Roofs That Work. Building Science Insight '89, National Research Council of Canada, Ottawa, Ontario, Canada.

NRCC (1995). National Building Code of Canada 1995 (NBCC). 11th ed.. Canadian Commission on Building and Fire Codes, National Research Council of Canada, Ottawa, Ontario, Canada.

NRCC (2001). Proposed changes to NBCC 1995 - Part 4. National Research Council of Canada, Institute for Research in Construction, Ottawa, Ontario, Canada.

PATTERSON S.; MEHTA M. (2001). Roofing Design and Practice. Prentice Hall Inc, Upper Saddle River, NJ, USA.

PEULER, M. (2002). Inelastic response of arc-spot welded deck-to-frame connections for steel roof deck diaphragms. Master's Degree Project Report, Department of Civil Engineering and Applied Mechanics, McGill University, Montreal, QC, Canada.

PEULER, M., ROGERS, C.A., TREMBLAY, R., (2002a). Inelastic Response of Arc-Spot Welded Deck-to-Frame Connections for Steel Roof Deck Diaphragms. Research Report No. G01-03, Department of Civil Engineering & Applied Mechanics, McGill University, Montreal, Canada.

PEULER, M., ROGERS, C.A., TREMBLAY, R., (2002b). Inelastic Response of Arc-Spot Welded Deck-to-Frame Connections for Steel Roof Deck Diaphragms. 16th International Specialty Conference on Cold-Formed Steel Structures, Orlando, USA, 763-778.

PRAKASH, V., POWELL, G.H., CAMPBELL, S. (1993). DRAIN-2DX Base Program Description and User Guide. Version 1.10, Report No. UCB/SEMM-93/17, Berkeley, CA, USA.

ROGERS, C.A., TREMBLAY, R. (2000). Inelastic seismic response of frame and side-lap fasteners for steel roof decks. Research Report No. EPM/CGS-2000-09, Department of Civil, Geological and Mining Engineering, École Polytechnique de Montréal, Montréal, QC, Canada.

ROGERS, C.A., TREMBLAY, R., (2003a). Inelastic Seismic Response of Side Lap Fasteners for Steel Roof Deck Diaphragms. *Journal of Structural Engineering, ASCE, Vol. 129 No. 12, 1637-1646.*

ROGERS, C.A., TREMBLAY, R., (2003b). Inelastic Seismic Response of Frame Fasteners for Steel Roof Deck Diaphragms. *Journal of Structural Engineering, ASCE, Vol. 129 No. 12, 1647-1657.*

SHEPHERD, R., DONALD R.A.H. (1967). The Influence of in-Plane Floor Flexibility on the Normal Mode Properties of Buildings. Journal of Sound Vibration (1967) 5 (1), 29-36.

STEEL DECK INSTITUTE, SDI (1981). Diaphragm Design Manual. Canton, OH, USA.

STEEL DECK INSTITUTE, SDI (1991). Diaphragm Design Manual. Second Edition. Canton, OH, USA.

STEWART, W.G. (1987). The Seismic Design of Plywood Sheathed Shear Walls. Ph.D. Thesis, Department of Civil Engineering, University of Canterbury, Christchurch, New Zealand.

TENA-COLUNGA, A., ABRAMS, D.P. (1996). Seismic Behaviour of Structures with Flexible Diaphragms. Journal of Structural Engineering, ASCE, **122**: 439-445.

TREMBLAY, R. (1996). Influence of In-Plane Flexibility of Roof Diaphragm on the Seismic Response of Single-Storey Braced Frames. Paper No. 1100, 11th World Conference on Earthquake Engineering. Elsevier Science Ltd.

TREMBLAY, R. (1998). Development Of Design Spectra For Long-Duration Ground Motion from Cascadia Subduction Earthquakes. Canadian Journal of Civil Engineering, **25**: 1078-1090.

TREMBLAY, R. (2001). Seismic Behaviour and Design of Concentrically Braced Steel Frames. AISC Eng. J., 38 (3), 148-166.

TREMBLAY, R., ATKINSON, G.M. (2001). Comparative Study of the Inelastic Seismic Demand of Eastern and Western Sites. Earthquake Spectra, 17(2): 333-358.

TREMBLAY, R., BÉRAIR, T. (1999). Shake Table Testing of Low-Rise Steel building with Flexible Roof Diaphragm. Proc. 8th Can. Conf. on Earthquake Eng., Vancouver, B.C., 585-590.

TREMBLAY, R., LACERTE, M. (2002). Influence of the properties of bracing members on the seismic response of concentrically braced steel frames. Proc. of the 12th European Conference on Earthquake Engineering, Oxford, Elsevier: Paper Reference 481.

TREMBLAY, R., ROGERS, C., ESSA, H.S., MARTIN, E. (2002). Dissipating Seismic Input Energy in Low-Rise Steel Building Through Inelastic Deformations in the Metal Roof Deck Diaphragm. 4th Structural Specialty Conference of the Canadian Society for Civil Engineering, Montréal, QC, Canada.

TREMBLAY, R., ROGERS, C., NEDISAN, C. (2002). Use of Uniform Hazard Spectrum and Computed Period in the Seismic Design of Single-Storey Steel Structures. Proc. 7th U.S. National Conference on Earthquake Engineering, Boston, MA.

TREMBLAY, R., ROGERS, C.A., NEDISAN, C., (2003). Seismic Torsional Response of Single-Storey Steel Structures with Flexible Roof Diaphragms. Advances in Structures, Hancock et al. (eds), Swets & Zeitlinger, Sydney, Australia, 1299-1305.

TREMBLAY, R., STIEMER, S.F. (1996). Seismic Behaviour of Single-storey Steel Structures with a Flexible Roof Diaphragm. Canadian Journal of Civil Engineering, **23** P.49-62.

TRI-SERVICE TECHNICAL MANUAL (1982). Seismic Design for Buildings. Depts. of Army, Navy and Air Force, US Government Printing Office, Philadelphia, PA, USA.

US ARMY CORPS OF ENGINEERS (1998). Seismic Design for Buildings. Engineering Division, Directorate of Military Programs, Washington, DC, USA. www.hnd.usace.army.mil/techinfo/ti.htm

YARNELL, R.S., PEKOZ, T., (1973). Tests on Field Weld Puddle and Fillet Welded Connection. Department of Structural Engineering, Cornell Univ. Ithaca, NY, USA.

ZIENKIEWICZ, O.C. (1977). The Finite Element Method. Third edition. McGRAW-HILL Book Company (UK) Ltd. Maidenhead, Berkshire, England.

APPENDIX 1: MATERIAL TEST RESULTS

The material properties of the steel sheets in the large-scale diaphragm tests (Table 4.2 of Section 4.1.6) were the same as found for Martin (2002) because the deck panels were from the same coil (tests 38 to 42).

For tests 43 to 49, the deck panels were from different coils. To verify that these materials conformed to ASTM A653M (2002), tension coupon specimens were tested according to ASTM A370 (2002). Four specimens were prepared and tested for each group in case some results might be not usable.

Table A1.1 Tension Coupon Tests

Group		Width	Coated Thickness	Uncoated Thickness	Ultimate load	Elongation	Yield stress	Ultimate stress	Young's modulus	% Elongation
		mm	mm	mm	N	mm	Mpa	Mpa	Mpa	
P3615/ 0.76 mm	1	12.5	0.76	0.72	3359	19.2	314	373	174462	38.4
	2	12.5	0.77	0.72	3398	18.2	314	378	196035	36.4
	3	12.5	0.77	0.72	3402	18.2	320	378	201237	36.3
	4	12.5	0.75	0.71	3369	17.4	322	380	210344	34.8
	Mean	12.5	0.76	0.72	3382	18.3	317	377	195520	36.5
	C.o.V.	0.00066	0.0109	0.0060	0.0054	0.0354	0.0110	0.0069	0.0675	0.0354
P2436/ 0.76 mm	1	12.5	0.78	0.74	3519	N/A	319	382	184600	N/A
	2	12.5	0.79	0.74	3523	N/A	316	382	187836	N/A
	3	12.4	0.78	0.73	3516	14.4	324	389	195161	28.72
	4	12.5	0.76	0.73	3529	15.0	325	387	171394	29.92
	Mean	12.4	0.78	0.74	3522	14.7	321	385	184748	29.32
	C.o.V.	0.00347	0.0140	0.0068	0.0014	0.0205	0.0107	0.0079	0.0466	0.0205
P2436/ 0.91 mm	1	12.5	0.91	0.86	4099	N/A	313	380	202282	N/A
	2	12.5	0.91	0.87	4123	N/A	319	379	N/A	N/A
	3	12.4	0.89	0.86	4062	13.5	314	380	N/A	26.90
	4	12.5	0.90	0.87	4054	15.1	N/A	373	N/A	30.28
	Mean	12.5	0.90	0.87	4085	14.3	316	378	202282	28.59
	C.o.V.	0.0031	0.0092	0.0058	0.0068	0.0591	0.0084	0.0084	0.0000	0.0591

Note: Elongation is based on 50 mm gauge.

APPENDIX 2: THE INSTALLATION QUALITY OF STRUCTURAL CONNECTORS

The intent of listing the installation quality of structural connectors is for future re-evaluation of test results and to explain some abnormal phenomenon relating to unexpected installation quality.

The qualified nail head standoff (NHS) is from 5.0 to 9.5 mm. All nails were measured after installation. Any nail whose head height was out of this range was deemed as not qualified and was removed and reinstalled. Prior to a test, all nailed connections conformed to this requirement.

The nominal diameter of welded connection was 16 mm. All diameters were measured after welding. The weld quality is represented by equivalent weld diameter in Table 4.21, which has been corrected with connection efficiency. The so-called connection efficiency is the percent of connected circumference, evaluated visually by the author. The equivalent diameter equals the measured diameter modified by connection efficiency.

General notes:

1. Bold typed values in all following Tables represent fasteners are at side-laps.
2. Italic typed values in all following Tables represent connections were reinstalled since the original installation was not qualified.
3. The values for both north side and south side fasteners are not shown because they will endure only very small deformations and remain elastic all the time.

Table A2.1 Test 38: Nail installation quality index (stand off height)

Test 38

The nail install quality index before replaced

Position	1	6	11	16	21	Average	C.o.V.
B	7.08	7.61	8.14	6.41	7.79	7.41	0.09
C	6.82	6.91	7.02	8.91	9.66	7.86	0.17
D	**10.09**	**9.25**	**7.78**	**8.62**	**9.44**	**9.04**	0.10
E	7.08	7.18	7.46	7.48	8.99	7.64	0.10
F	8.68	7.02	8.42	6.74	7.33	7.64	0.11
G	**8.23**	**7.95**	**N/A**	**6.07**	**N/A**	**7.42**	0.16
H	8.10	6.74	7.02	6.67	7.56	7.22	0.08
I	9.54	7.51	9.01	7.01	8.80	8.37	0.13
J	**9.55**	**8.43**	**8.77**	**7.47**	**7.73**	**8.39**	0.10
K	9.67	6.09	7.40	8.48	N/A	7.91	0.19
L	7.05	9.08	6.77	7.19	N/A	7.52	0.14
Average	8.35	7.62	7.78	7.37	8.41	7.86	0.12
C.o.V.	0.147	0.130	0.100	0.128	0.109		
					At sidelap	8.28	0.12
					Except Sidelap	7.70	0.13

Table A2.2 Test 39---Final nail installation quality index (stand off height)

Test 39

The nail install quality index after replaced

Position	1	6	11	16	21	Average	C.o.V.
B	6.39	6.43	7.93	6.06	7.77	6.92	0.13
C	**8.65**	**6.03**	**8.48**	**7.11**	**6.69**	**7.39**	0.15
D	8.44	7.92	5.66	6.24	5.72	6.80	0.19
E	5.27	5.87	6.39	5.44	7.02	6.00	0.12
F	**6.28**	***5.45***	**7.31**	**6.41**	**6.65**	**6.42**	0.10
G	6.65	5.67	6.35	7.20	9.34	7.04	0.20
H	5.64	6.22	6.11	5.88	8.71	6.51	0.19
I	**6.84**	**6.98**	**7.85**	***8.67***	**7.05**	**7.48**	0.10
J	*N/A*	9.30	6.83	6.25	5.94	7.08	0.22
K	6.76	5.75	6.62	6.35	*6.26*	6.35	0.06
L	**6.61**	**6.38**	**7.96**	**6.72**	**6.41**	**6.82**	0.10
M	6.65	5.41	7.67	6.18	7.40	6.66	0.14
Average	6.74	6.45	7.10	6.54	7.08	6.79	0.14
C.o.V.	0.157	0.185	0.125	0.131	0.158		
					At sidelap	7.03	0.11
					Except Sidelap	6.67	0.16

Table A2.3 Test 40--- Final nail installation quality index (stand off height)

Test 40

The nail install quality index after replaced

Position	1	6	11	16	21	Average	C.o.V.
B	6.93	7.05	6.91	5.40	5.31	6.32	0.14
C	**6.66**	**6.32**	**6.19**	**5.74**	**6.28**	**6.24**	0.05
D	5.30	5.28	6.75	6.70	5.40	5.89	0.13
E	5.90	6.14	7.69	4.85	6.08	6.13	0.17
F	**6.08**	***5.73***	***6.96***	**6.53**	**5.24**	**6.11**	0.11
G	5.42	5.02	6.97	5.09	5.62	5.62	0.14
H	5.53	6.26	6.13	5.31	4.54	5.55	0.12
I	**6.38**	**6.56**	**6.62**	***5.92***	**6.47**	**6.39**	0.04
J	5.05	5.68	6.32	5.30	*5.46*	5.56	0.09
K	5.16	5.92	8.47	5.13	5.03	5.94	0.25
L	**6.85**	**8.04**	***5.83***	***5.19***	**5.03**	**6.19**	0.20
M	5.20	6.06	8.03	6.37	9.01	6.93	0.22
Average	5.87	6.17	6.91	5.63	5.79	6.07	0.14
C.o.V.	0.109	0.128	0.122	0.114	0.208		
					At sidelap	6.23	0.10
					Except Sidelap	5.99	0.16

Table A2.4 Test 41---Weld diameter (measured and equivalent)

Test 41

The Weld diameter measured

Position	1		6		11		16		21	Average	C.o.V.
B	13.87		17.09		15.51		18.30		16.47	16.25	0.10
C (north)	**17.52**		**17.12**		**18.26**		**18.51**		**18.36**	**17.95**	**0.03**
C (South)	**18.95**		**19.71**		**16.69**		**19.62**		**18.91**	**18.78**	**0.07**
D	14.89		14.06		17.19		14.56		15.91	15.32	0.08
E	15.32		15.72		16.59		15.19		18.24	16.21	0.08
F (north)	**20.26**		**18.67**		**21.21**		**17.62**		**17.32**	**19.02**	**0.09**
F (South)	**17.66**		**18.95**		**16.77**		**18.47**		**17.97**	**17.96**	**0.05**
G	16.43		15.20		15.38		15.72		15.91	15.73	0.03
H	15.60		14.30		16.02		15.70		16.58	15.64	0.05
I (north)	**16.13**		**17.43**		**19.01**		**19.29**		**14.61**	**17.29**	**0.11**
I (South)	**17.39**		**17.94**		**19.83**		**17.81**		**20.13**	**18.62**	**0.07**
J	16.93		15.96		17.50		16.67		16.28	16.67	0.04
K	19.81		15.01		16.51		18.15		15.92	17.08	0.11
L (north)	**19.91**		**19.82**		**15.96**		**20.08**		**18.68**	**18.89**	**0.09**
L (South)	**20.34**		**18.22**		***18.47***		**19.71**		**15.09**	**18.37**	**0.11**
M	14.82		14.31		15.13		14.65		13.87	14.56	0.03
Average	17.24		16.84		17.25		17.50		16.89	17.15	0.07
C.o.V.	0.122		0.116		0.099		0.106		0.102		
Max	21.21										
Min	13.87										

Table A2.4 Test 41--- (continued)

Test 41

The Weld diameter after consider connection quality

Position	1		6		11		16		21	Average	C.o.V.
B	13.87		17.09		15.51		18.30		16.47	16.25	0.10
C (north)	14.02		13.70		14.61		14.81		12.85	**14.00**	**0.06**
C (South)	18.95		15.77		16.69		19.62		13.24	**16.85**	**0.15**
D	14.89		14.06		17.19		14.56		15.91	15.32	0.08
E	15.32		15.72		16.59		15.19		18.24	16.21	0.08
F (north)	20.26		14.94		21.21		14.10		10.39	**16.18**	**0.28**
F (South)	17.66		18.95		16.77		18.47		12.58	**16.89**	**0.15**
G	16.43		15.20		15.38		15.72		15.91	15.73	0.03
H	15.60		14.30		16.02		15.70		16.58	15.64	0.05
I (north)	16.13		12.20		13.31		19.29		8.77	**13.94**	**0.29**
I (South)	17.39		17.94		19.83		17.81		20.13	**18.62**	**0.07**
J	16.93		15.96		17.50		16.67		16.28	16.67	0.04
K	19.81		15.01		16.51		18.15		15.92	17.08	0.11
L (north)	13.94		19.82		12.77		16.06		13.08	**15.13**	**0.19**
L (South)	16.27		14.58		18.47		13.80		15.09	**15.64**	**0.12**
M	14.82		14.31		15.13		14.65		13.87	14.56	0.03
Average	16.39		15.60		16.47		16.43		14.71	15.92	0.11
C.o.V.	0.123		0.128		0.132		0.117		0.195		
Max	21.21								North	14.81	
Min	8.77								South	17.00	

Table A2.5 Test 42--- Weld diameter (measured and equivalent)

Test 42

The Weld diameter measured

Position	1	6	11	16	21	Average	C.o.V.
B	17.41	15.51	16.22	19.85	16.90	17.18	0.10
C (north)	**18.24**	**19.38**	**16.00**	**22.49**	**18.20**	**18.86**	**0.13**
C (South)	**19.15**	**19.12**	**15.97**	**23.41**	**19.25**	**19.38**	**0.14**
D	17.07	16.01	16.95	18.28	16.55	16.97	0.05
E	17.35	17.63	17.13	21.47	15.38	17.79	0.13
F (north)	**16.38**	**18.93**	**21.52**	**16.65**	**18.42**	**18.38**	**0.11**
F (South)	**17.01**	**18.62**	**15.51**	**18.36**	**18.86**	**17.67**	**0.08**
G	17.60	17.62	17.58	18.20	15.25	17.25	0.07
H	15.92	16.16	16.12	17.41	16.06	16.33	0.04
I (north)	**16.35**	**19.16**	**17.24**	**17.29**	**17.92**	**17.59**	**0.06**
I (South)	**18.05**	**17.62**	**16.01**	**17.36**	**19.21**	**17.65**	**0.07**
J	16.94	17.59	18.45	15.85	15.01	16.77	0.08
K	17.32	17.85	15.96	18.40	16.48	17.20	0.06
L (north)	**19.00**	**18.08**	**17.17**	**17.38**	**14.32**	**17.19**	**0.10**
L (South)	**16.44**	**15.58**	***16.19***	**16.81**	**18.59**	**16.72**	**0.07**
M	17.99	18.65	20.11	16.14	17.19	18.02	0.08
Average	17.39	17.72	17.13	18.46	17.10	17.56	0.08
C.o.V.	0.053	0.073	0.096	0.121	0.093		
Max	23.41						
Min	14.32						

Table A2.5 Test 42---(continued)

Test 42

The Weld diameter after consider connection quality

Position	1	6	11	16	21	Average	C.o.V.
B	17.41	15.51	16.22	19.85	16.90	17.18	0.10
C (north)	16.42	11.63	16.00	22.49	18.20	**16.95**	**0.23**
C (South)	19.15	15.30	15.97	23.41	19.25	**18.62**	**0.17**
D	17.07	16.01	16.95	18.28	16.55	16.97	0.05
E	17.35	17.63	17.13	17.18	15.38	16.93	0.05
F (north)	14.74	11.36	19.37	14.99	18.42	**15.77**	**0.20**
F (South)	17.01	18.62	15.51	16.52	18.86	**17.30**	**0.08**
G	17.60	17.62	17.58	18.20	15.25	17.25	0.07
H	15.92	16.16	16.12	17.41	16.06	16.33	0.04
I (north)	16.35	19.16	17.24	17.29	17.92	**17.59**	**0.06**
I (South)	18.05	17.62	16.01	17.36	19.21	**17.65**	**0.07**
J	16.94	17.59	18.45	15.85	15.01	16.77	0.08
K	17.32	17.85	15.96	14.72	16.48	16.47	0.07
L (north)	13.30	10.85	15.45	13.90	7.16	**12.13**	**0.27**
L (South)	16.44	14.02	16.19	16.81	18.59	**16.41**	**0.10**
M	17.99	18.65	18.10	12.91	13.75	16.28	0.17
Average	16.82	15.97	16.77	17.32	16.44	16.66	0.11
C.o.V.	0.081	0.169	0.068	0.162	0.182		
Max	23.41				North	15.61	
Min	7.16				South	17.50	

Table A2.6 Test 43--- Final nail installation quality index (stand off height)

Test 43

The nail install quality index after replaced

Position	1		6		11		16		21	Average	C.o.V.
B	6.97		7.05		7.24		6.09		6.90	6.85	0.06
C	**5.22**		**6.56**		**5.80**		**6.11**		**7.35**	**6.21**	**0.13**
D	6.96		6.59		6.33		5.17		6.91	6.39	0.11
E	6.93		6.51		5.68		5.52		6.04	6.14	0.10
F	**6.66**		**7.11**		**6.60**		**7.70**		**7.32**	**7.08**	**0.07**
G	6.36		6.50		5.70		7.69		6.04	6.46	0.12
H	7.10		6.52		5.72		5.80		6.31	6.29	0.09
I	**7.13**		**7.52**		**6.96**		**7.10**		**8.46**	**7.43**	**0.08**
J	6.52		6.33		7.01		6.09		6.96	6.58	0.06
K	6.31		5.63		6.36		6.02		7.37	6.34	0.10
L	**9.44**		**7.70**		**6.90**		**5.57**		**7.55**	**7.43**	**0.19**
M	6.93		7.00		6.06		6.59		7.01	6.72	0.06
Average	6.88		6.75		6.36		6.29		7.02	6.66	0.10
C.o.V.	0.140		0.083		0.090		0.131		0.097		

Max	9.44
Min	5.17

At sidelap	7.04
Except Sidelap	6.47

Table A2.7 Test 44--- Final nail installation quality index (stand off height)

Test 44

The nail install quality index after replaced

Position	1		6		11		16		21	Average	C.o.V.
B	6.75		6.75		6.56		6.99		7.39	6.89	0.05
C	**7.12**		**8.72**		**7.23**		**6.55**		**6.43**	**7.21**	**0.13**
D	5.58		9.06		6.00		5.57		7.12	6.67	0.22
E	6.37		6.67		6.13		6.84		5.98	6.40	0.06
F	**7.32**		**7.05**		**5.86**		**6.50**		**7.76**	**6.90**	**0.11**
G	6.13		7.71		6.78		5.57		5.11	6.26	0.16
H	6.16		7.22		7.62		5.72		7.13	6.77	0.12
I	**8.78**		**7.26**		**6.91**		**5.54**		**8.20**	**7.34**	**0.17**
J	6.71		6.24		6.44		8.84		7.34	7.11	0.15
K	6.12		6.75		6.67		6.59		7.11	6.65	0.05
L	**7.98**		**6.64**		**6.30**		**6.99**		**8.75**	**7.33**	**0.14**
M	7.26		6.61		6.07		8.05		6.75	6.95	0.11
Average	6.86		7.22		6.55		6.65		7.09	6.87	0.12
C.o.V.	0.131		0.120		0.081		0.154		0.136		

Max	9.06
Min	5.11

At sidelap	7.19
Except Sidelap	6.71

Table A2.8 Test 45--- Final nail installation quality index (stand off height)

Test 45

The nail install quality index after replaced

Position	1		6		11		16		21	Average	C.o.V.
B	6.54		6.10		7.23		5.81		6.24	6.38	0.08
C	**7.03**		**6.09**		**7.34**		**8.05**		**7.71**	**7.24**	**0.10**
D	6.06		6.10		7.58		6.75		5.99	6.50	0.10
E	5.87		6.44		6.48		6.42		6.18	6.28	0.04
F	**7.38**		**6.88**		**6.81**		**7.58**		**7.24**	**7.18**	**0.05**
G	6.35		6.07		8.41		6.09		5.51	6.49	0.17
H	6.40		6.77		5.58		6.39		6.23	6.27	0.07
I	**6.78**		**6.72**		**6.78**		**7.67**		**6.52**	**6.89**	**0.06**
J	6.95		7.17		7.61		6.33		5.14	6.64	0.14
K	6.16		5.70		6.54		6.26		5.48	6.03	0.07
L	**6.05**		**5.93**		**7.00**		**7.00**		**6.54**	**6.50**	**0.08**
M	6.58		5.55		6.48		6.96		7.42	6.60	0.10
Average	6.51		6.29		6.99		6.78		6.35	6.58	0.09
C.o.V.	0.070		0.079		0.103		0.102		0.125		

Max	8.41
Min	5.14

At sidelap	6.96
Except Sidelap	6.40

Table A2.9 Test 46--- Final nail installation quality index (stand off height)

Test 46

The nail install quality index after replaced

Position	1		6		11		16		21	Average	C.o.V.
B	6.50		5.86		6.54		7.66		6.07	6.53	0.11
C	**7.08**		**6.14**		**5.93**		**6.28**		**7.52**	**6.59**	**0.10**
D	5.34		6.14		6.66		5.43		7.05	6.12	0.12
E	5.84		6.64		6.68		6.10		6.30	6.31	0.06
F	**7.09**		**6.94**		**6.57**		**6.95**		**N/A**	**6.89**	**0.03**
G	5.38		5.65		6.82		6.97		6.55	6.27	0.11
H	6.20		7.58		5.96		6.71		6.64	6.62	0.09
I	**6.38**		**7.54**		**7.20**		**6.00**		**7.33**	**6.89**	**0.10**
J	5.57		6.20		5.95		6.23		5.80	5.95	0.05
K	5.38		5.50		7.20		6.79		5.80	6.13	0.13
L	**7.03**		**6.21**		**7.83**		**6.75**		**7.07**	**6.98**	**0.08**
M	7.34		6.18		7.51		6.24		7.56	6.97	0.10
Average	6.26		6.38		6.74		6.51		6.70	6.52	0.09
C.o.V.	0.120		0.105		0.091		0.089		0.098		

Max	7.83
Min	5.34

At sidelap	6.84
Except Sidelap	6.36

Table A2.10 Test 47--- Weld diameter (measured and equivalent)

Test 47

The Weld diameter measured

Position	1	6	11	16	21	Average	C.o.V.
B (north)	**18.27**	**19.74**	**18.40**	**15.93**	**14.45**	**17.36**	**0.12**
B (south)	**19.50**	**21.51**	**19.37**	**17.63**	**16.40**	**18.88**	**0.10**
C	18.40	16.43	16.67	17.88	16.20	17.12	0.06
D (north)	**19.03**	**16.07**	**17.48**	**17.64**	**19.34**	**17.91**	**0.07**
D (south)	**16.82**	**19.46**	**19.00**	**19.33**	**20.83**	**19.09**	**0.08**
E	18.04	15.66	15.90	18.71	18.16	17.29	0.08
F (north)	**19.39**	**17.92**	**16.77**	**16.39**	**16.36**	**17.37**	**0.07**
F (south)	**18.20**	**16.99**	**16.46**	**16.19**	**18.61**	**17.29**	**0.06**
G	18.73	17.22	15.44	18.65	19.95	18.00	0.10
H (north)	**18.69**	**18.63**	**17.00**	**18.35**	**16.95**	**17.92**	**0.05**
H (South)	**18.61**	**16.60**	**17.32**	**17.86**	**19.97**	**18.07**	**0.07**
I	17.31	15.98	16.35	17.00	17.00	16.73	0.03
J (north)	**18.05**	**17.61**	**17.34**	**18.47**	**19.80**	**18.25**	**0.05**
J (south)	**15.55**	**15.70**	**18.55**	**17.03**	**18.10**	**16.99**	**0.08**
K	16.28	15.68	*16.58*	18.92	19.26	17.34	0.09
L (north)	**17.18**	**16.09**	*16.65*	**17.69**	**14.79**	**16.48**	**0.07**
L (south)	**17.18**	**16.09**	**16.65**	**17.69**	**15.97**	**16.72**	**0.04**
Average	17.95	17.26	17.17	17.73	17.77	17.58	0.02
C.o.V.	0.061	0.098	0.063	0.055	0.108		

Max	21.51	Side lap (north)	17.549
Min	14.45	Side lap (south)	17.839
		Except Side lap	17.296

Table A2.10 Test 47--- (continued)

Test 47

The Weld diameter after consider connection quality

Position	1	6	11	16	21	Average	C.o.V.
B (north)	**18.27**	**19.74**	**14.72**	**14.34**	**10.12**	**15.44**	**0.24**
B (south)	**15.60**	**21.51**	**19.37**	**17.63**	**13.12**	**17.45**	**0.19**
C	18.40	16.43	16.67	17.88	16.20	17.12	0.06
D (north)	**19.03**	**16.07**	**17.48**	**14.11**	**13.54**	**16.05**	**0.14**
D (south)	**16.82**	**19.46**	**19.00**	**19.33**	**14.58**	**17.84**	**0.12**
E	18.04	15.66	15.90	18.71	18.16	17.29	0.08
F (north)	**13.57**	**17.92**	**15.09**	**11.47**	**13.09**	**14.23**	**0.17**
F (south)	**14.56**	**16.99**	**16.46**	**12.95**	**14.89**	**15.17**	**0.11**
G	18.73	17.22	15.44	13.06	11.97	15.28	0.18
H (north)	**18.69**	**14.90**	**17.00**	**18.35**	**11.87**	**16.16**	**0.17**
H (South)	**18.61**	**16.60**	**17.32**	**17.86**	**19.97**	**18.07**	**0.07**
I	17.31	15.98	16.35	13.60	17.00	16.05	0.09
J (north)	**18.05**	**12.33**	**17.34**	**14.78**	**13.86**	**15.27**	**0.16**
J (south)	**15.55**	**15.70**	**14.84**	**17.03**	**18.10**	**16.24**	**0.08**
K	16.28	15.68	16.58	18.92	19.26	17.34	0.09
L (north)	**17.18**	**16.09**	**16.65**	**17.69**	**11.83**	**15.89**	**0.15**
L (south)	**17.18**	**16.09**	**14.99**	**17.69**	**12.78**	**15.74**	**0.12**
Average	17.17	16.73	16.54	16.20	14.72	16.27	0.06
C.o.V.	0.092	0.124	0.081	0.155	0.197		

Max	21.51	Side lap (north)	15.50543
Min	10.12	Side lap (south)	16.7524
		Except Side lap	16.617

Table A2.11 Test 48--- Weld diameter (measured and equivalent)

Test 48

The Weld diameter measured

Position	1	6	11	16	21	Average	C.o.V.
B (north)	**18.61**	**18.69**	**19.56**	**24.27**	**20.12**	**20.25**	**0.12**
B (south)	**19.93**	**17.18**	**19.21**	**17.19**	**15.27**	**17.76**	**0.10**
C	16.39	17.24	17.35	19.05	17.90	17.59	0.06
D (north)	**18.39**	**19.85**	**20.03**	**19.21**	**20.35**	**19.57**	**0.04**
D (south)	**19.65**	**19.06**	**19.83**	**18.56**	**17.25**	**18.87**	**0.05**
E	17.66	15.25	15.84	17.58	18.26	16.92	0.08
F (north)	**18.63**	**16.76**	**20.56**	**20.53**	**18.95**	**19.09**	**0.08**
F (south)	**20.30**	**17.64**	**17.90**	**14.78**	**17.47**	**17.62**	**0.11**
G	17.85	16.21	17.65	17.38	17.60	17.34	0.04
H (north)	**20.05**	**18.69**	**18.27**	**16.73**	**19.07**	**18.56**	**0.07**
H (South)	**21.36**	**17.04**	**17.40**	**19.86**	**16.55**	**18.44**	**0.11**
I	17.03	18.62	15.98	18.44	17.97	17.61	0.06
J (north)	**18.79**	**19.23**	**20.97**	**21.99**	**22.05**	**20.61**	**0.07**
J (south)	**17.99**	**18.11**	**18.05**	**18.92**	**19.71**	**18.56**	**0.04**
K	18.88	19.23	*16.81*	17.74	16.79	17.89	0.06
L (north)	**18.84**	**19.80**	***17.40***	**15.53**	**18.38**	**17.99**	**0.09**
L (south)	**18.04**	**16.81**	**18.36**	**14.56**	**18.62**	**17.28**	**0.10**
Average	18.73	17.97	18.30	18.37	18.37	18.35	0.01
C.o.V.	0.067	0.074	0.083	0.135	0.088		
Max	24.27				Side lap (north)	19.34	
Min	14.56				Side lap (south)	18.09	
					Except Side lap	17.47	

Table A2.11 Test 48--- (continued)

Test 48

The Weld diameter after consider connection quality

Position	1	6	11	16	21	Average	C.o.V.
B (north)	**18.61**	**18.69**	**19.56**	**24.27**	**20.12**	**20.25**	**0.12**
B (south)	**11.96**	**17.18**	**19.21**	**17.19**	**15.27**	**16.16**	**0.17**
C	**16.39**	**17.24**	**17.35**	**19.05**	**17.90**	17.59	0.06
D (north)	**18.39**	**13.90**	**20.03**	**19.21**	**20.35**	**18.38**	**0.14**
D (south)	**13.76**	**11.44**	**11.90**	**18.56**	**17.25**	**14.58**	**0.22**
E	**17.66**	**15.25**	**15.84**	**17.58**	**18.26**	16.92	0.08
F (north)	**18.63**	**13.41**	**20.56**	**20.53**	**18.95**	**18.42**	**0.16**
F (south)	**20.30**	**14.11**	**14.32**	**14.78**	**17.47**	**16.20**	**0.16**
G	**17.85**	**16.21**	**17.65**	**17.38**	**17.60**	17.34	0.04
H (north)	**20.05**	**18.69**	**12.79**	**16.73**	**19.07**	**17.47**	**0.16**
H (South)	**14.95**	**13.63**	**13.92**	**19.86**	**16.55**	**15.78**	**0.16**
I	**17.03**	**18.62**	**15.98**	**18.44**	**17.97**	17.61	0.06
J (north)	**18.79**	**19.23**	**20.97**	**21.99**	**22.05**	**20.61**	**0.07**
J (south)	**14.39**	**18.11**	**18.05**	**18.92**	**19.71**	**17.84**	**0.11**
K	**18.88**	**19.23**	**16.81**	**17.74**	**16.79**	17.89	0.06
L (north)	**18.84**	**19.80**	**17.40**	**15.53**	**11.03**	**16.52**	**0.21**
L (south)	**18.04**	**16.81**	**18.36**	**14.56**	**18.62**	**17.28**	**0.10**
Average	17.32	16.56	17.10	18.37	17.94	17.46	0.04
C.o.V.	0.133	0.152	0.157	0.135	0.134		
Max	24.27				Side lap (north)	18.61	
Min	11.03				Side lap (south)	16.31	
					Except Side lap	17.47	

Table A2.12 Test 49--- Weld diameter (measured and equivalent)

Test 49

The Weld diameter measured

Position	1		6		11		16		21	Average	C.o.V.
B (north)	**14.93**		**15.69**		**17.17**		**12.83**		**13.48**	**14.82**	**0.12**
B (south)	**14.47**		**18.83**		**17.02**		**13.13**		**11.32**	**14.95**	**0.20**
C	16.01		15.28		17.45		13.03		14.05	15.16	0.11
D (north)	**16.93**		**15.73**		**18.71**		**18.87**		**17.14**	**17.48**	**0.08**
D (south)	**14.63**		**16.86**		**17.53**		**15.52**		**14.40**	**15.79**	**0.09**
E	18.64		15.86		18.43		17.86		16.64	17.49	0.07
F (north)	**17.53**		**17.68**		**18.41**		**17.07**		**18.18**	**17.77**	**0.03**
F (south)	**15.18**		**17.35**		**15.41**		**15.08**		**14.66**	**15.54**	**0.07**
G	15.92		15.72		15.13		17.93		15.81	16.10	0.07
H (north)	**17.13**		**18.66**		**17.36**		**17.20**		**17.17**	**17.50**	**0.04**
H (South)	**14.31**		**15.19**		**14.28**		**16.86**		**16.97**	**15.52**	**0.09**
I	14.30		18.59		18.14		15.68		17.75	16.89	0.11
J (north)	**14.72**		**15.43**		**16.86**		**20.14**		**18.36**	**17.10**	**0.13**
J (south)	**16.25**		**16.04**		**17.44**		**15.98**		**17.10**	**16.56**	**0.04**
K	15.42		15.77		*15.49*		15.73		15.63	15.61	0.01
L (north)	**16.79**		**15.77**		***14.06***		**15.26**		**13.60**	**15.10**	**0.09**
L (south)	**13.83**		**14.86**		**16.79**		**17.46**		**17.51**	**16.09**	**0.10**
Average	15.71		16.43		16.80		16.21		15.87	16.20	0.03
C.o.V.	0.086		0.079		0.085		0.125		0.125		

Max	20.14	Side lap (north)	16.63
Min	11.32	Side lap (south)	15.74
		Except Side lap	16.25

Table A4.12 Test 49--- (continued)

Test 49

The Weld diameter after consider connection quality

Position	1		6		11		16		21	Average	C.o.V.
B (north)	**14.93**		**15.69**		**17.17**		**12.83**		**13.48**	**14.82**	**0.12**
B (south)	**10.13**		**18.83**		**13.62**		**13.13**		**11.32**	**13.41**	**0.25**
C	**16.01**		**15.28**		**17.45**		**13.03**		**14.05**	15.16	0.11
D (north)	**15.24**		**12.58**		**18.71**		**18.87**		**12.00**	**15.48**	**0.21**
D (south)	**10.24**		**13.49**		**12.27**		**15.52**		**14.40**	**13.18**	**0.15**
E	**13.05**		**15.86**		**18.43**		**17.86**		**11.65**	15.37	0.19
F (north)	**17.53**		**17.68**		**18.41**		**17.07**		**18.18**	**17.77**	**0.03**
F (south)	**12.14**		**13.88**		**10.79**		**15.08**		**14.66**	**13.31**	**0.14**
G	**15.92**		**15.72**		**15.13**		**17.93**		**15.81**	16.10	0.07
H (north)	**15.42**		**18.66**		**17.36**		**17.20**		**17.17**	**17.16**	**0.07**
H (South)	**14.31**		**12.15**		**10.00**		**16.86**		**13.58**	**13.38**	**0.19**
I	**10.01**		**18.59**		**18.14**		**15.68**		**17.75**	16.03	0.22
J (north)	**11.78**		**15.43**		**13.49**		**20.14**		**12.85**	**14.74**	**0.22**
J (south)	**13.00**		**16.04**		**12.21**		**15.98**		**11.97**	**13.84**	**0.15**
K	**15.42**		**11.04**		**15.49**		**15.73**		**15.63**	14.66	0.14
L (north)	**13.43**		**12.62**		**14.06**		**15.26**		**13.60**	**13.79**	**0.07**
L (south)	**12.45**		**11.89**		**13.43**		**17.46**		**12.26**	**13.50**	**0.17**
Average	13.59		15.03		15.07		16.21		14.14	14.81	0.07
C.o.V.	0.166		0.166		0.188		0.125		0.152		

Max	20.14	Side lap (north)	15.63
Min	10.00	Side lap (south)	13.44
		Except Side lap	15.47

APPENDIX 3: DATA TREATMENT (FILTER SIGNALS)

As suggested by Martin (2002), in order to obtain the real forces acting on the deck panels, it is recommended that the test results be treated before being used in evaluating the diaphragm properties. The treatment includes filtering signals and removing inertial forces. Martin suggested a filter frequency value of 10 Hz for the load, and 3 Hz for the acceleration, and he also gave an effective mass of 18.6 kN/g to remove inertial forces.

In this thesis, this procedure is also applied but with some modifications in considering the specific situations in the tests. In Table A3.1, "M" is a monotonic load, "C+M" is cyclic plus monotonic load, "a" is the acceleration measured. It is noted that not all the test results were treated, only those which were deemed to be necessary, for example, when the time history curve was not very smooth. The effect of filtering is quite obvious, as can be seen in Figure A3.1 for example. For additional information refer to Martin (2002).

Table A3.1 Filter frequency and inertia forces

Test number	Load type	Run 1			Run 2			Removal of inertia forces
		Time duration (sec)	Filter frequency		Time duration (sec)	Filter frequency		
			Load	Acceleration		Load	Acceleration	
38	SD	25.2			25.2			
39	M	5365						
40	SD	505	0.500	0.150	513	0.500	0.150	(-18.6*a)
41	M	4207						
42	SD	25.3	10	3	25.3	10.0	3.00	(-18.6*a)
43	M	4349	0.020					
44	C+M	913			3548	0.020	0.020	(-18.6*a)
45	M	5508						
46	C+M	934			5431			
47	M	5051	0.020	0.020				(-18.6*a)
48	SD	468	0.500	0.150				
49	M	4639	0.020					

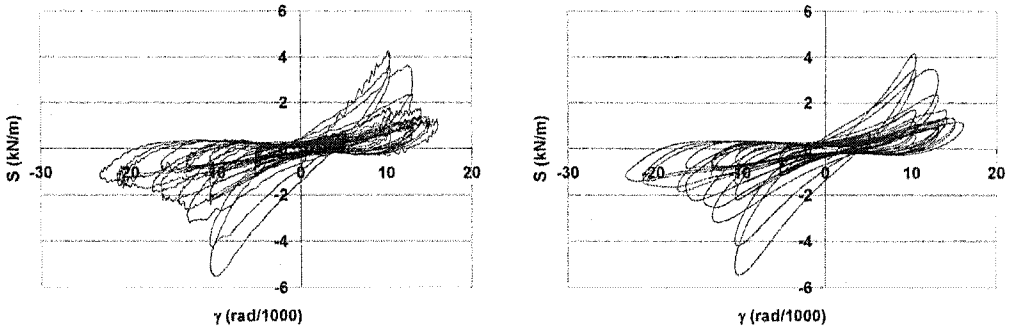

a) Before-filter b) After-filter

Figure A3.1 Comparison of before-filter and after-filter for test 48

APPENDIX 4: DYNAMIC ANALYSIS RESULT OF 2-R-I AND 2-F-I (I=2 TO 8)

The results of torsion analysis for 2-R-1 and 2-F-1 were discussed in Chapter 6 in detail. The other results are placed here to give a more conclusive comprehension of how torsion effects are influenced by roof flexibility.

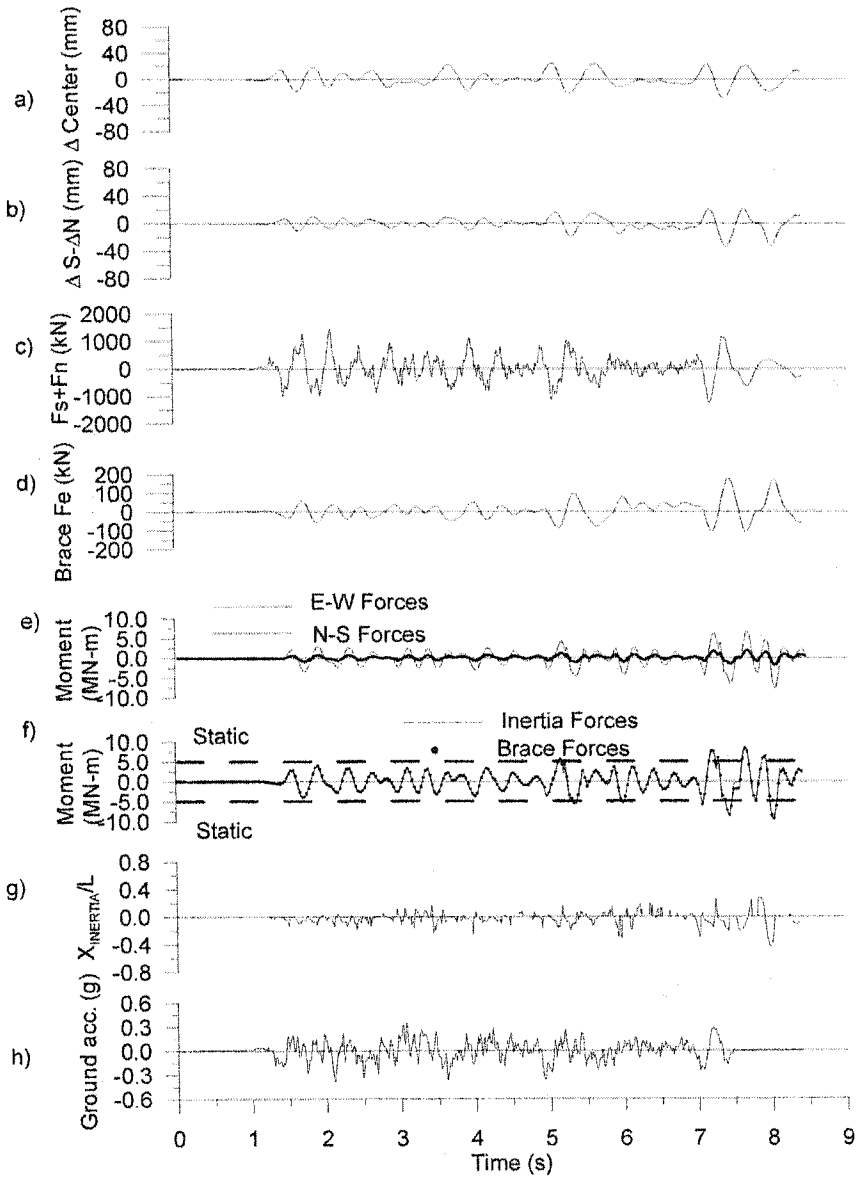

Response of 2-R-2 (Model 2-R to Seismic event No.2)

a) Storey drift at mid-length of the building; b)Difference between storey drifts at South and North walls;
c) Sum of inertia forces in E-W direction; d) Sum of brace force horizontal components in East wall;
e) Torsional moments due to E-W and N-S inertia forces;
f) Torsional moments due to total inertia forces and brace forces;
g) Location of E-W inertia center (CI); h) Selected ground motion

Figure A1. Result of 2-R-2

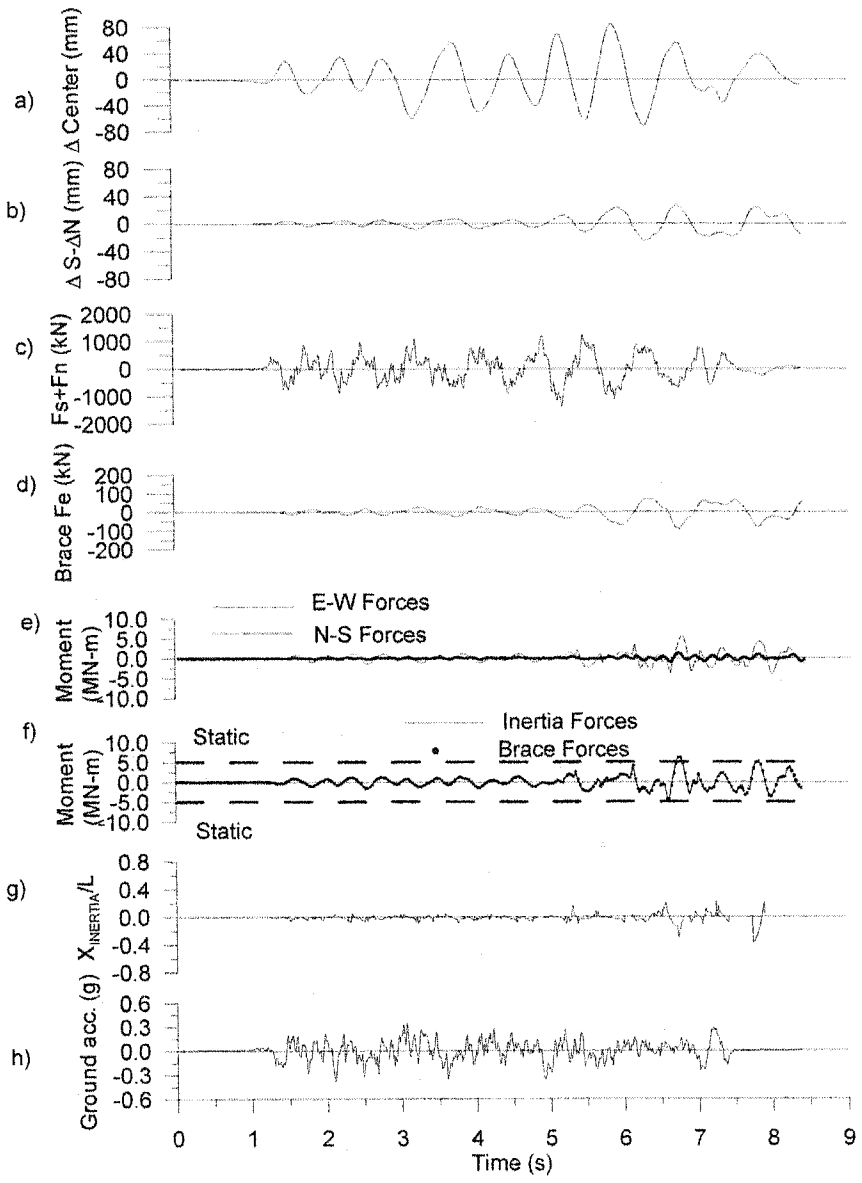

Response of 2-F-2 (Model 2-F to Seismic event No.2)

a) Storey drift at mid-length of the building; b)Difference between storey drifts at South and North walls;
c) Sum of inertia forces in E-W direction; d) Sum of brace force horizontal components in East wall;
e) Torsional moments due to E-W and N-S inertia forces;
f) Torsional moments due to total inertia forces and brace forces;
g) Location of E-W inertia center (CI); h) Selected ground motion

Figure A2. Result 2-F-2

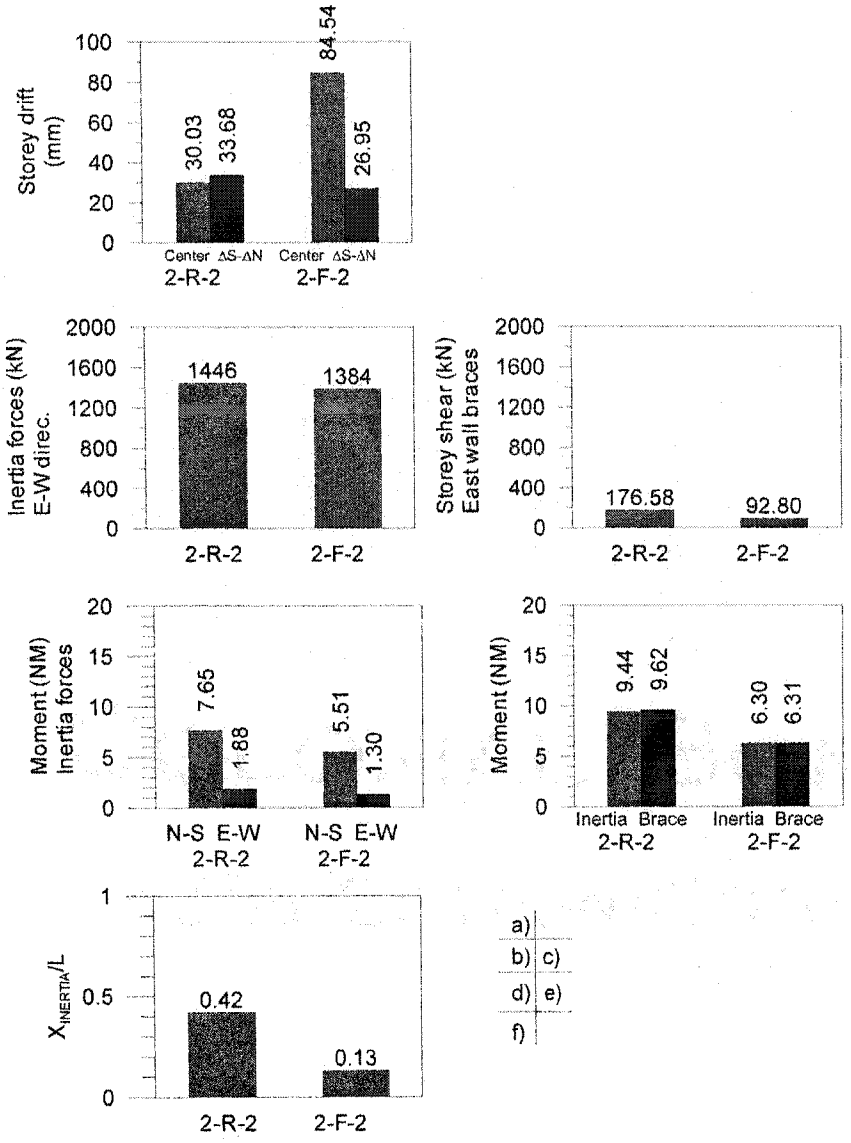

Maximum Response of 2-R-2 & 2-F-2 (Absolute value)

a) Storey drifts (at mid-length; Difference between South and North walls);
b)Sum of E-W direc. inertia forces; c) Storey shear by East wall braces;
d) Torsional moments due to inertia forces (North-South; East-West);
e)Torsional moments due to inertia forces and due to brace forces;
f) Location of E-W inertia center (CI) at maximum inertia torsion moment

Figure A3. Comparison of 2-R-2 to 2-F-2

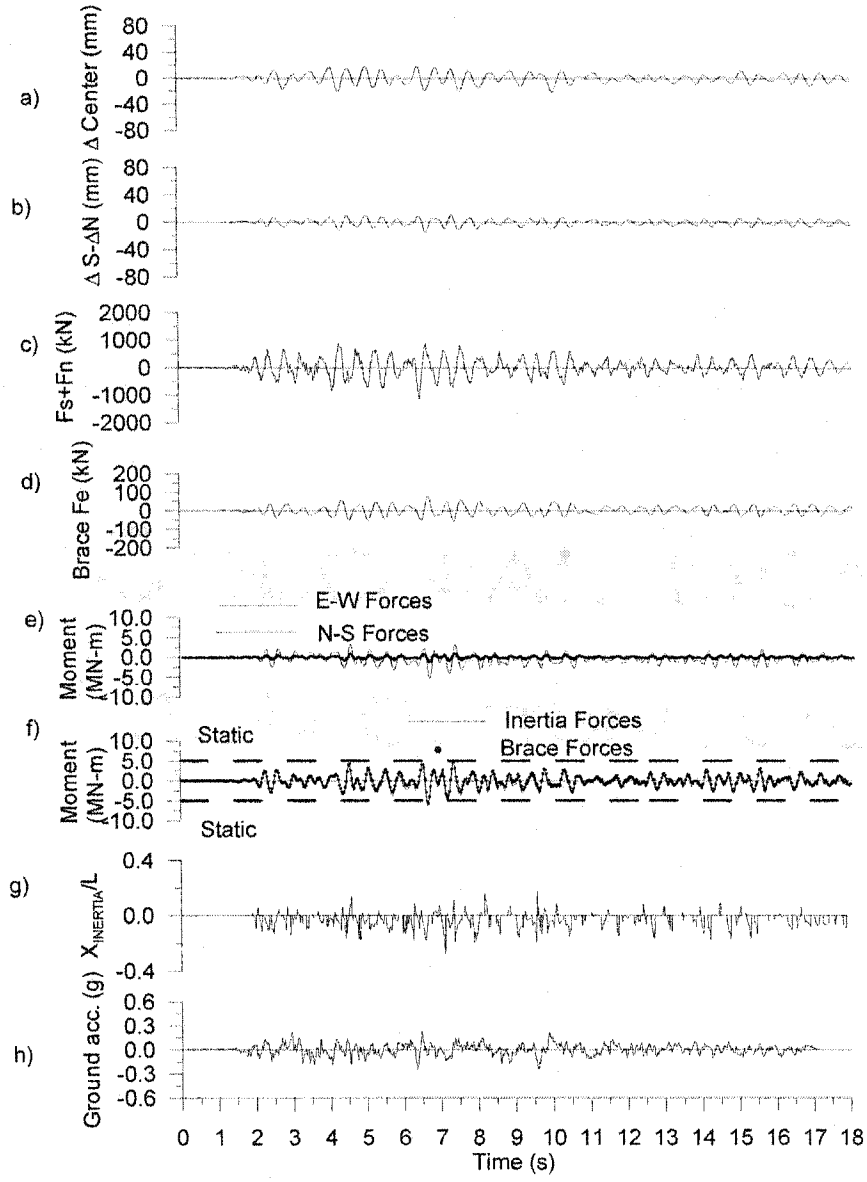

Response of 2-R-3 (Model 2-R to Seismic event No.3)

a) Storey drift at mid-length of the building; b)Difference between storey drifts at South and North walls;
c) Sum of inertia forces in E-W direction; d) Sum of brace force horizontal components in East wall;
e) Torsional moments due to E-W and N-S inertia forces;
f) Torsional moments due to total inertia forces and brace forces;
g) Location of E-W inertia center (CI); h) Selected ground motion

Figure A4. Result of 2-R-3

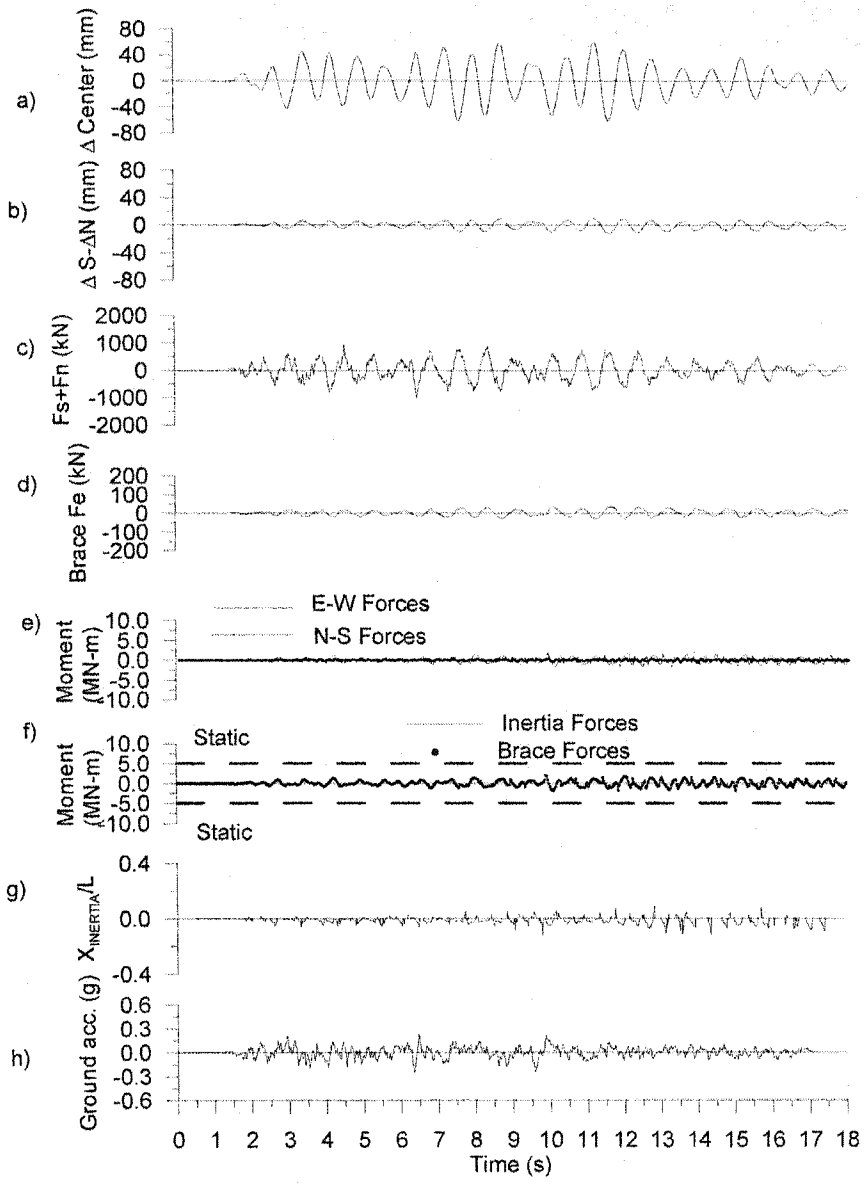

Response of 2-F-3 (Model 2-F to Seismic event No.3)

a) Storey drift at mid-length of the building; b)Difference between storey drifts at South and North walls;
c) Sum of inertia forces in E-W direction; d) Sum of brace force horizontal components in East wall;
e) Torsional moments due to E-W and N-S inertia forces;
f) Torsional moments due to total inertia forces and brace forces;
g) Location of E-W inertia center (CI); h) Selected ground motion

Figure A5. Result of 2-F-3

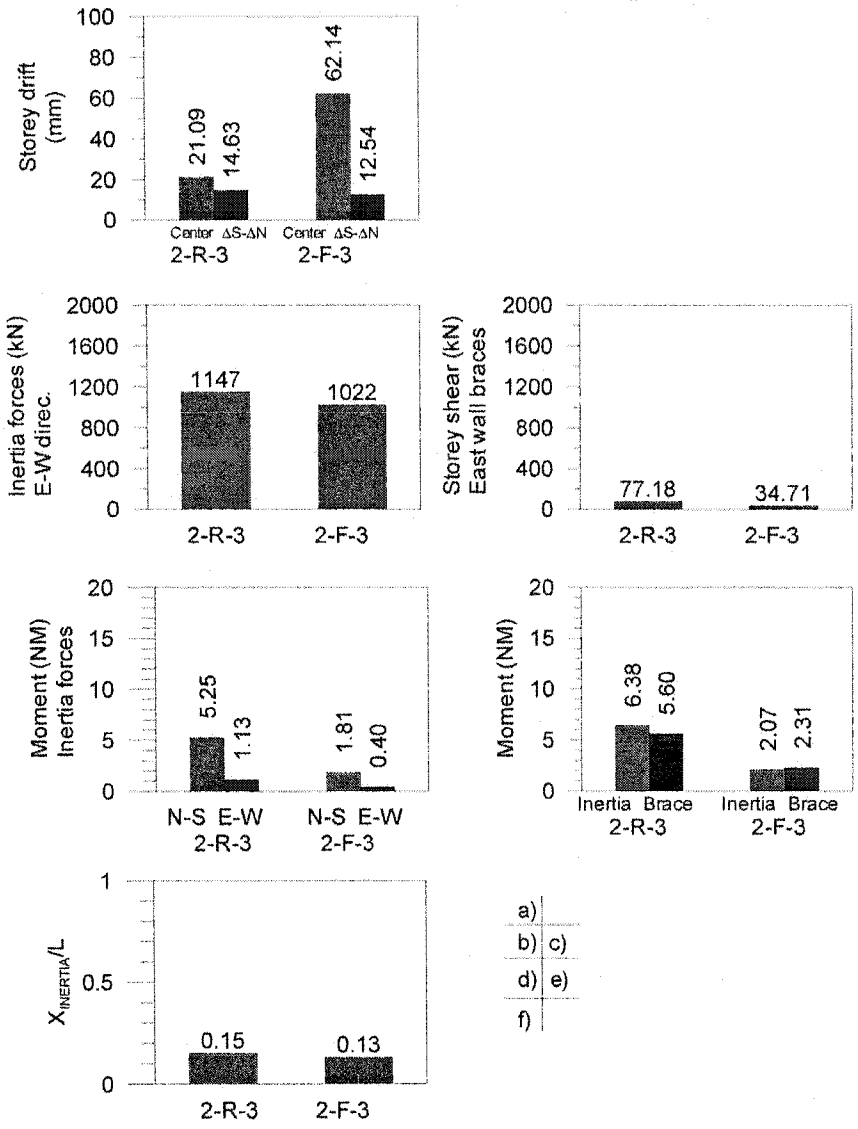

Maximum Response of 2-R-3 & 2-F-3 (Absolute value)

a) Storey drifts (at mid-length; Difference between South and North walls);
b)Sum of E-W direc. inertia forces; c) Storey shear by East wall braces;
d) Torsional moments due to inertia forces (North-South; East-West);
e)Torsional moments due to inertia forces and due to brace forces;
f) Location of E-W inertia center (CI) at maximum inertia torsion moment

Figure A6. Comparison of 2-R-3 to 2-F-3

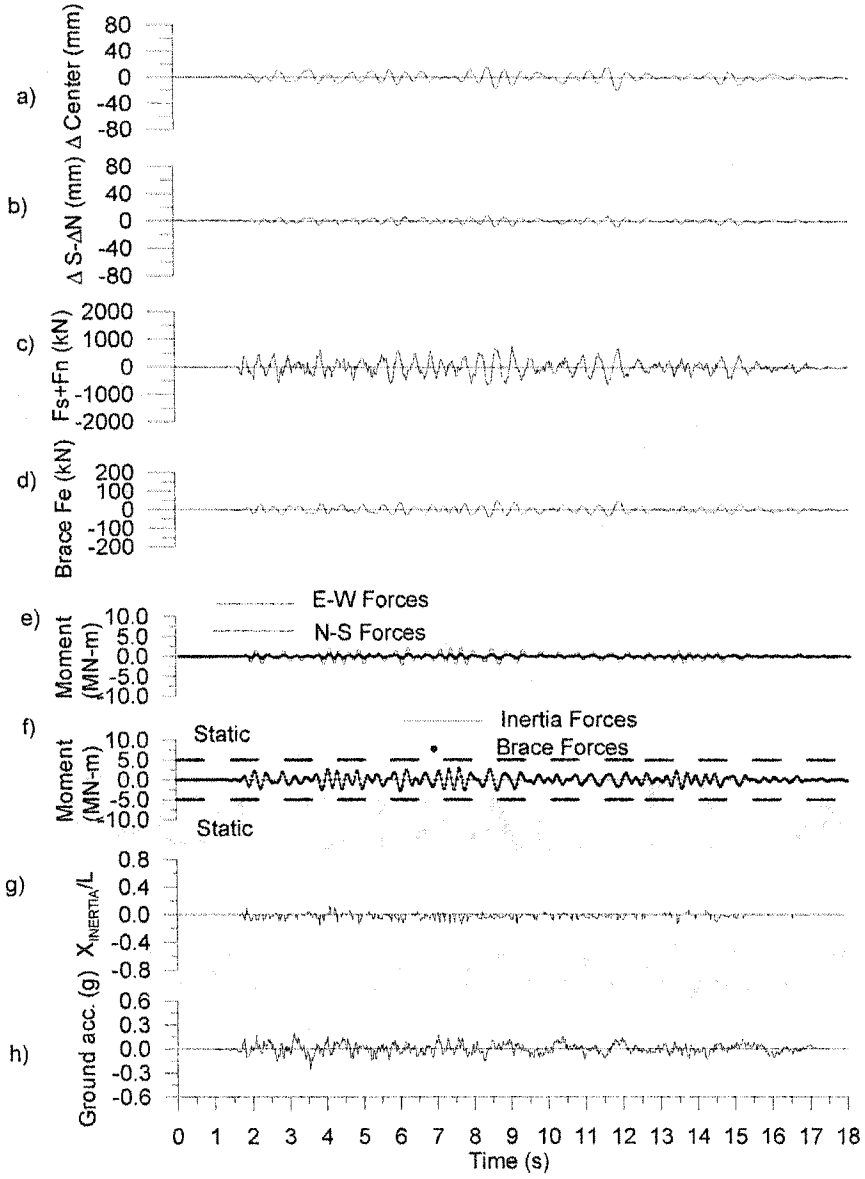

Response of 2-R-4 (Model 2-R to Seismic event No.4)

a) Storey drift at mid-length of the building; b)Difference between storey drifts at South and North walls;
c) Sum of inertia forces in E-W direction; d) Sum of brace force horizontal components in East wall;
e) Torsional moments due to E-W and N-S inertia forces;
f) Torsional moments due to total inertia forces and brace forces;
g) Location of E-W inertia center (CI); h) Selected ground motion

Figure A7. Result of 2-R-4

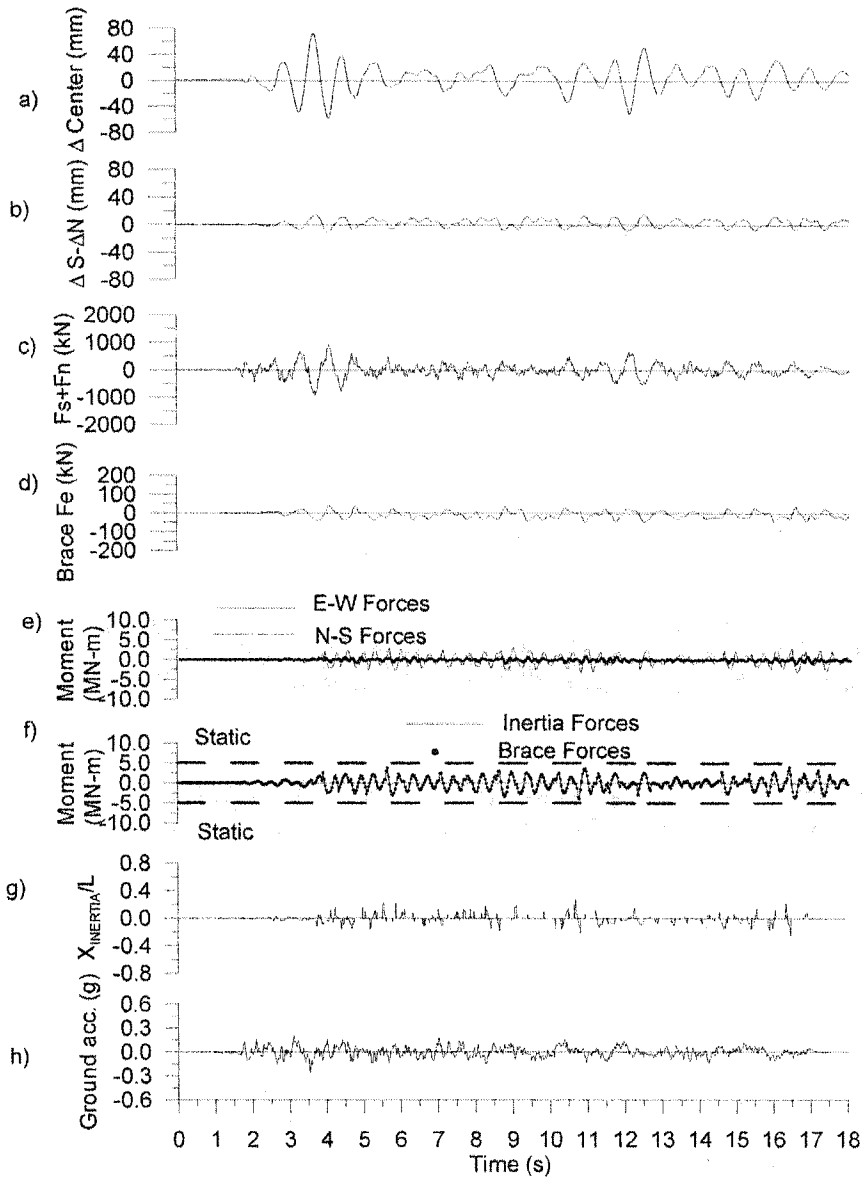

Response of 2-F-4 (Model 2-F to Seismic event No.4)

a) Storey drift at mid-length of the building; b)Difference between storey drifts at South and North walls;
c) Sum of inertia forces in E-W direction; d) Sum of brace force horizontal components in East wall;
e) Torsional moments due to E-W and N-S inertia forces;
f) Torsional moments due to total inertia forces and brace forces;
g) Location of E-W inertia center (CI); h) Selected ground motion

Figure A8. Result of 2-F-4

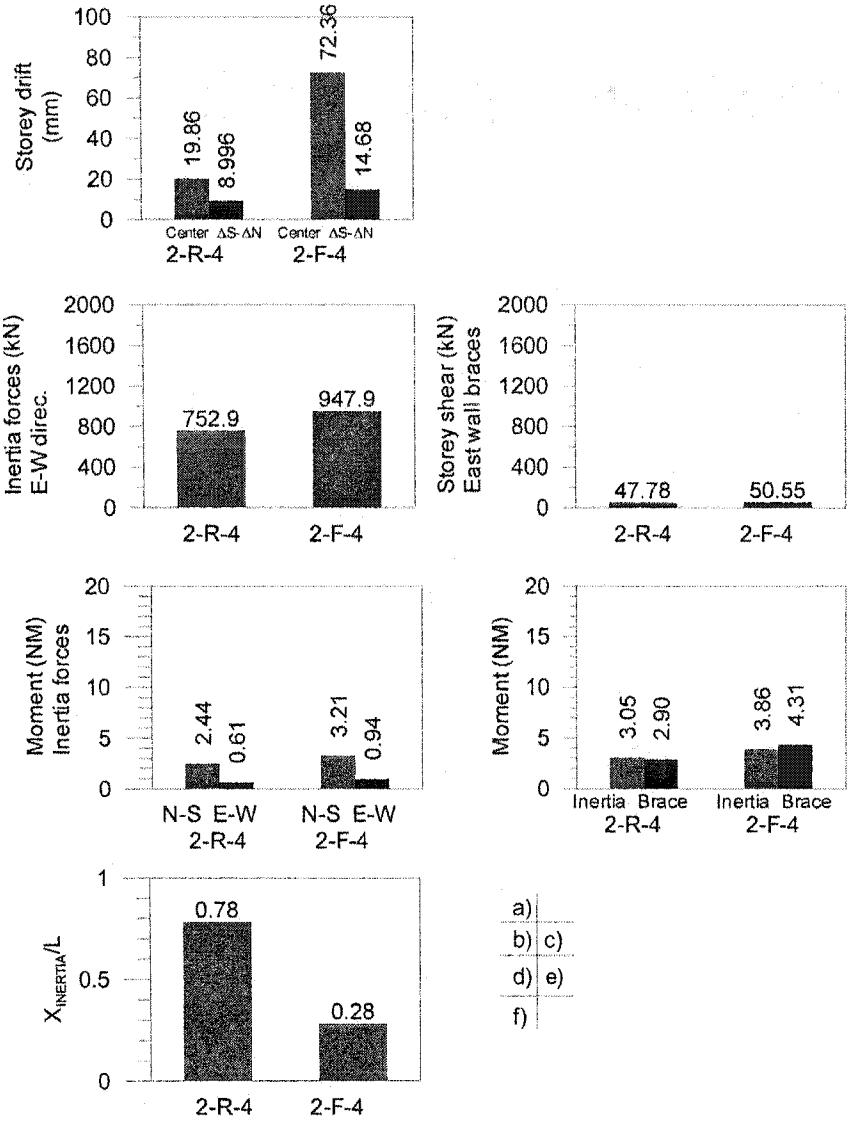

Maximum Response of 2-R-4 & 2-F-4 (Absolute value)
a) Storey drifts (at mid-length; Difference between South and North walls);
b)Sum of E-W direc. inertia forces; c) Storey shear by East wall braces;
d) Torsional moments due to inertia forces (North-South; East-West);
eTorsional moments due to inertia forces and due to brace forces;
f) Location of E-W inertia center (CI) at maximum torsional inertia moments

Figure A9. Comparison of 2-R-4 to 2-F-4

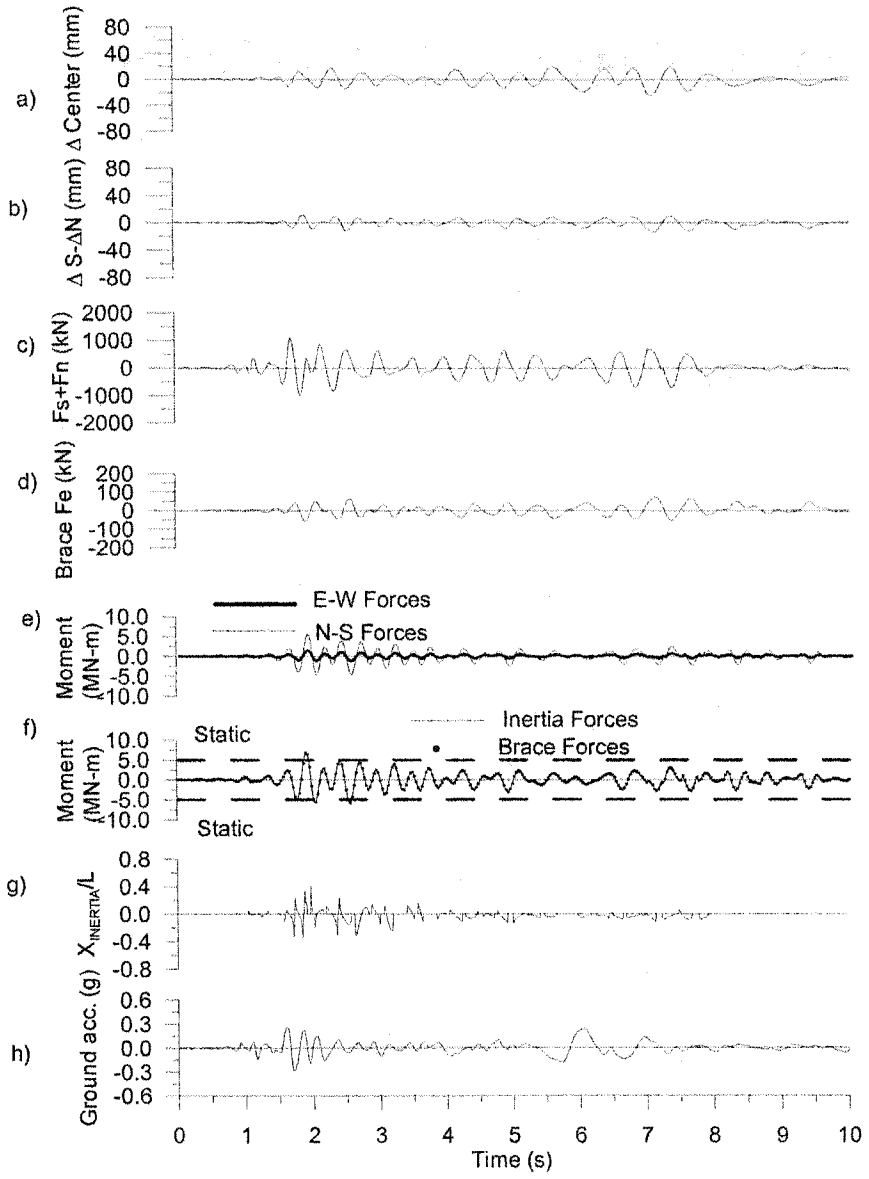

Response of 2-R-5 (Model 2-R to Seismic event No.5)

a) Storey drift at mid-length of the building; b)Difference between storey drifts at South and North walls;
c) Sum of inertia forces in E-W direction; d) Sum of brace force horizontal components in East wall;
e) Torsional moments due to E-W and N-S inertia forces;
f) Torsional moments due to total inertia forces and brace forces;
g) Location of E-W inertia center (CI); h) Selected ground motion

Figure A10. Result of 2-R-5

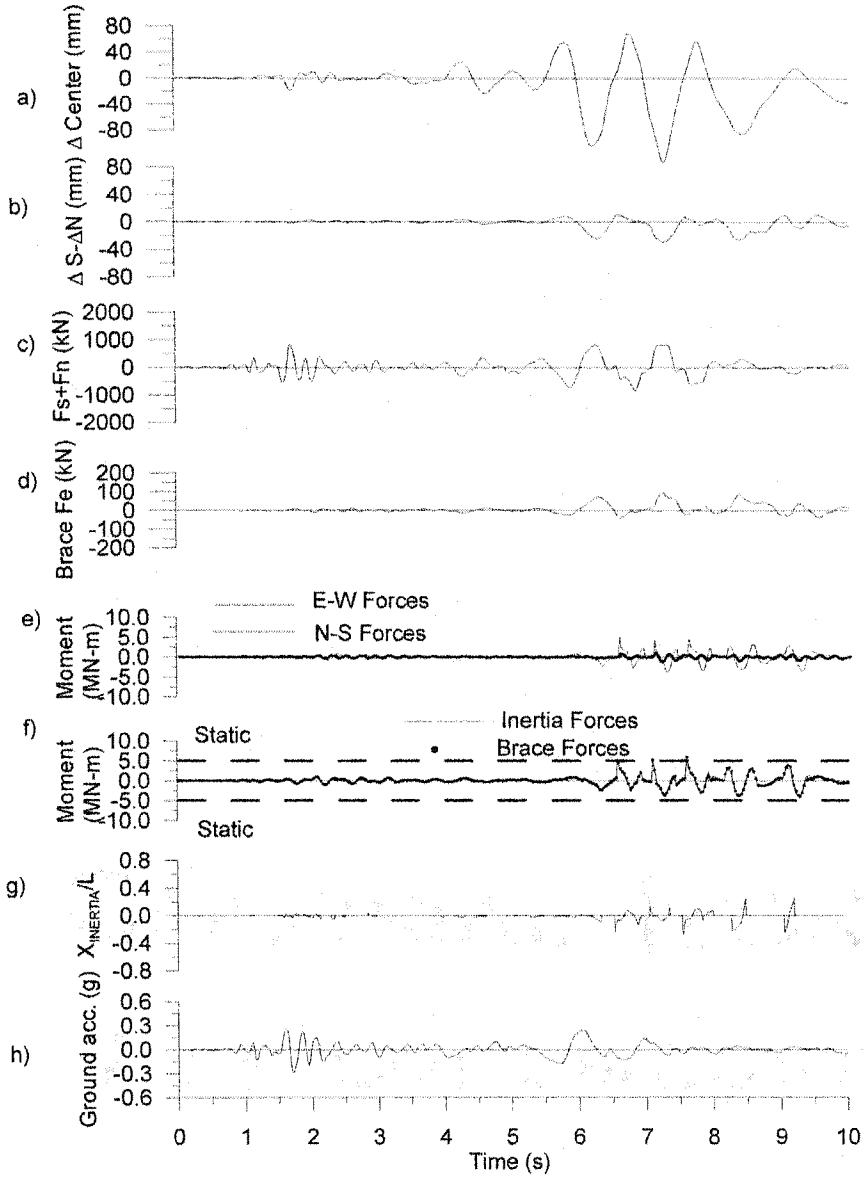

Response of 2-F-5 (Model 2-F to Seismic event No.5)

a) Storey drift at mid-length of the building; b)Difference between storey drifts at South and North walls;
c) Sum of inertia forces in E-W direction; d) Sum of brace force horizontal components in East wall;
e) Torsional moments due to E-W and N-S inertia forces;
f) Torsional moments due to total inertia forces and brace forces;
g) Location of E-W inertia center (CI); h) Selected ground motion

Figure A11. Result of 2-F-5

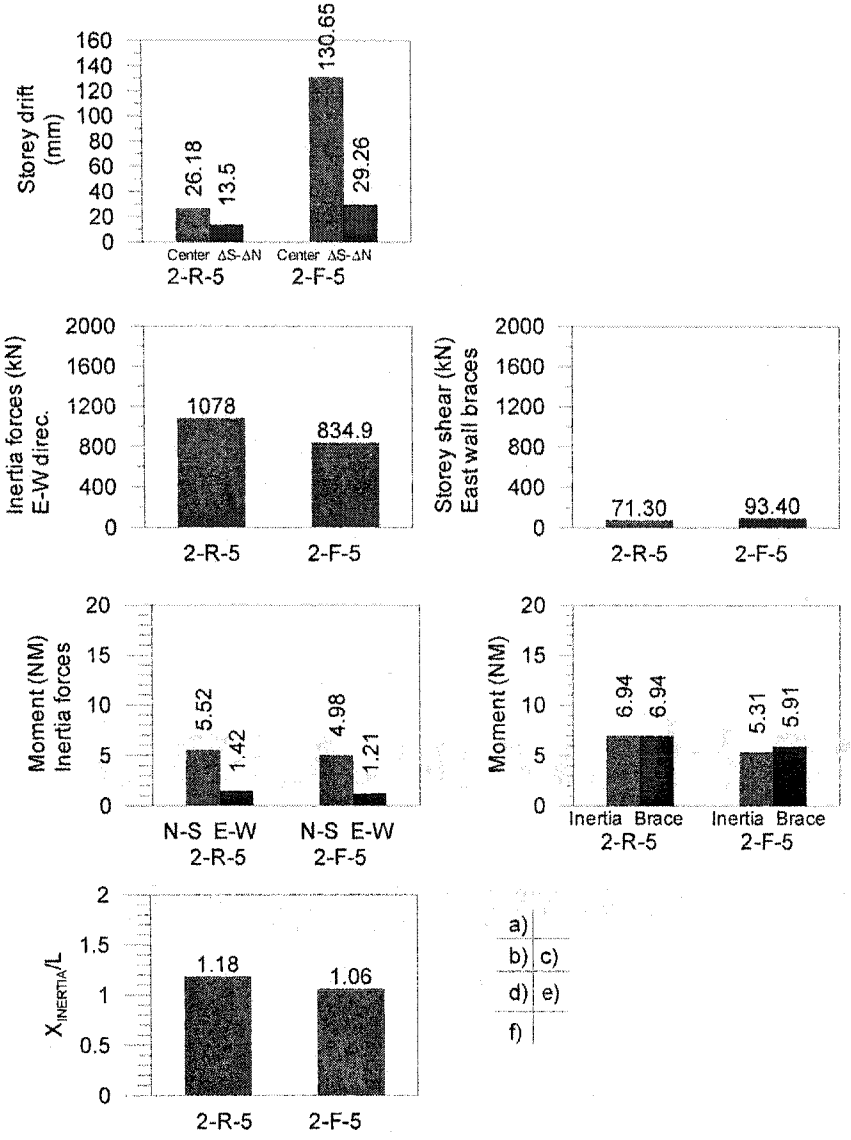

Maximum Response of 2-R-5 & 2-F-5 (Absolute value)

a) Storey drifts (at mid-length; Difference between South and North walls);
b)Sum of E-W direc. inertia forces; c) Storey shear by East wall braces;
d) Torsional moments due to inertia forces (North-South; East-West);
e)Torsional moments due to inertia forces and due to brace forces;
f) Location of E-W inertia center (CI) at maximum torsional inertia moments

Figure A12. Comparison of 2-R-5 to 2-F-5

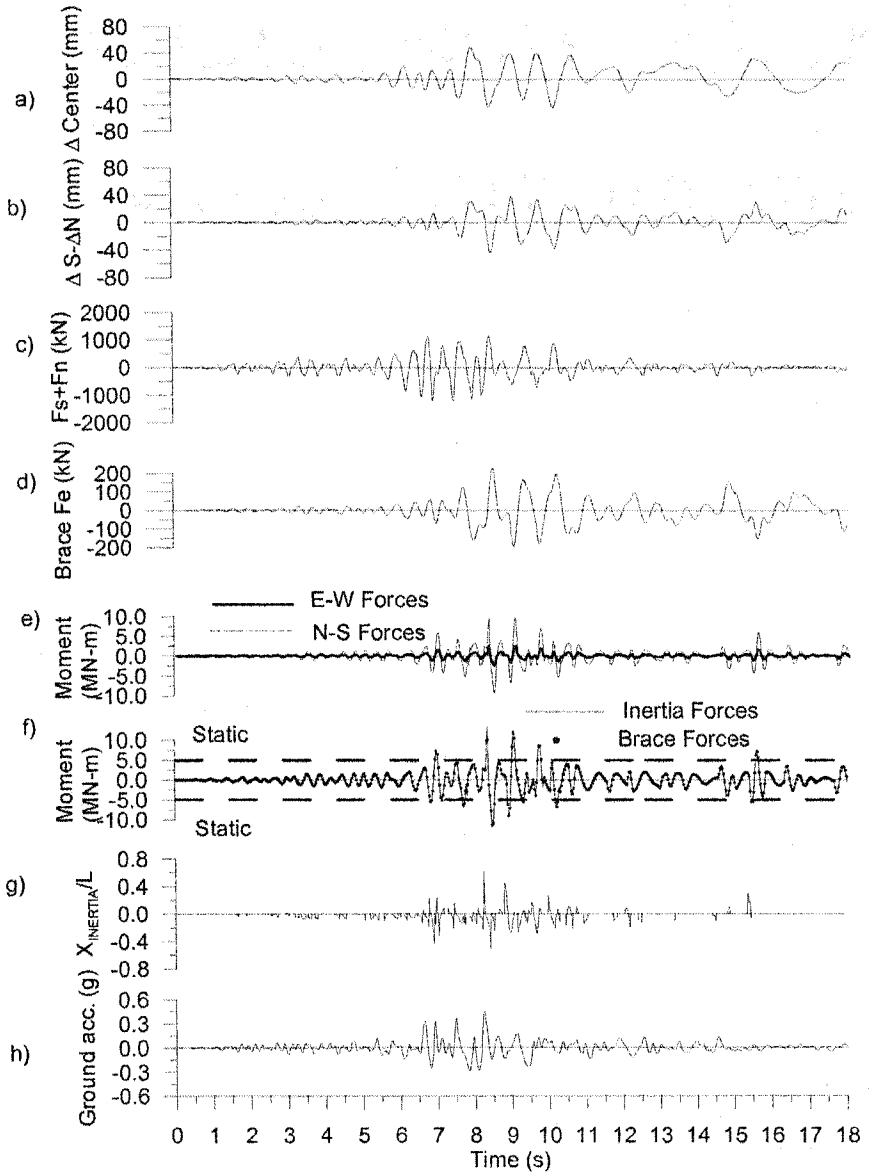

Response of 2-R-6 (Model 2-R to Seismic event No.6)

a) Storey drift at mid-length of the building; b)Difference between storey drifts at South and North walls;
c) Sum of inertia forces in E-W direction; d) Sum of brace force horizontal components in East wall;
e) Torsional moments due to E-W and N-S inertia forces;
f) Torsional moments due to total inertia forces and brace forces;
g) Location of E-W inertia center (CI); h) Selected ground motion

Figure A13. Result of 2-R-6

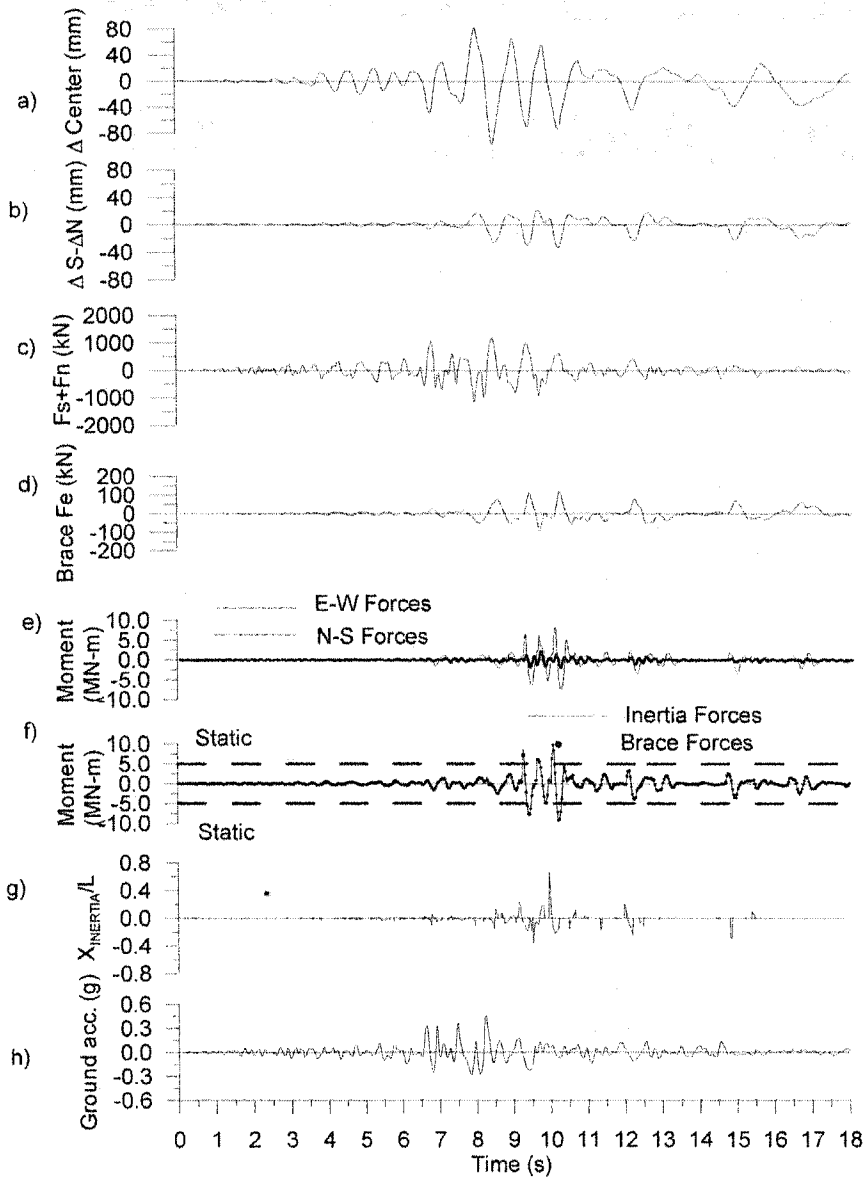

Response of 2-F-6 (Model 2-F to Seismic event No.6)

a) Storey drift at mid-length of the building; b)Difference between storey drifts at South and North walls;
c) Sum of inertia forces in E-W direction; d) Sum of brace force horizontal components in East wall;
e) Torsional moments due to E-W and N-S inertia forces;
f) Torsional moments due to total inertia forces and brace forces;
g) Location of E-W inertia center (CI); h) Selected ground motion

Figure A14. Result of 2-F-6

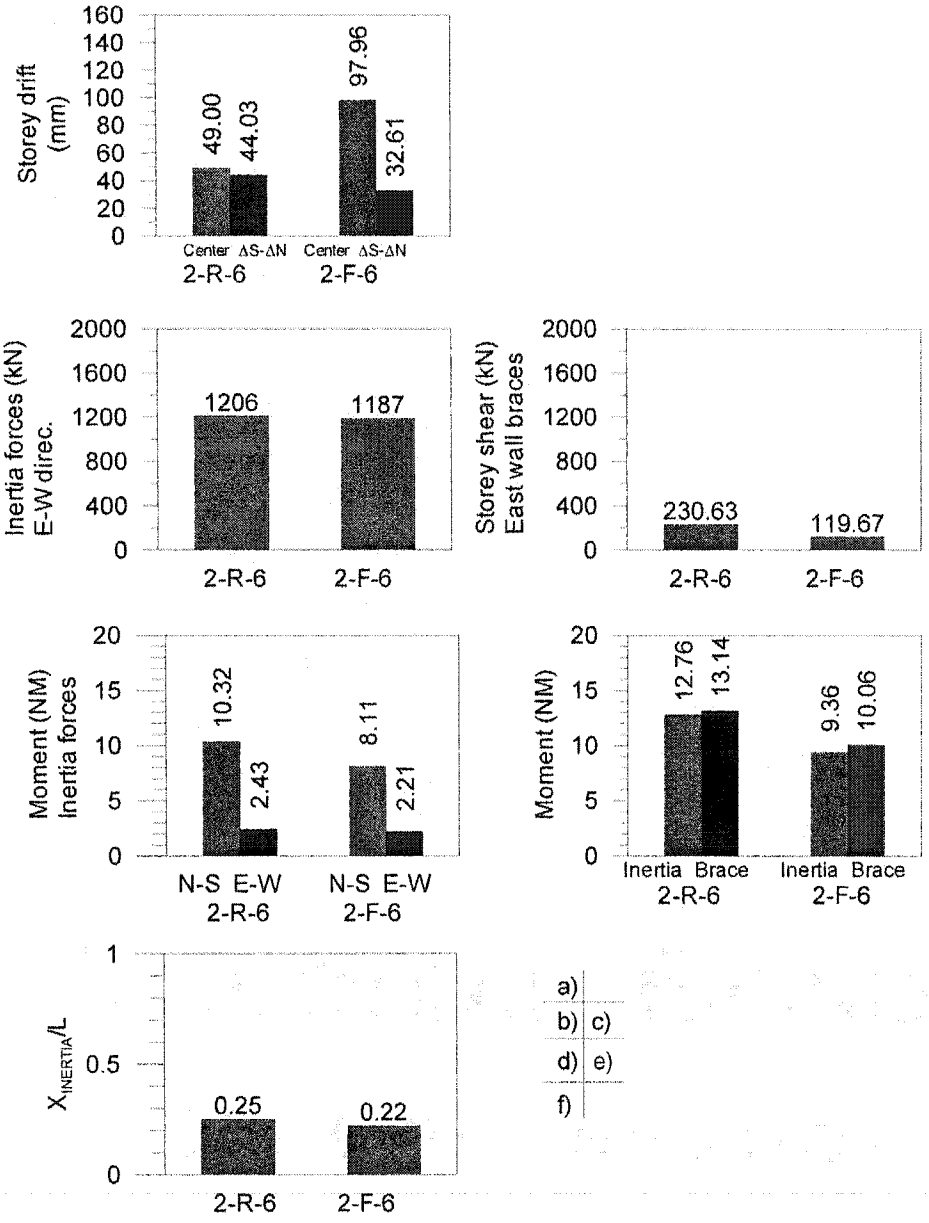

Maximum Response of 2-R-6 & 2-F-6 (Absolute value)

a) Storey drifts (at mid-length; Difference between South and North walls);
b)Sum of E-W direc. inertia forces; c) Storey shear by East wall braces;
d) Torsional moments due to inertia forces (North-South; East-West);
e)Torsional moments due to inertia forces and due to brace forces;
f) Location of E-W inertia center (CI) at maximum torsional inertia moments

Figure A15. Comparison of 2-R-6 to 2-F-6

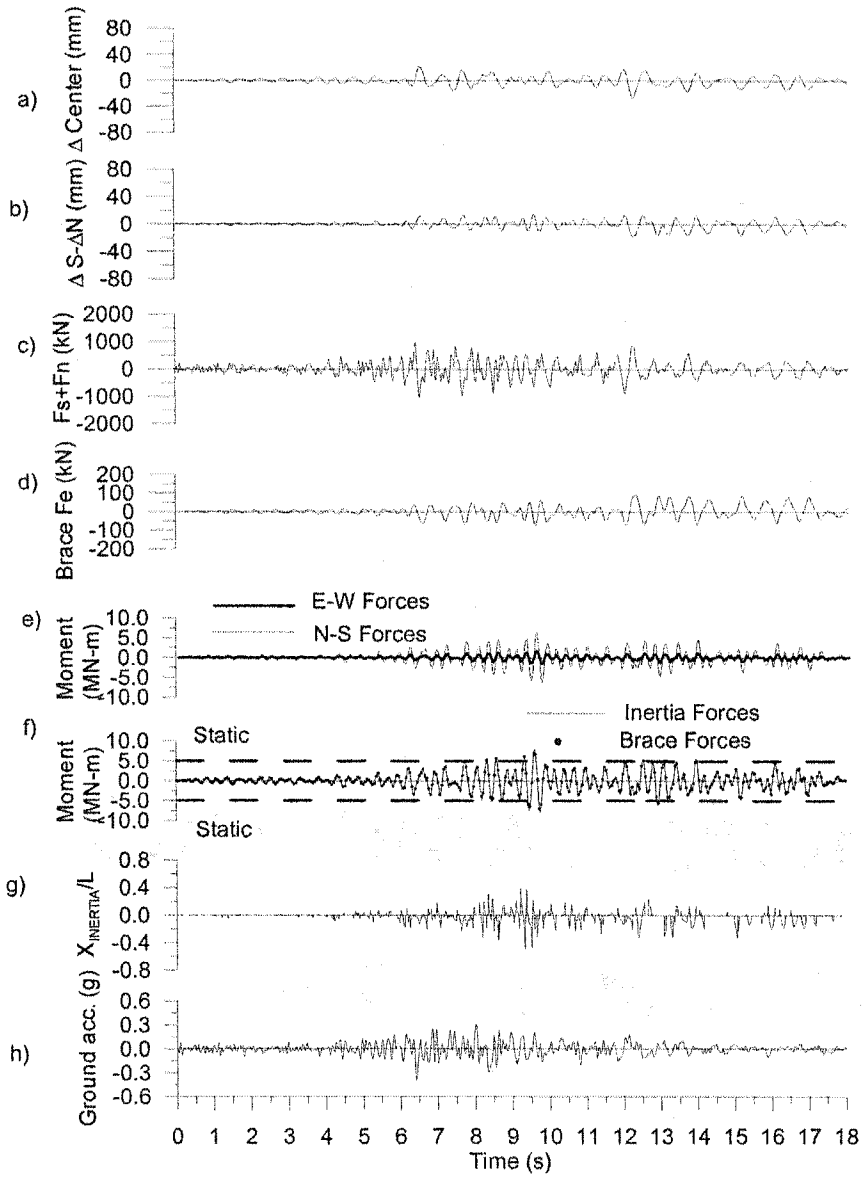

Response of 2-R-7 (Model 2-R to Seismic event No.7)

a) Storey drift at mid-length of the building; b)Difference between storey drifts at South and North walls;
c) Sum of inertia forces in E-W direction; d) Sum of brace force horizontal components in East wall;
e) Torsional moments due to E-W and N-S inertia forces;
f) Torsional moments due to total inertia forces and brace forces;
g) Location of E-W inertia center (CI); h) Selected ground motion

Figure A16. Result of 2-R-7

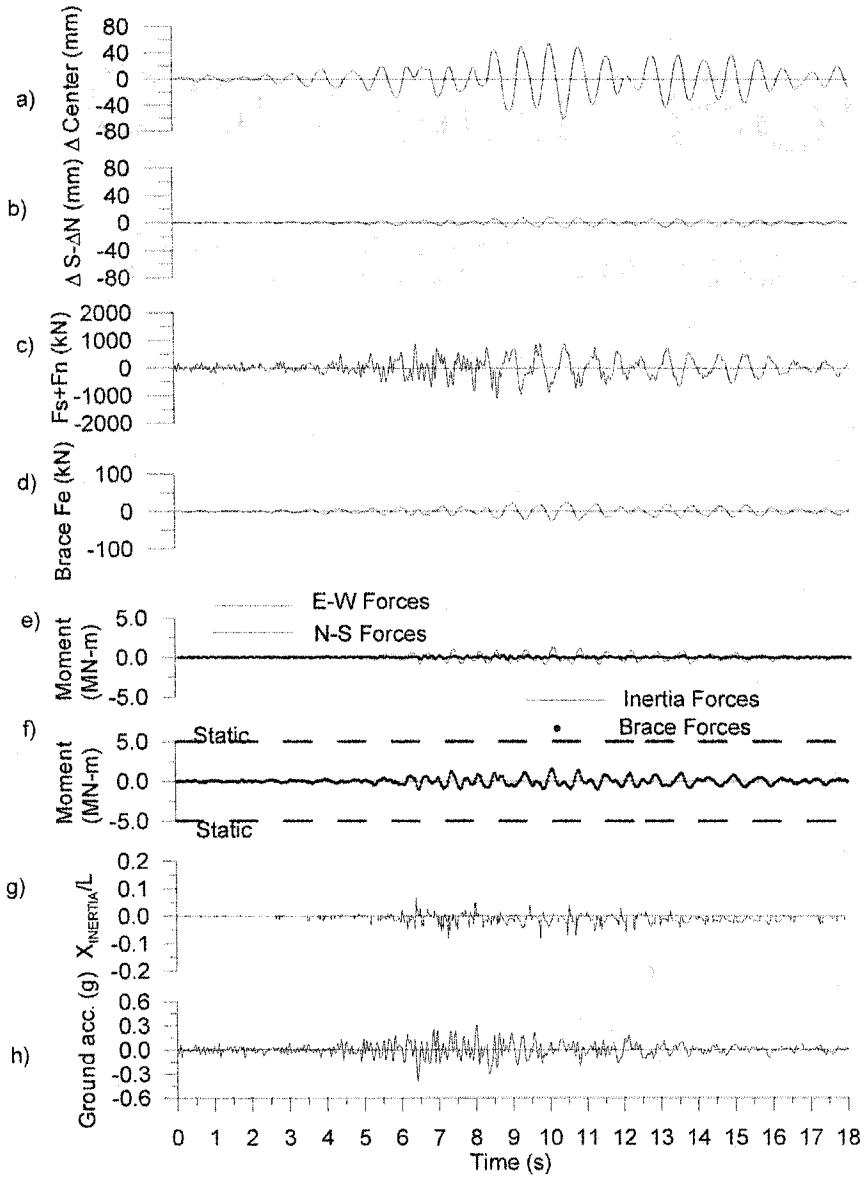

Response of 2-F-7 (Model 2-F to Seismic event No.7)

a) Storey drift at mid-length of the building; b)Difference between storey drifts at South and North walls;
c) Sum of inertia forces in E-W direction; d) Sum of brace force horizontal components in East wall;
e) Torsional moments due to E-W and N-S inertia forces;
f) Torsional moments due to total inertia forces and brace forces;
g) Location of E-W inertia center (CI); h) Selected ground motion

Figure A17. Result of 2-F-7

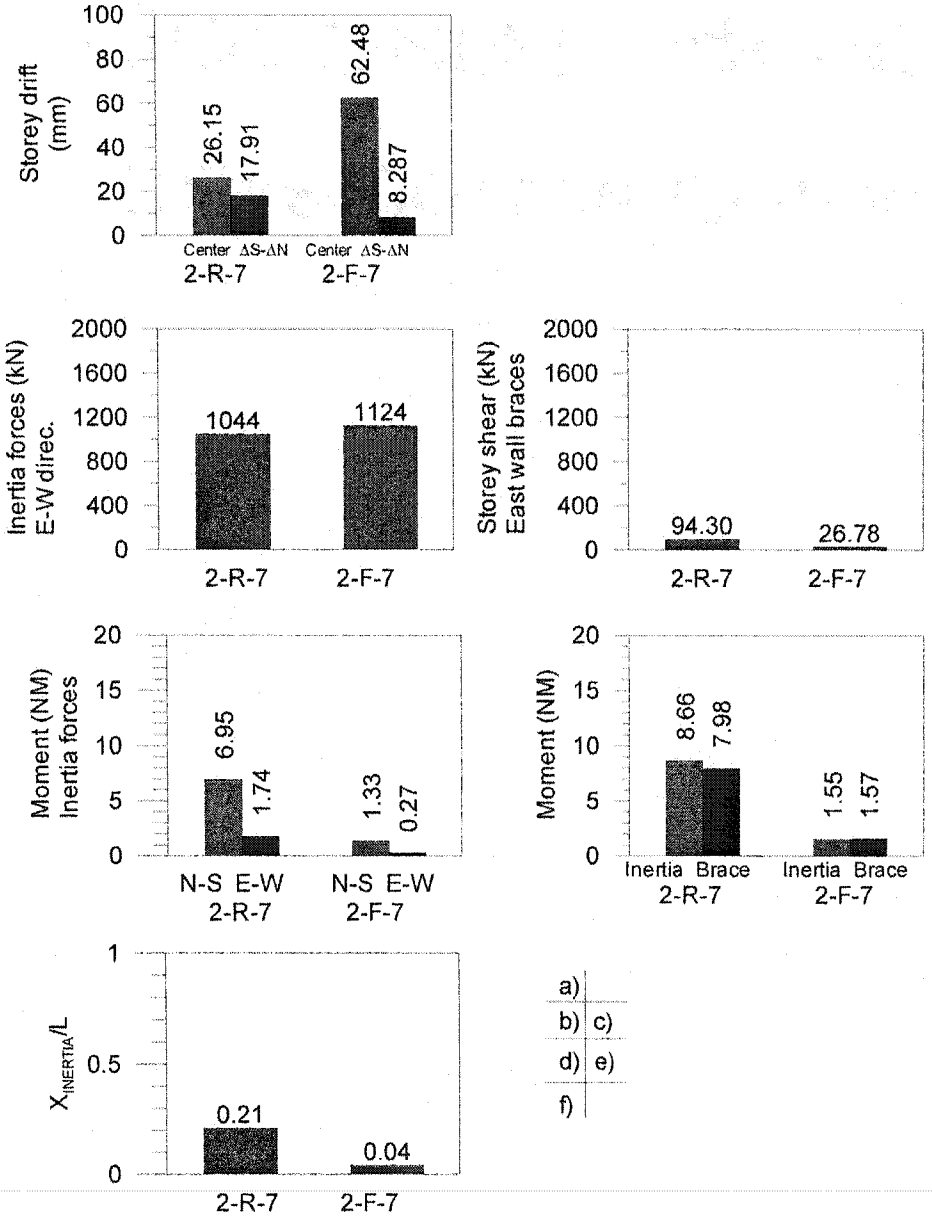

Maximum Response of 2-R-7 & 2-F-7 (Absolute value)

a) Storey drifts (at mid-length; Difference between South and North walls);
b)Sum of E-W direc. inertia forces; c) Storey shear by East wall braces;
d) Torsional moments due to inertia forces (North-South; East-West);
e)Torsional moments due to inertia forces and due to brace forces;
f) Location of E-W inertia center (CI) at maximum torsional inertia moments

Figure A18. Comparison of 2-R-7 to 2-F-7

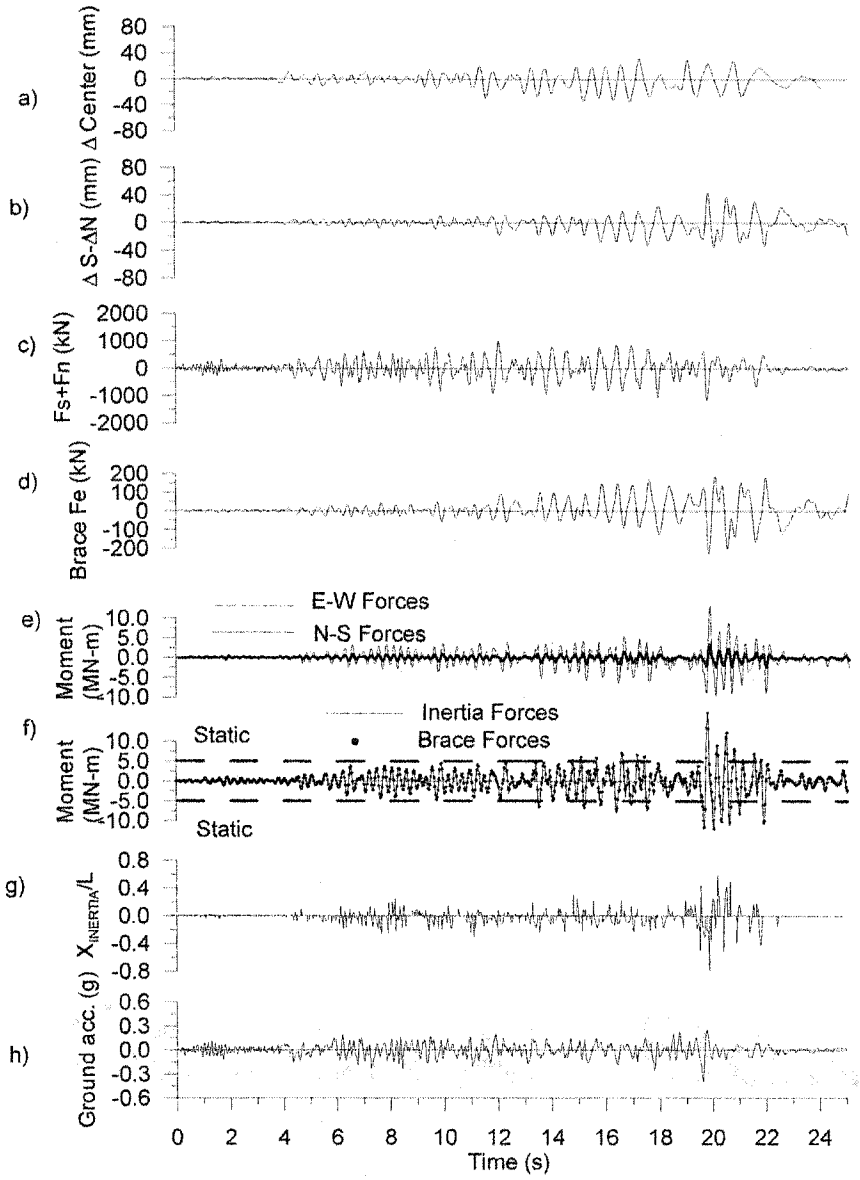

Response of 2-R-8 (Model 2-R to Seismic event No.8)

a) Storey drift at mid-length of the building; b)Difference between storey drifts at South and North walls;
c) Sum of inertia forces in E-W direction; d) Sum of brace force horizontal components in East wall;
e) Torsional moments due to E-W and N-S inertia forces;
f) Torsional moments due to total inertia forces and brace forces;
g) Location of E-W inertia center (CI); h) Selected ground motion

Figure A19. Result of 2-R-8

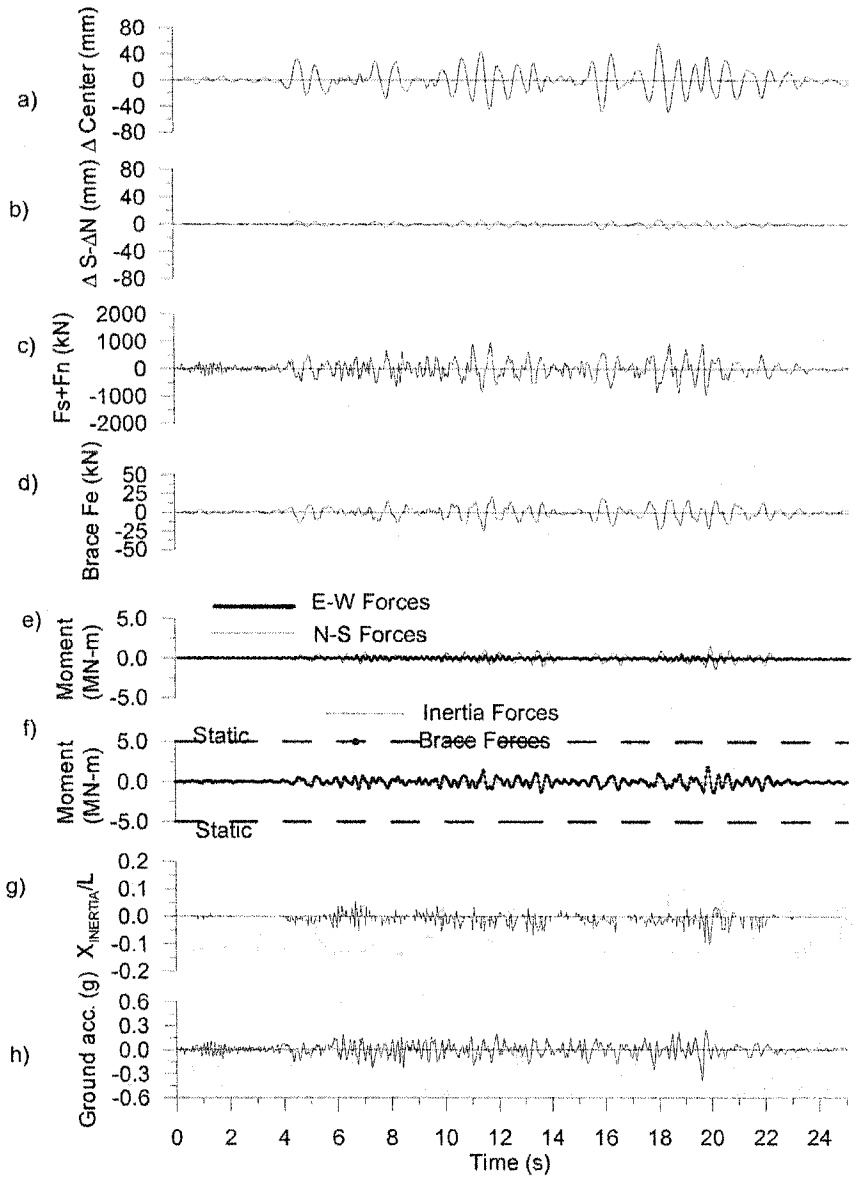

Response of 2-F-8 (Model 2-F to Seismic event No.8)

a) Storey drift at mid-length of the building; b)Difference between storey drifts at South and North walls;
c) Sum of inertia forces in E-W direction; d) Sum of brace force horizontal components in East wall;
e) Torsional moments due to E-W and N-S inertia forces;
f) Torsional moments due to total inertia forces and brace forces;
g) Location of E-W inertia center (CI); h) Selected ground motion

Figure A20. Result of 2-F-8

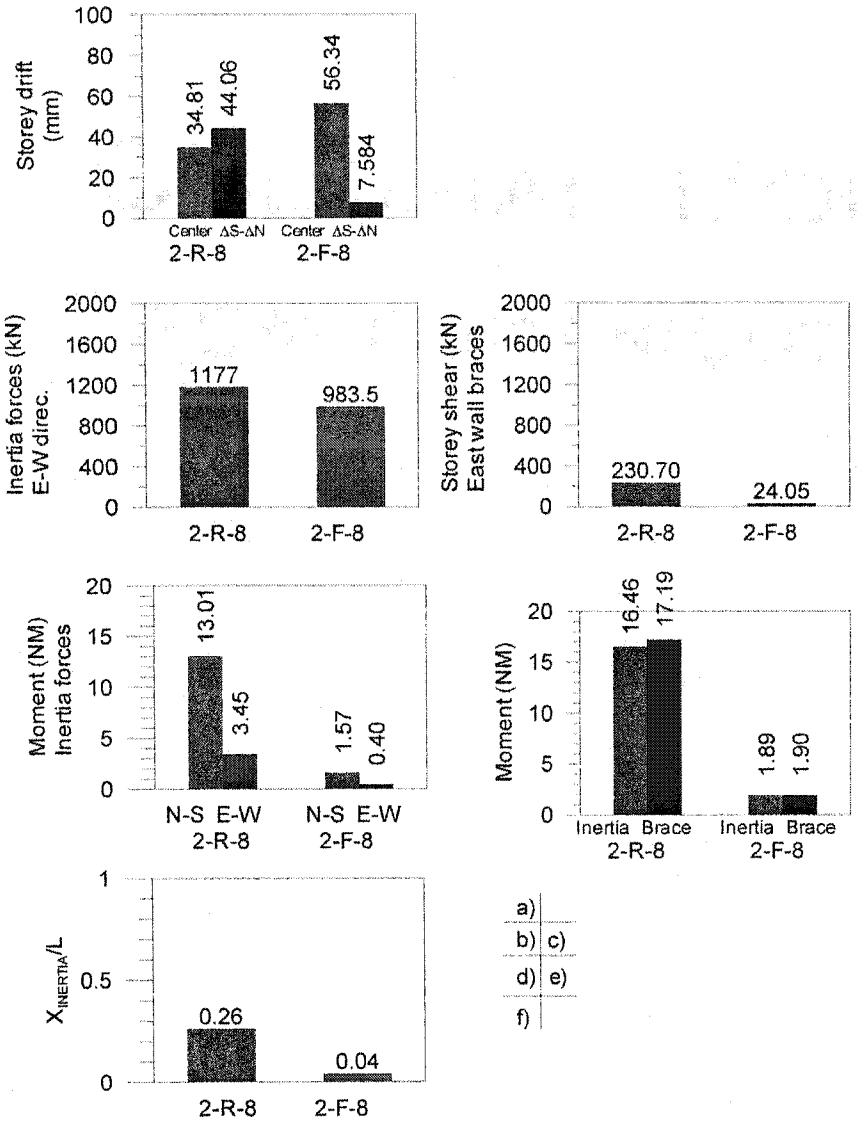

Maximum Response of 2-R-8 & 2-F-8 (Absolute value)

a) Storey drifts (at mid-length; Difference between South and North walls);
b)Sum of E-W direc. inertia forces; c) Storey shear by East wall braces;
d) Torsional moments due to inertia forces (North-South; East-West);
e)Torsional moments due to inertia forces and due to brace forces;
f) Location of E-W inertia center (CI) at maximum torsional inertia moments

Figure A21. Comparison of 2-R-8 to 2-F-8

APPENDIX 5: TORSIONAL MOMENT DRIFT PHENOMENON AND THE SOLUTIONS

A5-1. Phenomenon

Over the course of carrying out the dynamic analyses and determining the torsion response from inertia forces at the diaphragm nodes, a drift phenomenon was found for some cases, *i.e.* a noticeable difference between $T_{CM,D}$, the torsion response from inertia forces, and $T_{CM,B}$, the torsion response from brace forces. Figure A22 shows the drift phenomenon for case 2-R-5, while Figure A23 for case 2-R-7.

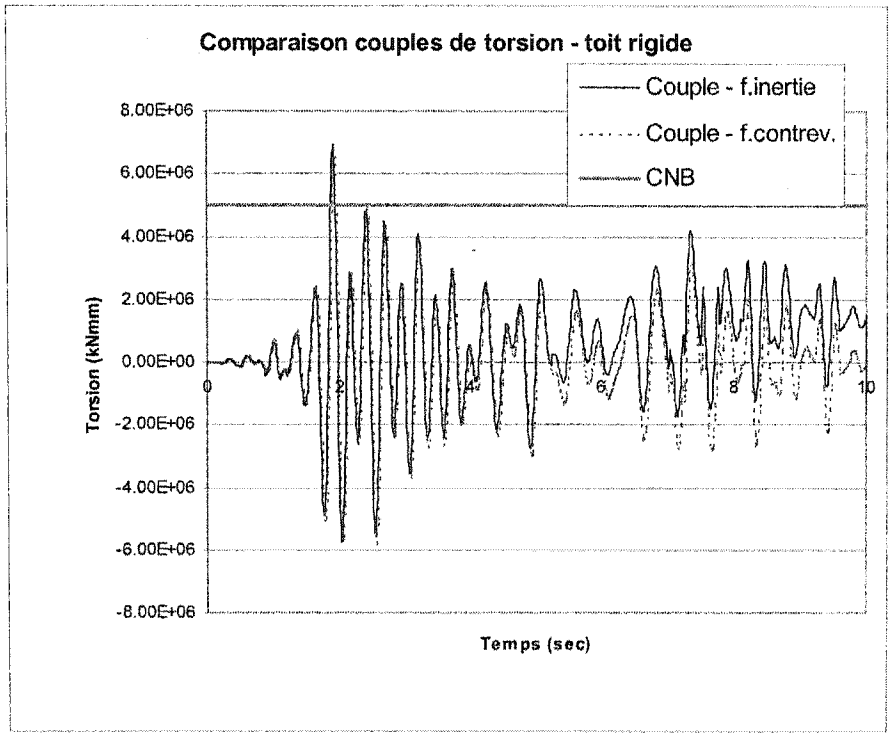

Figure A22. The drift phenomenon for case 2-R-5

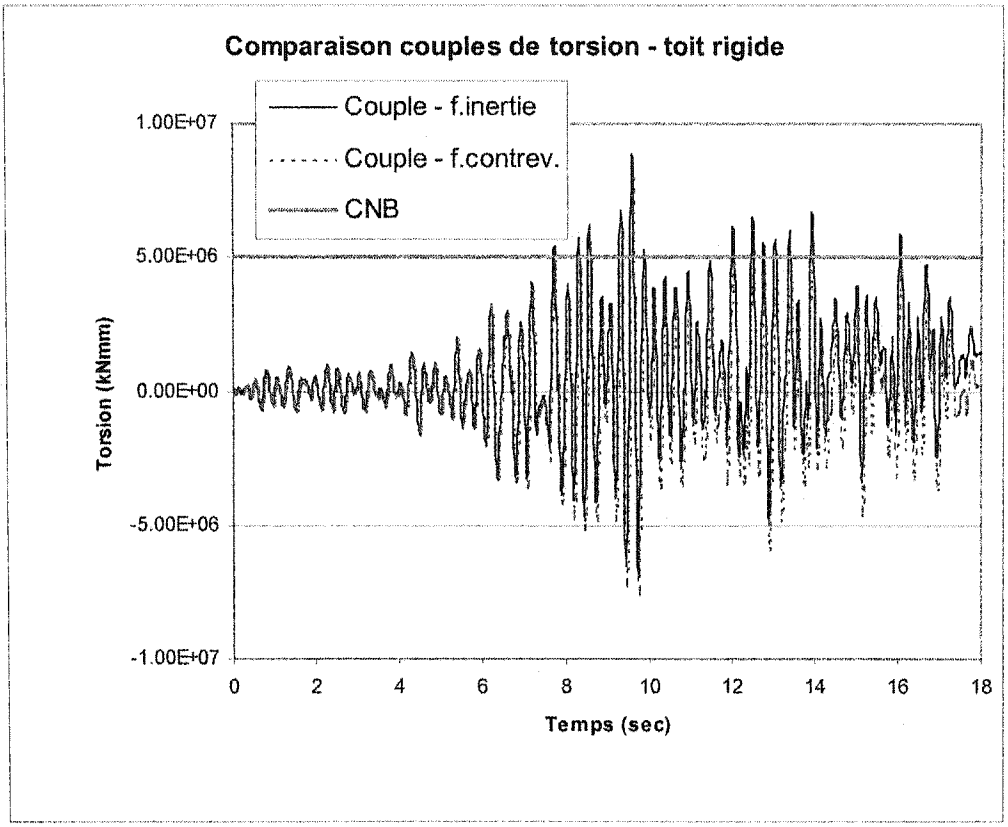

Figure A23. The drift phenomenon for case 2-R-7

Since the torsional moment is calculated from nodal accelerations, the torsional moment drift phenomenon can be attributed to the drift of these accelerations. An example of a continuously increasing acceleration for a representative node is shown in Figure A24.

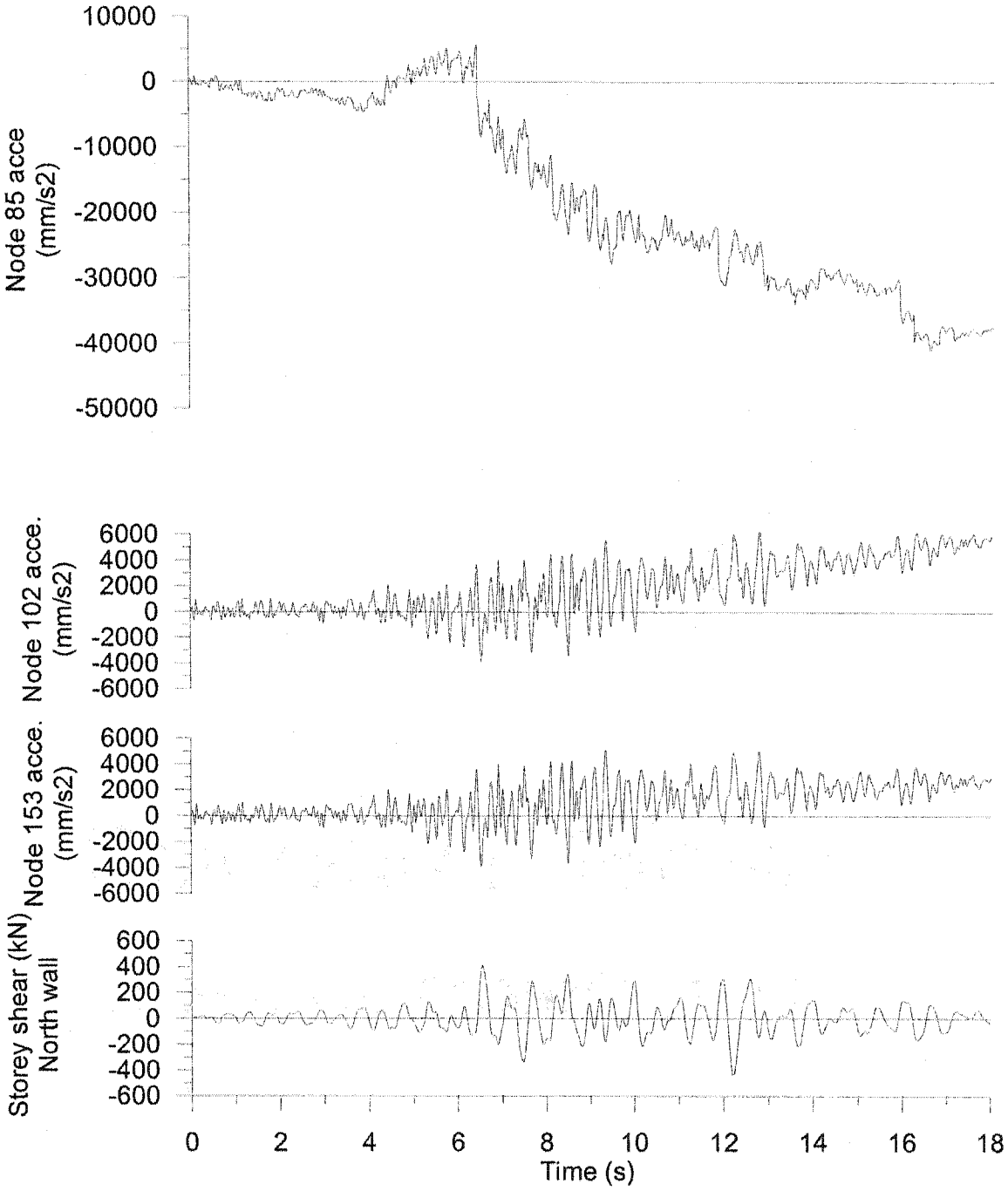

Note: The positions of these nodes refer to Figure 6.2

Figure A24. The drift phenomenon of nodal accelerations of 2-R-7

A5-2. Solution 1---reduce the roof stiffness

The above figures were obtained by assuming in the analyses that the deck diaphragm is very rigid, equalling 10^6 times the stiffness for a flexible roof.

Since no drift phenomenon was found in the flexible roof cases, one possible reason may be the stiffness difference between the deck and brace being excessive. This may have resulted in an "*ill-conditioned*" stiffness matrix (McGuire and Gallagher, 1979). Based on this consideration, the roof stiffness was reduced from the 10^6 level to the 10^3 level. For example, the G' for the flexible roof was 6.486 kN/mm was changed to 6486 kN/mm instead of 6000000 kN/mm.

For G'=6486 kN/mm, the roof was still quite stiff according to the SDI standard (1987). An improvement of node Y-direction acceleration was obtained as shown in Figure A25, where the drift phenomenon of node acceleration disappeared.

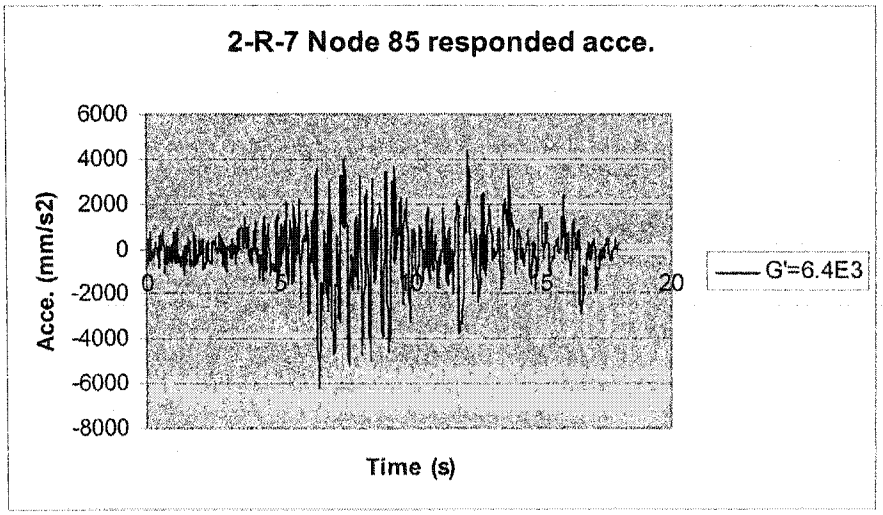

Figure A25. The improved response acceleration at node 85 with G'=6.4E3

By replacing with the new nodal accelerations from the new rigid roof (10^3 times stiffer than the flexible roof), the torsion response from the inertia forces is shown in Figure A26 for case 2-R-7.

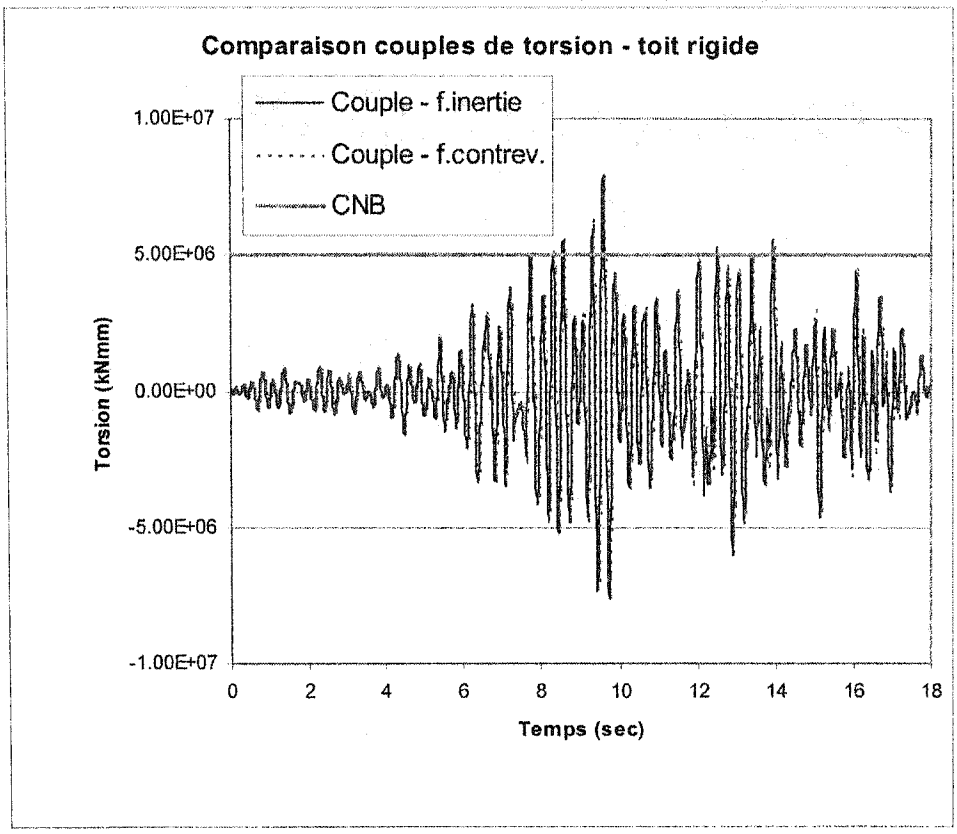

Figure A26. The torsion history of 2-R-7 at G'=6400 kN/mm

In above Figure, the drift phenomenon has disappeared and the two curves based on the deck inertia forces and the brace forces matched quite well.

Furthermore, a comparison of the storey drifts (Figure A27), relative displacements (Figure A28), and the torsional moment obtained from brace forces (Figure A29) all

provide evidence that the use of a reduced diaphragm stiffness, G'=6400 kN/mm, can maintain the same accuracy of that from G'=6.4 x 10^6 kN/mm.

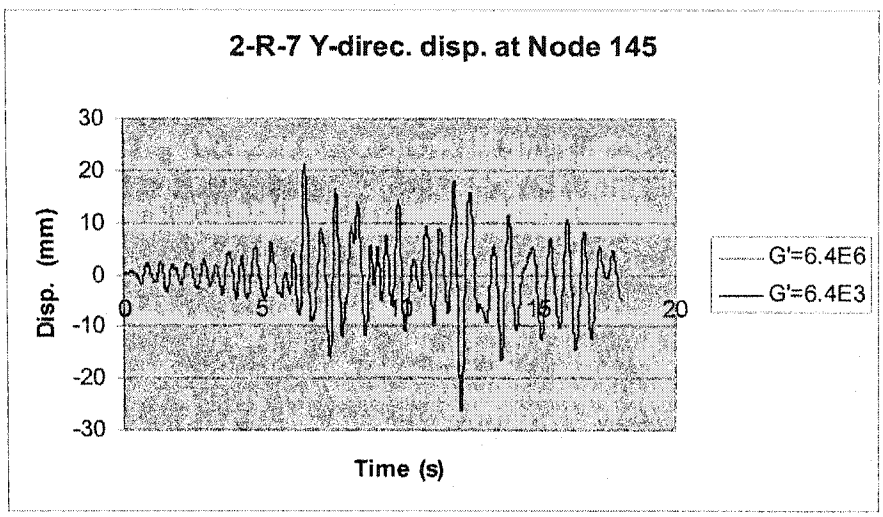

Figure A27. Comparison of peak story drift at mid-length

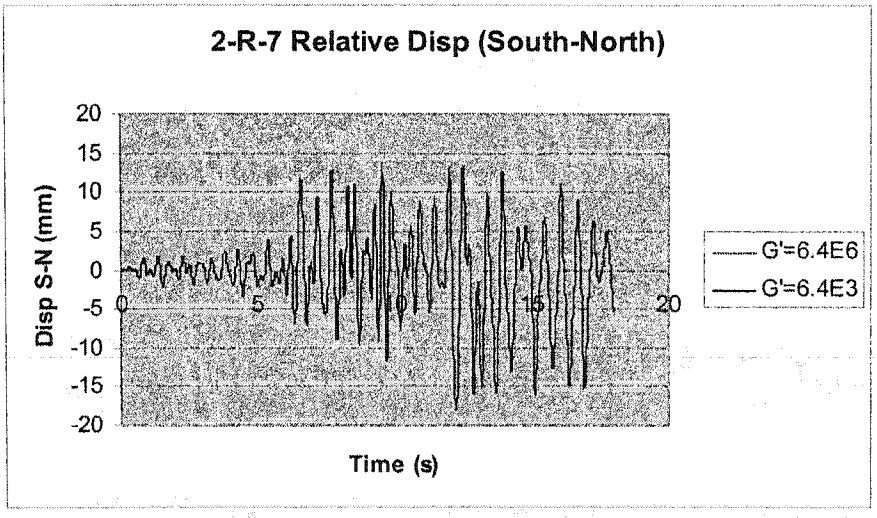

Figure A28. Comparison of relative displacement

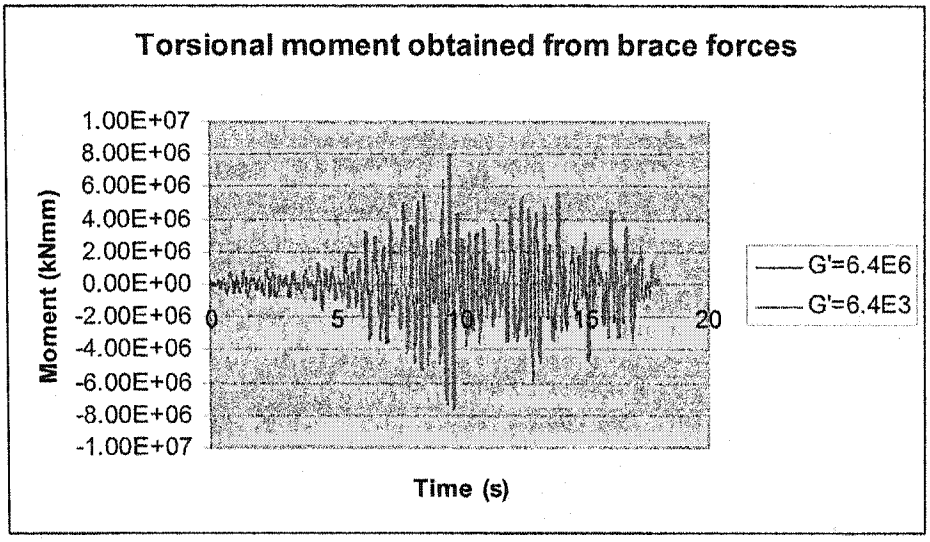

Figure A29. Comparison of torsional moment obtained from brace forces

A5-3. Solution 2----DRAIN acceleration corrections

In the step-by-step dynamic analysis of DRAIN-2DX (Prakash et al, 1993), "*equilibrium may not be satisfied at the end of a time step. Modifying the accelerations can satisfy it. This correction will usually improve the accuracy*". This correction or modification of the nodal accelerations was initially included in the input commands for the building models that were analysed, as suggested by Nedisan (2002). However, in this case the software correction did not improve the accuracy of the results, but rather resulted in the drift phenomenon presented above. Hence, this command was removed from the new DRAIN input file, resulting in a near match of the torsional moment calculated from the deck inertia forces and the brace forces (Figure A30), even when a high diaphragm shear stiffness, G'=6x10^6 kN/mm, was specified.

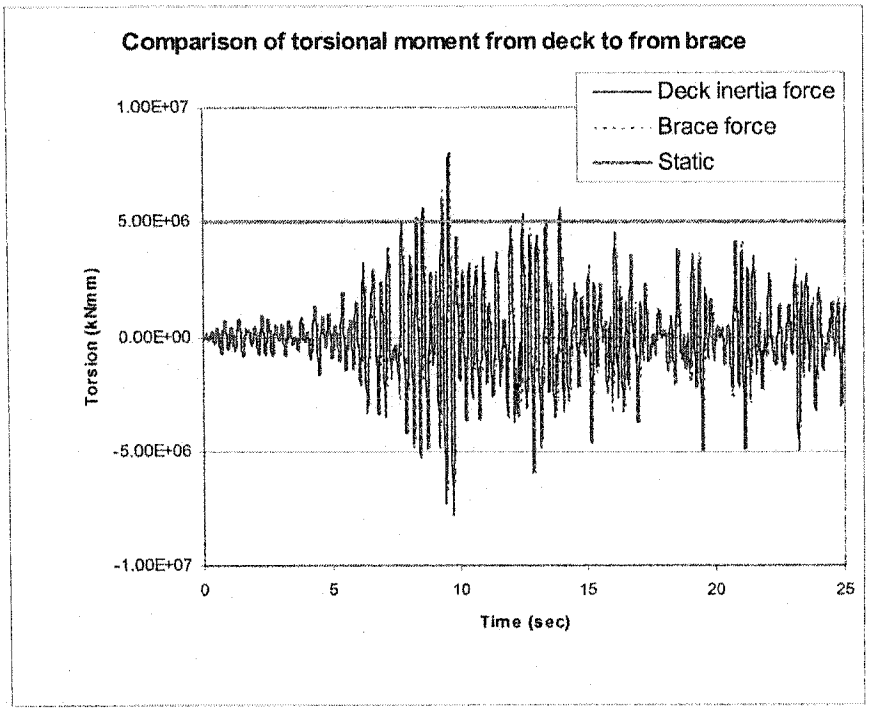

Figure A30. The torsional moment for G'=6x10^6, when node acceleration was not modified

It is important to realise that when the DRAIN command for modification of the nodal accelerations is not used, the equilibrium may not be satisfied at the end of a time step. But it was found that the maximum unbalanced force obtained in the analyses was 6.39 kN for model 2-R-7, and for most time steps, it was very small ($\approx 10^{-8}$ level). This unbalanced force (6.39 kN) should be acceptable if compared to the maximum inertia force in the Y-direction that was equal to 1044 kN for 2-R-7 case, the relative error is less than 1%.